Current Trends in International Fusion Research

Proceedings of the Second Symposium

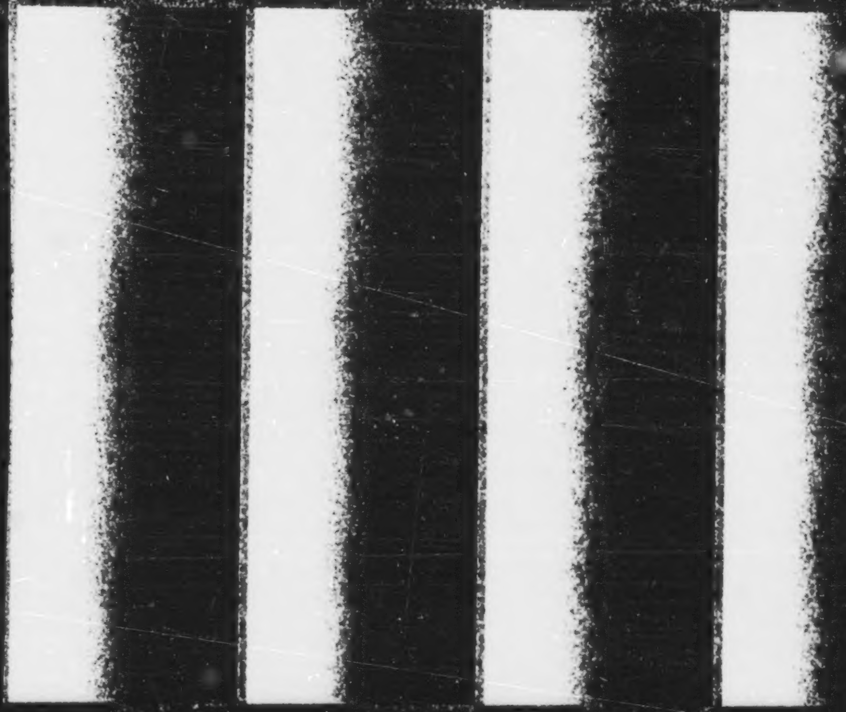

Edited by
Emilio Panarella

Current Trends in International Fusion Research

Proceedings of the Second Symposium

© 1999 National Research Council of Canada

All rights reserved. No part of this publication may be reproduced in a retrieval system, or transmitted by any means, electronic, mechanical, photocopying, recording or otherwise, without the prior written permission of the National Research Council of Canada, Ottawa, Ontario K1A 0R6, Canada.
Printed in Canada on acid-free paper.

This publication was produced from camera-ready copy provided by the editor.

ISBN 0-066-17522-3
NRC No. 41654

Canadian Cataloguing in Publication Data

Current trends in international fusion research — proceedings of the second symposium

Held in Washington, D.C. on March 10–14, 1997. — Intro.
Issued by the National Research Council of Canada
Includes bibliographical references
Includes in index
ISBN 0-660-17522-3
NRC No. 41654

1. Nuclean fusion — Congresses. 2. Plasma (Ionized gases) — Congresses.
I. Panarella, E. (Emilio) II. National Research Council of Canada

QC790.97C87 1999 539.7'64 C98-980241-8

Inquiries: Proceedings Program, NRC Research Press, National Research Council of Canada, Ottawa, Ontario K1A 0R6, Canada.

Correct citation for this publication: Panarella, E. (*Editor*). 1999. Current Trends in International Fusion Research — Proceedings of the Second Symposium. NRC Research Press, Ottawa, Ontario, Canada. 492 p.

Current Trends in International Fusion Research

Proceedings of the Second Symposium

Edited by

Emilio Panarella

Advanced Laser and Fusion Technology, Inc.
189 Deveault Street, Unit 7
Hull, Québec J8Z 1S7, Canada

NRC-CNRC
NRC Research Press
Ottawa, 1999

2nd SYMPOSIUM ON CURRENT TRENDS IN INTERNATIONAL FUSION RESEARCH

Review and Assessment

INTERNATIONAL ADVISORY BOARD

Bruno Coppi
Department of Physics
Massachusetts Institute of Technology
Rm. 26-217
Cambridge, MA 02139, U.S.A.

George H. Miley
216 Nuclear Engineering Laboratory
University of Illinois
103 S. Goodwin Avenue
Urbana, IL 61801, U.S.A.

Hans Persson
Fusion Plasma Physics
Alfvén Laboratory
Royal Institute of Technology
S- 100 44 Stockholm, Sweden

Richard F. Post
Lawrence Livermore National Laboratory
P.O. Box 808, L-644
Livermore, CA 94550, U.S.A.

Shenggang Liu
The University of Electronic Science
and Technology of China
Chegdu, Sichuan Province, 610054
People's Republic of China

R. N. Sudan
Laboratory for Plasma Studies
Cornell University
369 Upson Hall
Ithaca, NY 14853, U.S.A.

Edward Teller
Herbert Hoover Memorial Bldg.
Room 208
Stanford University
Stanford, CA 94305, U.S.A.

Guillermo Velarde
Instituto de Fusion Nuclear
Universidad Politecnica de Madrid
José Guitiérrez Abascal, 2
Madrid 28006, Spain

Chiyoe Yamanaka
Institute for Laser Technology
Yamadaoka 2-6
Suita, Osaka 565, Japan

Masaji Yoshikawa
Japan Atomic Energy Research Institute
2-2, Uchisaiwaicho 2-chome
Chiyoda-ku Tokyo 100, Japan

STEERING COMMITTEE

Michel de Peretti
Centre d'Études de Limeil Valenton
94195 Villeneuve-St. Georges, France

Francesco Giammanco
Department of Physics
University of Pisa
56100 Pisa, Italy

Julio Herrera
Instituto de Ciencias Nucleares
Universidad Nacional Autonoma de Mexico
Circuito Exterior C.U. A.P. 70-543
045 10 Mexico DF, Mexico

Ronald C. Kirkpatrick
MS B229
Los Alamos National Laboratory
Los Alamos, NM 87544, U.S.A.

Behram Kursunoglu
Global Foundation, Inc.
P.O. Box 249055
Coral Gables, FL 33124-9055, U.S.A.

Vincenzo Molinari
Department of Nuclear Engineering
University of Bologna
Via dei Colli, 16
40136 Bologna, Italy

Sadao Nakai
Institute of Laser Engineering
Osaka University
2-6 Yamada-oka
Suita Osaka, 565 Japan

Emilio Panarella
Advanced Laser and Fusion Technology, Inc.
189 Deveault St., Unit No. 7
Hull, P.Q., J8Z I S7 Canada, and
Department of Electrical Engineering
University of Tenneessee
Ferris Hall
Knoxville, TN 37996-2100, U.S.A.

Francesco Pegoraro
Dipartimento di Fisica
Universitá di Torino
10125 Torino, Italy

Hafiz-Ur Rahman
Institute of Geophysics and Planetary Physics
University of California
Riverside, CA 92521-0412, U.S.A.

Norman Rostoker
Department of Physics
University of California
Irvine, CA 92697-4575, U.S.A.

J. Reece Roth
Department of Electrical Engineering
The University of Tennessee
Knoxville, TN 37996-2100, U.S.A.

Nikos A. Salingaros
Division of Mathematics
The University of Texas
San Antonio, TX 78249-0664, U.S.A.

Y. Chia Thio
Massey University at Albany
Mathematics Department
Private Bag 102-904
North Shore MSC, Auckland, New Zealand

Moreno Vaselli
Scientific Attache
Embassy of Italy
Uliza Jesnina, 5
121002 Moscow, Russia

PANEL OF EVALUATORS

Stirling A. Colgate
MS-B275
Los Alamos National Laboratory
Los Alamos, NM 87545, U.S.A.

Edward C. Creutz
P.O. Box 2757
Rancho Santa Fe, CA 92067, U.S.A.

Arthur R. Kantrowitz
4 Downing Road
Hanover, NH 03755, U.S.A.

Joseph E. Lannutti
515 Keen Building
Florida State University
Tallahassee, FL 32306-3016, U.S.A.

Hans J. Schneider-Muntau
National High Magnetic Field Laboratory
Florida State University
Tallahassee, FL 32306-4005, U.S.A.

Glenn T. Seaborg
Bldg. 70/A Rm. 3307
Lawrence Berkeley Laboratory
1 Cyclotron Road
Berkeley, CA 94720, U.S.A.

Frederick Seitz
The Rockfeller University
1230 York Ave.
New York, NY 10021-6399, U.S.A.

CONTENTS

1. Opening Remarks 1
E. Panarella

SECTION I

2. Fusion Research: The Past is Prologue 5
Richard F. Post

Magnetic Confinement

3. Recent Progress in Plasma Focus Development: from an Existing 3 MJ to Projected 100 MJ Plasma Focus Installation 27
N.V. Filippov, T.I. Filippova V.I. Krauz, E.A. Azizov, L.G. Golubchikov, A.P. Lototsky, A.F. Nastoyashchy, N.G. Makeev and V.G. Rumyantsev

4. Review on a Dense Plasma Focus Research Line and Projections in the Nuclear Fusion Field 41
Jorge 0. Pouzo

5. The International Center for Dense Magnetized Plasmas: An Outline 59
A. Bernard, H. Bruzzone, P. Choi, H. Chuaqui, V. Gribkov, J. Herrera, K. Hirano, K. Kolácek, S. Lee, C. Luo, F. Mezzetti, M. Sadowski, H. Schmidt, K. Ware, C.S. Wong and V. Zoita
(The ICDMP Steering Committee)

6. Heliotron Research at Kyoto University 65
T. Obiki, S. Besshou, K. Hanatani, K. Kondo, T. Mizuuchi, K. Nagasaki, Y. Nakamura, M. Nakasuga, H. Okada, F. Sano and M. Wakatani

Inertial Confinement

7. Inertial Confinement Fusion at the Los Alamos National Laboratory 77
E. Lindman, D. Baker, C. Barnes, B. Bauer, J.B. Beck, R. Berggren, B. Bejzzerides, P. Bradley, R.E. Chrien, M. Clover, J. Cobble, C.A. Coverdale, M. Cray, N. Delamater, D. DuBois, B.H. Failor, J.C. Fernandez, L. Foreman, R. Gibson, P. Gobby, S.R. Goldman, D. Harris, A. Hauer, J. Hoffer, N. Hoffman, W.W. Hsing, R. Johnson, K. Klare, R. Kopp, W. Krauser, G. Kyrala, G. Magelssen, R. Mason, D. Montgomery, T.J. Murphy, J. Oertel, G. Pollak, H. Rose, K. Schoenber, D.P. Smitherman, M.S. Sorem, F. Swenson, D. Tubbs, W. Varnum, H. Vu, J. Wallace, R. Watt, R. Weaver, B. Wilde, M. Wilke, D. Wilson and W.M. Wood

8. Dissipative Phenomena in Shock Wave Implosion 93
F. Giammanco

9. The Spherical Pinch as a Radiation Source for EUV Lithography 103
J. Zhao and E. Panarella

10. Magnetized Target Fusion in a Spheroidal Geometry with Standoff Drivers 113
Y.C.F. Thio, E. Panarella, R.C. Kirkpatrick, C.E. Knapp, F. Wysocki, P. Parks and G. Schmidt

11. Geometry of the Spherical Pinch 133
Nikos Salingaros

SECTION II

12. Physics of Fusion Burning Plasmas, Ignition and Relevant Technologies 135
Bruno Coppi

Magnetic Confinement

13. High Confinement Regime in TFTR Configurations with Reversed Magnetic Shear 137
Ernesto Mazzucato and TFTR Group

14. FRC Fusion Reactor for Deep Space Propulsion 145
John Slough and Kenneth Miller

15. Experimental Initiation of Field-Reversed Configuration (FRC) Toward Helium-3 Fusion 155
Seiichi Goto

16. Helium-3 Fusion Based on a Field-Reversed Configuration 163
Hiromu Momota and Yukihiro Tomita

17. A User Facility for Research on Fusion Systems with Dense Plasmas ... 171
Dmitri D. Ryutov

Other Confinement

18. IEC Neutron Source Development and Potential Well Measurements ... 177
George H. Miley and Yibin Gu

19. A Prospect of the Tandem Mirror Fusion Approach 197
Teruo Tamano

20. Magnetic Pressure Driven Spherical Liner Implosion Experiments 203
James H. Degnan, Sean K. Coffey, Donald G. Gale, Jack D. Graham, James J. Havranek, Thomas W. Hussey, Gerald F. Kiuttu, Bret Kreh, F. Mark Lehr, Dane Morgan, Robert E. Peterkin, Jr., David Platts, Norman F. Roderick, Edward L. Ruden, Wayne Sommers and Peter J. Turchi

21. The Advances in Programming Compact Torus (PCT) Physics and Conceptual Design 209
Rustam Kh. Kurtmullaev

22. Innovative Confinement Concepts Workshop 211
Ronald C. Kirkpatrick

SECTION III

23. Present Status and Future Prospect of Inertial Confinement Fusion in Japan 213
Tatsuhiko Yamanaka

Inertial Confinement

24. Inertial Fusion Targets Ignition by Hypervelocity Plasma Jets 227
J.M. Martinez-Val, P.M. Velarde and S. Eliezer

25. Numerical Simulation of ICF Experiments and Conceptual Designs 239
Pedro Velarde

26. Prospects for Inertial Fusion Energy Based on a Diode-Pumped Solid-State Laser (DPSSL) Driver: Overview and Development Path 241
Charles D. Orth

27. Status of Direct-Drive Inertial Confinement Fusion Research at the Laboratory for Laser Energetics 251
Robert L. McCrory and John M. Soures

28. Magnetized Compression/Magnetized Target Fusion (MAGO/MTF) – An Update 261
Ronald C. Kirkpatrick and Irvin R. Lindemuth

29. Staged Z Pinches for Controlled Thermonuclear Fusion: Theoretical Studies 279
H.U. Rahman, P. Ney, F.J. Wessel and N. Rostoker

30. UCI Staged Z-Pinch 281
F.J. Wessel, B. Moonsman, N. Rostoker, Y. Song, A. Van Drie, P. Ney and H.U. Rahman

31. Study of ICF-Energy Conversion Schemes with Magnetic Field with Magnetic Field in Laser-Produced Plasma Experiments and PIC-Simulation 287
Yu. P. Zakharov, A.G. Ponomarenko, H. Nakashima and Y. Nagamine

SECTION IV

32. The Colliding Beam Fusion Reactor I. Solution to the Problem of Anomalous Transport with Beams in a Field Reversed Configuration Plasma 291
N. Rostoker, M.W. Binderbauer and H.J. Monkhorst

Magnetic Confinem

33. An Overview of Reversed-Field Pinch Research 303
D.A. Baker and J.A. Phillips

34. The Colliding Beam Fusion Reactor II. Atomic and Nuclear Physics of Spin Polarized H and B^{11} Fuel Beams 317
Hendrick J. Monkhorst, Michl W. Binderbauer and Norman Rostoker

35. Kinetic Ballooning Modes in Tokamaks 341
A. Hirose, M. Elia, M. Yamagiwa and L. Zhang

36. The Role of Magnetic Turbulence in the Sawtooth Relaxation Process in SINP Tokamak 351
Amit Kumar Hui, Ratan Kumar Paul and Dipark Banik

Other

37. Breakeven Criteria for DT Plasmas in Reactor-Type Conditions 353
E. Panarella

38. Issues of Fusion Burn Control 373
Hans Persson

39. Fusion of Deuterium Nuclei and Other Nuclear Processes in a Metallic Lattice 383
David W. Kraft and Lloyd Motz

40. New Physics for Fusion Energy 395
J. Reece Roth

41. The Los Alamos Intense Neutron Source 411
R.A. Nebel, D.C. Barnes, R. Bollman, G. Eden, L. Morrison, M.M. Pickrell and W. Reass

42. On the Possibility to Duplicate in the Laboratory Fusion Relevant Ball Lightnings 427
Mircea Sanduloviciu and Emilia Lozneanu

SECTION V

Other

43. Advanced Analyzers and Probes for Fusion-Plasma Diagnostics 431
Edbertho Leal-Quiros and Mark A. Prelas

44. Centrifugally Confined Plasmas: Enhanced Stability Scenarios 455
M.G. Jackson, B.R. Osborn, R.F. Ellis and A.B. Hassam

45. Confinement of a Rotating Degenerate Gas of Ions in a Magnetic Field 461
Vincenzo Molinari and Domiziano Mostacci

Inertial Confinement

46. Magnetic Compression/ Magnetized Target Fusion (MAGO/MTF): A Marriage of Inertial and Magnetic Confinement 463
Irvin R. Lindemuth, Carl Ekdahl, Ronald C. Kirkpatrick, Robert Reinovsky, Richard Siemon, Peter Sheeney, Frederick Wysocky, Vladimir Chernyshev, Vladislav Mokhov, Anatoli Demin, Sergei Garaniin, James Hammer, Dmitri Ryutov, Arthur Toor, Chris Deeney, Dillon McDaniel, James Degnan, Gerald Kiuttu and Robert Peterkin, Jr.

47. Hohlraum Targets Driven by Cluster Ion Beams for Inertial Confinement Fusion 467
C. Deutsch, N.A. Tahir, 0. Geb and J.A. Marhun

SECTION VI

48. Concluding Remarks 469
Emilio Panarella, Chairman of the Steering Committee

SECTION VII

49. Report of the Evaluators 471
Stirling A. Colgate, Edward C. Creutz, Arthur R. Kantrowitz, Joseph E. Lannutti, Hans J. Schneider-Muntau, Glenn T. Seaborg and Frederick Seitz

50. Biographies of Evaluators 475

Participants 481

Index 487

101-03315/

OPENING REMARKS

Emilio Panarella, Chairman of the Steering Committee

Advanced Laser and Fusion Technology, Inc.
189 Deveault St., No. 7, Hull, P. Q. Canada, and
Department of Electrical Engineering
University of Tennessee
Knoxville, Tennesee 37996-2100, U.S.A.

Before I begin my opening address to you, Dr. Edward Teller, a member of the International Advisory Board of this Symposium, who is not here for health reasons, has asked me to read the following comments on fusion research:

> "I would like to limit my comments mainly to what I feel are the most likely near-term consequences of research in inertial fusion and magnetic fusion. I will not speculate on whether or not in the foreseeable future either of these approaches will turn into a major source of electrical power. However, an enduring consequence of these researches will be their contribution to our understanding of the behaviour of matter under unusual conditions. Out of this understanding will, I am sure, flow consequences that we cannot foresee."

These remarks by Dr. Teller are very appropriate within the context of the nature of this Symposium, which I now take great pleasure in opening. This 2nd Symposium "Current Trends in International Fusion Research: Review and Assessment" is organized under the auspices of the Global Foundation. This is a nonprofit organization for global issues and frontier problems in science, which is guided by three objectives:

1. To make definitive impact by disseminating and effectively communicating its research and incisive analyses;
2. To offer its research results on strategic issues to interested governments, and
3. To recommend appropriate sources of energy which are compatible with environmental protection and economic development.

These objectives are clearly our own because we want to have with this Symposium a definitive impact of our research analyses. We want to offer to interested governments our recommendations on the strategic issues of fusion energy production and spinoff benefits, and we definitively want to recommend fusion as an appropriate source of energy compatible with environmental protection and economic development.

If we look at the past, I would like to quote from the Concluding Remarks of the Symposium of two years ago, when I said, and I quote:

Current Trends in International Fusion Research – Proceedings of the Second Symposium
Edited by E. Panarella. NRC Research Press, National Research Council of Canada, Ottawa, ON K1A OR6, Canada. 1999.

> "What we have done in the past five days cannot go unnoticed. With the demonstration of the individual and collective value of our work, we have left a strong mark of our presence within the plasma and fusion community. In the past five days we have proclaimed that plasma and fusion science has a value per se, independent of the ultimate goal, be it energy production or industrial applications. We have proclaimed that the basic value of the physics of plasmas has predominance over other considerations. We have also demonstrated that, while our desire to increase our knowledge in the physics of plasmas should be acknowledged and accepted, this does not distract us from the ambitious goal of reaching the objective of controlled fusion. We have sent a strong signal that the methodology of science, which can be expressed in a few simple words, namely 'one step at a time', is what guides us in our progression towards scientific and technological goals. We have also sent a signal that the selection criterion in 'big versus small science' should be used with exponentially increasing care when one moves from small to big."

If we pause therefore for a moment, and consider what we have achieved with the 1st Symposium of two years ago, we find that the impact of that meeting has been significant. Firstly, the wealth of fusion concepts presented at that meeting demonstrated that fusion is not a static science, but it is an evolving discipline where creativity and innovation are as much ingredients to achieve energy from fusion as engineering and technology are. Secondly, we demonstrated that a balanced approach to fusion is the most appropriate way to deal with this challenge, rather than concentrating the effort in one or perhaps two lines of research, because the risk of failure is thus greatly reduced. Thirdly, we demonstrated that the fusion community, irrespective of the research program in which one works, is united in this endeavour to achieve controlled thermonuclear fusion, because all fusion programs were represented, unevenly perhaps, but still sufficiently strong to make their case. Most importantly, two years ago we initiated an irreversible process of revision of the policies governing the approach to the fusion problem.

The impact of our gathering of two years ago can be assessed from a number of elements. Firstly, an extensive report of that meeting was published, following an invitation by its editor, in a special issue of the *Journal of Fusion Energy*, the September 1995 issue. As to the Proceedings of the 1st Symposium, they are now being published by Plenum Press, and the galley-proofs are available for your examination at the reception desk. The Proceedings contain all the presentations made at the 1st Symposium, as well as the recommendations from the Panel of Distinguished Scientists and Engineers who evaluated our work. You will read that the Panel looked favourably at our work and recommended a diversified approach to fusion. Another sign of the impact of our work of two years ago is given by the request by the editor of *Physics Today* to write an article on the strategic issues surrounding the fusion problem. Three members of the organization of this conference, Bruno Coppi, Norman Rostoker, and Chiyoe Yamanaka, initiated an effort to satisfy this request, but, because of the pressure on their time, they could not complete their effort. However, this was sufficient to persuade the editor of *Physics Today* that the problem of fusion needed to be aired, and the debate on the ITER program carried out in the pages of the June 1996 issue of this magazine has still a significant repercussion today through the flow of the letters to the Editor commenting on that debate. Thirdly, the U.S. Department of Energy has revised by a large extent its funding policy for fusion energy programs, and the once neglected programs of basic science and alternative concepts, which two years ago received less than 5% of the overall budget, will now receive, from what I understand, at least 29%, a significant increase. DoE itself is now following our lead and is organizing its own meetings, similar in purpose to our own. Last week a DoE supported meeting has taken place in California titled "Workshop on Innovative Confinement Concepts". The organizer of that meeting, Dr. Robert

Goldston from Princeton, following some discussions with me and clarification of the objectives of our respective meetings, agreed to have Dr. Ron Kirkpatrick, a member of our Steering Committee, to be included in his team. Tomorrow night, Dr. Kirkpatrick will report to us on the outcome of that workshop. While the DoE workshop is mainly a national gathering, our Symposium is truly international in nature. At the 1st meeting of two years ago we had 8 countries represented. Today, 15 countries are represented, and I particularly welcome the new representatives from Argentina, China, India, New Zealand, Pakistan, Romania, and Sweden.

What is the most immediate objective of this Symposium? The Statement of the Symposium Objectives is summarized in the following words:

> "The objectives of the Symposium are to identify, review, and assess the benefits, uncertainties and potentialities of the conventional, alternative, and exploratory approaches to fusion energy production and assess industrial spinoffs and other applications".

This Statement therefore leads to a review and analysis of the fusion concepts that have made possible, individually and collectively, to be where we are now in fusion research and to understand the nature of the fusion problem, thus paving the way for solutions.

Since the Symposium is basically an assessment, its distinct feature relative to other conventional conferences is the presence of a Panel of Distinguished Scientists and Engineers who will comment on our works with respect to direction, balance and synergism of the research programs, and will recommend measures to increase public understanding and support for fusion energy.

In conclusion, while we have to be proud of our achievements of the past, it is however important that we continue our effort of promoting fusion as a viable energy option and of providing meaningful recommendations to interested governments on the best strategic approach to the solution of the fusion energy problem.

On behalf of the International Advisory Board and Steering Committee, I wish you good work in the coming days.

FUSION RESEARCH: THE PAST IS PROLOGUE*

Richard F. Post

Lawrence Livermore National Laboratory
Livermore, CA 94550, U.S.A.

ABSTRACT

At this juncture fusion research can be viewed as being at a turning point, a time to review its past and to imagine its future. Today, almost 50 years since the first serious attempts to address the daunting problem of achieving controlled fusion, we have both an opportunity and a challenge. Some predictions place fusion research today at a point midway between its first inception and its eventual maturation – in the middle of the 21st century – when fusion would become a major source of energy. Our opportunity therefore is to assess what we have learned from 50 years of hard work and use that knowledge as a starting point for new and better approaches to solving the fusion problem. Our challenge is to prove the "50 more years" prophesy wrong, by finding ways to shorten the time when fusion power becomes a reality. The thesis will be advanced that in the magnetic confinement approach to fusion open-ended magnetic confinement geometries offer much in responding to the challenge. A major advantage of open systems is that, owing to their theoretically and experimentally demonstrated ability to suppress plasma instabilities of both the MHD and the high-frequency wave-particle variety, the confinement becomes predictable from "classical," i.e., Fokker-Planck-type analysis. In a time of straitened budgetary circumstances for magnetic fusion research now being faced in the United States, the theoretical tractability of mirror-based systems is a substantial asset. In pursuing this avenue it is also necessary to keep an open mind as to the forms that mirror-based fusion power plants might take. For example, one can look to the high-energy physics community for a possible model: This community has shown the feasibility of constructing large and complex particle accelerators using superconducting magnets, vacuum chambers and complicated particle-handling technology, housed in underground tunnels that are 20 or more kilometers long. In the paper examples of mirror-based fusion power systems resembling long "linear colliders" will be discussed.

It is not the intent of this paper to present detailed proposals for next-generation experiments in magnetic fusion research, but rather to encourage a return to the ambiance of an earlier era of fusion research, when innovative thinking and a spirit of scientific adventure prevailed. In that way we can realistically build a new era of fusion research, an era that would be firmly undergirded by the scientific and technological foundation that was laid in fusion's first half-century.

Current Trends in International Fusion Research — Proceedings of the Second Symposium
Edited by E. Panarella. NRC Research Press, National Research Council of Canada, Ottawa, ON K1A 0R6, Canada. 1999.

1. INTRODUCTION

The title of this paper, "Fusion Research; The Past is Prologue," is intended to focus the reader's attention on two aspects of the fusion quest as it is viewed by the author today. The first of these aspects, one that is especially apparent to anyone who has been involved in this research from its early days, is the maturity of today's understanding of the complexities of plasma behavior as compared to those early days. Starting, in the 1950s, with a relatively primitive knowledge of the plasma state that arose mainly from the study of electrical discharges in gases, fusion and space-physics researchers built a whole new scientific discipline; the physics of high-temperature plasmas. In the fusion-related case of the magnetic confinement of plasmas there exists today theory and computational expertise undergirding a truly prodigious data base on the behavior of plasmas at fusion-relevant densities and temperatures. And yet, despite this knowledge base we find ourselves without the means to define a fully satisfactory practical implementation of this understanding in the form of a viable fusion power system.

Thus the second aspect of the title, "prologue," is intended to address the question of the future of magnetic confinement fusion, in particular the issue of innovation aimed at finding better, simpler, less expensive approaches to fusion power than the present ones that are based on the "closed" or toroidal approaches such as the tokamak or the stellarator. As such it will represent an appeal to "cast a wider net" in our search for better approaches. Out of the author's biases and predilections, it will also represent an appeal to the fusion community to explore the potentialities of open-ended systems in this search.

Looking back over the history of magnetic fusion research it is not difficult to discern how closed systems, such as the tokamak, came to dominate the research scene. Their relative simplicity, their appealing empirical scaling laws (confinement time increasing as the square of the plasma radius) and their theoretical intractability (which forced an empirically based approach to progress) led to the construction of larger and larger facilities. The central theme of the tokamak campaign was, and still remains, "better confinement, hotter temperatures, and closer approach to the Lawson Criterion (i.e., $n\tau$, the product of plasma density and plasma confinement time, must exceed a critical value) for plasma ignition." In a time of uncertainty as to the viability of the basic concept of the magnetic confinement of hot plasmas, this theme was certainly a valid one. However, in seeking to achieve the ultimate goal of fusion research, namely, economic fusion power, that campaign theme is too simplistic.

While the world-wide emphasis on the tokamak approach has resulted in major achievements in plasma temperatures and confinement times, now approaching those needed for fusion power, it has at the same time led to a sobering circumstance: Based on the extrapolation of those same results, results that were so painstakingly achieved, the tokamak in its present form is seen by significant numbers of the fusion research community as being too large and cumbersome, and too fraught with serious practical problems, to ever become an economical source of fusion electrical power.

Thus a paradox: The positive aspect of the tokamak, i.e., that it has demonstrated the viability of the concept of the magnetic confinement of fusion-relevant plasmas, has been accompanied by a negative result: If the tokamak in fact does not represent a viable fusion power system, the decades-long preoccupation of the fusion community with research on closed systems has meant that research on the "orthogonal" alternative, that is, open-ended magnetic systems, has languished. Specifically it has languished to the point that today only one or two research groups in the world are seriously studying this alternative. With this diminution in effort there also comes an erosion of the understanding of the physics of such systems on the part of the fusion community. One purpose of this paper will therefore be to review some critical aspects of the concept of plasma confinement in open systems.

However, if it accomplishes no other objective, the main message that this paper is aimed at delivering is to encourage the fusion community, particularly its younger members, to take a serious look at the open-ended magnetic field topology, its characteristics and its inherent advantages (and its problems to be overcome) from a fusion standpoint. From this vantage point there may then be seen to exist new approaches to fusion power, ones that are simpler and less demanding than the closed-geometry genre, and ones that have a more promising future than those systems. The example system sketched in the concluding sections of this paper is included to illustrate a small subset of the many opportunities for innovation possessed by open-ended fusion systems. The type of system envisaged in this example may or may not represent a viable fusion approach in the long run.

2. DEFINING THE GOALS OF FUSION RESEARCH

The pursuit of magnetic fusion research has had many different goals over the nearly 50 years that it has been conducted. In the earliest days "the first thermonuclear neutrons" was a chimerical goal that was only a diversion. This goal was replaced by a more reasonable, but still stultifying one: the pursuit of ever-higher density-confinement-time products ($n\tau$ values). A positive effect of pursuing this new goal (which originated from the previously mentioned "Lawson Criterion" for net fusion power) was to focus the research on plasma instabilities and on ways to ameliorate their destructive effect on confinement. In time a negative effect of this goal was to cause, worldwide, the near abandonment of approaches that did not obviously extrapolate to high confinement $n\tau$ values, e.g. open systems such as the mirror machine. Now, after the tokamak has come to dominate the research scene, the research goal has shifted toward the achievement of the "ignition" of a deuterium-tritium (D-T) plasma, even if it is to be achieved in systems whose long-range economic viability is questionable. The D-T plasma ignition concept is, in turn, narrowly defined as that circumstance when the kinetic energy deposited (and retained) in the plasma by the 4.5 MeV alpha particle fusion reaction product is sufficient to maintain the plasma in steady state at fusion temperatures in the face of the cooling effects of radiation losses, transport losses across the confining magnetic field, and the energy required to heat up injected cold D-T fuel. Pictured as the long-awaited victory in "lighting the fusion fire," this goal is easily understood by everyone, but it, too, misses the real mark.

In charting a possible new course for fusion research the research goals chosen should not be ones that unnecessarily restrict the types of fusion systems that are to be investigated. They should also be goals that are seen to be compatible with the long range goal of fusion research itself. That broader goal, one that has been implicit in all that has been done to date, could be stated as follows: "To generate net power from fusion reactions at a competitive cost, and with superior environmental and safety characteristics as compared to other energy sources." Within this goal, the goal of "net power" is clearly the first step of the task. If we then, as is the convention, define a fusion parameter "Q" as the ratio of the fusion power produced to that required to sustain the fusion reactions, this first step is to achieve the condition $Q > 1$. This goal is not the same as, and is much less restrictive than, the one presently adopted by tokamak community: Their goal, that is, the one of plasma ignition, corresponds to achieving the condition $Q = \infty$.

Systems with finite Q values, especially including ones with Q values not much larger than unity, are so-called "driven" systems. They are ones where a substantial portion of the generated fusion power is recirculated in order to heat the fuel to fusion temperatures. We have discussed the implications of operating at low Q values in open-ended fusion systems in previous publications [1,2]. Operation at low-Q values clearly places much more modest demands on plasma $n\tau$ confinement parameters than does the requirement for ignition, shifting the burden to the technological tasks of achieving efficient plasma heating and efficient energy recovery from both fusion reaction products and the unreacted fusion fuel ions. In this sense driven fusion power systems are analogous to a well-known thermal-mechanical system, the gas turbine. This highly successful net-power producer is one in which the amount of power internally recirculated (from the turbine to the compressor) is actually substantially larger than the net output power. In the development of the gas turbine achieving useful net power required the steps of maximizing the efficiencies of both the compressor and the turbine.

Freeing fusion research from the goal of achieving ignition and substituting the long-range goal of achieving net power allows the consideration of a much wider range of possible systems, while at the same time reducing the requirements on the most intractable part of magnetic fusion research, that of extending the confinement time up to the limit $Q = \infty$. Once this new goal is accepted the task of fusion research becomes more evenly divided between the plasma-science-related goal of extending plasma confinement times and the technological goals of developing efficient means for injecting and heating fuel ions and of efficiently converting particle kinetic energies into electricity. In the next section I will recapitulate some of the attributes of open-ended magnetic fusion systems that seem to me to make them prime candidates for an era of new beginnings in fusion research.

3. OPEN-ENDED FIELD TOPOLOGY: DISTINCTIVE CHARACTERISTICS

Although perhaps not evident at first glance, the topological distinction between "closed" and "open" magnetic confinement systems is the source of profound differences in their attributes in confining plasmas. These differences are reflected in both the plasma-physics aspects of their confinement and in the practical aspects of their incorporation into fusion systems. To review the special characteristics of open systems that are relevant to the present discussion, they are:

1. Open-ended field configurations exist that permit MHD-stable confinement at high beta values. As shown by theory [3] and by experiment [4] in open-field geometry it is possible to form true "magnetic wells" within which plasmas whose plasma pressure approaches that of the confining field (i.e. $\beta = 1.0$) can be confined. Figure 1 illustrates the field configuration of a quadrupole magnetic well as produced by a "baseball" coil (a coil whose windings resemble the seam on a baseball). Such coils, first suggested at the Culham Laboratory in the United Kingdom, were employed in many mirror experiments.
2. In open-ended systems, where there exist two loss channels (transverse, across the field lines, and longitudinal, out the open ends) it is not necessary for the confined plasma to terminate, either in the radial direction or axially, on a nearby physical surface. In closed systems, having only a single loss channel, i.e. across the field lines, the plasma must terminate on a close-lying material surface, resulting in steep temperature and density gradients. These gradients can represent an important source of turbulence and cross-field losses for closed systems, one that need not occur in open systems. In an open system the radial plasma boundary can be far inside the chamber wall and the end-leaking plasma can be made to terminate on a large surface located far from the confinement zone.
3. Taking advantage of the ambipolar nature of plasma end losses from open-ended systems it is possible to establish localized regions of elevated plasma potential, thus controlling

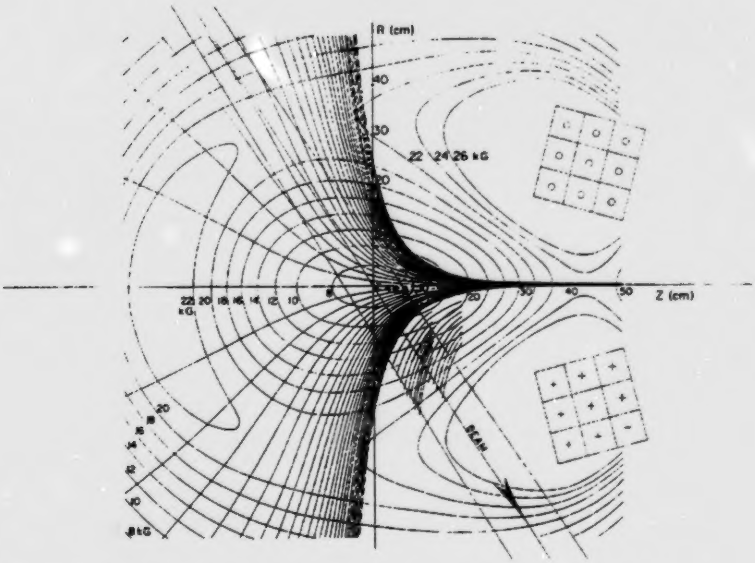

Figure 1. Field lines and field intensity contours calculated for a "baseball" coil

or inhibiting the loss of particles out the ends, as in the tandem mirror [5,6]. Also, the fact that the end-exiting plasma can be caused to terminate on surfaces whose potential can be controlled externally means that it is possible to vary the plasma potential with radius in a pre-determined way, allowing the suppression of certain classes of drift instabilities, as has been demonstrated in the Gamma 10 tandem mirror experiment [7] at Tsukuba University in Japan.

4. The end-loss channel of open systems makes them especially adaptable to the use of high-efficiency direct converters [8.9] located at the ends and intercepting the flow of charged fusion reaction products and energetic fuel ions that escape before fusing. The use of direct converters is an essential element in achieving operation at low fusion Q values.
5. Open systems, particularly ones operating at low Q values, can contain plasmas that are characterized by ion distribution functions that are non-maxwellian, i.e., ones that are less randomized than those normally encountered in closed systems. This property is important when it is desirable to suppress satellite neutron-producing reactions (for example, in a D-He^3 fueled system [10]), or to increase the efficiency of direct conversion systems, whose efficiency is higher the narrower the ion energy distribution.

In summary, it should be evident that removing the topological constraint that is imposed on closed systems, namely, that the flux surfaces of the confining field must close on themselves within the confinement chamber, has a profound effect on the "living space" of open-ended systems. This non-quantifiable characteristic of flexibility means that there is much more room for innovation and adaptation to particular requirements in open-ended systems than there is with closed systems.

In trying to understand why these listed advantageous characteristics of open-systems, ones that seem so apparent, have not been adequately recognized and exploited by the fusion research community, we return to the issue of goals alluded to earlier. From the onset of research in open-ended systems the issue of controlling end losses has been a stumbling block. As long as there existed uncertainty as to the viability of the whole idea of magnetic confinement those who made fusion policy were likely to come down on the side of systems for which the problem of end losses did not exist. This bias was not a serious problem as long as fusion budgets were healthy enough to allow breadth in the program, but when belts are tightened conservatism tends to have the upper hand. However, today we are presented with a new situation, one in which the conservative approach is seen to possibly lead to a dead end, and when new thinking is required. As illustrated by the distinctive characteristics that have been listed, I believe that open systems represent a fertile area for such new thinking.

4. OPEN-ENDED FIELD TOPOLOGY: PLASMA PHYSICS CHARACTERISTICS

As a result of now nearly fifty years of research on open-ended systems there exists a large body of information, including theory and corroborating experimental data, on such systems. In fact, throughout the history of research on open-ended systems there has always been a close affinity between the theory and experiment. By contrast, closed systems have often been found to be intractable to analysis, owing to the complexity of the plasma physics issues involved.

In this section I will briefly review the main theoretical developments in open systems and their corroboration by experiment.

4.1 Mirror Confinement and Adiabatic Invariants

This section briefly reviews the history of the particle-dynamic aspects of the confinement of plasmas in mirror systems. In this connection, one of the earliest-considered issues in the confinement of plasmas in mirror-based systems related to the constancy of the magnetic moment, μ, of the plasma particles as they gyrated back and forth between the mirrors. The magnetic moment is defined as the ratio of the particle's kinetic energy associated with the component of its velocity perpendicular to the field lines to the local value of the magnetic field:

$$\mu = \frac{W\perp}{B} \quad \text{Joules / Tesla} \tag{1}$$

Early theoretical work, for example that by Kruskal [11] established the validity of the concept of the adiabatic invariant (asymptotic invariance of the quantities, such as the magnetic moment, under slow changes of parameters). Later work (described below) related this to the problem of mirror confinement of charged particles.

The repelling force on a gyrating particle that is exerted by the magnetic mirrors (regions of increased magnetic field) is given by the equation:

$$F_z = -\nabla(\mu B) = -\mu\nabla(B) \text{ Newtons} \tag{2}$$

The quantity (μB) thus acts as a "potential energy" for motion along the field lines. When, in an increasing magnetic field, this potential energy becomes equal to the parallel component of energy at the lowest point in the field, the particle will be stopped and reflected, analogous to the back-and-forth motion of a rolling ball trapped between two hills. An equivalent statement of this condition is that the pitch angle made by the particle as it traverses the midplane must be greater than the "loss cone" angle, θ_c, where

$$\mathrm{Sin}(\theta_c) = (1/R)^{1/2}, \tag{3}$$

where R is the "mirror ratio," B_m/B_o, the ratio of the magnetic field at the peak of the mirror, B_m, to that at the midplane, B_o.

The first question to be asked, the one addressed by Kruskal, is the following: Under what conditions is it valid to assume that the magnetic moment remains constant as the particle bounces back and forth between the mirrors? As was shown by Kruskal, and by others following him, the magnetic moment is an adiabatic invariant. That is, its fluctuations during the course of its motion between the mirrors becomes exponentially small with the reciprocal of an "adiabatic parameter," α, equal to the ratio of the magnetic gradient scale length, L_m, to the gyroradius, a, of the particle, i.e., $\alpha = a/L_m$. The relationship therefore takes the form

$$\frac{\delta\mu}{\mu} = A\exp(-B/\alpha), \tag{4}$$

with constants A and B being of order unity in typical cases. As can be seen, the fluctuations become vanishingly small in the limit of small α. At typical fusion-relevant magnetic field strengths, particle energies, and apparatus physical dimensions, the adiabatic parameter is indeed quite small and fluctuations in μ arising from this source are usually unimportant.

Although the adiabatic invariance of μ insures that, in the absence of other perturbing effects (such as particle-particle collisions), trapped particles will remain trapped between the mirrors as far as their axially directed motion is concerned, it does not answer a subtler question: In bouncing back and forth between the mirrors, will the particles perform a random walk across the flux surfaces of the field until they hit the wall? This problem was addressed, and elegantly solved by Northrop and Teller [12]. They recognized that, in addition to the adiabatic invariant μ there is also operative another adiabatic invariant, *J*, the "action" integral, defined as the integral of the parallel velocity component of the particle between the turning points of the longitudinal bouncing motion of the particle as it is reflected by the mirrors. Specifically,

$$J = \int_{-L}^{L} v_{par}\, ds \quad \mathrm{m^2\ sec^{-1}} \tag{5}$$

The existence of the *J* invariant insures that bouncing particles, though drifting azimuthally, will, in absence of other perturbing forces, remain on a closed surface (corresponding to a flux surface in the limit of small cyclotron radius of the particle). One therefore has a situation where in the limit of sufficiently weak extraneous perturbations (for example, collisions), particles trapped between the mirrors will remain trapped "forever." This situation is in marked contrast to that in closed systems, for example the stellarator, where there exist classes of initially trapped particles that are compelled to drift across the field to the container wall.

The power of the two invariants to maintain trapping was dramatically illustrated, in 1958, in the ARGUS experiment, proposed by N. Christofilos. In this experiment, one that will in all likelihood never be repeated, a rocket launched a payload consisting of a small nuclear weapon into the ionosphere. When detonated, the nuclear explosion released a cloud of energetic electrons (from beta decays). Electrons from this cloud were mirror-trapped in the earth's magnetic field, and drifted azimuthally to form an artificial Van Allen belt which could be detected by sounding rockets. Ten years later it was still possible to observe the presence of such electrons, after they had made some billions of reflections.

Similarly striking confirmations of the power of the invariants to insure long-time confinement of energetic electrons in mirror fields were made in 1959 in an experiment by

Rodionov [13], and in 1962 in experiments by Gibson, et al. [14]. In both experiments electrons from the beta decay of a radioactive gas were trapped in situ between mirrors and their confinement times were measured and compared to the predicted lifetime from collisions of the electrons with background gas atoms. Confinement times corresponding to millions of reflections, in close agreement with those predicted by scattering theory, were found.

While collective effects, such as those discussed later, can certainly vitiate confinement in mirror-based systems, it is also true, as has been demonstrated in the laboratory, that when these collective effects are suppressed by choice of the field geometry and plasma parameters, confinement times are found approaching those predicted from "classical" inter-particle collisional effects expected in a quiescent plasma. To my knowledge this situation has never been encountered in a closed confinement geometry. In closed systems of all types there seems always to exist, at some level, turbulence that results in cross-field transport substantially in excess of the "classical" predictions.

Having determined the good confinement characteristics of mirror-based systems in the absence of collisional processes, the next necessary step is to calculate the effect of inter-particle collisions in causing losses through the end mirrors. It was early on recognized that in a simple mirror machine the confinement time would be limited to times of order of a mean ion-ion collision time, at which time there would be a high probability of an ion to have been scattered into the loss cone. To perform a meaningful calculation of the loss rate the Fokker-Planck equation was employed, incorporated into computer codes. Early fundamental work in this area includes work by Rosenbluth, McDonald and Judd [15], who formulated the problem and deduced the nature of the solution. As a result of their work, and of later work by many others [16,17], the steady-state "classical" density-confinement-time product for mirror systems with a mirror ratio, *R*, was found to be relatively accurately expressed by a relationship of the form:

$$n\tau = k_i E_i^{3/2} \log_{10}(R) \;\; m^{-3}\,\mathrm{sec.} \tag{6}$$

Here E_i is the mean ion energy, and the constant k_i depends on the ion type and on the details of the means by which the ions are introduced into the system (i.e. whether as monoenergetic beams and at what angle of injection relative to the field lines. For deuterons and perpendicular injection k_i was found to be approximately 2.5×10^{16}. As an example of the implications of this result, one must plug in a mirror ratio as high as 10 and an ion energy of 100 keV to achieve an nt value of 2.5×10^{19}, marginal as far as allowing the production of net fusion power ($Q > 1$) from the D-T reaction. This marginality hung over the Mirror Machine as a Sword of Damocles throughout its development. One result was to stimulate the invention of high-efficiency direct converters to increase the effective *Q* value of mirror-based systems. Another, and very significant, result was the invention of the Tandem Mirror concept by Dimov and Fowler and Logan. Still another was the introduction of the idea of multiple mirror systems (a linear array of linked mirror cells) by Post [18] and Budker [19].

Despite the marginality of the confinement time in simple mirror systems as predicted by the Fokker-Planck analyses, the confinement time predicted by this means stood as a well-defined "standard" against which to compare experimental results. To achieve confinement times approaching this standard required understanding and avoiding (or stabilizing) collective effects in the plasma, including both MHD modes and high-frequency instabilities. The fact that this feat was accomplished represents a major achievement of the mirror research community.

4.2 MHD Interchange Modes

From early on the issue of MHD stability has been addressed in open-ended systems of the mirror type. The first mirror machines employed simple axially symmetric fields. In such fields although the field-line curvature near the mirrors is convex toward the plasma, i.e., stabilizing for MHD interchange modes, the curvature near the midplane is concave toward the plasma (field weakens with radius). As shown in the original paper of Rosenbluth and Longmire [20], except for special ion distributions ("sloshing ions") that have density maxima near the mirrors, the line-averaged pressure-weighted curvature of such fields, is net negative, i.e., unstable. Since some early experiments, such as the "Table-Top" experiment at Livermore exhibited stable behavior when the theory indicated instability [21], other stabilizing mechanisms were postulated, which, under special circumstances could overcome the destabilizing effects of bad curvature. One such mechanism, predicted theoretically [22], is the so-called "line tying" effect, resulting from plasma electrical conductivity, along the field lines and through the mirrors to an external conducting surface, suppressing interchange modes by "shorting out" their electrically driven drifts. Still another stabilizing mechanism, effective against higher-order interchange modes, is that arising from the so-called "finite-orbit" effects, as predicted by Rosenbluth, Krall, and Rostoker [23]. They showed that the relative azimuthal drifts of ions and electrons (because of their different cyclotron radii), as they move up and down between the mirrors, can stabilize MHD interchange modes.

Although the above stabilizing mechanisms (line-tying and finite-orbit effects) may be operative in some experiments, they are not as potent as the field-configuration-related stabilizing effect, first demonstrated in the now-famous experiments by Ioffe [24]. In these experiments Ioffe showed that by introducing non-axially symmetric field components (created by axial conductors - the "Ioffe bars" - a "magnetic well" could be created within which the plasma was rendered robustly stable against all MHD-type modes. As later demonstrated theoretically by Taylor and Hastie [3], and subsequently verified in the 2XII experiment [4] of Coensgen et. al. at Livermore, the stabilizing effect of a magnetic well is so strong that plasmas with energy densities approaching that of the confining field ($\beta = 1$) can be stably contained. In a further extension of the idea of stabilizing by magnetic wells, Furth and Rosenbluth [25] showed that the linked series of mirror cells of a multiple mirror system could be rendered MHD-stable by proper design of the transition regions between the cells.

Recently, experiments in the Gas-Dynamic Trap mirror experiment [26] at the Budker Institute of Nuclear Physics in Novosibirsk, Russia have shown an additional stabilizing effect, related to the line-tying effect mentioned earlier. In these experiments, in agreement with theoretical predictions, it was shown that if the plasma coming through the mirrors in an axially symmetric mirror cell is exposed to a sufficiently long region of "good-curvature" field lines, the denser plasma inside the mirrors will be rendered MHD stable, even though contained in a configuration predicted to be MHD unstable by the Rosenbluth-Longmire criterion or its equivalent. A detailed discussion of this and other means for the stabilization of MHD modes in axially symmetric open-ended systems is given in a paper by Ryutov [27].

In summary to this point, there now exists a thorough theoretical understanding of MHD instabilities and their stabilization in open-ended systems, backed up by an extensive experimental data base. If required, situations can be created in open systems that suppress MHD-type modes of all orders. This is a situation that cannot be attained in closed systems such as the tokamak, where even under the best of circumstances there remain residual driving effects for higher-order MHD modes, in some cases resulting in plasma turbulence that unfavorably influences particle transport.

4.3 High-Frequency Instabilities of Velocity-Space Origin

Though capable of being rendered robustly stable against MHD modes, open systems may under some circumstances be susceptible to non-MHD modes of the wave-particle type. The source of these instabilities resides in the non-maxwellian nature of the plasmas that may be confined in open-ended systems. If certain critical conditions are satisfied by the plasma parameters then waves of electrostatic or electromagnetic nature may grow within the plasma, drawing energy from the "free energy" associated with the departures in velocity space of the ion (or electron) distribution functions from a maxwellian distribution. The critical conditions include the length of the plasma and the degree of departure of the distribution functions from an isotropic maxwellian. Early treatments of this type of instability in open-ended systems were given by Harris [28], Rosenbluth [29], Post and Rosenbluth [30], and by numerous other authors. As a result of these theoretical analyses not only were velocity-space instabilities well understood, but the required conditions for their suppression were clearly defined. A summary of the work on velocity-space instabilities and a more detailed bibliography is contained in a review article by the author [31].

As an early example of the appearance of velocity-space instabilities and their stabilization by Landau-damping effects Fig. 2 shows the results of an experimental determination of the stabilizing effects of Landau damping on a particular high-frequency instability encountered in the Baseball I mirror experiment at Livermore [33]. The plot shows the boundary between stability (below the line) and instability (above the line). The ordinate of the plot is proportional to plasma density. The parameter plotted on the abscissa, from the theory, is

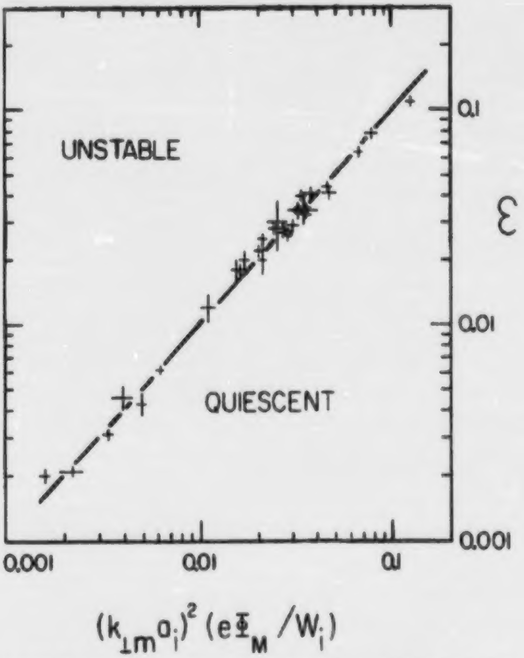

Figure 2. Landau-damping stabilization of ion-cyclotron mode in the Livermore Baseball I experiment: comparison between experiment and theory.

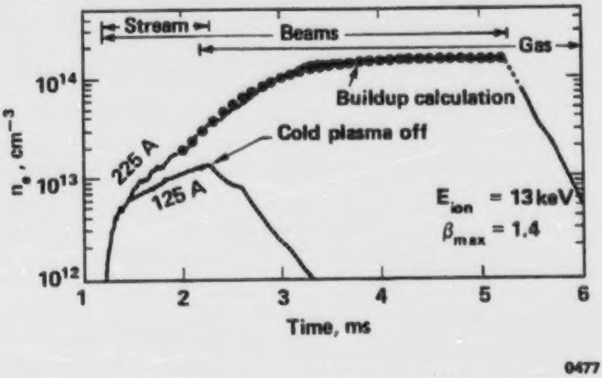

Figure 3. Plasma density buildup vs time in Livermore 2XII experiment showing stabilization of velocity-space instabilities by injecting a plasma stream.

proportional to the product of the plasma potential (determines the peak energy of the electrons producing the Landau damping) and the square of the wave number of the unstable mode. The agreement between theory and experiment is seen to be close, confirming the analysis.

Later, and in a similar way, the effectiveness of warm plasma stabilization of velocity-space modes was shown in the 2XIIB experiment at Livermore. In this experiment neutral beams were employed to build a trapped plasma in a deep quadrupole magnetic well. The results are shown in Fig. 3. In the absence of the warm plasma component the buildup is seen to be interrupted by the growth of instabilities. With the warm plasma stream the plasma now builds up in close agreement with the theoretically predicted buildup curve, reaching high density with no evidence of instabilities of either MHD or velocity-space origin.

Following the invention of the tandem mirror idea the concern for velocity-space instabilities in the confined plasma diminished. In a tandem mirror the central plasma, being electrostatically trapped between the end mirror cells, can more nearly approach an isotropic maxwellian state, one that is stable against such instabilities. In this situation another check on the agreement between experiment and "classical" mirror confinement theory can be made. Pastukhov [34] had predicted the parametric variation of plasma loss, over the potential barriers of the tandem mirror, with plasma potential. Figure 4 shows a comparison between Pastukhov's theory and experiment as found in the Gamma 10 experiment at Tsukuba. Again, the agreement between experiment and theory is seen to be close.

In summary to this point, not only have open systems been found to be tractable for theoretical analysis, but this analysis has been largely confirmed experimentally. In important cases it has been found possible to create confined plasmas that approach quiescence, in that confinement times come close to "classical" values, with fluctuation levels believed to be little above thermal values. There is good reason to believe that this situation, that is, confinement close to that determined by purely classical (i.e., collision-related) processes can be achieved at fusion-relevant conditions. However, owing to the reduction of effort on open-ended systems no experimental facilities of sufficient size to explore this possibility exist at the present time. The largest operating mirror facilities are the previously mentioned Gamma 10 tandem mirror experiment at Tsukuba University in Japan and the Gas Dynamic Trap and Ambal experiments at the Budker Nuclear Physics Institute in Novosibirsk, Russia. All three of these experiments, although capable of producing very significant data, are much smaller than the large tokamaks in the US, Europe, and Japan, too small to contain plasmas at the

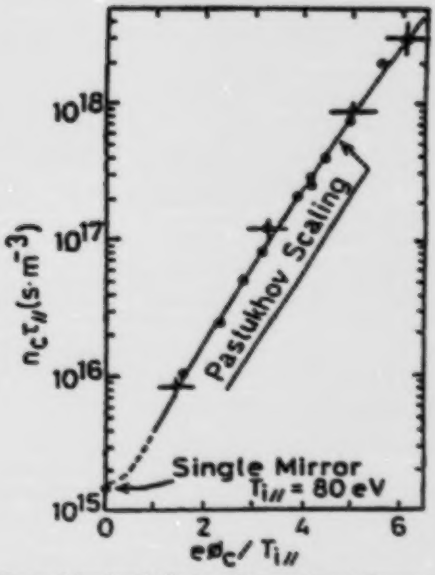

Figure 4. Ion longitudinal confinement time in Gamma 10 experiment: comparison between experiment and Pastukhov theory.

temperatures and densities that would be required in fusion power systems.

5. CHARTING A NEW COURSE FOR FUSION RESEARCH: SOME GROUND RULES

If we believe that there is now an opportunity to take a new look at the fusion problem with a broader view than that provided by considering only closed magnetic confinement systems, we then need to establish some new ground rules. The first one concerns our mental picture of a fusion system: Closed systems, such as the tokamak or the stellarator, bring with them the picture of a complex coil system of roughly spherical outward shape. Buried inside this structure is a fusion reaction chamber penetrated by beam lines and rf antennas. Access is limited, wall power densities are high, and there is little flexibility for innovative changes of any kind, for example, for the introduction of direct converters.

Contrast this mental picture with that for open-ended systems. Here one can contemplate a whole spectrum of possibilities. At one end of this continuum is a single mirror cell with quadrupolar mirror fields produced by a "baseball" coil, at each end of which would be placed direct converters. Such a system was studied conceptually many years ago by Moir et al. [35]. The next possibility, also studied in the past in the MARS reactor study [36], is a tandem-mirror system, having plugging cells and direct converters at each end, with modular coils and a long cylindrical confinement chamber located between them. At the far extreme of possible systems would be a long linear system, perhaps many kilometers long, composed of modular sections, and located in a tunnel deep underground. Such a system would resemble the SLAC linear accelerator at Stanford or the "linear colliders" being proposed for high-energy physics research. In what follows I will give as an example a long linear system employing mirror fusion concepts.

In addition to broadening our visualizations of what a fusion power plant might look like our ground rules should include broadening our view of the plasma regimes where such systems might operate. By "regimes" is implied such items as the degree of randomization of the ions of the plasma, and the types of ions present in the system. In closed systems such as the tokamak, particularly those aimed at ignition, collisional randomization insures that the ions and electrons exist close to a maxwellian state. However, in open systems, as noted earlier, the ions may exist far from a maxwellian state, to the point that they approximate directed beams. In such cases the physics issues involved come closer to those encountered in particle accelerators than those pertaining to a gas of maxwellian particles. As far as the fusing ions are concerned, however, since fusion is a binary reaction the particles in undergoing fusion are indifferent as to whether their energy distribution is a maxwellian or whether they are members of colliding monoenergetic beams: Their reaction probability will simply be given by the product of their reaction cross-section and their relative velocity. If it turns out to be advantageous, and in those cases where there are not substantive disadvantages, our ground rules for looking for new approaches should therefore consider the whole spectrum of plasma regimes.

Finally, as has already been discussed, in setting our new ground rules we should abandon the goal of plasma ignition as a requirement, substituting for it the simple requirement of net positive fusion power. In addition, we should be open to consider pulsed systems whose time-averaged energy release is positive. This latter proposition opens the door to "batch processing" types of fusion power generators. It also implies the possibility of taking advantage of time-dependent effects, such as time-of-flight of the particles, or in the extreme limit, inertial confinement effects, however, here in the context of magnetic confinement systems.

The point of laying out some ground rules for a new look at magnetic fusion systems is to attempt to break old habits of thinking. The relationship of this attempt to the subject of this paper is that I am endeavoring to point out the advantages of applying these new ground rules to open-ended systems. In this connection it would be presumptuous of me to try to enumerate a comprehensive list of possible variations on the open-ended theme where investigations might be aimed. I will instead give a simple example of a system that breaks with past tradition and that might be worthy of future study. The main criteria that will be applied to the example system is that it should be capable in theory of yielding net power within the assumptions made in analyzing it, that it does not require extreme extrapolations of technology to implement, and that it is not obviously too expensive ever to compete with other energy sources. The linear system that will be described is an evolutionary descendant of ones that I have discussed before [37,38,39]. Its appearance in this paper is for the purpose of giving substance to my plea for "casting a wider net" in looking for new directions for fusion research, in particular in looking at open systems.

6. LONG LINEAR OPEN-ENDED SYSTEMS FOR FUSION

The high-energy research community has paved the way for the fusion research community to consider the possibility of constructing fusion power systems in underground tunnels many kilometers long. They have shown the way to solve the land-use problem of locating very large and complex particle-handling systems in an economical way. An example is the 27 kilometer-long Large Electron-Proton Collider at CERN in Switzerland. The tunnel containing the magnets and vacuum chamber of this facility runs below farmland and villages in both Switzerland and France with no interference with those land uses.

The example that we will give, also a "collider," is comprised of a long axially symmetric central solenoidal superconducting magnet coil together with its cryogenic housing and a blanket assembly, inside of which is the fusion reaction chamber. The magnetic field strength tapers up smoothly from each end, approaching its maximum value asymptotically, so that the field lines converge inwardly from each end. Such a field configuration, having positive field line curvature throughout its length, should be stable against MHD modes of the interchange type. As such it represents the simplest possible MHD-stable field configuration for an open-ended system. The issue now becomes one of how one deals with end losses in such systems. In our example we will discuss one possible (very simple) solution involving the time-of-flight of two mutually-colliding ion beams, a system that might therefore be called a "linear collider." In this collider ions are injected, nearly parallel to the direction of the field lines, near the ends of the solenoid, where the field is weak. In traveling up the magnetic gradient the injected ions are compressed radially, increasing the particle density up to that required to achieve net power.

Critical to such colliders are ion injectors and direct converters located at the ends. These provide the means to create the colliding beams and to recover energy from ions that did not fuse. The technical and economic feasibility of such systems depends on whether or not these elements can achieve high efficiencies in their operation. In the case of the direct converters, previous work [9] has shown that conversion efficiencies of ion kinetic energies to electricity of order 90 percent are achievable, the higher the efficiency the narrower the energy distribution. Well-designed ion sources are also capable of achieving comparable efficiencies. The consequence of achieving high efficiencies in the injectors and the direct converters is, in effect, to multiply the Q_{fus} factor of the fusion reactions by an "electrical Q" that can permit the Q associated with the recovered fusion energy, Q_{fus}, to be actually smaller than unity, still allowing the system Q, to be larger than unity, i.e., indicating net power production. Here we have defined the parameter $Q_{fus} = Q_{fr} \cdot \eta_{f}$, where η_f is the efficiency of conversion of the fusion reaction energy to electricity, and Q_{fr} is the usual Q value, i.e., the ratio of the fusion energy released to the energy input required to maintain the plasma at fusion temperatures.

$$Q = Q_E \cdot Q_{fus} \qquad Q_E = \frac{\eta_i}{1 - \eta_i \eta_{dc}} \tag{7}$$

If the injection efficiency, η_i, and the direct conversion efficiency, η_{dc}, are both equal to 0.9, then $Q_E = 4.7$. In this way a trade-off between confinement requirements and technological development can be accomplished.

7. A LINEAR COLLIDER

In this section we will sketch an example of an open-ended system that illustrates the flexibility of this geometry for application to systems that are very different from conventional approaches. The example does not represent a detailed "proposal," but is instead aimed at showing the potential advantages of making a tradeoff that reduces the importance of achieving good confinement in fusion systems in exchange for solving some well-defined technological problems.

The example we will describe probably represents the simplest open system that one could propose that could conceivably become a viable fusion power plant. A particular version of the idea has been described in previously published reports [37,38,39]. In the earlier versions ion sources at one end of the solenoid inject Type A ions and other ion sources at the opposite end inject Type B ions. These ions collide with each other in passing through the tube, and a small fraction of them would fuse with the release of energy. Those ions that did not react would exit the system and enter the direct converters to accomplish the Q amplification described above. If the Type A ions were deuterons, and the Type B ions tritons, then the optimum injection energies for each would be 36 keV and 24 keV, respectively, giving an energy in the center-of-mass corresponding to the maximum point in the D-T reaction cross-section (at 100 keV), at a minimum total ion energy (64 keV). While the ion energies chosen represent optimum values from a colliding-beam standpoint, the configuration carries with it a certain technological problem: With ion sources and direct converters at both ends the problem arises of how to minimize the interception of the escaping ions on the structures of the ion sources so as to maximize their probability of interception by the direct converters. Molecular ion or neutral beam sources might help this endeavor, but they would carry with them additional technical challenges.

Given the issues just described we will here take a somewhat different tack. We will assume a less-than-optimum situation for colliding beams in return for the elimination of the problems just described, as follows: Assume that both the D and the T ion sources are located at one end, and the direct converters are located only at the far end. Here the T ions are injected, up the magnetic gradient, at such an initial angle that they end up spiraling down the field at a tightly-wound pitch angle. In this way they form a tritium "target" with which the injected D ions, moving down the field also at small pitch angles, can collide. If the energy of the T ions is substantially smaller than that of the D ions the optimum energy of injection of the D ions will be approximately 100 keV. For example, if we choose the energy of the T ions to be of order 10 keV, their velocity is small enough relative to the velocity of the D ions to be ignored in estimating the average reaction cross-section, which will be close to its peak value of 5.0×10^{-28} m^2. Choosing $W_D = 100$ keV and ignoring the azimuthally averaged velocity of the T ions relative to the D ions in the calculation then leads to a mean reaction parameter $\sigma_{DT} v_{rel} = 1.6 \times 10^{-21}$ m^{3}sec^{-1}. This value is about 4 times higher than the maxwellian-averaged reaction parameter for fusion reactions in a DT plasma at 20 keV kinetic temperature. The fusion power density is correspondingly higher than that for maxwellians, being about 60 megawatts/m^3 for D and T ion densities of 10^{20} m (assuming 22.4 MeV for the total energy release per DT fusion reaction, including capture energy in a Lithium-containing blanket).

7.1 Constraints Imposed by the "Firehose" Instability

In estimating the source parameters needed to achieve the desired densities of T and D ions in the collider it is necessary to consider the limitations that are imposed by the "firehose" MHD instability [40]. The firehose instability is driven by the existence of a parallel pressure component, above a critical value, in a frame in which the net momentum is zero. Thus, if in the configuration we have chosen we were to inject monoenergetic ions of only one species the firehose instability could not occur, as there is zero parallel pressure in the frame in which the net momentum is zero. Also, even if we were inject two different species of ion, if their relative energies were such that they moved down the field at the same velocity, the firehose instability would not be stimulated. However, in the present case we are injecting two types of ions at different energies and at different initial densities. Assuming that these beams co-mingle in flight the possibility of the firehose instability arises. In the calculations below we will make a "worst case" assumption, namely that the two beams co-mingle immediately upon exiting their respective ion sources.

For ions injected nearly parallel to the field lines an approximate condition for stability against the firehose instability, stated in terms of the total parallel ion pressure component and the local strength of the magnetic field, is given by equation 8:

$$\Sigma \mathrm{p}_{\mathrm{par}} = M_D n_D \left(\mathrm{v}_D'\right)^2 + M_T n_T \left(\mathrm{v}_T'\right)^2 < \frac{B^2(0)}{\mu_0}, \text{stable} \qquad (8)$$

Here the primed velocities of the deuterons and tritons are their velocities in the frame moving at velocity v_0, defined through equation 9:

$$(M_D n_D + M_T n_T) v_o = M_D n_D v_D + M_T n_T v_T \tag{9}$$

The most unstable region for this instability is in the vicinity of the sources, the point where the magnetic field is weakest and the ion kinetic energy is directed almost entirely along the field lines. The criterion given by equation 8 can be rephrased as a condition on the ion-source current density, ion energy, and the magnetic field (at its maximum) required to achieve a given compressed ion density. In the expressions below we express the ion-source current densities for both types of ions in units of 3 amperes/cm^2, the deuteron energy in units of 100 keV, the triton energy in units of 10 keV, the magnetic field in units of 10 Tesla, and the ion densities in units of $10^{20}\,\mathrm{m}^{-3}$. In other words, we set $j_D = j_T = 3.0\,\alpha$ amps/cm^2, $W_D = 100\,\lambda$ keV, $W_T = 10\,\lambda$ keV, $B_{max} = 10\,\Gamma$ Tesla, $n_D = 1.0 \times 10^{20}\gamma_D\,\mathrm{m}^{-3}$ and $n_T = 1.0 \times 10^{20}\,\gamma_T\,\mathrm{m}^{-3}$. We will also assume that both species of ions are injected at a small angle with respect to the field lines such that after moving up the magnetic gradient to the high-field region they are spiraling down the field at a pitch angle θ (rad.). With these assumptions the triton density is determined by the deuteron density through the ratio $\gamma_T/\gamma_D = 3.833$.

Considering now the calculation of the parallel pressures in the moving frame we find from equation 9 the velocity of this reference frame as having the value $v_0 = 0.3680\ v_D$. This and the other parameters may now be inserted into the stability condition, inequality 8, to yield a condition on the deuteron density after magnetic compression:

$$\text{For deuterons:} \quad 27.\left[\frac{\lambda^{3/2}\,\gamma_D^2\cos^2(\theta)}{\alpha\,\Gamma^2}\right] < 1.0,\ \text{stable,} \tag{10}$$

with the triton density being 3.833 times that of the deuteron density.

The choice of 3.0 amperes/cm^2 for the unit of ion-source current density has its origin in pioneering studies of ion-source current limitations in 1979 by Dembrinski and John [41]. In their paper these authors reported the achievement of light-ion current densities in excess of this value by extraction of the ions from a flowing plasma. Using this technique they overcame the usual Bohm-sheath limitation (of order 1 ampere/cm^2) on the current density of conventional ion sources.

The choice of 10 Tesla for the unit of magnetic field is that this level of field can be routinely obtained with large superconducting magnet coils. If justified on economic grounds, even higher fields than 10 Tesla could be obtained for a linear collider. For superconducting coils a long solenoid represents a much more favorable geometry for obtaining high fields than that of closed systems such as the tokamak.

In addition to the constraints imposed by the firehose instability there is a constraint imposed on the pitch angle after compression by the necessity to avoid the "mirror" MHD instability mode for the tightly spirally ions. An approximate condition for stability against the mirror mode is given by the inequality [40]:

$$\frac{\Sigma p_{perp}}{B^2/2\mu_0 + \Sigma p_{perp}} < \frac{\Sigma p_{par}}{\Sigma p_{perp}},\ \text{stable} \tag{11}$$

where $\Sigma p_{perp} = \left[n_D M_D v_D^2 + n_T M_T v_T^2\right]\sin^2(\theta)$ and $\Sigma p_{par} = \left[n_D M_D v_D^2 + n_T M_T v_T^2\right]\cos^2(\theta)$. In the limit of $\cos^2\theta \ll 1$ condition 11 becomes:

$$\cos^2\theta > \frac{0.111\,\lambda\gamma_{\mathcal{D}}}{\Gamma^2}, \text{ stable} \tag{12}$$

Now inserting this constraint (as an equality) into equation 10 results in a revised criterion that, insures stability against both modes for both the deuterons and the tritons. The new criterion is:

$$\text{For deuterons: } 3.01\left[\frac{\lambda^{5/2}\,\gamma_D^3}{\alpha\Gamma^4}\right] < 1.0, \text{ stable} \tag{13}$$

with the triton density, as before, being 3.833 times the deuteron density

7.2 Fusion-Related Parameters

Using the peak value of the reaction cross-section and taking into account the effect of the pitch angle on the deuteron path length we may estimate the reaction probability of a deuteron per meter of the solenoid, finding:

$$R_{DT} = 5\times10^{-8}\left[\frac{\gamma_T}{\cos(\theta)}\right] = 1.9\times10^{-7}\left[\frac{\gamma_D}{\cos(\theta)}\right] \text{ m}^{-1} \tag{14}$$

Inserting the constraint on cos(θ) implied by inequality 12 results in an equation reflecting the limits on the reactivity imposed by the mirror instability:

$$R_{DT} = 5.8\times10^{-7}\left[\frac{\gamma_D^{1/2}\,\Gamma}{\lambda^{1/2}}\right] \text{ m}^{-1} \tag{15}$$

Similarly, the fusion power density, using the value assumed above for the fusion reaction parameter, is given by the equation:

$$p_{DT} = 57\cdot[\gamma_D\gamma_T] = 218.\,[\gamma_D]^2 \text{ megawatts/m}^3 \tag{16}$$

We may use equation 14 to estimate a "breakeven length" of our linear collider, i.e., the minimum length of high field solenoid required to yield an amount of electrical power, (converted from the fusion energy released to electricity at an efficiency η_f), equal to the electrical power required to inject the deuteron ion beam (i.e., including ion source and direct converter efficiencies). For this rough estimate we will ignore the lesser power required to inject the low-energy T beam. This length is then given by the equation:

$$L_{min} = 2.3\times10^4\left[\frac{\cos(\theta)\lambda}{\gamma_D Q_E\,\eta_f}\right] \text{ meters} \tag{17}$$

Again, inserting the constraint (inequality 11) on cos(θ) gives a new relation reflecting the limitation imposed by the mirror instability:

$$L_{min} = 7.8\times10^{3}\left[\frac{\lambda^{3/2}}{\gamma_D^{1/2}Q_E\ \eta_f\ \Gamma}\right]\ \text{meters} \tag{18}$$

The expression for the breakeven length may also be used to estimate the breakeven "confinement time" (flight time) of the deuterons through the system, as an index of the diminished confinement time requirements of this linear collider, as compared to conventional fusion systems, such as the tokamak. From equation 17 and the velocity of the deuterons we find the result:

$$\tau_{min} = 7.4\times10^{-3}\left[\frac{\lambda^{1/2}}{\gamma_D Q_E \eta_f}\right]\ \text{sec.} \tag{19}$$

7.3 An Example Case

We may now use equations 13 through 19 to calculate an example linear collider case. In equation 13 we will assume values for all the parameters except the density parameter, γ_D, finding then the limiting deuteron and triton densities stable against the firehose mode and the mirror mode at all points in their trajectories. We take $\lambda = \alpha = \Gamma = 1.0$ in equation 13 finding $\gamma_D = 0.69$ and $\gamma_T = 2.66$. Inserting these ion density values into equation 16 we find $p_{DT} = 105$ megawatts/m^3, a rather high power density, one having implications as to the smallness of the diameter of the plasma column that will be needed in the linear collider.

For comparison with conventional fusion systems we may use these same parameters in equation 19 to evaluate the breakeven confinement time of the deuterons. Taking the efficiency of conversion of the fusion energy, $\eta_f = 0.33$ (i.e., assuming a conventional thermal cycle is used), taking the source and direct converter efficiencies, $\eta_i = \eta_{dc} = 0.9$, so that $Q_E = 4.7$, we find $t_{min} = 7.$ ms. To be sure the confinement times required for practical net power would be substantially longer than this value, but still would be small compared to those required in a conventional tokamak-based fusion power system.

Equation 18 may be used to estimate the breakeven length of the linear collider. With the parameters assumed above we find $L_{min} = 6.0$ kilometers. As a first cut for the length of our linear collider we might assume $L = 15.$ kilometers, i.e., 2.5 times the breakeven length. Associated with this length would be a deuteron confinement (flight) time of 17.5 ms, and a triton flight time (estimated from the ratio of the deuteron velocity to the triton velocity) of about 45 ms.

If one assumes, for example, that the net power output of the plant is to be 1000 MWe the minimum plasma radius may then be estimated approximately by using the power density as calculated from equation 17 and the fusion energy conversion efficiency that was assumed above. The minimum radius of the column (assumed to be at constant density as a function of radius out to its boundary), is then found to be a (min) = 2.4 cm. This almost ridiculously small radius is a consequence of the projected high fusion power density of our linear collider, coupled with the necessity to have a long plasma column in order to achieve net power. Even if one assumes that the density distribution of the plasma column is parabolic with radius the column diameter would only be of order 10 cm. This diameter is to be contrasted with the plasma diameter of several meters projected for fusion power plants based on the tokamak.

While the example that we have given is for a D-T fusion system, the linear collider idea or its variants could in principle be applied to other fusion fuel cycles, such as D-He^3. An economic penalty would be paid because of the smaller fusion cross-section and the higher ion energies required, but other advantages, such as the near-absence of satellite neutron-producing reactions and the elimination of the need for a breeding blanket, could ameliorate this penalty. In fact a case could be made that it should be much easier to scale up an open-ended system, such as a linear collider, to operate with alternate fusion cycles than it would be to contemplate scaling up tokomak-based systems for such cycles.

7.4 Electron Physics and Other Plasma-Related Issues

In the simple calculations that have been presented some potentially important plasma-related and other issues have not been discussed. It is beyond the intent of this article to deal with such issues definitively, so that the discussion here will be limited to brief comments. One issue, perennially brought up in the discussion of open-ended systems, is the question of end thermal losses associated with the electrons of the plasma. To reduce the effects of electron drag on the ions to acceptable levels the electron temperature of the plasma has to be of order a few keV. To illustrate the point, in the example case the characteristic slowing-down time of the deuterons by electron drag becomes equal to their flight time of 17.5 ms. at an electron temperature of 3.0 keV, representing a probable lower bound to the operating electron temperature.

The issue is the following one: If anything like the normal heat conductivity of the electrons were to prevail at kilovolt electron temperatures the resultant energy loss through the ends would be enormous. Fortunately, as was predicted theoretically [42], and recently confirmed experimentally in the Gas Dynamic Trap experiment [43] at Novosibirsk, the situation is much better than this. In an open-ended system with a central dense plasma that expands into a weakening magnetic field the rate of loss of electrons is controlled by the ambipolar potential that arises naturally in preserving quasi-neutrality. This potential, if it is allowed to rise to its asymptotic value, holds in the electrons, effectively inhibiting their loss rate. Furthermore as the theory predicted and experiment confirmed, if the expansion ratio of the field, that is the ratio of the field at its maximum to that where it terminates on a physical surface is larger than the square-root of the ion-to-electron mass ratio, the electron population becomes decoupled from any interaction with the wall, becoming insensitive to, for example, the emission of secondary electrons at the wall. In this case the energy losses per electron associated with the electron channel are limited to some multiple (of order 5) of the electron mean energy in the plasma. The number of electrons being lost is in turn limited to that associated with any source terms that are present in the plasma.

In the linear collider case here the expansion ratio of the magnetic field at the ends will be substantially larger than Mirnov and Ryutov's critical value. Also, since only completely ionized ions are being injected by the ion sources, the primary source of the electrons in the plasma column is the ionization of the background gas in the system. This source could in principle be made quite small in steady state. We conclude that it may be possible to create a situation where the energy loss through the electron channel out the ends is acceptably small.

Another area where electron-physics issues might impact the operation of a linear collider is the presence of turbulent transport. Although we have addressed all of the "killer" MHD modes (interchange, firehose, and mirror modes) there might still be present small-scale turbulence that could cause excessive cross-field transport. The usual way to estimate this transport is compare it with the Bohm diffusion rate, which represents an approximate upper bound to the rate of diffusion caused by such turbulence. For our example case, assuming a parabolic density distribution with an outer radius of 5 cm., the calculated Bohm diffusion velocity at 3.0 keV is approximately 18 cm./ms. It follows that for the linear collider example that we have given the rate of cross-field transport by turbulence would have to be a substantial fraction of the Bohm rate before it seriously interfered with the operation of the system.

Another effect of the ambipolar potential of the electrons on the collider would be to require that in order to have the ion energies within the collider equal to those assumed above, namely 10 keV for the tritons and 100 keV for the deuterons, the actual ion-source accelerating voltages would have to be increased by an amount equal to the ambipolar potential. At an electron temperature of 3 keV this potential would be of order 15 keV. Of course the injected ions, though losing energy through climbing up the ambipolar potential, would be accelerated by the same potential as they exited. Thus the direct converters would still be operating on D and T ions having energies comparable to the accelerating energy input at the sources. In the interest of simplicity the corrections to the equations for ion source densities, etc., required to take into account the effect of the ambipolar potential, have not been introduced.

7.5 Some Economic Considerations

If the above physics and engineering considerations are found to be valid, then the calculations presented for the linear collider example would be a reasonable representation of its size and other characteristics. However, whether such a system, even if it proved technically feasible, would ever be built depends on its economic viability. While it is not within the scope of this article to attempt to present a detailed cost analysis of the linear collider that has been described, it is possible to make some simple cost estimates that are informative.

We have already noted that locating a fusion linear collider in an underground tunnel is a feasible means of solve the siting and land-use problem, the way having been paved by the high-energy physics community. Moreover, the cost of tunneling itself is minuscule compared to the cost of the structures within the tunnel and can be neglected. As to the cost of the linear collider itself, a starting point can be obtained by reference to studies that have been made of the cost of large-scale SMES (Superconducting Magnetic Energy Storage) systems for utility use. One particular study [44] involved long solenoidal magnets of the same general character as the ones proposed for our linear collider fusion power system. The results of their study may be used to obtain a rough estimate of the costs of the solenoid for the linear collider. If we assume that the solenoid is 2 meters in inner diameter, is 15 kilometers in length, and operates at 10 Tesla it will be storing about 2.0×10^{12} Joules of magnetic energy. From the reference the cost per megajoule of an entire large SMES system is shown as about \$250. If we make the upper-limit assumption that 100 percent if the cost resides in the solenoid our 15 kilometer solenoid would, under this assumption, be estimated to cost $\$5.0 \times 10^{8}$ (\$33,000/meter). If we multiply this figure by 3.0 to account for the other components (blanket, vacuum chamber, etc.) and assume an equal cost for the "balance of plant" we arrive at a capital cost estimate of $\$3.0 \times 10^{9}$ for the entire 1000 megawatt fusion system, or \$3000/kilowatt. This figure is not inconsistent with the present-day capital cost of nuclear power plants.

7.6 General Comments

The foregoing discussion of a simple linear collider outlines an extreme case of open-ended systems that might be of value for fusion power purposes. As noted earlier, our linear-collider example is at one end of a continuum of systems at the other end of which is are systems such as the tandem mirror or the "field-reversed mirror" (a field-reversed configuration contained in a mirror cell). In another paper [39] I have discussed a concept, the "kinetic tandem," that represents the melding of the tandem mirror idea with the linear collider. The kinetic tandem utilizes the same mirror compression effect described in this paper to create ion-density peaks at each end of a long reaction chamber. These peaks, in the same manner as was employed in the original tandem mirror idea, generate potential maxima that confine a target plasma through which other injected ions pass to produce fusion reactions. However, as its name implies, the kinetic tandem employs only particle kinetic effects to produce its density peaks, thus requires no end mirror cells to accomplish its purposes. Its field is the same tapered solenoidal field that is utilized in the linear collider. As with this paper, however, the main point in discussing these variants on open-ended systems is to drive home the point of the flexibility of such systems for innovative improvements.

8. SUMMARY AND CONCLUSIONS

In magnetic fusion research we find ourselves in a new situation, one fraught with both problems and opportunities. Fifty years of research has resulted in enormous progress in the understanding of the plasma-physics problems of fusion and in movement toward achieving the plasma conditions required for fusion. And yet we are faced with the situation that the scientific front-runner in fusion - the tokamak - may not be a viable approach to economic fusion power. Our opportunity is therefore to utilize our scientific knowledge base in an informed search for better ways to solve the fusion problem. In this paper some of the characteristics and the physics history of open-ended systems has been presented. The argument has been made that open-ended systems are much more amenable to innovative approaches than are closed ones. To support this thesis an extreme example - the linear collider - has been sketched out. Only time will tell whether it, or other variations on this theme, will prove to be economically viable systems. Our real point here is to attempt to reinstill the spirit of innovation and adventure that marked the early days of fusion research. The major difference between then and now is the understanding of the plasma state, gained by 50 years of hard work and reflected in the choice of the title for this paper. A sub-title might have been: "Fusion's Great Opportunity is Now." The underlying truth is that fusion still represents the best option for meeting our civilization's long-term energy needs.

ACKNOWLEDGMENTS

I wish to acknowledge valuable help from Dimitri Ryutov in resolving important plasma physics issues that I encountered in writing this article.

REFERENCES

*Work performed under the auspices of the U. S. Department of Energy by the Lawrence Livermore National Laboratory under contract number W-7405-ENG-48.

1. R.F. Post and J.F. Santarius. Fusion Technology. **22**, 13 (1992).
2. R.F. Post and D.D. Ryutov. Current Trends in International Fusion Research. 153, Plenum Press (1997).
3. R.J. Hastie and J.B. Taylor. Phys. Fluids. **8**, 323 (1965).
4. D.L. Correll, J.F. Clauser, F. H. Coensgen, et al. Nucl. Fusion. **20**, 655 (1980).
5. G. I. Dimov, V.V. Zakaidov and M. E. Kishinevskii. Sov. J. Plasma Phys. **2**, 326 (1976).
6. T.K. Fowler and B.G. Logan. Comments Plasma Phys. Controll. Fusion. **2**, 167 (1977).
7. T.Tamano, T. Cho et al. Open Confinement Systems for Fusion. World Sci. Pub. Co. (1994) p. 1.
8. R.F. Post. Nuclear Fusion Reactors. Proc. British Nuc. Eng. Soc., (1969) p. **88**.
9. R.W. Moir, W. L. Barr and G. A. Carlson. Plasma Phys. and Controll. Nucl. Fusion Research 1974, **3**, IAEA, Vienna (1975) p. 583.
10. R.F. Post and D.D. Ryutov. Comments Plasma Phys. Controll. Fusion. **16**, 375 (1995).
11. M. Kruskal. J. Math. Phys. **3**, 806 (1962).
12. T.G. Northrop and E. Teller. Phys. Rev. **117**, 215 (1960).
13. S.N. Rodionov At. Ehnerg. **6**, 623 (1959).

14. G. Gibson, W. Jordan and E.J. Lauer. Phys. Fluids **6**, 116 (1963).
15. M.N. Rosenbluth, W.M. McDonald, D.C. Judd. Phys. Rev. **107**, 1 (1957).
16. T.K. Fowler and M. Rankin. Plasma Phys. **8**, 121 (1966).
17. A.W. Futch, J.P. Holdren, J. Killeen and A.A. Mirin. Plasma Phys. **14**, 211 (1972).
18. R.F. Post. Phys. Rev. Lett. **18**, 232 (1967).
19. G.I. Budker, V.V. Mirnov, D.D. Ryutov. JETP Lett. **14**, 214 (1971).
20. M.N. Rosenbluth and C.L. Longmire. Ann. Phys. **1**, 120 (1957).
21. R.F. Post, R.E. Ellis, F.C. Ford and M.N. Rosenbluth. Phys. Rev. Lett. **4**, 166 (1960).
22. J. Berkowitz, H. Grad and H. Rubin. Peaceful Uses of Atomic Energy (Proc. 2nd Int. Conf., Geneva 1958) Vol. **31**, UN, New York, **177** (1958).
23. M.N. Rosenbluth, N.A. Krall and N. Rostoker. Nucl. Fusion Supplement Part 1, 143 (1962).
24. Y.V. Gott, M.S. Ioffe and V.G. Tel'kovskii. Nucl. Fusion Supplement Part 3, 1045 (1962).
25. H.P Furth and M.N. Rosenbluth. Phys. Fluids **7**, 764 (1964).
26. A.V. Anikeev et al. Open Plasma Confinement Systems for Fusion. World Scientific Pub. Co. 303 (1994).
27. D.D. Ryutov. Physics of Mirrors, Reversed-Field Pinches and Compact Tori. **2** 791, Societá Italiana di Fisica (1980).
28. E.G. Harris. Phys. Rev. Lett. **2**, 34 (1958).
29. M.N. Rosenbluth. Plasma Physics (Lectures at Seminar at International Centre for Theoretical Physics, Trieste, 1964), IAEA, Vienna, 485 (1965).
30. R.F. Post and M.N. Rosenbluth. Phys. Fluids **9**, 730 (1966).
31. R.F. Post. Nuclear Fusion **27**, 1579 (1987).
32. R.F. Post. Plasma Confined in Open-Ended Geometry. (Proc. Int. Conf. Gatlinburg, 1967) Rep. CONF-671127, ORNL, Oak Ridge, TN, 309 (1967).
33. C.C. Damm, J.H. Foote, A.H. Futch et al. Phys. Rev. Lett. **24**, 495 (1970).
34. V.P. Pastukhov. Nucl. Fusion **14**, 3 (1974).
35. R.W. Moir, W.L. Barr, D.J. Bender et. al. Plasma Physics and Controlled Fusion Research 1976, **3**, IAEA, Vienna, 223 (1977).
36. B.G. Logan. Mirror-Based and Field-Reversed Approaches to Fusion (Proc. Workshop Varenna, 1983) Vol. **1**, Int. School of Plasma Physics, 347 (1984).
37. R.F. Post. Physics of Alternate Magnetic Confinement Schemes (Proc. of Workshop, Varenna 1990), Societá Italiana di Fisica, 63 (1991).
38. R.F. Post and D.D. Ryutov. Current Trends in International Fusion Research, Plenum Press, 153 (1997).
39. R.F. Post. Plasma Physics Reports **23**, 756 (1997).
40. W.A. Newcomb. J. Plasma Phys. **26**, 529 (1981).
41. M. Dembinskii and P.K. John. J. Appl. Phys. **50**, 6113 (1979).
42. V.V. Mirnov and D.D. Ryutov. Itagi Naukii Tekhniki, Fisika Plasmy, (V.D. Shafanov, Ed.) Moscow, **8**, 77 (1988) (in Russian).
43. P.A. Bagryansky et al. Proc. of Open Systems '98 Conf., Novosibirsk, Russia, 27-31 July 1998. Transactions of Fusion Technology **35**, 79 (Jan. 1999).
44. C.A. Luongo. IEEE Trans. on Magnetics **32**, 2214 (1996).

RECENT PROGRESS IN PLASMA FOCUS DEVELOPMENT: FROM AN EXISTING 3 MJ TO PROJECTED 100 MJ PF INSTALLATION

N.V. Filippov, T.I. Filippova V.I. Krauz, E.A. Azizov[1], L.G. Golubchikov[1], A.P. Lototsky[1], A.F. Nastoyashchy[1], N.G. Makeev [2], and V.G. Rumyantsev[2]

RRC "Kurchatov Institute"
Moscow, 123181, Russia
[1]TRINITI
Troitsk, Moscow Region, 142092, Russia
[2]VNIIEF
Sarov, 607190, Russia

ABSTRACT

A given study deals with an analysis of one of the possible ways of using the Plasma Focus (PF) - type facilities for solving the tasks of Controlled Fusion. The facility at issue is based on a Filippov's type Plasma Focus with an inductive energy storage. Some estimates show that 300 MJ energy storage is needed to provide the 50 MA plasma current in order to achieve a "breakeven". The Project discussed here propose instead to use the existing inductive storage, TIN-900, from the power supply of the TSP - tokamak coupled to a Filippov's type of PF machine. This new facility "MINIK" (60 - 100 MJ deposited into the discharge at the plasma current > 30 MA) will allow to directly approach the solution of the task under consideration. In this Project it is expected that number of scientific studies and engineering physics developments will be performed by the efforts of scientists from three Russian Scientific Centers, RRC KI, SRCRF - TRINITI and RFNC -VNIIEF, under support by International Science and Technology Center (ISTC) with a wide involvement of foreign specialists.

1. INTRODUCTION

The controlled fusion program based on pulsed - high current - discharges (PHCD) has reached the point where DEMO test are required. A number of different diagrams for realizing PHCD is known. Plasma Focus systems are one of the most developed variant in this direction.

These systems have been well known since the end of the fifties, when - independently - N.V. Filippov [1] in the USSR and J. Mather [2] in the USA reached an essential progress in the studies of rather different, from the general viewpoint systems, i.e. Z-pinch and coaxial plasma accelerators, respectively. As the result, Plasma Focus were developed yielding a

Current Trends in International Fusion Research — Proceedings of the Second Symposium
Edited by E. Panarella. NRC Research Press, National Research Council of Canada, Ottawa, ON K1A 0R6, Canada. 1999.

plasma with the highest (by that time) specific energy content. This was an intense source of neutrons, X-ray radiation and charged particle beams that attracted the attention of a large number of researchers.

In spite of external differences in the electrodes arrangement both types of Plasma Focus (i.e., Filippov's and Mather's) the results produced with them were very close to each other. This can be explained by the presence of one general - very important - property: non-cylindrical plasma-current sheath (PCS) cumulating toward the axis at the final stage of the discharge in both systems. Hence, the origin of the second name to these systems: «non-cylindrical Z-pinch».

It is possible to single out three main stages of a discharge in both systems. Since there are some differences in these stages for the PF Mather and Filippov types, let us illustrate the principle of operation for these systems , to make it clear, using the Filippov type.

Its structure is based on the so-called «flat» set of electrodes (Fig.1). The anode (1) of a comparatively - large diameter is separated from the cathode (2) with a ring-like insulator (3). The vacuum chamber (4) is filled with a gas (deuterium or heavy gases, dependent on the tasks to be solved) under pressure in the range from a few tenths of Torr up to a few Torr. The capacitor banks (C_0) with the stored energy in the range from a few kJ to a few MJ are usually used at present as a power supply source. After triggering the switch (S), the breakdown in the discharge gap along the insulator (3) takes place, and PCS is produced (stage I). This is the first and a very important stage of the discharge, since the quality of the created sheath essentially affects the further discharge process. Under the effect of ponderomotive forces the sheath realizes the complicated motion along the electrode gap accompanied by the shock wave production. When a part of the PCS attains the anode surface, the accelerated PCS-motion towards the chamber axis starts to occur (stage II). At this point the current rises attaining its maximum for the time of the order of 10 μs. The anode dimensions are chosen from a condition for attaining the chamber axis by PCS at the maximum of a current. In the Mather approach, the stage of a long radial compression is replaced by an axial PCS-acceleration along the anode. Note that there is an important instant, when, at this very phase of motion, the plasma-magnetic storage with a moving current jumper is actually realized under conditions of spatial current peaking.

In the process of PCS-cumulating at the chamber axis (stage III), a fast plasma compression (~ 10^{-7} s) up to the densities of ~ 10^{19} cm^{-3} and heating occur. At the stage of

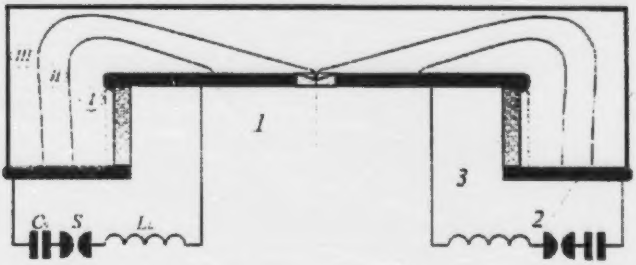

Figure 1. Schematic view of PF machine - Filippov type: (1) anode; (2) cathode; (3) insulator; (4) vacuum chamber; C_0 - energy storage (capacitive bank); L_0 - external inductance; S - rink-like vacuum switch. I-stage of breakdown along the insulator and plasma-current sheath formation; II-stage of PCS radial acceleration; III-stage of radial compression and dense plasma focus formation.

a dense pinch, the current density of about > 10^8 A/cm^2 is attained that results in a drive of strong current instabilities and in an abrupt current disruption. Actually, we have an effective plasma switch, and the energy stored in the magnetic field of a pinch is released into the «loading» , i.e. an anomalous plasma heating, intense neutron and X-ray radiation and the charged particle beam drive occur. An essential point in this is that the physics of the processes at the final nuclear-active stage is similar for different devices of a given type. Hence, the general nature of scaling laws takes place, i.e. dependence of the main plasma parameters and those of radiation characteristics on the discharge current magnitude and, respectively, on the results attained by the present time.

In particular, from an analysis of the experimental results produced in various laboratories for a wide range of initial discharge parameters, the following experimental dependence of a neutron yield on the pinch current (See, e.g., [3]) follows:

$$Q_N\,(\text{D-D}) = (1\text{-}5)\ 10^{11}\ I_p^4,\ [I] = \text{MA} \tag{1}$$

When PF is supplied from a capacitor storage, another - experimental - scaling law is usually used, as a dependence on the initial energy, W_0, of the power supply source (e.g. [4], [5]):

$$Q_N(\text{D-D}) = (0.5\text{-}1.0)\ 10^7\ W_0^2,\ [W] = \text{kJ} \tag{2}$$

Since W_0 is the characteristics of initial discharge conditions, and I_p, of its final stage, it is natural that these two scaling laws coincide only in the case, when one manages to pass whole discharge current through the pinch. It is a rather complicated task, and its solution is related to the proper organization of the initial discharge stages. The measurements of a current passing through the central pinch zone - they will be discussed bellow - are not easy and, as a rule, they are not carried out, in general. Usually, the experimenters limit themselves by registration of a total discharge current, although the problem of a current cumulating in the plasma column is always present.

The best results at present are: the neutron yields of about 10^{12} neutrons at W~500 kJ (Los-Alamos [6], Limeil [7], Frascati [8]). Thus one of the highest specific neutron yields, ~$3\text{x}10^{13}$ n/cm^3 for D-D reaction at a comparatively-low energy consumption, ~ $5\text{x}10^{-7}$ J/$n_{D\text{-}D}$, has been realized by PF. Since the neutron cost drops with an increase in the deposited energy and in the current through a pinch, one can rely on the achievement of $W_0/W_{D\text{-}T}$ ~ 1 at the respective increase in the power of the facilities. Some rough estimates show that the break-even can be attained at W~300 MJ and at the current of ~ 50 MA. This digits are not fantastic, they are really-achievable at the present stage of engineering. The only problem is the expenses associated with the solution.

2. PROBABLE DIAGRAMS FOR REALIZING THE CONTROLLED FUSION ON THE BASIS OF THE FACILITIES, PF-TYPE

As noted above, the results attainable at the PF-facilities are determined, to a considerable degree, by the magnitude of a current passing through a non-cylindrical pinch at the final stage of a discharge. Various modifications of the facility differ mainly by the technique of an approach to the problem of power peaking. At the last Symposium, the potential opportunities for the pulsed - high current - discharges to solve the controlled fusion problem were discussed, using two circuit-diagrams [5]. One of the circuit-diagrams is based on the technique of delivering the current to the plasma compression zone with compact tori (CT) at the MARAUDER - facility, using the capacitor storage of the SHIVA-STAR (Phillips Laboratories) as a power supply source. Very interesting results were recently produced at this facility [9]. The main goal of those experiments was to study the efficiency of current transportation to the PF-zone. It has experimentally-shown that the delivery to the compression zone up to 3 MA of a discharge current with the CT produced in the argon plasma is possible at the energy of the power supply source equal 1–2 MJ. The magnetic probes and the speedy photo registration (in a visible range and in a soft X-ray one) show the classical PF-evolution behavior. The result of no less importance is the registration of a neutron radiation. It confirms an effective current transfer from CT to the deuterium plasma injected along the system axis.

This report represents the alternative approach (second circuit-diagram) based on PF of the Filippov-type with an inductive storage. Previously, in the experiments on small PF - facilities with an inductive storage, a noticeable current pulse peaking was attained [10]. That resulted in a 3–4 - times increase in the neutron yield in comparison with the yield produced, when the traditional capacitor storage were used at the same stored energy and at the same current levels. It is related to the fact that, as noted, PF-itself is a magnetic storage with the power peaking at the final stage of the discharge. Thus, PF is an optimal plasma loading for the inductive energy sources, and it can be considered as the final stage of the power peaking in the circuit-diagram of the current generator. This greatly reduces the engineering requirements.

With the increase in the discharge current and in the energy deposited into PF, the radial dimensions of the discharge system should be proportionally enhanced to retain the optimal conditions (working gas density and the linear current density) for the discharge start-up at the insulator under which a symmetric current sheath is produced. For the current with the amplitude, $I > 10$ MA, e.g., the chamber radius should exceed 1 m. At such a size the leading edge duration of a current pulse, $t \sim 20$ μs long, is quite acceptable. During this time, according to the calculations, the current sheath after its production and after the start-up of its drive is rather far away from the chamber center, and its inductance is still very small. Since the needed current pulse duration is increased with an increase in the stored energy and in the current, it becomes possible to use large inductive storage. Moreover, we consider this way as the only possible one for PF in the energy range of a few tens MJ and higher.

3. MINIK - PROJECT

The construction of a special energy set for a large PF-facility is a rather expensive enterprise. However, at present we possess of an unique opportunity to essentially-approach the solution to such a problem and to propose to use for the existing energy set for TSP-tokamak, at TRINITI (Troitsk), an inductive storage TIN-900 [11].

TIN-900 includes 32 coils mounted into a toroidal magnetic system. Each coil has 13 turns in the primary winding. The maximal charging current of the storage, at the connection of the primary windings in series, is I_{ch}= 150 kA. This corresponds to the stored magnetic energy W=900 MJ. Each coil is supplied with a secondary, single turn winding with the permissible current of 2 MA through it. The highest voltage which is capable of withstanding the primary winding insulation is equal Uc=40 kV. However, to operate this storage under design conditions only four switches are provided, they are built-in among the groups with eight coils in each. Therefore the operating power of the storage does not exceed $2{,}4 \times 10^{10}$ W.

It is evident that in the present stage the TIN-900 storage power is not sufficient for the PF-type systems under consideration. It is necessary to adopt special systems for its peaking. The concrete solutions for these peaking systems will be discussed below, but now let us note that the estimates show that one can obtain up to 100 MJ of the energy deposited into the plasma and the plasma current greater than 30 MA, taking account of the losses at different stages of the energy conversion. These values exceed the possibilities of the now-existing PF-systems by about an order of magnitude.

Nevertheless, the creation of such a facility is a rather complicated task. It requires a great number of preliminary work for its solution. For this purpose, a Proposal has been prepared aiming towards the development of the pulsed - high power - neutron source based on the TSP - power supply set (ISTC, Proposal # 734). This Proposal is an unique opportunity to use the scientific and technical potential of three largest scientific centers of Russia - RRC "Kurchatov Institute", VNIIEF (Sarov) and TRINITI (Troitsk) to solve the fundamental problems in the physics of the pulsed-high current-discharge and to develop the corresponding pulsed engineering.

The Project is expected to be realized in two years with the participation of about 90 qualified specialists. The Project Leader is Prof. E.Azizov, Division Director at TRINITI. The works at RRC KI are headed by Professor N.Filippov; those at VNIIEF, by Dr. N. Makeev, Head of Department and at TRINITI by Dr. A. Lototsky.

The main goal of the Project is to find the ways of resolving physical and engineering problems of PF-systems transition into a GJ - energy range of the power supply source.

The expected structure of the facility named MINIK (Russian abbreviation for the Neutron - High power - Source with an Inductive Cascade) is shown in Fig.2. It provides a two-staged inductive storage (IS) with the first stage of a transformer type - current amplifier (rising current from 150 kA at input to 1.8 MA at output). The second stage of the IS with the time of the energy input and its "keeping", t ~ 20 ms, can be a mechanically-stressed small-sized toroid with the total current of about 45-50 MA. The PF - chamber is made as a monounit with the second stage of the IS.

The primary inductive stage (TIN-900) is charged with two turbogenerators, TDK-200, through current converters system. After charging with a set of switches (TIN-900 - design switches), the current, $I_0 > 1.5$ MA, is exited in the secondary winding of the first stage. Then, the pulsed energy transfer (200 MJ) to the second stage, with the power amplification from 10^{10} W to 10^{12} W, is realized via the second level switches (32 modules), according to a special circuit-diagram. The magnetic energy transfer process duration is t ~ 20 - 30 ms under voltage of current switching no more than 5 kV. After charging the second stage, its input is

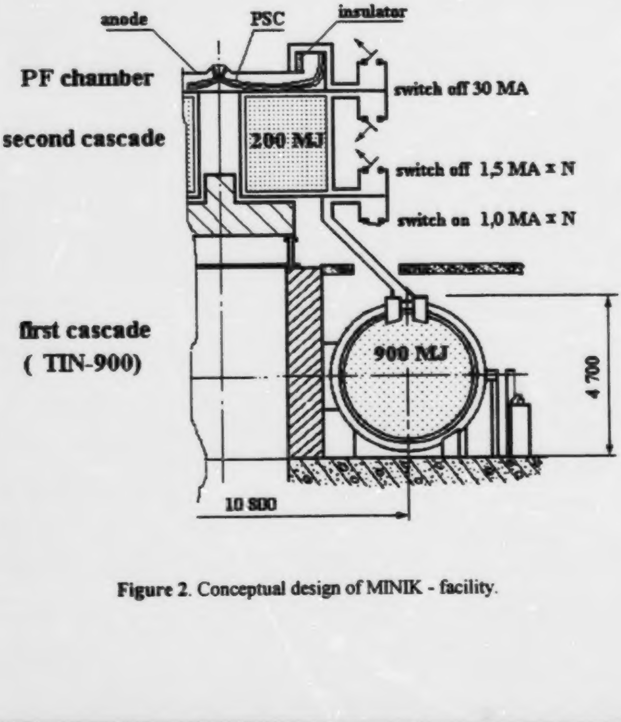

Figure 2. Conceptual design of MINIK - facility.

short-circuited, preventing, later on, the high voltage transfer to the coils of the first stage.

With the system of the third level switches the amplified current of the second stage (~40 MA) is applied to the PF-chamber. The system switches are placed in azimuthally-symmetric pattern along the chamber perimeter to improve the conditions for shaping the PCS. The primary breakdown occurs in a medium of a heavy gases (Ar, Ne). The breakdown voltage, U_{br}, does not exceed 25 kV and, after it, the voltage drops with an increase in the current. With a current rise the plasma sheath acceleration along the anode starts to take place. The specific features of the inductive storage operation require a rather fast completion of the current switching "ON" until the current sheath velocity is not great. On the basis of the above - given estimate for the current switching (30 μs) one can show that the current switching voltage will not exceed 25 kV and the energy losses will be lower than 10 MJ.

At the cumulating phase, a part of the second stage energy (~ 60 MJ) will be introduced directly into the chamber, the left 130 MJ are reserved, waiting for the development of a PCS-collapse culmination stage. The efficiency of this energy fraction conversion into radiation of a Plasma Focus depends on an opportunity to prevent the secondary breakdown across the insulator surface.

4. MAIN CONTENT OF WORKS ON MINIK - PROJECT

The works on Project can be divided into two parts:

- Studies of plasma physics and radiation PF-characteristics under forced conditions of a current pulse in order to predict the parameters of the proposed facility.
- Studies in the range of the pulsed - high current - power supply production.

4.1 Background and feasibility of project

The first item above is closely related with the feasibility of this Project. The main work will be performed at RRC KI and VNIIEF, since these Centers have a great experience in the PF-systems studies. The results produced in the recent years at the Lab headed by N.V.Filippov at the PF-3 facility with the total stored energy of 2.8 MJ and two auxiliary experimental stands (W=180 kJ) will be the basis for these works.

The main goals of the realized investigations was to study the PCS - dynamics in the discharges of heavy gases (Ar, Ne). The last circumstance has a principal significance for MINIK Project. For matching the power supply source with the discharge system we need to select such dimensions of the anode that the sheath compression at the axis would occur at the current maximum. In the case of deuterium operation with the current of some tens of MA, the anode dimensions should be very large. Therefore Ne is expected to be used as the main working gas at the initial discharge stages (breakdown and a radial compression) with the subsequent compression of the deuterium jet injected along the system axis. This concept is close to that used in the mentioned above experiments at the MARAUDER - facility.

As noted, one of the main problems in the PF discharge is the total current compression towards the system axis. This problem was studied at the PF-3 - facility, presently the largest PF. A photograph of PF-3 is shown in Fig.3. For studying the PCS-dynamics we used a special anode insert with the built-in calibrated Rogowski coils at the radii 3.5 cm and 6.5 cm from the anode center (Fig. 4). Oscillograms of the signals from these coils are shown in Fig. 5. One can see that the current compression from the radius 6.5 cm to the radius 3.5 cm occurs practically without losses. A decay of the current is caused not by the current loss but by its reduction, as a result of an increase in the discharge loop inductance, i.e. the energy is stored in the magnetic energy of the pinch. One should pay attention to the fact that at the radius 3.5 cm we have a current rise > 10^{13} A/s due to the spatial power peaking. Thus one can

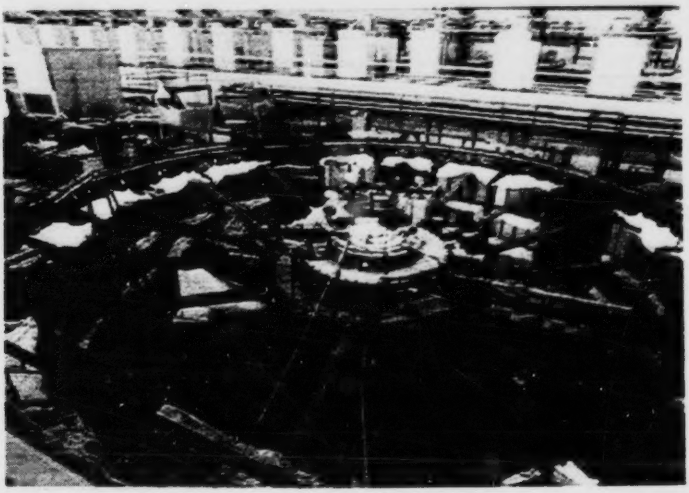

Figure 3. General view of the PF-3 facility.

declare that at the PF-3 - facility, in the Ne - discharge at the stored energy of about 1 MJ, it is possible to accumulate the current of about 3 MA in the zone close to the system axis from the initial diameter of 100 cm.

The radial compression phase and the pinch phase evolution at the PF-3 - facility, under discharge in Ne, are shown in Fig. 6. The photographs were produced in a visible light, the exposure time was 10 ns (*). A given sequence of images shows the classical plasma behavior, typical for small PF- facilities operating with deuterium.

Since the discharge system dimensions are not optimal a priori for discharge in deuterium we had no chance to verify the scaling laws by the neutron yield. However, for a quantitative estimate of the PF-3 operation efficiency, one can note that up to 10% of the capacitor bank energy is transferred into the energy of soft X-ray radiation under the conditions optimized for the X-ray production [13].

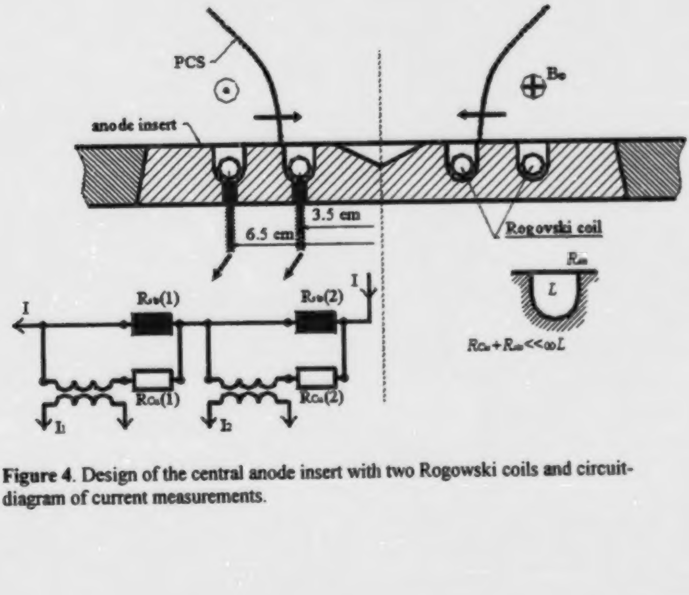

Figure 4. Design of the central anode insert with two Rogowski coils and circuit-diagram of current measurements.

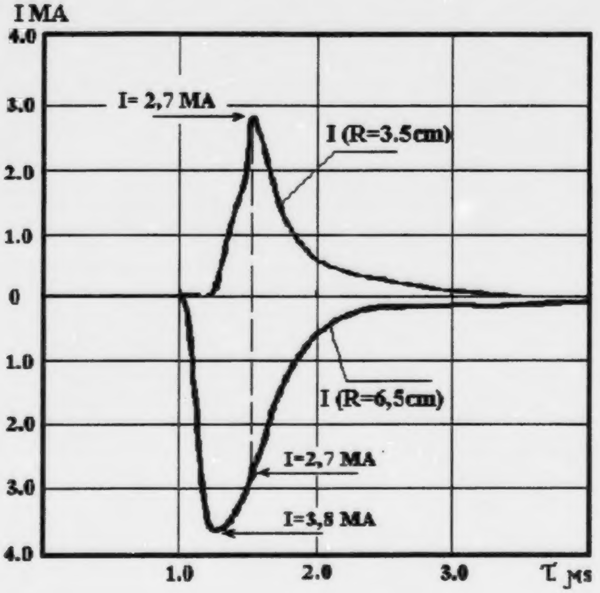

Figure 5. Traces of Rogowski coils signals.

Thus from the produced results, it follows that at present there are no serious problems in mastering the power production at the MJ-level. Within the ISTC-Project framework the studies of the initial discharge stages, depended on the energy loading onto the insulator, will

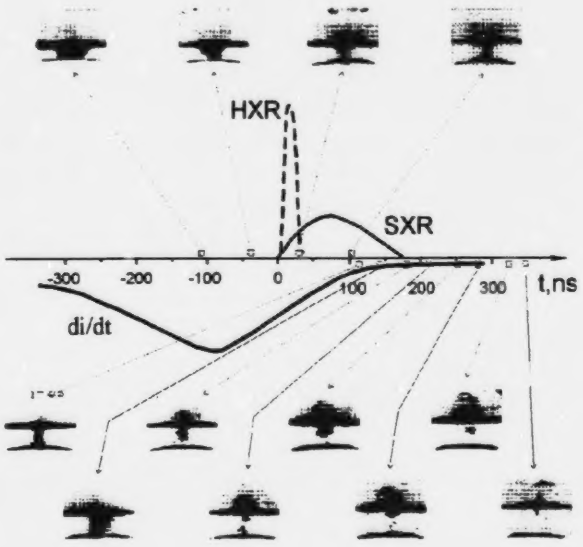

Figure 6. Evolution of radial compression and pinch phases in PF-3. Pictures are recorded in visible light, exposition time is 10 ns. Discharges occur in Ne (1 Torr).

be continued. One of the most important tasks will be the development of the pulsed deuterium feed to the discharge volume (together with VNIIEF) and the study of the plasma current sheath dynamics in the complicated multicomponent gaseous medium with large gradients of the initial gaseous distribution. At the same time, in VNIIEF the studies of the scaling law, spatial-temporal and spectral characteristics of the neutron radiation will be done at the functioning facilities. The theoretical studies of a final discharge phase assume the development of a pinch compression model at high current, I > 10 MA, where a noticeable effect of the radiation compression mechanism is already possible.

4.2 Engineering physics developments

Some works in the field of pulsed - high current - power production will be done by the efforts of the specialists from TRINITI and from VNIIEF.

As known, the power of the energy removal from the inductive storage is limited by technical parameters of the multistage current switches. The main problem for the current switches is the necessity of combining a low voltage conditions for the continuous charging of the magnetic energy storage (MES) with a current for time, τ_{ch}, with its fast switching to the loading for the time, τ_l, under high discharge voltage. The time ratio, τ_{ch}/τ_l, determines the coefficient of the MES-power amplification which does not exceed $k = 5x10^2$ even with the use of two-staged or three-staged current switches.

In order to increase k, the two-cascaded MES has already been proposed [14], its block-diagram is given in Fig. 7. In this circuit - diagram there are two stages of a switch, K1 and K2, between which an intermediate storage cascade (2nd cascade in Fig. 8) is built-in. After transferring the energy to the intermediate storage cascade, the stage K1 can be short circuited and should not withstand the discharge voltage across the loading under operation of K2. In that case, the calculated power amplification coefficient is the product of the cascade amplification factors, $k= k_1 \cdot k_2$. A great power amplification is attained due to separation of the function between the switch stages.

The successful operation of the two-cascaded magnetic energy storage directly depends on the applied technique for the pulsed magnetic energy transfer between the 1st storage cascade and intermediate one. In the simplest case of a direct current switching from one inductance to another, the theoretical efficiency of the magnetic energy transfer is limited by the factor 0.25. The technique for the radical efficiency rise have been previously considered [15,16,17]. Their common basis is the organization of the discrete multistep transfer process which can be realized in the known circuit-diagrams with the MES - sections connected in parallel.

The theory of the systems for highly-effective magnetic energy transfer, developed at TRINITI was confirmed in a number of experiments. The general view and design of the original switching system with which the energy of a three-sectioned inductive storage was transferred to the pulsed magnetic coil with a strong field, at the efficiency equal 0.41, are

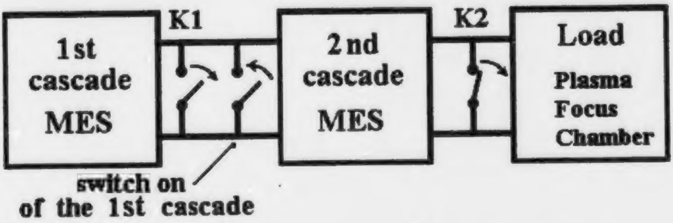

Figure 7. Block-diagram of two-cascaded Magnetic Energy Storage (MES).

shown in Figs. 8 and 9. Each of the switches included two stages of the current interruption: mechanically-destroyed conductor at the first stage and an electrically - exploded wire at the second one. Their mutual disposition is shown in Fig. 9. This disposition has one structural feature: the stages are located in the different frames filled with a mineral oil. The set of three switches operated in an automatic mode: exploding wire excited the shock wave in the oil which, in its turn, cut the conductor of the next switch, by its pressure, upon the finned dielectric barrier. The current of this conductor was switched to a parallel wire etc.

The transfer efficiency of such sets essentially depends on the discreteness of the process, i.e. on the number of inductive storage sections, according to the relationship:

$$\eta \geq \lambda/(1+\lambda)\{1-1/2N[\sqrt{\lambda}\cdot\mathrm{arctg}\sqrt{\lambda}+\lambda/(1+\lambda)]\} \qquad (3)$$

where N is the number of sections, $\lambda=L_2/L_1$ is the parameter of matching between the inductances of second (L_2) and first (L_1) cascades.

When the number of section in TIN-900 is N = 32, one can obtain an efficiency higher than 0.8. However, the detailed analysis has shown that the calculation of real characteristics for the pulsed device can be carried out, taking account of some features in the system of magnetic storage and in its elements, as well as those of a PF-loading, only.

Some preliminary results of calculating the magnetic energy transfer process from TIN-900 to the second cascade of the storage (and, then, to the PF-chamber), dependent on the loading inductance, L_2, in the second inductive cascade, are represented in Fig.10. The quantity F is the product of the energy transfer coefficient, η, by the current through the loading, I, to the fourth power and by the power, P, developed in the loading:

$$F = \eta \cdot I^4 \cdot P \qquad (4)$$

Let us discuss some feasibility consideration in the choice of the function F which, in a given case, is the special aim function for optimizing the current generator. From some previously done studies it is known that the maximal efficiency, η, of the energy transfer and

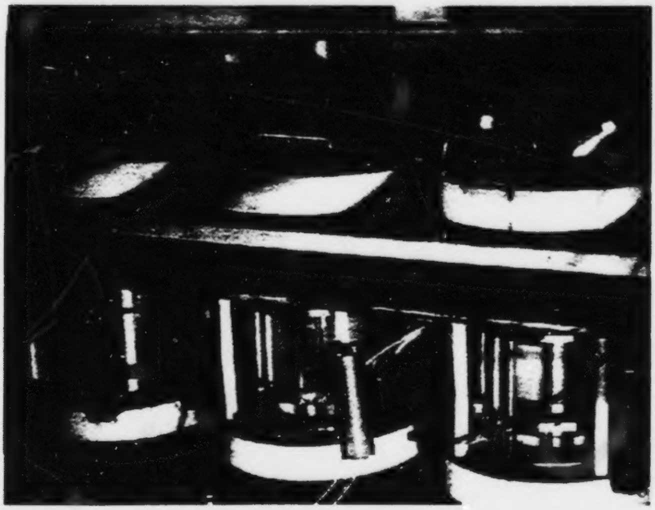

Figure 8. General view of an experimental set of switches for the three sectioned inductive storage used in the experiments at TRINITI for the energy transfer into the magnetic coil with the efficiency η=0.41.

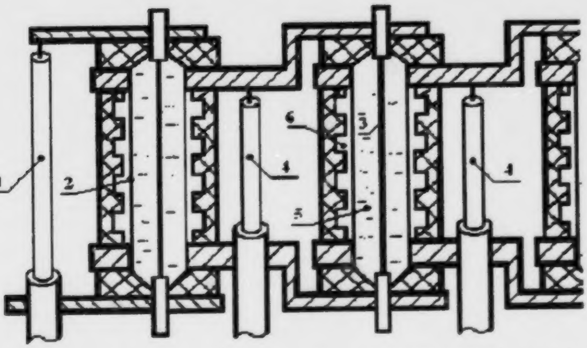

Figure 9. Design of a set of switches for the three-sectioned magnetic storage: (1) cable for the pulsed drive of a switch; (2) mechanically destroyed conductor of the first stage of the switch; (3) electrically-exploded wire (second stage); (4) cable current lead-ins from the magnetic storage sections; (5) mineral oil (arc quenching medium).

the maximal power of the transfer system, P, are realized at different values of the parameter of matching the inductances, λ. It would be natural to introduce some function, $f = \eta \cdot P$, representing an acceptable compromise solution for selecting electromagnetic (efficiency and power) parameters of the inductive storage. Then, we would look for an optimum source of a current on the basis of the above-represented scaling law (Eq. 1). Let us take account of the fact that the neutron yield is proportional to the fourth power of a current. In other cases (e.g. in the X-ray source design) the optimization function can be different. Note that all the quantities in the relationship (4) can be easily reduced to the dimensionless form (e.g. the current can be expressed in the units of a charging current, I_{ch}, and the power can be related to the total disruptive power of all the switches). This allows one to optimize the power supply source structure as a whole and then, to take account of the quality of its matching with the loading.

In a given case inductance, L_2, defines the energy transfer efficiency (see, Eq. 3) to the second cascade only at the present inductance of the first cascade (TIN-900). However, we should clearly understand that, with a rise in L_2 and with a rise in the efficiency, η, the current through the system should be reduced. It is seen in Fig. 10.

But the choice of the inductance L_2 also determines the conditions of matching with PF-chamber. Let us consider now the energy transfer process into the plasma loading (PF). Today we do not know what will be the inductance of the 100 MJ-pinch at the final stage of its cumulating. However, we assume that its value will not be much different from L = 150 nH which corresponds to the MJ-experimental facilities. Therefore it seems to be natural to look for an optimum with the expression (4), using the current through the PF-pinch, not through the inductive cascade. To estimate one can neglect the active impedance of a current sheath at the stage of its radial compression and assume that a magnetic flux is retained in the L_2 - PF - circuit. The pinch current dependence at the phase of maximal compression for the same range of changes in the inductance of the second cascade as that in Fig. 10, taking account of the above-said assumption on the pinch inductance (~ 150 nH), is given in Fig. 11. We see that, within the framework of the considered - relatively simple - solution for the current drive system, its amplitude is limited by 30 MA. Optimization function for this case is also given in Fig. 10 (dotted curve). Its maximum practically coincides with the I_{PF} - maximum because of a comparatively-slow change in other quantities in comparison with I^4.

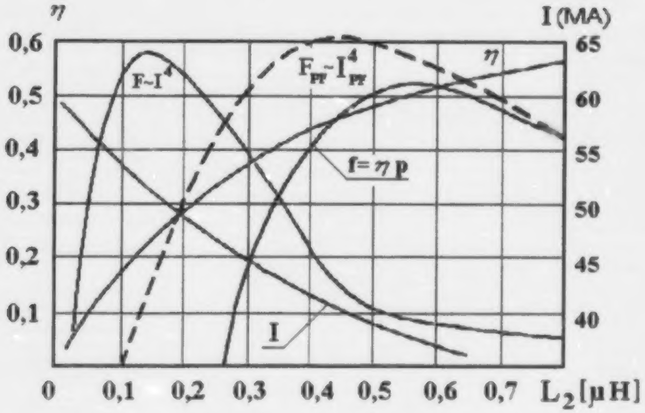

Figure 10. Current, I, efficiency of energy transfer, η, and the optimization function, F, vs. second cascade inductance, L_2; solid line - cascade I - cascade II transfer, dotted line - cascade II-plasma loading transfer.

Besides that, we see the opportunity to increase the current up to 50 MA. This can be realized by using a two-turn toroidal storage of the second cascade and switching of the turns, in parallel, during the PF - discharge. Such an opportunity should be involved into the studies of the large PF-facility design.

If one recapitulates our preliminary consideration of the power supply system, one will realize that one could rely on the current 30-50 MA (the upper limit corresponds to the additional doubling of the current), at the efficiency of energy transfer to the PF - power supply cascade equal about 0.3-0.5.

The structure of works on energy part for the ISTC - Project is very wide, being the detailed study of the energy transfer systems, taking account of the magnetic system geometry, determination of the parameters for switches, development and the tests of the mock-up samples. The works on matching of a magnetic current generator with an initial PF-discharge stage compose a considerable part in these activities. Therefore the construction, at TRINITI, of a small (200 kJ) experimental PF-stand with its power supply from an inductive storage is planned to be realized for studying the PCS-behavior at steep leading edges of a current.

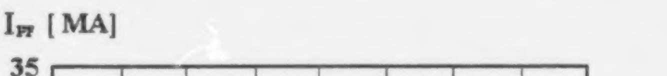

Figure 11. Plasma current in PF at the phase of maximal compression vs. second cascade inductance, L_2.

5. SUMMARY

Thus one can make a statement that the PF-systems, Filippov-type, are a real alternative to the existing approaches for solving the controlled fusion problem. The proposed Project is intended for the development and production of the MINIK-facility, the engineering parameters of which exceed those of the existing PF-systems by more than order of magnitude and closely-approach the expected parameters of the DEMO-fusion facilities. An important feature of Project is that it is based on the existing - functioning - power supply set to the TSP-tokamak. This circumstance makes the Project cost considerably smaller and makes it presently realizable.

The physical principle upon which Project is based is of no less importance. According to it, the power supply and the direct plasma loading are unified so that PF is one of the stages in the general circuit-diagram of the energy conversion. This allows one to optimize the system, as a whole, dependent on the problem under solution (source of neutrons, X-ray radiation, particle beams etc.), to essentially-enhance the utilization efficiency of the energy stored in the power supply source.

The proposed MINIK-facility parameters allow one not only to solve the fundamental controlled fusion physics problems but to produce a unique - high power- source of neutron and X-ray radiation. Under corresponding Project study with the optimization respective to a definite radiation, one can rely, in particular, on the production of the about 10^{19} D-T neutrons per pulse, at the flux density of about 10^{22} n/s×cm^2 in the zone, ~ 20 cm in radius.

The potential applications of such a neutron source are rather wide:

- tests of materials and an equipment in a strong radiation field;
- cancer neutron-boron-capture-therapy (substitution of fission based neutron sources);
- production of short-lived isotopes for medical and biological use;
- transmutation of nuclear wastes;
- driver for safe fission reactors, etc.

The authors of this Project posses of the necessary material basis, qualified Personnel and of the distinct organizational structures for the Project realization. At present the Project is submitted to ISTC.

ACKNOWLEDGMENTS

Presentation of this paper has been possible due to financial support from ISTC (Project # 734) and Avogadro Energy Systems Inc., NY. The authors are grateful to Dr. J.S. Brzosko from AES Inc. for discussion and comments on this project and to J.R.Brzosko for assistance in preparation of the text.

REFERENCES

* Photographs were produced by Dr. A.N. Mokeev (RRC KI) [Ref. 12].

1. N.V.Filippov, T.I.Filippova and V.P.Vinogradov. Dense, High Temperature Plasma in a Non-Cylindrical Z-Pinch Compression, Nuclear Fusion, Suppl., part 2, p. 577 (1962).
2. J.W.Mather. Phys. Fluids. **8**, 366 (1965).
3. J.P.Rager. The Plasma Focus, Com. Naz. Energ. Nucl. Cent. Frascati (Pap.), 81.19/cc, (1981).
4. L.Michel, K.H.Schönbach and H. Fisher, Appl. Phys. Lett. **24**, 57 (1974).
5. J.S. Brzosko, J.H. Degnan, N.V. Filippov, B.L. Freeman, G.F. Kiuttu and J.W. Mather. Comments on the Feasibility of Achieving Scientific Breakeven with a Plasma Focus Machine, Current Trends in International Fusion Research (Proc. of the First

International Symposium of Current Trends in Fusion Research (1994), Washington, D.C.), Plenum Press, New York, pp. 11-32 (1997).

6. K.D. Ware, A.M. Williams and R.W. Clark. Bull. APS **1**, 1364 (1973).
7. A. Bernard et al. Microinstabilities Connected with Neutron Emission and Electromagnetic Radiation in the Plasma Focus, 7th Europ. Conf. on Contr. Fus. and Plasma Phys., Lausanne, **1**, 60 (1975).
8. J.S.Brzosko, B.V.Robouch and J.Klobukowska. Fusion Technology **12**, 71 (1987).
9. G.F. Kiuttu, J.D. Graham, J.H. Degnan, J.S. Brzosko, S.K. Coffey, D.D. Gale, C.D. Holmberg, B.B. Kreh, J.W. Meyers, C.A. Outten, E.L. Rude and K.D. Ware. New Method of Initial Multi-Megaampere, Multi-Megajoule Plasma Focus Discharges Using Magnetized Plasma Flow Switches. 1996 IEEE ICOPS, p. 238 (4D05-06).
10. V.K.Chernyshev, V.A.Tsukerman and V.M.Gerasimov et al. Sov. J. Tech. Phys. **31**, 558 (1986).
11. E.A. Azizov, Yu.A. Alekseev and N.N. Brevnov et al. Atomnaya energia (Rus.J.) **52**, 108 (1982).
12. A.N. Mokeev, V.V. Mialton, N.V. Filippov, Plasma Sheath Dynamic in the Filippov-Type Plasma Focus Facility. Preprint IAE, 1998, RRC "Kurchatov Institute", Moscow, in press.
13. N.V. Filippov, T.I. Filippova, I.V. Khutoretskaia, V.V. Mialton, and V.P. Vinogradov, Physics Lett. **211**, 168 (1996).
14. E.A. Azizov, I.A. Ivanov, A.P. Lototsky. Electrichestvo (Rus.J) **4**, 35 (1990).
15. A.P. Lototsky. Prospects for the inductive energy storage usage as the power supply to the magnetic - high power - systems. IAE - Preprint, 3714 (1982).
16. A.P. Lototsky. On the magnetic energy transfer efficiency from inductive storage. Electrichestvo (Rus.J) **6**, 64 (1985).
17. A.P. Lototsky. Generation of strong magnetic fields in the chamber of a fusion facility with adiabatic plasma compression. Reports of the third All-Union Conf. on engineering problems of fusion reactors, 1984, June, 20-22. Leningrad, M., Central Sci. Res. Atom. Inform. Institute **3**, 127 (1984).

REVIEW ON A DENSE PLASMA FOCUS RESEARCH LINE AND PROJECTIONS IN THE NUCLEAR FUSION FIELD

Jorge Pouzo*

Instituto de Física Arroyo Seco
UNCPBA
Tandil BA (7000) Argentina

ABSTRACT

In this work a review of a twenty five years research line on DPF is presented. This line can be characterized by four objectives: a) Obtain some possible explanation of the empirical scaling law for neutron yield with the pinch current, in terms of both thermal and non-thermal nuclear fusion processes; b) Explain the reasons of the existence of high and low deuterium pressure limits beyond which the neutron yield drops even when the pinch current is increasing (in the first case), or monotonously decreasing (in the lower pressure limit); c) In base of the results obtained in these two first stages, find criteria of design for DPF devices improving its performance of nuclear fusion production; d) Finally, arrive to a proposal of a DPF experiment in which the possible extrapolation of the neutron yield scaling law could be clarified. The experimental and theoretical results obtained in this research line are described in this paper. From an accurate measurement of neutron energy spectra, evidences of the coexistence of thermal and non-thermal fusion mechanisms in the plasma focus were obtained. Developing relative simple models, the neutron yield scaling law was explained in terms of a superposition of both fusion mechanisms. Respect to the upper pressure limit, it was found that an insufficiency in the energy available for ionize the swept gas during the roll-off stage, can produce an inefficient pinch compression, with the consequent drop in the neutron yield. The lower pressure limit was explained in terms of the presence of a radiative wave produced by an excess of the plasma energy during the radial compression stage. As a conclusive result, it was shown that both pressure limits can be avoided, and a good matching factor can be obtained applying appropriate criteria of design. On the base of this criteria, a proposal of a DPF experiment with a focus current over 1 MA is presented. The main scope of this experiment would be to clarify the extrapolation feasibility of the neutron scaling law and, in consequence, the DPF chances as alternative scheme into the NF international efforts, or its applications as intense neutron source.

Current Trends in International Fusion Research — Proceedings of the Second Symposium
Edited by E. Panarella. NRC Research Press, National Research Council of Canada, Ottawa, ON K1A 0R6, Canada. 1999.

1. INTRODUCTION

Since the days of the early 60's when N. Fillippov in the USSR [1] and J. Mather in the USA [2] reported on neutrons emitted from D-D nuclear fusion reactions by both types of dense plasma focus (DPF), continuous and successful research work was made with such devices. The plasma focus device consists in a capacitor bank discharging on a coaxial gun electrodes configuration (see Fig. 1). After a run-down phase (with axial and radial steps) the plasma sheath is (in part) focused in a very small zone (plasma focus) on the axis. This concentration of plasma reaches densities of 10^{19} cm^{-3} and temperatures of several keV, remaining confined by 100 – 200 ns. The high performance of DPF in D-D neutron yield in terms of electrical energy inverted by nuclear fusion (NF) reaction, is so high that was not overcome by other NF devices. Its simplicity and this high NF performance was the main attractive facts for the DPF research, but also, the results obtained with DPF in the last 25 years of researches, demonstrated its applications in other very important fields. In one of the most complete reviews [3], H. Conrads gives an entire panorama on multiple technological applications of this devices, specially talking on the German activities. The main scope of the present work is to talk about a research line oriented to obtain design criteria for DPF optimization as NF reactor, in which our team had an active participation.

2. THE EARLY PROPOSALS OF NEUTRON YIELD SCALING LAWS AND ITS LIMITS

In the German laboratory of Darmstadt was presented the first scaling law of the average of fusion neutrons yield Y with the energy E stored in the capacitors: $Y \propto E^2$ [4]. In Limeil (France), Bernard founds the correlation between Y and the focus current I, based only in a few French DPF and Z-pinch experiments : $Y \propto I^{3.3}$ [5]. Just at the same time, the Plasma Physics Laboratory of Buenos Aires University, presented a scaling law of the type : $Y \propto W^2$, where W is the electromechanical work exerted on the plasma for its heating and acceleration [6]. Not much later, the scaling law: $Y \propto I^4$, was presented by Buenos Aires Lab. [7,8], and this is the most generally accepted up to the present. A big DPF experiment starts in 1974 at Frascati into the EURATOM program, under direction of Ch. Maisonnier [9]. The 1 MJ DPF

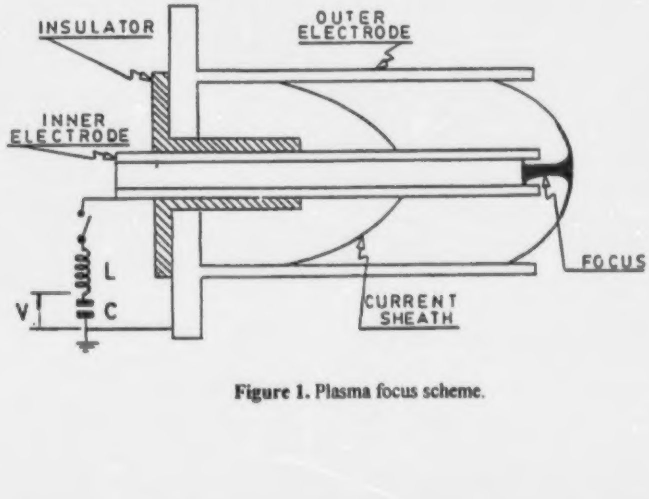

Figure 1. Plasma focus scheme.

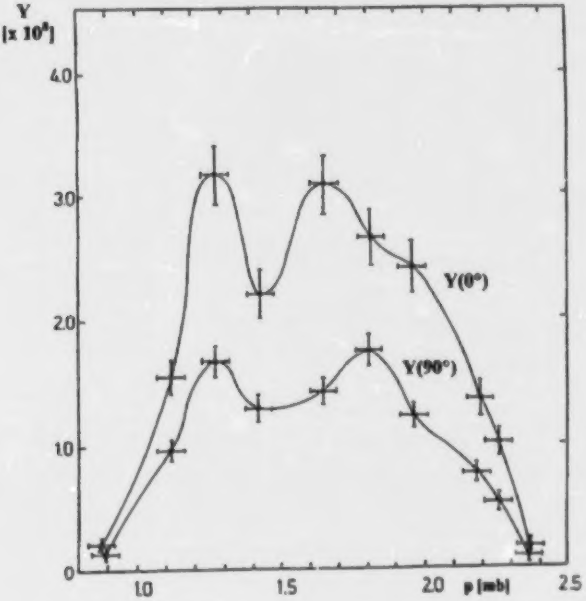

Figure 2. Neutron yield Y vs filling pressure p in PACO device. The upper curve corresponds to a detector located in the axial direction. The lower one to a detector at 90° of the axis.

device was designed as an extrapolation of other successful previous experiment, the "Mirapi" device . In the "Mirapi" (100 kJ) a mean neutron yield $Y \sim 10^{10}$ neutrons per shot in pure D_2 discharges was obtained with a focus current I of around 700 kA [10]. Then, a production of $Y \sim 10^{14}$ was expectable for the big device. Instead, the best Y value obtained in the 1 MJ was of around 10^{12} neutrons.

The second large device was the Poseidon which put in operation in the Stuttgart University's Plasma Physics Institute at 1980 [11]. This experiment ($E = 500$ kJ), under the conduction of H. Herold and H. Schmidt, do not reach the expected performance respect to the Y but, as will be commented later, by different type of problems that those of the Frascati 1 MJ.

When Y is measured at different values of D_2 pressure p, there are an upper and lower pressure limit of p in which Y drops event when I do not presents same fast variation whit p. Then, such limits can not be explained in terms of the above mentioned scaling law. As an example of a narrow p range with neutron production, in Fig. 2 it is show Y vs. p reported in [12] for PACO device at Tandil. In the next paragraphs the results obtained in the research of both limits and its consequences on the scaling law interpretation and the Y optimized design of DPF devices are explained.

3. THE *Y* UPPER PRESSURE LIMIT

The first well defined limit for the scale of Y with I was obtained as is described in [13]. In the present paragraph it is transcribed the main parts of that work.

By means of two-dimensional numerical MHD models it is possible to calculate the dynamic evolution of the current sheath (CS) from the coaxial stage up to radial compression.

Generally, the models gives the time evolution of the characteristic discharge variables, such as the current I, the discharge self-inductance L, the gas mass M swept up by CS, etc. To this purpose, the electromechanical work

$$W = \tfrac{1}{2} \int (dL/dt).I^2\, dt$$

exerted by the electromagnetic forces on the CS can be computed ([14] contains some analytic approximation of W in the run-down stage of Mather-type guns). Here W is the sum of the kinetic energy E_k and the internal energy E_i, the latter mainly including thermal and ionization energies. If ohmic heating can be neglected it can be easily demonstrated that:

$$E_i = \tfrac{1}{2} E_k$$

so that the specific internal energy per unit of collected mass: $\varepsilon = E_i/M$, can also be calculated. The function $\varepsilon(t)$ behaves as it is shown in Fig. 3a: first ε increases with t and reaches a relative

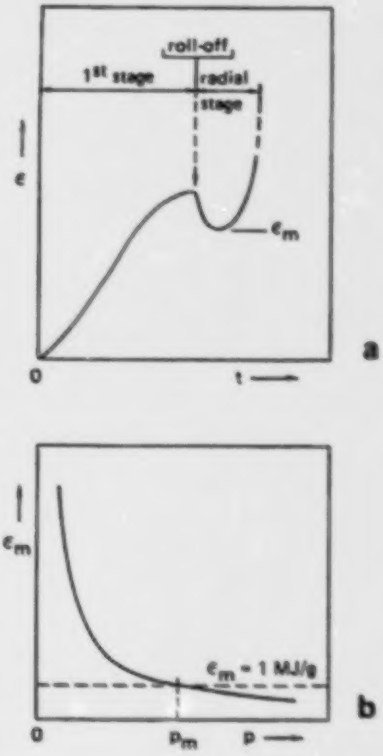

Figure 3. a) Typical sheath energy by unit of swept mass (ε) vs time curve, for a fixed deuterium filling pressure. **b)** Qualitative curve of ε minimum (ε_m) during the radial compression phase of function of deuterium filling pressure.

Table I. Main parameters and values of I_f and ε_m (for $p = p_M$) of experiments in which neutron cut-off appears when I_f (p) is still increasing.

Laboratory and device	C (μF)	V (kV)	L_0 (nH)	R (cm)	ℓ (cm)	I_f (kA)	ε_m ($MJ \cdot g^{-1}$)
Frascati: Mirapi	45	34	30	2.5	23	700	1.00
		32				650	0.95
		30				640	0.85
		28				600	0.80
		26				560	0.75
Frascati: I MJ	1250	20	20	8	56	1415	1.10
		30	20	8	56	2060	1.02
		20	16	18.5	35	1340	0.90
Świerk	21	36	75	2.5	23	447	1.5
Stuttgart: Nessi	225	13	20	3.3	18	600	1.03
		13			26	530	1.08
		16			18	720	0.93
		16			22	670	0.98
		16			26	650	1.01
Stuttgart: Minifocus	60	20	60	2.5	25	430	1.46
Darmstadt	6.7	10	24	0.8	10	104	1.20
		12				120	1.30
		13				133	0.97
		15				149	0.74
		16				159	0.74
		18				181	0.81
		20				202	0.82
Los Alamos	90	16	16	2.5	22	494	1.39
			20			632	1.19
Buenos Aires: PF I	6	17	33	1	10	151	0.92
			43			147	0.91
			51			143	1.00
Limeil	90	18	32	5	18.5	479	1.04
	30	33	53	5		504	1.61
	30	45	53	5		688	1.84
	60	33	27	7.5		828	1.50
	60	40	27	7.5		1011	1.42

maximum at the roll-off time; during the radial compression, ε decreases to a relative minimum ε_m and then increases strongly again during the final stage of the pinch compression. The drop of ε during the radial compression is more pronounced as larger is the inner electrode diameter. The value of ε_m decreases monotonously with the pressure, as can be seen in Fig. 3b.

By using a snow-plow model , it was studied the behavior of several machines which cover a wide range of energies and electrode dimensions. In the standard experiments, is observed that, when the neutron cut-off appears at a value of p_m for which $I(p)$ is increasing with p, ε_i has a value ε_m of about 1 MJ/g (see Table I).This value results significantly close to the specific ionization energy for deuterium. Y as a function of I (when only p is varied) for

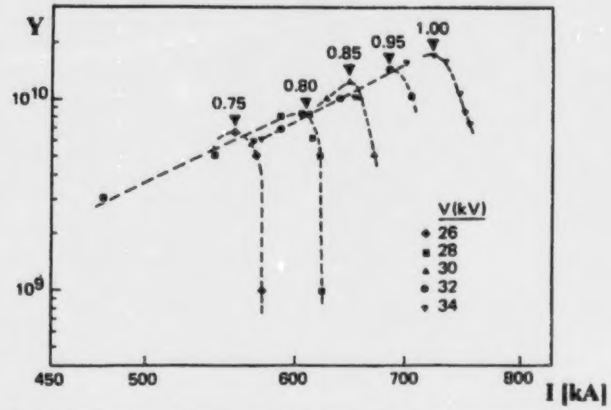

Figure 4. Experimental neutron yield vs focus current for several experiments on Frascati's Mirapi device. The value of ε_m (in MJ/g) corresponding to each curve maximum is indicated.

several important experiments, is shown in Figs. 4 to 6. Note that *Y* drops for values of ε_m very close to 1 MJ/g.

Due to its relevance, here it is considered in particular the Frascati 1 MJ case. In Fig. 7, it is shown I and ε_m as a function of p in three experiments with different gun geometries and electrical parameters. The point for which *Y* starts to decrees is indicated in each experiment. As it can be seen *Y* drops - even with I increasing - just at the pressure in which the curve ε_m (p) crosses the 1 MJ/g line.

For values of p under p_m , the scaling law $Y \propto I^4$ is fulfilled in all the studied cases. An example in which this limit was avoided through an adequate design, is the SPEED *I* device

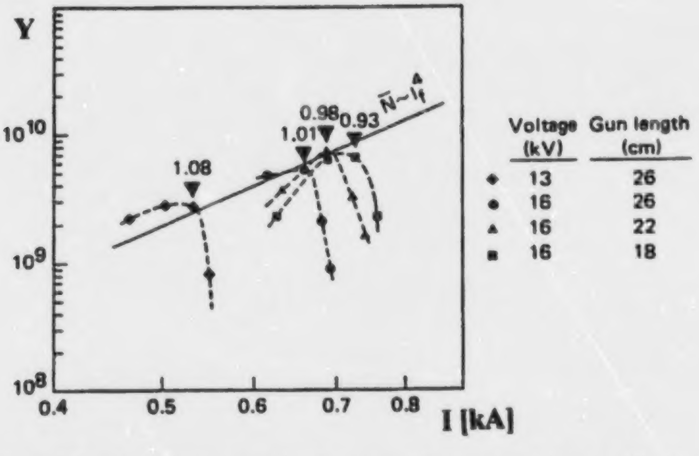

Figure 5. Experimental neutron yield vs focus current for several experiments on Nessi's Stuttgart device. The value of ε_m (in MJ/g) corresponding to eaach curve maximum is indicated.

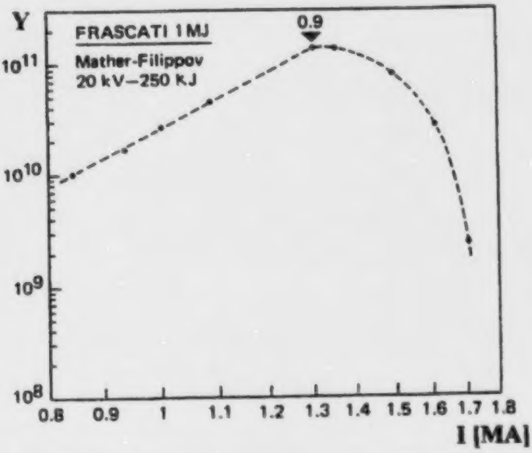

Figure 6. Experimental neutron yield versus focus current for Mather-Flippov geometry in Frascati's 1 MJ plasma focus. The value of ε_m (in MJ/g) corresponding to each curve maximum is indicated.

at Düsseldorf. In Fig. 8, the measured in SPEED *I* of *Y* versus *p* are presented, together with *I*(*p*) and ε_m (*p*) and, as it can be seen, the maxima of *Y* and *I* are in coincidence according with the scaling law. In this last case must be mentioned that the optimized geometry, calculated

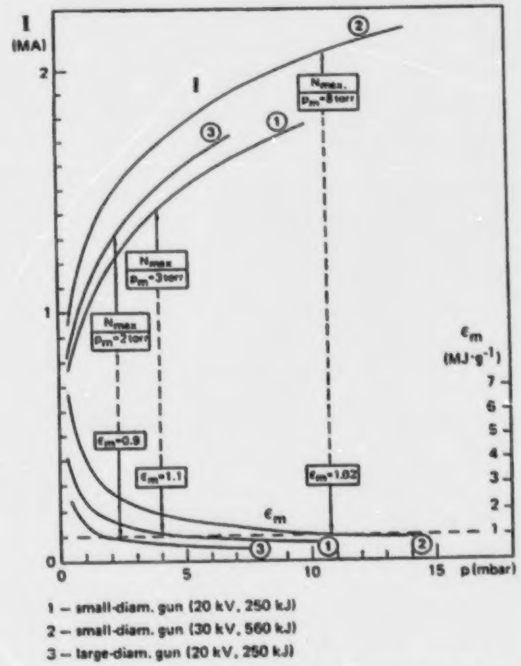

Figure 7. Computed current and ε_m as function of p for three groups of electrical and geometrical parameters of Frascati's 1 MJ. Measure p corresponding to the Y cut-off in each experiment is indicated.

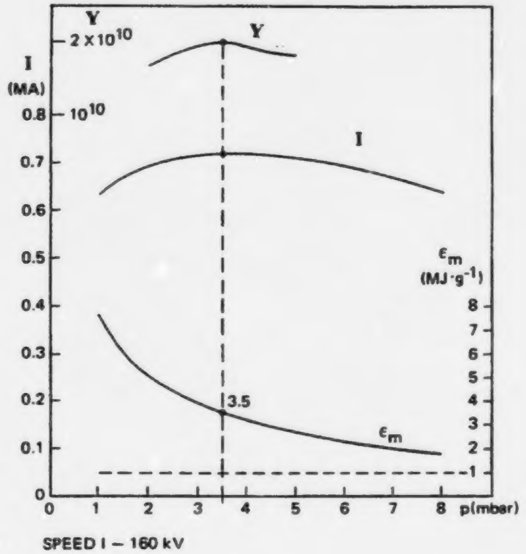

Figure 8. Computed focus current and ε_m in the SPEED 1 device at Düsseldorf. The upper curve shows the experimental values of the neutron yield as function of p.

through the MHD model (searching a maximum value of *I* with $\varepsilon_m > \varepsilon_i$) was confirmed with the experimental optimization.

4. HYPOTHESIS ON THE UPPER PRESSURE LIMIT ORIGIN

The fact that ε_i is approximately equal to the specific ionization energy of deuterium suggests that the neutron cut-off is connected with the ionization process in the shock wave during the radial compression. One hypothesis aiming at an explanation of the upper pressure limit is the following: if the energy which the shock wave can transfer to the collected neutral gas is not sufficient to ionize it completely, the plasma becomes transparent to the magnetic field, and the 'magnetic piston' loses its efficiency just in the most critical phase. If the high ion temperature in the focus is mainly due to randomization of the kinetic energy acquired by the ions during the radial acceleration [15], such a reduction in piston efficiency can strongly diminish the NF reactions rate. If, instead the ion heating is mainly connected with turbulent processes [9], the effect may be explained in terms of the spatial current distribution.

During the first moment of the discharge (when ε_m increases from zero), ε_m is still smaller than ε_i , but in general this insufficiency of ε_m affect the shock wave only during the axial propagation, and ε_m reaches values higher than ε_i before the radial stage start. However, if ε_m remains very small during the initial phases, a significant portion of neutral gas could remain in the insulator region, producing the frequently observed second breakdown on the insulator during the maximal pinch compression.

In a recent work [16], through series of image converter (IC) pictures performed in Tandil PACO device, it is shown that the CS presents a structure of filaments at all the time in which $\varepsilon_m<\varepsilon_i$. So that, from the beginning of the discharge, when de CS starts to move from the insulator surface, the CS presents a clear filamentation and this 'disappears' (at least it takes a such fine structure that the filaments cannot be observed with the IC device) when ε_m reaches the ε_i value (see Fig. 9). Into the neutron production pressure range (p =1.5 mb), this change of the CS structure is produced before the roll-off, and the focus presents the aspect shown in Fig. 9a). Instead, for $p>p_m$ (p = 2.1 mb), ε_m remains lower than ε_i after the roll-off, and the CS filamentation remains up to the focus, and has the aspect shown in Fig. 9b).

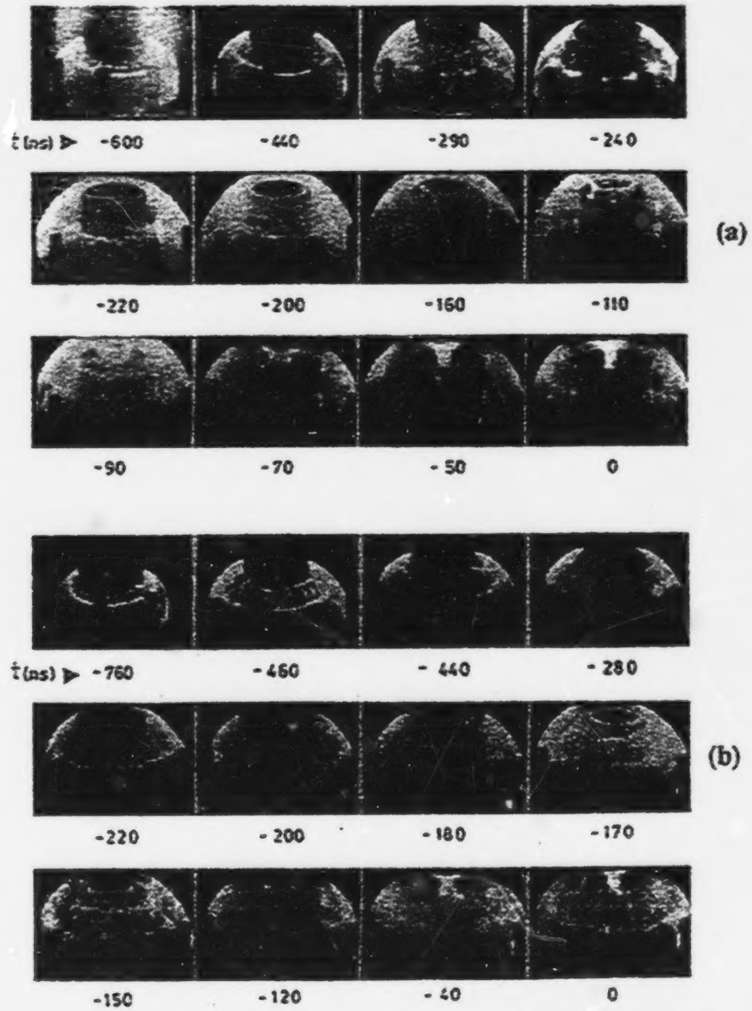

Figure 9. Sequence of plasma sheath image converter pictures in PACO device. a) for p = 1.5 mb (best neutron production); b) for p = 2.1 mb (high pressure Y cut-off)

5. EVIDENCES AND HYPOTHESIS ON THE *Y* LOWER PRESSURE LIMIT

As above mentioned, there is also a lower *p* limit under which *Y* drops even when I remains still in a high value. This effect was observed clearly in PACO device where the neutrons drop for *p* lower than 1 mb, approximately. The first hints about the reasons of this *p* lower limit for *Y* were obtained at 1987-88 (see [12] and [17]). In these works it is experimentally measured the velocity of the CS light front (by use of fast photodiodes) simultaneously with *Y* measurements. The main results was that, for $p \leq 1$ mb, a correlation of *Y* cut-off with an increment of CS light front velocity - during the radial compression phase is clearly observed.

In a more recent work [18], through a large series of IC pictures taken in the lateral and frontal gun direction during the radial compression stage, it was obtained, respectively, the time evolution of the external radius r_e and the internal radius r_i of the plasma sheath. The experimental functions r_e (*t*) and r_i *t*) reported in [18] are shown in Fig. 10. The analysis of these functions are as follows: At a *p* value into the range of neutron production (fig. 10 a), the r_e and r_i move in similar way, and both r_e (*t*) and r_i (*t*) functions fulfill a typical selfsimilar equation : $r \sim t^n$, with $n = 0.8$ (see Fig. 11a), which corresponds [19] to a strong shock wave with $\gamma = 5/3$ (just the ideal gas γ value). At the pressure around 1 mb (Fig. 10 b), the r_e moves in the same way, but the r_i has a different behavior The radius r_i (*t*) also follows a selfsimilar

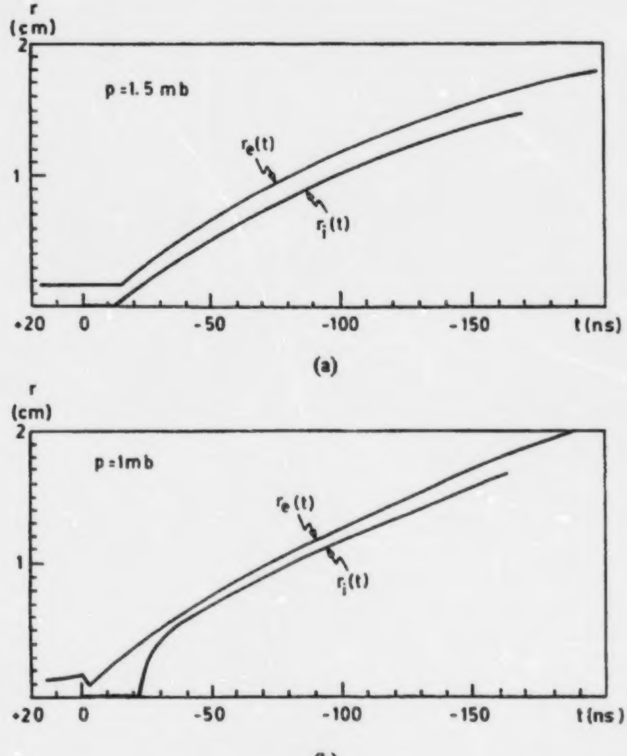

(a)

(b)

Figure 10. a) Superposition of re(t) and ri(t) mean curves for p = 1.5 mb. b) Idem for p = 1 mb.

equation, but with $n = 0.5$ (see Fig. 11b). So that, a sudden acceleration of r_i respect to r_e is observed in the last instants of the radial compression stage. The value and $n = 0.5$ does not correspond to a γ finite value for a material wave, and this suggest the following picture for the phenomenon:

At lower pressure, ε_m can reaches values very larger than ε_i , and the plasma sheath temperature becomes very high; in this conditions a temperature or radiation wave advances on the neutral gas (as a precursor) and preheating the focus zone before the maximal compression. Such preheating inhibits a good plasma compression, with a corresponding *Y* decreasing (the same type of phenomenon is well known in laser fusion),.

In the opinion of this author, the above described effect could be the main reason for the low performance of Poseidon device in Stuttgart (see paragraph 2).

6. THE *Y* VS. *I* SCALING LAW TAKING INTO ACCOUNT THE *Y* PRESSURE LIMITS

A first review of *Y* vs. *I* scaling law taking into account both pressure limits for *Y*, was made in [20]. Experimental values of *Y* are usually reported in the literature, not so the corresponding values of I . Anyway, using the same two-dimensional MHD model mentioned

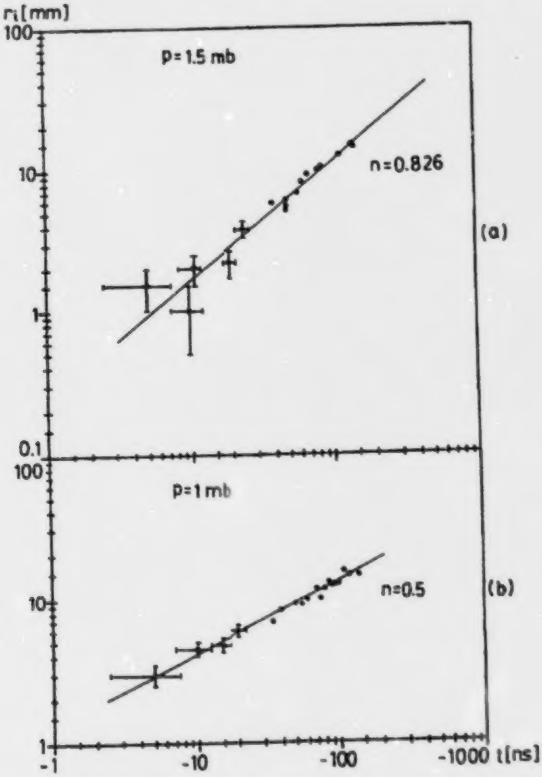

Figure 11. Logarithmic graph of $r_i(t)$: a) for p = 1.5 mb; b) for p = 1 mb.

in paragraph 3, it is possible to calculate I values with an accuracy better than 10%. Besides, the same model allows to check if the experiment is affected (or not) by the pressure limits. This methodology was used in the elaboration of a new study on the empirical correlation between Y and I . In Fig. 12, the logarithmic graph of Y vs. I values of 117 experiments (performed in 14 devices) not affected by the pressure limits, is shown. The points are positioned along the straight line $Y \sim I^{1.7}$ with a correlation coefficient better than 0.9. On the other hand, if they are selected only those points corresponding to "small" machines (about 1 kJ of bank energy), the slope of the "best-fit" straight line is significantly higher. It must be pointed out that, in the considered experiment, E ranges from 1 to 650 kJ, V from 17 to 160 kV and geometrical cross-section length ratio of the inner electrode ($\pi.r^2/z$) goes from 0.2 up to 31 cm. A remarkable fact is that the dependence of Y on I seems to be valid for experiments in which evidences of non-thermal effects have been reported, and also for experiments in which this evidences are weak or absent. On this point deals the following paragraph.

7. POSSIBLE ROLE OF THERMAL AND NON-THERMAL MECHANISMS IN THE NEUTRON YIELD AND THE *Y* vs. *I* SCALING LAW

The main mechanism responsible of the D-D nuclear reactions in the focus are not totally clarified up to date but, from the measurements of the energy neutron spectra in the 1 MJ Frascati device [21], was established that both thermal and non-thermal mechanisms take part in the nuclear reactions in a similar way. In this paragraph, the analysis of the possible incidence of each mechanism in the scaling law of Y with I, given in [20], is summarized.

From experimental measurements of deuteron and electrons beams generated in the focus, it can be assumed that deuteron beams with energy between 50 to 300 keV (in the case of the highest population of energetic ions), in currents of about 1% of I and duration of some nanoseconds, are crossing a bulk of thermal plasma with a density of the order of 10^{19} cm^{-3}. Under the beam-target hypothesis (for a monoenergetic ion beam), taking into account the classical formula for D-D beam-target reactions, it results:

$$Y\,(\text{beam-target}) \propto I$$

In a quantitative way, taking the typical values of 10 ns and 150 keV for the duration and mean energy of the beam, respectively, it results :

$$Y\,(\text{beam-target}) = 9.3 \times 10^2\, I$$

(with I in A).

This simple analysis gives as a result that this mechanism cannot explain the empirical scaling law but, the above written numerical expression gives, for example, in a small DPF with $I = 100$ kA, a relative high value of $Y \sim 10^8$. In other words, from this analysis it can be interpreted that a beam-target mechanism cannot explain the Y scaling law, but it can produce a relevant part of the neutrons in the small and middle devices into the energy range operated up to date.

Under the hypothesis of a thermal mechanism is possible to obtain a correlation between Y and I if the focus is considered as a quasi-stationary pinch in which the Bennett equation $I \propto NT$ (N: linear density, T: temperature) is fulfilled in average. Assuming the hypothesis of a magnetic confinement in radial direction and inertial confinement in axial direction, and supposing that T reaches the order of 1-2 keV, Y by thermonuclear reactions results:

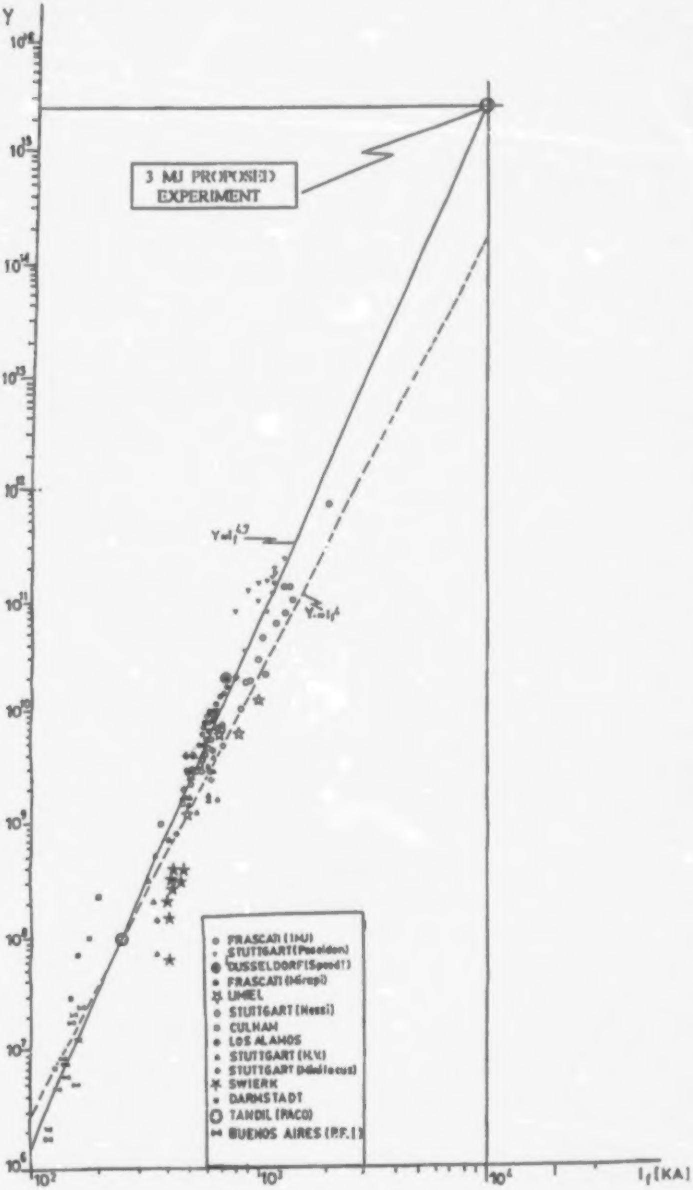

Figure 12. Experimental values of *Y* vs. *I* in different experiments not affected by the pressure limits.

$$Y \propto (n/n_0)\, I^4$$

where n/n_0 is the ratio between the final pinch density n and the density of filling gas n_0. This thermonuclear model has a good fit with the empirical scaling law. Taking $T \geq 2$ keV, $n = 10^{19}$ cm^{-3} and $(n/n_0) = 100$, results:

$$Y \cong 2x10^{10} \,.\, I^4$$

(with I in MA. In Fig. 12 it is shown the straight line corresponding to this equation .

The differences between the main straight line and the line given by the thermal model can be explained by the relative weight of the non-thermal neutron production in the small DPF experiments. With I over 500 kA the law $Y \propto I^4$ is fulfilled very well in the experiments. But the actual extrapolation possibilities of this law should be checked in an experiment where the current value $I \sim 10$ MA could be reached without effects of higher or lower pressure limit. The next two paragraphs deals on the proposal of such experiment.

8. THE ENERGY EFFICIENCY IN AN OPTIMIZED DESIGN

The energy efficiency of the DPF as NF reactor is roughly estimated from the expression:

$$\eta = e_f \,.\, Y / E^2$$

where e_f is the energy of each emitted neutron and E is the energy initially stored in the capacitor bank. From the energy balance in the plasma focus discharge can be easily found the following relation:

$$I^2 = k\, E$$

where k is a constant depending on the design involving the selection of electrical and geometrical parameters as well as the optimum value of p (matching). Assuming the scaling law $Y \propto I^4$, it results:

$$Y \propto k^2 . E^2$$

and then it is:

$$\eta \propto Y/E^2 \Rightarrow k^2 \propto Y/ E^2$$

The global efficiency η depends on the scale factor E, but the ratio Y/ E^2 represents a merit factor of an optimized design independent of the device scale. In a I optimized design, the higher value of k must be reached in order to obtain the higher value of Y/ E^2 and, in such design, it is essential the condition $\varepsilon_m \geq \varepsilon_i$ In the Table II the values of Y/ E^2 for several DFP experiments are shown. As it can be seen, the best values of this merit factor correspond to the SPEED I and PACO, devices, designed according to the condition $\varepsilon_m \geq \varepsilon i$

9. A PROPOSAL OF HIGH SCALE EXPERIMENT: THE R05 DEVICE

As it was seen before, in order to discriminate what of both mechanisms, thermal or non-thermal, is preponderant in the DPF neutron yield and rend possible to extrapolate the scaling law, would be very useful to have an experiment in the scale of 10 MA. From the Table II and equation $I^2 = kE$ it can see that a value of k corresponding to a good matching is $k \sim 30$ MA/MJ. Then, if one plans an experiment with I of the order of 10 MA with a good matching, E must be approximately 3 MJ. Extrapolating the scaling law $Y \sim I^4$, this experiment could produce $Y \sim 2x10^{15}$ D-D neutrons/pulse. It was previously experimentally proved that using 50% D-T mixture, the Y in the DPF increases by a factor 100 [22, 23]. Then, this experiment

Table II. Quality factors for different DPF devices

LABORATORY	DEVICE OR YEAR	Eo (kJ)	Y max	Y/Eo^2 (neutr./J^2)
LOS ALAMOS	1966	38	1×10^{10}	6.9
FRASCATI	MIRAPI	26	1.6×10^{9}	2.4
FRASCATI	1 MJ	562	7×10^{11}	2,2
STUTTGART	MINIFOCUS	12	8×10^{8}	5.5
STUTTGART	H. V.	12	3.8×10^{9}	26
STUTTGART	POSEIDON	280	1.6×10^{11}	2
BUENOS AIRES	P. F. 1	0.86	2×10^{7}	27
LIMEIL	1970	30	6.5×10^{9}	7.2
CULHAM	1968	29	7×10^{9}	8.3
SWIERK	1974	13.6	3.8×10^{8}	2
DUSSELDORF	SPEED 1	19.2	2×10^{10}	54
TANDIL	PACO	1.9	2×10^{8}	55

operated with D-T could produce $Y \sim 10^{17}$ neutrons of 14 MeV per shot, which represents a fusion energy of the order of 200 kJ. In other words, this experiment would be a D-T reactor with an energy efficiency of (as minimum) 5%. This estimated efficiency suggested the name R05 for a such experiment, which was proposed by the first time in [24].

Choosing previously the capacity C, the charging voltage V and parasitic inductance L, it is possible to calculate ε_m and the total current I, in all instant of the discharge, for different geometries of the gun and different values of p, as it is commented in the beginning at this paper. In a first attempt to obtain an I optimized design of a 3 MJ experiment was arrived to the following values for the main parameters:

- Charging voltage $V = 240$ kV
- Capacity $C = 104$ μF
- Parasitic inductance (estimated) $L = 10$ nH
- Deuterium pressure (optimum) $p = 90$ mb
- Total length of the gun $l = 170$ mm
- Length of the insulator $l = 70$ mm
- Diameter of internal electrode $d = 160$ mm
- Diameter of external electrode $d = 400$ mm

In Fig. 13 it is shown the calculated curves $I(t)$ and $\varepsilon_m(t)$ in a discharge at $p = 90$ mb of D_2. The minimum value of ε_m during the radial compression stage results 1.08 MJ/g but, in all this phase, ε_m remains less than 1.25 MJ/g.

In this first design was obtained a value $I = 5.5$ MA which, according with $I^2 = kE$, represents a matching quality $k = 10$. With this design, according with the scaling law, the neutron output of 10^{13} - 10^{14} could be expected with pure deuterium. This represents a minimum efficiency $\eta = 0.5\%$ for D-T mixture.

10. FINAL REMARKS

This first conceptual design may be improved in order to obtain, with the same value of E, a better value of k fulfilling the condition $\varepsilon_m > \varepsilon_i$, and may be possible to reach η (D-T) > 5%.

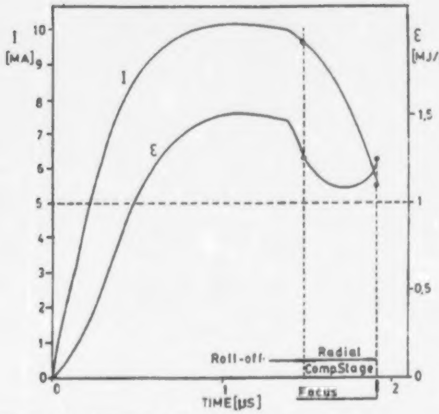

Figure 13. Computed characteristic curves of the proposed experiment R05.

Taking into account that in an hybrid fusion-fission reactor the fusion energy output is multiplied by a factor 20, a goal with the proposed experiment would represent the possibility to reach the break-even with an hybrid system based in a plasma focus device. On the other hand, the possibility to use the DPF as driver of pellet implosions in inertial confinement system at a level of R05 proposal was theoretically demonstrated [25]. Moreover, the relative low cost of this type of device, converts the R05 proposal in a very interesting facility in NF research.

One of the more hard technical problems is to obtain adequate materials for the gun in order to resist currents of the order 10 MA. One of the possible solutions could be to make electrodes detachable in each shot, for example, with liquid lithium dynamically conformed.

Finally, it must be pointed out the very pessimistic assumption for the energy performance η here calculated: it is taken as output energy only the corresponding to the flux of 14 MeV neutrons emitted by D-T reactions. A more fine calculation would give very much promissory results.

REFERENCES

* Researcher of CONICET.

1. N.V. Filippov et al. Nucl. Fusion, suppl. 2, 77 (1962).
2. J.W. Mather. Phys. of Fluids, **8**, 366(1965).
3. H. Conrads. Proc. of III Latin-American workshop in Plasma Phys., Santiago de Chile (1988), Book of Invited Lectures, pp. 27–44.
4. L. Michel, K. Schonbach and H. Fisher. Appl. Phys. Letters, **24**, 57 (1974).
5. A. Bernard. Proc. 3 Top. Conf. on Pulsed High Beta Plasmas, Culham (1975) p. 69.
6. H. Bruzzone, H. Kelly, M. Milanese, J. Pouzo. Nucl. Fus., **16**, 870 (1976).
7. J. Pouzo. The Plasma Focus as alternative Nuclear Fusion Line, Doctoral Thesis, Buenos Aires University, 1979.
8. R. Gratton, C. Ferro Fontan, H. Kelly, J. Pouzo et al. Proc. of Spring College on Plasma Phys., ICTP (Trieste, 1981) p. 274.
9. Ch. Maisonnier. Pulsed Fusion Reactors, Pergamon Press (1974) p. 131.
10. Ch. Maisonnier, C. Gourlan, G. Luzzi, L. Papagno et al. Proc. of Int. Conf. on Plasma Phys. and CNFR (Madison, 1971), IAEA ,**1**, 523(1971).

11. H. Herold and A. Hayd. Proc. of 3 Int. Workshop on Plasma Focus Research, (Stuttgart, 1983) p. 131.
12. J. Pouzo, D. Cortázar, R. Milanese, R. Moroso and R. Piriz, Small Plasma Physics Experiments, World Sci. Publ., London 80, (1988).
13. M. Milanese and J. Pouzo. Nucl. Fus. **25**, 840 (1985).
14. J. Vargas, F. Gratton and J. Gratton, Proc. of Int. Conf. on Plasma Phys. and CNFR (Berchtesgaden, 1976), IAEA, **3**, 483 (1976).
15. Artsimovich. Controlled Thermonuclear Reactions, Oliver & Boyd Pub. (London 1964) p. 129.
16. M.Milanese, R. Moroso and J. Pouzo. IEEE Transactions on Plasma Sc., **21**, 606 (1993).
17. D. Cortázar, M. Milanese, R. Moroso and J. Pouzo. 3rd Latin-American Workshop in Plasma Physics, Santiago de Chile (1988), Book of Contributed Papers, p. 19.
18. M. Milanese, R. Moroso and J. Pouzo. IEEE Transactions on Plasma Sc., **21**, 373 (1993).
19. G. B. Whitham. Linear and Non-linear Waves, Whiley & Sons Pub., 143 (1974).
20. M. Milanese and J. Pouzo. Small Plasma Physics Experiments, World Scientific Publications, London, 66 (1988).
21. M. Milanese and J. Pouzo. Nucl. Fusion **18**, 533(1978).
22. C. Patou, A. Simonnet and J. Watteau. Le Journal du Physique, **29**, 973(1968).
23. J. Mather. Proc. of Int. Conf. on Plasma Phys. and CNFR. (Culham, 1966), IAEA, **1**, 385, (1966).
24. J. Pouzo. Proc. of Energy Independence Conference: Fusion Energy and Plasma Physics (Rio de Janeiro, 1987), World Sc. Publ., London(1988) p. 521.
25. R. Gratton, R. Piriz and J. Pouzo. Nucl. Fus., **26**, 483(1986).

THE INTERNATIONAL CENTER FOR DENSE MAGNETIZED PLASMAS: AN OUTLINE

The ICDMP Steering Committee

Alain Bernard[1], Horacio Bruzzone[2], Peter Choi (Executive Secretary)[3], Hernán Chuaqui[4], Vladimir Gribkov (Secretary)[5], Julio Herrera[6], Katsumi Hirano[7], Karel Kolácek[8], Sing Lee[9], Chengmu Luo[10], Franco Mezzetti[11], Marek Sadowski[12], Helmut Schmidt[13], Kenneth Ware[14], Chiow San Wong[15] and Vasile Zoita[16]

[1]Commisariat à l'Energie Atomique, France
[2]Universidad de Buenos Aires, Argentina
[3]Ecole Politechinique, France
[4]Pontificia Universidad Católica de Chile, Chile
[5]Lebedev Physical Institute, Russia
[6]ICN-Universidad Nacional Autónoma de México, Mexico
[7]Gunma University, Japan
[8]Institute of Plasma Physics, Czech Republic
[9]Nanyang Technical University, Singapore
[10]Tsinghua University, People's Republic of China
[11]Universitá di Ferrara, Italy
[12]Soltan Institute for Nuclear Studies, Poland
[13]Universität Stuttgart, Germany
[14]Defense Nuclear Agency, U.S.A.
[15]University of Malaya, Malaysia
[16]Institute of Technology of Radiation Devices, Rumania

ABSTRACT

The present situation of Plasma Physics research has raised the need of close collaboration between scientists worldwide. Yet the contribution some groups can make, particularly those from developing countries, is severely limited by their lack of human or economic resources. On the other hand, the sharing of technology and scientific knowledge which is able to improve the quality of life can be a significant factor in the progress of humanity. This calls for a joint effort that could be channeled through the creation of an international Center where research and training could be pursued on an open and equal rights basis. The research in such a Center should be aimed at some specific area which may provide challenging problems to be solved, and a training environment in which useful skills can be acquired. Since the dense magnetized plasmas meet these criteria, a proposal has been made

Current Trends in International Fusion Research – Proceedings of the Second Symposium
Edited by E. Panarella. NRC Research Press, National Research Council of Canada, Ottawa, ON K1A OR6, Canada. 1999.

to create the International Center for Dense Magnetized Plasmas, as a Center of excellence, with the first and foremost purpose of studying this subject.

1. INTRODUCTION

The present situation of plasma physics research has raised the need of close collaboration between scientists worldwide. Yet the contribution some groups can make, particularly those from developing countries, is severely limited by their lack of human or economic resources. On the other hand, the sharing of technology and scientific knowledge which is able to improve the quality of life can be a significant factor in the progress of humanity. This calls for a joint effort that could be channeled through the creation of an International Center, where research and training could be pursued on an open and equal rights basis. Its visitors would be given an equal status, in terms of position, contribution of ideas and exchange of knowledge. Scientific collaboration between partners of different backgrounds and cultures on the equal platform provided by such a Center is the best way to respond to the urgent challenge which face the nations of the world. The research in such a Center should be aimed at some specific area which may provide challenging problems to be solved, and a training environment in which useful skills can be acquired. Since the dense magnetized plasmas described below meet this criteria, a proposal is being made on the request of UNESCO to create the International Center for Dense Magnetized Plasmas (ICDMP) as a Center of excellence, with the first and foremost purpose of studying this subject.

This is meant to be a Center on an international scale, that would attract some of the world's best scientists working in the field of dense plasmas produced by large currents. However, it would also be a Center with a mission, which would extend beyond the traditional research institute, as it would cross national boundaries, providing training in the subject. As a clear-cut objective, it should help to bridge the North-South divide. It could also be an important part of the growing solidarity between the technologically advanced countries and those engaged in the process of industrialization, because it would help the latter to develop their own research capacities and participate in the world research effort. Yet, international scientific co-operation cannot simply reduce to one way relations between those countries which provide scientific knowledge and those who benefit from it. It must be done as a scientific joint venture for mutual benefit. This requires that the subject to be studied a the Center is such that the research groups at developing countries can be able to make a contribution in it, with resources they can afford. The Center would be subject to supervision from an international panel of experts that would meet periodically to assess the advancement of projects. It would also advise regarding its life-span, which is proposed to be limited.

As a first phase, a global twinning program has been promoted, where a network of groups working in different countries join efforts to study in various laboratories phenomena of current interest.

2. THE DENSE MAGNETIZED PLASMAS

Matter of extreme energy density in the plasma state is found in a significant fraction of the universe. Such plasmas can be created in the laboratory through a natural concentration of energy in a high current discharge. These high temperature, high density plasmas, commonly referred as Dense Magnetized Plasmas, are copious sources of electromagnetic radiation, as well as high energy ions and electrons. These Dense Magnetized Plasmas are also rich sources of thermonuclear reactions. Thus, they provide a wealth of phenomena that present challenging problems, as well as the opportunity to train scientists in a wide variety of experimental methods and techniques.

The Dense Plasma Focus (DPF) has been selected as the initial Dense Magnetized Plasma load for a primary 1 MJ system of the Center for several reasons. The DPF pulsed power technology is less complicated, operating in the 10-100 kV range of simple conventional capacitor bank designs, than more sophisticated megavolt power conditioning technologies to drive on Ohm type loads to a few Mega-Amperes. For the DPF this is accomplished through an electromagnetic process of converting the stored electrical energy over a time scale of several microseconds. At the final phase of this inductive energy storage (IES) a few Mega-Amps of a cylindrical current sheath collapse radially at a rate of $5x10^7$ cm/sec within a centimeter diameter. The rapid increase in inductance during these few nanoseconds of current pinching are not accompanied by a similar reduction in the inductively locked current. The result is a built-in, constant current inductive generator capable of coupling the Mega-Amps current into a 1 Ohm axial load with high efficiency.

A comparable state of the art pulsed power generator designed to produce a few Mega-Amps at the Mega-Volt level would cost several million $US and would require a high and costly level of sophistication in operation and maintenance, beyond the budget envisioned for the ICDMP. On the other hand, the DPF system would be more economical to maintain and operate, and cost five to ten times less to construct.

On the other hand, the choice of the DPF as a research subject is supported by the fact that it is one of the few in Plasma Physics that has widely spread in developing countries, due in part to its affordability. Thus it guaranties the viability of establishing scientific joint ventures of mutual benefit on equal rights terms.

3. TRAINING AND SCIENTIFIC EXCHANGE PROGRAMS

One of the main goals of global significance of the Center is to provide training to candidates from laboratories of developing nations on pulsed power technology and dense magnetised plasma physics. This includes organising a training programme for a selected number of candidates on a range of basic theory and methods of dense magnetised plasmas based on a specific device, providing hands on experience in the use of modern sophisticated diagnostic equipment. For this purpose the DPF is an excellent device due to its capability to produce extremely hot and dense plasma conditions, despite its relatively simple set up and operation. At the end of the training programme, the trainees would take back to their home institutions a small DPF device which they become fully acquainted, and confident to research with. Once this phase is completed, scheduled visits could be arranged, so that the former trainee can keep up his production and contribution to the field within an established program. Simultaneously, a network of those researchers associated to the Center can be set up. The achievements of the group should be assessed through workshops that would include the participation of best qualified experts in the field. In this way, the Center would be able to accelerate the dissemination of knowledge and transfer of technology. Another important function of the Center is to provide opportunity for PhD students, specially from developing countries, to pursue their research projects on DPF devices.

4. EXTENSION OF BASIC UNDERSTANDING OF THE DPF

At present, the DPF community has reported in the literature a wealth of phenomena, whose evolution often depends on the constructional specifications of each device, as well as their operational parameters. The complexity of the plasma focus phenomenon, combined with its sensitivity to certain operational conditions, makes it almost impossible to compare results originating in different facilities. The progress achieved during the past few years, based on collaborative work between different groups, shows the need of an organized approach to the problem, if a qualitative step in understanding the physics behind the DPF is to be made. The design of a new set of devices, with reference specifications, proposed by a group of well recognized experts in the field, may allow this goal. At the same time, reliable data must be collected by means of the best possible available diagnostics. The generation of an appropriate data base on these reference experiments will stimulate the formulation of better theories upon which they can be tested. The concentration of the best hardware in the proper atmosphere for joint collaboration of experts in the field will allow feasible and efficient conditions for addressing the main issues to be solved, taking advantage of cross-fertilization of experiences and knowledge. This venue may stimulate the synergism of different scientific cultures, nurtured by the continued influx of ideas and experiences from scientists worldwide, and the exposure to new ideas through interaction. Simultaneously, the concentration of efforts and resources would provide high quality conditions for training of inexperienced personnel, as stated in the previous section, who would have access to state of the art equipment and borderline knowledge.

As it stands, the devices required need not go beyond the size and operational parameters of existing ones, but the quality of their design should be improved according to present day technology and knowledge. It is important at this stage, not to leap to a major machine of larger dimensions and operational parameters than those existing, but rather to leap to a better device whose quality will allow better results than those obtained so far, and designed in such a way that comparison with theory can be best accomplished.

A series of DPF devices, covering practically the whole energy and current ranges, as well as operating regimes (fusion plasmas, heavy gas discharge radiation and high repetition rate), will be designed and built. The main DPF facility will be built using advanced design concepts and techniques, such as new materials (sintered ceramics, alloys) and technologies, new techniques (CAD and optimization techniques), and new simulation codes. It should be a system that integrates in a compatible way the new advanced diagnostics. This machine should represent a genuine synthesis of collective knowledge realized by designing it, using in an unbiased way, the new concepts obtained from recent research results around the world. Such a device will respond to the strongly felt need for a qualitative step beyond the presently available hardware.

As a distinctive goal, this device will also operate as a reference facility to be used for standardization and calibration of measurement techniques, as well as normalization of operating parameters.

5. APPLICATIONS AND TECHNOLOGY TRANSFER

There is a large number of possible technological applications for the DPF at different stages of development. These rely on some salient features of this kind of device, such as its strong X-ray, ion, electron or neutron emissions, or its large changes of impedance. Amongst the most interesting ones we could mention ion beam implantation, gas laser pumping, pulsed ion and electron beam sources, pulsed neutron sources for biological and materials research and analysis, X-ray lithography and microscopy, and fast opening switches. In many cases, the DPF is seen as an alternative to other technologies, what is lacking is the possible development into an everyday working application. At this stage of development of possible applications, countries with large differences in technological capabilities are on a very similar footing. It is apparent that the Center as envisaged would provide an ideal environment to advance the state of development to achieve practical devices.

Apart from the development of new technology, there is a wide array of well proven technological developments which would be used in the Center on different experiments. High voltage technology, pulsed power as well as a vast array of diagnostics, such as X-ray detection, laser interferometry and other optical techniques, electrical and magnetic measurements. All these aspects would be used by scientists and trainees, resulting in a very efficient way of transfer of know how from advanced to developing countries.

Although only a quick reference to DPF applications has been made here, it is important to point out that other small plasma physics devices made available for research at the Center have a great potential for application. As an example, one could mention the use of pulsed power technology to produce short lived plasmas for high intensity UV radiation. Such sources can be used for food sterilisation, and would be of special significance for developing countries, where food conservation is an outstanding problem.

6. THE GLOBAL TWINNING PROGRAM AND THE ICDMP

As mentioned in the introduction, a global twinning programme has been promoted as a first phase for the establishment of the Center. This has promoted close collaboration among the existing research groups in the field of DPF, and hold its own value. However, this approach cannot represent an alternative to the proposed Center, since it would only allow partial support to the solidarity between technologically advanced countries and those engaged in a development and industrialization process. Under these circumstances a real global consciousness would not be achieved because of the everlasting unbalance between resources and possibilities.

In practical terms, the development of joint experiments and the interaction of scientists from several countries for long periods of time would be more efficient within an established site, than in the context of global twinning. The running cost of a Center would be far lower than the one of a global twinning program.

It should also be noted that one of the main features of the proposed Center is the guarantee equal rights of all partners to access to scientific and technological knowledge, as a prerequisite for full scientific interaction. This would be difficult, and probably impossible in a global twinning scheme under the present world circumstances.

7. CONCLUSIONS

Motivated on the fact that dense magnetized plasmas offer an appropriate ground for collaborative effort between developed and developing countries, a Center of excellence is being proposed on the request of the UNESCO along this line of research. Its three pillars would be: i) fundamental research on dense magnetized plasmas, ii) education and training, and iii) development of technology applications and transfer. The kind of device which has been chosen to establish this Center is the Plasma Focus, because its pulsed power technology is less complicated, operating in the 10–100 kV range of simple conventional capacitor bank designs, than more sophisticated MV power conditioning technologies to drive 1 Ohm type loads to a few MA. On the other hand, a Plasma Focus is more economical to maintain and operate, allowing a larger number of shots per year than other devices. In addition, several countries have developed a good working knowledge of Plasma Focus, in part, thanks to its affordability.

What is planned for the new Center is to have experimental facilities that will act as reference standards to which the results obtained in various co-operating laboratories will be compared in the frame of the visiting scientists program. This would allow a unique database available to all, which may help to formulate better theories, and compare them with experiments. Not least important is the development of modern diagnostic techniques and have a proper calibration of them, using recent technology which a has already been applied in other areas of plasma research. Standards would be set in the general operation of experiments, as well as everyone of the diagnostics methods. The philosophy is that, facing the challenge of complex physics, one has to resort to modes of collections of data which encompass more measurements with greater accuracy.

This work can stimulate training in a wide array of well proven technologies used at the Center, resulting in an efficient transfer of know how from advanced to developing countries. Namely, high voltage technology, pulsed power, x-ray detection, electric and magnetic measurements, neutron and charged particle investigation methods, and laser interferometry and other optical techniques.

The salient features of the Plasma Focus, such as its strong x-ray, ion, electron and neutron emissions, as well as its large changes of impedance, make it a feasible candidate for a number of applications in which training would be most valuable. A few outstanding ones would be ion beam implantation, gas laser pumping, pulsed ion and electron beam sources, pulsed neutron sources for biological and materials research and analysis, x-ray lithography and microscopy, and fast opening switches.

The statements expressed in this outline are those of the Steering Committee, and not necessarily of the above mentioned institutions.

HELIOTRON RESEARCH AT KYOTO UNIVERSITY

T. Obiki, S. Besshou[1], K. Hanatani, K. Kondo[1], T. Mizuuchi, K. Nagasaki,
Y. Nakamura[1], M. Nakasuga[1], H. Okada, F. Sano and M. Wakatani[1]

Institute of Advanced Energy
Kyoto University
Gokasho, Uji, Kyoto 611, Japan
[1] A Graduate School of Energy Science
Kyoto University
Gokasho, Uji, Kyoto 611, Japan

ABSTRACT

Heliotron magnetic confinement system is attractive for fusion reactor, because no ohmic current is necessary and the magnetic configuration has an inherent divertor structure without divertor coils. Plasma Physics Laboratory of Kyoto University has been conducting the heliotron research over thirty years. Experimental studies on Heliotron-E is briefly reviewed, and future prospect of heliotron system is also discussed.

1. INTRODUCTION

The Plasma Physics Laboratory of Kyoto University has been conducting plasma research over thirty years in order to carry out the experimental and theoretical studies on the plasma confinement, stability and transport in helical heliotron magnetic configuration. We have designed and manufactured Heliotron devices, that is, Heliotron A, B, C, D, DM, DR and E. Heliotron-E, one of the largest helical devices in the world has started the plasma experiment since 1980 and obtained many fruitful experimental results. A large number of experimental and theoretical reports for Heliotron-E has been published so far. A historical overview is seen in Ref.[1], and recent experimental results are reported in Ref.[2]. The successful demonstration of stable confinement of high density and high temperature currentless plasmas in Heliotron-E encouraged the same type of experiments in other helical devices such as ATF, W7-AS and CHS. Now, the helical system is recognized as a promising magnetic confinement scheme for fusion reactor.

Heliotron-E was constructed for the following principal purposes,

1. to demonstrate proof-of-principle experiment for steady-state fusion reactor and obtain plasma performance comparable to tokamaks
2. to establish scaling law of the plasma confinement in helical system

Current Trends in International Fusion Research – Proceedings of the Second Symposium
Edited by E. Panarella. NRC Research Press, National Research Council of Canada, Ottawa, ON K1A OR6, Canada. 1999.

Main research objectives are:

1. analysis of helical heliotron magnetic configurations;
2. confinement of high temperature and high density plasmas without ohmic current;
3. development of heating schemes and study of heating mechanism;
4. divertor research for helium ash exhaust and heat removal;
5. confinement study of high energy particles.

Several kinds of heating schemes have been applied in Heliotron-E to produce and heat currentless plasmas, such as electron cyclotron heating (ECH), neutral beam injection (NBI) and ion cyclotron heating (ICH). Since no ohmic plasma current is necessary, the helical system has a potential for steady state operation using superconducting coils without dangerous current driven disruption. Since the magnetic surface, produced by external helical coils, has an inherent separatrix, the divertor configuration can be obtained without any additional coils. We have obtained high density, high electron and ion temperatures, high energy confinement and high β plasmas in Heliotron-E. The highest plasma parameters are listed up in Table 1. Plasma parameters of T_e and $T_i \geq 1$keV, $\bar{n}_e \geq 10^{20}$m^{-3}, $<\beta>=2\%$ were achieved. Based on the Heliotron-E experimental results, the Large Helical Device (LHD) has been designed as the first helical device with superconducting coils and is now under construction at National Institute for Fusion Science.

In this paper, we will briefly review the Heliotron-E experimental results and discuss the future prospect of heliotron fusion system. The hardware of Heliotron-E device and related developed technology are described in Sec.2. Confinement study of currentless plasma and improvement of plasma confinement are shown in Sec.3 and 4. Collaboration works, especially, scaling study is shown in Sec. 5. Future prospect in Kyoto University related to fusion study is discussed in Sec. 6. Conclusion can be found in Sec.7

2. HELIOTRON-E DEVICE

Heliotron-E is one of heliotron/torsatron configurations, which is characterized by large aspect ratio, R/a~11, large rotational transform, $\iota(0)=0.5$ and $\iota(a)=2.5$ and large magnetic shear, $\Theta=(a^2/R)(d\,\iota/dr)|_{r=a}=0.5$. The major and minor radii are 2.2m and 0.2m, respectively, and the plasma volume is about 1.7m^3. The maximum strength of central magnetic field is 2.0T. The closed magnetic surfaces are formed by external coils such as helical coil and vertical coils. The characteristic parameters of magnetic surfaces such as plasma volume, magnetic axis position, rotational transform, magnetic shear and magnetic well depth can be controlled by the auxiliary vertical and toroidal coils.

The fluorescence method and the two dimensional beam impedance method, which are

Table I

plasma parameters	maximum values	heating schemes
n_e	1.8×10^{20} m^{-3}	NBI+pellet
T_e	3.1 keV	ECH
T_i	1.2 keV 1.6 keV	NBI ICH
$n_e\,\tau_E$	3.0×10^{18} m^{-3}s	NBI
<b>	2 %	NBI

developed in our laboratory, visualized the magnetic field structure. The last closed magnetic surface is surrounded by an intrinsic ergodic region. This region is expected to function as a divertor layer without any additional coil system. The peripheral field structure including 'built-in' divertor configuration is also confirmed experimentally.

Development of plasma heating technology and plasma diagnostic has also been made as well as plasma experiments, including the mode conversion and transmission system for ECH, TV Thomson scattering system , heavy neutral beam probe and pellet injector. The transmission components for ECH power have been developed and utilized for the plasma heating in Heliotron-E. The improved Vlasov converter has a high efficient mode conversion from the whispering gallery mode to the Gaussian beam which is favorable for the high power long transmission. This type of converter is now installed in the 84GHz CW gyrotron for LHD. The pellet injector was developed for plasma density control and diagnostics. The solid hydrogen pellet is accelerated by a two-stage gas gun method. The bare pellet had a world record velocity of v=3.2km/sec. This is due to the successful development of wide-caliber fast high-pressure valve and the optimization of piston.

3. CONFINEMENT OF CURRENTLESS PLASMAS

Currentless plasmas are successfully produced and heated by ECH using gyrotrons of 28GHz, 35GHz, 53GHz and 106GHz frequencies for fundamental and second harmonic resonance. It was demonstrated that the electron confinement is improved with decreasing the plasma current. With the higher frequency, the target plasmas with higher electron density and higher electron temperature are available. The radiation loss is small for ECH plasmas, and there is no strong impurity accumulation, so that it is easy to keep the quasi-steady state plasma. These experiments indicate a potential of steady-state operation without dangerous current driven disruption. In the 106GHz second harmonic ECH experiment, the accessible density expands to $7.0\times10^{19}\mathrm{m}^{-3}$ (T_e=0.5keV) and the highest electron temperature T_e=3.1keV (n_e=$0.5\times10^{19}\mathrm{m}^{-3}$) is obtained. The ion temperature does not increase with the increase of the electron density in contrast to the collisional coupling even at the medium density. Otherwise, it increases at the low density regime ($n_e \leq 1\times10^{19}\mathrm{m}^{-3}$), possibly related to the transport improvement by the positive electric field. In W7-A and W7-AS low shear machines, a drastic confinement degradation was observed when the rotational transform coincides with the low-order rational number, while such a degradation did not happen in Heliotron-E with high magnetic shear.

NBI is an effective heating scheme for obtaining high density or high temperature plasmas. The neutral beams with perpendicular and tangential injection angles are injected into ECH target plasmas to obtain currentless plasmas in a wide range of density and temperature. The collisionless plasma with high ion and electron temperature can be sustained by NBI heating. Figure 1 shows the dependence of ion temperature measured with neutral particle analyzer on the NBI power[3]. The ion temperature of NBI plasmas is scaled as

$$T_i(0)(\mathrm{keV})=0.2P_{abs}(\mathrm{MW})/n_e(10^{20}\mathrm{m}^{-3})$$

for a wide range of NBI conditions including co- or counter-injection and perpendicular injection, where P_{abs} is absorbed power. The heating efficiency is almost the same for both perpendicular and tangential injection. This seems consistent with the heating efficiency calculation using orbit following Monte Carlo code. The ion and electron temperatures of

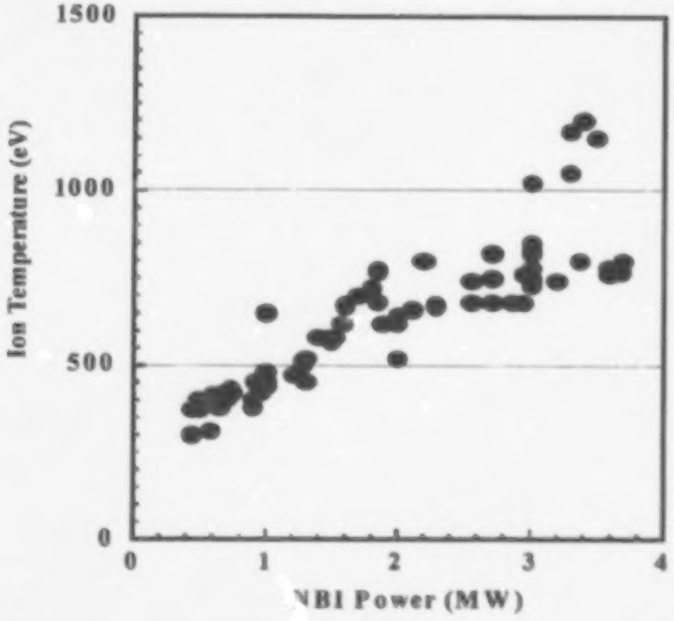

Figure 1. Dependence of ion tgemperature on NBI power.

$T_i(0)=1.2$keV, $T_e(0)=0.7$keV are achieved at the medium density, $n_e=2.5\times10^{19}m^{-3}$. We should note that all the highest parameters were attained under the condition without ohmic current. The highest density, $n_e\leq1.8\times10^{20}m^{-3}$, is stably attained in NBI plasmas for 60msec, which is limited by the power supply, with additional gas puffing and further pellet injection. The dominant energy loss channel in NBI plasmas is anomalous electron transport, which increases with the increase of NBI power. The ion thermal transport coefficient is consistent with a neoclassical value within a factor of three. The electron thermal transport coefficient scales as the gyro-reduced Bohm scaling law. The mechanisms of radial transport and density limit are still under investigation, but the density is not severely restricted like tokamaks (no clear density limit has been observed).

Ion cyclotron frequency range wave heats both ions and electrons. Three kind of RF heating are applied to the ECH target plasma, (a) fast wave heating using minority hydrogen ions at the medium density deuterium plasma, (b) second harmonic wave and ion Bernstein wave heating at the low density deuterium plasma and (c) slow wave heating at the low density level of hydrogen plasma. The RF frequencies are 26.7MHz and 28.2MHz corresponding to the proton cyclotron frequency at 1.75T and 1.85T, respectively. ^{3}He minority heating using 17.8MHz RF is also available. The plasma can be sustained only by ICH without ECH. In case of fast wave heating (H minority), a high energy tail of minority proton is clearly seen up to 100keV as shown Fig.2[4]. The deuteron bulk ion temperature is also confirmed to increase. With a slow wave heating of 400kW at the fundamental proton frequency, the ion temperature is increased from 0.3keV to 1.6keV at $n_e=0.6\times10^{19}m^{-3}$.

The electron collisionality regime ranges widely from the collisional regime through the

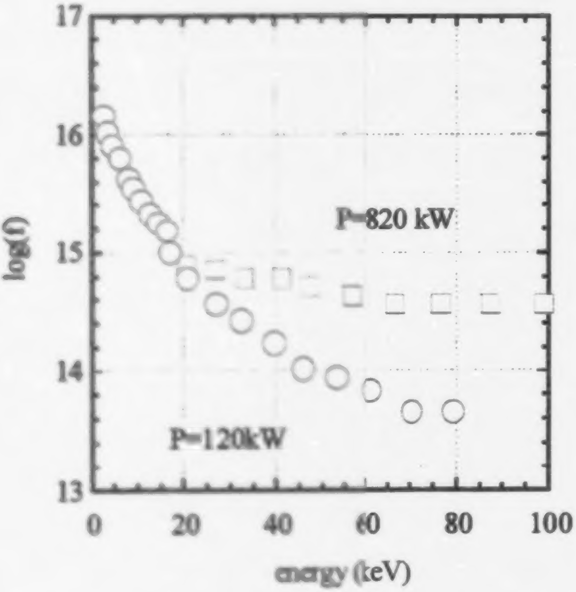

Figure 2. Ion energy distribution perpendicular totoroidal magnetic field in ICH plasma.

plateau regime to the collisionless regime by scanningthe density and heating power. Figure 3 shows the electron collisionality at half radius for ECH, NBI and ICH plasmas[5]. The low collisional regime up to the collisionality, $\nu^{**}\sim10^{-2}$, normalized by the bounce frequency of helically trapped particles are experimentally investigated. According to one dimensional transport calculation code, the electron thermal transport coefficient is close to the one

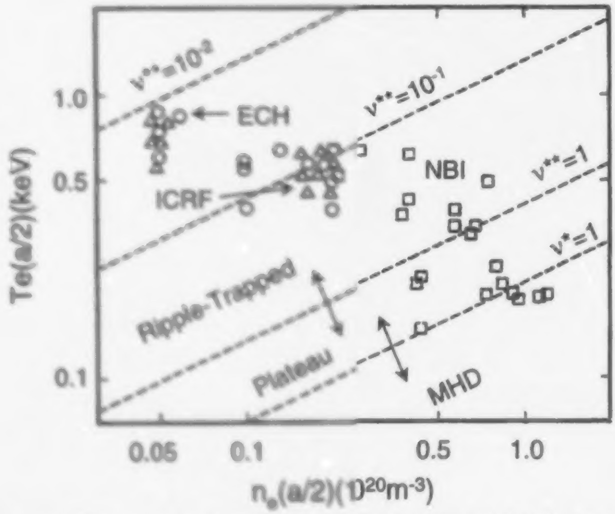

Figure 3. Electron collisionality at half radius for ECH, NBI, and ICH plasma.

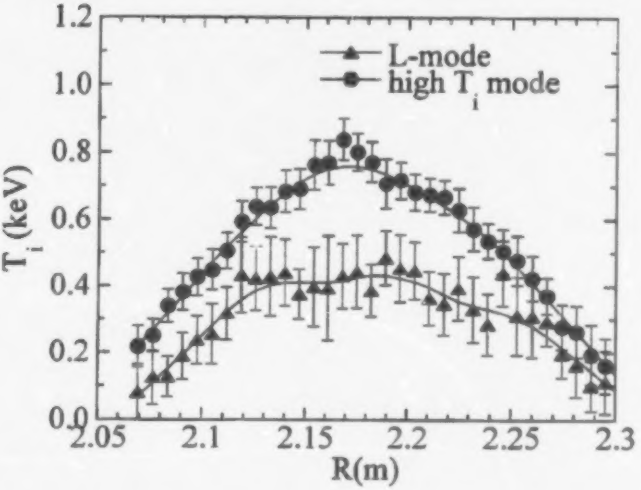

Figure 4. Ion temperature profiles in high Ti and L-modes.

predicted from the neoclassical theory in the plateau regime including the ripple diffusion.

4. IMPROVEMENT OF PLASMA CONFINEMENT

Peaked electron temperature profile is realized in the 106GHz second harmonic ECH, using a focused Gaussian beam with linear polarization. The 1/*e* beam power radius at the magnetic axis is less than 2cm, which is much smaller than the plasma radius. The highest electron temperature, $T_e(0)=3.1$keV, is obtained at the low density, $n_e=0.5\times10^{19}m^{-3}$. Compared with the 53 GHz fundamental ECH, the electron temperature profile is more peaked and the energy confinement is improved. This may be associated with the localized power absorption profile.

The improvement of ion confinement, "high T_i mode" is observed in collisionless (low density) NBI plasmas. Figure 4 shows ion temperature profiles at both high T_i and L-modes[6]. The high T_i mode is characterized by a peaked n_e and T_i profiles with a reduction of the ion thermal diffusivity. The ion thermal conductivity at the core region is improved by one order of magnitude. The improvement of ion transport can be explained by the radial electric field shear due to large density gradient (density peaking). The Er shear may be more important than the bulk plasma velocity shear in reducing the turbulence and improving ion transport.

The magnetic axis position can be shifted by additional vertical field. When the magnetic axis was shifted inwardly, then the plasma confinement was found to be improved. The inward shift localizes the helical field ripple at the inner side of the torus and improves the confinement of ripple trapped particles in the velocity space. The improvement in energetic trapped particle confinement leads to the improvement in the bulk plasma. Additional toroidal field also affects the energy and particle confinement as shown in Fig.5 [7]. The maximum plasma energy is obtained when the toroidal field is superposed so as to increase the plasma radius (decrease the rotational transform). The energy confinement time is improved by 50% more than that without the toroidal field. In addition to the confinement improvement, the MHD stabilization effect is also observed. The pressure-driven interchange modes with m/n=2/1 and 1/1 are suppressed.

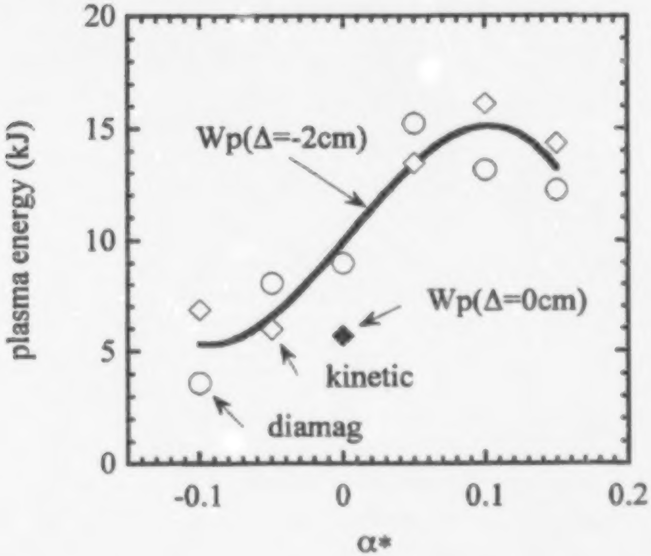

Figure 5. Dependence of plasma energy on additional toroidal field.

Reduction of impurity influx and control of hydrogen recycling are important issues for plasma confinement. Several wall conditioning schemes have been performed, titanium gettering, carbonization and boronization. In the early phase of Heliotron-E experiments, titanium gettering has been very effective for improving plasma operation, where oxygen

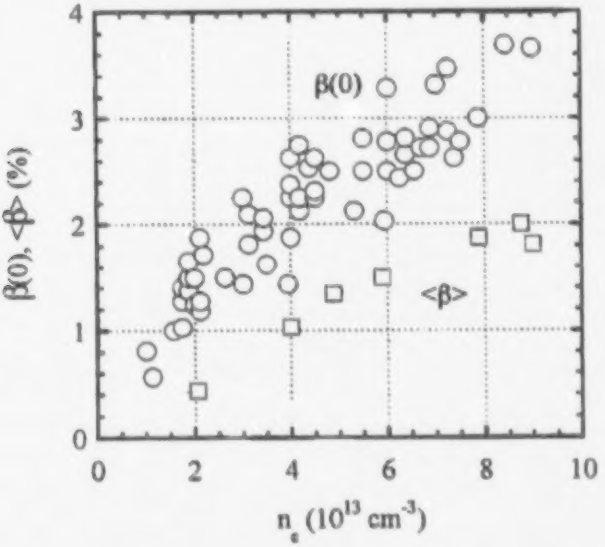

Figure 6. Volume averaged beta denoted by open square and central beta by open circle as a function of density.

impurities are reduced, and also the recycling of hydrogen from the wall is suppressed. Carbonization has been applied to reduce metal impurities, with wall surfaces coated by low-Z materials. The iron impurities are clearly reduced. The radiation loss is suppressed even in the high density regime, and the quasi-steady state is achieved at the medium density. The highest density operation is achieved with a combination of pellet injection and carbon-coated wall surfaces, in which the electron density is kept as high as $1.8\times10^{20}\mathrm{m}^{-3}$. Profile measurements show that the volume-averaged beta $\langle\beta\rangle$ reaches 2.0%, where the central beta, $\beta(0)$ is 3.6% as shown in Fig.6 [8]. According to the MHD calculation, the maximum beta value is not limited by the pressure driven instability but by the heating power. One can see that a lower magnetic field operation is very effective for obtaining higher β . Profile effects on energy confinement have also been investigated. The density profile is peaked by the pellet injection, while the temperature profile also changes through the density modification. Boron coating has been applied to Heliotron-E since 1993 by using 2.45GHz ECR discharge of Helium and $B_{10}H_{14}$ gases. After boron coating, light impurities such as oxygen and carbon are remarkably

Table II. International collaboration works in Helitron-E.

Organization	Titles	year
ANU	Development of electron cyclotron heating system	1995-1997
IAP (Russia)	Development of high power millimeter wave transmission line	1995-1996
MPI, ORNL	International Stellarator Scaling 95	1995
Kharkov Institute	Measurement of divertor plasma	1996-1997
MIT	Impurity transport study using laser blow-off method	1983-1985
PPPL	Study of MHD equilibrium and stability by STEP code Study of low n TAE in helical plasmas	1988-1993
PPPL, ORNL, Keldysh IAM, Univ. Carloso III, MPI, CRPP	Benchmark of 3D MHD stability code	1993-1996
ORNL	Soft X -ray measurement Pumped Limiter Divertor Experiment Magnetics measurement Heavy Neutral beam probe measurement Neutral Beam Injection Benchmark Studies for Stellarators/Heliotron Optimization of l=2 helical system 35GHz ECH experiment	1983 1984-1988 1984-1986 1987-1991 1987-1989 1989 1993-1994
St. Petersburg Univ.	Lithium pellet experiment	1994-1997
Univ. Wisconsin	ECE measurement	1982

suppressed, and the plasma reproducibility is greatly improved. In contrast to the carbon coating, the hydrogen recycling is suppressed to a low level, leading that the low collisional plasma is easily available. The high T_i mode plasma with a reduced thermal conductivity was obtained in the $1/\nu_i$ low collisional regime.

5. COLLABORATION WORKS

We have made many international collaboration works in both experimental and theoretical fields as a collaboration fusion research together with Australian National University (ANU), Centre de Recherches en Physique des Plasma (CRPP), Keldysh Institute of Applied Matehmatics (IAM), Institute of Applied Physics (IAP, Russia), Masachussech Institute of Technology (MIT), Max Planck Institute für Plasma Physik (MPI), Oak Ridge National Laboratory (ORNL), Princeton Plasma Physics Laboratory (PPPL), St. Petersburg Univ., Univ. Carloso III and Univ. Wisconsin. The international collaboration works are listed in Table II. We have also made domestic collaboration works with many universities and organizations.

An empirical scaling for the global energy confinement has been proposed, based on the regression analysis for the database initially of Heliotron-E and lately including other stellarators/heliotrons. This scaling law is known as the LHD scaling [9],

$$\tau_E=0.17\,P^{-0.58}\,n_e^{0.69}\,B^{0.84}\,a^{2.0}\,R^{0.75}.$$

Figure 7 illustrates the LHD scaling law. The global energy confinement time, τ_E, is increased with the increase of the density and magnetic field strength although it is degraded with the input power. These characteristics are commonly observed in both tokamaks and helical systems. The difference from tokamaks is a strong dependence on the magnetic field strength

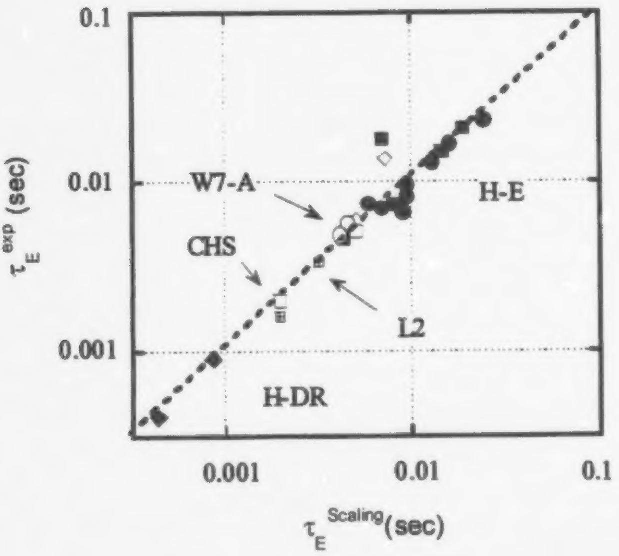

Figure 7. LHD scaling of global energy confinement.

and the density, $\tau_E \propto n_e^{0.6} B_t^{0.8}$, and size scaling, $\tau_E \propto a^2 R^1$. Recently the LHD scaling has been extended to a new scaling law, International Stellarator Scaling (ISS95) [10] by combining the W7-AS,CHS and ATF data as

$$\tau_E = 0.079\, P^{-0.59}\, n_e^{0.51}\, B^{0.83}\, a^{2.21}\, R^{0.65}\, \iota^{0.4}.$$

The scaling laws for β and particle confinement are also derived, and are confirmed with experimental data of other helical devices.

6. FUTURE PROSPECT

The Japanese government approved to establish the Graduate School of Energy Science and the Institute of Advanced Energy at Kyoto University in 1996. According to this approval, the Plasma Physics Laboratory was reorganized, and it participated in these two organizations, Institute of Advanced Energy and Graduate School of Energy Science. Institute of Advanced Energy is devoted mainly to the research on the physical and technological aspects of advanced energy science in cooperation with the Graduate School of Energy Science.

In order to contribute to the development of fusion science and technology from the viewpoint of advanced energy research and to investigate the further improvement of helical systems, we are now designing an advanced magnetic confinement system, which should satisfy the physically necessary properties for fusion reactor, in particular, good confinement of high energy particle, MHD stability and divertor operation. The concept of a new machine is based on helical-axis heliotron with $\ell = 1$ field component. Figure 8 shows schematic of helical coil and plasma. The designed device parameters are R=1.2m, a=0.14-0.2m. The maximum magnetic field on axis is 1.2T. The external coil system is composed of $\ell=1$ helical coil, toroidal and vertical coils. Compared to the modular coil system such as W7-X and HSX, the characteristic parameters of magnetic surface such as rotational transform, magnetic well, bumpiness and magnetic axis position, can be varied in a wide range, resulting in the flexible magnetic configuration.

Absolute trapping of helically trapped particles are one of major task in helical system,

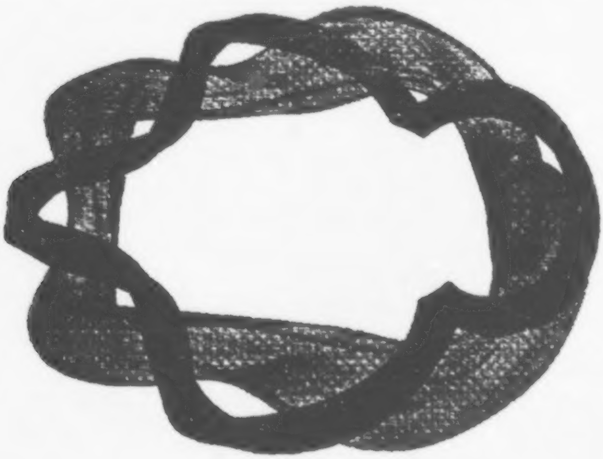

Figure 8. Configuration of helical coil and plasma helical-axis heliotron.

because the ripple transport is enhanced in the low collisional regime. The restoration of helical symmetry reduces the ripple transport. The magnetic axis shift experiment, as described in Sec. 4, showed that the energy confinement was improved when the drift surface coincides with the magnetic surface. At present design study, the field spectrum is optimized so as to make bumpiness component reduce the neoclassical transport due to the helical ripple component. Stabilization of pressure-driven instability is also important for stable operation. Since the magnetic well is effective for the stabilization of pressure-driven instability, the magnetic surface is designed to have a magnetic well up to the last closed magnetic surface. According to the numerical calculation, the equilibrium beta, $<\beta>\sim 5\%$, is expected.

7. CONCLUSION

Helical system is recognized as one of leading candidates for fusion reactor comparable to tokamaks. Since the magnetic configuration is constructed only by external coils, the helical system has a potential of steady state operation without dangerous current-driven major disruption. Plasma Physics Laboratory of Kyoto University has been conducting the fusion research using heliotron devices. Heliotron-E experiment showed that the currentless plasma is successfully produced and heated by several heating methods. It was also shown that the plasma confinement is improved by the optimization of heating and magnetic configuration, and the wall conditioning. Our experimental results would contribute to the understanding of common physics in magnetic confinement system. Extending to the Heliotron-E results, the advanced helical system is proposed and designed in Kyoto University. Compatibility among confinement of high energy particles, MHD stability and divertor operation is under investigation.

ACKNOWLEDGMENTS

Authors acknowledge the late Prof. K. Uo, the founder and first director of the PPLK, and Prof. A. Iiyoshi, the former director of PPLK, for their kind encouragement. They thank the Heliotron-E staff and many collaborator from universities and organizations for supporting the Heliotron-E project. Without their help, they could not have made any experimental progress toward a heliotron fusion reactor.

REFERENCES

1. M. Wakatani and S. Sudo, Plasma Phys. Control. Fusion **38**, 938(1996).
2. T. Obiki, et al., Proc. 16th Conference on Fusion Energy, Montreal, IAEA-CN-64/C1-3 (1996).
3. K. Uo et al. Proc. Plasma Physics and Controlled Nuclear Fusion Research (Kyoto) **2**, 355 (1986).
4. T. Mutoh et al. Proc. Plasma Physics and Controlled Nuclear Fusion Research (Kyoto) **2**, 473 (1986).
5. T. Obiki, et al., Proc. Plasma Physics and Controlled Nuclear Fusion Research (Seville) **1**, 757 (1994).
6. K. Ida et al. Phys. Rev. Lett. **76**, 1268 (1996).
7. T. Obiki et al. Proc. Plasma Physics and Controlled Nuclear Fusion Research (Washington, D. C.) **2** , 425 (1990).
8. O. Motojima et al. Nucl. Fusion **25**, 1783 (1985).

9. S. Sudo et al. Nucl. Fusion **30**, 11 (1990).

10. U. Stroth et al. Nucl. Fusion **36**, 106 (1996).

INERTIAL CONFINEMENT FUSION AT THE LOS ALAMOS NATIONAL LABORATORY

Erick Lindman, D. Baker, C. Barnes, B. Bauer, J.B. Beck, R. Berggren, B. Bezzerides, P. Bradley, R.E. Chrien, M. Clover, J. Cobble, C.A. Coverdale, M. Cray, N. Delamater, D. DuBois, B. H. Failor, J.C. Fernandez, L. Foreman, R. Gibson, P. Gobby, S.R. Goldman, D. Harris, A. Hauer, J. Hoffer, N. Hoffman, W.W. Hsing, R. Johnson, K. Klare, R. Kopp, W. Krauser, G. Kyrala, G. Magelssen, R. Mason, D. Montgomery, T.J. Murphy, J. Oertel, G. Pollak, H. Rose, K. Schoenberg, D.P. Smitherman, M.S. Sorem, F. Swenson, D. Tubbs, W. Varnum, H. Vu, J. Wallace, R. Watt, R. Weaver, B. Wilde, M. Wilke, D. Wilson and W.M. Wood

Los Alamos National Laboratory
Los Alamos, NM 87545, U.S.A.

ABSTRACT

The Los Alamos National Laboratory is contributing to the resolution of key issues in the US Inertial-Confinement-Fusion Program and plans to play a strong role in the experimental program at the National Ignition Facility when it is completed.

1. INTRODUCTION

The goal of the Los Alamos Inertial-Confinement-Fusion (ICF) Program is to achieve fusion in the laboratory. And, we believe that the facility, in which this goal is most likely to be achieved, is the National Ignition Facility (NIF). The NIF [1], which is currently scheduled for completion in 2004, is a 192-beam laser operating at 0.35 μm wavelength. It is capable of delivering 1.8 MJ to a mm size target at a peak power of 500 TW. It will be capable of direct- and indirect-drive illumination and is expected to achieve a maximum of 45 MJ of fusion yield per pulse.

1.1 Direct Drive

In direct drive the energy of the laser is deposited spherically symmetrically on the surface of the spherical capsule containing the deuterium-tritium (DT) fuel. The laser energy diffuses into the capsule and produces a region of high pressure which accelerates the outer layer outward and the inner layers inward. The inward acceleration causes the fuel in the capsule to be compressed and heated to ignition conditions. Los Alamos has a small effort

Current Trends in International Fusion Research — Proceedings of the Second Symposium
Edited by E. Panarella. NRC Research Press, National Research Council of Canada, Ottawa, ON K1A 0R6, Canada. 1999.

in support of this approach. It is primarily directed toward the investigation of the use of foam layers on the outside of the capsule to improve the drive symmetry. Experimental results [2] and theoretical calculations [3] suggest that some improvement is achievable using foam layers.

1.2 Indirect Drive

In indirect drive the capsule is located inside a high-Z container called a hohlraum. The laser energy is deposited on the walls of the hohlraum where it is absorbed and converted to x-rays. These x-rays then carry the energy to the capsule and ignition conditions are achieved as before. The bulk of the Los Alamos program is directed towards achieving ignition with indirect drive. Since existing lasers cannot achieve the conditions expected in indirect drive targets on the NIF, it is necessary to use computer codes such as LASNEX [4] to predict the conditions that will be achieved and the subsequent behavior of the capsule and DT fuel. To check the reliability of the predictions of the code, extensive experiments are carried out in the parameter ranges accessible to existing lasers and compared to code predictions for these cases. LASNEX predictions of NIF-target behavior and comparisons of LASNEX calculations with experiments will be discussed in more detail below.

2. PREDICTIONS OF NIF-TARGET PERFORMANCE

2.1 Integrated Modeling and the LASNEX Computer Code

Integrated modeling refers to the practice of calculating all of the dynamics inside the hohlraum simultaneously, rather than calculating parts of the problem separately. Physical effects included in such calculations are (1) laser-ray propagation, refraction, absorption and x-ray conversion, (2) laser-entrance-hole (LEH) effects such as window (the thin membrane covering the LEH to hold in the gas) expansion and hole closure, (3) x-ray transport with typically 70 energy groups, (4) wall and channel plasma dynamics, spot motion, stagnation, filling and hydro coupling and (5) capsule dynamics such as preheat, implosion and burn. Physical effects that are currently not included in the calculations, because they are not in the LASNEX code, include plasma interpenetration and laser-plasma instabilities. Hydrodynamic instabilities are not included either, but for different reasons. The fine zoning required to resolve the small perturbations on the capsule which grow as the result of Rayleigh-Taylor instabilities would make the calculation prohibitively expensive to carry out. These effects are calculated with the LASNEX code in separate capsule-only calculations.

2.2 NIF-Target Calculations

Integrated modeling with the LASNEX code has been used to calculate the performance of, and demonstrate the attainment of ignition for, a variety of indirect-drive targets for the NIF. The targets consist of a gold hohlraum in which laser energy is deposited and converted to x-rays and a capsule that is imploded by the x-rays. The same hohlraum was used in all of the indirect-drive targets. It was a gold cylinder, 10 mm long by 5.5 mm in diameter, with concentric laser-entrance holes (LEH's) in the gold endcaps. The LEH's were 2.75 mm in diameter and were covered with a thin polyimide window to hold in the hydrogen-helium gas whose density was approximately 1.3 mg/cm^3. The hohlraums were then irradiated with either two or three cones of beams from either side.

The calculation of the Livermore PT (point target) design, shown in Fig. 1, was first

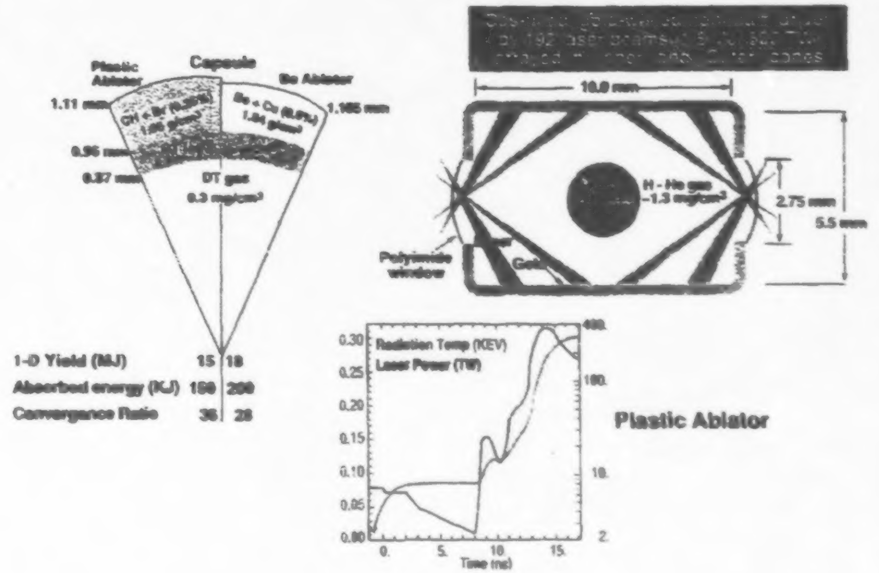
Plastic Ablator
Capsule
Be Ablator
1.11 mm
CH + Br (0.25%)
1.05 g/cm³
Be + Cu (0.9%)
1.105 mm
0.95 mm
0.87 mm
DT gas
0.3 mg/cm³
1-D Yield (MJ) 15 18
Absorbed energy (KJ) 150 200
Convergence Ratio 36 28
10.0 mm
H - He gas
~1.3 mg/cm³
2.75 mm
5.5 mm
Polyimide window
Gold
Radiation Temp (KEV)
Laser Power (TW)
0.30
0.25
0.20
0.15
0.10
0.05
0.00
400.
100.
10.
2.
0.
5.
10.
15.
Time (ns)
Plastic Ablator

Figure 1. Calculated performance of the Livermore PT (point target) and the Los Alamos beryllium-ablator capsule designs. The results for the two capsules were obtained in calculations using the same hohlraum and laser-beam pointing.

repeated, and the results were compared to Livermore results [5—8]. The capsule in this target was a bromine-doped plastic (CH) shell with an inner radius of 0.95 mm, an outer radius of 1.1 mm and a density of 1.05 g/cm^3. A layer of deuterium-tritium (DT) ice having a density of 0.25 g/cm^3 extended from a radius of 0.87 mm to the inner radius of the plastic shell. Inside the DT-ice layer the rest of the volume is filled with DT gas at a density of 0.3 mg/cm^3. Two cones of beams whose intensities were varied independently to achieve the required time-dependent drive and symmetry were used in the calculation. This target calculated to ignite with two-cone illumination and gave a fusion yield of 12 to 15 MJ with a laser energy of 1.3 MJ and a peak power of 360 TW.

An alternate design, also shown in Fig. 1, was then proposed at Los Alamos in which the plastic shell was replaced with a copper-doped beryllium shell [8]. All dimensions remained the same except for the outer radius of the beryllium shell which dropped slightly to 1.105 mm. Again two cones of beams whose intensities were varied independently to achieve the required time-dependent drive and symmetry were used in the calculations. This target calculated to ignite with two-cone illumination and gave a fusion yield of 16 MJ with a laser energy of 1.4 MJ and a peak power of 400 TW. The advantages of this design over the original PT design is a reduced sensitivity to the growth of surface perturbations and a reduced sensitivity to thermal errors during the process of forming and symmetrizing the DT-ice layer. The disadvantages are associated with fabrication procedures. A seamless sphere cannot be made as easily with beryllium as it can with plastic. Instead two hemispheres may have to be made and joined. In addition the beryllium capsule cannot be diffusion filled with DT. Instead it must be filled through a hole which then must be plugged. The resulting perturbations at the joint and the fill hole may lead to jetting of the beryllium into the fuel.

Ignition was achieved with another variation of the PT design involving the use of three

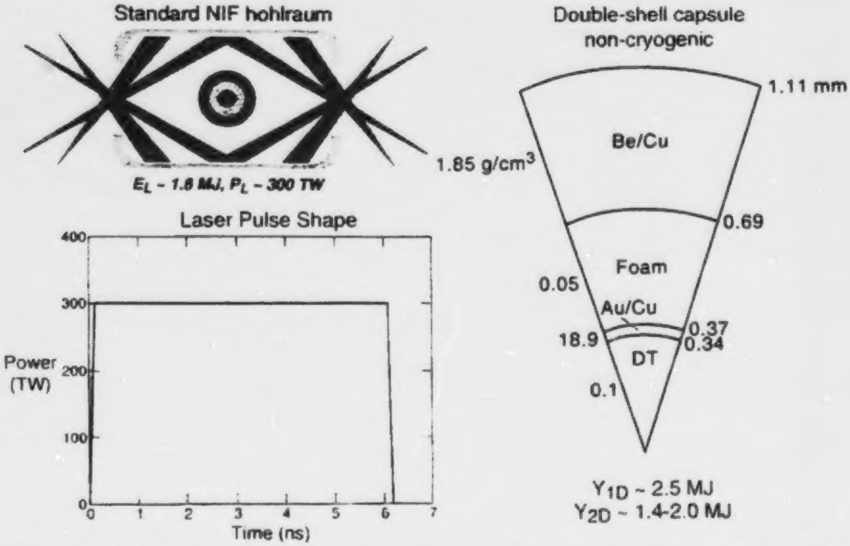

Figure 2. Calculated performance of the Los Alamos double-shell capsule design. The results were obtained using the same hohlraum and laser-beam pointing that was used in Figure 1. The simple laser pulse shown here with no beam phasing was used in place of the tailored pulse.

beam cones instead of two. Drive symmetry was easier to obtain with this approach, and a fusion yield of 12 MJ was obtained with 1.3 MJ in at a peak power of 360 TW.

More recently another alternate design has been proposed at Los Alamos, a double-shell design [9], shown in Fig. 2, whose principal advantages are that it is non-cryogenic and does not require a shaped laser pulse. Its disadvantages are lower yield and greater sensitivity to hydrodynamic instabilities. The outer shell is copper-doped beryllium with an inner radius of 0.69 mm and an outer radius of 1.11 mm. Inside of the ablator is a layer of plastic foam with density 0.05g/cm^3 which extends from a radius of 0.37 mm to 0.69 mm. This layer plays the role of a cushion allowing the imploding outer shell to smoothly accelerate the inner shell which contains the DT fuel. The inner shell is made of a gold-copper alloy with a density of 18.9 g/cm^3 and inner and outer radii of 0.34 and 0.37 mm respectively. The gaseous DT fuel is contained with the inner shell at a density of 0.1g/cm^3. When this target is driven with a 6 ns flat-top pulse at 300 TW, 1.8 MJ is delivered to the target and a calculated yield of 1.4 to 2 MJ is obtained. It is not a high-gain target, but ignition is obtained.

2.3 Pulse Shaping and Beam Phasing

In order to compress the fuel to high density and raise its temperature to the required value, it must first be adiabatically compressed and then shock heated symmetrically. The laser pulses necessary to do this, shown in Fig 3, are complicated functions of time. Significant deviation from the resulting drive will prevent ignition of the PT target.

Adequate symmetry is required as well. The laser energy is deposited in the region where the laser beam first encounters material from the hohlraum wall. Because of the blow-off of the wall, this region moves. This spot motion along with the changing relative x-ray emission intensity from the rest of the hohlraum introduces time-dependent asymmetries in the capsule drive. The laser pointing cannot be changed on these time scales, so an alternate

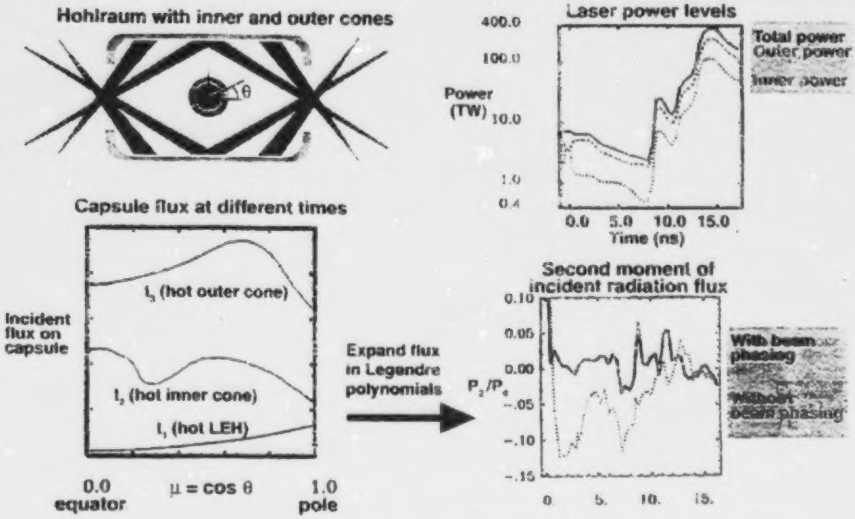

Figure 3. Beam phasing. The power vs. time for the inner and outer beam cones are plotted on the same graph and compared to the total power. The flux on the capsule as a function of the polar angle is shown at different times. Data such as this are used to generate the coefficient of the Legendre function, P_2, in an expansion of the drive vs. polar angle. Typical values of P_2 as a function of time are shown for cases with and without beam phasing.

strategy to compensate for these time-dependent asymmetries has been devised. Two cones of beams are used to give two rings of laser spots. The "center of irradiance" can then be moved towards or away from the capsule by changing the relative intensity of these rings. This concept is called beam phasing and is used to reduce time-dependent asymmetries. Thus the sum of the intensities of the two rings determines the capsule drive, and the difference is used to control time-dependent symmetry.

The laser power levels that were used in the calculations of the PT target are shown in Fig. 3. A measure of the drive symmetry with and without beam phasing is presented as well. The improvement in drive symmetry with beam phasing is quite apparent. If the calculation with beam phasing is repeated without beam phasing, i.e. with the total power unchanged and the ratio of the powers in the inner and outer cone held constant, the PT target does not ignite [5—8]. This result is true for the beryllium target as well. When three-cone illumination is employed, beam phasing is not required to obtain ignition. However, in the absence of beam phasing the target is much more sensitive to tiny errors in pointing and beam intensity.

Neither beam phasing nor a special laser pulse is required to obtain ignition in the double-shell target [9]. The previously quoted results were obtained with a 6-ns flat-top pulse, shown in Fig. 2, with a fixed power ratio between the inner and outer cones. The smooth acceleration of the inner shell, driven by the rising pressure in the cushion material between the shells, plays the same role as the shaped laser pulse required for the PT target.

2.4 Hydrodynamic Instabilities and Surface Irregularities

The LASNEX code can also be used to perform direct-numerical-simulation (DNS) calculations of the growth of perturbations from fabrication surface irregularities [10].

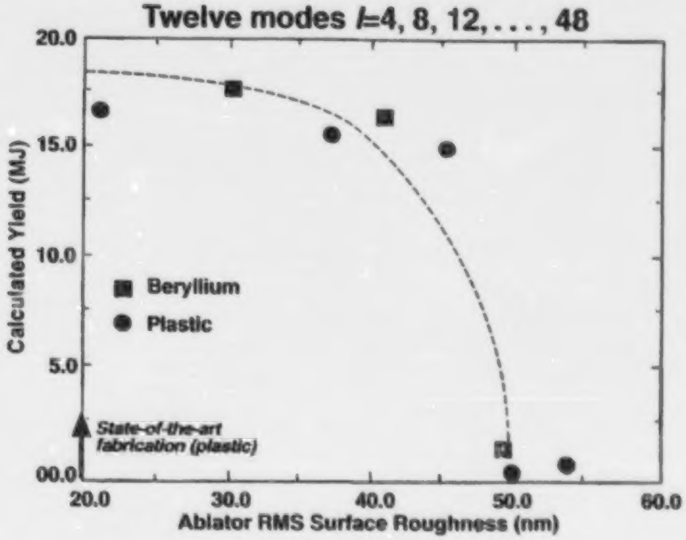

Figure 4. Calculated yield vs. ablator surface roughness. Initial DNS calculations for NIF suggest that both the beryllium and plastic capsules tolerate ablator roughness up to 40 nm.

Accurate calculations of these effects are not included in integrated-modeling calculations because the zoning requirements exceed the capacity of the computer. Instead they are evaluated in separate capsule-only calculations in which high resolution is obtained by putting all the zones in the capsule.

Many spherical-harmonic modes can then be included in the calculation simultaneously. No adjustable model parameters are used, and the initial amplitudes are chosen to represent a spectrum measured from capsules that were made using state-of-the-art technology. The finite initial amplitudes lead to nonlinear growth, and the shape of the imploded fuel and its self-consistent yield are obtained.

Initial DNS calculations for NIF suggest that both the beryllium and the plastic capsules

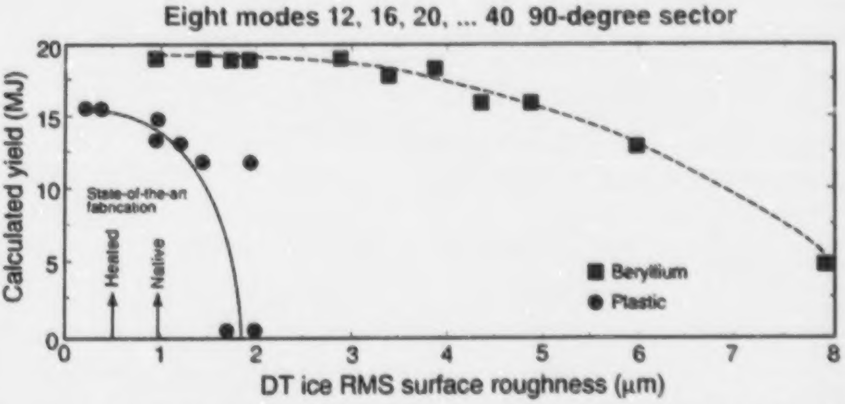

Figure 5. Calculated yield vs. DT-ice surface roughness. 2-D multimode calculations show that the Beryllium capsule tolerates greater DT-ice surface roughness than the plastic capsule.

tolerate ablator roughness up to 40 nm. Fig. 4 shows yield plotted against surface roughness for a series of such calculations. At 40 nm surface roughness the yields have dropped by only as much as 10%, while at 50 nm the capsules no longer ignite. For plastic capsules 20 nm surface roughness is attainable with current state-of-the-art fabrication techniques.

The other surface which has been studied in some detail is the inner DT-ice surface. Here two dimensional multimode calculations show that the beryllium capsule tolerates greater DT-ice surface roughness than the plastic capsule. Fig. 5 shows yield plotted against ice-surface roughness for the two capsules. The plastic capsule fails to ignite at a surface roughness of 2 μm, while the beryllium capsule is still showing 5 MJ of yield at 8 μm. Using a process called beta layering, DT-ice layers can be formed inside a capsule with surface roughness less than 2 μm.

3. EXPERIMENTS AND FUTURE RESEARCH

Experiments are being carried out in a number of different areas to increase our understanding of the physical processes occurring in these hohlraums and to verify the accuracy of our code predictions. One such area which will not be discussed in detail is that of laser-plasma instabilities [11-21]. In this area questions currently being addressed include: What saturates stimulated Brillouin scattering? And can we limit stimulated Brillouin (SBS) and stimulated Raman (SRS) scattering for relevant NIF plasma conditions? The answers to these questions will give us more confidence in our ability to predict backscatter levels on the NIF. Other areas of current research, that will be discussed in detail, include drive symmetry, hydrodynamic instabilities and beta layering.

3.1 Drive Symmetry

The discrepancies between Nova experiments in vacuum and gas-filled hohlraums, shown in Fig. 6, and LASNEX modeling of capsule-implosion symmetry in gas-filled hohlraums were first reported in 1994 [22] and are now well established [23-28]. A number of physical mechanisms which might contribute to these effects have been evaluated [29,30].

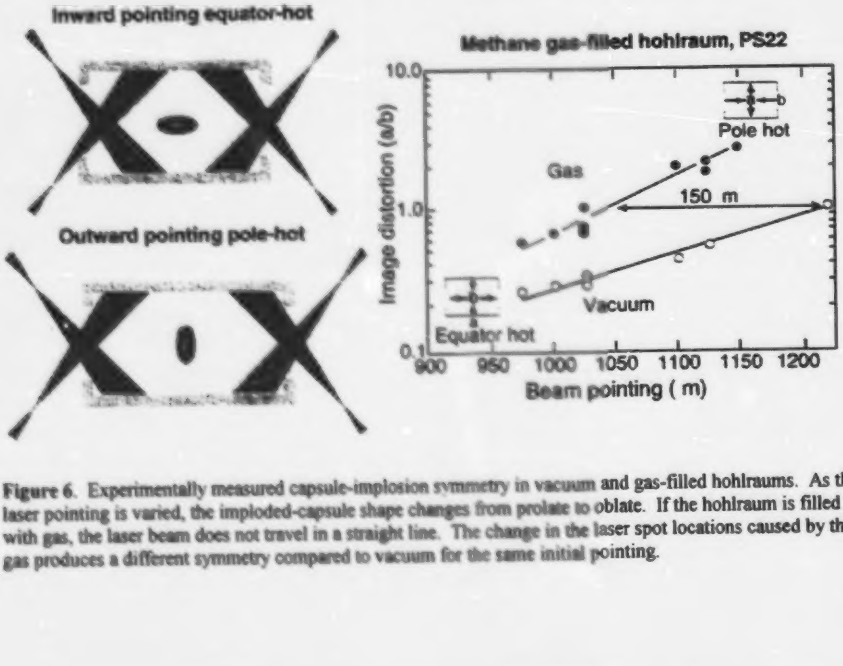

Figure 6. Experimentally measured capsule-implosion symmetry in vacuum and gas-filled hohlraums. As the laser pointing is varied, the imploded-capsule shape changes from prolate to oblate. If the hohlraum is filled with gas, the laser beam does not travel in a straight line. The change in the laser spot locations caused by the gas produces a different symmetry compared to vacuum for the same initial pointing.

One of these is currently thought to be responsible for essentially all of the effect on capsule-implosion symmetry. This mechanism, laser-beam propagation in filaments bent by plasma flow, is being studied intensively at Los Alamos [30] and Livermore [31], and a bending of the laser beam by as much as 9 degrees has been theoretically predicted under idealized conditions [31].

The strongest evidence for the conclusion that "beam steering" is the dominant effect on capsule-implosion symmetry, however, comes from recent calculations of Nova experiments. Using thin-wall hohlraums in Nova experiments (150 micron thick epoxy cylinders with 2 microns of Au deposited on the inner surface), it is possible to see through the walls of the hohlraum with gated x-ray imagers and see the location of the laser spots as a function of time. This diagnostic can be simulated in LASNEX calculations to get the equivalent spot motion.

The spot shifts seen in experiments differ by as much as 300 microns from those seen in calculations when no additional deflection is included. The X's in Fig. 7 show the shift in the location of the hot spot from nominal pointing in a recent Nova shot as a function of time. When a LASNEX calculation with no additional deflection is done, some spot motion occurs because of the wall motion. The spot shift as a function of time for this case is given by the dotted curve in Fig. 7. The disagreement between experiment and calculation is thought to result from bending of the laser beam by the plasma [30,31]. The effect is strongest at a point in the plasma where the transverse Mach number of the flow is one and is a complicated function of the local plasma parameters.

The effect can be mocked up in LASNEX calculations, however, by bringing the laser beam in at a different angle as shown in Fig. 8. The bottom half of the Figure shows the laser beam propagating at 50 degrees from the hohlraums axis as they do at Nova. The upper half of the Figure shows a laser beam that is propagating at 58.75 degrees through the same intersection point with the hohlraum axis. The laser spot is shifted roughly 20 microns per

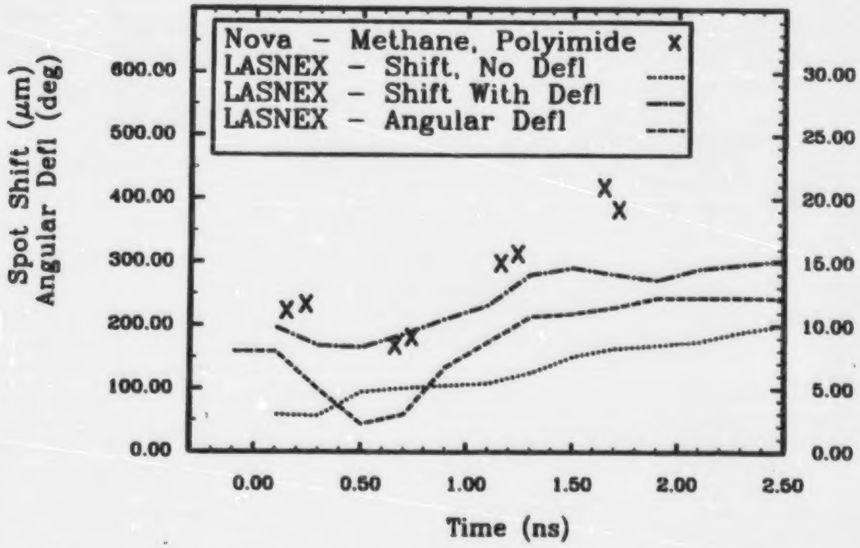

Figure 7. Spot motion in gas-filled hohlraums. Spot motion can be measured in gas-filled thin-wall hohlraums at Nova. The observed shift in a LASNEX calculation with no externally applied additional deflection disagrees with experiment. The additional shift can be added by changing the laser propagation angle as a function of time. The added angular deflection produces a shift with deflection which agrees with the Nova spot-position data at early time.

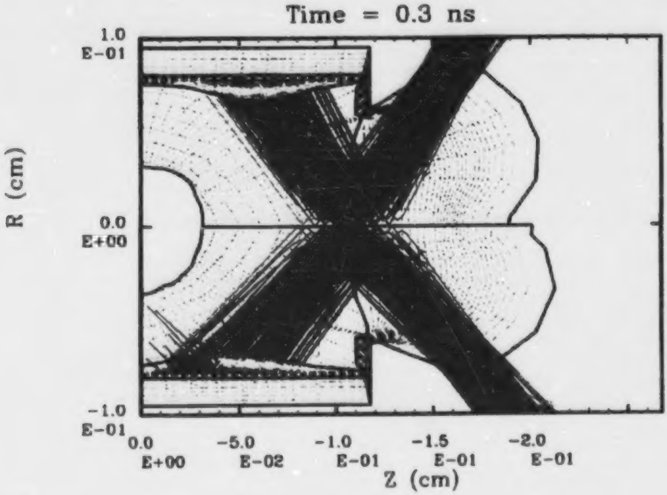

Figure 8. Raytrace with and without added deflection. In the lower half hohlraum, the laser is propagating initially at 50° to the axis of the hohlraum as the Nova beams are designed to do. In the upper hohlraum the central ray intersects the axis of the hohlraum at the same point but the initial angle of propagation of the beam has been rotated 8.75° to approximate the additional beam deflection required at early time to match the experimentally measured hot-spot position.

degree or approximately 175 microns. This angle is changed in the calculation as a function of time to give the time dependence shown in the dashed curve in Fig. 9. The resulting spot shift, shown in the dash-dot curve in Fig. 7, matches the experimental data quite well over the early part of the time interval. The discrepancy at late time is thought to be due to an artifact in the experimental data reduction.

When the additional angular deflection is included in the calculation in such a way as to match the spot motion seen in the experiment, the imploded-capsule symmetry agrees well with the experimental data. Figure 9 shows experimental data and calculations for a pointing scan at Nova in which the length of the hohlraum and the laser pointing were varied simultaneously. The distortion is the ratio of the length of the semi-major axis of the ellipsoid transverse to the hohlraum axis divided by the length of the semi-major axis along the hohlraum axis. The laser pointing is defined here as the distance from the center of the hohlraum to the intersection of the central ray of the laser beam with the hohlraum's axis, and the length of the hohlraum is always adjusted so that this intersection is in the plane of the inside surface of the laser-entrance hole. The symmetry of the imploded capsule changes from prolate (sausage) at inner pointing at the left to oblate (pancake) at outer pointing at the right. The discrepancy between the experimental data and LASNEX calculation is quite apparent. When the calculation is done with the additional angular deflection, however, the resulting distortion of the imploded capsule is consistent with the experimental values.

Smoothing the beams using random phase plates or kineform phase plates is expected to reduce this problem substantially. Preliminary results from ongoing experiments seem to confirm this hypothesis. Physics packages which could calculate these effects have not been added to LASNEX. If beam smoothing eliminates these effects, there will be little interest in adding the additional physics packages to LASNEX.

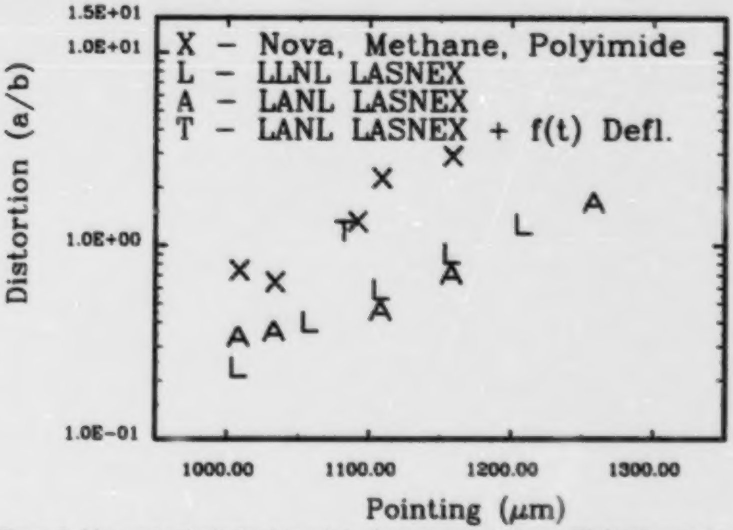

Figure 9. Measured and calculated capsule-implosion symmetry. In gas-filled hohlraums the calculated imploded-capsule symmetry differs from experimental measurements and is much closer to the experimental data for vacuum hohlraums. However, when the laser propagation angle in the LASNEX calculation is adjusted to reproduce the spot motion observed in a gas-filled hohlraum, the calculated imploded-capsule symmetry (plotted with T in the figure) agrees with experiment.

3.2 Hydrodynamic Instabilities

Indirect-drive Rayleigh-Taylor experiments in a cylindrical geometry are being carried out at Nova by Los Alamos investigators [32-36]. The use of a cylindrical geometry retains convergent effects while providing diagnostic access to the inside surface. These experiments are an important check on the planar Rayleigh-Taylor experiments which have been carried out by others. In a converging geometry the mode numbers of the perturbations are conserved and the wavelengths change. As a result the growth rates change with radius and simple exponential growth is not expected. In addition growth in amplitude can occur from convergence alone. These effects are included in LASNEX calculations which agree well with the experimental results.

A typical experimental arrangement is shown in Fig. 10. A cylindrical scale-1 hohlraum is driven by 8 of the 10 Nova beams. The cylindrical implosion structure is located at the center of the main hohlraum with its axis perpendicular to the axis of the main hohlraum. One of the unused beams is used to irradiate the backlighter. A time-resolved x-ray pinhole camera is then used to record images of the imploding cylindrical structure.

Experimental data from a recent experiment [36] is shown in Fig. 11. This experiment was designed to measure the feed through of a perturbation imposed on the outer surface of a cylindrical shell to its inner surface and its subsequent growth. The initial target was a 40 mm thick plastic shell with an inner diameter of 430 mm. It had a 4 mm thick layer of chlorinated plastic on its inner surface to act as a marker layer by absorbing x-rays. Its interior was filled with plastic foam, and it had an m=12 perturbation machined onto the outer surface with a peak-to-valley ratio of 9 μm. In Fig. 11 at 2.11 ns the black marker layer in the images has expanded to a thickness of about 20 μm and shows structure which came from the perturbation machined onto the outer surface of the plastic shell. At later time the growth of

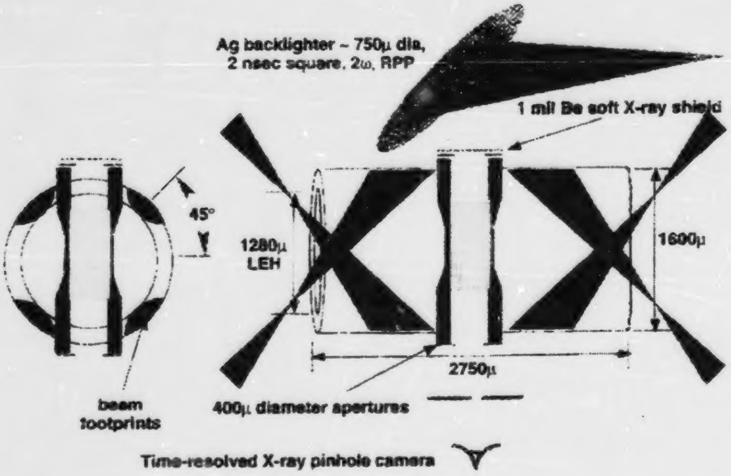
Ag backlighter ~ 750μ dia,
2 nsec square, 2ω, RPP
1 mil Be soft X-ray shield
45°
1280μ
LEH
1600μ
2750μ
beam
footprints
400μ diameter apertures
Time-resolved X-ray pinhole camera

Figure 10. Experimental layout for Rayleigh-Taylor experiments in a cylindrical geometry. The cylindrical structure to be imploded is placed in the main hohlraum with its axis at right angles to the axis of the main hohlraum. Eight beams are used to illuminate the hohlraum and a ninth is used to illuminate the backlighter.

these perturbations is seen as the shell decelerates because of the pressure buildup in the foam inside the shell.

A control experiment, in which no perturbation was machined on the outer surface of the cylindrical shell, was performed for comparison. A single image from this latter experiment is shown at the bottom of Fig. 11. The marker layer in it shows no m=12 structure as expected. LASNEX calculations of these experiments reproduce these images quite well.

3.3 Beta Layering

NIF ignition designs employ uniform spherical layers of cryogenic fuel. The preferred mechanism for producing such layers in capsules filled with DT gas, and subsequently cooled, is called beta layering. It uses re-absorption of the β emission from the tritium in the DT fuel to drive an ice layer to uniformity. Optimization of this mechanism for different capsule designs is currently an active area of research at Los Alamos [37–40].

The beta-layering procedure begins with the freezing of the fuel inside a capsule into an irregular mass. The self-heated DT then establishes a parabolic radial temperature profile. The temperature of the outer surface is held approximately constant by the continuous heat extraction. As a result the temperature of the inner surface varies with the radial thickness of the layer: the thicker the layer, the warmer the surface. DT sublimes from the thick regions to re-freeze at the thin regions. Layer uniformity increases 10-fold every 61 minutes. The interior surface reaches equilibrium when it follows an isotherm. Since the interior isotherm will be concentric to the external surface at equilibrium, the interior surface of the DT fuel will be concentric and uniform as well.

An rms roughness of the order of 2 μm is typically seen in experiments. The measured power spectrum [39,40] of a 139 μm thick layer at 18.8K is shown in Fig. 12. The roughness as a function of spherical-harmonic mode number shows the largest contribution at low mode number with a dramatic decrease at high mode number. Two-dimensional realizations of spectra such as this are used in the DNS calculations mentioned earlier. These data plus the

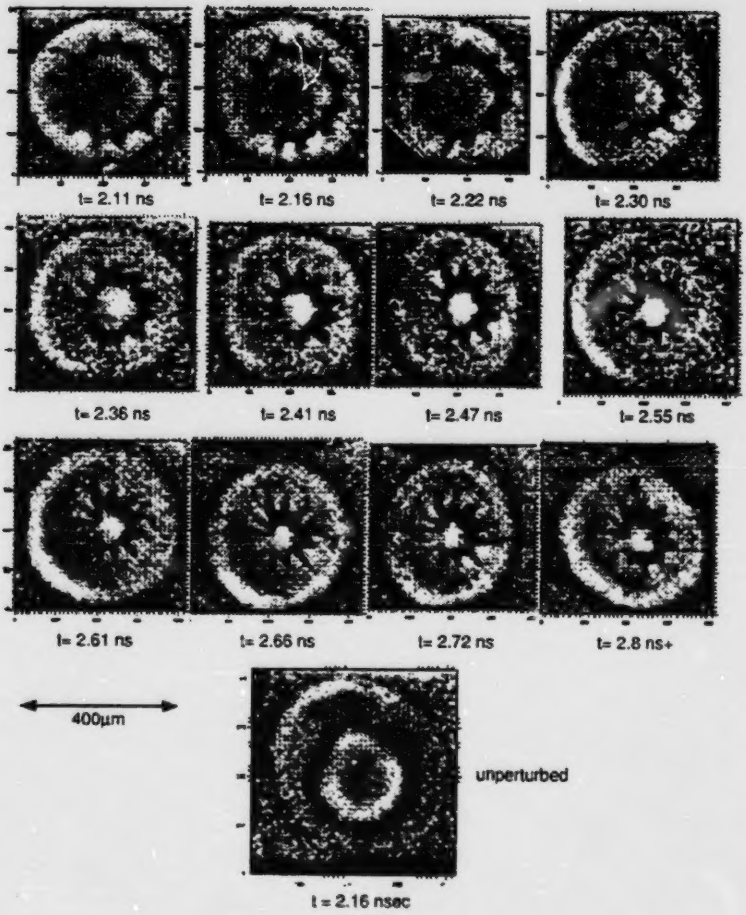

Figure 11. A sequence of gated X-ray images of the cylindrical backlit implosion. Emission appears on center at 2.30 ns, which is when the shock wave converges at the origin. The backlighter spatial extent is limited by the 400-μm-diameter circular apertures at each end of the cylinder, and the deviation from circularity is a measure of the effect of parallax. Shown in the bottom panel is an image of an imploding shell with no initial perturbations.

calculations support the contention that ignition is achievable on the NIF.

4. CONCLUSIONS

The National Ignition Facility will be an important research facility for the study of fusion energy, astrophysical phenomena, plasma physics, atomic physics and hydrodynamics. It will, indeed, become the center for research in many of these areas. Researchers from laboratories and universities in the United States and from around the world will be able to participate in projects that can not be done elsewhere.

Every effort is being made to assure the achievement of ignition at the National Ignition Facility. Research workers at Los Alamos are contributing extensively to this effort.

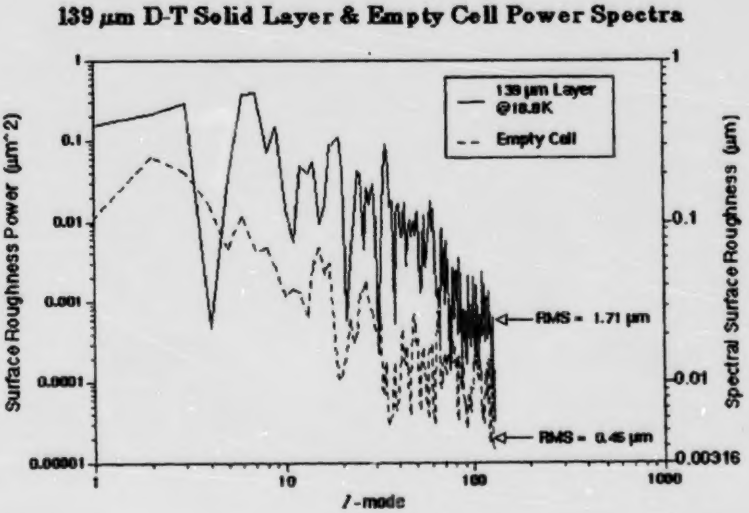

Figure 12. DT ice layer roughness characterized in spherical harmonics. Surface roughness is measured with and without a layer of DT-ice. The surface roughness of the cell in which the measurement is taken is negligible compared to the surface roughness of the DT ice when it is present.

Researchers at Los Alamos and elsewhere look forward to playing a strong role in the research work that will be performed at the National Ignition Facility when it is complete.

Work performed for the U. S. Department of Energy under Contract No. W–7405–ENG–36.

REFERENCES

1. "National Ignition Facility Conceptual Design Report," Lawrence Livermore National Laboratory Proposal, UCRL-Prop-117093, NIF-LLNL-94-113, L-16973, August 1994.
2. R.G. Watt, D.C. Wilson, R.E. Chrien, R.V. Hollis, P.L. Gobby, R.J. Mason, R.A. Kopp, R.A. Lerche, D.H. Kalantar, B. MacGowan, B.B. Nelson, P.W. McKenty and O. Willi. Foam Buffered Spherical Implosions at 527 nm. to be published in Physics of Plasmas.
3. R.J. Mason, R.A. Kopp, H.X. Vu, D.C. Wilson, S.R. Goldman, R.G. Watt, M. Dunne and O. Willi. Computational Study of Laser Imprint Mitigation in Foam-Buffered ICF Targets. to be published in Physics of Plasmas.
4. G.B. Zimmerman and W.L. Kruer. Plas. Phys. **2**, 51 (1975).
5. S.W. Haan and S.M. Pollaine. LLNL Research Monthly **93-1**, 5 (1993) (unpublished).
6. S.W. Haan, S.M. Pollaine, J.D. Lindl, L.J. Suter, R.L. Berger, L.V. Powers, W.E. Alley, P.A. Amendt, J.A. Futterman, W.K. Levedahl, M.D. Rosen, D.P. Rowley, R.A. Sacks, A.I. Shestakov, G.L. Stroebel, M. Tabak, S.V. Weber, G.B. Zimmerman, W.J. Krauser, D.C. Wilson, S. Coggeshall, D.B. Harris, N.M. Hoffman, and B.H. Wilde. Phys. Plasmas **2**, 2480 (1995).
7. W.J. Krauser, N.M. Hoffman, D.C. Wilson, B.H. Wilde, W.S. Varnum, D.B. Harris, F.J. Swenson, P.A. Bradley, S.W. Haan, S.M. Pollaine, A.S. Wan, J.C. Moreno and P.A. Amendt. Phys. Plasmas **3**, 2084 (1996).

8. W.J. Krauser, B.H. Wilde, D.C. Wilson, P.A. Bradley, and F.J. Swenson. Proc. 12th Int. Conf. on Laser Interaction and Related Plasma Phenomena, **369**, 186(AIP Press, 1996).
9. D.B. Harris and W.S. Varnum. Bull. Am. Phys. Soc. **41**, 1479 (1996).
10. N.M. Hoffman, D.C. Wilson, W.S. Varnum, W.J. Krauser and B.H. Wilde. Proc. 12th Int. Conf. on Laser Interaction and Related Plasma Phenomena, 369, 166 (AIP Press, 1996).
11. B. Bauer, R.P. Drake, K.G. Estabrook, J.F. Camacho, R.G. Watt, M.D. Wilke, B.E. Busch and S.E. Caldwell. Phys. Plasmas **2**, 2207 (1995).
12. B.S. Bauer, R.P. Drake, K.G. Estabrook, R.G. Watt, M,D. Wilke and S.A. Baker. Phys. Rev. Lett. **74**, 3604 (1995).
13. J. Cobble, J.C. Fernandez, B.H. Wilde, S. Evans, J. Jimerson, J. Oertel, D.S. Montgomery and C.C. Gomez. Rev. Sci. Instrum. **66**, 4204 (1995).
14. R.P. Drake, R.G. Watt and K.G. Estabrook, Phys. Rev. Lett. **77**, 79 (1996).
15. B. Bezzerides, H.X. Vu and J.M. Wallace. Phys. Plasmas **3**, 1073 (1996).
16. H.X. Vu. J. Comp. Phys. **124**, 417 (1996).
17. J.C. Fernandez, J.A. Cobble, B.H. Failor, W.W. Hsing, H.A. Rose, B.H. Wilde, K.S. Bradley, P.L. Gobby, R. Kirkwood, H.N. Kornblum, D.S. Montgomery and M.D. Wilke. Phys. Rev. **E 53**, 2747 (1996).
18. J.C. Fernandez, J.A. Cobble, B.H. Failor, D.F. DuBois, S.S. Montgomery, H.A. Rose, H.X. Vu, B.H. Wilde, M.D. Wilke and R.E. Chrien. Phys. Rev. Lett. **77**, 2702 (1996).
19. H.A. Rose. Phys. Plasmas **2**, 2216 (1995).
20. R.G. Watt, J. Cobble, D.F. DuBois, J.C. Fernandez, H.A. Rose, R.P. Drake and B.S. Bauer. Phys. Plasmas **3**, 1091 (1996).
21. B.H. Wilde, J.C. Fernandez, W.W. Hsing, J.A. Cobble, N.D. Delamater, B.H. Failor, W.J. Krauser and E.L. Lindman. Proc. 12th Int. Conf. on Laser Interaction and Related Plasma Phenomena **369**, 255 (AIP Press, 1996).
22. E.L. Lindman, N. Delamater, G. Magelssen and A. Hauer. Laser Interaction with Matter. Proc. 23rd European Conf. (IOP Press, 1995) p. 329.
23. N.D. Delamater, T.J. Murphy, A.A. Hauer, R.L. Kauffman, A.L. Richard, E.L. Lindman, G.R. Magelssen, B.H. Wilde, D.B. Harris, B.A. Failor, J. Wallace, L.V. Powers, S.M. Pollaine, L.J. Suter, R. Chrien, T.D. Shepard, H.A. Rose, E.A. Williams, M.B. Nelson, M.D. Cable, J.B. Moore and K. Gifford. Phys. Plasmas **3**, 2022 (1996).
24. N.D. Delamater, T.J. Murphy, A.A. Hauer, R.L. Kauffman, A.L. Richard, E.L. Lindman, G.R. Magelssen, B.H. Wilde, D.B. Harris, B.A. Failor, J. Wallace, L.V. Powers, S.M. Pollaine, L.J. Suter, R. Chrien, T.D. Shepard, H.A. Rose, E.A. Williams, M.B. Nelson, M.D. Cable, J.B. Moore and K. Gifford. Proc. 12th Int. Conf. on Laser Interaction and Related Plasma Phenomena **369** (AIP Press, 1996).
25. N.D. Delamater, G.R. Magelssen and A.A. Hauer. Phys. Rev. **E 53**, 5240 (1996).
26. A.A. Hauer, N.D. Delamater, E.L. Lindman, G.R. Magelssen, T.J. Murphy, H.A. Rose et al. Proc. 24th Eur. Conf. on Laser Interaction with Matter. Madrid, Spain, 1996.
27. A.A. Hauer, N.D. Delamater, D. Ress, W. Hsing, L. Suter, L. Powers, O. Landen, D. Harris, R. Thiessen, G. Magelssen, E. Lindman, D. Phillion, P. Amendt, R. Watt and B. Hammel. Rev. Sci. Instrum. **66**, 672 (1995).
28. A.A. Hauer, L. Suter, N. Delamater, D. Ress, L. Powers, G. Magelssen, D. Harris, O. Landen, E. Lindman, W. Hsing, D. Wilson, P. Amendt, R. Thiessen, R. Kopp, D. Phillion, B. Hammel, D. Baker, J. Wallace, R. Turner, M. Cray, R. Watt, J. Kilkenny and J. Mack. Phys. Plasmas **2**, 2488 (1995).
29. E.L. Lindman, G.R. Magelssen, S.M. Pollaine, L.V. Powers, N.D. Delamater, T.J. Murphy, B.H. Wilde, L.J. Suter, A.A. Hauer and R.L. Kauffman. Proc. 12th Int. Conf. on Laser Interaction and Related Plasma Phenomena **369**, 263 (AIP Press, 1996).

30. H.A. Rose. Phys. Plasmas **3**, 1709 (1996).
31. D.E. Hinkel, E.A. Williams and C.H. Still. Phys. Rev. Lett. **77**, 1298 (1996).
32. J.B. Beck, W.W. Hsing, N.M. Hoffman and C.K. Choi, Proc. 12th Int. Conf. on Laser Interaction and Related Plasma Phenomena **369**, 160 (AIP Press, 1996).
33. R.E. Chrien, C.W. Barnes, W.W. Hsing, G.T. Schappert, N.M. Hoffman, J.B. Beck, G.R. Magelssen and D.P. Smitherman. Proc. 24th Eur. Conf. on Laser Interaction with Matter, Madrid, Spain, 1996.
34. N.M. Hoffman, F.J. Swenson, W.S. Varnum, D.C. Wilson, C.W. Barnes, J.B. Beck, C.K. Choi, R.E. Chrien, W.W. Hsing, G.R. Magelssen, G.T. Schappert and D.P. Smitherman. Proc. 24th Eur. Conf. on Laser Interaction with Matter, Madrid, Spain, 1996.
35. W.W. Hsing, C.W. Barnes, J.B. Beck, N.M. Hoffman, D. Galmiche, A. Richard, J. Edwards, P. Graham, S. Rothman and B. Thomas. Phys. Plasmas **5**, 5 (1997).
36. W.W. Hsing and N.M. Hoffman. Phys. Rev. Lett., to be published (1997).
37. J.K. Hoffer. in Laser Plasma Interactions 5: Inertial Confinement Fusion, ed. M.B. Hooper (IOP Press, 1995) p. 209.
38. K. Hoffer, L.R. Foreman, J.J. Sanchez, E. Mapoles and J.D. Sheliak. To be published in Proc. 12th Topical Mtg. on Fusion Technology, Reno, NV (1996).
39. J.D. Sheliak, J.K. Hoffer, L.R. Foreman and E.R. Mapoles. Fus. Tech. **30**, 83 (1996).
40. E.R. Mapoles, J. Sater, J. Pipes and E. Monsler. Phys. Rev. **E 55**, 3473 (1997).

DISSIPATIVE PHENOMENA IN SHOCK WAVE IMPLOSION

F. Giammanco

Dipartimento di Fisica e Istituto di Fisica della Materia
Unità di Pisa, Università di Pisa
Piazza Torricelli 2,
56126 Pisa, Italy

ABSTRACT

In this work we analyze the influence of dissipative phenomena due to electron thermal diffusion and radiative losses which occur after collapse of implosive shock waves in a preformed plasma. Dissipative phenomena affect seriously the rate of nuclear yields when plasma parameters are close to ignition values unless alpha-particle heating is taken into account.

1. INTRODUCTION

The generation and propagation of shock waves in laser plasma interaction are of great importance in view of achieving plasma compression and heating comparable to those obtained in inertial confinement fusion [1-5]. Many experimental and numerical studies have been devoted to analyse diverging and converging shock waves in different geometries. The formation of shock wave during the plasma expansion process, in laser breakdown of gas, has opened up new regimes of state of matter where the equation of state of dense and hot material can be studied [6]. In this context, the interaction of spherical converging shock wave with the expanding plasma/diverging shock wave occupies a distinctive place due to its direct applicability in analysing the feasibility of the plasma fusion scheme "Spherical Pinch" [3], where a hot central plasma is confined and compressed by imploding shock wave.

In a previous paper [7], the attention was focused on the problem of plasma evolution in laser induced gas breakdown, the formation of diverging shock wave and, under appropriate conditions, their interaction with the converging shock wave. It was demonstrated that reflection of diverging shock wave by an implosive front leads to the compression of central plasma and enhancement of plasma temperature to very large values during the collapse phase of implosive piston. The generation of neutrons in these conditions was also studied and a scaling law for neutron generation in appropriate cases also derived. Particularly, the scheme based on a central shock wave reflected by a strong converging shock wave was compared with the usual scheme of pellet implosion. It was recognized that this scheme offers several advantages and seems to lower noticeably the ignition threshold. First of all, it makes it easier

Current Trends in International Fusion Research — Proceedings of the Second Symposium
Edited by E. Panarella. NRC Research Press, National Research Council of Canada, Ottawa, ON K1A 0R6, Canada. 1999.

to compress the central plasma because of the reduction of internal pressure due to the shock wave expansion. Moreover, the reflected shock wave provides a first heating and compression (by a factor of 10) of central plasma, before the final implosion takes place.

The motion of strong converging shock wave and diverging shock wave produced by energy deposition in the central plasma was analyzed in Ref. 7 by using an analytical hydrodynamic approach. We assumed that the converging shock wave is generated by the laser induced breakdown, or by discharge of capacitor banks as in Ref. 3, of a thin spherical shell, which propagates in a radially inward direction. During the converging motion, it meets the preformed central plasma or diverged shock wave detached from it. Therefore subsequent interaction physics depends on two different physical situations. In the first case, the converging shock wave has reached the vicinity of the cell well before the formation of the explosive shock wave and the central plasma is compressed if the pressure at the front of the converging shock wave is greater than the fireball pressure. This situation is of particular interest due to its applicability. Maximum central plasma compression obtainable is $(\gamma + 1)/(\gamma - 1)$, but the central plasma temperature may reach enormous values comparable to those obtained in inertial confinement scheme. This scheme is classified as "Spherical Pinch" [3]. Actually, experimental results of Ref. 3 showed that compression and heating of central plasma is greatly enhanced if the implosive shock wave meets the central explosive shock wave already formed, before the collapse takes place. Again similar to the preceding case, if the pressure at the converging front exceeds the pressure at the diverging shock front, the latter wave is reflected back and heats the central plasma, and may further lead to multiple reflections. Scaling laws carried out from the model in both cases show that the reflected shock front produced a noticeable pre-heating and compression of fireball and hence leads to a gain in efficiency of 2 or 3 orders of magnitude. Relevant neutron production occurs after the collapse of strong converging shock wave and the subsequent re-explosion. In Ref. 7, we considered cooling and expansion of central plasma behind the re-explosive front only due to the hydrodynamic expansion, neglecting dissipative phenomena due to electron thermal diffusion, and electron-ion thermal exchange, and radiative losses. In Ref. 9, these phenomena were analyzed in a similar case, i.e. a central plasma with uniform density and temperature at relatively low charge density (atmospheric density) and temperature of 10 keV. In these conditions, dissipative phenomena do not play a relevant role during the effective time when nuclear reactions take place. Nevertheless, for ignition experiments plasma density must be at least two orders of magnitude higher. It turns out that electron cooling might induce a faster decrease of ion temperature than that due to hydrodynamic expansion.

In the following, we analyze the role of electrons taking into account electron thermal diffusion and radiative losses. We assume that plasma density and temperature are uniform in a volume whose radius is initially the minimum radius reached during the collapse of implosive shock wave. Temperature and density are then determined according to Ref. 7 by an hydrodynamic model. Ion and electron density time evolution is due to fireball expansion. Actually, electrons are linked to ions because of the very short Debye length and thermal diffusion is due to the short-range electron-electron collisions so that it does not lead to an additional electron expansion compared with ion motion.

2. MODEL AND DISCUSSION

After the collapse, an explosive shock wave propagates outwards according to a second-kind self-similar motion [10], so that the shock front position is given by

$$R_s = R_{\mathrm{lim}}\left(1+\frac{V_o}{\alpha R_{\mathrm{lim}}}t\right)^{\alpha} \tag{1}$$

where R_{lim}, V_o and α are accordingly the minimum radius reached at the implosion, the shock explosive velocity immediately after the implosion and the exponent of self-similar motion, i.e. $\alpha = 0.687$ [1,10]. Behind the shock front, in the central part of plasma, i.e. the fireball, whose radius is R_{lim} after the implosion, density and temperature are almost constant because of ion thermal diffusion [7,9]. The time evolution of fireball radius is related to the shock front position by [7,9]

$$\mathcal{R}_f = \mathcal{R}_{\mathrm{lim}}\left(\frac{\mathcal{R}_s}{\mathcal{R}_{\mathrm{lim}}}\right)^{\frac{\varepsilon}{2(\varepsilon+3)}} \tag{2}$$

where $\varepsilon = \frac{2\frac{1-\alpha}{\alpha}}{\gamma-\frac{2}{3}\frac{1-\alpha}{\alpha}}$. The fireball plasma density is given by

$$\mathcal{N}_f = \mathcal{N}_o\left(\frac{\mathcal{R}_{\mathrm{lim}}}{\mathcal{R}_s}\right)^{\delta} \tag{3}$$

where $\delta = \frac{\varepsilon(\varepsilon+6)}{2(\varepsilon+3)}$ and N_o is the density at the first instant of re-explosion. The fireball temperature, neglecting dissipative phenomena, decrease due to hydrodynamic expansion according to equation

$$\mathcal{T}_{\mathrm{fhy}} = \mathcal{T}_o\left(\frac{\mathcal{R}_{\mathrm{lim}}}{\mathcal{R}_s}\right)^{\beta} \tag{4}$$

where $\beta = 2\frac{1-\alpha}{\alpha}\frac{\varepsilon(\varepsilon+6)}{2(\varepsilon+3)}$ and T_o is the temperature at the first instant of re-explosion.

In a pure hydrodynamic approach, also the electron temperature is assumed to evolve according to eq. 4. In this work, we assume an electron temperature evolution essentially due to thermal diffusion, radiative losses by recombination and bremssthralung, and electron-ion thermal exchange. Moreover, we neglect the influence of hydrodynamic motion on electron temperature. Actually, ion velocity decreases behind the shock front towards the center of fireball. On the other hand, electron temperature evolves according to eq. 4 when characteristic time constant of dissipative phenomena is longer than that due to hydrodynamic expansion.

When the thermal diffusion coefficient χ depends on temperature as in a plasma, i.e $\chi = \frac{aT_e^{5/2}}{N_e}$. with $a \sim 1.4\times10^{16}$ in electrostatic units (esu), the time-space profile of electron temperature is given by a self-similar thermal wave [10] in a spherical geometry, i.e.

$$\mathcal{T}_{\mathrm{eth}} = \mathcal{T}_C\left(1-\frac{r}{r_{\mathrm{th}}}\right)^{2/5} \tag{5}$$

r$_{th}$ represents the position of thermal front which in our case is $r_{th} = \mathcal{R}_f + \left(\frac{a\mathcal{T}_c^{5/2}}{\mathcal{N}_f}t\right)^{2/19}$. $\mathcal{T}_c$ is the central temperature of electrons given by the energy conservation, i.e., $\mathcal{T}_C = \mathcal{T}_f\left(\frac{\mathcal{R}_f}{r_{th}}\right)^3$. Eq. 5 requires a uniform plasma density and a negligible temperature beyond the thermal front compared with $\mathcal{T}_C$. Both conditions are fulfilled well in our scheme.

Eq. 5 shows that electron temperature has an almost flat profile except for $r \sim r_{th}$. It turns out that we can simplify the diffusion coefficient, in the equation of electron energy conservation, i.e.

$$\frac{1}{r^2}\frac{\partial}{\partial r}\left(r^2\frac{a\mathcal{T}_e^{5/2}}{\mathcal{N}_f}\frac{\partial \mathcal{T}_e}{\partial r}\right) = -\frac{12}{5}\frac{a\mathcal{T}_C^{7/12}}{\mathcal{N}_f r_{th}} \tag{6}$$

Eq. 6 holds true for $r = r_{th}$. Simplification of diffusion term allows us to carry out the electron temperature of center of fireball, i.e. the maximum temperature, by time integration of energy conservation equation for electrons. Then, during the re-explosive phase, the electron temperature is solution to the equation

$$\frac{d\mathcal{T}_e}{dt} = -\frac{12}{a}\frac{a\mathcal{T}_e^{7/12}\mathcal{R}_f^{21/2}}{\mathcal{N}_f r_{th}^5} - \frac{\mathcal{N}_f}{k_B}\left(\frac{\mathcal{D}_{ric}}{\mathcal{T}_e^{1/2}} + \mathcal{D}_B\mathcal{T}_e^{1/2}\right) - \frac{\mathcal{T}_e - \mathcal{T}_i}{\tau_{ei}} \tag{7}$$

The electron-ion thermalization time is $\frac{1}{\tau_{ei}} = \frac{\beta\mathcal{N}_f}{\mathcal{T}_e^{3/2}}$ where β ~ 3 × 10^{-7} in esu. k_B is the Boltzmann constant. As an effect of thermal exchange the ion temperature decreases according to

$$\frac{d\mathcal{T}_i}{dt} = \frac{\mathcal{T}_e - \mathcal{T}_i}{\tau_{ei}} \tag{8}$$

Actually, ion temperature decreases also because of hydrodynamic expansion according to Eq. 4. Nevertheless, in this approach we assume that decrease due to hydrodynamic expansion occurs at a slower rate. On the other hand, when Eq. 4 decreases faster than Eq. 8 dissipative phenomena do not play a relevant role.

Larger number of nuclear reactions occurs during the re-explosive phase just after the collapse of converging shock wave. Moreover, we assume that the main contribution to the generation of neutrons comes from the central fireball, where T and N can be assumed spatially uniform. Then, neutron yields are given by

$$\mathcal{N}_n = \frac{4\pi}{3}a\int_0^\infty \mathcal{R}_f^3\mathcal{N}_f^2\frac{\exp\left(-b/\mathcal{T}_f^{1/3}\right)}{\mathcal{T}_f^{2/3}}dt \tag{9}$$

a and b are coefficients of cross section of nuclear reaction. For a D+T mixture a ~10^{-7} (esu) and $b \sim 4.3 \times 10^3$ (esu). In the case of pure hydrodynamic expansion, T_f is given by Eq. 4 while by solution of system of Eqs. 7 and 8 when dissipative phenomena are taken into account.

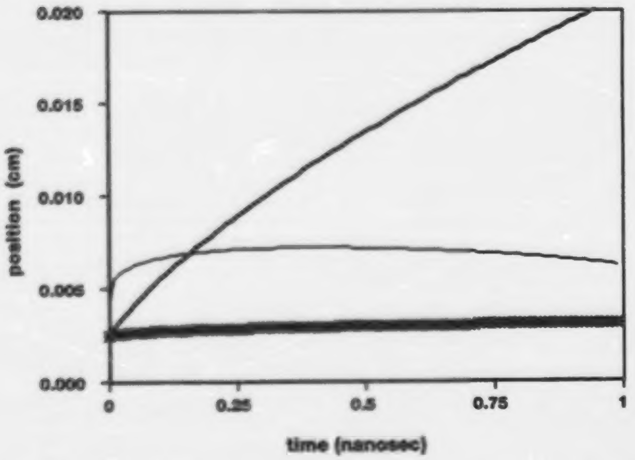

Figure 1. Time evolution of re-explosive shock front (thick line), thermal front (thin line) and fireball front (line with stars).

First, we test the influence of dissipative phenomena in the case of experimental results given in Ref. 3. Central and peripheral shock waves are produced by capacitor bank discharges whose duration overcomes typical laser pulse duration. The central plasma energy 30 J is deposited in a sphere of radius $R_0 = 2$ cm filled with deuterium at 8.2 atm. An energy of 1 kJ is deposited at the periphery of the gas. The imploding shock wave meets the central plasma after about 0.8 μs. During the collapse, about 10^7 neutrons were emitted by central plasma, whose maximum temperature was ~ 0.7 KeV. Central plasma time evolution was measured by

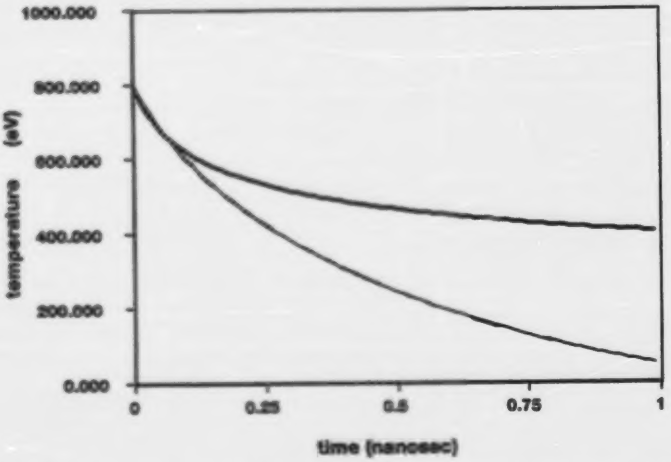

Figure 2. Time evolution of ion and electron temperature in the presence of dissipative phenomena (thin lines) and for hydrodynamic expansion (thick line).

recording the plasma luminosity with an image converter camera. After collapse, the luminous front of central plasma had a rather constant radius of about 8×10^{-2} cm for about 5 μs. An average density of about 3×10^{19} ions/cm^3 was carried out from total emitted neutrons, and measured temperature, volume, and confinement time of central plasma. At the collapse, temperature and density reach the values of 0.8 keV and 10^3 Atm, respectively, for a minimum radius $R_{LM} = 2.5 \times 10^{-3}$ cm. After the collapse, central plasma is quite stable for about 3 μs neglecting effects due to further implosions.

Figure 1 shows the time evolution of re-explosive shock front (thick line), thermal front (thin line) and fireball front (line with stars).

Figure 2 shows the time evolution of ion and electron temperature in the presence of dissipative phenomena. In this case, both temperature overlap (thin lines). Thick line is the time evolution for pure hydrodynamic expansion.

In the experiment of Ref. 3, nuclear yields are barely affected by thermal diffusion in spite of temperature decreases faster. However, relevant number of fusion reactions occurs during about 0.1 ns (see Fig. 3) where dissipative phenomena play a negligible role (Fig. 2).

According to the numerical example of Ref. 7, we apply the model to investigate the role of dissipative phenomena under conditions which would lead to break-even following the hydrodynamic approach. In this case, an energy of 300 kJ is assumed to be deposited in 0.5 μs at the periphery of a sphere of radius $R_0 = 2$ cm, filled by deuterium-tritium at 700 atm. An energy of 300 J is absorbed by central plasma in 0.1 μs. Data correspond to a simulation performed by using scaling laws given in Ref. 11. During the collapse, the maximum density and temperature are 8×10^5 atm and 7 keV, respectively. The expected total neutron number from simulation of Ref. 11 is $N_n = 10^{16}$. The following figures show the time evolution of relevant parameters.

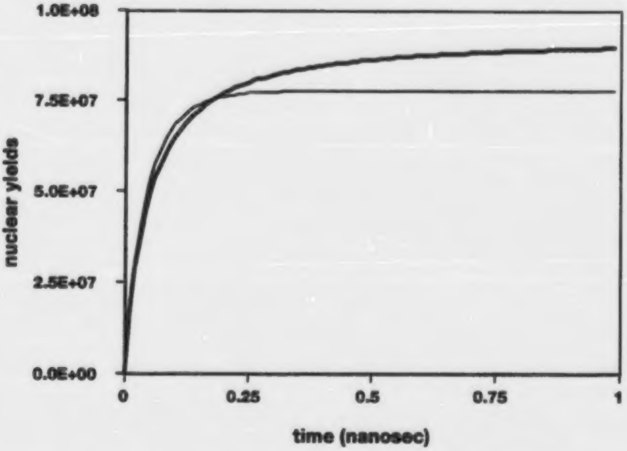

Figure 3. Shows the nuclear yields. Thick line-hydrodynamic motion. Thin line-dissipative phenomena.

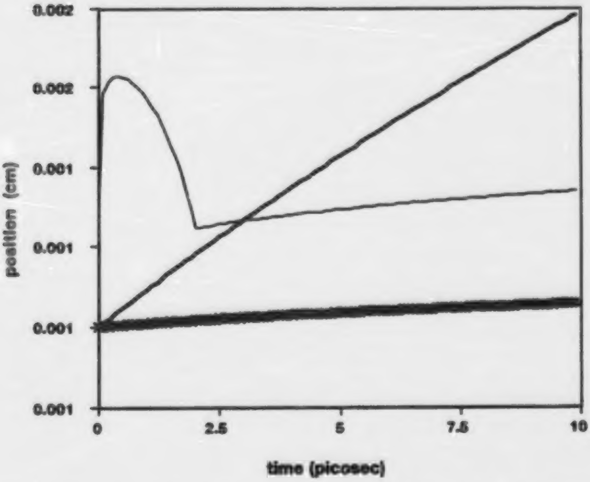

Figure 4. Time evolution of re-explosive shock front (thick line), thermal front (thin line) and fireball front (line with stars).

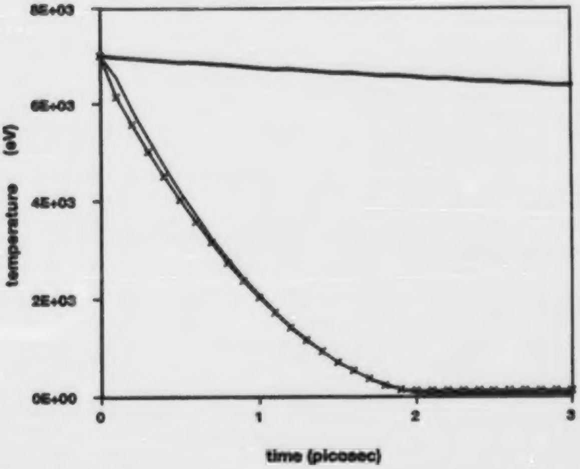

Figure 5. Time evolution of ion and electron temperature in the presence of dissipative phenomena - Ion temperature-thin line. Electron temperature-thin line with stars. Ion temperature from hydrodynamic expansion-thick line.

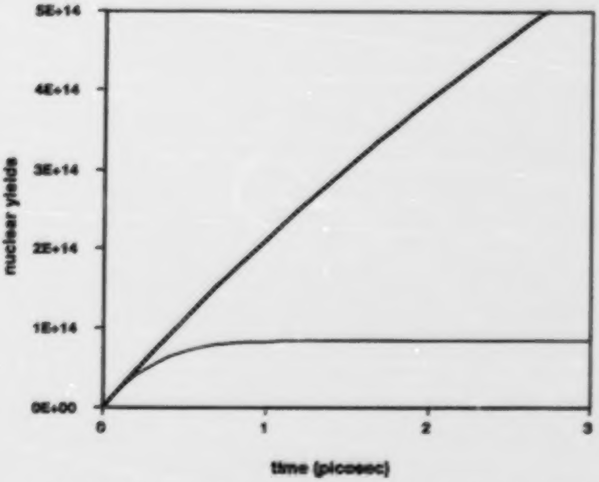

Figure 6. Nuclear yields. Thick line-hydrodynamic motion. Thin line-dissipative phenomena.

Figure 6 shows that dissipative phenomena, mainly due to radiation losses, strongly affect the rate of nuclear reactions. In the hydrodynamic model, nuclear reaction are effective along about 300 ps leading to a final value of 4 × 10^{15} which is in a good agreement with computer simulation. Nevertheless, once losses are included, nuclear yields jump to a value of 8 × 10^{13} since the effective time is less than 1 ps (Fig. 6). The product of fireball density (Eq. 3) times the time (Fig. 7) fulfils the Lawson criterium 5 picoseconds after the re-explosion takes place.

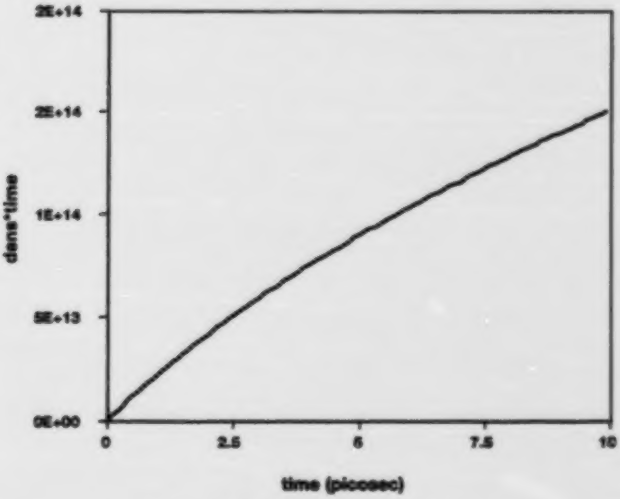

Figure 7. Fireball density times time.

Figure 5 shows that plasma temperature is high enough to maintain nuclear reactions for less than 1 picosecond because of overall losses.

From the above discussion, it turns out that a simple hydrodynamic approach, although useful to carry out scaling laws, gives an overestimation of nuclear yields. Nuclear yields scale approximately linearly with the time in which ion temperature is high enough to sustain nuclear reactions. In spite of the disruptive effects of dissipative phenomena, we stress that model does not include alpha-particle trapping. Alpha particles produced by nuclear reactions could provide, in case of efficient trapping, an additional source of energy which prevent ion temperature from strong cooling. Actually, in the previous example, although partially trapped, energy released by alpha particles could compete with fireball cooling.

REFERENCES

1. Y. Fujimoto and E.A. Mishikin. Phys. Fluids **21**, 1933 (1978).
2. J. Nuckolls, L.Wood, A. Thiessen and G. Zimmermann. Nature **239**, 139 (1972).
3. E. Panarella. J. Fusion Energy **6**, 285 (1987) and references therein.
4. M.A. Harith, V. Palleschi, D.P. Singh, G. Tropiano and M. Vaselli. Optics Communications **71**, 76 (1989).
5. B. Ahlborn and M.H. Key. Plasma Physics **23**, 435 (1981); B. Ahlborn, M.H. Key and A.R. Bell. Phys. Fluids **25**, 541 (1982).
6. D. Salzmann, S. Eliezer, A. D. Krumbein and L. Gitter. Phys. Rev. **A 28**, 1738 (1983).
7. F. Giammanco, S. Del Tredici, D.P. Singh, M. Vaselli. Fusion Tech. **27**, 221 (1995).
8. G. Einaudi, F. Giammanco, A. Giulietti and M. Vaselli. Il Nuovo Cimento, **51B**, 280 (1979).
9. F. Giammanco. Il Nuovo Cimento, **54B**, 297 (1979).
10. Ya.B. Zel'dovich and Yu.P. Raizer. Physics of Shock Waves and High Temperature Hydrodynamic Phenomena. Academic Press, New York (1966).
11. E. Panarella Ed. Current Trends in International Fusion Research. Plenum Press, New York (1997), p. 67.

THE SPHERICAL PINCH AS A RADIATION SOURCE FOR EUV LITHOGRAPHY

J. Zhao and E. Panarella

Advanced Laser and Fusion Technology, Inc. (ALFT)
189 Deveault St. Unit No. 7
Hull, PQ J8Z 1S7, Canada

ABSTRACT

The prospects for plasma radiation sources to be used in the next generation lithography (NGL) is appealing. Among a few candidate lithography systems, extremely ultraviolet lithography (EUVL) is considered a promising one. The stringent requirements by EUVL for radiation sources present, however, great challenges. In this paper we demonstrate a pinched plasma system, the SPX IV system, which has characteristic features that satisfy the basic requirements for EUVL. The machine converts 20% of stored electric energy into plasma energy. The diagnostics of the radiation generated were carried out by dosimetry measurements using radiachromic films. The results show that the system can deliver about 80 joules of radiation energy per pulse in a narrow bandwidth in the EUV region. Since the machine can be pulsed at 1 Hz, this means that 80 watts of EUV radiation is available for lithography. The center of the photon energy distribution is around 100 eV or 13 nm.

1. INTRODUCTION

The field of plasma physics is a mature one, its history dating back to the end of last century. More specifically, interest in ionized gases began in the late nineteenth century with experiments on gas discharges. Later, the term "plasma" was introduced by Langmuir in the 1920s. Between 1925 and 1927, Appleton and coworkers discovered the existence of electrically conducting layers known as the ionosphere. Appleton himself played a major role in developing a theory of wave propagation in cold plasmas to explain the reflection and refraction of radio waves in the ionosphere which were vital for long distance radio transmission. Since most matter outside the lower layers of the Earth's atmosphere is ionized, a major impetus for the development of plasma physics came from space scientists studying a variety of phenomena such as aurora, ionosphere, Van Allen belt, the corona of the sun, pulsars, etc. [1,2] In recent times, another major stimulus came from research in controlled thermonuclear fusion for energy production. This research, which started at the beginning of the 50s, came soon to the realization that energy generation from fusion would materialize

Current Trends in International Fusion Research — Proceedings of the Second Symposium
Edited by E. Panarella. NRC Research Press, National Research Council of Canada, Ottawa, ON K1A 0R6, Canada. 1999.

only after long and fundamental research was done on the heating and confinement of a plasma. A few key concepts such as magnetic confinement fusion (MCF) [3,4] and inertial confinement fusion (ICF) [5,6] have since emerged in which significant progress has been made in plasma research towards a practical fusion reactor.

The study of plasmas requires diagnostics possibly with non-perturbing tools. The most natural of these tools is provided by the plasma itself because it emits copious radiation. Hence, the study of radiation emission from plasmas is a favored diagnostic. On the other hand, although the main effort in fusion research is to minimize radiation losses because of their cooling effect on the plasma, one finds that the same radiation from a plasma can be put to advantageous industrial use. As a consequence, there has been recently a trend towards shifting emphasis from the study of plasma for fusion research to other areas of plasma industrial applications, such as plasmas as neutron sources, or X-ray and EUV generators. Interestingly, the theoretical analysis has shown that more than 90% of the plasma energy can be converted into radiation energy [7]. Since for most laboratory generated plasmas the energy deposited in the plasma is electrical energy, if the conversion of this energy into plasma energy is achieved with a sufficiently high efficiency, then indeed a plasma device can be a powerful radiation source.

One of the potential industrial applications of plasma radiation sources is microlithography. Lithography has become increasingly important as a key driver for the microelectronics industry. The realization that optical lithography is being pushed to its threshold limits of imaging has demanded new means to achieve enhanced circuit miniaturization. A major industrial direction has been focused on the next generation lithography (NGL) to manufacture sub 130 nm features. A brief review on the current status of the lithography industry and its trend will be given in the next section. Among a few potential candidates, extreme ultraviolet lithography (EUVL) is a promising one. The EUV lithography system is made up, as usual, of the following components: wafers, mask, projection tools, stepper and radiation source. We are concerned in this paper with the radiation source, which is a plasma source. There are many plasma radiation sources depending on the mechanism of plasma formation [8]. The spherical pinch system SPX IV developed at ALFT (Advanced Laser and Fusion Technology) has demonstrated characteristic features that satisfy most of the requirements for EUVL. Motivated initially by fusion research, the SPX machine has a high efficiency of plasma compression and is capable of generating a spot of hot plasma [9,10]. The system has evolved into an industrial prototype machine for X-rays and EUV generation [7,11,12]. With recent modifications, the machine has been configured as a EUV radiation source.

In the following sections, we will give a brief review of the current status of microlithography, describe in detail the experiments we carried out on our SPX IV system, and present results on spectral and radiation intensity diagnostics.

2. MICROLITHOGRAPHY

Microlithography has become an increasingly important key driver for the microelectronics industry. The explosive growth of the semiconductor industry over the last two decades is the result of the industry ability to increase the density of circuits at a faster rate than the cost to fabricate smaller, faster, and more reliable circuit elements. On the other hand, the lithography industry has been coming to the realization that the current optical technology is being pushed to its threshold limits of imaging. The 193 nm DUV lithography technology is believed to be able to manufacture down to a limit of 130 nm critical dimension (CD) features. Although there exists two further optical extensions at 157 nm and 126 nm, there is the concern that any gain will only provide "one generation node". A major industry effort has therefore been directed towards the next generation of lithography (NGL) to support manufacturing of sub 130 nm technologies whose capability would span several generation nodes down to linewidths as small as 30 nm. Possible next generation lithography alternatives are: proximity X-ray (1X X-ray, synchrotron), e-beam direct write (EBDW), ion projection lithography (IPL), projection e-beam (SCAPEL), and extreme ultraviolet lithography (EUVL). The latter has several advantages over other candidate techniques. Among them, EUVL is based on the optical experience and does not require central facilities such as a synchrotron. The essential requirements for a EUV radiation source are: sufficient radiation energy flux, proper spectral range and proper spatial dimensions. According to a white paper produced by Charles Gwyn et al. from Extremely Ultraviolet Limited Liability Company, [13] a point-like plasma source with radiation power output of 30–40 W centered at 13 nm (~100 eV) is required for EUVL applications. Since EUV radiation is absorbed by most materials, reflective optics at EUV wavelength is necessary. Multi-layer condenser mirrors are therefore used to filter and direct the desired wavelength to the optical mirror train down to the wafer. A common property of plasma EUV sources (either produced by laser or by spark discharges) is the high number of particulates generated which will deposit onto the mirrors causing the system to deteriorate over time. Thus a debris-free plasma source is highly desirable to eliminate the need for precision cleaning of condenser mirrors.

Recently, substantial progress has been made in all technical areas of EUVL. Reflective optics using multilayer coating with >67% reflectivity has been achieved. Photoresists used by 193 nm are extendible to EUV wavelengths and high sensitivity resists (13 mJ/cm^2) already exist. Development of a point-like plasma source with sufficient radiation power (30–40 W output), centered at 13 nm (~100 eV peak temperature) remains a key point for the success of EUVL. Laser produced plasma based on gas jets provides a debris-free EUV source [14]. However, the efficiency of converting laser power to EUV radiation power is only about 0.1. The spherical pinch system SPX IV developed at ALFT has the characteristic features that satisfy most of the requirements of EUVL. It delivers about 80 joules of radiation energy per pulse, in a narrow band centered at 10–13 nm. This is equivalent to 80 watts of radiation power when the machine is operated at the repetition rate of 1 Hz.

3. EXPERIMENTAL

3.1 Experimental Setup

The SPX system operates on the principle of inductive electrical discharge (inductive pinch). The energy storage system for the SPX IV consists of five capacitors which retain 30 kJ of electrical energy when charged to 30 kV. Normally, for fusion research, the SPX has been operated with a spherical inductance [9]. However, it was found convenient in our case to use a cylindrical, rather than spherical pinch coil (theta pinch) for the following reasons. Firstly, for EUV generation, only a moderately hot plasma ($T \sim 100$ eV) is required and the theta pinch is sufficient for compressing the plasma to such a temperature. Secondly, EUV is absorbed by most materials, and requires a vacuum system in order to be transported to the target. A cylindrical geometry offers an easier way than the spherical to create such a vacuum system. Thirdly, with a cylindrical geometry it is possible to obtain more efficient preionization in the center of the pinch through an inductive discharge.

The SPX IV machine can be operated in single discharge mode or in the automatic mode. In the latter mode, a repetition rate of 1 Hz is achieved at full charging voltage.

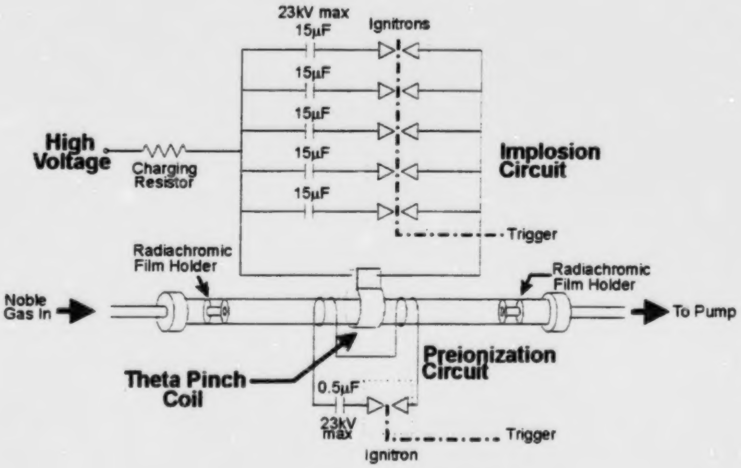
23kV max
15μF
Ignitrons
15μF
15μF
High Voltage
Charging Resistor
15μF
Implosion Circuit
15μF
Trigger
Radiachromic Film Holder
Radiachromic Film Holder
Noble Gas In
To Pump
Preionization Circuit
Theta Pinch Coil
0.5μF
23kV max
Trigger
Ignitron

Figure 1. Schematic of the SPX IV experimental apparatus.

A schematic diagram showing the experimental apparatus is given in Fig. 1. A single turn pinch coil is wrapped around a glass tube where constant gas flow is maintained with the gas pressure normally well below 1 Torr. A preionization circuit using an inductive electrical discharge provides sufficient ionization of the gas to facilitate the deposition of the main implosion energy. For this purpose a separate capacitor is used to store 132 J (at a charging voltage of 23 kV) of energy which is discharged through two inductive coils connected in series on both sides of the pinch coil. Thus, a uniform gas preionization is obtained in the center of the pinch, before the energy in the main condenser bank is discharged. The spectrum and the intensity of the preionization plasma were carefully analyzed in order to determine the time of maximum preionization. This is the time when the strong implosion phase was initiated. Different noble gases, such as Ne, Ar, Kr and Xe, have been used in the experiments. The machine was operated mainly at its lower limits (15–18 kV) of voltage levels.

The diagnostic of the radiation consisted mainly of integrated dose measurements done with calibrated radiachromic film whose exposure was filtered by the gas itself, as described in the next section.

4. RESULTS AND DISCUSSION

Various measurements have been carried out on the SPX IV. They are described as follows.

4.1 Energy Transfer Efficiency Measurement

The knowledge of the efficiency of converting electrical energy into plasma energy is of great importance in understanding the physical processes in the plasma. It offers valuable information for system improvement. For a plasma created by electromagnetic inductance (or *RCL* discharge), Makomaski et al. [15] have proposed that the plasma be considered as a secondary circuit, the primary circuit of such transformer being the pinch coil itself. With the approximation that the discharge oscillation frequency is much higher than the decay rate of the current amplitude, they have been able to derive a simple expression for the instantaneous amount of energy deposited in the plasma as a function of the total stored electrical energy:

$$E(t) = \frac{1}{2} C V_o^2 \left(1 - \frac{\alpha_o}{\alpha}\right)\left(1 - e^{-2\alpha t}\right) \qquad (1)$$

where C is the total capacitance of the condenser bank, V_o is the charging voltage, and α, α_o are respectively the damping coefficients corresponding to the discharges with and without plasma. Therefore the only parameters required to determine the energy transfer efficiency are the two damping coefficients.

A procedure based on the method reported in Ref. 15 has been developed to determine the energy transfer efficiency. The discharge currents were recorded when the plasma was induced in the system and when it was not. The discharge without plasma was obtained by keeping all experimental conditions identical except filling the vessel with air at atmospheric pressure. At this pressure, inductive breakdown of the gas does not occur. The damping coefficients, together with other system parameters, were then obtained by fitting the experimental discharge data to a curve using non-linear least square method. Figure 2 shows the running efficiency calculated using Eq. (1). Also shown in Fig. 2 are the two curves of discharge currents. When operating at 22 kV, the SPX IV system has an energy transfer efficiency of 20% in one discharge cycle.

4.2 Radiation Diagnostics

The radiation output from the SPX IV was characterized by dosimetry and spectral analysis. A radiachromic film manufactured by Far West Technology Inc. was used for the

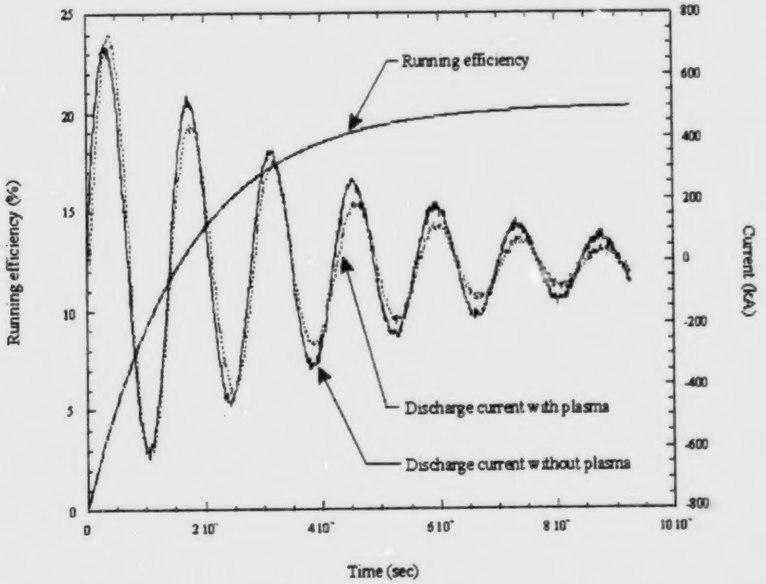

Figure 2. Running energy transfer efficiency, namely the instantaneous percentage of the total energy stored in the condenser bank that has been deposited into plasma. For comparison, the discharge currents with and without plasma are also shown.

diagnostics. This film has photosensitivity similar to that of the photoresist used in the lithography industry. It has an energy independent response to photons with wavelengths shorter than 345 nm (UV) and has very low response to visible light. The optical density O.D. is related directly to the transmission of the irradiated film, T, as follows:

$$\text{O.D.} = \text{Log}_{10}(1/T) \qquad (2)$$

Calibration with X-rays dosimetry shows that a unit of optical density change corresponds to ~125 mJ/cm^2 of incident radiation [16]. Since the SPX IV is a broadband radiation source, various filters including quartz, thin mylar, beryllium and aluminum foils were used for spectral band identification. These filters have known transmission characteristics in the relevant energy range. The transmission of inert gases at given pressures and path lengths were calculated using the absorption data available in the available literature [17]. A comparative method was used to identify the main distribution of the radiation. As mentioned earlier, the SPX machine is a broadband radiation source, ranging from UV, EUV into the tail of soft X-rays. Two cameras loaded with radiachromic films were positioned on each side of the pinch coil at equal distance from it. A quartz filter was used in one of the cameras. In the other camera the film was unfiltered. The optical densities (hence the total radiation energy) with and without quartz filter were compared and the difference gave an indication of the radiation energy beyond UV (i.e. wavelength shorter than 120 nm). It was found that under the operation conditions described above, a small fraction of the total radiation is in the visible/UV region. This small contribution was subtracted from the total measured optical density. Beryllium and mylar filters were then used to make measurements of the X-ray ($E \geq$ 1 keV) content. It was found that it is very small. Thus, most of the radiation energy must fall in the EUV region. Over the EUV range, i.e., at peak wavelength ~13 nm and narrow bandwidth around the peak, the radiation energy output was estimated to be about 80 J per pulse. The total radiation energy contained between 120 nm and 10 nm is about 800 J in one pulse of machine operation.

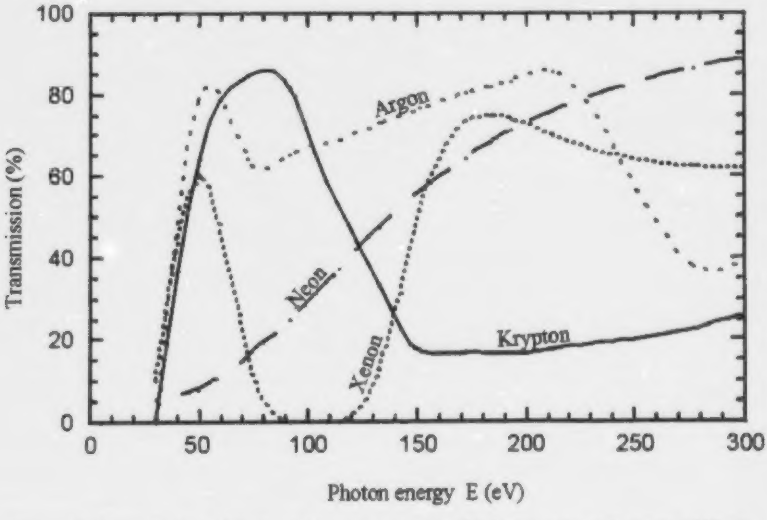

Figure 3. Transmissions of the inert gases at a pressure of 0.5 Torr and a path length of 27 cm.

4.3 Temperature Measurement

The attempt to determine the plasma temperature or the peak radiation energy has been based on the assumption that the radiation is of pure bremsstrahlung origin, which is a reasonable assumption. If line emissions are present, this assumption generally results in a lower value of the plasma temperature. The transmission of noble gases was calculated using the published absorption data [17]. Figure 3 shows the transmissions of various inert gases at a pressure of 0.5 Torr and a path length of 27 cm. The actual absorption attenuation over 27 cm at the same gas pressure was also determined experimentally. This was carried out using a dual channel method. Two film cameras were positioned on each side of the pinch coil at the distances of 27 cm and 54 cm, respectively. The ratio of the measured intensities at 54 cm and 27 cm represents the total transmission of the radiation over a distance of 27 cm, as the following calculations show:

$$I(27\text{cm}) = I_0 e^{-\gamma 27}$$
$$I(54\text{cm}) = I_0 e^{-\gamma 54}$$

$$\frac{e^{-\gamma 54}}{e^{-\gamma 27}} = e^{-\gamma 27} = \frac{I(27\text{cm})}{I_0} = T(27)$$

where I_0 is the intensity of the plasma radiation source, and I(27cm), I(54cm) are the intensities at 27 and 54 cm, respectively, γ is the transmission coefficient through the gas and T(27cm) is the transmission at 27 cm. By comparing this value with the calculated transmission curve and assuming that the transmission at the peak temperature dominates the overall transmission, then the position of this peak was determined. Of course, this approach is approximate. It is also based on the assumption that the gas, except at the center of the

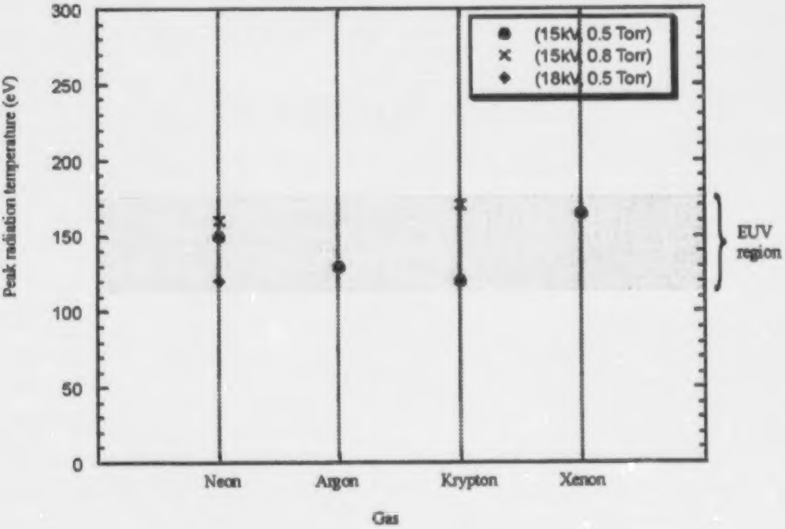

Figure 4. Peak radiation temperature from SPX for various gases and charging voltages. The radiation peak fall in the EUV region (~150 ev).

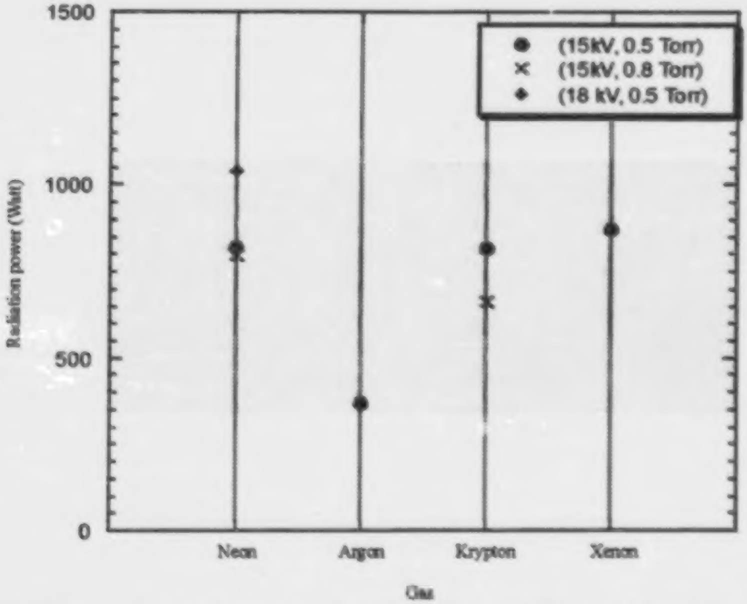

Figure 5. Integrated radiation power from SPX for different gases and charging voltages, when the machine is operated at 1 Hz.

pinch, is neutral. There is always a certain degree of ionization of the gas when radiation passes through. The above approximations will generally result in a lower estimate of the plasma temperature and the radiation flux. Fig. 4 shows the results of the temperature measurements. Fig. 5 shows the results of the power measurements. Table 1 summarizes the results.

Further improvements of the SPX machine have been planned. Efforts will be made to increase the energy transfer efficiency from condenser bank to plasma. Due to the nature of the pinched plasma there will be fluctuations between shots. Therefore a relatively low dose per pulse at a relatively high repetition rate are future objectives aimed at gaining better control over the exposure dosage of wafers.

Table 1. Diagnostic results of the EUV radiation from SPX IV system.

Voltage (kV)	Gas	Pressure (Torr)	Total energy per pulse (J)	Peak position (eV)
15	Ne	0.5	820	150
15	Ne	0.8	795	160
18	Ne	0.5	1041	120
15	Ar	0.5	370	130
15	Kr	0.5	817	120
15	Kr	0.8	660	170
15	Xe	0.5	870	165

5. CONCLUSIONS

The SPX IV system has demonstrated great potential as a simple, compact and powerful EUV radiation source. An energy transfer efficiency of 20% has been achieved to convert electrical energy into plasma energy. The radiation output in a narrow band in the EUV region has been estimated to be about 80 joules per pulse from the more than 800 joules of total energy in the extended EUV region, equivalent to 80 W of power when the SPX IV is operated at a repetition rate of 1 Hz. The center of the EUV photon energy distribution is around 100 eV (or ~ 13 nm).

ACKNOWLEDGMENTS

Albert Phillippe, Steve Drew, and Andrew McLellan have participated in this work, and their technical contribution is appreciated and acknowledged.

REFERENCES

1. E.N. Parker. Cosmetic Magnetic Fields. Clarendon Press, Oxford (1979).
2. E.R. Priest. Solar Magnetohydrodynamics. Cambridge University Press (1982).
3. J.G. Cordy, R.J. Goldston and R.R. Parker. Phys. Today (January 1992).
4. K. Miyamoto. Plasma Physics for Nuclear Fusion. MIT Press, Cambridge (1980).
5. J.D. Lindl, R.L. McCrory and E.M. Campbell. Phys. Today (September 1992).
6. W.L. Kruer. Laser-plasma Coupling. Chapter 5 of Proceedings of the IEEE Mini-course on Inertial Confinement Fusion, edited by G.H. Miley. University of Illinois Fusion Studies Laboratory (1980).
7. P. Savic and E. Panarella. Jour. of Appl. Phys. **59**, 3990 (1986).
8. Juan R. Maldonado. SPIE **2523**, 2 (1995).
9. E. Panarella. Jour. of Fusion Energy **6**, 285 (1987).
10. H.B. Chen, J. Chen, B. Hilko and E. Panarella. Jour. of Fusion Energy **13**, 45 (1994).
11. S. Aithal, K. Kawai, L. Lamari and E. Panarella. SPIE **1671**, 383 (1992).
12. L. Zhang, E. Panarella, B. Hilko and H. Chen. SPIE **2437**, 356 (1994).
13. Charles Gwyn et al. A White Paper, Extremely Ultraviolet Limited Liability Company (EUV LLC), Livermore, California, September (1997).
14. Kubiak et al. OSA TOPS on EUV **4**, 66 (1996).
15. H. Makomaski, E. Panarella and P. Savic. C.A.S.I. Transactions **3**, 95 (1970).
16. J.R. Maldonado, A. Reisman, H. Lezec, B. Bumble, C.K. Williams and S.S. Iyer. J. Vac. Sci. Technol. **B5** (1), 248 (1987).
17. B.L. Henke, P. Lee, T.J. Tanaka, R.L. Shimabukuro and B.K. Fujikawa. Atomic Data and Nuclear Data Tables **27**, 1 (1982).

MAGNETIZED TARGET FUSION IN A SPHEROIDAL GEOMETRY WITH STANDOFF DRIVERS

Y.C.F. Thio*, E. Panarella[1], R.C. Kirkpatrick[2], C.E. Knapp[2], F. Wysocki[2],
P. Parks[3] and G. Schmidt[4]

CSPAR
University of Alabama
Huntsville, Alabama, 35899, U.S.A.
[1] Advanced Laser & Fusion Technology
189 Deveault St., Unit No. 7
Hull, P.Q., J8Z 1S7, Canada
[2] Los Alamos National Laboratory
Los Alamos, New Mexico, 87544, U.S.A.
[3] General Atomic, Inc.
P.O. Box 85608, MS15-114H
San Diego, California, 92186-5608, U.S.A.
[4] NASA Marshall Space Flight Center
Huntsville, Alabama, 35899, U.S.A.

ABSTRACT

An embodiment of magnetized target fusion (MTF) with the potential that the drivers can be positioned in a standoff distance from the site of the fusion burn is proposed. The magnetized target plasma is formed out of two merging compact toroids, and is imploded by a spherical plasma liner formed out of the merging of a number (nominally 60) of high momentum density plasma jets. These plasma jets are produced by highly efficient electromagnetic accelerators. They also carry the main fusion fuel. The implosion dynamics is studied in three phases: the preliminary shock heating and compression, the acoustic compression, and the containment of the burning target and liner. Mathematical models are developed to model these three phases of the implosion dynamics, and have been implemented in a suite of computer codes. Preliminary results produced by the models have been very encouraging, showing the great potential of the proposed MTF scheme. The scheme has a low energy threshold for economic breakeven, and has the potential of high wall-plug energy gain of more than 50 or so. Moreover, the pulsed power drivers are very modest and can be accommodated with current state of the art and existing facilities. The embodiment thus potentially provides a low-cost and fast R&D path towards demonstrating practical fusion energy and followed-on commercialization.

Current Trends in International Fusion Research — Proceedings of the Second Symposium
Edited by E. Panarella. NRC Research Press, National Research Council of Canada, Ottawa, ON K1A 0R6, Canada. 1999.

1. INTRODUCTION

In magnetized target fusion (MTF), an imploding material liner is used to compress a magnetized plasma to fusion condition and to confine the resulting burning plasma inertially to obtain the necessary energy gain. By choosing a physics and engineering regime intermediate between the two extremes of conventional magnetic confinement fusion (MFE) and inertia confinement fusion (ICF), MTF seeks to avoid the physics and engineering problems of these two conventional approaches to fusion.

Specifically, the density regime and time scale of MTF is intermediate between MFE and ICF. This regime is important for three reasons. (1) Fusion reactivity scales as density squared, which is increased by many orders of magnitude over conventional MFE. (2) All characteristic plasma scale-lengths decrease with density. Hence, system size is naturally reduced at high density. (3) The presence of the magnetic field in the target plasma greatly slows down the thermal conduction losses to the material liner, thus allowing relatively slow compression to be used with liner produced by highly efficient electromagnetic drivers. It reduces the required power and precision to compress and heat plasma to fusion-relevant conditions compared with ICF, and brings the pulsed-power requirements within reach of current state of the art. For these reasons, MTF promises to be a low-cost approach to fusion [1,2,3].

Solid liners have been proposed for compressing the target for MTF, especially for a near-term demonstration of the scientific principles of MTF. One frequent criticism of solid-liner driven MTF relates to its reactor potential. Though reactor scenarios have been proposed for solid-liner driven MTF, critics of MTF have pointed out three potential practical difficulties with solid-liner driven MTF. Firstly, the drivers for imploding the liner need to have sufficient stand-off distance from the point of the fusion combustion for the hardware to be re-usable, and this might be difficult to achieve in the case of solid liners. Secondly, the cost of manufacturing the solid liner tends to drive the economic breakeven energy level into the multi-gigajoule range, thus increasing the initial capital cost of the power plant. Thirdly, the solid debris from the liner might present a problem to the first wall of the reactor.

This paper is a response to these criticisms of MTF, by proposing an embodiment of MTF that will avoid all these difficulties. In the proposed embodiment, a gaseous (plasma) liner is used instead, and is formed in a standoff manner. It has a low energy threshold for economic breakeven, and has the potential of high wall-plug energy gain of more than 50 or so. Moreover, the pulsed power drivers are very modest and can be accommodated with current state of the art and existing facilities. The embodiment thus potentially provides a low-cost and fast R&D path towards demonstrating practical fusion energy and followed-on commercialization.

2. THE PROPOSED APPROACH

Figure 1 illustrates the scheme. Two compact toroids containing fusionable materials are introduced into a spherical reactor vessel (typically about 2 m or more in radius) in a diametrically opposing manner [4,5]. Embedded in the compact toroids are magnetic fields in force-free Woltjer-Wells-Taylor's state of minimum energy [6] which are known experimentally to be extraordinarily stable. They collide in the center to form an initial magnetized plasma. A spherical distribution of plasma jets are then launched from the periphery of the vessel, coalescing to form a spherically converging plasma liner. On impact with the central plasma, the plasma liner sends a shock wave through it, shock heating it to some elevated temperature (above a few hundreds eV). The high temperature immediately raises the electrical conductivity of the plasma to the extent that it traps the magnetic flux

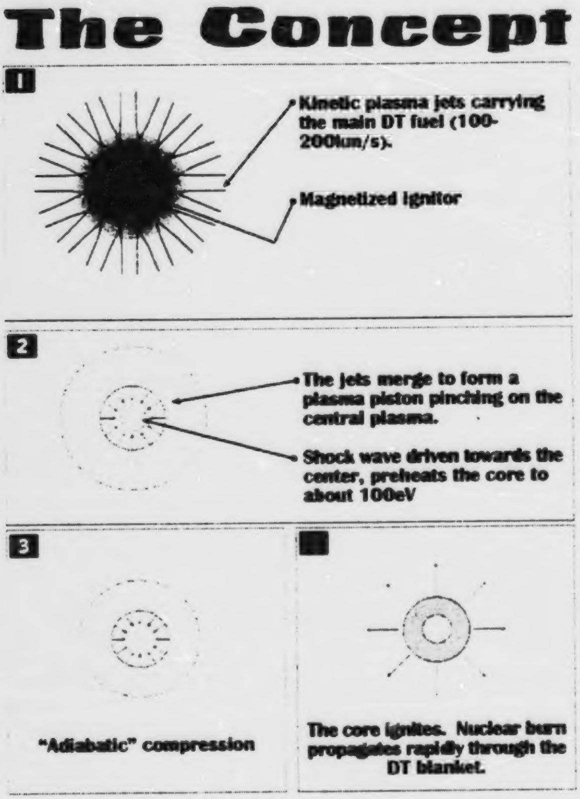
The Concept
1
Kinetic plasma jets carrying the main DT fuel (100-200km/s).
Magnetized ignitor
2
The jets merge to form a plasma piston pinching on the central plasma.
Shock wave driven towards the center, preheats the core to about 100eV
3
"Adiabatic" compression
The core ignites. Nuclear burn propagates rapidly through the DT blanket.

Figure 1. Magnetized target fusion with an imploding plasma liner.

inside the central plasma. Because of the dominant radial momentum density of the plasma liner, it continues to implode towards the center. The target plasma is further compressed by the plasma liner and heated near-adiabatically to conditions for thermonuclear burn, the magnetic flux being compressed with it, raising the magnetic fields towards megagauss levels. The compression is near adiabatic for two reasons: (1) the presence of the megagauss magnetic field strongly inhibits electron thermal conduction losses by several orders of magnitude, (2) the plasma density of the central plasma is kept relatively low so that bremsstrahlung losses are small. Synchrotron radiation losses can also be shown to be negligible. The thermal loss rates are sufficiently low that the compression heating can be achieved relatively slowly using plasma jets with velocity of the order of 10 - 100 cm per microsecond. These plasma jets can be produced using Lorentz force coaxial plasma guns as shown in Figure 2. The possibility of forming a plasma liner out of the merging of plasma jets has been demonstrated experimentally by Degnan using a cylindrical array of plasma guns [7].

The plasma liner is a composite structure consisting of two layers, an inner layer carrying the main fusion fuel, and an outer tamping layer carrying a heavy gas such as argon. This composite structure can be formed either as part of the process of refueling the plasma guns, or by a properly synchronized launch of two sets of spherically distributed plasma jets, each set carrying the required gas. The radial convergence of the plasma liner is halted abruptly by

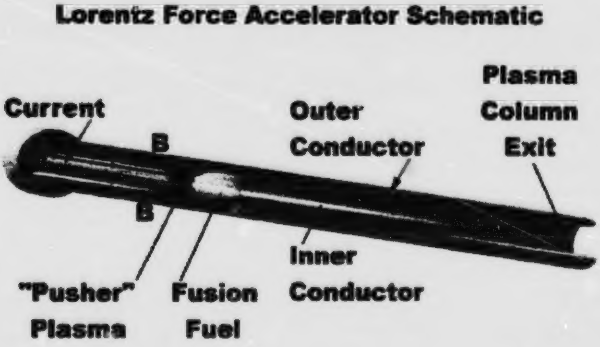

Figure 2. Coaxial plasma guns for producing the high velocity plasma jets.

the nuclear burning central plasma sending a stagnating shock expanding outwards through the plasma liner, compressing the plasma liner to form a highly dense cold fuel layer on the inside. The cold fuel layer is ignited by the nuclear burning central plasma serving therefore as a "hot spot". The pressure and the inertia of the shocked and compressed liner provide the inertia confinement for itself and the nuclear burning hot spot. When the expanding shock wave reaches the outer boundary of the plasma liner, the liner expands and a rarefaction wave emanates radially inwards from the surface of this outer boundary. This results in the expansion and the disassembly of the plasma liner, terminating the confinement of the nuclear burning fireball. The fusion confinement time is approximately the sum of the transit time of the stagnating shock and twice the transit time of the rarefaction wave through the cold fuel layer. If the cold fuel layer is sufficiently thick and dense to trap and re-deposit a fraction of the energy of the charged particles from the fusion reactions, it is possible for a fusion burn wave to spread through the cold fuel, and thus multiplying the energy gain of the hot spot. Excessively high gain is not required here as plasma accelerators are relatively efficient.

The conditions of the plasma liner and the target plasma at the instant of impact (engagement) determines the subsequent dynamics of implosion. Typical parameters for the plasma liner at this instant of impact are: velocity – 125 km/s, particle density – 10^{20} cm^{-3}, total energy – 10 MJ. Typical parameters for the target plasma at the instant of impact are: density – 10^{18} cm^{-3}, temperature – 2 eV, magnetic field – 1 T. Typical parameters for the target plasma at peak compression to produce gainful fusion burn are: temperature – 10 keV, density – 10^{21} cm^{-3}, pressure – 30 Mbar, radius – 2.5 mm, confinement time – 0.05 µs.

The concept is an evolution from a combination of previously studied concepts including impact fusion [8], compression of compact toroids [9], theta and spherical pinches [10], and electromagnetic accelerators [11].

3. THE CONTACT SURFACE AND FLUX TRAPPING

A few fundamental questions about scheme need to be addressed at the outset: (1) Would a contact surface be formed between the plasma liner and the target plasma to provide a "piston head" in imploding the target plasma, or would the interpretation of plasmas prevent such a contact surface from being formed? (2) Would the magnetic flux be trapped in the target plasma and be compressed by the liner?

The thickness of the contact surface is of the order of the collision length scales of the particles in the liner. The collision length (mean free path) between the same species of particles in a plasma is given by [12],

$$\lambda = \frac{25\pi\varepsilon_0^2 (kT)^2}{Z^4 n e^4 \ln \Lambda}$$

As we shall later, the shocked temperature of the liner initially is about 100 eV. With a density of the order of 10^{20} cm^{-3}, the collision length can be estimated at about 10 μm. Since this is small relative the spatial scale of compression, the formation of a reasonably well defined contact surface can be expected. The stability of this contact surface during the implosion, however, is a separate matter which is much more complex an issue and should be addressed in a future study of the concept.

In order for the magnetic flux to be trapped within the target plasma during the implosion, the plasma conductivity must be sufficiently high so that magnetic diffusion across the contact surface is sufficiently slow compared to the velocity of implosion. The ratio of the rate of implosion to the rate of magnetic diffusion is given by the magnetic Reynolds number of the process,

$$R_m = \mu \sigma v \ell$$

where μ, σ, and ℓ are the permeability, conductivity and the spatial scale of the implosion. Using a temperature of about 100 eV and a velocity of 100 km/s for the contact surface, and setting ℓ to be about half of the target radius, the Reynolds number is conservatively estimated to be at least 500. This is sufficiently large to ensure that magnetic flux leakage from the target plasma is negligible during the implosion.

4. IMPLOSION DYNAMICS: PHYSICAL DESCRIPTION

The parameter space relevant to MTF has been extensively studied by Lindemuth and Kirkpatrick, and Kirkpatrick [13], Lindemuth and Ward [14]. Presenting the results in a plane with the ion temperature and areal density (density-radius product) as coordinates (a Lindl-Widner diagram), the emphasis of these studies is in identifying the region of the parameter space in which fusion ignition would occur in the target, i.e. the condition of a positive rate of temperature rise (dT/dt > 0) in the target is maintained by the fusion reactions occurring in the target alone without further external energy input. Though target ignition is not a strict requirement for a workable scheme here, it is desirable. Our first objective in the following discussion is to explore the existence of practical target implosion trajectories leading to ignition.

There is, however, another important energetic consideration here, namely, the energy of the liner required to achieve the target ignition conditions. This issue has been examined for solid liners [15] where it is found that typically less than one-fifth of the initial liner energy is transferred to the target. We could expect a lesser proportion of the energy going into the target in the case of a plasma liner as more energy would be expended as thermal energy in the plasma liner during the implosion. On the other hand, the target gain has the potential of being amplified many times by the fusion burning of a thin but dense inner layer of the plasma liner. Our second objective in the following discussion is to provide estimates of the liner energy required to achieve the desired implosion, and to provide some indications of the possibility of the fusion burning of a thin inner layer of the liner.

A definitive study of these issues requires an accurate accounting of the energy deposition by the fusion α particles in a strong magnetic field. While efforts are underway to develop more accurate theoretical approaches and the computing methods to treat α-transport in a strong magnetic field, for convenience, we will adopt here an approximate model of Kirkpatrick in which an uniform azimuthal magnetic field is assumed to exist within the spherical volume of the target plasma.

To begin the discussion, assume a plasma liner in the form of a spherical shell of finite thickness converging on a target plasma which is also assumed to be spherical. As the plasma liner and the target plasma are initially relatively cold with relatively low sound speed, when they collide, shock waves are produced in both the target plasma and the liner. The shock in the target plasma converges spherically towards the center and is reflected near the center. In time, the reflected shock meets the radially converging contact surface giving rise to a second radially ingoing shock in the target which is again reflected near the center. The process is repeated until the radial momentum of the liner is totally dissipated, at which point the target and the liner have reached their peak compression. By design, the first ingoing and reflected shocks in the target are strong. The passage of these two shocks, however, heats the target to a sufficiently high temperature that the subsequent reflected shocks are relatively weak. The associated compression of the target plasma resulting from these weak shocks is more or less acoustic. If the magnetic field in the plasma is sufficiently high to provide the required degree of magnetothermal insulation, then the subsequent acoustic compression is nearly adiabatic.

The stability of this acoustic implosion phase is critical to the success of the scheme, and is determined by the Rayleigh-Taylor instability. In this study, we assume that the Rayleigh-Taylor instability becomes significant only for implosion with radial convergence of more than a factor of 10. Accordingly we limit the radial convergence during the acoustic implosion to be less than 10. It must be appreciated that the driver of Rayleigh-Taylor instabilities during the implosion is the significant deceleration of the liner due to the pressure build-up in the target and the adverse density gradient across the target-liner interface. During the merging and coasting of the liner towards the target prior to impact, both the deceleration and density gradient are not sufficiently adverse to produce any significant growth rate for the Rayleigh-Taylor instabilities in the liner. Thus the radial convergence of the liner itself prior to its interaction with the target is not significantly subjected to this mode of instability.

After peak compression is reached, further advance by the liner is halted by the immense pressure developed in the target. A stagnating shock propagates outward in the liner with a "piston" speed approximately equal to the local inward flow speed before the arrival of the stagnating shock. When this stagnating shock reaches the outer boundary of the liner, a rarefaction wave propagates backwards towards the center. The confinement time for the target plasma is approximately the transit time of the stagnation shock plus twice the transit time of the rarefaction wave. During this period, the target plasma is designed to ignite or burn. Furthermore, the fusion α-particles leaving the target plasma still carry sufficient energy to cause an inner layer of the liner to burn (ignition is not required for the liner) to produce amplification of the energy gain of the target. The burn time for this inner "cold fuel layer" of the liner is approximately twice the transit time of the rarefaction wave.

5. IMPLOSION DYNAMICS: THE MATHEMATICAL MODELS

A succinct presentation of the mathematical models for analysing the concept is given here in support of the objectives of the present paper. Detailed discussion of the mathematical models are presented elsewhere.

5.1 The Preliminary Shock Heating and Compression of the Target Plasma

For the first ingoing shock, the Hugoniot jump conditions across the shock give the density (ρ_i), pressure (p_i), and temperature (T_i) behind the shock front in terms of the initial target density (ρ_0) and temperature (T_0) as,

$$\rho_i = \left(\frac{\gamma+1}{\gamma-1}\right)\rho_0, \quad p_i = \left(\frac{\gamma+1}{2}\right)\rho_0 u_c^2, \quad kT_i = \left(\frac{\gamma-1}{1+Z_i}\right)\left(\frac{1}{2}m_i u_c^2\right) \tag{1}$$

assuming the shock to be infinitely strong (upstream Mach number $M \to \infty$) where m_i is the ion mass, u_c is the velocity of the contact surface, and Z_i is the effective charged state of the ions. The radially converging flow following the shock compresses the gas adiabatically by another factor of 4.719 for a gas with $\gamma = {}^5/_3$ according to Lazarus and Richtmyer [16]. The temperature rises by a factor of 2.813 associated with this adiabatic compression. The interaction of the ingoing flow with the stagnating flow near the center produces a reflected shock with a strength (pressure ratios) of 2.55. The corresponding upstream Mach number is 2.24, giving rise to a density multiplication factor of 1.71 and a heating factor of 1.49667. The net density compression factor after the passage of the first ingoing and reflected shock is thus 32, whereas the target plasma temperature is raised to the value T_{2s} given by,

$$kT_{2s} = \frac{2.797}{1+Z_i}\left(\frac{m_i u_c^2}{2}\right) \tag{2}$$

Denote the liner velocity before its collision with the target plasma by $u_{\ell,o}$. On impact with the target plasma, the liner sees a "piston" velocity of $u_{\ell,p} = u_{\ell,o} - u_c$ producing a shock propagating outwards relative to the liner. The resulting velocity of the contact surface u_c is one that results in a shock pressure in the liner that maintains pressure continuity across the contact surface. If the initial unshocked (upstream) pressure in the liner is $p_{\ell,o}$, applying the shock Hugoniot across the shock front in the liner gives the relationship,

$$\frac{1}{2}\rho_{\ell,0}u_{\ell,p}^2\left[(\gamma+1)p_i + (\gamma-1)p_{\ell,0}\right] = \left[p_i - p_{\ell,0}\right]^2 \tag{3}$$

Together with the expression (1) for the interfacial shocked pressure p_i, the two equations may be solved for the initial velocity of the contact surface u_c and the pressure p_i. In dimensionless form, the two equations may be reduced to one in terms of the upstream Mach number, $M_{\ell,s}$, of the shock front in the liner:

$$\begin{gathered}\frac{1}{2}\gamma(\gamma-1)M_{\ell,s}^2\left[\left(\frac{\gamma+1}{\gamma-1}\right)\delta(M_\ell - M_{\ell,s})^2 + 1\right] = \left[\delta(M_\ell - M_{\ell,s})^2 - 1\right]^2 \\ M_{\ell,s} = \frac{u_{\ell,p}}{c_{\ell,0}}, \quad M_\ell = \frac{u_{\ell,0}}{c_{\ell,0}}, \quad \delta = \frac{\gamma(\gamma+1)}{2}\left(\frac{\rho_0}{\rho_{\ell,0}}\right)\end{gathered} \tag{4}$$

where $c_{\ell,0}$ is the acoustic speed in the liner before colliding with the target plasma. We note that, in equation $M_{\ell,s} = 0$ (4), when the right hand side $\delta(M_\ell - M_{\ell,s})^2 - 1 = 0$, or equivalently, when $\delta = 1/M_\ell^2$. This is the case when the impact is perfectly matched "acoustically" for the liner, resulting in no shock ($M_{\ell,s} = 0$) in the liner. For the case $\gamma = 5/3$, this condition reduces to $\mathrm{r}u_\ell = \sqrt{(9/20)(\rho_{\ell,0}/\rho_0)}\, c_{\ell,0}$ requiring the liner velocity to be given by. The resulting instantaneous velocity of the contact surface equals this velocity. Equivalently, the resulting instantaneous shocked pressure in the target plasma at the interface is equal to the liner pressure ($p_{\ell,0}$) prior to impact. The liner velocity and pressure refers to these quantities at the inner surface of the liner.

5.2 The Acoustic Implosion Phase With Magnetic Thermal Insulation

The D-T reaction is selected for this first study, though the mathematical model developed may be extended to apply to other fusion reactions. The evolution of the target plasma temperature is governed by the energy equation,

$$\frac{d}{dt}(kT_t) = \frac{1}{6N}\left\{\Delta E_\alpha \dot{N}_r - \dot{Q}_c - \dot{Q}_{rad} - p\dot{V} - \dot{E}_B - \dot{E}_k\right\} \tag{5}$$

where N is the number of deuterons in the target plasma ΔE_α, is the amount of energy deposited by an α-particle in the targe $\dot{N}_r$ t, is the rate of fusion reactions $\dot{Q}_c$, is the thermal conduction loss rate, $\dot{Q}_{rad}$ is the radiative loss rate, p is the target plasma pressure and $\dot{V}$ is the rate of change of the target volume, $\dot{E}_B$ is the rate of increase of the target magnetic energy, and $\dot{E}_k$ is the rate of change in the target kinetic energy. An equal mixture of D and T is assumed. The expressions for these quantities are given respectively by,

$$\dot{N} = -\dot{N}_r = -\frac{N^2}{V}\langle\sigma v\rangle,$$

$$\dot{Q}_c = 4\pi r_b^2 g\kappa\left(\frac{T_t - T_b}{r_b}\right),\quad \kappa = \kappa_{\perp e} + \kappa_{\perp i},\quad \kappa_{\perp e} = \frac{n_e k(kT_e)\tau_{ee}}{m_e}\,\frac{4.66\omega_{ce}^2\tau_{ee}^2 + 11.92}{\omega_{ce}^4\tau_{ee}^4 + 14.79\omega_{ce}^2\tau_{ee}^2 + 3.77},$$

$$\kappa_{\perp i} = \frac{n_i k(kT_i)\tau_{ii}}{m_i}\,\frac{2\omega_{ci}^2\tau_{ii}^2 + 2.64}{\omega_{ci}^4\tau_{ii}^4 + 2.7\omega_{ci}^2\tau_{ii}^2 + 0.68},\quad \tau = \frac{25\pi m^{1/2}\varepsilon_0^2(kT)^{3/2}}{\sqrt{3}Z^4 ne^4 \ln\Lambda},\quad \omega_c = \frac{eB}{m}$$

$$\dot{Q}_{rad} = \dot{Q}_{bremsstrahlung} + \dot{Q}_{synchrotron},$$

$$\frac{\dot{Q}_{bremsstrahlung}}{V} = 1.445\times10^{-40} g_{ff} n_e T_e^{1/2}\sum n_i Z_i^2,\quad \frac{\dot{Q}_{synchrotron}}{V} = 6.2\times10^{-17} B^2 n_e T_e(keV)\left[1 + \frac{T_e(keV)}{204} + \dots\right],$$

$$\dot{E}_B = \left(\frac{2\pi}{3\mu}\right)\left(\frac{r_0}{r_h}\right)^2 (B_0 r_0)^2 u_b,\quad E_k = \frac{3}{10}m_t u_b^2,\quad p\dot{V} = \frac{3N_p kT_t u_b}{r_b},\quad N_p = 4N. \tag{6a}$$

where r_b is the target plasma radius, V is its volume, u_b is its surface radial velocity, m_t is its mass, and T_b is the temperature of the "cold" boundary in contact with the liner (about 100 eV). N_p is the total number of particles (deuterons, tritons, and electrons) in the target plasma, and we have assumed that any fusion α-particles are instantaneously lost from the target after depositing a certain amount of energy ΔE_α in the target. SI units are used in the expressions throughout this Section, including the expressions that follow, except in the expression for synchrotron radiation above where the electron temperature is given in keV. The parameter g in the thermal conduction loss rate is a shape factor for the temperature profile within the target. For a parabolic temperature profile, g = 1.25. The thermal conductivities,

$\kappa_{\perp e}$ and $\kappa_{\perp i}$, are Braginskii conductivities in the form given by Sheehey [17]. For the electron-electron (τ_{ee}) and ion-ion (τ_{ii}) collision times, we adopt the form for the collision time (τ) between like species given by Gross [18]. For α energy deposition ΔE_α in the presence of a magnetic field, Kirkpatrick [19] provides the following expression for the fractional α-deposition,

$$f_\alpha\left(Br, \rho r; f_0\right) = f_0(\rho r)\left[\frac{1+3(Br)^2}{1+3(Br)^2 f_0(\rho r)}\right], \tag{6b}$$

where B is the constant azimuthal magnetic field, r is the radius of the plasma sphere, ρ is its mass density, and $f_0(\rho r)$ is the fractional α-deposition in the absence of the magnetic field. Expression (6b) was obtained by Kirkpatrick by fitting the analytical expression to the numerical results from an extensive run of a particle-tracking code. For α-deposition in the absence of the magnetic field, we use Evans' theory [20] in which the average spatial loss rate in energy by an ion of energy E, mass m and charge Ze to a particle species j in a plasma at a temperature T_j, mass m_j and charge $Z_j e$, is found to be,

$$\begin{gathered}
-\left\langle\frac{dE}{dx}\right\rangle_j = 2\pi Z^2 Z_j^2\left(\frac{e^2}{4\pi\varepsilon_0}\right)^2 \frac{m}{m_j E} F_j\left(y_j\right) \ln\Lambda_j, \\
F_j\left(y_j\right) = erf\left(y_j\right) - \left[1+\frac{m_j}{m}\right] y_j\left(\frac{2}{\sqrt{\pi}}\right)\exp\left(-y_j^2\right) \quad y_j^2 = \frac{m_j}{m}\frac{E}{kT_j}.
\end{gathered} \tag{6c}$$

5.3 The Structure of the Plasma Liner

The loss rates to the ions and electrons are computed separately and then summed. Assuming the jets merge to form a steady-state gas shell with radial flow prior to impact, the flow velocity and density profiles may be computed by solving the steady-state fluid equations for mass and momentum conservation,

$$\frac{\partial}{\partial r} r^2 \rho u_r = 0, \quad \frac{\partial p}{\partial r} + \frac{1}{r^2}\frac{\partial}{\partial r}\rho r^2 u_r^2 = 0 \tag{7}$$

Furthermore, if we assume that the flow is polytropic with a polytropic index of Γ, these equations can be reduced to a single ordinary differential equation for the velocity profile, $\psi(\xi)$, in dimensionless form,

$$\frac{\xi}{2\psi}\frac{d\psi}{d\xi} = \frac{1}{M^2-1}, \quad M^2 = \left(\frac{u_r}{c}\right)^2 = M_b^2 \psi^{\Gamma+1}\xi^{2(\Gamma-1)}, \quad \psi = \frac{u_r}{u_b}, \ \xi = \frac{r}{r_b}, \quad \psi(1) = 1, \tag{8}$$

where c $(= \gamma p/\rho)$ is the local sound speed at the position r, u_b, r_b, and M_b are the velocity, radial coordinate and the local Mach number of the inner surface of the liner respectively. The pressure, density and local sound speed at a point interior to the liner are given respectively by,

$$\frac{\rho}{\rho_b}=\left(\psi\xi^2\right)^{-1},\quad \frac{p}{p_b}=\left(\frac{\rho}{\rho_b}\right)^{\Gamma},\quad \frac{c}{c_b}=\left(\frac{\rho}{\rho_b}\right)^{(\Gamma-1)/2} \tag{9}$$

where the subscript *b* refers to the inner surface of the liner. The velocity and density profiles obtained by a numerical solution of equation (8) for the case $M_b = 1^+$ are shown in Figure 5.1. Note the very steep gradient of both the density and the velocity profile near the interface. Note also that the knee of the velocity profile occurs around $\xi \sim 4$ and asypmtotes to a value twice its value at the interface. For $M^2 >> 1$, the equation has the asymptotic solution,

$$\psi \rightarrow \left\{1+\frac{1}{M_b^2}\left(\frac{\Gamma+1}{\Gamma-1}\right)\left[1-\frac{1}{\xi^{2(\Gamma-1)}}\right]\right\}^{1/(\Gamma+1)} \tag{10}$$

If the flow within the liner is adiabatic, then the polytropic index coincides with the ratio γ for the specific heats of the gas.

The total mass, thermal energy and kinetic energy of the liner are given respectively by,

$$\begin{gathered} m_\ell=\int_V \rho\, dV=3\rho_b V_b \int_1^{\xi_a}\frac{1}{\psi}\, d\xi, \\ E_{\ell,T}=\int_V \frac{p}{\gamma-1}\, dV=\frac{3p_b V_b}{\gamma-1}\int_1^{\xi_a}\frac{\xi^2}{\left(\psi\xi^2\right)^{\gamma}}d\xi,\quad E_{\ell,k}=\int_V \frac{1}{2}\rho u_r^2\, dV=\frac{3\gamma}{2}M_b^2\int_1^{\xi_a}\psi\, d\xi. \end{gathered} \tag{11}$$

5.4 Target Confinement

The flow in the liner starts out highly supersonic with the local mach number M_b at the inner surface of the liner exceeding the value of 10 typically. By design, the initial momentum density of the liner is chosen to be such that compression of the target proceeds with very little resistance until near the point of turn-around. Near the point of turn-around, the sudden build up of pressure in the target and in the liner causes the flow in the liner to experience a rapid transition to a subsonic flow. A singularity is apparent in equation (8) at $M = 1$. Before the subsonic transition, equation (8) gives a reasonable approximation to the flow. It is used to compute the liner profile (velocity $u_r(r)$, density $\rho(r)$, and pressure $p(r)$) down to the point when the local mach number M_b at the inner liner surface is nearly 1. At this point maximum compression in the target and liner is essentially attained, and a stagnation shock propagates outwards halting the converging flow in the liner. The "piston" speed of this stagnation shock is the local flow speed u_r. Thus, assuming that it is a strong shock, the local speed of the stagnation shock front is $(\gamma+1)u_r/2$. The transit time for this stagnation shock is approximated by the integral,

$$t_s=\left(\frac{2}{\gamma+1}\right)\int_{r_b}^{r_a}\frac{dr}{u_r}=\left(\frac{r_b}{u_b}\right)\left(\frac{2}{\gamma+1}\right)\int_1^{\xi_a}\frac{d\xi}{\psi(\xi)}\equiv\frac{r_b}{u_b}\tau_s(\xi_a). \tag{12}$$

where the dimensionless velocity profile $\psi(\xi)$ is calculated from equation (8) with $M_b = 1^+$, as shown in Figure 5.1.

When the stagnation shock reaches the outer boundary of the liner ($r = r_a$), a rarefaction wave propagates backwards. The rarefaction wave speed is approximately the local speed of sound. Hence an estimate of its transit time may be given by,

$$t_r = \int \frac{dr_s}{c_s(r_s)},$$

where $c_s(r_s)$ is the local sound speed at the shocked radial position r_s. After the passage of the stagnation shock, the shocked density $\rho_s(r_s)$ and the shocked pressure $p_s(r_s)$ at the shocked position r_s, are given respectively by,

$$\rho_s(r_s) = \left(\frac{\gamma+1}{\gamma-1}\right)\rho(r), \; p_s(r_s) = \left(\frac{\gamma+1}{2}\right)\rho(r)u_r^2(r), \tag{13}$$

where $\rho(r)$ and $u_r(r)$ are the density and velocity at the unshocked position r before the passage of the stagnation shock. The shocked (r_s) and unshocked (r) coordinates are related by mass conservation as,

$$4\pi r^2 \rho(r)\, dr = 4\pi r_s^2 \rho_s(r_s)\, dr_s, \quad \text{or,} \quad dr_s = \left(\frac{\gamma-1}{\gamma+1}\right)^{1/3} \frac{\xi^2}{\left(\xi^3 + \frac{2}{\gamma-1}\right)^{2/3}}\, dr. \tag{14}$$

The rarefaction wave transit time integral is accordingly given by,

$$t_r = \left(\frac{r_b}{u_b}\right)\left(\frac{\gamma-1}{\gamma+1}\right)^{1/3}\left(\frac{2}{\gamma(\gamma-1)}\right)^{1/2} \int_1^{\xi_a} \frac{\xi^2}{\left(\xi^3 + \frac{2}{\gamma-1}\right)^{2/3}\psi}\, d\xi \; . \equiv \left(\frac{r_b}{u_b}\right)\tau_r(\xi_a) \tag{15}$$

The target confinement time is taken to be,

$$t_{conf} = t_s + 2t_r = \frac{r_b}{u_b}\left(\tau_s(\xi_a) + 2\tau_r(\xi_a)\right) \tag{16}$$

5.5 Estimating the Yield from the Burning of the Cold Fuel Layer

Let $\varepsilon_s(r_s)$ be the energy density at the position r_s after the passage of the stagnation shock, but before the passage of the alpha particles streaming outwards from the fusion burning target. After the passage of the alpha particles, the energy density at the point is increased by the energy deposition by the target alpha particles. The resulting energy density and temperature at the position r_s in the liner are,

$$\varepsilon = \varepsilon_s + \left(-\frac{dE_\alpha'}{dr}\right)\frac{N_\alpha}{4\pi r_s^2} = \frac{1}{2}\rho_s(r_s)u_r^2 + \left(-\frac{dE_\alpha'}{dr}\right)\frac{N_\alpha}{4\pi r_s^2} = \frac{1}{2}\rho_b u_b^2\left(\frac{\gamma+1}{\gamma-1}\right)\frac{\psi}{\xi^2} + \left(-\frac{dE_\alpha'}{dr}\right)\frac{N_\alpha}{4\pi r_s^2},$$
$$kT = \frac{(\gamma-1)\varepsilon}{2n_{DT}}, \tag{17}$$

where $n_{DT} = \frac{\rho_s(r_s)}{m_{DT}}$, and N_α is the cumulative (total) number of alpha particles passing through the spherical shell at position r_s. The spatial rate of energy deposition by the alpha particles to the plasma, $\left[-\frac{dE'_\alpha}{dr}\right]$, is given by Evans' theory, expression (6c). This is calculated using the density and temperature profile of the liner before the passage of the alpha particles. The decrease in the energy of the alpha particle is accounted for by integrating Evans' equation (6c) over this profile for the passage of the alpha particles through the liner. Knowing the temperature T, the local fusion reactivity $\langle \sigma v \rangle$ and the fusion reaction rate can be determined. The burn fraction f_b at this position follows if the burn time is known.

We have not taken into account the increase in the temperature of the liner and the fusion reactivity due to the energy deposition of the new alpha particles born of the fusion in the liner. Thus yield enhancement of a propagating burn through the liner has not been included here. On the other hand, this increase in temperature and pressure would lead to a local expansion and a consequent reduction of fusion reactivity and its yield. Overall we expect that the results produced here are a conservative approximation and the overall fusion yield is likely to be larger than what we present here.

Most of the burn in the liner occurs in a very thin inner layer (of the order of several to a few tens of μm's) of the liner where the density is high. The burn time for this thin inner layer is taken to be twice the rarefaction wave transit time t_r as given by expression (15). The total fusion yield from the burning of the cold fuel layer is estimated by integrating the fusion energy density over the volume of the burning layer in the liner, thus,

$$E_{Fl} = N_r \varepsilon_F = \varepsilon_F \int 4\pi r_s^2 f_b n_D \, dr_s, \quad \varepsilon_F = 17.6 \text{ MeV for D-T reactions.} \tag{18}$$

5.6 Implementation

The mathematical models were implemented in a suite of MATLAB codes. Detailed documentation of the codes is given elsewhere [21]. The analysis begins by specifying the target radius, ion density, temperature and magnetic field at the moment of impact with the liner. The impact is assumed to be acoustically matched for the liner. The shock compression and heating are calculated according to the theory developed in section 5.1. The resulting target conditions are then used as the initial conditions for the set of ordinary differential equations (5) and (6) of section 5.2 governing the acoustic compression of the target.

The differential equations are integrated using a 4th-order Runge-Kutta method. During the early stages of the acoustic compression, because of the overwhelming momentum density of the liner, the trajectory is more or less linear. In the calculation, a linear trajectory is assumed until desired peak compression is nearly reached. To provide a smooth transition to the state in which the liner is stationary, when the time is within 10% of the instant of peak compression, a quartic time dependence of the target radius is assumed until the target radius reaches a pre-assigned minimum value. After this instant, the target radius is kept constant computationally for a length of time which is the target and liner confinement time as defined in Section 5.4. Time integration of the differential equations is continued until a preset instant, giving the temperature, the cumulative number of fusion reactions, and the alpha energy deposition in the target versus time. The p-dV work done on the target is also accumulated versus time.

The peak pressure of the nuclear burning target and the confinement time together determines the pressure, density and the thickness of the stagnated liner, and hence the energy in the liner at stagnation. Adding to this the energy required to perform the p-dV work on the target, and the shock heating and compression due to the first ingoing and reflected shock, gives the minimum kinetic energy the liner must have initially. The maximum pressure experienced by the target up to a particular instant t determines the inner pressure p_b of the liner required to confine the target. Following Section 5.3 above, the profile of the liner at peak compression is taken to be its profile when the mach number M_b of the flow at the inner liner surface is ~ 1^{+}. By similarity of the flow, the flow velocity at the inner surface at impact is approximately the asymptotic value of its velocity profile at peak compression, assuming a compression ratio > 4. The flow velocity at the inner liner surface at peak compression is thus about half the contact surface velocity at impact ($u_b \sim 0.5\ u_c$). The inner liner density is determined from these data as $\rho_b = \gamma p_b / c_b^2$. With the value of u_b known, the required confinement time determines the dimensionless position ξ_{α} of the outer boundary of the liner through the relationship (15). The integrals (11) then give the mass and energy of the liner at this position required to confine the target in pressure and time. The fusion yield of the liner follows from the expressions (16) and (18) of Section 5.5 given the fusion yield from the target and the liner profile.

Finally, the structure of the liner prior to impact is calculated by requiring mass and energy conservation. Thermal losses from the liner are ignored (liner performance is expected to improve if thermal losses from the liner are taken into account as they would produce a colder and denser liner). The energy of the liner prior to impact is the sum of the energy required to produce the first ingoing and reflected shocks in the target, the p-dV work on the target during the acoustic compression of the target, and the energy of the liner at peak compression.

6. IMPLOSION DYNAMICS: THE NUMERICAL RESULTS AND DISCUSSION

Computations are conducted here only to show the existence of realizable implosion trajectories to produce substantial fusion yield and meaningful gain, and to illustrate the profound effect the magnetic field has on the outcomes. Extensive parametric studies are left for the future. A small number of cases are computed here for an almost arbitrarily chosen implosion velocity of 125 km/s. The radius and the DT ion density of the target at impact with the liner are chosen to be 50 mm and 10^{24} m^{-3} respectively. After the first ingoing and reflected shocks, the target shrinks to a radius of 15.8 mm and a shock heated temperature of about 283 eV, quite independently of its initial temperature. The computation proceeds to model the thermal evolution of the target plasma as it is acoustically compressed down to a preset radius of 2.5 mm. The acoustic radius compression ratio is 6.3. The target is then computationally maintained at the minimum radius for a length of time which is the confinement time of the target as defined in Section 5.4. The thermal evolution of the target and the consequent fusion yield from the target and the liner is critically affected by the presence of the magnetic field and is illustrated here for four cases of the initial magnetic field in the target at impact. The computation then proceeds to determine the total liner energy required to confine the target as a function of the confinement time. For the same peak target pressure, the longer the confinement time required, the thicker is the liner and thus the larger is its thermal energy at stagnation. The principal computational results are summarized in Table 1.

A typical set of the modeling results are shown in Figures 3(a) – (f), in which the case for an initial magnetic field B of 2 T in the target is illustrated. The target temperature (labeled T), the burn fraction of the target (labeled f_b) and the mean fractional alpha deposition in the target (labeled f_a) versus time measured from the end of the first ingoing and reflected shocks are shown in Figure 3(a). The temperature rises sharply when the target radius falls below

3 mm. When the compression stops, the target temperature is 12 keV. However, the target temperature continues to increase after the compression stops, climbing to about 36 keV after a target confinement time of 200 ns. Ignition occurs because of the high magnetic field of 800 T present in the target at peak compression. The high magnetic field gives rise to a high degree of α-deposition, reaching almost 40% just after peak compression is reached when the density is high and the temperature is not so high. The target burns rapidly generating a yield of nearly 216 MJ after having been confined for 200 ns, as shown in Figure 3(b). The same figure shows also that the total amount of energy invested in the target is 2.8 MJ. Defining self gain of the target as the ratio of target fusion yield to the energy invested in the target, the self gain of the target in this case is around 80.

The fusion yield from the target is amplified by the burning of a thin but very dense layer in the inner surface of the liner. The ion density in the inner surface of the liner reaches over 3.7 ´ 10^{30} m^{-3} at peak compression in this case as shown in Figure 3(f). At this density, the α-energy is rapidly absorbed in an extremely thin layer of the liner. The DT in this thin layer burns rapidly releasing nearly 1.2 GJ of fusion energy in less than 200 ns as illustrated in Figure 3(d). However, in order to provide a confinement time of 200 ns, the total energy required by the liner is 94 MJ. Defining the net gain Q_{net} to be the ratio of the total fusion yield to the total liner energy required, this gives a net gain of only 15 if a liner is used to provide a confinement time of 200 ns.

We note, however, that in this case, a confinement time of 200 ns is excessive and is not optimum with respect to net gain of the system. This is illustrated in Figure 3(c) in which the net gain is shown as a function of confinement time. The net gain peaks at a value of 56 for a confinement time of about 29 ns. The liner that provides this confinement time requires only 11 MJ of energy. The total fusion yield in this case is 619 MJ. The liner amplification, defined

Table 1. Summary of cases computed and discussed.

Case #	#1	#2	#3	#4
Target B field at impact (T)	2	1	0.5	0
Target B field after the first two shocks	20.2	10.1	5	0
Radial convergence factor due to acoustic compression	6.3	6.3	6.3	6.3
Maximum target temperature (keV)	>36	9.96	8.3	1.5
Confinement time allowed (ms)	0-0.2	0-0.2	0-0.20	0-0.2
Target fusion yield (MJ)	0-216	0-52	0-9.1	0.0023
Liner fusion yield (MJ)	0-1220	0-1150	0-646	0
Liner energy (MJ)	0-94	0-38	0-32	4.4
Maximum system (target + liner) net gain	56	70	28	0.0017
Confinement time at max. gain (ms)	0.029	0.057	0.085	0.0078
Liner energy at max. gain (MJ)	11	13.7	15.7	1.1
Fusion yield at max. gain (MJ)	619	962	433	0.0019
Minimum liner thickness at max. gain (mm)	1.6	3.1	4.5	0.42
Ion density at the inner liner surface at peak compression at max. gain (m^{-3})	3.7´10^{30}	2.6´10^{30}	2.2´10^{30}	4´10^{29}
Target system gain (target yield/total input)	1.4	1.3	0.54	0.002

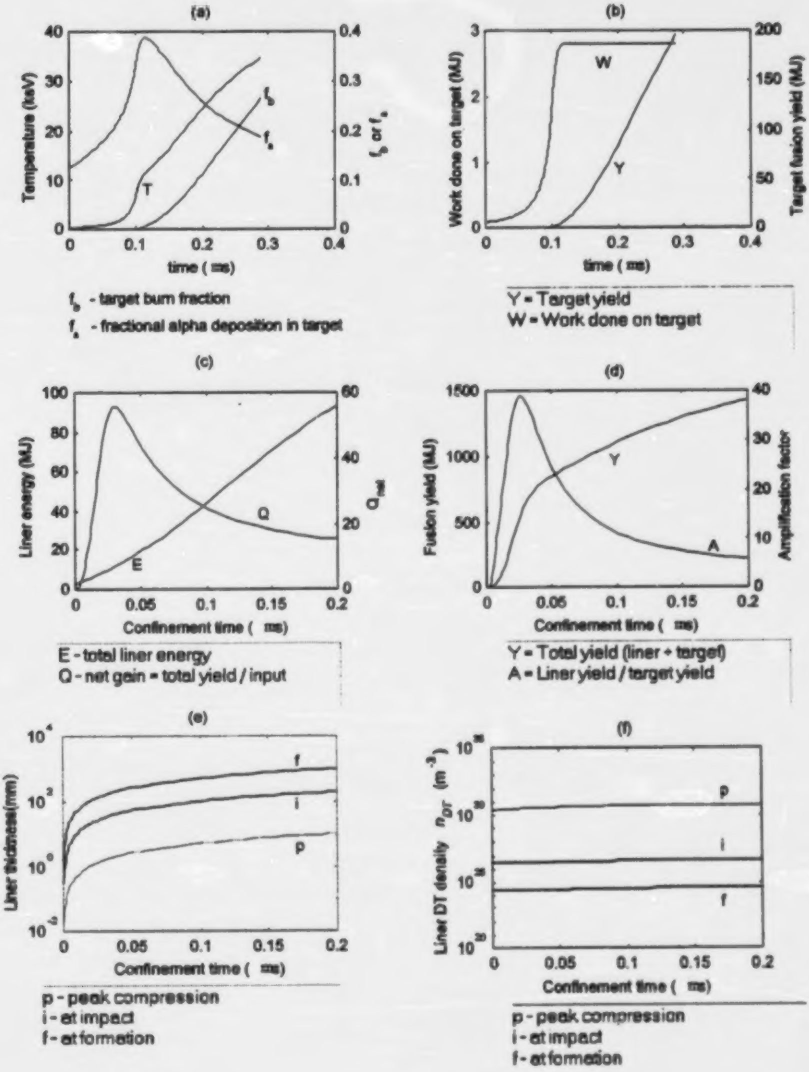

Figure 3. Case A-1: $B(0) = 2T$, $n_i(0) = 1\times 10^{24}\ m^{-3}$, $v_s(0) = 125$ km/s, $T(0) = 10$ eV, $r(0) = 50$ mm, $r_p = 2.5$ mm.

as the ratio of the liner yield to the target yield, is shown in Figure 3(d) as the curve labeled A. It peaks at a value of about 39 for about the same confinement time also. The burning of the liner occurs only in an extremely thin inner layer of the liner in which the α-particles originating from the target are totally absorbed because of the high density and the low temperature in the layer. Since burn propagation is not provided for in the present model, the fuel in this layer becomes depleted with increasing degree of burn. Therefore, the yield from this liner layer gradually plateaus (Figure 3(d)) while the required liner energy increases almost linearly with confinement time. This leads to a decline in liner amplification and net gain with confinement time after a peak is reached.

Finally, the liner thickness and density at various radial position as a function of confinement time are shown in Figure 3(e) and (f) respectively. The mathematical model as developed in Section 5.3 assumes that the flow profile in the liner is self similar with respect to its radial position. Thus its thickness scales linearly and its density inversely with the cube of its radial position. If the liner is formed at 0.25 m away from center, then its thickness and density at formation are shown by the curves labeled *f* in Figure 3(e) and (f) respectively. Though the density of the compressed liner is high, its density at formation by the merging of the plasma jets, is relatively low, of the order of 2.4×10^{24} m^{-3}. The velocity of the liner at this position is about 128 km/s. These numbers of are indicative of the properties of the plasma jets required to form the liner.

In Figure 4 (a) – (d), the performance of the system is studied as a function of the initial target *B* field, as well as the target confinement time. Four values of the initial *B* field ($B(0)$) are used: 2, 1, 0.5 and 0 T, with the case of 2 T treated in Figure 3 included as a reference. The thermal evolutions of the target for the various initial B fields are shown in Figure 4(a), the net gains in Figure 4(b), the required liner energies in Figure 4(c), and the total fusion yield in Figure 4(d).

As expected, in the case $B(0) = 0$, there is no magnetothermal insulation and the target hardly gets above 1.5 keV in temperature. No meaningful fusion yield occurs in this case. In the cases where $B(0) = 0.5$, 1, and 2 T, the effects of magnetothermal insulation are clearly in

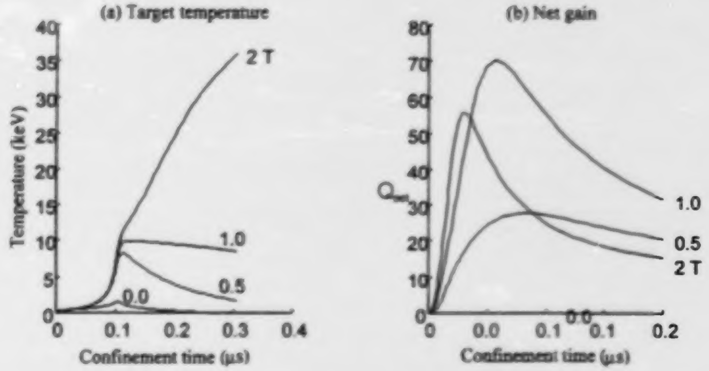

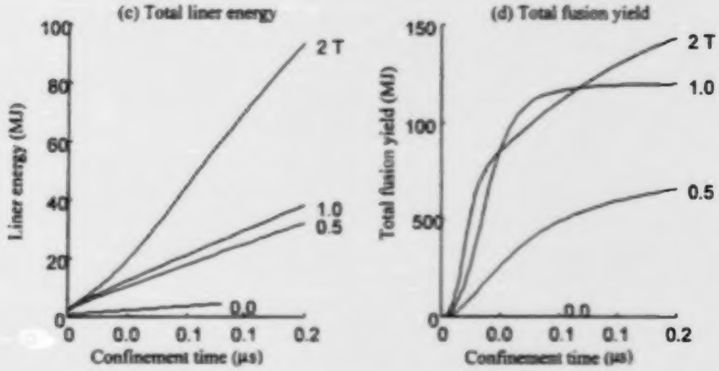

Figure 4. Performance as a function of the initial magnetic field in the target and confinement time. The curves are for four different values of the intial target field: 0, 0.5, 1, and 2T.

evidence. The temperature development follows similar trajectories for the three cases up to the point when the compression stops. At this point, the target with a $B(0) = 0.5$ T cools rapidly, indicative of the high rate of the thermal losses despite the presence of relatively strong magnetic field (200 T). Although the target temperature reaches 8.3 keV, the fusion rate and the α-deposition rate were not sufficiently high to maintain the temperature and the burning of the target. No target ignition occurs in this case. However, we note that the system consisting of the target and the liner together still gives rise to a significant net gain which peaks at about 28 for 85 ns of confinement, giving a total fusion yield of 433 MJ and requiring only about 16 MJ of liner energy. For the case with the highest $B(0)$ of 2T, the target temperature continues to rise because, with the target magnetic field at 800 T at peak compression, the α-deposition rate and the magnetothermal insulation are sufficiently high to produce ignition in the target. The net gain peaks in this case at 56 after 29 ns of target confinement, yielding 619 MJ of fusion energy with 11 MJ of energy input into the liner.

The real surprise is the existence of an intermediate value between 0.5 and 2 T, namely the case with $B(0) = 1$ T, where the net gain of the system actually rises above that of the case with $B(0) = 2$ T. A net gain of 70 was attained in this case after a target confinement time of 57 ns, yielding 962 MJ of fusion energy for only 13.7 MJ of energy input. The reason for this is that, while the fusion and α-deposition rate was such that the burning occurs below but at the verge of ignition, the fractional α-deposition rate in the target was lower than the case for $B(0) = 2$ T, allowing therefore a higher α energy flux into the liner. This gives rise to a higher heating rate of the inner layer of the liner. The necessary burn temperature in the liner for maximum fusion yield was reached in a shorter confinement time, requiring therefore less energy for the liner, resulting in a higher net gain. Notice that the total fusion yield plateaus in this case after the maximum gain was reached as illustrated in Figure 4(d). This is evident of the 'burn-out' of the inner liner layer due to a combination high temperature and high density. In the present model, radiative and conductive thermal transport in the liner are neglected, so also the effect of local hydrodynamic expansion. These assumptions are likely to break down under these circumstances. Future studies should address these effects.

7. CONCLUSIONS

An embodiment of magnetized target fusion (MTF) with the potential that the drivers can be positioned in a standoff distance from the site of the fusion burn is proposed. The magnetized target plasma is formed out of two merging compact toroids, and is imploded by a spherical plasma liner formed out of the merging of a number (nominally 60) of high momentum density plasma jets. These plasma jets are produced by highly efficient electromagnetic accelerators, the efficiency of which is expected to exceed 50%. They also carry the main fusion fuel. The implosion dynamics is studied in three phases: the preliminary shock heating and compression, the acoustic compression, and the containment of the burning target and liner. Mathematical models are developed to model these three phases of the implosion dynamics, and have been implemented in a suite of computer codes. Preliminary results produced by the models have been very encouraging, showing the great potential of the proposed MTF scheme. The presence of the magnetic field in the target has profound effects on the implosion trajectories and the consequent fusion yield. The liner requirement to confine a specific target is a function of the confinement time and the initial magnetic field in the target, which together dictates the fusion yield from the target.

The model is applied to study the liner requirements to implode a specific target with an initial radius (50 mm), an initial DT density (10^{24} m^{-3}) to a final radius (2.5 mm) with an initial implosion velocity (125 km/s) at impact with the liner, versus the length of confinement time. Carrying out the computation for four discrete values of the initial target magnetic field (0, 0.5, 1 and 2 T), we found that: (1) The target temperature exceeds 8 keV in all cases except the case of no magnetic field, in which case, the temperature hardly exceeds 1.5 keV; (2) All cases produce substantial fusion yield with a significant system net gain except for the case with no initial magnetic field; (3) Substantial fusion yield with a significant system gain exceeding 28 can occur even without ignition in the target; (4) Ignition occurs for an initial magnetic field > 1 T; (5) For a particular value of the initial magnetic field, the system net gain increases at first with confinement time, reaches a peak and then declines with further increase in confinement time. (6) The maximum gain achievable does not increase indefinitely with increasing initial magnetic field; rather, the maximum gain peaks at some value of the initial magnetic field; in the present case, it peaks near an initial magnetic field of 1 T; for this value, the maximum system gain occurs for a confinement time of 57 ns, with a total fusion yield of 962 MJ, requiring only 13.7 MJ of energy input into the liner and target, giving a net system gain of 70. Because electromagnetic accelerators are highly efficient, gains such as this or lower are more than adequate for a practical system for economical power generation. In this sense, these gains are relatively high for practical purposes. If the liner is formed at 25 cm from the center of implosion, the DT density of the liner is of the order of 1.6×10^{24} m^{-3}, which is indicative of the density of the plasma jets required.

The results show that further exploration of the concept are highly warranted. Parametric studies are needed to elucidate the scope of the practical potentials of the concept. The feasibility of merging the jets to form a spherical and/or cylindrical liner is a fundamental issue that warrants immediate attention theoretically and experimentally. The stability of the contact surface during the shock and acoustic compression phase should be investigated, so also are the effects of radiative and conductive thermal transfer on the structure of the liner. The potential enhancement of the nuclear burn produced by a secondary implosion of the target caused by the burning of the inner layer of the liner should also be explored.

ACKNOWLEDGMENTS

The development of the concept has benefitted from the opportunities of presenting the concept at a number of meetings and conferences, including the IAEA TC Meeting in Pleasanton, California, October 20-23, 1997, the First International Workshop in MTF in the same place and time, the DoE Innovative Confinement Concepts Workshop at Princeton Plasma Physics Laboratory in April 1998, and the IEEE ICOPS at NCSU, Raleigh, North Carolina, June 1998. It has benefitted greatly through the numerous discussions with a great number of people, among them, Richard Siemon, Irv Lindemuth, Pete Sheehey, Dan Barnes and Fred Ribe of Los Alamos National Laboratory, Jim Degnan and Gerry Kyuttu of the Air Force Research Laboratory at Kirtland AFB, Albuquerque, George Miley of the University of Illinois at Urbana-Champaign, Dimitri Ryutov and Ralph Moir of Lawrence Livermore National Laboratory, Nikos Salingaros of the University of Texas at St. Antonio, and others. We also like to thank Fleur Daniels (formerly) at Massey University, Auckland, New Zealand and Brent Freeze at the University of California at Los Angeles for assisting with the art work for Figures 1 and 2 respectively.

REFERENCES

*Also of Massey University, Auckland, New Zealand.

1. I. R. Lindemuth and R.C. Kirkpatrick. Fusion Technology **20,** 829 (1991).
2. R.C. Kirkpatrick and I.R. Lindemuth. Magnetized Target Fusion, An Overview of the Concept, Current Trends in International Fusion Research, ed. E. Panarella, Plenum Press, New York (1997).

3. R. Siemon et al. A Proposal for a Proof-of-Principles Experiment for Magnetized Target Fusion. Paper presented at the American Physical Society Division of Plasma Physics Meeting, New Orleans, LA., Nov 16 – 20, 1998.
4. D.R. Wells, P.E. Ziajka and J.L. Tunstall. Fusion Technology 9, 83 (1986).
5. J.H. Degnan. Phys. Fluids B 5, 2938 (1993).
6. J.B. Taylor. Phys. Rev. Lett. 33, 1139 (1974).
7. J.H. Degnan, W.L. Baker, M. Cowan, J.D. Graham, J.L. Holmes, E.A. Lopez, D.W. Price, D. Ralph, and N.F, Roderick. Operation of cylindrical array of plasma guns.
8. F. Ribe ed. Proceedings of the Workshop in Impact Fusion, Los Alamos National Laboratory, Los Alamos, NM (1978).
9. D.R. Wells et al (1986); C.W. Hartman and J.H. Hammer. Phys. Rev. Lett., 48: 929 (1982).
10. E. Panarella. J. Fusion Energy 6, 285 (1987).
11. Y.C. Thio et al. "Feasibility Study of Railgun as a Driver for Impact Fusion, Final Report," Report DoE/ER/13048-3, Contract DE-AC02-83ER13048, U.S. Department of Energy, Germantown, Washington, D.C. (1986).
12. R.A. Gross. Fusion Energy, John Wiley, New York, (1984).
13. I.R. Lindemuth and R.C. Kirkpatrick. Nucl. Fusion 23, 263 (1983).
14. R.C. Kirkpatrick, I.R. Lindemuth and M.S. Ward. Fusion Technology 27, 201 (1995).
15. S.A. Colgate, A.G. Petschek and R.C. Kirkpatrick. Minimum Energy for Fusion Ignition, A Realistic Goal, Los Alamos National Laboratory Report LA-UR-92-2599 (1992).
16. R.B. Lazarus and R.D. Richtmyer. Similarity Solutions for Converging Shocks, Los Alamos Scientific Laboratory Report, LA-6823-MS, Los Alamos, New Mexico, USA (1977).
17. P.T. Sheehey. Magnetohydrodynamic Simulation of Solid-Deuterium-Initiated Z-Pinch Experiments, Los Alamos National Laboratory Report LA-12724-T, 39, (3.1.7), (3.1.8), Los Alamos, New Mexico, USA, (1994).
18. R.A. Gross. Fusion Energy, 53, (4.18), John Wiley (1984).
19. R.C. Kirkpatrick, private communication (1998).
20. F. Evans. Note on the Calculation of Energy Deposition of Alpha Particles in a DT Plasma by Rutherford Scattering, Los Alamos National Laboratory Report LA-5448-MS (1973).
21. Y.C.F. Thio. Computer Codes for Modeling the Implosion of a Magnetized Target Plasma by a Spherical Plasma Liner, Center for Space Plasma and Aeronomic Research Report, University of Alabama, Huntsville, Alabama (1998).

GEOMETRY OF THE SPHERICAL PINCH

Nikos Salingaros

Division of Mathematics
Computer Science and Statistics
University of Texas at San Antonio
San Antonio, TX 78249, U.S.A.

The spherical geometry is critically compared to a toroidal geometry for plasma confinement. The latter is found to be deficient in several fundamental aspects, including stability, compactness, vessel stresses, and ability to undergo pressure scaling [1]. The success of the spherical pinch in several size working prototypes is contrasted to the inability of small tokamaks to perform. Using results from systems theory, we argue that any complex system, such as a fusion reactor, must succeed first on the small scale. Only then can it have any chance of success after being scaled up in size. The present attempt to build a toroidal reactor of the complexity of the ITER model contradicts well established results in systems theory. If this program were not supported against numerous scientific objections, perhaps it would have been declared unrealistic, and canceled. Our conclusion is that the fusion program can progress only if it is driven by scientific motivations, and attention is paid to engineering rules of thumb such as the scaling of working models.

On the positive side, the spherical pinch is one of the by-products of the fusion program. Already, there are industrial spin-offs such as a neutron generator, and a soft X-ray source that can be used for microlithography, or other industrial applications. These devices are natural steps in the evolution of the spherical pinch towards a working fusion device. In sharp contrast to other geometries, industrial spherical pinches are now available as a technological product. This leads the strongest possible optimism for the continued success of the spherical geometry coupled with the concept of converging spherical waves. In its basic mechanism, the spherical pinch links with the highly successful, though still classified, inertial confinement fusion devices used to mimic the performance of thermonuclear devices.

REFERENCES

1. N. A. Salingaros. Fusion Tech. **27**, 230 (1995).

Current Trends in International Fusion Research – Proceedings of the Second Symposium
Edited by E. Panarella. NRC Research Press, National Research Council of Canada, Ottawa, ON K1A OR6, Canada. 1999.

PHYSICS OF FUSION BURNING PLASMAS, IGNITION AND RELEVANT TECHNOLOGIES*

Bruno Coppi

Massachusetts Institute of Technology
Cambridge, MA 02139, U.S.A.

The importance of demonstrating both to the scientific community and the general public that ignition can be achieved in a magnetically confined plasma has been underlined recently both in the scientific literature as well as in policy documents. At the same time, the degree of common awareness of the number of requirements that have to be met and of their complexity, has increased. Therefore, there has been more appreciation for the efforts that has been undertaken in order to achieve ignition conditions and also more realistic restraint in claiming that certain classes of experiments (the large-scale ones) can be designed to reach these conditions with very high degrees of probability.

The main set of requirements to be met for D-T fusing plasmas to reach the (ignited) regime where the heating of the plasma by the 3.5 MeV produced α-particles is sufficient to compensate for all the losses of thermal energy include: the electron temperature exceeding that of the nuclei, the α-particle slowing down time being shorter than the electron energy confinement time, the degree of plasma purity corresponding to values of *Zeff* typically not in excess of 7/4, the confinement parameter $n_{eo}\tau_E$ being about 4×10^{20} sec/m^3 or larger and the peak plasma temperature exceeding 12 KeV. Here n_{eo} is the peak electron density. In addition, the assumption is commonly made that nearly all the energy carried by the produced α-particles is deposited in the plasma.

"Surrogate" experiments, such as those carried out in the so called "hot-ion mode" regime, have given important contributions to basic plasma physics, such as providing evidence for the existence of a large enhancement of the angular momentum transport rate ("anomalous viscosity") relative to that predicted by the collisional theory. On the other hand, they have introduced rating parameters (e.g., the so called break-even Q, the triple product $n_{io}T_i\tau_E$, the power produced by fusion reactions) which are not sufficient to measure progress toward ignition regimes.

Since a multiple contribution of plasma parameters has to be attained for this, relevant experiments do not necessarily have to be of large scale, as it would be necessary if the energy containment time alone had to be maximized. In addition, the present knowledge of the conditions for the macroscopic stability of plasmas, combined with the requirement of high plasma currents to ensure the appropriate confinement time, indicates clearly that high field machines are the only ones expected, in principle, to be able to reach ignition.

Current Trends in International Fusion Research – Proceedings of the Second Symposium
Edited by E. Panarella. NRC Research Press, National Research Council of Canada, Ottawa, ON K1A OR6, Canada. 1999.

As a consequence, a parallel strategy for fusion is suggested: one directed at developing high field superconducting magnets and the other employing normal conducting high field magnets to investigate, in the near term, the physics of fusion burning plasmas. Within this strategy, the state of the Ignitor machine, the first proposed and designed to demonstrate ignition, is described. The completed construction of the prototypes of the key machine components and the relevant results on confinement produced by Alcator C-Mod experiments, are discussed.

A view of a world effort in fusion research is offered which preserves the needed scientific spirit, and involves a valid technology component aimed at developing new advanced kinds of hardware in contrast to the "paper technology" deviations of the recent past.

* Sponsored in part by the U.S. Department of Energy.

HIGH CONFINEMENT REGIME IN TFTR CONFIGURATIONS WITH REVERSED MAGNETIC SHEAR

E. Mazzucato and the TFTR Group

Princeton University
Princeton Plasma Physics Laboratory
Princeton, New Jersey 08543, U.S.A.

ABSTRACT

Turbulent fluctuations in plasmas with reversed magnetic shear have been investigated in TFTR. Under intense auxiliary heating, these plasmas are observed to bifurcate into two states with different transport properties. In the state with better confinement, it has been found that the level of fluctuations is very small throughout most of the region with negative shear. By contrast, the state with lower confinement is characterized by large bursts of fluctuations which suggest a competition between the driving and the suppression of turbulence. These results are consistent with the suppression of turbulence by the **E**×**B** velocity shear.

1. INTRODUCTION

Recent results [1–4] point to the beneficial effects of negative magnetic shear on plasma performance in tokamaks. In these experiments, magnetic configurations with a non-monotonic safety factor q have been obtained using a variety of techniques. The common result is a strong peaking of the pressure profile, which indicates a reduction of plasma transport in the central region with negative shear. Since short scale turbulence is considered to be the source of anomalous losses in tokamaks, these results appear to be consistent with theoretical predictions that negative shear can suppress geodesic curvature driven instabilities, such as trapped particle modes [5], the toroidal ion temperature gradient mode [6], and high-n ballooning modes [7].

In order to study the effects of negative magnetic shear on plasma turbulence in tokamaks, we have conducted an experimental study of turbulent fluctuations in plasmas with reversed magnetic shear on the Tokamak Fusion Test Reactor (TFTR). These are deuterium plasmas with a major radius R=2.6 m, a minor radius a=0.94 m, a toroidal magnetic field B=4.6 T, and a plasma current I_p=1.6 MA. The central plasma region with negative shear is created early in the discharge by a combination of heating and current drive. Under intense

Current Trends in International Fusion Research — Proceedings of the Second Symposium
Edited by E. Panarella. NRC Research Press, National Research Council of Canada, Ottawa, ON K1A 0R6, Canada. 1999.

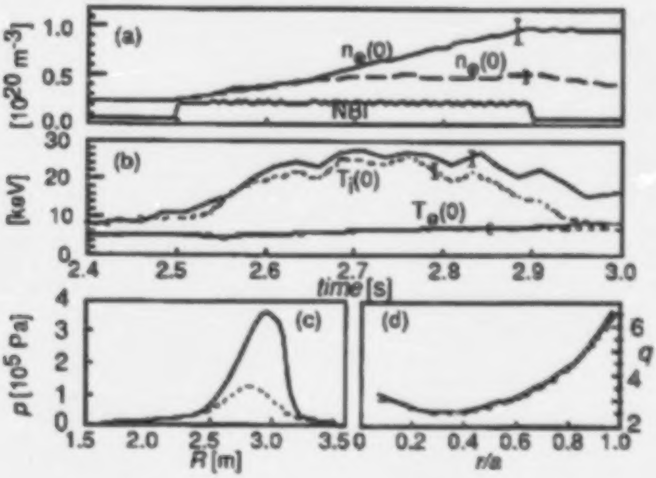

Figure 1. Time evolution of central electron density (a) and temperatures (b) in ERS (solid line) and RS (dashed line) plasmas with 29 and 27 MW of balanced NBI, respectively. The bottom graphs show the radial profile of the plasma pressure (c) at t=2.9 s, and the safety factor (d) at the bifurcation time.

auxiliary heating with neutral beam injection (NBI), these plasmas are observed to bifurcate into two different states, the reversed shear (RS) and the enhanced reversed shear (ERS) mode [3]. The RS mode is similar to the *supershot regime* which is normally observed in TFTR with monotonic q-profiles. The ERS mode is characterized by highly peaked density and plasma pressure profiles which indicate the formation of a transport barrier (Fig. 1). Since at the time of bifurcation (t≈2.65 s) the q-profiles are very similar in the two plasma modes (Fig. 1), the observed phenomenon cannot be ascribed solely to the negative magnetic shear.

A transport analysis, ignoring particle pinches, gives the electron particle diffusivity (D_e)

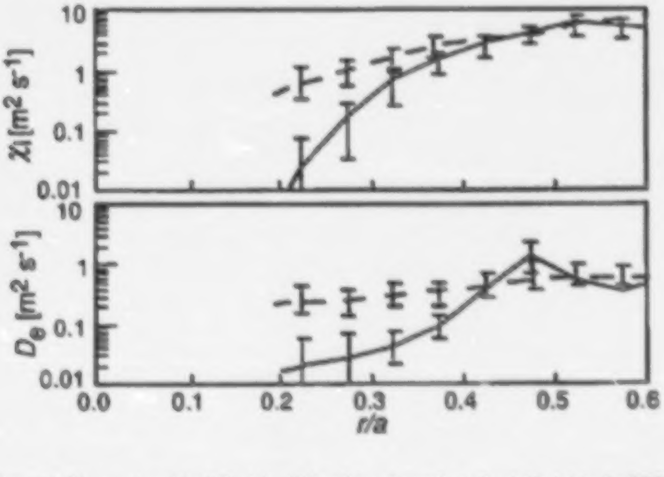

Figure 2. Electron particle diffusivity (D_e) and ion thermal conductivity (χ_i) in the ERS (solid line) and RS (dashed line) plasmas of Fig. 1 (t=2.75 *s*).

and the ion thermal conductivity (χ_i) of Fig. 2, which shows a greatly reduced plasma transport in the ERS mode. In particular, the precipitous drop of χ_i inside the reversed shear region to values below those of conventional neoclassical theory [3] reveals the formation of a transport barrier. This improvement of the ion thermal transport in the ERS mode derives from the ion temperature which remains larger than in the RS mode (Fig. 1) in spite of a stronger ion-electron coupling.

2. TURBULENT FLUCTUATIONS

The short scale turbulent fluctuations of these plasmas have been investigated with microwave reflectometry. The reflectometer system operated in the X-mode on the frequency range 123-142 GHz. Well collimated beams with a diameter of ≈5 cm were launched into the plasma using scalar guides and Gaussian optics.

The interpretation of reflectometry measurements is relatively simple when the amplitude of plasma fluctuations is small and their scale length is larger than the wavelength of the probing wave [8,9]. The latter assumption is satisfied in TFTR where the wavenumber of previously observed fluctuations is ≈1 cm^{-1} [9]. This allows the use of the geometrical optics approximation, and guarantees that the effects of turbulent fluctuations on the probing wave come predominately from a narrow region near the cutoff (<1 cm). At very small levels of fluctuation, the electromagnetic field can be separated into a large coherent reflection and small amplitude scattered waves (Born approximation) [8]. Under these conditions, the level of density fluctuations can be inferred from either the fluctuations in the phase of the received signal, or from the ratio between the power of the scattered waves and the power of the coherent reflection. Unfortunately, the first method is of limited use in tokamaks because, as the level of fluctuations increases and the scattered waves rise in amplitude and angular divergence, a complicated interference pattern makes the phase of the received signal completely chaotic and, therefore, useless for fluctuations measurements. The second method has a wider range of applicability, but it too breaks down when the amplitude of the coherent reflection decreases below detectable levels. This sets the maximum value of measurable density fluctuations, which in the present experiment is in the range $\tilde{n}_e/n_e \approx 0.5-1.0\times10^{-2}$.

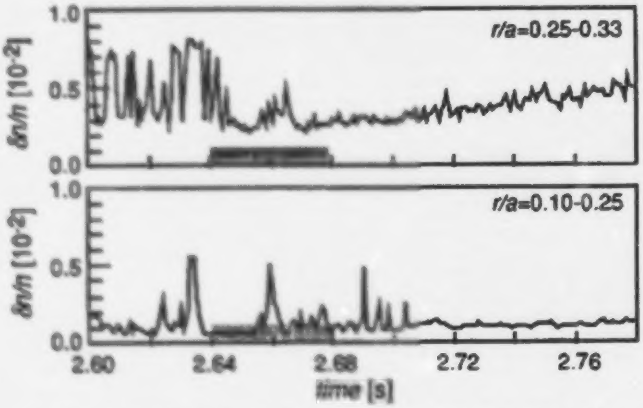

Figure 3. Time evolution of density fluctuations in the ERS mode. The shaded area represents the time of bifurcation.

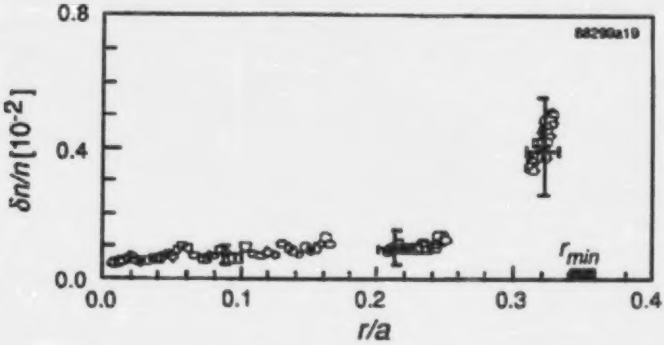

Figure 4. Amplitude of density fluctuations in the ERS mode of Fig. 1 at t=2.72-2.78 *s*; r_{min} is the radial position with minimum q.

Figure 3 shows the time evolution of density fluctuations at two radial locations inside the negative shear region of an ERS plasma. From these results, it appears that large bursts of turbulence, initially present in the discharge, disappear after the transition into the ERS mode.

By using the displacement of the reflecting point of the probing wave, caused by the plasma density rise, we get the amplitude of density fluctuations shown in Fig. 4 as a function of the normalized minor radius r/a. The abscissas in this figure are the calculated positions of the reflecting cutoff on the low field side of the equatorial plane, including a relativistic correction [10] which ranges from 2 to 6 cm. As described elsewhere [9], to obtain the amplitude of density fluctuations from reflectometry measurements requires the knowledge of the shape of the radial spectrum of fluctuations. Unfortunately, in the rapidly evolving plasmas of the present experiment, this is difficult to obtain with radial correlation measurements. Fortunately, all previous theoretical and experimental studies of short scale fluctuations in large tokamaks indicate that the bulk of the turbulent activity occurs at wavelengths larger than the ion Larmor radius (ρ_i), typically in the range of radial wave

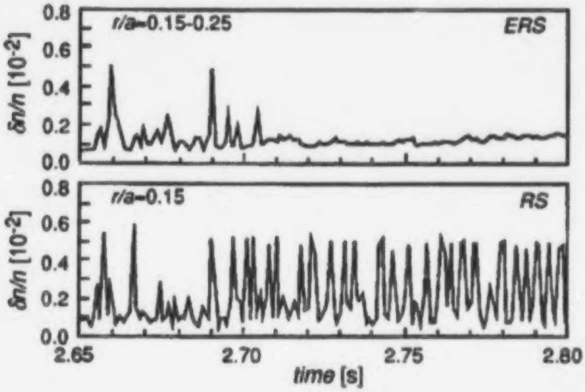

Figure 5. Time evolution of density fluctuations in ERS (top) and RS (bottom) modes.

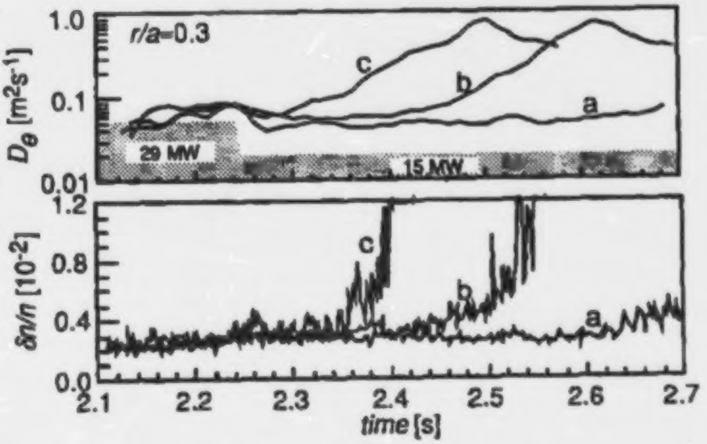

Figure 6. Electron particle diffusivity and amplitude of density fluctuations at r/a=0.3 ; a - balanced injection, b - co/counter=5/1, c - co/counter=6/0.

numbers $0.2<k_r\rho_i<1$. Accordingly, the values in Fig. 3 and 4 have been obtained assuming k_r = 1 cm^{-1}, which corresponds to $k_r\rho_i \approx 0.5$, and we have calculated the error bars by taking the extreme values of $k_r\rho_i$=0.2 and 1, respectively. In spite of these uncertainties, we draw the conclusion that the level of fluctuations is very small in the main core of ERS plasmas, and that it rises near the point where q reaches its minimum value. Both of these phenomena are reminiscent of the radial dependence of the plasma transport coefficients (Fig. 2).

Turbulent fluctuations in the RS mode are substantially different from those in the ERS mode, as illustrated in Fig. 5 which shows the time evolution of the fluctuation amplitude in the middle of the negative shear region. From these data, it appears that bursts of turbulence, reaching the maximum detectable level, persist throughout the entire plasma pulse. Closer to the plasma center ($r/a<0.1$), this phenomenon disappears and the measured level of fluctuations becomes similar to that in the ERS mode. This indicates that a central quiescent region exists in the RS mode as well, but with a much smaller radial extent than in the ERS mode.

The observed correlation between the decrease in fluctuations and the transition into the ERS mode implies that a surge of turbulence must occur at the back-transition from the ERS to the RS mode. This is indeed what is observed, as illustrated in Fig. 6, which shows the time evolution of the electron particle diffusivity and the level of turbulence across a back-transition. The latter occurs when, for achieving steady state conditions, the NBI power is lowered from 29 to 15 MW. The three cases shown in Fig. 6 differ on the co-counter NBI power ratio. It has been found [11] that, while balanced (case *a* in Fig. 6) and counter-dominated injection produces plasmas which remain in the ERS mode until the end of NBI, co-dominated injection causes a back-transition into the RS mode (cases *b* and *c* in Fig. 6). Figure 6 illustrates very clearly that the loss of ERS confinement, which is represented by the rise in the value of D_e, coincides with a sharp increase in the level of turbulent fluctuations.

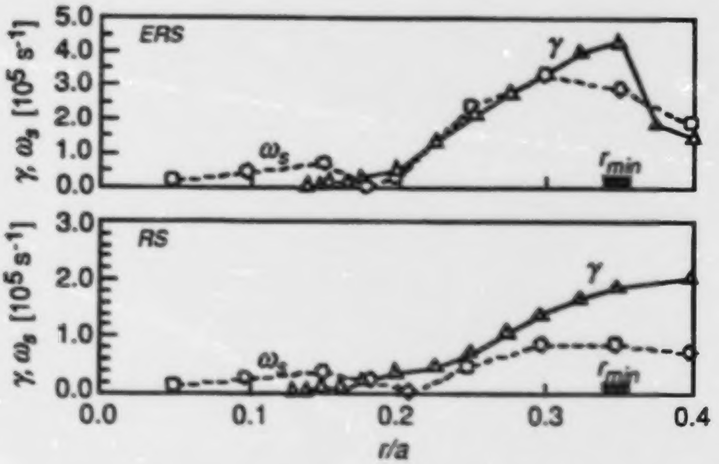

Figure 7. Maximum linear growth rate γ (triangle), and shearing rate ω_s (circles) for the ERS (top) and the RS (bottom) plasmas of Fig. 1 at t=2.75 *s*.

3. DISCUSSION

We have compared the experimental observations with the theoretical predictions for toroidal electrostatic drift-type modes. Figure 7 shows the linear growth rate of the most unstable mode (γ) which was calculated with a kinetic toroidal eigenvalue code [12]. Surprisingly, we find the largest values of γ in the ERS mode, which provides further evidence that shear reversal is not the only cause of turbulence suppression in these plasmas. Furthermore, the size of the central stable region is the same in both plasma regimes. These results, which were confirmed by those obtained with a toroidal gyrofluid code [13], demonstrate that other phenomena, besides the reversed shear, play a role in the ERS/RS dynamics.

A possible mechanism for the suppression of turbulence is the decorrelation of turbulent fluctuations by a large **E×B** velocity shear which may exist in regions of large pressure gradient [14–22]. This mechanism, which in the past has been invoked for explaining the reduction in the level of fluctuations at the edge of plasmas in the H-mode [14–18], might also be at work in the central plasma region with negative magnetic shear [19–22]. The numerical simulations in Ref. [19] indicate that turbulence is suppressed when the linear growth satisfies the condition $\gamma \leq \omega_S$, where ω_S is the characteristic **E×B** shearing rate which was derived in Ref. [20]. On the tokamak midplane, we obtain $\omega_S = \left|(RB_\theta/B)\partial(E_R/RB_\theta)/\partial R\right|$, where B_θ is the poloidal magnetic field, and E_r is the radial electric field. The latter can be obtained from the radial component of the force balance equation, using measured quantities and the neoclassical poloidal velocity. In the unstable part of the reversed shear region, where $\gamma>0$, we obtain $\gamma \leq \omega_S$ for the ERS mode, and $\gamma > \omega_S$ for the RS mode (Fig. 7). Similarly, we find that the ERS relaxation in Fig. 6 is caused by a decrease in the shearing rate below the calculated value of γ [11]. The observed difference in the co/counter NBI injection is, then, explained by the sign of the term containing the toroidal velocity in the force balance equation, which in the case of co-injection causes a reduction in E_r.

From these results, we draw the conclusion that the observed reduction of fluctuations in ERS plasmas is consistent with the suppression of turbulence by the **E×B** velocity shear.

4. CONCLUSION

In conclusion, the results presented in this paper provide the first experimental evidence of a correlation between the low level of turbulent fluctuations and the improved confinement in the main core of plasmas with reversed magnetic shear (ERS). We have also detected large bursts of fluctuations in plasmas with similar magnetic shear but with a poorer confinement (RS), suggesting a competition between the driving and the suppression of turbulence.

These observations are consistent with the suppression of turbulence by a decorrelation of turbulent fluctuations from the **E×B** velocity shear.

ACKNOWLEDGMENT

This work was supported by U.S. Department of Energy Contract No. DE-AC02-76-CHO3073.

REFERENCES

1. M. Hugon et al. Nucl. Fusion **32** (1992) 33.
2. E.A. Lazarus et al. Phys. Fluids **B 4** 3644 (1992).
3. F.M. Levinton et al. Phys. Rev. Lett. **75** (1995) 4417.
4. E.J. Strait et al. Phys. Rev. Lett. **75** (1995) 4421.
5. B.B. Kadomtsev and O.P. Pogutse. Sov. Phys. JETP **24** (1967) 1172.
6. B. Coppi et al. Phys. Fluids **10** (1967) 582.
7. M.S. Chance and J.M. Green. Nucl. Fusion **21** (1981) 453.
8. E. Mazzucato and R. Nazikian. Plasma Phys. Controlled Fusion **33**, (1991), 261.
9. *Idem*. Phys. Rev. Lett. **71** (1993) 1840.
10. E. Mazzucato. Phys. Fluids **B 4** (1992) 3460.
11. E.J. Synakowski et al. Phys. Rev. Lett. **78** (1997) 2972.
12. G. Rewoldt et al. Phys. Fluids **30** (1987) 807.
13. M.A. Beer. Ph. D. Thesis, Princeton University (1994).
14. H. Bigliari, P.H. Diamond and P.W. Terry. Phys. Fluids **B 2** (1989) 1.
15. K.C. Shaing et al. Phys. Fluids **B 2** (1990) 1492.
16. B. Basu and B. Coppi, Phys. Fluids **B 4** (1992) 2817.
17. J. Dong and W. Horton. Phys. Fluids **B 5** (1992) 1581.
18. F.L. Hinton and G.M. Staebler, Phys. Fluids **B 5** (1993) 1281.
19. R.E. Waltz et al. Phys. Plasmas **1** (1994) 2229.
20. T.S. Hahm and K.H. burrell. Phys. Plasmas **2** (1995) 1648.
21. L.L. Lao et al. Phys. Plasmas **3** (1996) 1951.
22. P.H. Diamond et al. Phys. Rev. Lett. **78** (1997) 1472.

FRC FUSION REACTOR FOR DEEP SPACE PROPULSION

John Slough and Kenneth Miller

University of Washington
Seattle, Washington 98195, U.S.A.

ABSTRACT

It is difficult to dispute that only nuclear power has the potential of making other than modest explorations of space feasible. Fusion research in recent years has focused on the tokamak concept which, while reaching break-even thermonuclear conditions, has resulted in large, expensive reactor designs. This dictates exploring novel, simpler and less costly configurations. A leading candidate is the field-reversed configuration (FRC), a compact toroidal (CT) geometry which is the geometrically simplest, most compact, and highest power density of all currently studied magnetic fusion confinement schemes. It has also been recognized that the linear geometry, high plasma pressure, and linear exhaust of the FRC make it the ideal candidate for propulsion applications.

For propulsion applications, and even for space power generation, it is desirable that most of the fusion reaction products be charged ions, rather than neutrons as they are for the standard D-T fuel cycle. The plasma exhaust can then be used for both propulsion and direct energy conversion.

The D-^{3}He reaction produces ^{4}He and a proton, rather than the ^{4}He and neutron produced by D-T. However, due to the higher required burn temperatures of such fuels, magnetic confinement schemes with even moderate internal magnetic fields can not use them due to high synchrotron radiation preventing ignition. The FRC has negligible internal magnetic fields and could readily burn aneutronic fuels. The discovery of large deposits of ^{3}He on the moon (deposited by the solar wind) has spurred renewed interest in aneutronic fusion. A magnetic fusion reactor must reach a product of density and energy confinement time, $n\tau_E$ 10^{20} m^{-3}sec for break-even power output from fusion. This has so far only been achieved in large tokamaks, but the lifetime scaling in small FRC experiments looks favorable. The key issues for a FRC fusion engine are startup and sustainment. For space applications, one must form a high temperature FRC (kT ~ 70 keV) using RF antennas alone.

FRCs are presently made in a high voltage pulsed device called a field-reversed theta pinch (FRTP). For space applications, the FRTP initiation method is too massive and cumbersome, and it will be necessary to create FRCs with RF fields. This has been done previously in small devices, but only at very low power levels, with resultant low plasma

Current Trends in International Fusion Research — Proceedings of the Second Symposium
Edited by E. Panarella. NRC Research Press, National Research Council of Canada, Ottawa, ON K1A 0R6, Canada. 1999.

temperatures. The FRC was generated however, and sustained for as long as a rotating magnetic field (RMF) was applied. There is no inherent limit to the confining flux that can be generated by the RMF system. The electrons are heated by Ohmic dissipation from the currents driven by the RMF. To raise the ion temperature to fusion conditions, an additional RF Alfven wave, generated by a simple m=0 excitation of the axial field coils, would be used to heat the ions simultaneously. A new experiment, STX, is currently being constructed at the University of Washington to explore generation techniques based on RF magnetic fields.

The start-up conditions reflect the final conditions after preionization and ion heating have occurred. The synchronous current driven by the RMF is defined as $I'_{sync} = ne\omega r_s^2/2$. It should be noted that the transverse RMF field B_ω is small for both the start-up experiment as well as the reactor. The power required to sustain the FRC after start-up is quite modest with only 260 kW needed to sustain the confining flux in the reactor case. This is due to the small transverse field required to entrain the electrons and produce the megamp currents needed. It should be noted that the magnitude of the driven current does not depend on the RMF field strength. Only the RMF frequency, plasma density, and size determine the magnitude of the confining poloidal field. Since the RMF field, $B_\omega << B_e$ (the axial field generated), the radial energy confinement should not be unduly influenced by this small transverse field.

The experimental question then becomes one of maintaining penetration conditions in addition to FRC equilibrium as the plasma is ionized and heated by both the RMF (Ohmic) and Alfven wave systems, as well as what effect the RF fields have on FRC confinement

This paper will present progress on the experiment as well as analysis of the basic efficiency of a FRC fusion propulsion system.

1. INTRODUCTION

It can hardly be disputed that only nuclear power has the potential of making other than modest explorations of space feasible. Fusion must eventually be developed if extensive space exploration is ever to be a reality. The prodigious fuel and energy requirements for space missions beyond Mars are illustrated in Fig. 1. Trips to the outer planets must be accomplished on sub-year timescales if man is to be a participant. Trips to other planetary systems, even with fusion propulsion, must be looked on as space colonization as Fig. 1 illustrates for a 300 year trip to Alpha Centauri. These are the realities of the known sources of energy applied to space

Destination	x_{trip} ~ 10 A.U. (Jupiter) x_{trip} ~ 4 L.Y. (Alpha Centauri)	t_{trip} ~ 1/3 year t_{trip} ~ 300 years
Characteristic Velocity	$v_{Jupiter}$ ~ 300 km/sec v_{alpha} ~ 8000 km/sec	
Specific Energy	$\varepsilon_{Jupiter}$ ~ $4x10^{10}$ J/kg ε_{alpha} ~ $3x10^{13}$ J/kg	
Specific Power	$\alpha_{Jupiter}$ ~ 4 kW/kg α_{alpha} ~ 4 kW/kg	
Assumptions:	α=constant=$v_{char}^2/2t_{trip}$ $v_{ship}=v_{exhaust}$ $v_{char}=2x_{trip}/t_{trip}$, $\varepsilon=v_{char}^2/2$.	

Propulsion System	Exhaust (km/s
Chemical	5
Electric	30
FRC at RPPL	200
Thermal Fusion	2000
Fusion Proton	50000
Fuel	**Specific Ener**
Chemical	$1x10^7$ J/kg
Fission	$5x10^{13}$ J/kg
Fusion	$1x10^{15}$ J/kg

Figure 1. Velocity and energy constraints for deep space missions to Jupiter and Alpha Centauri.

travel. The power requirements demand a fusion engine that must in addition be very low mass (i.e. simple and low maintenance). Fusion research in recent years has focused on the tokamak concept which, while reaching break-even thermonuclear conditions, has resulted in large, expensive reactor designs. This has led the Department of Energy (DOE) to reevaluate the program and shift its focus to exploring novel, simpler, and less costly configurations. The leading candidate is the Field-Reversed Configuration (FRC), a compact toroidal (CT) plasma that is the geometrically simplest, most compact, and highest power density of all magnetic fusion confinement configurations (see Fig. 2). It has also been recognized, both in the United States and Russia, that the linear geometry, high plasma pressure, and linear exhaust of the FRC make it the ideal candidate for propulsion applications. In fact, the unique promise of the FRC fusion reactor for deep space missions was recognized in a NASA study [1].

2. TECHNICAL BACKGROUND

FRCs are compact toroidal plasmas confined usually in a cylindrical magnetic chamber, and without any significant toroidal magnetic field. A sketch of the geometry is shown in Fig. 1, and a review of the subject before the LSX experiments is given in Ref. [2]. The FRC has such unique properties that it appears to have been designed solely with propulsion applications in mind. These properties are listed below.

Simple, linear, low field magnet system.

1. High plasma pressure. Radial pressure balance requires the plasma energy density, nkT, $\cong B^2/2\mu_0$, that of the axial magnetic field.
2. Directed, unobstructed linear exhaust of detrapped plasma that can be ejected out either end with a simple magnetic mirror field.
3. Unique ability to burn advanced fuels with low neutron output.

The same attributes that make FRCs ideal for propulsion applications also make them the most attractive engineering option for terrestrial fusion power generation. Relative to the tokamak, the development of the concept has not been vigorously pursued. This has been due partly to the early historical success of the tokamak and partly for political reasons (rapid development of a scientifically proven confinement scheme). It had always been assumed that a toroidal field was necessary to provide magnetohydrodynamic (MHD) stability. The

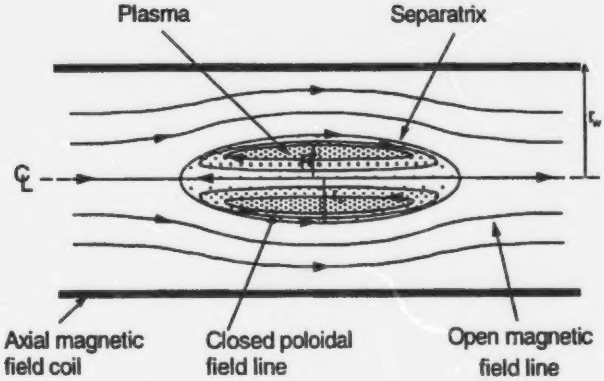

Figure 2. FRC geometry showing flux surfaces

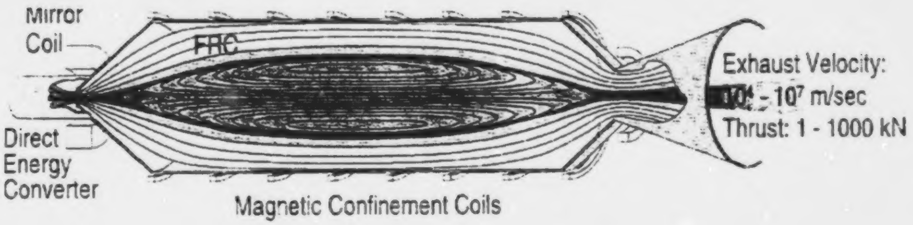

Table 3. FRC as power source and ion engine for deep space missions

observed stability of FRCs has been attributed to kinetic effects represented by the parameters, (a ratio of the number of internal ion gyroradii to plasma radius), and these stabilizing effects diminish for s >> 1. Recent experimental results on LSX [3,4,5] have shown that FRCs are robustly stable at large s values (above 4), where reactors must operate (s~20). Recent theoretical developments have shown that kinetic effects are much less important than previously thought [6]. The latest theoretical work has concentrated on showing that the FRC may represent a fundamental minimum energy state, and thus develop naturally out of initial chaos [7]. There is experimental evidence for this in recent Japanese experiments.

For propulsion applications, and even for space power generation, it is desirable that most of the fusion reaction products be charged ions, rather than neutrons as they are for the standard D-T fuel cycle.

The plasma exhaust can then be used for both propulsion and direct energy conversion (see Fig. 3 above). The extensive shielding, blanket, and thermal power equipment required for a D-T burning reactor would not be required. D-T is thought of as the primary fuel for first generation fusion reactors since it has the largest fusion cross-section and lowest ignition temperature.

There has been a realization in the fusion community for some time that other fuel cycles, utilizing low or zero neutron-producing fuels, would be far more desirable. The D-^{3}He reaction produces ^{4}He and a proton, rather than the ^{4}He and neutron produced by D-T. However, due to the higher required burn temperatures of such fuels, magnetic confinement schemes with even moderate internal magnetic fields can not burn them due to high synchrotron radiation losses preventing ignition. The FRC has low internal magnetic fields and could readily burn aneutronic fuels. The discovery of large deposits of ^{3}He on the moon (deposited by the solar wind) has spurred renewed interest in aneutronic fusion. In fact, a group of Japanese researchers has spent several years designing an FRC reactor using D-^{3}He for terrestrial power generation [8]. The use of D-^{3}He in an FRC would thus be the ideal fusion system for space [9].

A magnetic fusion reactor must reach a product of density and energy confinement time, $n\tau_E \sim 1020\ m^{-3}$sec for break-even power output from fusion. This has so far only been achieved in large tokamaks, but the lifetime scaling in small FRC experiments looks very favorable. Lifetime scaling results from FRC experiments are shown on Fig. 4. The most recent LSX results exhibit very strong scaling with the plasma radius rs, with also a strong dependence on the ion gyroradius ρ_i (which is generally about 3-5 mm). Most of the data points were at $1\text{-}5\times10^{21}\ m^{-3}$ densities, about an order of magnitude higher than for any other magnetic fusion device due to the inherently high β - the ratio of plasma energy to external confining magnetic field energy ($\langle\beta\rangle \sim 1$ for the FRC).

Although LSX was highly successful in forming stable FRCs with good confinement, the internal flux ~ 10 mWb, decayed away on a msec time-scale since there is no transformer threading the 'toroid' as there is in a tokamak. Confinement times in the 100 msec to 1 sec. range are needed to achieve the $n\tau_E$ confinement parameter needed for fusion burn. To achieve

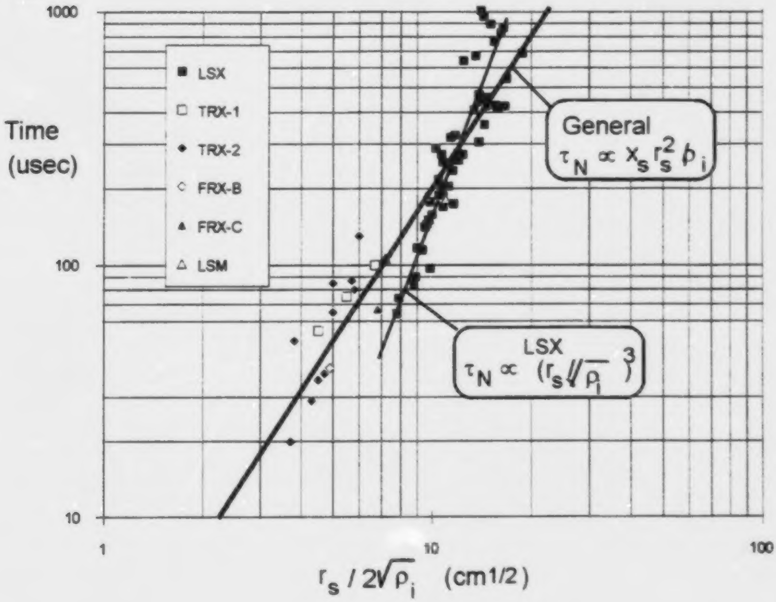

Figure 4. Measured FRC particle lifetime scaling

these confinement times, flux levels will have to be ~ 1Wb, which is most likely beyond the capabilities of the field-reversed θ-pinch (FRTP) formation used in virtually all FRC experiments. Under the NASA sponsored program an experiment, the Star Thrust eXperiment (STX), has been constructed to investigate the use of rotating magnetic fields (RMF) to form, sustain, and increase the flux of FRCs. The key questions involve generation of the RMF in the plasma, and synchronous drive of the electrons. This flux generation mechanism is similar to an induction motor, and would produce the large fluxes necessary for reactors. Previous RMF experiments, conducted at low power in small facilities, had generated FRCs without using a FRTP, but the low available powers and poor preionization methods prevented hot, fusion relevant plasmas from being achieved [10].

3. RF CURRENT DRIVE

The FRC configuration is produced by a strong azimuthal current, which reverses the external axial magnetic field direction. In FRTPs this current is induced by applying a high azimuthal voltage. A rotating magnetic field, applied as sketched in Fig. 5, is a much simpler, and far more efficient method of generating this current. It also has the advantage of being a steady state technique for current sustainment. In order to drive only the electrons, and not the ions, the rotation frequency ω must also be less than the electron cyclotron frequency ω_{ce} = eBω/me, with respect to the wave field Bω, and greater than the ion cyclotron frequency ωci = eBω/mi The electron-ion collision frequency vei must be much lower than ω_{ce} so that the electrons will stay magnetized and be dragged along with the rotating field. When this is the case, the current density is given by j_θ = -eneωr. This plasma current in combination with the external coil current (in the opposite direction) results in the confining poloidal field depicted in Fig. 5. The applied magnetic field Bω can penetrate into such a collisionless plasma since

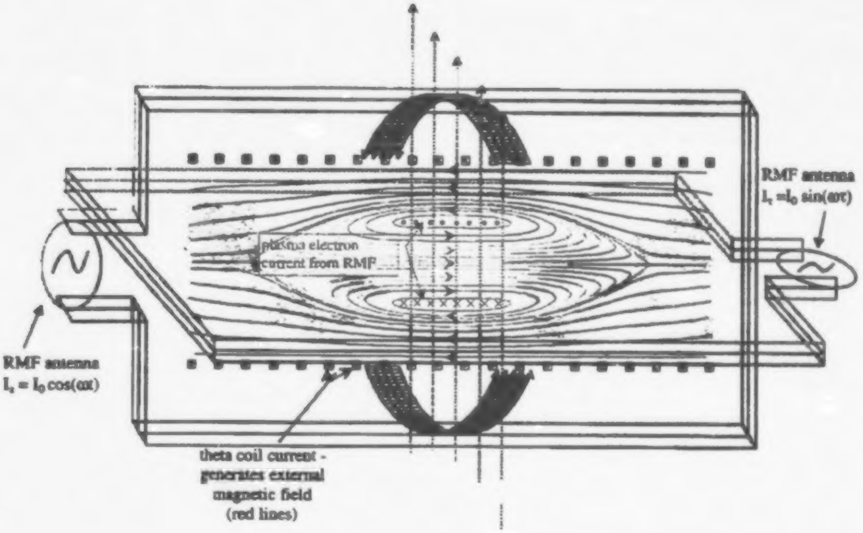
RMF antenna
$I_s = I_0 \sin(\omega t)$
plasma electron current from RMF
RMF antenna
$I_c = I_0 \cos(\omega t)$
theta coil current - generates external magnetic field (red lines)

Figure 5. Coil, antenna, and plasma currents with the resultant magnetic fields.

the electrons see a nearly stationary field in their own frame of reference. Current drive in this manner has been demonstrated experimentally and explained theoretically by Hugrass [10].

Penetration of the RF field into an existing plasma is more complicated in that the FRC screens out the RMF with image currents on the diffusion timescale which is comparable to the configuration lifetime. If the RMF fields are present and embedded in the plasma during the initial preionization a much simpler picture arises. Assuming that one has full RMF penetration in a plasma with a quasi-steady current drive, one can then examine the conditions that must be satisfied for this state to persist. The frequency condition: $\omega_{ci} < \omega < \omega_{ce}$ clearly becomes the first condition as explained above. From the electron equation of motion

$$-e/m[\mathbf{E} + (\mathbf{u} \times \mathbf{B})] - \mathrm{vei}\,\mathbf{u} = \omega\mathbf{u}.$$

With the plasma resistivity and current density defined in the usual way:

$$\eta = \frac{m\nu_{ei}}{ne^2} \qquad \mathbf{j} = -ne\,\mathbf{u},$$

yields the following for a plasma where $\omega << \mathrm{vei}$:

$$\mathbf{E} = \eta\mathbf{j} + \frac{1}{ne}\mathbf{j} \times \mathbf{B}. \ \text{(Ohm's Law)} \tag{1}$$

The solution is characterized by the field penetrating a distance

$$\delta = \left(\frac{2\eta}{\mu\omega}\right)^{1/2}.$$

For = 1×10^6 sec^{-1}, n = 1×10^{20} m^{-3} and T_e = 100 eV, $\eta_c = 10^{-6}$, one has $\delta \approx 2$ mm. This is the usual skin depth for a conductor in an external RF field. However, for a hot, low resistivity plasma in the presence of a magnetic field, the Hall term (second term in eq. 1) can dominate over the resistive term. From eq. 1 this occurs when $\eta << B_\omega/ne$ or equivalently $v_{ei}/\omega_{ce} <<1$. This is of course the regime of interest for RMF current drive. Solution of the nonlinear Ohm's law with the resistive term now as a correction yields [10]:

$$j_q = \frac{\nu\varepsilon\rho w}{1+2\left(\dfrac{n_{\varepsilon\iota}}{w_{\chi\varepsilon}}\right)^2}.$$

The Hall effect causes the electron fluid to rotate with the magnetic field. This synchronous rotation produces a current density $j_\theta \approx ner\omega$. The effect of collisions is to cause a slip between the electron fluid and the RMF. The solution for the axial current density is

$$j_z = \frac{E_z}{h\left(1+\dfrac{1}{2}\left(\dfrac{n_{\varepsilon\iota}}{w_{\chi\varepsilon}}\right)^2\right)}.$$

This suggests that an effective resistivity η_{eff} can be defined such that

$$\eta_{eff} = \eta\left(1+\frac{1}{2}\left(\frac{\nu_{ei}}{\omega_{ce}}\right)^2\right)$$

so that $E_z = \eta_{eff} j_z$. The effective skin depth is thus

$$\delta_{eff} \approx \frac{\delta}{\left(\dfrac{\nu_{ei}}{\omega_{ce}}\right)}.$$

If maximum current is to be driven, this skin depth must be comparable or greater than the plasma radius, or $\underline{\delta_{eff} \geq r_s}$, which becomes condition 2.

The synchronous rotation of the electrons with the RMF is interrupted only by collisions that, in a sense, de-magnetize the electrons and allow them to slip from the rotating field. Thus RMF penetration and current drive is more effective with decreased collisionality or higher conductivity. Another way to view this seemingly contradictory dependence is to consider the RMF in the electron frame of reference. The increased penetration is due to the Doppler shifted frequency of the RMF to near zero in the reference frame of the co-rotating electrons. Only the slippage off the RMF field lines from collisions that prevents perfect penetration. The previous assumption that $v_{i\theta} << v_{e\theta}$ is equivalent to not having the ions rotate with the RMF. It was already mentioned that the ions must not be magnetized to the RMF, which sets an upper limit on ω, but it is also necessary that the electrons do not transfer their momentum to the ions over a long time-scale. Two fluid calculations show this is easy to achieve with even minimal fueling rates since the fuel ions are deposited with zero angular momentum, and they diffuse out much faster than they gain momentum from collisions with electrons [11]. The two conditions that must be met for effective current drive are then

1) $\omega_{ci} < \omega << \omega_{ce}$
2) $\delta_{eff} > r_s$.

Many experiments and calculations show the latter criterion to be the key requirement [12]. For deuterium with the RMF measured in gauss,

$$\omega_{ci} = 4.8x103\ B_\omega(G)\ sec^{-1}$$
$$\omega_{ce} = 1.8x107\ B_\omega(G)\ sec^{-1}.$$

In numerical units these conditions can be written as a constraint on the RMF field in terms of the FRC density collisionality and size:

$$B_\omega(G) > 55\ n_e(1020\ m^{-3})\ \nu_{ei}(10^6\ s^{-1})\ r_s^2(m)$$

The classical electron-ion collision frequency is $\nu_{ei} = 10^5 n_e(10^{20} m^{-3})/T_e^{3/2}(keV)\ sec^{-1}$, and very low wave field strengths are thus sufficient for hot plasmas. For typical steady state FRC

Table I

	Start-up Experiment	**D-He^3 Reactor**
Fuel	D	D-He^3
r_s (m)	0.18	1.0
B_e (T)	0.3	5
n_e (10^{20} m^{-3})	1	5
T_e (keV)	0.1	30
T_i (keV)	0.7	70
ν_{ei} (10^6 s^{-1})	1	0.0025
ω (10^6 s^{-1})	3	0.25
B_ω (T)	0.01	0.0025
ω_{ci} (10^6 s^{-1})	0.5	0.10
ω_{ce} (10^6 s^{-1})	1800	450
δ (m)	0.002	0.02
δ_{eff} (m)	1.2	1.4
I'_{sat} (MA/m)	0.5	10
ϕ_p (Wb)	0.008	2.5
τ_ϕ (sec)	0.0023	44
P'_{rmf} (MW/m)	1.2	0.26

conditions in the proposed experiment, $n_e = 10^{20}$ m^{-3}, T_e = 100 eV, the classical collision frequency is vei = 3x106 s-1 and the classical resistivity is $\eta_c = 1\text{x}10^{-6}$ Ω-m. For an RMF with B_ω = 100 G (0.001 T), and $\omega = \pi\text{x}10^6$ s^{-1} one has δ_{eff} = 1.2 m (>> r_s ~ 0.2 m) as well as $\omega_{ci} < \omega << \omega_{ce}$.

For a reactor it is necessary that the effective electron collision frequency be much lower in order to provide for longer penetration distances. A listing of RMF parameters and required collisionality for the proposed start-up RMF experiment and a full scale D-He^3 reactor is given in table I.

The start-up conditions reflect the final conditions after preionization and heating have occurred. The synchronous current driven by the RMF is defined as $I'_{sync} = ne\omega r_s2/2$. It should be noted that the transverse RMF field is small for both the start-up experiment as well as the reactor. The power required to sustain the FRC after start-up is quite modest with only 250 kW needed to sustain the confining flux in the reactor case. This is because only a small transverse field is required to entrain the electrons and produce the megamp currents needed. It should be noted that the magnitude of the driven current does depend on the RMF field strength, only the RMF frequency, plasma density and size determine the magnitude of the confining poloidal field. Since The RMF field, $B_\omega << B_e$, (the axial field generated) the radial energy confinement should not be unduly influenced by this small transverse field.

4. D-T FUSION ENGINE

In the near term the use of ^{3}He as a fuel will be quite limited. It is possible to meet the requirements laid out in Fig. 1 however with the D-T reaction. The efficiency of the engine is decreased by roughly a third since 80% of the fusion energy is in the form of neutrons that must be thermalized. The lower fusion temperature and densities required for the D-T reaction translate into a confinement field that would not need to be superconducting, which would considerably reduce the complexity and additional mass required for the cryogenic systems. The parameters for such an engine producing 500 MW of fusion power are given below in table II.

Table II. FRC D-T fusion engine reactor parameters

L_{con} R_{con}	8 m 2.5 m	Plasma Density n_e	3x10^{20} m^{-3}
L_{FRC} R_{FRC}	6 m 1.2 m	Plasma T_{ion}	13 keV (1.5x10^8 °K)
B_e (field ext. to FRC)	1.7 T	Plasma Inventory	32 mg D,T
Fusion Power	500 MW	Plasma Radiated Power	12 MW
P_{Jet} $P_{Thermal}$	80 MW 414 MW	Magnet Mass (Alum.)	30 MT
$\alpha = \Pi_{Thrpower}/M_{Prpwr}$ 218 MΩ/60 MT = 3.6 κΩ/κγ			

REFERENCES

1. N.R. Schulze. Fusion Energy for Space Missions in the 21st Century. NASA Technical Memorandum 4297, Executive Summary (1991), p. 39.
2. M. Tuszewski. Nucl. Fus. 28, 2033 (1988).
3. A.L. Hoffman and J.T. Nucl. Fus. 33, 23 (1993).
4. J.T. Slough et al. Phys. Rev. Lett. 69, 2212 (1
5. J.T. Slough et al. Phys. Plasmas 2, 2286 (1995).

6. A. Ishida, R. Kanno and L.C. Steinhauer. Phys. Fluids **B 4**, 1280 (1992).
7. L.C. Steinhauer, A. Ishida and R. Kanno. Phys. Plasmas **1**, 1523 (1994).
8. H. Momota, A. Ishida, Y Kohzaki, G.H. Miley, S. Ohi, M. Ohnishi, K. Yoshikawa, K. Sato, L.C. Steinhauer, Y. Tomita and M. Tuszewski. Fusion Tech. **21**, 2307 (1992).
9. R. Chapman, G. Miley, W. Kernbichler and M. Heinder. Fusion Technology **15**, 1154 (1989).
10. W.N. Hugrass. J. Plasma Physics **28**, 369 (1982).
11. M. Ohnishi and A. Ishida. Effects of Radial Flow on Current Drive in Field-Reversed Configurations by Rotating magnetic Field - to be published in Nuclear Fusion.
12. H.A. Blevin and P.C. Thonemann. Nucl. Fusion: 1962 Supplement, Part 1, 55 (1962).

EXPERIMENTAL INITIATION OF FIELD-REVERSED CONFIGURATION (FRC) TOWARD HELIUM-3 FUSION

Seiichi Goto

Plasma Physics Laboratory,
Osaka University
Yamada-Oka 2-1, Suita
Osaka 565-0871, Japan

ABSTRACT

Many kinds of experimentally progressive works are summarized in the FIX-FRC device, which aim to approach the D-^{3}He fusion reactor. Physics and technique of translation of the FRC formed in the theta pinch coil are presented. The confinement properties of the FRC are given together with the nature of the scraped plasma and the loss flow. This suggests the existence of different scaling from the nominal one. New experiments are also tried to open the near future prospect in FRC studies.

1. INTRODUCTION

Field-reversed configuration (FRC) has obtained a promising position as unique candidate for the deuterium-Helium-3 fusion core plasma, since the conceptual design of the FRC-based reactor "ARTEMIS" appeared [1]. The design is initiated from the intrinsic properties of the FRC. The following three properties with the FRC are essential for the helium-3 fusion plasma core. First, the extreme high beta (≥90%) nature can avoid the electron synchrotron radiation loss problem. The existence of the natural open divertor around the core, secondly, enables to exert the fusion protons of 15 MeV toward the direct energy convector which will be located at the big open space on the geometrical axis of the core. As the third, the shape and position control of the FRC can be realized by the translation technique. This could be necessary to overcome the reactor design problems.

Present achievements of experimental and theoretical works on the FRC are, however, insufficient for allowing the worldwide fusion society to promote a big project of the FRC experiment. This may not deny the proposed potentiality of the FRC-based Helium-3 fusion but indicates the need of much more financial support as recommended by R.F. Post at the former meeting [2]. The main requirement from the ARTEMIS design is to solve the

Current Trends in International Fusion Research — Proceedings of the Second Symposium
Edited by E. Panarella. NRC Research Press, National Research Council of Canada, Ottawa, ON K1A 0R6, Canada. 1999.

various issues for the production of a seed FRC plasma to have the feasibility of the post-evolution up to the fusion ignition. If this is resolved, the way to a Helium-3 reactor may quickly open even as for the problems on engineering, economy and environment. This is called by "Goal Oriented Strategy" , and suggested by the ARTEMIS design work.

In this paper, the author will present a systematic experiment in our FIX-FRC apparatus at Osaka [3], which aims to approach the realization of a kilovolt sustained FRC plasma as a seed FRC mentioned above. In the following sessions, the translation of FRC into a metal chamber from the formation region, some transport characteristics of the confined FRC in a mirror field, and some new trial experiments for heating will be described.

2. EXPERIMENTAL APPARATUS

The experiments are conducted on the FIX apparatus which is shown in the schematic drawing of Fig 1. The main part consists of two regions. One is the FRC formation region and the other the confinement region into which the formed FRC plasma can be translocated as explained later.

2.1 Formation Region

The formation scheme is based on the inverse-biased theta-pinch method. The inner diameter and the length of the main theta coil are 0.31m and 1.17m, respectively. At each end of the pinch coil a driven mirror coil is mounted, which can operate to make the forced reconnection of the end field and also to push the plasma down to the confinement area. The typical field is 1T at the main with the bias field of 0.04T, and the rising time is ~4μs. Inside the quartz tube of 0.27 m inner diameter, deuterium gas puff is pre-ionized and quickly made to be the FRC plasma with (T_e+T_i) ~450eV, n_e~$6\times10^{21}m^{-3}$, r_s ~0.04m and $2l_s$ ~0.90m. Although the FRC can be contained here, this compact toroid is forced to move by the driven coils for the translation experiment.

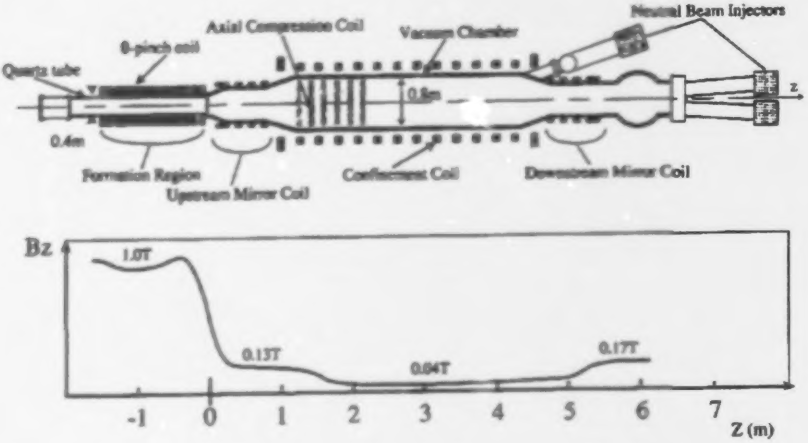

Figure 1. Schematic drawing of FIX-FRC apparatus. The axial magnetic field distribution is also presented. The vertical and the horizontal scales are the same as z-axis of the field distribution.

2.2 Confinement Region

This is composed by a central straight part of 3m length, two tapered parts which make a pair of magnetic mirrors and neutral beam (NB) injectors at the down-stream side. The central metal vacuum chamber of 0.80 inner diameter can hold the decompressed FRC plasma with (T_i+T_e) ~ 150eV, n_e ~ $5\times10^{19}m^{-3}$, r_s ~ 0.2m and $2l_s$ 3.0m, in the quasi-steady magnetic field of 0.04T after the translation process. Note that the mirror ratio can be chosen to be 2 ~ 8 under the 0.04T straight field and then the contained plasma state is sometimes sensitive to that. Typical mirror ratio is 3.0 for the experiment described here.

3. TRANSLATION PROCESS

It is still unknown what kind of relation between the initial formation and the final confinement stages holds. Only a simple scaling [4] has been given according to the conservation of magnetic flux, internal energy and total inventory together with some supposed equilibrium formula. However this relation breaks for the experiment here. Then our work concentrates to the study of the dynamical process during the FRC movement. Fig. 2 represents the time and space evolution of the excluded flux radius r_s of the FRC measured by

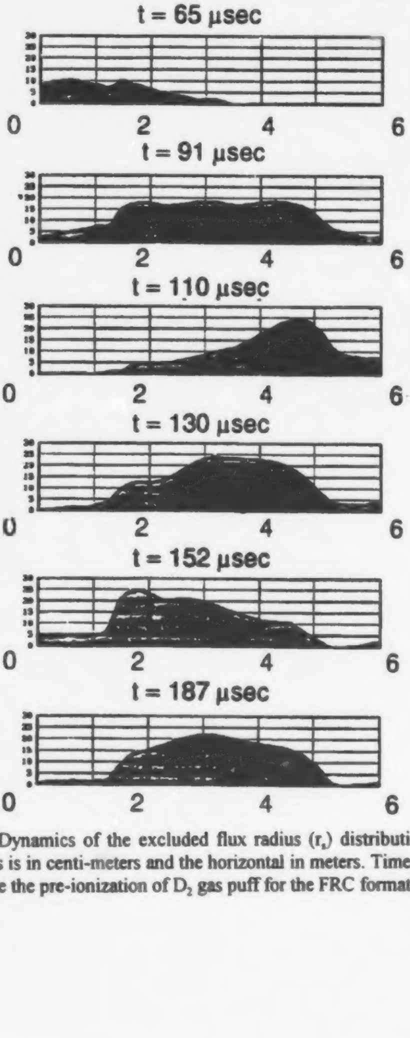

Figure 2. Dynamics of the excluded flux radius (r_s) distributions. The vertical axis is in centi-meters and the horizontal in meters. Time origin is chosen to be the pre-ionization of D_2 gas puff for the FRC formation.

a magnetic pick-up probe array with 30 channels along z-axis. An FRC is produced in the formation region at t~50 μs and pushed out to the confinement region, where the traveling velocity is around 2 × 10^5 m/s in the 0.04T guiding field. This directed kinetic energy with super-Alfvenic speed can be converted into the internal thermal energy when the FRC is reflected at the down-side mirror field (t = 90~120 μs). The conversion efficiency is estimated to be 50 ~ 80% against the various mirror ratios, and its rethermalization mechanism is found to be a shock-like process in the collisionless regime [5], [6]. This may promise that the same translation sheme is adaptable for the future FRC reactor core production.

Another type of translation experiment has been performed on the control of deflecting the FRC movement across a curved magnetic field. In the transverse field of 0.007T added to Bz ~0.04T, the FRC plasmoid moves as crossing the curved guide field with holding the configuration [7]. This suggests some applicability of a new seed FRC injection, for example, that is a steering injection. Moreover, This result is contrary to that for the movement of plasma without closed magnetic flux lines. The examination of this type of experiment will give a scientific sound to many branches of plasma physics.

4. CONFINEMENT

The usual evaluation of the confinement characteristics in the FRC experiments relies on the nominal scaling $\tau_N \propto R^2/\rho_i$ as a reference [8], where τ_N is the decay time of inventory, R the major radius $\left(=r_s/\sqrt{2}\right)$ and ρ_i the ion Larmor radius in the external field. In our case, the observed τ_N=0.2~0.3 ms and this is 3~5 times larger than the predicted value by the scaling. It may be, however, pointed out that the experimental value of τ_N has a serious question because of the short time span of the signals for the estimation or since the exponential filing is sometimes not well. The most good fitting of the data to the exponential curve can be obtained for the case of the flux decay signal as shown in the curve of Fig. 3. In this case, the obtained value of τ_N~120 μs is again out of the scaling up to now. This suggests the existence of a new scaling law in the low density range of FRC in comparison with the usual range of $n_e \geq 1\times10^{21}m^{-3}$.

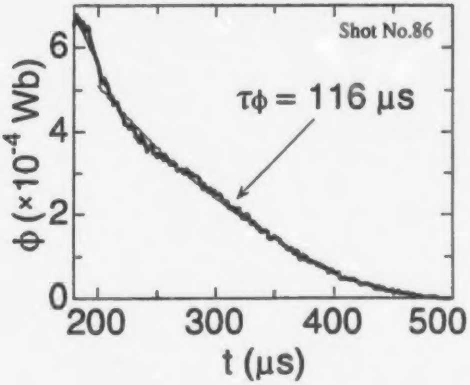

Figure 3. Flux decay signal during the quiescent phase after the translation movement. The value of τ_ϕ = 116 μs is the fitting is the fitting constant.

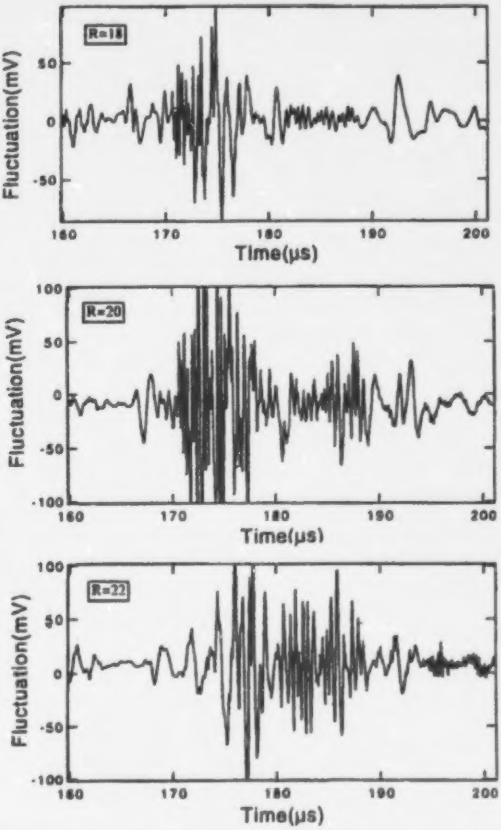

Figure 4. Magnetic fluctuation signals on the radial position of 18 cm, 20 cm, and 22 cm in one shot discharge. $\tilde{B}/B = 10^{-3} \sim 10^{-4}$ for f = 1 - 10 MHz ($3\ \Omega_i$ ~ $0.4\ f_{LHD}$).

The anomalous transport in FRC has been thought to be caused by the lower-hybrid-drift (LHD) instability [8]. In the FIX experiment, there have been performed the measurements of the fluctuation by several methods such as the forward scattering, the Fraunhofer diffraction of CO_2 laser with 10 μm, and some small-size internal magnetic probe [9]. However, no LHD fluctuations have been detected with the serious level over 1% of the density. Only the magnetic probe gives the fluctuations of ~1% in several hundred KHz which is near to the ion cyclotron frequency, and that of ≤0.1% below LHD frequency, as shown in Fig. 4.

In order to reveal the particle loss channels, we have extensively studied on the scraped-off layer and the end-loss plasmas [10], [11], using the various kinds of diagnostics such as the single, the double and the triple electrostatic probes, the Mach probe, magnetic probes, the special Faraday cup, the Doppler shift and the interferometer. These techniques can be applied because the confinement region is apart from the formation in the high voltage circumstance. The pressure profile just outside the separatrix shown in Fig. 5 is found to be exponent with the normalized thickness $\delta/\rho_i = 1.0$~1.2. The density and the temperature are ~2×10^{19} m^{-3} and magnetic line of force to the mirror throat. The flow velocity is estimated to be ~5×10^{3} m/s in

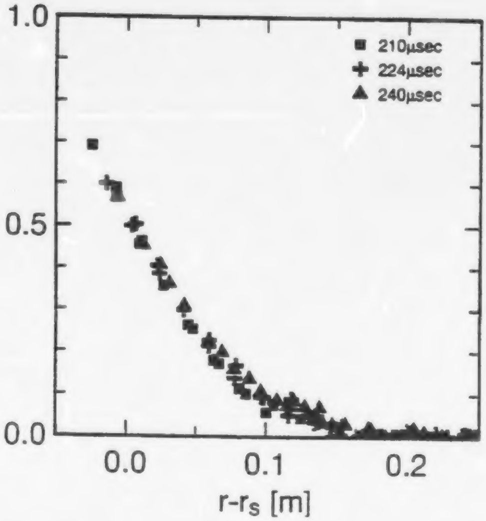

Figure 5. Radial profiles of the plasma pressure outside the separatrix radius.

the straight line by the Mach probe measurement. At the mirror throat where the flow behaves like as a jet stream, the measured parameters are as follows; the central density ~4 × 10^{19} m^{-3}, the jet velocity 5 × 10^4 m/s and the jet radius ~0.07 m for the mirror ratio of 3. Then, the particle loss rate from the two mirrors is estimated to be ~7 × 10^{22} /s. The decay rate of the particle number of the core FRC is, on the other hand, (5~10) × 10^{22} /s, which is consistent with the end loss measurement. Thus the loss measurement at the jet region is designated to be a powerful tool for particle confinement study of the FRC.

We have been also developing a novel particle energy analyzer to be able to measure the axial and the azimuthal velocity distribution simultaneously [12]. The average energy of ions lost from the mirror throat is ~100 eV derived from the measurement by the analyzer. This is the same value of the confined ion temperature, and so the ion energy loss in the FIX-FRC seems to be convection energy loss. The loss rate in this mirror throat is found to be (6~10) × 10^5 J/s [13]. However, the total energy decay of the core plasma is (3~5) times larger than this value from the diamagnetic measurement. This is quite different to the results discussed in other FRC's [8], [14].

5. ADDITIONAL EXPERIMENTS

In near future studies of the FRC, it is required to find the experimental technologies to realize a quasi-stationary FRC. For the purpose, heating techniques, fueling methods, seed current production, and confinement control will be expected. The following preliminary experiments are conducted in our FIX device. A trial to heat the held FRC plasma by a fast rising magnetic field has been performed [15]. This is found to excite some kind of magnetic wave in the FRC, and may lead to the RF wave application to the extreme high-beta plasma heating. A megawatt class of neutral beam injectors (NBI) have been already installed as shown in Fig. 1. This will be used to understand how to make the current seed and also to heat the plasma. In order to study the confinement scaling together with the heating, the axial magnetic slow-mode compression program is just undertaken. This technique can make the feasibility that the elongation factor of the FRC is changed in time. The compression or the length shortening has been already achieved without a deleterious effect.

6. SUMMARY

Although the goal of the D-^{3}He fusion reactor will be very far from the present status of the FRC study, it is insisted that the principal nature of the FRC may fit the requirement from the reactor study. The present experiment in the FIX shows that the translation technique will be applicable for the reactor case. The particle and the confinements are now in the critical level, but some improvements are in progress. Further heating and seed current application begin to be explored by the experiment.

REFERENCES

1. H. Momota, A. Ishida, Y. Kohzaki, G.H. Miley, S. Ohi, M. Ohnishi, K. Sato, L.C. Steinhauer, Y. Tomita and M. Tuszewski. Fusion Techn., **2**, 2307 (1992).
2. B. Coppi, C. Deutsch, E. Panarella, F. Pegoraro, R.F. Post, H. Rahman, N. Rostoker, J.R. Roth, N.A. Salingaros, G. Velarde and C. Yamanaka. J. Fus. Energy, **14**, 285, (1995).
3. H. Himura, S. Okada, S. Sugimoto and S. Goto, J. Plasma Phys., **2**, 191 (1995).
4. T. Tanjyo, S. Okada, Y. Ito, M. Kako, S. Ohi, S. Goto, T. Ishimura and H.Ito. Tech. Reports Osaka Univ., **34**, 201 (1984).
5. H. Himura, S. Okada and S. Goto, Trans. Fusion Technol., **27**, 345 (1995).
6. H. Himura, S. Ueoka, M. Hase, R. Yoshida, S. Okada and S. Goto, Proc. 1996 Int. Conf. Plasma Phys., **2**, 1190 (1996).
7. H. Himura, H. Wada, S. Okada, S. Sugimoto and S. Goto. Phys. Rev. Lett., **78**, 1916 (1977).
8. M.Tuszewski, Nucl. Fus., **28**, 2033 (1988).
9. S. Okada, S. Ueki, H. Himura and S. Goto. Trans. Fus. Tech., **27**, 341 (1995).
10. S. Goto, K. Matsumoto, H. Himura, D. Sadahiro, Y. Suzuki, M. Okubo, S. Sugimoto and S. Okada. Proc. 1994 Int. Conf. Plasma Phys., **1**, 165 (1994).
11. T. Ohtsuka, M. Okubo, S. Okada and S. Goto, J. Plasmas Phys., **5**, 10 (1998) to be published.
12. M. Okubo, S. Okada and S. Goto. J.Plasma and Fusion Research, **70**, 1102 (1994).
13. M. Okubo, A. Ozaki, S. Okada and S. Goto. Proc. Int. Conf. Plasma Phys., **2**, 1186 (1996).
14. J.T. Slough, A. Hoffman, R.D. Milroy, E.A. Crawford, M. Cecik, R. Maqueda, G.A. Wurden, Y. Ito and A. Shiokawa. Phys. Rev. Lett., **69**, 2212 (1992).
15. S. Okada, H. Taniguchi, H. Sagimori, Y. Miyawaki, M. Hase, R. Yoshida, S. Sugimoto and S. Goto. Proc. 16th Int. Conf. Fusion Energy, **2**, 229 (1997).

HELIUM-3 FUSION BASED ON A FIELD-REVERSED CONFIGURATION

Hiromu Momota and Yukihiro Tomita
National Institute for Fusion Science
Toki 509-5292, Japan

ABSTRACT

An attractive characteristics of helium-3 fusion based on a field-reversed configuration is studied. A conceptual design of D-^{3}He fueled FRC reactor "ARTEMIS" [1] has been carried out showing that bases of engineering needed for achieving a commercial reactor are conventional and the cost of electricity from "ARTEMIS" is estimated as cheap as approximately 30 mills/kW·h. A low neutron yield allows us large freedom of reactor materials and reduces the problem of disposal of radioactive waste. Critical issues lie on the way to the target are clarified. A possible method to improve plant performances by applying polarized fuels is discussed too. A favorable characteristic of polarized fuels lies on the reduction of neutron yield and the compactness of the fusion core. Because of the enhancement of reactivity of D-^{3}He reaction by applying polarization, the neutron fraction in the total fusion power decreases to 1.3% with the same volume of "ARTEMIS" and consequently neutron wall loading is as low as 72 kW/m^2. Consequently, this low neutron mode gives us large freedom of choosing reactor materials. The fusion reactor using polarized fuels with the same neutron yields as "ARTEMIS" decreases its size from 196 m^3 to 33 m^3. This operation mode gives us the possibility of developing an economic fusion reactor.

1. INTRODUCTION

Nuclear fusion researches have been developed towards D-T fuel because of its large cross-section (5 barns for D-T; 1 barn for D-^{3}He). Among various confinement systems of plasma, especially a tokamak concept demonstrated good confinement results. Construction of "International Thermonuclear Experimental Reactor: ITER" is scheduled on the bases of this concept, which is programmed to demonstrate controlled thermonuclear fusion. The estimated cost for constructing ITER, however, is as expensive as around 10 billion dollars. The heat load on the divertors is estimated as 20 MW/m^2, which is one order higher than what

Current Trends in International Fusion Research — Proceedings of the Second Symposium
Edited by E. Panarella. NRC Research Press, National Research Council of Canada, Ottawa, ON K1A 0R6, Canada. 1999.

conventional technology allows. The high neutron flux of 10 MW/m^2 on the first wall requires the development of structural materials, which are sound during 100 MWy/m^2 of neutron flux for a commercial reactor. Some of these problems come from the 14 MeV neutrons from D-T reactions. To avoid these problems neutron-lean fusion research has been done [2], where the D-D and D-^{3}He fusion reactions are representative candidates. The D-D fusion produces neutrons of 2.5 MeV from D-D reaction as well as 14 MeV from D-T reaction. Since the production of neutrons from D-D fusion is half that from D-T fusion, this reaction unresolves the problems attributed to the neutrons. For the purpose of mitigating above the engineering problems a conceptual design of a commercial fusion reactor "ARTEMIS" [1] has been carried out on the bases of a field-reversed configuration (FRC) with D-^{3}He fuels. This design of "ARTEMIS" demonstrates several attractive characteristics: 1) The high beta value (= plasma pressure / magnetic pressure > 0.9) of an FRC and the application of direct energy converters should enable us to construct a cheap 1 GWe power plant of about 1 billion dollars. 2) Because of its low neutron flux (~ 0.2 MW/m^2) conventional materials allow us to keep the reactor sound during its full life of 30 years. 3) Because of its low neutron yields the reactor is intrinsically safe and environmentally acceptable in view of the disposal of radioactive waste. There are issues for developing "ARTEMIS" : 1) Physics understanding of plasma confinement in an FRC is still poor. 2) Helium-3 fuel must be obtained from the lunar surface. 3) Development of highly efficient direct energy converters is needed.

2. D-HELIUM-3 FUELED FRC REACTOR "ARTEMIS"

A comprehensive design study of the 1 GWe D-^{3}He fueled FRC fusion reactor "ARTEMIS" [1] was carried out for the purpose of examining its attractive characteristics and clarifying the critical issues for a commercial fusion reactor. The "ARTEMIS" is composed of a formation chamber, a burning chamber, and a pair of direct energy converters (DECs), all of which are connected by magnetic lines of force. In Fig.1, a whole view of the "ARTEMIS" is exhibited. The total length and the maximum radius of the device are 160 m and 10 m, respectively. An initial FRC plasma is produced by a fast reversed theta-pinch method in the formation chamber. With a fast acting gas puff for feeding mixed gas of D_2 and ^{3}He at 52 mPa and an axial contraction of an initial FRC, we obtain a plasma with an averaged electron density of 4×10^{20} m^{-3} and a plasma temperature of 3 keV. To produce an FRC plasma reliably, the aluminum oxide vacuum chamber must keep its axisymmetry as perfectly as possible to avoid unwanted magnetic disturbances. Just after the initial formation of the FRC plasma, an applied unbalance magnetic field gradient transfers the FRC plasma to the adjacent burning chamber. Injection of 1 MeV —100 A deuterium atom beam, injection of D-^{3}He fueled ice pellets, and a slow magnetic compression in the burning chamber evolves the volume, the number density, and the temperature of the plasma up to those for the D-^{3}He burning state. The representative parameters of the burning plasma is listed in Table 1. Most of the D-^{3}He fusion energy is carried by charged particle along the magnetic lines of force, which connect to a pair of direct energy converters, each of which has a cusp type DEC and a traveling wave DEC (TWDEC) [3]. The former is a double cusped shape for controlling the energy carried by leaked fuels and ashes components. The first cusp acts as an electron separator that separates electrons from ion components and introduces them to collector plates installed at the first line cusp. Ions pass through the first cusp because of its large moment of inertia and go to the second line cusp. Due to the applied electrostatic field, ions decrease their kinetic energy and then arrive at an ion collector plate. A conversion efficiency of 65 % is estimated to this cusp type DEC. Directly lost fusion protons with 15 MeV pass through the cusp type DEC because of their large inertia and are guided to the TWDEC. As energy of

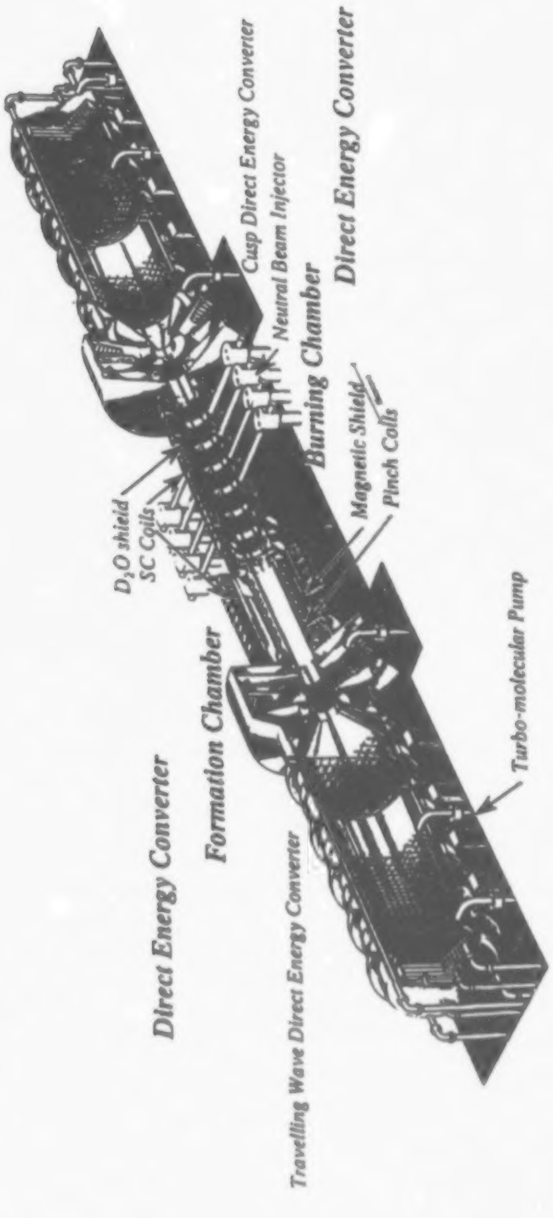
Direct Energy Converter
Formation Chamber
Travelling Wave Direct Energy Converter
D$_2$O shield
SC Coils
Burning Chamber
Magnetic Shield
Pinch Coils
Turbo-molecular Pump
Neutral Beam Injector
Cusp Direct Energy Converter
Direct Energy Converter

Figure 1. Whole view of 1 GWe D-^{3}He/FRC reactor "ARTEMIS"

Table 1. Representative parameters of D-^{3}He burning plasma in "ARTEMIS"

Plasma Volume (Radius × Length)	197 m^3 (1.68 m × 22.2 m)
Electron Density	5.1×10^{21} m^{-3}
Density Ratio of ^{3}He to D	1.35
Averaged Plasma Temperature	83.5 keV
Averaged Plasma Beta-Value	0.98
Energy Confinement Time	6.9 sec.
NBI Power	1 MeV × 100 A
Plasma Current	189 MA

15 MeV carried by fusion protons is too high to handle with an electrostatic method, a TWDEC is adopted on the basis of the principle of a Linac. The TWDEC consists of a modulator, which modulates the velocity of incident proton beams, and a decelerator with external transmission-circuits for energy recovery. The estimated conversion efficiency of this TWDEC is as high as 75 %. A small fraction of the fusion energy is carried by neutrons and photons to the first wall of the burning chamber. This energy is converted to electricity by turbine generators. The overall conversion efficiency is estimated as high as 70 %.

The representative power plant parameters of 1 GWe D-^{3}He FRC reactor "ARTEMIS" are listed in Table 2 where the same parameters from 'SSTR (Steady State Tokamak Reactor)', which was designed as a demonstration reactor in Japan Atomic Energy Research Institute [4], are listed as a reference. In the reactor "ARTEMIS" the plant efficiency (= output electricity / fusion power) is as high as 57 %. The fusion power of 1,757 MW is distributed almost in the same ratio to heat converters, TWDECs, and cusp DECs, which suggests that the development

Table 2. Representative plant parameters of "ARTEMIS"

	ARTEMIS	SSTR
Output Electricity (MW)	1000	1000
Fusion Power (MW)	1757	3000
Power Guided to Heat Converters (MW)	668	3710
Power Guided to TWDECs (MW)	526	x
Power Guided to Cusp DECs (MW)	573	x
Annual Consumption of Helium-3 (kg/years)	63.7	D - T
Heat Load on the First Wall (MW/m^2)	2	4.5 (Divertor)
Neutron Load on the First Wall (MW/m^2)	0.18	2.6
Radius of the First Wall (m)	2.28	2.2
Total Weight of the Reactor (tons)	4900	20,000 – 30,000

Table 3. Figure of merits from "ARTEMIS"

	ARTEMIS	SSTR
Total Capital Cost (Direct Cost)	1,800 M\$ (1,030 M\$)	8,640 M\$
Cost of Electricity	0.03 \$/kW·h	0.2 \$/kW·h
Level of Safety Assurance	1	2
Occupational Whole Body Exposure	1.4 mSv / 13 days	< 2,000 mSv / 13 days
Public Surface Exposure in Normal	4 mSv / 50 years	< 250 mSv / 50 years
Intruder Dose of Radioactive Wastes	0.0024 mSv / year	< 5 mSv / year

of highly efficient DECs is needed. The heat load on the first wall is around 2 MW/m^2. Since the life of the structural materials in a neutron irradiation is approximately 10 MW·y/m^2 with a ferritic steel, the neutron wall load of 0.18 MW/m^2 enables us to keep the first wall sound during the full reactor life of 30 years. The annual consumption of ^{3}He is estimated to be 64 kg for one 1 GWe reactor. The reactor "ARTEMIS" with a total weight of 4,900 tons is easy to construct and maintain because of its compactness and linear structure. Detailed studies on the reactor components are still needed to clarify their performances precisely. The cost of electricity (COE) from "ARTEMIS" [5], however, can be estimated on the basis of ESECOM studies [6] (Table 3). The estimated total capital cost and direct cost are 1,800 M\$ and 1,030 M\$, respectively. As we mentioned above, a ferritic steel as a first wall material appear to be appropriate for a 30 years operation. Thus we are able to assume a life of the reactor of more than 30 years. The cost of electricity would be 0.03 \$/kW·h as shown in Table 3, which must be compared to 0.2 \$/kW·h from a tokamak reactor. The estimated cost of helium-3 from the lunar surface is 0.15 – 0.30 M\$/kg [7]. This assumption of the cost of helium-3 slightly affects the COE and an expensive cost of helium-3 by a factor 5 gives still a low COE of 0.038 \$/kW·h. Since the D-^{3}He reactor has no breeding blanket for tritium production and the neutron yield is quite low, there is no nuclear heating of structural materials even in case of LOCA (loss of coolant accident) or LOFA (loss of flow accident). Consequently, the level of safety assurance is unity, i.e., the system is intrinsically safe. These aspects give the occupational whole body exposure and the public surface exposure in normal operations as low as 1.4 mSv/13 days and 4 mSv/50 years, which is two to three order lower than the allowable maximum.

The reactor "ARTEMIS" showed attractive characteristics by combining D-^{3}He fuels and an FRC as a plasma confinement system. The issues to be resolved for developing a commercial reactor are also clarified through the "ARTEMIS" design. Since we have poor understandings on an FRC plasma, the details of the transport phenomena in an FRC have to be clarified theoretically and as well as experimentally. The proof of principle of innovative DECs (cusp type DEC and TWDEC) is needed. The minable helium-3 on the lunar surface is estimated as about 10^6 tons [8], which corresponds to the amount of the energy demand in all of the world at the middle of the next century during 500 years. With regard to the Big-Bang originated ^{3}He the amount available in gaseous planets as Jupiter and Saturn is estimated to be as large as 10^{24} kg. Collaborative efforts between space engineers and fusion scientists are strongly recommended.

3. INTRODUCTION OF POLARIZED D-HELIUM-3 FUEL

The conceptual design "ARTEMIS" of 1 GWe D-^{3}He fueled fusion clarifies the attractive aspects for a commercial reactor. For developing a commercial reactor there are still issues to be resolved. By use of polarized fuels in a D-^{3}He fusion reactor the enhancement of reactivity brings a moderation of required plasma and engineering parameters. In order to see the polarization effects a parametric study of polarized D-^{3}He fueled fusion reactor in an FRC is carried out for the purpose of comparing the results with "ARTEMIS." In this study the cross-section of polarized D-^{3}He and D-T reactions is assumed to be 1.5 times larger than the respective unpolarized ones. Up to now there is no clear conclusion whether D-D reactions are suppressed by polarization or not. So we assume that D-D reactions are unaffected by the polarized fuels. The Hoffman's confinement scaling of FRC plasma [9] modified by Kurtmullaev [10] is also applied in the "ARTEMIS" study, where the particle confinement time is twice longer than the energy one. Operation conditions are obtained by analyzing the zero-dimensional continuity equations of particles and energy for respective species. Optimization studies are carried out for two modes, i.e., one minimizes neutron yields, another concerns the plasma volume. In these optimization studies the net output power is also 1 GWe and the heat load on the first wall of the device is limited to 2.0 MW/m^2, which level is applicable by the conventional engineering. In the small volume mode where neutron yield is the same as 56 MW of "ARTEMIS", plasma volume decreases to 33 m^3 and required energy confinement time is mitigated to 1.5 sec. The neutron wall loading, however, increases 2.4 times higher than "ARTEMIS." This wall loading level of 0.43 MW/m^2 corresponds to the 23 year-life of a ferritic structural materials (10 MW·y/m^2), which is shorter than the life of conventional reactor of 30 years. On the other hand the operation of low neutron mode, where plasma volume of 196 m^3 is the same as "ARTEMIS", gives us a reduced neutron yields as 23 MW. The required energy confinement time is similar to that of "ARTEMIS." For both of operation modes optimum plasma temperature is 84 keV, which is almost the same as "ARTEMIS."

4. CONCLUSIONS

The conceptual design of D-^{3}He FRC fusion reactor "ARTEMIS" has clarified the attractive characteristics for a commercial fusion reactor: 1) The high beta value (> 0.9) of an FRC and the application of direct energy converters enable us to construct a cheap 1 GWe power plant of about 1 billion dollars. 2) Because of its low neutron flux (~ 0.2 MW/m^2) conventional materials allow us to keep the reactor sound during its full life of a reactor. 3) Because of its low neutron yields the reactor is intrinsically safe and environmentally acceptable in view of the disposal of radioactive waste. 4) The cost of electricity is estimated as low as 0.03 $/kW·h.

The issues to be resolved for developing a commercial reactor were also clarified through the "ARTEMIS" design: 1) Details of the transport phenomena in an FRC have to be clarified theoretically and as well as experimentally. 2) Proof of principle of innovative DECs (cusp type DEC and TWDEC) is needed. 3) As helium-3 fuel must be obtained from the lunar surface, collaborative efforts between space engineers and fusion scientists are strongly recommended. A favorable characteristics of polarized fuels lies on the reduction of neutron yield and the compactness of the fusion plasma core. The neutron fraction in the total fusion power decreases to 1.3 % by applying polarization with the same volume of "ARTEMIS" and consequent neutron wall loading is 72 kW/m^2. The fusion reactor using polarized fuels with the same neutron yield as "ARTEMIS" decreases its size to 33 m^3. The depolarization effects in a magnetized fusion plasma are left to be studied. The developments of reliable method and cost to produce the large amount of polarized helium-3 and deuterium are also required.

REFERENCES

1. H. Momota et al. Proc. Seventh Int. Conf. on Emerging Nuclear Energy Systems. Makuhari, Chiba, Japan 20 - 24 September 1993 p.16.
2. H. Momota. Kakuyugo Kenkyu. **61**, 5 (1987) [in Japanese].
3. H. Momota. LA-11808-C, Los Alamos National Laboratory, New Mexico, USA (1989).
4. M. Kikuchi. Nucl. Fusion **30**, 265 (1990).
5. H. Momota. J. of Energy Society of Japan **72**, 91 (1993) [in Japanese].
6. J.P. Holdren et al. UCRL-53766, Univ. of California (1989).
7. H.E. Thompson. Proc. of Second Wisconsin Symp. on Helium-3 and Fusion Power (1993) 159.
8. L.J. Wittenberg, J.F. Santarius, and G.L. Kulcinski. Fusion Technol. **10**, 167 (1986).
9. A.L. Hoffman and J.T. Slough. Nucl. Fusion **26**, 1693 (1986).
10. B.B. Bogdanov et al. Proc. 13th Int. Conf. Plasma Physics and Controlled Nucl. Fusion Research. Washington D.C., October 1990, IAEA **2**, 739 (1991).

A USER FACILITY FOR RESEARCH ON FUSION SYSTEMS WITH DENSE PLASMAS

Dmitri D. Ryutov

Lawrence Livermore National Laboratory,
Livermore, CA 94551, U.S.A.

ABSTRACT

There are fusion systems whose dimensions can be scaled down to a few centimeters, if the plasma density and confining magnetic field are raised to sufficiently high values. These systems include the FRC, spheromak, Z-pinch, multiple mirrors, etc. The fusion-grade plasma in these systems can be obtained with the energy deposited to the plasma as low as 10–100 kJ. This prompts a "user-facility" approach to the studies of this class of fusion systems. The user facility would consist of a pulsed energy source (presumably, a Marx generator), and a set of diagnostics permanently deployed at the facility site. Research groups could bring their own "targets" (experimental assemblies of a few centimeter size) to perform series of experiments at the facility. Because of their small size, the targets will be relatively inexpensive and thus well within the reach of the university groups. The paper describes several specific experiments on creation and subsequent adiabatic compression of centimeter-size closed field line configurations. We also discuss possible development of stand-off energy sources suitable for pulsed fusion reactors with such "targets".

1. INTRODUCTION

There are a number of fusion systems whose dimensions can be scaled down to a few centimeters, if the plasma density and confining magnetic field are raised to sufficiently high values. These systems include the field-reversed configuration (FRC), spheromak, Z-pinch, multiple mirrors, and some others. The fusion-grade plasma in these systems can be obtained with the energy deposited to the plasma as low as 10–100 kJ. This prompts a "user-facility" approach to the studies of this class of fusion systems. The concept of such a user facility was first briefly mentioned in Ref. 1. Here we present a more detailed description.

The user facility would consist of a pulsed energy source (presumably a Marx generator) and a set of diagnostics permanently deployed at the facility site. Research groups could bring their own "targets" (experimental assemblies of a few centimeters size, see below for some specific examples) to perform a series of experiments at the facility. Because of their small size, the "targets" would be relatively inexpensive, and thus well within the reach of the university groups. The concept and design of the targets would be entirely the mission of the

Current Trends in International Fusion Research — Proceedings of the Second Symposium
Edited by E. Panarella. NRC Research Press, National Research Council of Canada, Ottawa, ON K1A 0R6, Canada. 1999.

participating groups. The availability of such a user facility for performing experiments should have a strong favorable effect on the creative potential of fusion research.

The main energy source could be a Marx generator with the stored energy up to 1 MJ and the pulse-length in the microsecond range. Certain pulse-shaping capacity would increase the range of possible experiments. A couple of separate energy sources with the energy content up to 100 kJ, for generating the bias magnetic field, would be desirable. The interface of the Marx generator and the load can be made very flexible.

The set of diagnostics should include optical, UV, and x-ray spectroscopy; neutron diagnostics (for both DD and DT neutrons, with tritium used as a trace element); optical imaging; and x-ray backlighting. The typical time-scale of plasma processes for the aforementioned fusion systems will not be shorter than 30–50 ns. Particular research groups might also provide their own diagnostics.

There is a similarity between the concept of a user facility presented in this paper and the concept of international center for the studies of plasma focus presented by Herrera [2]. Perhaps, a combination of the two would rise the chances for the actual creation of such a facility. There already exist examples of large facilities which serve, at least in part, as user facilities. The Nova laser in the Lawrence Livermore National Laboratory is used by a numerous university groups; the Z facility at Sandia National Laboratories (fast Z pinch) is a site of a number of collaborative multi-institutional experiments. The proposed facility would allow research groups with limited resources to contribute in a significant way to development of several fusion concepts.

2. EXAMPLES OF POSSIBLE EXPERIMENTS

To be more specific, we consider in more detail two possible experiments related to the FRC. The first is the study of the formation and properties of an FRC with the density $n \sim 10^{18}$ cm^{-3}, the temperature $T \sim 100$ eV, and the magnetic field strength $B \sim 100$ kG. This set of parameters corresponds to

$$\beta \equiv \frac{16\pi nT}{B^2} \sim 1 \tag{1}$$

The radius of the FRC can be $a \sim 1$ cm, and the length $L \sim 4$-6 cm. Such an object could then be adiabatically compressed by an imploding liner (see Ref. 3 for a more detailed discussion and further references).

Magnetic coils of a radius $\sim 1.5a$ would be used for creating the bias magnetic field and for the field reversal. The bias coil can have a relatively long pulse, up to a hundred microseconds. There should not be any problems in creating such a coil. The field-reversal coil should be turned on within a time of order of several axial Alfven transit times [4],

$$\tau = \alpha L / v_A \tag{2}$$

with α being of the order of 2. For the aforementioned set of parameters, and for a deuterium plasma, one has $\tau \sim 1$ μs. This estimate sets the time-scale for the controlled changes of the magnetic field.

The total energy content in the plasma will be ~ 1 kJ, and the magnetic energy will be several times higher, ~ 3 kJ (because the magnetic field occupies a larger volume). For $\tau \sim 1$ μs, the power level involved into the process of field reversal will be ~ 3 GW. The current in the coil,

$$I \sim \frac{cBL}{4\pi}, \tag{3}$$

should be ~ $1.5 \cdot 10^{15}$ CGS ~ 0.5 MA (for B~100 kG and L = 6 cm). The required loop voltage will be of the order of 7.5 kV. All these parameters are not very demanding and can be reached even without use of the main energy source. In this experiment, the pulsed magnetic system can possibly be designed so as to survive multiple shots.

At the temperature of 100 eV, the plasma will be fully ionized, and its radiative losses will be [5]:

$$P_{rad}(W) = 1.7 \cdot 10^{-32} n^2(cm^{-3}) T^{1/2}(eV) \cdot \pi a^2(cm) L(cm) \tag{4}$$

For the parameters given above, this power will be only 2.5 MW, much less than the total power delivered to the plasma during the reconnection event, 1 kJ/1 μs ~ 1 GW. This means that radiative losses from a pure plasma are negligibly small. For radiative losses to become considerable, the plasma should become very dirty, with the amount of heavy impurities (of the type of iron) in the range of 1%.

The FRC with the aforementioned parameters will have a ratio of plasma radius to a characteristic ion gyro-radius of ~ 30–50, much higher than in the existing experiments and very close to the values of this parameter expected for a FRC-based fusion reactor [4].

If successful, this experiment will pave the road to the second one, where the pre-formed FRC will be translated into an imploding liner of the type described in [3] and then adiabatically compressed. We conceive of a scenario where the on-axis hole through which the FRC will be injected will be closed early in the implosion, thereby trapping the FRC inside the liner. This can be achieved by using a liner whose linear density (mass per unit length) on the injection end is smaller than over the rest of its length (Cf. Ref. 6)

The compression should be 3-dimensional, because in 3D implosions the energy is delivered predominantly to the plasma, not to the embedded magnetic field (Cf. Ref. 3). The feasibility of quasi-spherical implosions has been demonstrated in the experiments by Degnan et al [7]. In geometrically self-similar 3D implosions, the plasma temperature scales as

$$T = T_0 C^2 \tag{5}$$

where C is a linear convergence (the ratio of the initial dimension to the instantaneous dimension). If one starts with the plasma with the temperature T_0 = 100 eV, the fusion-grade plasma needs reaching C ~ 7–10. Note that, in the aforementioned experiments by Degnan et al, the maximum linear convergence was close to 7. According to the analysis carried out in Ref. 3, the life-time of the hot dense state is determined by the liner expansion under the action of the plasma pressure. For the liners with a mass of a few grams, one can obtain the fusion gain Q ~ 1. The energy delivered to the liner should be in the range of 100-200 kJ. Assuming that the efficiency of the energy transfer from the condenser bank to the liner is ~ 10%, one sees that the energy stored in the condenser bank should be 1–2 MJ. This sets the scale for the main energy source for the user facility.

The experimental assembly will now have to be replaced after every shot (for this reason, we have used the word "target" to designate the experimental assembly). But since the target is compact (with the maximum dimension not exceeding 10–15 cm), manufacturing a few dozen targets for one experimental campaign should be inexpensive. We imply that the experimental group will bring these targets to the user facility and "shoot" them out within a couple of weeks.

3. DIAGNOSTICS ISSUES

The possibility of providing a set of sophisticated diagnostics permanently deployed at the user facility is one of the most attractive features of the user facility approach (the diagnostics constitute, possibly, the most expensive part of the hardware). For the configurations where the plasma is not obscured by the liner, one can use spectroscopy to measure relative line intensity, Stark broadening, Doppler broadening, possibly with a deliberate adding of trace impurities. The electron density and temperature could be measured by Thomson scattering. Faraday rotation could be used for the measurements of the magnetic field. Optical and UV imaging could be used to view an overall structure of the plasma configuration. For the configurations obscured by the liner, one could perform X-ray imaging (provided the liner material is transparent in the chosen spectral band) as well as detect fusion neutrons. X-ray backlighting could be used to observe the interface between the plasma and the liner. In some cases (in particular, if one implodes a mirror-like configuration), the presence of the liner would still allow using axial viewing ports.

4. DEVELOPMENT OF STAND-OFF ENERGY SOURCES

An important part of the activities centered around the user facility, could be development of stand-off energy sources for pulsed fusion devices based on liner implosions. A problem with such devices is that, in every implosion, a large amount of energy is released from the fusion plasma. If implosion occurs at the tips of the electrodes of the power supply system, an unacceptable thermo-mechanical damage to an expensive hardware occurs. Certainly, a commercial fusion reactor cannot operate in such a mode.

A possible way of solving this problem was delineated in [3], where it was suggested that the fusion reactor would work in the following way: the experimental assemblies will be dropped into explosion chamber (whose walls would be protected by liquid lithium, very much as in ICF reactors [8]), and the energy required to drive the implosion will be delivered from the distance of tens of meters (see below).

It is assumed that the assembly in this case will contain the following elements: i) the system for pre-forming the FRC (or other configuration to be adiabatically compressed); ii) the liner; iii) the on-board circuitry required to energize various systems in a required sequence (formation of pre-plasma, translation it into the liner, liner implosion).

There are at least two ways of delivering the energy to the assembly dropped into the explosion chamber. The one is to use the "inverse diode" system [3], where the assembly would be energized by an 1-MeV electron beam, penetrating through the entrance foil, being absorbed by a cathode, and generating a voltage between the foil and the cathode. With an appropriate circuitry (including, possibly, a pulse transformer) installed in the assembly, this energy source could be used to drive some fast circuits. The second way is based on the use of fast flyers accelerated either electromagnetically [9] or explosively [10]. These flyers could then be used to compress the conducting flux conserver enclosing some seed magnetic field (which could be generated, in particular, by the inverse diode system). The kinetic energy of the flyer would be converted into the magnetic energy and the latter would drive a circuit of the imploding liner. The flyers with velocities of order of 10^7 cm/s were obtained in electromagnetic accelerators, with the flyer energy ~ 100 kJ [9]. Explosively driven cumulative jets with velocities up to $9 \cdot 10^6$ cm/s were obtained [10].

The studies of detached energy sources are at present in their infancy, and the contribution of the groups working at the user facility could be very important. All the diagnostics deployed for the studies of plasma physics issues can be used effectively also for the studies of operation of the prototypical energy conversion systems (inverse diode, magneto-explosive generators, etc).

5. DISCUSSION

The 3D liner implosions can also be used to adiabatically compress some other closed-field-line configurations, like the spheromak and even a spherical tokamak (with a central post mounted inside the liner). Although an imploded spherical tokamak may not have a great future as a fusion reactor, it may allow reaching a new parameter domain in terms of plasma density and thereby add substantial new information to the physics of tokamaks.

Purely radial liner implosion on a multimirror system with a dense plasma would provide favorable experimental conditions for the studies of the wall confinement [11] – an issue of great importance for many pulsed systems with dense plasmas, including MAGO [12]. The advantage of the open-ended system is the presence of an axial access.

All in all, creation of a user facility for studies of pulsed systems with a dense plasma would add a new dimension to fusion research. It would give opportunity to numerous university research groups to fully develop and demonstrate their creative potential. It would also be an excellent way to build up an international collaboration on innovative fusion concepts.

ACKNOWLEDGMENTS

This work was performed under the auspices of the U.S. Department of energy by Lawrence Livermore National Laboratory under contract W-7405-Eng-48.

REFERENCES

1. D.D. Ryutov. Reinventing Fusion, Plenary talk at 12th American Nuclear Society Topical Meeting on the Technology of Fusion Energy, Reno, NV, June 16-20, 1996.
2. Bernard et al. The International Center for Dense Magnetized Plasmas, (these Proceedings, p. 59).
3. R.P. Drake, J.H. Hammer, C.W. Hartman, L.J. Perkins, D.D. Ryutov. Fus. Tech. **30**, 310 (1996).
4. M. Tuszhewski. Nucl. Fusion **28**, 2033 (1988).
5. J.D. Huba. NRL Plasma Formulary, NRL/PU/6790-94-265 (1994).
6. S.G. Alikhanov, S.G., V.P. Bakhtin, V.M. Brusnikin, I.S. Glushkov, R.Kh. Kurtmullaev, A.L. Lunin, A.D. Muzychenko, V.P. Novikov, V.V. Pichugin, V.N. Semenov, G.E. Smolkin, E.G. Utyugov and I. Ya. Shipuk. Investigation of model thermonuclear systems with liners, In Proc. 6th Conf. on Plasma Phys. and Contr. Nucl. Fusion Res., (1977); Berchtesgaden Germany, October 6-13 1976, **3**, 517, International Atomic Energy Agency, Vienna (1977).
7. J.H. Degnan et al. Phys. Rev. Lett. **74**, 98 (1995); J.H. Degnan, (these Proceedings, p. 203).
8. R. Moir. Phys. Plasmas **2**, 2447 (1995).
9. J.E. Osher, G. Barnes, H.H. Chau, R.S. Lee, C. Lee, R. Speer and R.C. Weingart. IEEE Trans. Plasma Sci. **17**, 392 (1989).
10. M.A. Lavrent'ev and B.V. Shabat. Hydrodynamical Problems and their Mathematical Models, Moscow, Nauka Publishing House (1973) (in Russian).
11. D.D. Ryutov. Sov. Phys. Uspekhi **18**, 466 (1975).

12. R.C. Kirkpatrick. Magnetized Target Fusion (MTF): Relaxing the Driver Requirements, (these Proceedings, p. 263).

IEC NEUTRON SOURCE DEVELOPMENT AND POTENTIAL WELL MEASUREMENTS

George H. Miley and Yibin Gu

Fusion Studies Laboratory
University of Illinois
Urbana-Champaign Campus
103 S. Goodwin Avenue
Urbana, IL 61801, U.S.A.

ABSTRACT

The development of a spherical inertial electrostatic confinement (IEC) device for use as a low-yield portable neutron source for neutron activation analysis (NAA) is presented. This represents the first example of a commercial application of a confined fusing plasma. The spin-off of such fusing plasma applications is viewed as an important supporting element in the longer-term evolution of fusion power. For future development of the IEC, higher flux neutron devices are desired, with a fusion power unit being the ultimate goal. A key issue for such scale-up is the formation of a strong "double" potential well in the IEC plasma to improve ion confinement. Initial experimental measurements of a double well in the present device are described here. These results represent a first experimental study of such structures.

1. INTRODUCTION

The development of "spin-off applications" based on fusion research is one of the anticipated benefits from the large investment in fusion research. There are several different types of "spin-offs." One involves applications based on supporting technology such as magnets, neutral beams, optics, etc. [1]. A second category involves non-fusing plasma technology and associated diagnostics that arise from fusion plasma research, such as plasma processing of materials, new plasma-based light sources, new plasma and ion sources, etc. [2,3]. Yet a third type, which uniquely builds on fusion reactor research, employs *fusing* plasmas for applications such as neutron or proton production, plasma waste/material treatment with a "self-energized" plasma source, and fusion space propulsion. The variety of applications is largest for the non-fusing case and more specialized for fusing plasmas, although ultimately the economic benefits may be equally important for both.

As dependable high gain (i.e., high Q-value = fusion energy out/energy in) devices evolve, a wide variety of possible applications should progressively emerge in addition to electrical production. These include neutron sources for fusion materials testing [4], for tritium

Current Trends in International Fusion Research — Proceedings of the Second Symposium
Edited by E. Panarella. NRC Research Press, National Research Council of Canada, Ottawa, ON K1A 0R6, Canada. 1999.

production [5], and for both nuclear and chemical/biological waste management [6]. However, it is equally important, but more difficult to develop "immediate" applications to fill the "gap" between today's experiments and the future development of these more advanced high-Q devices. One fruitful avenue appears to be the development of low-Q inertial electrostatic confinement (IEC) units as low-level neutron sources for neutron activation analysis (NAA) [7,8], and that is the subject for the present paper.

2. THE IEC — BACKGROUND

The basic IEC concept traces back to Philo Farnsworth, the inventor of electronic television. However, the neutron source versions are a modification based on University of Illinois at Urbana-Champaign (UIUC) research where ion guns are replaced with a grid-produced plasma discharge, operating in the unique "star" mode [9]. In addition to spherical geometry used in earlier devices, a unique cylindrical version has been developed at the UIUC. In the spherical design, illustrated in Fig. 1, the transparent grid biased at ~–60 kV acts as a cathode relative to the grounded vacuum vessel wall.

When deuterium is used, ions produced in the discharge are extracted from the plasma by the cathode grid, accelerated, and focused in the center where reactions occur. The grid provides recirculation of the ions, increasing the power efficiency. At high currents, a potential structure develops in the non-neutral plasma, creating virtual electrodes that further enhance ion containment and recirculation [9,10] (see Fig. 2). This feature is essential for the good ion confinement required to develop future high power devices. In present IEC neutron sources, however, currents are too low to create the potential structure shown in Fig. 2. This, combined

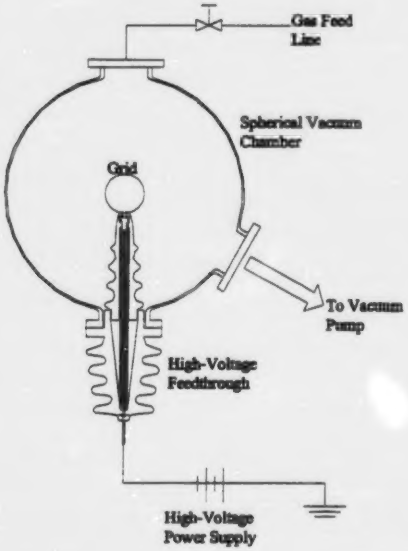

Figure 1. Cross section showing construction of the single-grid spherical IEC. This design, along with a special "open" grid design that provides a Star Mode plasma, are used in UIUC neutron source work.

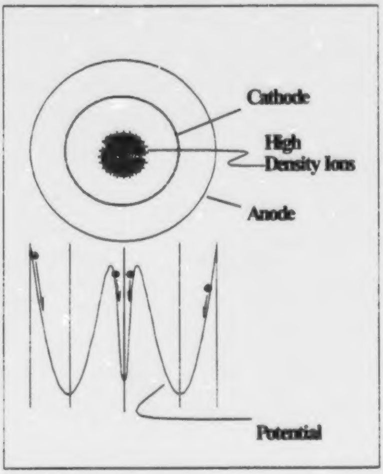
Cathode
High Density Ions
Anode
Potential

Figure 2. Illustration of the "double well" potential structure in the dense plasma core of an IEC. The central "well" traps ions, providing efficient local ion confinement and recirculation.

with a relatively high background neutral deuterium pressure results in a bulk of the fusion reactions being from beam-background gas collisions as opposed to beam-beam collisions which would dominate in an effective potential well "ion trap". Thus, the development of the potential structure of Fig. 2 is crucial for future IECs, and initial experimental measurements of such potential structures are described later.

Present steady-state IEC units produce 10^7 D-D n/s or (10^9 D-T n/s), while advanced pulsed versions extend to 10^{11} D-D n/s. The cylindrical version (Fig. 3) uses a hollow electrode design where ions recirculate between two outer anodes producing a "line-like" neutron source within the hollow cathode region. Thus the cylindrical version is especially useful for applications requiring a broad area extended source, e.g., luggage inspection, and NAA of materials, such as ores, on a conveyer belt. Neutron yields from the cylindrical design are

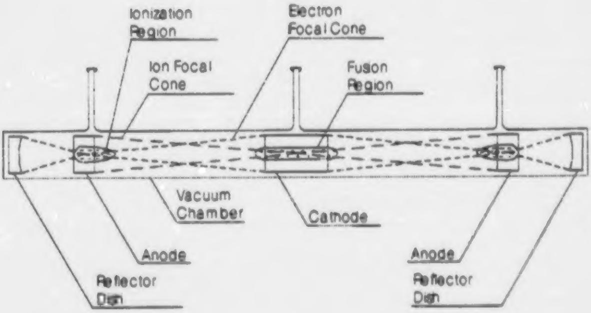
Ionization Region
Electron Focal Cone
Ion Focal Cone
Fusion Region
Vacuum Chamber
Cathode
Anode
Anode
Reflector Dish
Reflector Dish

Figure 3. Cross section of the cylindrical version of the IEC. The ion-electron optics are designed to provide a central beam through the hollow cathode.

comparable with those from the spherical IEC, but the lack of virtual electrode formation limits its ultimate fusion rate relative to future scale up. Thus the spherical version is the prime candidate for an ultimate high intensity neutron source or a power plant. Both the spherical and cylindrical sources are currently available commercially from Daimler-Benz Aerospace Corporation as portable neutron activation units [11].

The unique feature of the IEC is that it develops a "fusion-grade" plasma in a small volume (few cm^3) while avoiding bulky magnets, injectors, etc. In addition, the Star Mode [9] creates ion beams that reduce grid bombardment, which, combined with use of a "damage free" plasma target (the dense core of Fig. 2) provides long lifetime units. Thus, the IEC provides a "first step" in what will hopefully be a progression of uses for fusion-grade plasmas prior to actual fusion power plants.

3. IEC DEVELOPMENT STRATEGY

The present version of the IEC offers a competitive low-level portable neutron source for industrial NAA. However, it appears possible to extend the IEC to a variety of additional applications [7–16].

This future development can follow two routes. One path involves the development of higher yield ("intense") neutron sources for applications such as neutron tomography, isotope production, medical applications such as boron neutron capture therapy (BNCT), and studies of neutron damage of materials. The second path involves development of units for non-neutron applications such as a variable spectrum soft x-ray source (electron-injected spherical device); fullerene production (species separation in a recombining methane-helium plasma); jet heating (spherical device jet mode), plasma processing, cutting, and welding surface implantation. To follow one or more of these paths, however, requires extensive research and development devoted to specific issues related to each application.

4. HIGH INTENSITY FUSION NEUTRON SOURCES

The need for a high-intensity fusion neutron source for studies of neutron damage in fusion reactor materials is widely recognized [4]. Two approaches to this goal are generally being stressed by fusion researchers world wide being considered: an accelerator and flowing lithium target (or other suitable target capable of a high cooling rate) or alternately, an actual fusion device operating at a Q-value slightly less than unity. Examples of the latter include the gas dynamic mirror and the spherical tokamak. An advantage of the fusion device is that it would provide a larger volume for irradiation of samples. Hence, it is termed a "volumetric" neutron source. The disadvantage is that operation of this type will require intensive R & D to obtain a reliable fusion device which itself must face neutron damage issues. If such a neutron test facility can be achieved, it should also lead the way to additional important applications, such as tritium production, waste treatment, isotope production, etc. [5,6]. The IEC, if extended to high neutron intensities, might also compete in these areas, but would represent a remarkably different type of facility, being considerably smaller (hence lower cost) than the other magnetic type confinement devices. The IEC plasma scales in velocity space rather than in terms of plasma surface to volume ratio. Consequently, the IEC size is principally set by voltage breakdown and heat removal considerations [13–14]. Another distinctive advantage of a device like the IEC is that, due to its small size, hence modest unit cost, the required steps for experimental scale-up could be done relatively quickly. The key scale-up issue, however, involves uncertainties in the physics, including the ability to maintain required electrostatic potential structures in the central fusion volume and finding ways to control or avoid ion-beam instabilities. These issues have received some theoretical study, but benchmark experiments are essential to evaluate how large of a neutron yield can ultimately be obtained. The potential well measurements described later in the present paper represent a first step in this direction. A possible strategy for exploring such a development path is illustrated in Fig. 4.

Potential applications would expand at each step as the neutron yield (hence Q-value) is increased. In the effort at the UIUC, pulsed power techniques are under development in order to take advantage of the favorable scaling with ion current [17]. In addition, a technique (RIDO) to create bunching of the ions through re-circulation and acceleration is under development [15].

Development of an intense IEC source would compliment, not replace, the proposed fusion reactor "volume neutron source" facility. The IEC would lend itself to construction of small neutron units, placed in various laboratories desiring them for specialized research. The volumetric source would provide a large central facility capable of incorporating full-sized components for testing. It would also be a step toward other large-scale applications such as tritium production and waste treatment. The smaller IEC facilities would provide multiple groups with the capability of supporting research on basic aspects of neutron damage in materials. It would accommodate miniature samples and could also lead to other applications such as neutron tomography, special isotope production, etc. A variant would use energetic protons produced in D-^{3}He fueled IEC's for applications such as PET-scan isotope production and proton therapy [7,8]. Since the D-^{3}He and D-D cross sections are comparable in the current 60–100 kV operating range, IEC operation with D-^{3}He is a relatively straightforward variant of neutron source devices.

5. POTENTIAL WELL MEASUREMENT TECHNIQUE

As stressed earlier, confirmation of the existence of a potential well capable of trapping energetic ions is a key physics issue for development of higher power devices. Measurements of the potential structure in the UIUC device have recently been carried out which, for the first time, provide definitive data about the well and its behavior. Due to their importance, these measurements are described in some detail here.

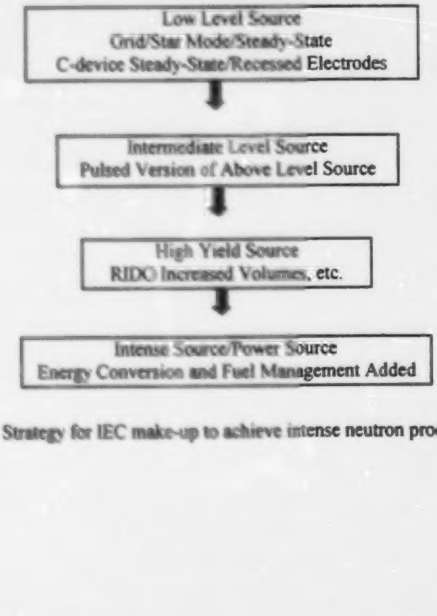
Low Level Source
Grid/Star Mode/Steady-State
C-device Steady-State/Recessed Electrodes
Intermediate Level Source
Pulsed Version of Above Level Source
High Yield Source
RIDO Increased Volumes, etc.
Intense Source/Power Source
Energy Conversion and Fuel Management Added

Figure 4. Strategy for IEC make-up to achieve intense neutron production.

5.1. Prior Studies and Considerations

The spherical IEC concept for confining energetic ions for fusion purposes arose in part from the theoretical prediction, based on solution of coupled Vlasov-Poisson's equations, of the existence of multiple electric potential wells (formed by a spatially oscillating space charge) inside a transparent spherical cathode into which ions and electrons are injected [18–21]. Energetic ions trapped in these potential wells are predicted to bounce back and forth (recirculate) in the trap formed by the virtual anode creating the well, resulting in intense fusion zones in the wells. The solution of these coupled equations also shows that when electrons and ions are well focused radially, for a fixed (secondary-electron)/(recirculating-ion) current ratio, the potential-well shape is essentially a function of the perveance K, ($K = I/V^{3/2}$, where I is the ion current, and V is the cathode voltage) [20]. Thus, in the following discussion, K is treated as a key parameter, although in practical systems, additional factors such as the ion energy-momentum distribution, the neutral ion density, impurities, etc., also enter. Farnsworth's and Hirsch's original solution employed the highly ideal assumption of zero angular momentum and monoenergetic particles. Consequently, the ability to achieve potential wells in practice was questioned. Still, because of the simplicity of the concept and the success of Hirsch's experiments [20] (where he reported anomously high fusion neutron rates and, using a collimator, found spatial peaks in Bremsstrahlung and neutron emission, suggesting multiple wells), a low level of both theoretical and experimental IEC studies continued in the 1970 and 1980s. However, prior to the present work, attempts to measure the potential well structure remained ambiguous.

After Hirsch's experiment, Hu and Klevan's [22] theoretical studies focused on the conditions needed for strong well formation, i.e., for strong ion trapping and fusion in the center of an IEC. They found that steady-state solutions of such wells could indeed be constructed. However, Hirsch's experiments fell into a somewhat different parameter system, raising questions about the interpretation of his experiment. Stability issues were also explored by Barnes [23] using computer simulations. He did not find any stable, deep ion-trapping wells, raising further questions. Subsequently, analyses by Baxter and Stuart [24] suggested that in this geometry, the phenomena of intersecting beams and ion-gas collisions dominated over the phenomena of initial electrostatic confinement. Thus, their interpretation of Hirsch's results attributed the neutrons observed to beam-background fusion reactions rather than electrostatic wells. Still, features such as the high neutron rate, the peaked Bremsstrahlung emission, and the increased fusion rate with lower pressure supported the view that well formation was responsible for Hirsch's results.

Experimental verifications of the existence of potential wells in spherical IEC were subsequently attempted by various experimentalists. Swanson [25] used an electron beam (from an electron gun) to probe an electron-driven IEC and Black [26] used an electron beam (from ^{109}Cd conversion electrons) to probe both an electron and an ion-driven confinement device. Later experiments all used ion-driven IECs which, based on Hirsch's experiments, appeared to be more stable. Gardner [27] used a microwave cavity technique to measure the electron density, while Nadler [28] used a new technique involving a collimated proton detector to measure proton source rate profiles. Satsangi [29] performed a measurement of the IEC core size using light intensity methods, and Thorson [30] used a collimated proton detector plus Langmuir probes for ion flow and fusion reactivity characterization. However, all of these experimental attempts to prove the existence of multiple potential wells were inconclusive and frequently contradictory.

A review of this prior work indicated that two problems had to be overcome to obtain improved measurements: 1) experimental conditions favoring well formation (e.g., $K >$

0.4 mA/kV$^{3/2}$) must be established, and 2) very good spatial resolution, on the order of millimeters, must be employed since in present research devices the well structure occurs over such dimensions. Thus, issues to be addressed relative to well formation include achieving sufficient perveance and avoiding ion beam defocusing due to grid asymmetries (or ion-gun misalignments when multiple ion guns are employed as the ion source). Further, theoretical studies by Cherrington [31], and Black and Klevans [32], who examined the "threshold" conditions needed to go from a shallow potential well to deep multiple potential wells, showed the need for a high recirculation of the ion current (i.e., high grid transparency) along with a low ion energy spread and low ion angular momentum, plus a tight ion beam focal point. While these requirements apply to the ions, by implication, similar restrictions must be placed on the electrons whose dynamics are controlled by the virtual cathode formed by the potential structure. These conditions were met in the present experiments by using the Star Mode operation [9,21] combined with use of a special floating "energy spread control" grid, along with operation at modest voltages but high currents to maximize the perveance, K.

The Star Mode represents an especially important aspect of the experiment since it insures a high grid effective transparency and a tight ion focus. This mode had been discovered earlier during experiments at the UIUC designed to study new IEC applications, e.g., studies of a portable neutron source for activation analysis [7,16,21]. Visual observation of the Star Mode showed that the beams in the spokes of the Star pattern formed a very tight focal spot at the center of the grid cage, significantly improving conditions favoring a double well. Indeed subsequent light profile measurements confirmed a very tight focus was achieved, the focus spot (or plasma "core") radius approaching theoretical "ballistic" limits [29].

5.2. Potential Well and Fusion Reaction Rate Relationship

Studies with the computer simulation code [33] (IXL) that solves the collisionless Vlasov equation and Poisson's equation in spherical coordinates showed earlier that "practical" spreads in ion energy and angular momentum limit the number of spatially alternating wells to two (termed here a "double well"). This double well is composed of a positive well formed by ions converging at the focal spot in the spherical cathode, with an inner negative well formed by electrons focused inside the positive well due to the virtual anode. While this double well falls short of the multiple well structure originally envisioned, as a practical matter, such a double well is capable of efficiently trapping ions within the virtual anode, much as hoped for in multiple wells. Thus the double well provides an attractive goal for future IEC devices designed for increased fusion rates.

Due to this trapping effect, the radial distribution of the fusion reaction rate density provides a means of distinguishing the double-well profile. This relation between the proton-source-rate density profile and the potential well structure is delineated in Fig. 5. A fixed voltage is assumed in the figures. The progression towards a double well is associated with increasing the ion current. At low ion current, where there is no significant positive charge build-up and the space-charge potential is low, a single sharp peak in the reaction rate density occurs in the central focus created by the spherically converging ions. As the height of this positive potential peak increases, ions are repulsed, causing a distinct dip in the center of the reaction rate density peak. However, as the ion current is further increased, the resulting virtual anode accelerates and focuses electrons in the center of the positive well, creating a potential "double-well". Consequently, a distinctive peak in the reaction rate density suddenly appears in the middle of the dip in the reaction rate density profile due to the fusion of ions trapped by

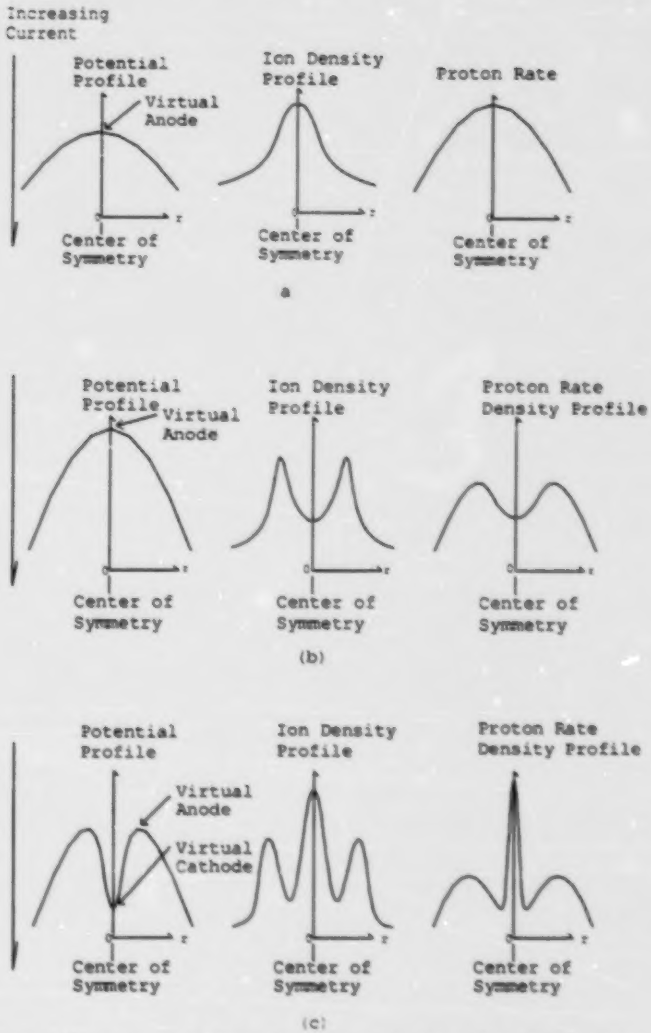
Increasing Current
Potential Profile
Virtual Anode
Ion Density Profile
Proton Rate
0
r
Center of Symmetry
a
Potential Profile
Virtual Anode
Ion Density Profile
Proton Rate Density Profile
Center of Symmetry
(b)
Potential Profile
Virtual Anode
Virtual Cathode
Ion Density Profile
Proton Rate Density Profile
Center of Symmetry
(c)

Figure 5. Illustration of the change in proton rate density profile as the ion current increases from a) to c). The change in proton rate density profile is correlated with the ion density and potential profiles. (a) A low single-peak potential when the proton rate density is the highest. (b) A high single-peak potential when the peak of proton rate density shifts outward in radius and dips at the center. (c) A sharp central proton peak emerges due to the high density created by trapped ions when the double well forms.

the double well. In the present experiment, a deuterium gas fill was used and the reaction rate was monitored using a collimated detector to scan for D-D protons. Because of this distinct reaction rate density relation illustrated by Fig. 5, the observance of two proton source rate peaks (cf. Fig. 5(c)) uniquely signals the existence of a double potential well. In addition, as discussed later, analysis of the peak amplitudes can provide a reasonable estimate of the well depth.

5.3. Proton Detection System

The system (Fig. 6) for measuring the proton rate profile consists of a semiconductor proton detector, a precision position aligner allowing pivotal movement of detector inside the vacuum chamber, a capillary collimator, and an electronic system to amplify and deliver signals to a multichannel analyzer. The detector, having a circular active window area of 1 cm^2, was seated on the outside edge of the vacuum chamber and connected to the outside electronic chain through an electrical feedthrough. During measurements, the acceptance cone of the detector-collimation assembly was pivoted across the dense plasma core by the position aligner.

A thin (1 mil) lead foil was used in front of the detector to provide strong attenuation and shielding of x-rays, mostly created when electrons hit the chamber wall. This prevented undesirable mixing between proton signals and the x-rays.

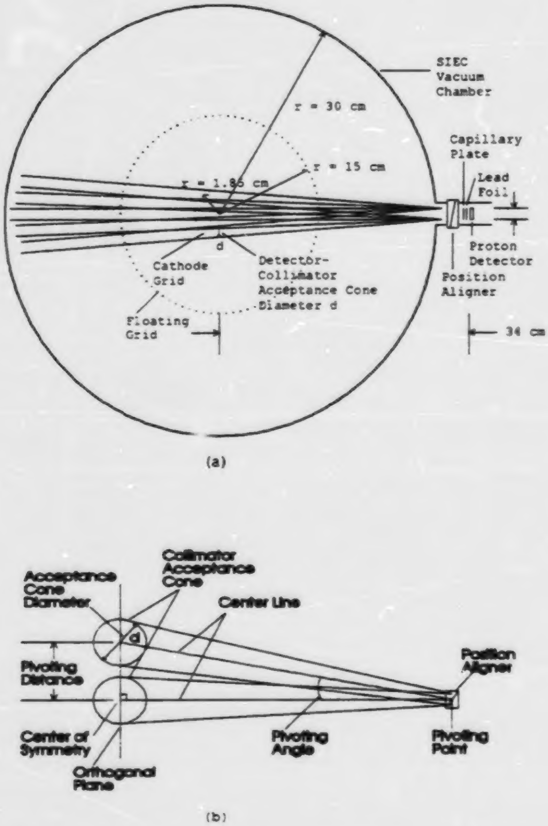
SIEC Vacuum Chamber
r = 30 cm
r = 15 cm
r = 1.85 cm
Capillary Plate
Lead Foil
d
Cathode Grid
Detector-Collimator Acceptance Cone Diameter d
Proton Detector
Position Aligner
Floating Grid
34 cm
(a)
Collimator Acceptance Cone
Acceptance Cone Diameter
Center Line
d
Pivoting Distance
Position Aligner
Center of Symmetry
Orthogonal Plane
Pivoting Angle
Pivoting Point
(b)

Figure 6. (a) Scanning proton-detector-collimator assembly layout. (b) During the measurements, the detector-collimation assembly was pivoted through the core of plasma by the position aligner.

The glass capillary plate employed for collimation contains micron-size holes perpendicular to the plate surface (~50% transparent from the holes). In order to optimize the collimation while maintaining a reasonable proton through-put, several collimators with a different capillary hole diameter D and plate thickness L were tried for optimal performance. In practice, if the D/L ratio (termed the "collimation") is large, the detector does not provide good spatial resolution; conversely if the D/L is too small, the proton through-put is reduced, making detection difficult. In the limit of extremely small D/L, small angle scattering of the protons off of the background gas before and in the holes can reduce the number of protons successfully passing through the collimator to values below the detector noise signal. In order to obtain the best collimation and still be able to detect protons, the smallest possible D/L = 1/40 was selected, although this selection resulted in lower count rates, hence required longer run times.

6. WELL MEASUREMENT RESULTS

6.1. Measurement of Total Proton Rate

Prior to spatial measurements, the total proton generation rate over the dense core region was measured as a function of current and voltage. This was done by replacing the capillary collimator with a single large tube collimator. The results from the measured total proton rates are used to compare with the total proton rates calculated by integrating the radial proton rate density profiles at a fixed current and voltage over the volume involved. The integrated rate using the capillary collimator data was expected to be somewhat less than half of the value using the single tube due to the 50% transparency of the capillary plate. In addition to the transparency effects, factors such as small angle collisions between protons and background gas further increase the collimator loss below 50%. The measured total rate was then used to normalize the absolute magnitude of the spatial measurements at each voltage-current condition. This result is employed later in estimates of the well depth.

6.2. Pivotal Proton Rate Profile

To collect proton rate scans, the collimated detector was pivoted at discrete steps with a step size of 1.8 mm, starting with the outer edge of the collimator line of sight on one side of the grid and ending on the other side. The pivotal profiles were measured in a steady-state mode at relatively low voltages (15 – 25 kV) and high currents (10 – 80 mA) where a double potential well might be expected according to IXL calculations and the previous light intensity measurements [12,17]. Qualitatively, the use of lower voltages (vs. those used in neutron source studies) results in slower ions, building up central space charge in conjunction with the higher currents.

The lower bound voltage (15 kV) was chosen to achieve high perveance and the strong ion accumulation in the center core necessary to create the potential well structure, while still providing sufficient fusion reaction rate to allow a reasonable proton count rate. Still, a significant amount of time (30 minute time interval per data point) was needed to collect data at each point to reduce the statistical variation. Under these conditions, ~300 protons were recorded at 15 kV and 80 mA with the collimator centered. Around 1200 counts were recorded at 25 kV and 20 mA. Care was taken to adjust any conditions (voltage, current, pressure) that might drift from the set point during these extended runs. Fortunately, the IEC configuration exployed was relatively stable so such adjustments were minor in nature.

Results form the pivotal collimation proton rate measurements are shown in Fig. 4.6. The x-axis origin in the figure represents the center of symmetry. The x-axis (horizontal) error bars represent the maximum uncertainty of 0.45 mm in locating the center of symmetry at $x = 0$. This assumes this location error (once the center of symmetry is determined with an error that is either to the left or to the right of the center of symmetry) is propagated to the rest of the positions in the pivotal scan, and the uncertainty associated with the positioning of each pivot point is small enough to be neglected. The y-axis (vertical) error bars represent the random error in the detector's output associated with the proton counting uncertainty where the distribution of the variation during the measurement is Gaussian. (Due to the quite stable operation noted earlier, changes due to drifts in settings during runs are discounted.) Thus, the proton counting error is statistical and equal to the square-root of the average value of the detector's output.

As expected, the proton counts on the two sides of center are symmetrical with respect to the center line. Also, as seen from the narrow curves, the focusing of ions at the sphere center is excellent. The half-width-half-maximum (HWHM) of the proton rate curves, i.e., the focused high-density core size, remains relatively constant over 4.5 – 5 mm (vs. a minimum achievable 3-mm core radius calculated from the ideal ballistic model [29]).

Figure 7 shows the proton rate profiles at 10, 20, 40, 60, and 80 mA at 15 kV fixed voltage, providing a range of $K = 0.17$ to 1.37 mA/kV$^{3/2}$. Again the amplitude of the profiles increases as the cathode current increases, and, as anticipated, a double peak structure is observed for the higher currents. At 10 mA, the proton rate profile has a flat distribution at the origin, similar to the profile at 20 kV, 20 mA. At 20 mA, two incipient proton rate peaks start to emerge on the "wings" of the profile. As the cathode current (hence the ion current) is increased further, the peaks become even more visible. At 80 mA, two peaks on the sides of the central peak are distinctly visible, and as shown later, this structure becomes even more distinct after inversion to obtain radial profiles.

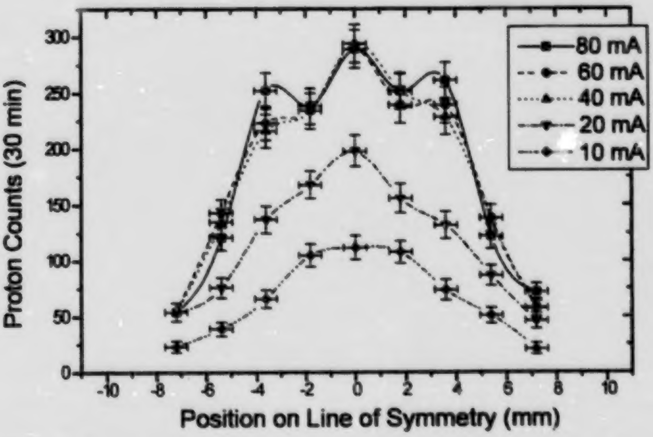

Figure 7. Proton rate profiles along the line of symmetry at the currents of 10, 20, 40, 60, 80 mA ($K = 0.17, 0.34, 0.68, 1.03, 1.37$ mA/kV$^{3/2}$ respectively) at the fixed voltage of 15 kV. The x-axis origin represents the center of symmetry. The peak amplitude increases as the current increases. The HWHM remains relatively constant over 4.5–5 mm. Notice that as the current increases, i.e., perveance increases, the profile evolves. Two distinct peaks in proton rate appear at 80 mA.

6.3. Radial Proton Rate Density Profile

The raw data from the pivotal sweep shown in Fig. 7 must be reformulated to obtain the desired radial profiles. When the collimator collects protons during a scan, they can originate from volumes defined by the intersection of the collimator's solid angle and each of the various spherical shells around the center point of the plasma core. Thus to determine the number of protons coming from a specific spherical shell (needed to find the radial profile), it is necessary to subtract off contributions from the other shells. That is possible using data about the other shells taken from different solid angles as the collimated detector is swept across the core. Formally, the calculation corresponds to a classical Abel inversion [33].

The fact that the collimator-detector diameter was larger than the core size (1 cm vs. 8 mm diameter, respectively) further complicates the analysis. This necessitated an additional calculation to obtain the solid angle rates needed for the Abel inversion. A correction for this effect in effect, makes use of the fact that contributions from each shell are successively removed as the edge of the collimator-detector moves across the core. Successive subtractions of these contributions gives the desired solid angle rates for use in the Abel inversion.

The amplitudes of the profiles after the inversions are normalized to the measured total proton rate discussed earlier. The assessment of errors in the final profiles requires consideration of variations in profile shape. A radial proton rate density profile drawn through the upper limits of the error bars is similar to the profile drawn through the lower limits. Thus, as illustrated in Fig. 8, to obtain extreme limits in profile shapes, it is necessary to draw curves through the upper and lower error bar limits in such a way that the largest variations in the profiles are created. That is, in the proton rate profile where there are two distinct or two incipient peaks, the profile with more significant peaks formed by the error bars was used to calculate the "upper error" curve. Then the profile formed by the opposite extreme (low limit) of the corresponding error bars was used to produce the "lower error" curve. Otherwise, in the case of a single peak, the profile with a less significant peak (indicating more ion accumulation) formed by the error bars is used to produce the upper error curve (denoting deeper single-well formation), and vice verse. When the limiting curves are defined in this way, the "upper" error curve implies that the curve shape could be obtained by a higher current than its nominal value, while the "lower" error curve implies a lower current is conceivable.

Figure 9 shows the proton rate density profile at 80 mA and 15 kV along with upper and lower limit error curves. A composite proton rate density profile for the varying current is shown in in Fig. 10. The curves drawn through the data points in these figures employ a third-order spline fit. The slight negative value in the mean curves is an inaccuracy associated with the spline fit. This does lead to a slight negative over shoot and some uncertainty in the exact location of the minimum proton rate density where the virtual anode exists. However closer spacing of data points would be necessary to properly correct this problem. The Abel inverted radial profiles in Fig. 10 show trends similar to the raw pivotal profiles, i.e. a single peak at low perveance and two peaks at high perveance. This evolution with current is consistent with the theoretical prediction shown earlier in Fig. 5.

Some further general observations can be made from Figs. 9–10. First, as seen from Fig. 9, even in the "worst case" relative to minimum peaking (labeled "lower" error), a definitive two-peak distribution remains. In the "upper" error case, the peaks become even more distinctive. A similar analysis has been done for all cases shown in subsequent graphs, but for clarity only the mean curves are shown. The variation due to error limits has not been found to significantly change the interpretation of any of these results. In Fig. 10, the evolution of the profiles with current at a fixed voltage of 15 keV follows the expected behavior where an orderly

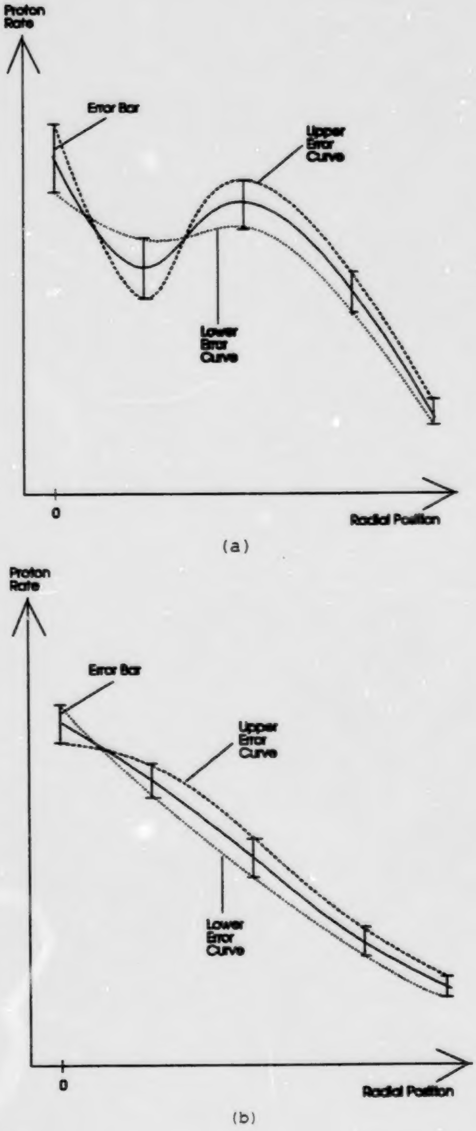
Proton Rate
Error Bar
Upper Error Curve
Lower Error Curve
0
Radial Position
(a)
Proton Rate
Error Bar
Upper Error Curve
Lower Error Curve
0
Radial Position
(b)

Figure 8. Illustration of upper and lower error curves to provide extreme profile shapes. (a) Error curves for profile of two peaks. (b) Error curves for profile of one peak.

increase in the peaks at the center (0 mm) and at ~4 mm occurs, representing a double well of increasing depth.

The theoretical studies by Hirsch [20] and Klevans [22] suggests that the vitual anode should shift outward with increasing current; however, with the wide spacing data points and the corresponding uncertainty in the location of the peak could mask this movement. Still, the present observation that the radius of the virtual anode remains fairly fixed over this range of currents is also consistent with earlier light emission measurements that indicated a roughly constant plasma core size [29]. Physically, over this range of currents the double well evolution with ion-electron space charge buildup allows an increase in local densities of both, at some point in evolution, a saturation is expected such that the virtual anode radius expands with added current. Indeed IXL code calculations by Tzonev [33] suggest that very high currents (>>10 A) and increased angular momentum will, as expected, increase the core size.

Next, returning to the detailed behavior in Fig. 10, note that starting at 10 mA, a small dip in the proton rate density occurs at the center position. As the cathode current is doubled to 20 mA, two distinct proton rate density peaks emerge, one sharp peak at the center of the core region and a smaller peak at about 3.6 mm. As the current is doubled again to 40 mA, and increased through 60 mA to 80 mA, the magnitudes of these peaks continually increase, the peak at the core center becoming much higher due to the deeper well formation with ion trapping and subsequent fusion inside the double well. The outer peak at 3.5 – 4.0 mm also slowly increases. That peak is mainly due to the increased ion density caused by lower energy ions converging towards the center core that are reflected by the virtual anode of the double well. The local fusion rate peaks slightly out from the virtual anode location when the ion velocity and increased density are maximum.

These results indicate a single peak (virtual anode formation) occurs for $K = 0.16 - 0.22$ mA/kV$^{3/2}$ while two peaks (one at $r = 0$, one at r ~ 3.6 mm), i.e. a double well, occur for $K \geq 0.34$ mA/kV$^{3/2}$. As stressed earlier, the appearance of two distinct peaks in the proton rate density profile, as obtained in Fig. 10, is the distinctive ("characteristic") signature of a double potential well. Thus this experiment clearly demonstrates the existence of a double potential well in the present IEC for $K \geq 0.34$ mA/kV$^{3/2}$. (Note, however, that K values are device specific because the current involved is a function of the ion recirculation factor. Thus application of this limiting K value to other IEC units requires a modification involving an estimate of the recirculation factor).

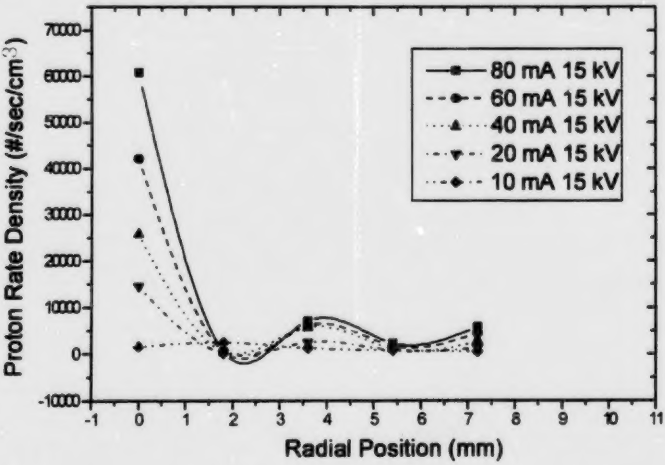

Figure 9. Radial proton rate density profile at 80 mA, 15 kV after the matrix inversions. The limiting results due to the error bars are shown in dotted and dashed curves, for $K = 1.38$ mA/V$^{3/2}$.

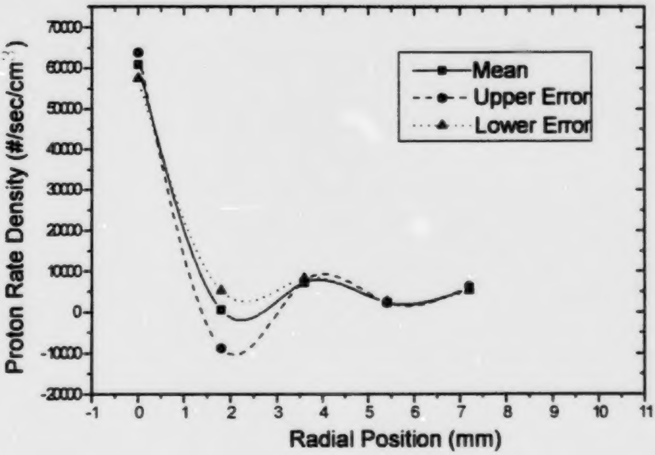

Figure 10. A comparison of radial proton rate density profiles (from mean value) at currents of 10, 20, 40, 60, 80 mA. The voltage is constant at 15 kV.

7. DOUBLE WELL DEPTH

While this experimental work has identified the definitive two-peak signature of the double-well, the question of how deep the well is remains. In this section we provide a calculation of the well depth; however, this calculation from the present data is complex and requires several assumptions since the potential is not measured directly with the present proton technique. Most importantly, the number of recirculations of a trapped ion in the double well, including charge-exchange losses must be estimated. Mean-free-path (MFP) considerations (e.g., number of recirculation = potential well diameter/MFP) provide a first approximation. Charge-exchange effects must be included in the MFP since this is a dominate effect at the gas pressure used in present experiments [30]. Another aspect, namely the dynamics of the well structure (e.g., possible well structure time oscillations [34]) and its possible effect on fusion reactions, i.e. on proton production, are not well understood. Thus in the present analysis, a steady-state well structure is assumed.

The spatial variation of the charge–exchange collisions must be considered in the calculation. Since the charge exchange $(D^+ + D^0 \rightarrow (D^0)' + (D^+)')$ cross section [35,36] decreases exponentially as the energy of the incoming ion, D^+, increases, the trapped ions are most likely to charge exchange as they approach the (virtual) anode where they have the lowest energy. In the case where a trapped ion (either in the double well or in the grid region) charge-exchanges at the (virtual) anode, the original low energy ion is replaced by a "cold" ion. Since the original ion will have a low energy due to deceleration as it approaches the virtual anode, the energy difference between it and the new "cold" ion is not too great. The new ion is then accelerated by the (virtual) cathode field and then continues to recirculate inside the well. Since the energy of the new ion is not significantly different from the original, in effect then, the original ion can still be considered to "exist" and recirculate despite the charge exchange collision. As a result, the space charge profile, hence the potential structure is not greatly effected. After a number of such collisions, however, the accumulated energy lost becomes significant and must be accounted for in evaluating the potential structure. This is done by using a charge exchange model where the ion still exists after charge–exchange collision but with some energy loss. As a first estimate, we assume that the average energy loss (energy of original ion - that of charge-exchanged ion), δE, during a charge-exchange collision is roughly the average energy of the ion undergoing collision. This can be calculated as

$$\delta E = \int_{1eV}^{E\,max} E\sigma(E)dE \Big/ E_{max} \int_{1eV}^{E\,max} \sigma(E)dE \qquad (1)$$

where $\sigma(E)$ is the D^+-D^0 charge-exchange cross section for deuteron and E_{max} is the maximum energy (prior to deceleration) of the ion undergoing charge exchange. In other words, an ion that charge exchanges at this average energy results in a "new" ion at zero energy. This latter ion is then reaccelerated by the (virtual) cathode, essentially replacing the original trapped ion, but with a slightly lower energy. For practical computation, $\sigma(E)$ was fit over a D^+ energy ranging from 1 eV to 20 keV.

Because the charge-exchange cross section is larger at low ion energies, a slow ion is more likely to charge exchange than a fast ion. Once a slow ion is accelerated to its maximum energy, it is likely to go to the other side of the potential well before it undergoes another charge-exchange collision. In the charge-exchange model, where an ion is replaced after a charge-exchange collision by a slow ion (of approximately thermal velocity), the slow ion is then reaccelerated and proceeds to recirculate to the other side of the well. In the following, we assume a charge exchange generally occurs when the ion is slowing down to turn. Thus, an initial confined ion of total energy ΔE_0 inside the negative potential well gives rise to a charge-exchange ion with $\Delta E_0 - \delta E_1$ (where δE_1 is calculated from Eq. 1) from the first charge exchange collision, and then that ion is replaced in the second charge exchange collision by one with $\Delta E_0 - \delta E_2$, and so on, as delineated in Fig. 11. The successive ions continue to recirculate

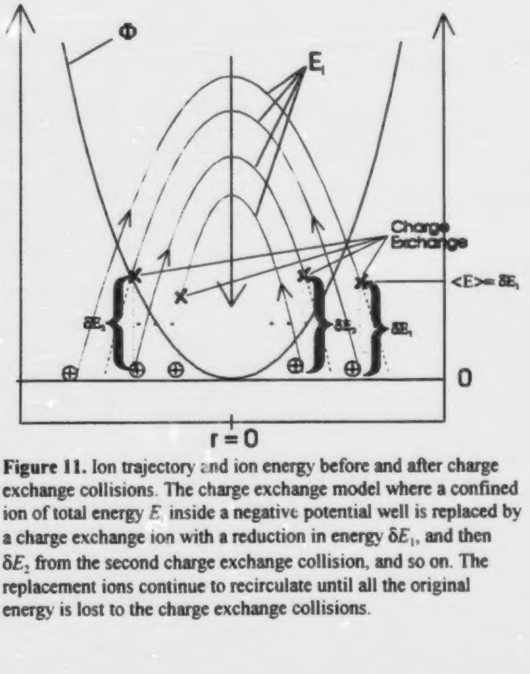

Figure 11. Ion trajectory and ion energy before and after charge exchange collisions. The charge exchange model where a confined ion of total energy E_i inside a negative potential well is replaced by a charge exchange ion with a reduction in energy δE_1, and then δE_2 from the second charge exchange collision, and so on. The replacement ions continue to recirculate until all the original energy is lost to the charge exchange collisions.

until all of the initial energy ΔE_0 is lost. The number of recirculations can be calculated from the number of collisions required to lose ΔE_0. For example, in the present case, a 15-keV ion is found to recirculate 20 times before all of its original energy is lost.

8. COMPARISON TO PRIOR WELL STUDIES

The present study represents the first definitive experimental measurement of the double well in a IEC. The early result by R. Hirsch [20] indicated a potential double well from a colliminated gamma measurement. However, his experimental conditions were quite different from the present, e.g. ion gun injectors were employed, the device dimensions were quite different, and the gas-fill pressure was about 1/5th of that used in the present experiment. Also, since the gamma spatial resolution was not as good as that of the present proton collimator, it is difficult to directly compare results. But, it appears that the well structure observed here (4-mm radius) would fall within the center peak observed in Hirsch's measurements, hence would not have been resolved in the measurement. Alternately, the possibility that Hirsch's experiment had an unexpectedly large ion recirculation factor might have caused the potential structure to spread in radius. In any case, the interpretation of Hirsch's results has been an issue in the literature ever since his original measurements. While the present measurements do no fully resolve the interpretation issue, they do definitively demonstrate a double-well potential structure, which was a part of the debate about Hirsch's measurement.

There have also been several other measurements that showed incipient double-well formation. These include Swanson, et al. [25], Nadler [28], and Satsangi [29]. However, the measured double wells were generally within error bar limits for measurement and the earlier work used electron rather than ion injection. Thus these results have generally been viewed as not providing a definitive proof for double well formation. That view was further reinforced by attempts by others, e.g. Black and Klevans et al. [22,26], and Thorson, [30] who did not find a measurable double well structure. Thus, the present experiments provide a new insight to these earlier studies. The small size of the structure diameter is particularly crucial to recognize, forcing extremely good collimation and spatial resolution. It is not clear that the prior experiments had adequate spatial resolution. Further, it is important that measurements be carried out in the perveance regime above threshold with good ion energy-angular momentum control. Thus, for these reasons the present studies used the floating grid and were done at the lowest voltage possible and extended the current range to maximum available values. Again, such precautions were not always employed in earlier experiments.

9. SUMMARY, POTENTIAL WELL MEASUREMENT

Proton rate profiles were measured in the spherical IEC over cathode currents of 10 – 80 mA and voltages from 15 – 25 kV (perveance values of 0.08 – 1.38 mA/kV$^{3/2}$). The distinct signature of the double-well structure, namely a double-peaked proton rate density profile, was observed at the currents above 20 mA at 15 kV (perveance value >0.34 mA/kV$^{3/2}$). This value then is proposed as a threshold perveance for double-well formation (note it is somewhat lower than the previous prediction from pulsed measurements [37]).

While, the experiment has conclusively demonstrated the existence of a double-well potential structure, the potential well parameters, e.g. depth, involve interpretative calculations. This calculation requires an estimation of number of ion recirculations as controlled by charge-exchange collisions. Based on this model, the well depth for 80 mA, 15 kV is estimated to be ~3.3 – 4.1 kV, or about 22 – 27% of the applied cathode voltage. This depth is reasonably consistant with 1XL simulations, and "deeper" wells are predicted for higher currents [33]. Currents were limited in present experiments by available power supplies.

10. CONCLUSIONS

In view of the long-term nature of fusion power, the continued spin-off of "fusion-grade" technology such as the IEC portable neutron should enhance interest and funding for fusion research and development. This approach will also familiarize a larger segment of society with fusion prior to the introduction of power units. The latter is very important, both in terms of maintaining enthusiasm for the main-line program and in order to avoid "new technology shock" like that faced by fission power when it was suddenly turned over to the public. The development of such spin-off technology must rely both on the identification of market "niches" and on use of fusion concepts that can meet the market competition in terms of costs, reliability, and environmental compatibility.

The feasibility of scaling the present low level IEC neutron source up to higher neutron yields and ultimately to a fusion power device is uncertain. Considerably more research is needed to evaluate the physics issues involved. However, the potential-well measurement described here provides an important first step in that direction.

ACKNOWLEDGMENTS

Important contributions by the IEC group members (Robert Stubbers, Brian Jurczyk, John DeMora, Blair Bromley, and Mike Williams) at the UIUC are gratefully acknowledged. A vital collaboration with J. Sved, Daimler-Benz Aerospace, has been instrumental in the commercialization of the IEC neutron source. Collaboration with R. Anderel and J. Hartwell, INEEL, through the University Research Consortium has also been a vital factor in IEC development. This work was partially supported under contracts: DASA, No. 505013-D MIL, and INEEL, No. CC-S-622904-002-C.

REFERENCES

1. W. Ellis et al. U. S. Industry's Perspective on Fusions' Next Step. Proc. FPA Symposium on Plasma Science and Its Applications, Washington, D. C., June 3–5, (1998).
2. S.O. Dean. Near-Term Applications of Plasma Science and Fusion Research. Proc. FPA Symposium on Plasma Science and It's Applications, Washington, D. C., June 3–5, (1998).
3. S.O. Dean. The Plasma Touch. The World and I, pp. 146–153, June (1996).
4. M.A. Abdou et al. Fusion Technology, **29**, 1 – 57, (1996).
5. W.M. Stacey. et al. Fusion Technology, **32**, 563–589, (1997).
6. W. Gough and B. Eastland. IECNES 91. Trans. of Fusion Technology, **20**, Part 2, (1991).
7. G.H. Miley et al. Trans. of the ANS, **77**, 505– 6, (1997).
8. G. L. Kulcinski et al. Trans. of the ANS, **77**, 507, (1997).
9. G.H. Miley et al. IEEE Trans. on Plasma Science, **25**, 4, 733–739, (1997).
10. Y. Gu and G.H. Miley. Bulletin APS, **11**, 1851 (1995).
11. G.H. Miley, B. Bromley, B. Jurczyk, and Y. Gu. Progress in IEC Research for near-Term Thrusters and Future Fusion Propulsion. Proc. NASA JPL Space Propulsion Research Workshop, Pasadena, CA, May 20–22, (1997).
12. G.H. Miley et al. Scaling of the Inertial Electrostatic Confinement (IEC) for Near-Term

Thrusters and Future Fusion Propulsion, Proc. 15th Symposium on Space Nuclear Power and Propulsion (STAIF98), Part 3, pp. 1373–1375, Albuquerque, NM, January (1998).

13. G. Miley and L. Chacon. Engineering Issues for a Gridded IEC for Fusion Propulsion, Proc. NASA-JPL Ninth Advanced Space Propulsion Research Workshop and Conference, Pasadena, CA, March 11–13, (1998).
14. L. Chacon and G.H. Miley. Fusion Technology, **33**, pp. 182–209, March (1998).
15. B. Jurczyk, Y. Gu and G.H. Miley. Bulletin APS, **42**, 10, p. 1818, (1997).
16. J. Sved. Trans. of the ANS, **77**, 504, (1997).
17. G.H. Miley, Y. Gu, M. Ohnishi, Y. Yamamoto, M. Hasegawa, and K. Yoshikawa. Potential Well Structure and Scaling Studies for the IEC. International Sherwood Fusion Theory Conference, Madison, WI, April 23–26, (1997).
18. W. Elmore, J. Tuck, and K. Watson. Phys. Fluids **2**, 3, 239–246 (1959).
19. P.T. Farnsworth. U.S. Patent No. 3,386,883 (June, 1968).
20. R.L. Hirsch. J. Appl. Phys., **38**, 4522 (1967).
21. G.H. Miley et al. An Inertial Electrostatic Confinement Neutron/Proton Source. AIP Conference Proceedings 299: Third International Conference. AIP Press, 675 (1994).
22. K.M. Hu and E.H. Klevans, Phys. Fluids **17**, 227–231, (1974).
23. C.W. Barnes. Ph.D. dissertation, Stanford University, 1970.
24. D.C. Baxter and G.W. Stuart. J. Appl. Phys. **53**, 4601 (1982).
25. D.A Swanson, B.E. Cherrington, and J.T. Verdeyen. Phys. Fluids **16**, 1939 (1973).
26. W.M. Black and J.W. Robinson. J. Appl. Phys. **45**, 6, (1974).
27. A.L. Gardner. Measurements On A Spherical Electrostatic Confinement System Employing Six Ion Guns. The U.S. A.E.C. Final Report No. C00-2180-7 (1974).
28. J. H. Nadler. Space-Charge Dynamics and Neutron Generation in An Inertial-Electrostatic Confinement Device, Ph.D dissertation, University of Illinois at Urbana-Champaign, 1992.
29. A.J. Satsangi. Light Intensity Measurements of an Inertial Electrostatic Confinement Fusion Plasma, M.S. thesis, University of Illinois at Urbana-Champaign (1996).
30. T.A. Thorson. Ion Flow And Fusion Reactivity Characterization of a Spherically Convergent Ion Focus, Ph.D. dissertation, University of Wisconsin (1996).
31. B.E. Cherrington, J.T. Verdeyen, and D.A. Swanson. Recent Developments in Electrostatic Confinement – Theoretical, Annals New York Academy of Sciences.
32. W.M. Black and E.H. Klevans. J. Appl. Phys., **45**, 2502–2511, (1974).
33. I.V. Tzonev. Effect of Large Ion Angular Momentum Spread and High Current on Inertial Electrostatic Confinement Potential Structures, M.S. thesis, University of Illinois at Urbana-Champaign, (1996).
34. M. Ohnishi, Yasushi Yamamoto, Kiyoshi Yoshikawa and Kunihiro Sato. Mult-Potential Well Formation and Neutron Production in Inertial-Electrostatic Confinement Fusion by Numerical Simulations, Proceedings of 16th IEEE/NPSS Symposium on Fusion Energy, (1995).
35. B.P. Bromley. Approximate Modeling of the Inertial Electrostatic Confinement Cylindrical Device, M.S. thesis, University of Illinois at Urbana-Champaign, (1997).
36. R.K. Janev et al. Elementary Processes in Hydrogen-Helium Plasmas (Springer-Verlag, New York, 1987).
37. Y. Gu, M. Williams, R. Stubbers and G.H. Miley. Pulsed Operation of Spherical Inertial-Electrostatic Confinement Device, 12th Topical Meeting on the Technology of Fusion Energy, ANS, LaGrange Park, IL, (1996). Fusion Technology, **30**, No. 3, pp. 1342–1346, December (1996).

A PROSPECT OF THE TANDEM MIRROR FUSION APPROACH

Teruo Tamano

Plasma Research Center
University of Tsukuba
Tsukuba, Ibaraki 305, Japan

ABSTRACT

Mirror research in recent years is almost entirely represented by the tandem mirror approach which has the following distinguished characteristics:

- It uses both magnetic and electrostatic potential confinement.
- It is potentially a steady state confinement system with no instabilities due to plasma currents.
- It is an open end system with possibilities for good particle/energy handling and direct energy conversion.
- It is potentially a high beta system, accordingly a good candidate for a D-^{3}He system.

Recent results of the tandem mirror experiments are reviewed in Refs. 1 and 2. In this paper we intend to brief the major results of the recent tandem mirror experiments and to discuss their implications in the future of the tandem mirror approach. Details of the experimental results can be found in the references.

Recent tandem mirror experiments have mainly been carried out in Japan. The GAMMA10 device [1–3] is the world largest tandem mirror operating at the University of Tsukuba. The total length of the device is 27 m and the maximum magnetic field strength in the central cell region is 0.6 T. The HIEI device [4] is another tandem mirror located at the Kyoto University. The total length is 14 m with the magnetic field of 0.1 T in the central cell. The AMBAL-M device at the Budker Institute of Nuclear Physics in Novosibirsk, Russia has almost the same length as GAMMA10. However, it is still under conversion into a tandem mirror. Presently, only the one-side plug cell is completed and it is in preliminary operations. The HANBIT device at the Korea Basic Science Institute, Korea is a rebuilt of the TARA tandem mirror device formally used at Massachusetts Institute of Technology (MIT). It has just started its initial experiments.

The current goal of the tandem mirror research is to obtain the proof of principle of the tandem mirror approach and the research is mainly concentrated on physics understandings and their implications. The highlights of the major recent experimental results are briefed below and their implications are discussed for each key issue.

Current Trends in International Fusion Research — Proceedings of the Second Symposium
Edited by E. Panarella. NRC Research Press, National Research Council of Canada, Ottawa, ON K1A 0R6, Canada. 1999.

1. POTENTIAL FORMATION

One of the most important issues for the tandem mirror approach is formation of plug and barrier potentials to confine ions and electrons. It has been demonstrated that these potentials can be made by wave heatings, such as electron cyclotron resonance heating (ECRH) at GAMMA10 and ion cyclotron resonance heating (ICRH) at HIEI. The original proposal for the potential formation was to inject high energy sloshing ions [5,6], but these wave heating results have added great flexibility to the potential formation scheme. The maximum potential value created so far by ECRH in GAMMA10 is about 2 kV. However, the potential seems to increase approximately linearly with the electron temperature [1,2]. Since the electron temperatures in present day experiments are up to a few hundred eV, the potential could increase to tens of kV for a fusion plasma with an electron temperature of 10 keV. This assumes that the heating power, the plasma density and the plasma size are the same as those used in the present experiments.

The present-day experiments also indicate that the potential ϕ is proportional to the ECRH power divided by the plasma density. The ECRH power used for the formation of the potential in GAMMA10 is of the order of 100 kW at the plasma density of about $2 \times 10^{18}\ m^{-3}$. Therefore, this scaling indicates that a potential of tens of kV in a fusion plasma at a plasma density of $10^{20}\ m^{-3}$ seems feasible with an ECRH power of about 10 MW.

It is also very important to investigate whether these potentials can steadily be maintained or not. In order to study this issue, efforts are being made to lengthen the pulse length of GAMMA 10 discharges from 0.1 s to 0.5 s. Theoretical understanding of the potential formation with a wave heating is also under way [7,8]. Computer simulations with a simple model begin to demonstrate that a potential can be formed by a wave heating under a certain conditions. These results suggest that the potential formation mechanism is determined by the two fundamental conditions, i.e., the quasi-neutral condition of the plasma and the ambipolar condition of the plasma flow to the ends. In other words, the formation mechanism may be understood in the following manner: When hot electrons are created by a strong ECRH, they are mirror trapped and tend to generate a negative potential in the region. Then, some of the electrons flowing through the barrier to the end are reflected back due to the negative potential, i.e., the electron flow to the end is reduced. Therefore, the ion flow to the end must be reduced in order to maintain the ambipolar flow condition, which requires existence of a positive potential between the barrier region and the end region. Let us say that the ambipolar flow condition is satisfied at the peak of the positive potential (i.e., plug potential). Since the magnetic field reduces towards the ends, parallel velocities of electrons and ions increase as they flow towards the end. In order to keep the ambipolar condition in every place, the potential must be more negative towards the ends. Accordingly, the axial potential along the magnetic field lines has a well in the barrier region and a hill in the plug region.

2. PLASMA CONFINEMENT

The next important question about a tandem mirror system is confinement. Present-day experiments indicate that the axial loss is close to the classical loss based on the potential confinement. Since the potential confinement system is an absolute confinement system, this may not be a surprise. If this holds in a tandem mirror fusion system, an energy confinement time increases with the three halves power of a electron temperature and decreases linearly with a density. Therefore, the electron energy confinement is most important in the tandem mirror research. The present electron energy confinement time of a hot ion mode plasma in GAMMA 10 is about 2 ms for the electron temperature of 100 eV at the density of $2 \times 10^{18}\ m^{-3}$. Therefore, one can expect 40 ms for 10 keV at $10^{20}\ m^{-3}$ for the same ratio of a potential ϕ over an electron temperature T_e. If this ratio ϕ/T_e be improved by 50 % by increasing the wave heating power, the axial confinement time becomes 1 s which is close to a break-even condition.

A radial confinement time becomes an issue under this condition. Confinement in the present-day experiments is still determined by an axial loss. However, one can estimate the upper limit of the radial loss as the axial loss has recently become small. The estimated upper limit of the radial electron confinement time in terms of the Bohm time for GAMMA10 is more than 1000 Bohm time which is no worse than that of a typical tokamak [1,2]. Therefore, the radial confinement seems reasonably good. In particular, it is encouraging that this good confinement is considered to be an outcome of the suppression of drift instabilities due to a ExB sheared flow caused by radial electric fields [4,9]. This is very similar to that of the H-mode in a toroidal device. However, the radial electric fields are always naturally generated in a tandem mirror when plug/barrier potentials are formed. The amount of the sheared flow speed E/B in a tandem mirror fusion reactor plasma may increase by one order of magnitude, however, the electron thermal speed and the ion sound speed may also increase by the same order. Therefore, a similar effect of the sheared flow on plasma stability can be expected in a fusion reactor plasma.

Ion energy confinement of GAMMA10 in a hot ion mode is explained by the classical processes [1,2]. In the hot ion mode the ion-ion collision time is shorter than the ion-electron energy transfer time (electron drag time). Therefore, the mirror loss-cone loss due to ion scattering may not be a dominant ion loss mechanism. Indeed, in the core region of GAMMA10 the main energy loss mechanism for ions is found to be the classical electron drag, i.e., the energy transfer from ions to electrons due to the Coulomb collisions. This loss is inversely proportional to the three halves power of the electron temperature. In order to prove this point a second harmonic ECRH is applied to a plasma in the central cell [7]. When the ECRH power of 10 kW is applied to the electrons, the ion temperature is doubled from 2.5 keV to 5 keV. This is a remarkable demonstration of the ion loss mechanism. It is also experimentally observed that the ion temperature increases linearly with the absorbed ICRF power[1,2]. The ion temperatures of 10 keV perpendicular to B and of 0.5 keV parallel to B have been produced in GAMMA10. Thermonuclear fusion neutrons are observed in those plasmas [1,2,10]. (Perhaps more precisely, those should be called quasi-thermonuclear fusion neutrons because of the anisotropy in the ion temperature). In the periphery region of GAMMA10 the main ion energy loss mechanism is a combination of electron drags and charge exchange processes with neutral particles.

A plasma density in the present-day tandem mirror experiments is the farthest plasma parameter from a break-even condition. The cause for the low density is not clearly understood. Possible causes for the low density are the low magnetic field and the low electron heating power in the present experiments. Since no direct electron heating is typically involved, electrons gains energy only from ions through Coulomb collisions which is of the order of 10 kW at most. Therefore, a plasma cannot take too much neutral gas, which tends to limit the particle source. Only a gas puffing technique has been applied to the tandem mirror experiments so far. A hydrogen pellet injection may give a chance for a higher density plasma based on the experiences in toroidal systems. A pellet ablation code simulation shows that a particle source profile with a pellet injection can have a better match to the energy density profile of the GAMMA10 plasma, and thus more effective gas feeding is expected. An expected difficulty of a pellet injection in a usual open-end device is that a cold dense plasma tends to escape from the end right after pellet ablation before it has a chance to be heated. However, a tandem mirror could sustain the dense cold plasma by electrostatic potentials until the plasma is heated. A hydrogen pellet injection experiment is actually planned in GAMMA10. The Oak Ridge National Laboratory (ORNL) pellet injector used on the

Advanced Toroidal Facility (ATF) device has been offered to the GAMMA10 experiment by the courtesy of U.S. DOE and ORNL and it is being modified for the tandem mirror use.

The other remedy for the low density problem may be a direct electron heating. ECRH is a possible candidate for this. However, ECRH at the fundamental cyclotron frequency in GAMMA10 has a difficulty because of the cut-off frequency at the low magnetic field. In the case of ECRH with a second harmonic cyclotron frequency wave a heating power is preferentially absorbed by hot electrons and bulk electrons are not effectively heated[7].

3. PLASMA STABILITY

Another important issue in a tandem mirror plasma is plasma stability. It is supposed to be one of the advantage of the tandem mirror approach that a much higher beta plasma can stably be contained compared to that in a toroidal plasma. This makes a tandem mirror as a main candidate for a D-^{3}He reactor. Since there is no major plasma current associated with a tandem mirror, current driven instabilities can be excluded. Indeed, the main mhd instability observed in tandem mirrors is a flute instability. This is clearly suppressed in the average minimum-B tandem mirror experiments [11]. Since an ordinary average minimum-B mirror system involves a non-axisymmetric magnetic configuration such as a quadrupole field configuration, a locally high magnetic field region is required. This may limit the available magnetic field in the main confinement region. Therefore, a demonstration of a high beta plasma in an actual tandem mirror device is very important. The maximum beta values achieved in the recent tandem mirror experiments are 14 % in HIEI and 5% in GAMMA 10. It needs to be investigated whether this is an outcome of the low heating power system (up to about 100 kW), or the low magnetic field, or something else.

Stability studies of several axisymmetric mirror configurations have been proposed. However, answers for these configurations are not yet obtained at this point. As mentioned before, a hot ion mode [1,2] in GAMMA10 has produced a stable, very anisotropic plasma with ion temperatures of 10 keV perpendicular to B and 0.5 keV parallel to B. Therefore, the strong anisotropy does not seem to create a severe consequence. A mirror instability is predicted by a simple mhd theory for a strong anisotropic pressure distribution. This has not yet been identified experimentally in a tandem mirror system. Nonlinear nature of this instability must be understood.

As for micro-instabilities, Alfven ion cyclotron instabilities are observed at a high beta with a large anisotropy [12-15]. These tend to relax the anisotropy and to slightly increase the axial loss of ions [16], but the effect is relatively small according to the experiments with the anisotropy up to 15. If this is a general conclusion, one can create a fusion plasma with large anisotropy (i.e. with much larger perpendicular energy) which can generate a more fusion power than that in an isotropic plasma. This could be an advantage for a D-^{3}He ignition system. In particular, one can selectively heat a ^{3}He plasma near the mid plane of a tandem mirror which produces very few neutrons due to D-D reactions.

4. PROSPECT OF A TANDEM MIRROR SYSTEM

Based on the best knowledge obtained from the present day experiments, the following scaling can be used to extrapolate the performance of the tandem mirrors:

$$\phi \propto T_e P_w / n_e, \tag{1}$$

and

$$P_h \propto n_e T_e / \tau_E, \tag{2}$$

where the symbols denote the following parameters:

ϕ: Potential (difference between the plug potential and the barrier potential),
T_e: Electron temperature,
n_e: Electron density,
P_w: Wave power for potential formation,
P_h: Plasma heating power,
τ_E: Energy confinement time determined by the axial loss.

Accordingly, one can expect the following future plasma as an extrapolation of the present-day plasma.

	T_e (keV)	n_e (10^{20} m^{-3})	ϕ (kV)	P_w (MW)	P_h (MW)	τ_E (s)
Present:	0.1	0.02	1	0.05	0.1	0.002
Future:	10	1	150	8	0.5	1

This result seems very promising. It is interesting to note that the most of the power is used for the potential formation and the required heating power is very low because of the improved axial confinement due to the high potential. Of course, one may need to consider radial losses across the magnetic field under this condition.

There are some clear advantages in a tandem mirror system over a toroidal system. One of them is confinement of high energy particles such as alpha particles and ions injected by neutral beams. A fair amount of those particles in a toroidal system is lost due to toroidal drifts when they are trapped in toroidal ripple fields. Under certain conditions this can be comparable with a mirror loss cone loss. This is no concern for an axisymmetric mirrors. In a non-axisymmetric mirror system high energy particle loss across the magnetic field must be evaluated individually.

Another advantage is a control of heat flux to the mirror ends. Since the end region can be expanded as much as we like without increasing a volume of a high magnetic region, a heat load on the end plate can be much smaller compared to that on divertor plates in a toroidal system. In order to further reduce the heat loss to the end plates, the thermal dike approach[17] and the mesh bias approach have been investigated in GAMMA10[18,19]. The basic idea of these method is to reduce a cold electron flow from the end to the confinement region so as to prevent a warm electron flow towards the end as a return.

In summary, there are a number of possibilities in the tandem mirror approach that could make a fusion reactor quite different from a toroidal fusion reactor. Some of those possibilities can be investigated in the present-day tandem mirror devices with relatively minor additions.

ACKNOWLEDGMENTS

The author gratefully acknowledges contributions by the GAMMA10 Group: T. Cho, M. Hirata, H. Hojo, M. Ichimura, M. Inutake, K. Ishii, A. Itakura, I. Katanuma, R. Katsumata, Y. Kiwamoto, A. Mase, Y. Nagayama, Y. Nakashima, T. Saito, M. Shoji, E. Takahashi, Y. Tatematsu, K. Tsuchiya, N. Yamaguchi, and K. Yastu. The author also thanks to Prof. Y. Yasaka and Dr. O. Sakai, Kyoto University for their useful discussions and cooperation.

REFERENCES

1. T. Tamano. Physics of Plasmas **2**, 2321 (1995).
2. Teruo Tamano. Transactions of Fusion Technology **27**, 111 (1995).
3. M. Inutake et al. Phys. Rev. Lett. **55**, 159 (1985).
4. O. Sakai et al. Phys. Rev. Lett. **70**, 4071 (1993).
5. G. I. Dimov et al. Fiz. Plazmy **2**, 597 (1976).
6. T. K. Fowler and B. G. Logan. Comments Plasma Phys. Controlled Fusion **2**, 167 (1977).
7. T. Saito et al. Fusion Energy **2**, 105 (1996).
8. I. Katanuma et al. Phys. Plasmas **4**, 2532 (1997).
9. A. Mase et al. Nucl. Fusion **31**, 1725 (1991).
10. Y. Kiwamoto et al. Phys. Plasmas **3**, 578 (1996).
11. M. Inutake et al. in Proc. Invited Paper, International Conference on Open Plasma Confinement Systems for Fusion, Novosibirsk, 1993, edited by A. A. Kavantsev (World Scientific, Singapore, 1994), p. 51.
12. M. Ichimura et al. in Ref. 11, p. 69.
13. M. Ichimura et al. Phys. Rev. Lett. **70**, 2734 (1993).
14. M. Ichimura et al. Fusion Eng. Design **26**, 251 (1995).
15. A. Mase et al. Rev. Sci. Instrum. **68**, 454 (1997).
16. K. Ishii et al. in Proc. 1996 Conf. on Plasma Physics, Nagoya, 1996, edited by H. Sugai and T. Hayashi (Japan Soc. Plasma Science and Nucl. Fusion, Japan, 1997), p. 1322.
17. T. Ohkawa. J. Plasma Fusion Res. **64**, 305 (1990).
18. Y. Kiwamoto et al. Phys. Plasmas **1**, 3986 (1994).
19. T. Saito et al. Phys. Plasmas **2**, 352 (1995).

MAGNETIC PRESSURE DRIVEN SPHERICAL LINER IMPLOSION EXPERIMENTS

James H. Degnan, Sean K. Coffey[1], Donald G. Gale[2], Jack D. Graham[2], James J. Havranek, Thomas W. Hussey, Gerald F. Kiuttu, Bret Kreh, F. Mark Lehr, Dane Morgan[3], Robert E. Peterkin, Jr., David Platts[3], Norman F. Roderick, Edward L. Ruden, Wayne Sommars[2] and Peter J. Turchi

Air Force Research Laboratory
Phillips Research Site
Kirtland AFB, New Mexico 87117, U.S.A.
[1] NumerEx
Albuquerque, New Mexico, U.S.A.
[2] Maxwell Technologies Inc.
Albuquerque, New Mexico, U.S.A.
[3] Los Alamos National Laboratory
Los Alamos, New Mexico 87545, U.S.A.

ABSTRACT

We have imploded quasi-spherical aluminum shells by magnetic pressure from 12 MA discharges. These implosions achieved ~ 10 km/sec implosion velocity, and were used to compress unmagnetized hydrogen plasma with initial pressure above 100 atm and initial temperature above 1 eV. Multiple radiographs of the compression of an interior copper shell target indicate that the compressed fluid pressure reached the megabar range prior to contact of the imploding shell and target. A modification of these experiments is to allow the initial plasma to be magnetized, with lower density and higher temperature deuterium. This would constitute a magnetized target fusion experiment.

We have used the Shiva Star capacitor bank operated at 12 MA and 5 MJ to implode aluminum shells electromagnetically in tapered quasi-spherical geometry, achieving peak implosion velocities above 20 km/sec inner surface (~10 km/sec thickness-averaged) [1]. Lower velocity (up to 2 km/sec) quasi-spherical solid liner implosions have also been reported by Goloviznin et al [2] , Chernyshev et al [3], and Mokhov et al [4]. We have used the present implosions to compress a working fluid of hydrogen plasma with initial pressure above 100 atm and initial temperature above 1 eV. We use a working fluid of hydrogen that is initially

Current Trends in International Fusion Research — Proceedings of the Second Symposium
Edited by E. Panarella. NRC Research Press, National Research Council of Canada, Ottawa, ON K1A 0R6, Canada. 1999.

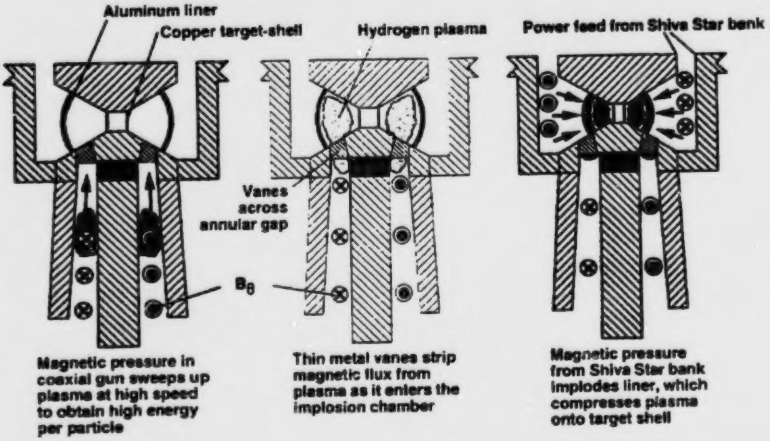
Aluminum liner
Copper target-shell
Hydrogen plasma
Power feed from Shiva Star bank
Vanes across annular gap
B_θ
Magnetic pressure in coaxial gun sweeps up plasma at high speed to obtain high energy per particle
Thin metal vanes strip magnetic flux from plasma as it enters the implosion chamber
Magnetic pressure from Shiva Star bank implodes liner, which compresses plasma onto target shell

Figure 1. A sequence of three processes creates pressures of 10–100 Megabars in the target shell.

hot enough to insure that the sound speed in the fluid will be greater than the velocity of the inner surface of the imploding solid liner; this avoids shock formation in the compressed fluid. In these experiments, we purposely prevent magnetization of the fluid, in an attempt to obtain uniform, isotropic fluid pressure. The goal is to obtain uniform fluid pressures in the 1 to 10 megabar range. We have obtained experimental (radiographic) evidence of compressing the working fluid to greater than a megabar prior to contact of the inner surface of the outer liner with the outer surface of an interior compression target.

The initial hydrogen plasma is obtained using a 1 MA, 100 KJ co-axial plasma gun, and is injected through a circular array of vanes to strip away azimuthal magnetic field [5,6]. This

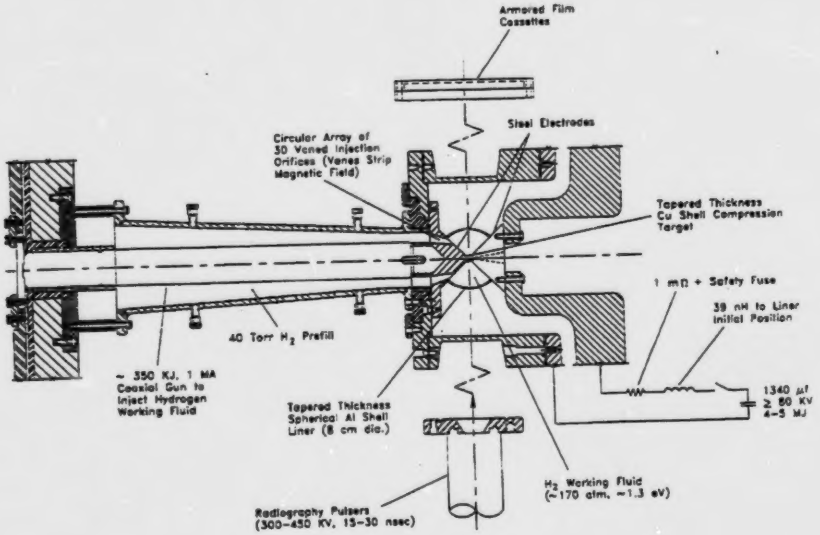
Armored Film Cassettes
Steel Electrodes
Circular Array of 30 Vaned Injection Orifices (Vanes Strip Magnetic Field)
Tapered Thickness Cu Shell Compression Target
1 mΩ + Safety Fuse
39 nH to Liner Initial Position
40 Torr H_2 Prefill
~ 350 KJ, 1 MA Coaxial Gun to Inject Hydrogen Working Fluid
Tapered Thickness Spherical Al Shell Liner (8 cm dia.)
1340 µf
≥ 60 KV
4–5 MJ
H_2 Working Fluid (~170 atm, ~1.3 eV)
Radiography Pulsers (300–450 KV, 15–30 nsec)

Figure 2. Working fluid injection and imploding linear hardware.

process is illustrated in Fig 1, and the hardware is illustrated in Fig 2. The working fluid injection was observed with auxiliary experiments, using chambers similar to the initial interior volume of the solid liner, but with greater diagnostic access. Working fluid diagnostics included time-gated optical spectroscopy, fast photography, and piezoelectric probes. Inductive magnetic probes are used to monitor current delivery to the vicinity of the injection vanes, and to confirm absence of magnetic field in the chamber. Piezoelectric probe signals indicate that working fluid with pressures up to 100 atmospheres is injected into the interior of cylindrical solid liners. This is consistent with 2D-MHD simulations. Such simulations indicate that working fluid at pressures of 170 atmospheres is injected into the interior of our quasi-spherical liners. Optical spectroscopy suggests that the fluid temperature is somewhat higher than 1 eV.

The imploding aluminum shell is observed with radiography. The effect of the compressed working fluid on a cylindrical shell of Cu, serving as a compression target, is also observed with radiography. The aluminum spherical-shell is initially 8 cm diameter, 1 to 2 mm tapered thickness, and is mounted between two conical electrodes of steel. The interelectrode gap converges at an included angle of 90 degrees to a minimum value of 1 cm. The Al shell thickness is proportional to the cosecant squared of the polar angle (co-latitude), and is thinnest at 90 degree angle from the central axis. To first order (the thin shell limit), this taper causes the ratio of magnetic pressure to liner mass per unit area (and therefore the spherically radial acceleration) to remain independent of polar angle during the implosion. The result is a nominally spherical implosion. The radiographs are taken through the 0.6 cm thick aluminum outer (return current) conductor. The target is a copper tube with tapered thickness (6 to 15 mil, or 0.15 to 0.38 mm). The operating parameters of the radiography source are 300 kilovolts, 5 kiloamps, 30 nanosecond pulse, with a tungsten anode. The apparent spatial resolution is approximately 0.2 mm. Radiographs, such as those shown in Fig 3, show compression of the target cylinder prior to contact of its outer surface with the inner surface of the imploding liner. One can see the reduced exposure indicating the compressed fluid layer between the imploding liner inner surface and the central target outer surface until very late in the compression, that is, until less than 0.1 µsec before contact of the two surfaces. A series

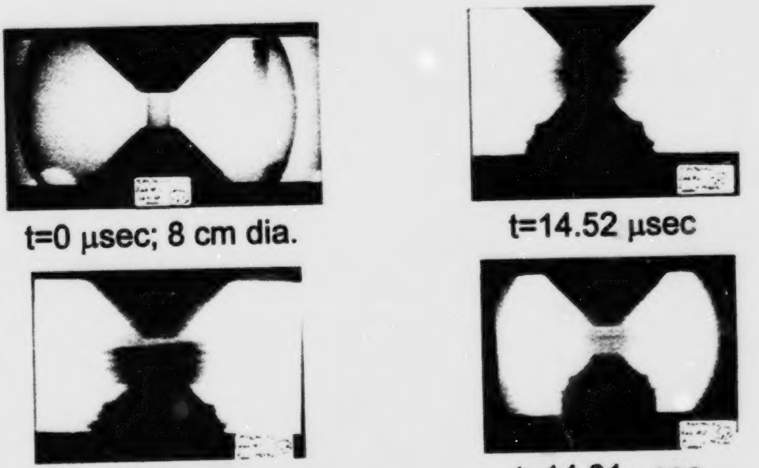

t=0 µsec; 8 cm dia.

t=14.52 µsec

t=14.44 µsec

t=14.61 µsec

Figure 3. Capacitor driven MTF experiments will be similar in energy and configuration to already achieved working fluid compression. (Radiographs of 5 MJ experiments shown.)

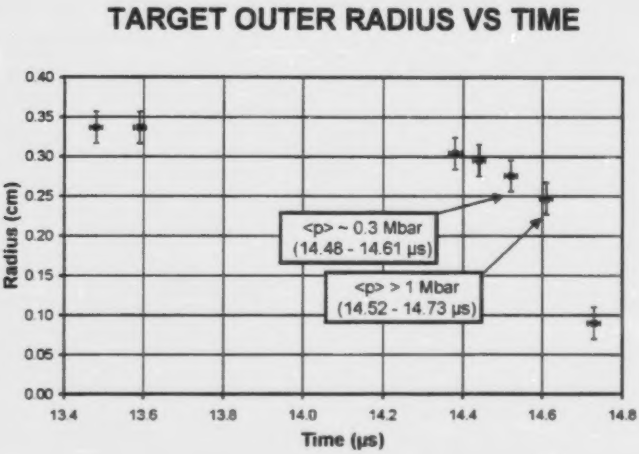

Figure 4. Central target compression data indicate time average fluid pressures approaching a megabar ~ 0.1 μsec prior to stagnation.

of such radiographs has enabled estimates of the average acceleration of the inner target surface and the fluid pressure during several time intervals late in the implosion - compression. These indicate that the fluid pressure exceeds a megabar prior to contact (see Fig 4).

Auxiliary experiments with such a target and with no working fluid, but with fluid injection ports in the electrode, and with sensitive magnetic probes outside the diagnostic target, indicate no target compression and no injected field. Thus, target compression, which is observed in imploding shell - working fluid compression experiments, is presumably due to the compressed hydrogen pressure.

We did some solid liner implosion experiments with tall cylindrical targets and highly converging electrode gaps, as a hedge against possible problems with spherical liners. Radiographs from such an experiment, which was also an auxiliary experiment with no working fluid, are shown in Fig 5. The earlier incidence of short wavelength instabilities in cylindrical liners, relative to quasi-spherical liners, may be due in part to the fact that the entire axial length of the liner has a cross section close to the critical one for avoiding melting and vaporization. In the quasi-spherical liners, only the portion of the liner near 90 degree polar angle (i.e., the "equator") has a cross section close to this critical one.

While these experiments were not done for fusion applications, they are relevant to magnetized target fusion (MTF), such as described by Lindemuth et al [7,8], and by

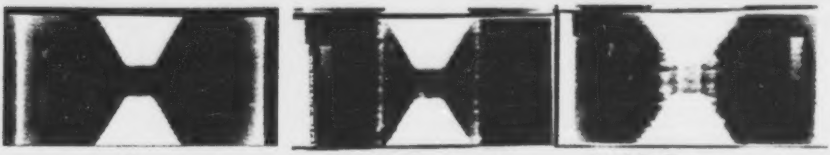
t=0 usec t=12.3 usec t=13.3 usec

Figure 5. No compression of central target observed when no working fluid is injected. Interior magnetic probes see no field.

Chernyshev et al [9]. A variant of the experiments we have done, using magnetized, lower density deuterium instead of unmagnetized, higher density hydrogen, would be an MTF experiment. With our existing laboratory arrangement, we are in an excellent position to evaluate critical problems with MTF concepts. In particular, the question of contamination of a magnetized, hot hydrogen working fluid by high Z material from the liner (and electrodes) may be answered.

ACKNOWLEDGMENTS

This work was supported by the Air Force Office of Scientific Research. We would like to acknowledge the support and interest of Dr. W. L. Baker, Dr. B. Godfrey, and Dr. R. Kelley.

REFERENCES

1. J.H. Degnan et al. Phys. Rev. Lett. **74**, 98 (1995).
2. V. Goloviznin et al. Megagauss Physics and Technology. Second International Conference on Megagauss Magnetic Field Generation and related Topics, ed. by P.J.Turchi Plenum Press, New York, NY, U.S.A. (1980) p. 415.
3. V.K. Chernyshev et al. Sixth International Conference on Megagauss Magnetic Field Generation and Related Topics, ed. by M. Cowan and R. Spielman Nova Science Publishers Inc., Commack, NY, U.S.A. (1994) p.815.
4. V. Mokhov et al. Sov. Phys. Dokl. **24**, 557 (1979).
5. F.M. Lehr et al. J. Applied Physics **75**, 3769 (1994).
6. F.M. Lehr et al. "Progress on the formation of a high density working fluid for solid liner implosions. Digest of Technical Papers, Ninth International IEEE Pulsed Power Conference, 21-23 June 1993, p.176, Eds. K.R. Prestwich and W.L. Baker, IEEE Catalog Number 93CH3350-6, LIBRARY OF CONGRESS 93-79733.
7. I. Lindemuth and R. Kirkpatrick. Nucl. Fusion **23**, 263 (1983).
8. I. Lindemuth et al. Phys. Rev. Lett. **75**, 1953 (1995).
9. V.K. Chernyshev and V.N. Mokhov. On the Progress in the Creation of Powerful Magnetic Energy Sources for Thermonuclear Target Implosion. Digest of Technical Papers: 8th IEEE International Pulsed Power Conference, pp. 395-410.

THE ADVANCES IN PROGRAMMING COMPACT TORUS (PCT) PHYSICS AND CONCEPTUAL DESIGN

Rustam Kh. Kurtmullaev

State Research Center "TRINITI"
Troitsk, 142092, Russia

The PCT conception was proposed in 70's as an alternative to conventional pinch systems, with new approaches directed against fundamental difficulties discovered on the way of compressionally heated high β plasmas application to fusion purposes.

The experimental design includes [1-3]:

- multi-element solenoidal systems with programming θ-currents to forming the elongated axially symmetrical antiparallel magnetic structure (AMS) and its guided evolution to Compact Torus (CT)
- axially channelized Z-current and impulsive / rotation multipoles replaced on side wall for magnetic insulation and radial distribution and losses control
- multi-chamber general design for separated procedures of CT formation, heating, translation, confinement (or additional compression by imploding solid liner)

The PCT scenario was tested in crucial experiments on TOR, TL, BN devices (TRINITI) [1] by parameters $B \sim 5 - 20$ kG, $n \sim (1 - 5) \times 10^{15}$ cm^{-3}, $T_e \sim 0,1 - 0,5$ keV, $T_i \sim 0,1 - 3$ keV.

The physical essence of scenario:

1. Controlling formation of elongated AMS and forced nontearing connection of its ends;
2. Slow AMS energy accumulation and forced switch on of shock axial contraction based on specific MGD "trigger" feature of balloon shaped CT.
3. Adjustment of Self-Organization Mode of the total relaxation, that gives simultaneously:
   - fast plasma flows acceleration (up to $V_z \sim 10^8$ cm/s) by means encounter MGD stable and lossfree poloidal pistons;
   - impulsive initiation ($\tau \sim 10^{-4}$ s) of anomalous viscosity, plasma flows thermalization and, as consequence of plasma pressure jump, - the axial contraction stopping;
   - sharp transformation of low $< \beta >$ AMS into equilibrium high $< \beta >$ CT with arbitrary structure (balloon shaped racetrack, ellipse or spheroid);
   - dominant ion heating with scaling $T_i \sim B^2$ without any saturation signs in studied range 0.1 – 3 keV. It is physical base to one-step shock achievement the fusion temperature in slow arose fields near the 30 – 50 kG.

Current Trends in International Fusion Research — Proceedings of the Second Symposium
Edited by E. Panarella. NRC Research Press, National Research Council of Canada, Ottawa, ON K1A 0R6, Canada. 1999.

4. Losses and instabilities damping and tearing-merging effects control both in dynamic and stationary phases founded on balloon shaping, inner "double currents ring" structure, plasma flows affect and toroidal field influence [4] . The special interest represents a long lived ($\tau \sim 10^2$ ms) sheared plasma flows in stationary confined CT [3].
5. CT translation and transforming of configuration by programming multi-coil system and AMS shaping, that gives the variation of directed/thermal energy relation $E_{kin}/E_{th} \sim 0 - 10$ and configuration ellipticity $\varepsilon = l_s / 2r_s \sim 1 - 5$.

The PCT next step conceptual and experimental design.

It based on asymmetrically shaped cone AMS (5) and gives equally with shock heating, stabilization and loss damping also the new attractive feature: Self organization final state with arbitrary expanded radial size r_s by conservation of final separatrix volume, maximum postshock energy density and temperatures. This approach, uses only cone AMS axial contraction and stable overcritical balloon phenomena (1,5) means an simplest and cheapest way to increasing the system lifetime $\tau \sim r_s^2$.

The recent crucial experiment on TL-cone device [5] confirms such kind production mirror fields supported large radius ($X_s = r_s / r_c \sim 0{,}9$), relative short ($\varepsilon \sim 2$) CT in continuous process of axial compression and relaxation, without any disruptive effects.

The paper contains the data for next step experiment project founded on combination of two encounter cone AMS systems and central stationary mirror trap, supporting the final CT configuration with double balloon shaping and "double current ring" inner structure, that is attractive because of its controlling stability features. This installation, named "Double Star", will have 40 cm diameter confinement region with shock heated in $T_i \sim 10 \ldots 100$ keV range plasma by fields $B \sim 30 - 50$ kG, excited by MJ's level energy source, corresponds to TOR installation data.

The "Double Star" program main aims:

1. Study of high beta plasmas fundamental physics, including life time scaling near the fusion temperatures range;
2. Conceptual modeling of fusion design tasks including advanced fuel problems.

The report concerns also to possible applications of PCT advances in solid liner compressed high energy dense CT approach [1,2] as well as in present MTF programs and other directions used accelerated dense CT and shaped intensive plasma flows.

REFERENCES

1. R.Kh. Kurtmullaev et al. In book "Results of Science ...," Plasma Physics Ser. 7, 80, Moscow (1985).
2. A.G. Eskov et al. in Proc. 10th Eur. Conf for Contr. Fusion and Plasma Phys. 319, Moscow, 1981; A.G. Eskov et al. Sov. Tech. Phys. Lett **38** (1983).
3. B.B. Bogdanov et al. in Plasma Phys. and Contr. Nuclear Fusion Research, 13th Conf, Washington, Proc. **2**, IAEA 739 (1991); B.B. Bogdanov et al. 12th Conf. , Nice, Proc. **2**, IAEA 527 (1989).
4. A.P. Kreshchuk and R.Kh. Kurtmullaev. Intern. Conf. on Plasma Phys., Nagoya, Japan, 1996. Proc. **1**, 478.
5. R. Kh. Kurtmullaev. Report on Intern. Workshop on Physics Bases for D-He^3 Fusion, Niigata, Japan, 1996 (to be published); A.G. Eskov et al. Report on the same Workshop, (to be published).

INNOVATIVE CONFINEMENT CONCEPTS WORKSHOP

Ronald C. Kirkpatrick

Los Alamos National Laboratory
Los Alamos, NM 87544, U.S.A.

ABSTRACT

The Innovative Confinement Concepts Workshop occurred in California during the week preceding the Second Symposium on Current Trends in International Fusion Research. An informal report was made to the Second Symposium. A summary of the Workshop concluded that some very promising ideas were presented, that innovative concept development is a central element of the restructured US DOE. Fusion Energy Sciences program, and that the Workshop should promote real scientific progress in fusion.

The Innovative Confinement Concepts Workshop held in Marina del Rey, California, during March 3-6, 1997 was sponsored by the US DOE Office of Fusion Energy Science to meet a need for assessment of alternate fusion concepts. Dr. Robert Goldston, now director of the Princeton Plasma Physics Laboratory, was the Workshop organizer. The program committee was comprised of about twenty individuals from a broad cross section of the US fusion community:

Rob Goldston (chair)
John Greenly
Steve Jardin
Jim Lyon
Bill Nevins
John Sarff
Bob Taylor
Roger Bangerter
Alan Hoffman
Jay Kesner
Farrokh Najmabadi
Martin Peng
Ron Stambaugh
Frank Wessel
Dan Barnes
Bick Hooper
Ron Kirkpatrick
Jerry Navratil
L. John Perkins
Joe Talmadge
Mike Zarnstorff

They suggested the names of individuals for concept presentation in several categories of concepts ranging from magnetic confinement to electrostatic confinement to inertial confinement.

Current Trends in International Fusion Research — Proceedings of the Second Symposium
Edited by E. Panarella. NRC Research Press, National Research Council of Canada, Ottawa, ON K1A 0R6, Canada. 1999.

The concept areas represented were:

Unconventional Magnetic
qa < 1 Toroidal Magnetic
Magnetic-Inertial
Inertial Fusion Energy
qa > 1 Toroidal Magnetic
3-d Toroidal Magnetic
Other (including sonoluminescence and muon catalyzed fusion)

The Workshop began with overview presentations from Stewart Prager on scientific benefits of alternative concepts, John Perkins on criteria for attractive fusion power, and Jerry Navratil on the FESAC committee meeting on stages of concept development.

During the first two days of plenary sessions there were about three presentations for each category, which were given by individuals representing specific concepts within each category. On the third day a poster session attracted over 50 contributions, some of which supported the presentations from the previous two days. In addition to the posters there were a few oral contributions. Many of the invited and poster papers presented at the ICC Workshop were also presented at the Second Symposium and appear in these proceedings.

In the afternoon of day three the Workshop broke into concurrent sessions for the consideration of several scientific and engineering topics:

Macrostability
Confinement
Suprathermal Particle Effects
Power and Particle Handling
Continuous Operation
Advanced Reactor Issues

On the morning of the fourth day concurrent informal concept area breakout sessions considered aspects of the concepts within each broad category of concepts. In these sessions the chief proponent of each concept that was not previously presented was invited to give a brief presentation, and then a general discussion followed which was aimed at answering several specific questions common to all the concept categories.

During the second part of the fourth day all the concept area breakout conveners reported at plenary session of all the attendees.

The Workshop organizers collected the view graphs for most of the presentations and bound them into five volumes. In addition, a summary of the oral presentations was posted on a web site by Steve Jardin [1]. The reports from the breakout sessions and the compilation of view graphs were used to assemble a report to be published in the near future [2].

REFERENCES

1. S. Jardin. Summary of Oral Talks at Innovative Confinement Concepts Workshop. posted on the web at http://w3.pppl.gov/~jardin/iccw.html.
2. R.C. Kirkpartick. Innovative Confinement Concepts Workshop, Marina del Rey, California, March 3-6, 1997. Fusion Technology, 34, pp. 170 (1998).

PRESENT STATUS AND FUTURE PROSPECT OF INERTIAL CONFINEMENT FUSION IN JAPAN

Tatsuhiko Yamanaka

Institute of Laser Engineering
Osaka University
2-6 Yamada-oka, Suita
Osaka 5650871, Japan

ABSTRACT

Inertial confinement fusion is a real alternative of the conventional Tokamak device for fusion energy because of its different scientific and technological approach from a magnetic confinement fusion. Described are the advantage of inertial fusion energy (IFE), key issues to be solved for IFE, present status and future plans in Japan. In term of the present status, implosion physics related to hydrodynamic instability, fundamental research of fast ignition, diagnostic technologies concentrated on 2D imaging with 10 ps resolution, laser technologies to achieve an irradiation nonuniformity of 3-5% rms in a solid state laser and fuel pellet technologies to fabricate capsules meeting to ignition experiments and future reactors are presented in some details.

1. INTRODUCTION

Inertial confinement fusion (ICF) truly represents a very different scientific and technological approach from a magnetic confinement fusion (MCF), and the developmental cost and the cost of electricity of inertial fusion energy (IFE) could be smaller than those of the conventional Tokamak device. IFE research has different spin-off areas from the magnetic fusion energy (MFE) and contributes to the advanced technologies in the optical industry, high density matter physics including the astronomical objects, diagnostics with highly temporal and spatial resolution, etc.. The great advantage of laser fusion is that the fusion plasma which meets to energy production can be demonstrated with relatively low cost using a conventional single-shot-base laser system.

Recent progress on high density compression to 600 times solid density [1] and of understanding of hydrodynamic instability are spurring the scientists to construction of burning plasma facility, so that United State and France are promoting the construction of ignition facilities.

The issues to be explored and developed for the demonstration of burning plasma are the detailed properties of hydrodynamic instabilities with relation to laser irradiation uniformity, the uniformity control of laser beams and the cryogenic target fabrication techniques. For those

Current Trends in International Fusion Research — Proceedings of the Second Symposium
Edited by E. Panarella. NRC Research Press, National Research Council of Canada, Ottawa, ON K1A 0R6, Canada. 1999.

issues IFE people already have concepts backed up by some experimental results. For the energy production excellent believable reactor designs are presented while a lot of R&D items exist since little technological development has yet occurred. Most challenging issues are the the cost effective, highly efficient, reliable energy driver, the problems related to the proposed liquid or granular blanket such as reliable configuration of blanket, vacuum recovery within a cycle time and the pointing of driver beams on fuel pellets.

In this paper attractive features of IFE, issues to be solved, present status of ICF research in Japan and future prospect based on the strategic design for inertial fusion energy development which is discussed by the professionals related areas [2] are presented.

2. ATTRACTIVE FEATURES OF IFE

IFE has a lot of attractive features from the stand points of the power plant and the developmental research. There are three great attractive features for the power plant.

1) Reactor chamber can be designed topologically simple.
2) Energy driver can be separable from the reactor chamber by any distance.
3) Liquid blanket can be used.

The first comes from that ICF does not need magnetic field for plasma confinement and the reactor chamber may be designed without complex equipments near the reactor chamber for the energy driver and the fuel pellet. The first and the second present easy maintenance of the reactor chamber which is activated by 14 MeV neutrons. The second will give us most attractive benefits. Complex energy driver can be maintained without radioactive hazard. One energy driver system, which will be most expensive part of the power plant, can supply energy for several reactor chambers. For instance in the laser fusion reactor design of "Koyo", [3] the energy driver operates with 12 Hz to drive four reactor chambers in series. This multi-reactor system offers flexible operation of power plant and reduces the cost of electricity. The third can contribute to reduce radioactive waste by protecting structural materials from 14 MeV neutrons by the thick liquid metal/ alloy or granular blankets.

Attractive points in developmental phase are summarized as follows;

1) Physics related to production of fusion energy or burning plasma may be established by relatively small facility such as the installation for hydrodynamic equivalent plasma demonstration. The energy and the cost for it may be enough 50–100 kJ and $100–200 M although fine diagnostics and laser system with supra-high irradiation uniformity, about 0. 1% in rms, have to be developed.
2) Reactor plasma can be demonstrated using already developed conventional laser technologies with low cost comparing to the Tokamak reactor. Note the construction cost of the National Ignition Facility (NIF) of US is $1,2 M.
3) Key reactor technologies such as laser and fuel pellet can be developed using a small scale modules.
4) Physics and R&D of technology can be developed parallel with relatively small facilities, and an integrated simulation code which predicts accurately gain scaling can be developed using data obtained from such facilities.
5) Laser fusion has a lot of spin-off in the fundamental physics as well as applied science and in the optical industry which will be one of the major industries in 21st century. High density implosion and new research of fast ignition will open laboratory experiments of astrophysics and new ultra intense field physics.

3. KEY ISSUES TO BE SOLVED

3.1 Fusion Plasma Physics

Demonstration of a high density compression [1] in 1989–90 was a remarkable mile stone in IFE. The next milestone is the demonstration of the ignition-and-burn in the area of plasma physics. There are two ways to achieve the ignition-and-burn condition. One is the conventional way in which ignition starts from a hot spark at the center of the isobarically compressed plasma. The other is a new approach and is called as fast ignition,[4] in which a small part of the isochorically imploded low temperature high density plasma is heated up to the ignition temperature by a ultra-intense laser pulse.

The most important physics to be solved for ignition-and-burn in the conventional way is quantitative understanding of hydrodynamic instabilities such as Rayleigh-Taylor (R-T) instability, and preheating of the main fuel. The energy of compressed core plasma E_p, fusion out put energy E_f are given as

$$E_p = 10^4 \left(\rho_h/\rho_s\right)^{-2} \left(\rho_h R\right)_\alpha^3 T + 0.35\, \alpha \rho^{2/3} M \qquad \text{(MJ)}, \qquad (1)$$

$$E_f = Q(=334\ GJ/g) M f_b \qquad \text{(GJ)}, \qquad (2)$$

where the first term of right hand side of eq. (1) is the hot spark energy and the second term is main fuel energy in Fig. 1(a). ρ_h, ρ_S, are mass density of DT plasma at hot spark, and solid DT in g/cm^3. $(\rho_h R)_\alpha$ is the density-radius product/areal density of hot spark which is equal to α particle range of 0.3 g/cm^2. T is the temperature of hot spark in keV. ρ and M are mass density and total mass of main fuel, and α is isentrope of main fuel given by [internal energy/ Fermi energy]. Q(= 334 GJ/g) is fusion energy obtained from unit fuel mass and f_b is burn fraction which depends upon ρR.

If one wants to make a plasma given by eq. (1), first of all the amplitude of R-T instability in acceleration phase must be at least less than the in-flight thickness of main fuel since a broken-up main fuel can not make a hot spark required and also main fuel density does not reach the value to attain the required gain. The acceptable amplitude of R-T instability is depend upon the isentrope factor α. Higher α by preheat makes thicker inflight fuel layer and moderates the condition of the main fuel break-up. But it increases main fuel internal energy and then requires higher ablation pressure and /or lower main fuel density which results in lower fusion gain of E_f/E_p. α has to be kept at least less than 3 for achieving an attractive fusion gain by a laser with output energy of several MJ and efficiency of 10%.

Second, the hot spark $\rho R = (\rho_h R)\alpha$ must be satisfied at stagnation phase under the existence of R-T instability. If the hot spark-main fuel mixing takes place at stagnation phase as shown in Fig. 1(b), the effective hot spark energy in eq. (1) will be $(R_e/R)^3$ times of the ideal case since the mixing layer (Re-R) does not act effectively as ignitor, so that bigger driver energy is required.

The physics of hydrodynamic instabilities and preheating have been studied extensively because they are closely related to the irradiation uniformity and pulse shape of the laser. It is, however, not studied yet enough to determine the features of laser and fuel pellet for IFE with the accuracy of engineering sense. Lawrence Livermore National Laboratory (LLNL) is promoting the NIF project to demonstrate the ignition-and-burn by the indirect implosion scheme. The LLNL approach is one way to obtain the required data for IFE. Laser fusion, however, has another approach, the so called hydrodynamic equivalent plasma of which hot core temperature and density are the same as those of the ignition plasma but the size is small.

This is a more scientific way and less expensive approach, although one has to prepare a better irradiation uniformity laser and higher resolution diagnostic techniques than those of the National Ignition Facility.

In the new approach of fast ignition no hot spark is required at the center of the compressed core, so that the required ablation pressure is reduced so much since the main fuel can be compressed without hot spark pressure. Therefore the requirement for hydrodynamic instability is moderated as demonstrated already by not so good uniformity laser. But one must study on the penetration of a ultra-intense laser beam into the high density compressed core plasma to deposit the energy in a small region at the center or some part of the compressed core plasma. The expected physics for laser penetration into over-dense plasma is a relativistic effect which increase the plasma frequency. So far no one has experimental data to judge the feasibility of this way, but the success of this method presents the higher fusion gain by a smaller laser system with moderate uniformity.

3.2 Fusion Technology

The issues of IFE which are key in the technological field for laser fusion are briefly summarized here since the laser fusion research can be carried out using already developed or under development conventional techniques in NIF and other implosion physics researches with some modifications until the experimental reactor phase. They are the energy driver, fuel pellet and reactor chamber. The energy driver must operate with repetition rate of several Hz and the efficiency of ≥10% for the expecting pellet gain of 100. The most promising laser is so far the diode laser pumped solid state laser (DPSSL) of which progress is so rapid in the industrial application. The efficiency is estimated to meet the IFE. Technology for mass production of laser diodes with low cost, laser architecture with high extraction efficiency and high cooling performance of elements, automatic beam quality control system and high damage-threshold optical components with long life have to be developed. One of the most difficulties is the development of the final optics which are set near the reactor chamber and are exposed by 14 MeV fusion neutrons, x-ray and plasma particles. Innovative ideas are expected for protecting the optics from radiation from the fusion plasma.

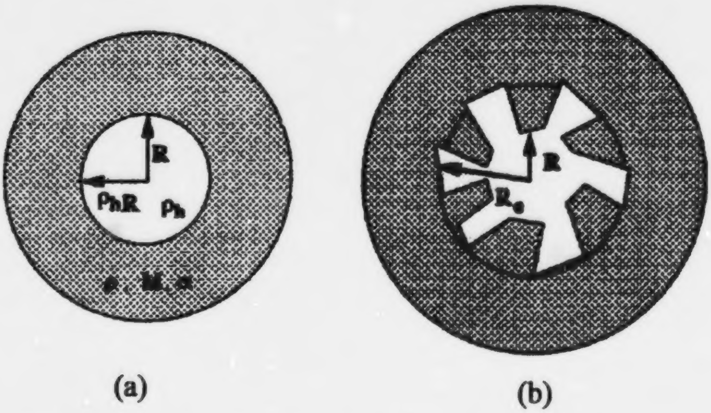

Figure 1. Schematic of imploded plasma. (a): Ideal case. (b): Realsistic case.

In term of the fuel pellets, the mass-production technology of fuel pellets which includes high pressure (up to several hundred bar) tritium gas handling and cryogenic techniques to make a uniform DT solid or liquid layers and the pellet injection system have to be developed. In direct drive system either for isobaric or fast ignition schemes fuel pellets have to be injected with velocity of ≥300 m/s and the position accuracy of about 1% of the pellet diameter at the center of the reactor chamber in order to keep the DT layer suitable for implosion and the required laser illumination uniformity. It requires an injection system with a tracking system predicting the pellet position with the above mentioned position accuracy.

Most suitable blanket of reactor chamber is liquid-metal or alloy containing lithium for tritium breading and protection of structural wall from 14 MeV neutrons, x-ray and plasma particles. The required thickness of liquid metal blanket will be about 1 m. For such a reactor chamber concept no experimental works has been done so far. Therefore fundamentals of liquid metal wall formation, reliability of the wall against the explosive pressure, vacuum recovery, etc. have to be studied. Protection of the final optics from neutrons, x-ray, plasma particles and liquid metal vapor is essentially important since it may decide the repetition rate of reaction, reliability of long term operation, etc.

4. PRESENT STATUS OF ICF RESEARCH IN JAPAN

4.1 Laser Implosion Physics

4.1.1 Hydrodynamic instability

In order to design a burning plasma it is essentially important to understand in detail the hydrodynamic instability, especially on the growth rate, saturation level, mode coupling and source of initial perturbation of R-T instability. Regarding to the initial perturbation, a perturbation imprinted by the irradiation nonuniformity of week leading edge of laser pulse is important as well as the intrinsic perturbation of the fuel pellets.

The growth rate of R-T instability at the surface where plasma ablates with velocity v is given theoretically [5] by

$$\gamma = 0.9(kg)^{1/2} - \beta kv \tag{3}$$

where k is wave number of perturbation, g the gravity acting on acceleration surface, β the reduction factor due to the ablation of plasma. The velocity v is given by m/ρ_a. Here m is mass ablation rate and ρ_a the density at ablation surface. Reduction factor β is theoretically estimated to be 3 which depends upon the structure of ablation surface [5].

The linear growth rate is measured for 530 n m laser irradiation on the polystyrene planar target with different surface modulation depth and wavelength [6] as shown in Fig. 2. Here the thickness of target is 16 μm and the initial perturbation amplitudes are 0.1–1 μm. The temporal change of the amplitudes are measured by x-ray back-lighting method with streak camera as an areal mass density change. Linear growth rates are determined in the condition that the amplitude is less than the compressed target thickness of ÷ 3 μm, The laser intensity is 7×10^{13} W/cm^2. Uniform irradiation is obtained using a partially coherent laser so that no R-T instability is observed with unperturbed target. The gravity g and the mass ablation rate measured are 4.9×10^{15} cm/s^2 and 2.9×10^5 g/cm^2 in the experimental conditions. The

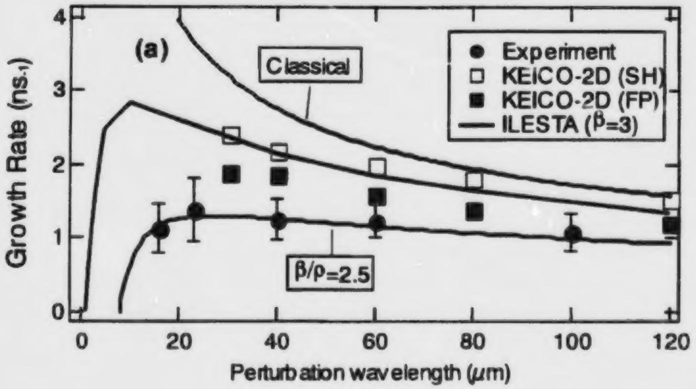

Figure 2. Growth rate of R-T instability. Experimentally observed growth rates are smaller than the theoretically predicted values.

observed growth rates for different wavelengths are shown in Fig. 2. The classical growth rate is given by $(kg)^{1/2}$ in the figure. The observed growth rates are smaller than the calculated values using m/ρ obtained from our standard 1D simulation code ILESTA by putting $\beta = 4$, and the values predicted by the 2D simulation code KEICO(SH). Here both codes are described using the Spitzer-Harm thermal conductivity but they can reproduce well the experimentally observed macroscopic hydrodynamic behaviors. Simulation results by KEICO(FP) with Fokker-Plank equation, in which the energy transport is treated by multi-group method, approach closer to experimental results but still give higher growth rates. The detailed discussion is in reference (6).

The initial imprint by laser irradiation nonuniformity is studied with a 16 μm thick polystyrene target by illuminating a sinusoidally modulated low intensity pulse (5 ×

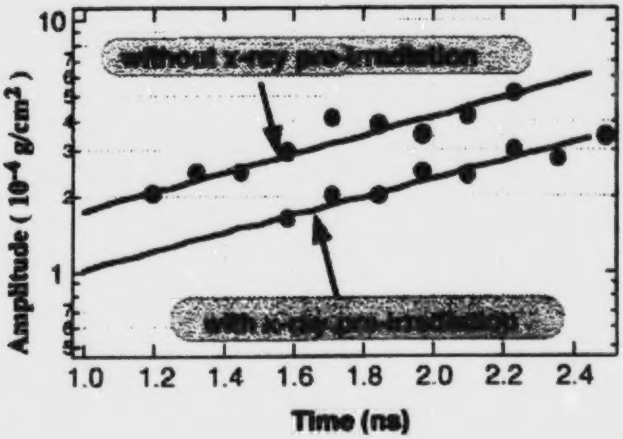

Figure 3. Initial imprint due to laser nonuniformity is suppressed by x-ray pre-irradiation.

10^{12} W/cm^2) followed by the non-modulated high intensity beam [6, 7]. The modulation intensity $\delta I/\langle I\rangle$ is given by a slit mask to be 10% and 40% with spatial wavelength l of 100 μm. The amount of the imprint is estimated by interpolating the areal mass density perturbation grown by the irradiation of high intensity beam. The areal mass density perturbation at the onset time of the high intensity beam is 9×10^{-5} and 2×10^{-4} g/cm^2 for $\delta I/\langle I\rangle$ = 10% and 40%, respectively. While no imprint is observed for the non-modulated beam.

The reduction of imprint by the uniform preformed plasma is studied in the same way [6][8]. The preformed plasma is produced by an external x-ray source. The perturbation amplitude imprinted is reduced to 60% of that without x-ray pre-irradiation in the case of 40% modulation imprint pulse as shown in Fig. 3. This reduction factor is discussed with cloudy model in which the reduction factor f is given by $f = \exp(-kD)$ where D is the stand-off distance. For k = 630 cm^{-1} (l = 100 μm and D = 14 μm), f becomes 0.4 which is close to the experimentally observed value. Here the irradiation x-ray intensity is estimated to be 7×10^{10} W/cm^2 and the stand-off distance D is given by $C_s\tau$ is 14 μm, where C_s is the sound velocity of x-ray preformed plasma (3.5×10^6 cm/s) and τ is the duration (400 ps). This hybrid method is useful to suppress the initial imprint in direct drive implosion.

The behavior of the ripple shock wave, which gives the areal density perturbation, is also studied using a surface modulated planar target [9, 10]. The phase inversion is observed when the shock traveling distance becomes equal to the perturbation wavelength. The areal density perturbation approaches to be 4 when shock front propagates more than a perturbation wavelength. These results agree well with the theoretical calculation [11].

4.1.2 Fundamental experiments of fast ignition

In the concept of fast ignition it is expected that an ultra-high intensity laser penetrates very near the isochorically imploded core plasma by a self-focusing due to the ponderomotive force and/or relativistic effect to produce high energy electrons and/or ions which heat locally small part of more than 1,000 times solid density region to the ignition temperature. A 1 μm, ~ 1 ps, petawatt laser will be used. Relativistic effect takes place at intensity of 5×10^{18} W/cm^2 for 1 μm laser. In order to clarify the feasibility of the fast ignition a lot of fundamentals have to be studied.

In our institute 2D simulation works on self-focusing and penetration into over-dense region are carrying out as well as experimental works. For the experimental studies 30 TW/ps beam and 100 TW/ps beam are developing. The 100 TW beam system has ability to deliver PW/ps by changing the pulse compression grating to bigger one.

Prechanneling or hole boring by a small energy prepulse may be required for sending an ultra intense beam efficiently into the over dense region. If an ultra-intense pulse is irradiated alone to the imploding plasma, it may dissipate most of the energy in the low density region without producing high energy electrons and ions effective for making an ignitor. Therefore hole boring experiments are carried out [12]. Target plasma is produced by irradiating two 350 nm laser beams (5 J/100 ps × 2) onto the planar plastic targets. A test beam with wavelength of 1 μm and pulse width of 100 ps is focused using f/3 lens normally to the target plasma after 0.9 ns of the target plasma formation pulse. The intensity at focal point is 2×10^{17} W/cm^2 for the spot size of 30 μm with focal depth of ± 80 μm at both sides of the best focus point. The position of density $3 \pm 2 \times 10^{20}$/cm^3 is measured to be at 200 ± 20 μm from the initial target surface by means of a diffractometry using a 263 nm, 10 ps UV probe beam. Note the cut-off density for 1 μm laser is 1×10^{21}/cm^3. The focusing points of the test beam are varied from 100–400 μm from the initial plastic target surface. When the test beam is focused at 250 μm from the initial target surface, a sharp red shifted back scattered spectrum and a tight x-ray emission with 30 μm in diameter at the target surface are observed. While they are not observed at 100 and 400 μm. From the detailed analysis of these phenomena with other experimental results it is concluded that hole boring reaching to the solid density region takes place by the whole beam self-focusing.

4.1.3 Diagnostics

Diagnostics of ICF plasma requires extremely high spatial and temporal resolution, and x-ray and fusion related particles are mainly used since the plasma density is so high for usage of optical probes and conventional high energy particles. The most important diagnostics are of density ρ, areal density or density-radius product ρR, temperature and structure of imploding plasmas. Required spatial and temporal resolutions should be a few μm and a few ps, respectively. A variety of diagnostic instruments and methods are developed. For ρR measurements methods used fusion products and their related particles are established for conventional use. They are the secondary reaction method [13], neutron activation method [14], neutron knock-on method [15], etc. Two dimensional x-ray imaging camera with temporal resolutions of 80 ps and <10 ps are conventionally used. 80 ps one records multi 2D images using a specially designed gated microchannel plate image intensifier [16]. The <10 ps one reconstructs multi 2D images from multi-images obtained by a large photo-cathode streak camera using a sampling technique [17]. A penumbral coded imaging method is developed for imaging of neutron source with spatial resolution of 30 μm [18]. For fusion bum time and duration measurements, two types of streak cameras are developed. One is the fiber-scintillator streak camera with 50 ps resolution [19] and the other is the streak camera with $U0_2$ cathode with 70 ps resolution [20]. A 920 channel single hit neutron detector is developed for ion temperature and ρR measurements [21].

There are two 10 ps 2D imaging systems named MIXS (Multi-image x-ray streak camera) [17] and 2D-SIXS (2 dimensional sampling image x-ray streak camera) [22]. The principle of MIXS and an example of obtained images are shown in Fig. 4. An array of same images having a separation distance s is given on a slit-photocathode of a streak camera (Fig. 4a). The direction of the array is tilted with a small angle θ with respect to the slit so that the 2D image can be decomposed into a set of 1D sliced images. After taking temporally varying images (Fig. 4b), the original image is decomposed from the streaked images (Fig. 4c) by the aid of a computer. The recomposed 2D images give a snapshot with the same resolution of the streak camera. Therefore temporal resolution of as short as that of streak camera is obtained ideally. For usual use 5–10 pinhole images are projected on the streak slit. In this case the spatial resolution is limited by diameter of pinhole camera.

2D-SIXS is developed to obtain better spatial resolution. A 2D image is projected on a photocathode of streak camera using a large clear aperture x-ray microscope with high spatial resolution. If a mask with a pinhole matrix is inserted in front of the photocathode instead of streak slit, one can obtain streak images corresponding to the pinhole position. The pinholes are so arranged that resultant streak images do not overlap each other. The temporally resolved 2D images can be recomposed by taking intensity data of each sampling points.

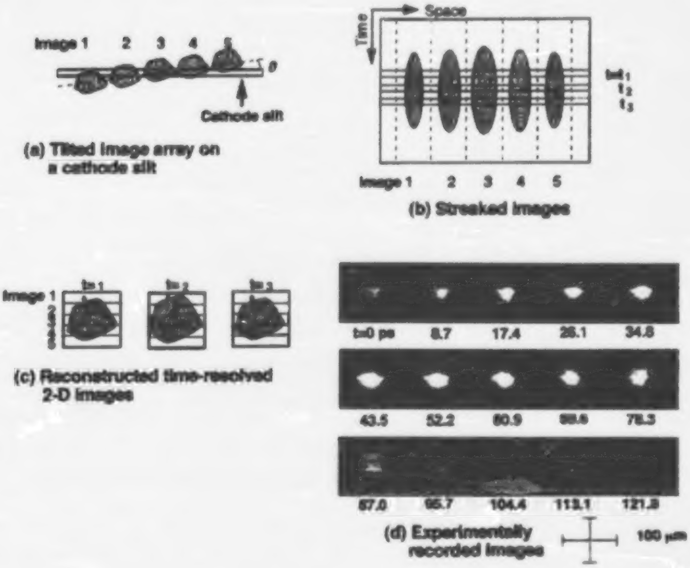

(a) Tilted image array on a cathode slit

(b) Streaked images

(c) Reconstructed time-resolved 2-D images

(d) Experimentally recorded images

Figure 4. Principle of multi 2D imaging using a streak camera and an example of recorded images.

4.2. Laser Technology

In direct drive implosion, laser irradiation uniformity is essentially important to achieve a high density compression and an ignitor at the center of compressed core. Laser irradiation uniformity is dependent upon the intensity profile of each beams, instantaneous power balance between beams and number of beams. A random phase plate (RPP) [23], which divides a beam into many beamlets with randomly distributed phase difference π, greatly contributes to the improvement of irradiation uniformity and it is used conventionally for implosion experiments in the world. High mode number nonuniformity, however, remains due to the speckles induced by the coherence of laser. In order to reduce speckle effects, a partially coherent light is developed by which nonuniformity in high modes is smeared out in time average with combination of RPP. The improvement of power balance between 12 beams of the Gekko XII laser system is improved by a detailed control of the charging voltage of the amplifiers and by introduce of an equipment to adjust the different conversion efficiency of frequency converters of KDP crystals.

Another important technique in laser is the tailoring of laser pulse since the implosion performances depend upon the temporal change of the ablation pressure. A pulse tailoring system used optical fibers is developed which can easily obtain almost of any pulse shapes. For the fast ignition experiments a petawatt-picosecond laser is developing. Development of DPPSL are also carrying on aiming the reactor driver.

A partially coherent light (PCL) technique is developed with a technique of pulse tailoring [24]. A single 100 ps pulse from the mode locked oscillator is sent to an optical fiber to make a broad band chirped pulse. The obtained chirped pulse is compressed to 50 ps pulse using a grating pair. This pulse is split into multi beams using a wave guide type fiber coupler. Then they are combined with different attenuation and different time delay to make a required pulse shape and duration. The obtained pulse is sent to multimode fiber to reduce the spatial coherence and the interference effect of overlapped part of the pulses.

The PCL is excellent for achieving a good irradiation uniformity but the frequency conversion efficiency decreases due to the broad spectrum and the beam divergence. A 2D-SSD (smoothing by spectral dispersion) technique is developed [25] in order to improve the conversion efficiency and to use for main drive pulse following the PCL pulse.

Power balance of 12 beams of Gekko XII is improved to be 3–5% rms in imbalance around the pulse peak and 10% at the leading edge (1/100 peak intensity) [24, 26]. Gekko XII green laser system includes two nonlinear elements. One is nonlinear power amplifiers and the other is crystals for second harmonic generation. Therefore, first of all, the pulse shapes of 12 beams are adjusted to be same in fundamental wavelength of 1 μm by controlling the gains of small size linear amplifier and large size nonlinear power amplifier. The output pulses of the outlet of amplifier chains are sent to the frequency conversion crystal, KDP, through variable attenuators. By controlling the power of each beam with variable attenuators, the shapes of 2nd harmonic light are adjusted to be identical. And then the power of each beam onto the target is adjusted by adjusting the laser beam aperture at linear amplifiers. Finally the intensity on the surface of the target is adjusted by slightly changing the focusing condition. These procedures are confirmed by improving the accuracy of energy monitors to be ± 1% and by introducing 4 GHz oscilloscopes for the pulse shape measurement.

The present target irradiation uniformity of Gekko XII green beam system is shown in Fig. 5. Here the segment shape of RPP is changed from the square to the hexagonal with better control of phase shift in order to reduce nonuniformity caused by 12 beams. The attained nonuniformity for irradiation on a 0.5 mm diameter spherical target is 3–5 % rms [26].

4.3. Fuel Pellet Technology

Techniques of fuel capsule fabrication, solid or liquid fuel layer formation inside the capsule, and target levitation and injection are investigating extensively. Capsules are traditionally fabricated by means of an emulsion method [27]. A continuous production method is developed, by which capsules almost meet the requirements for the ignition-and-burn experiments planned in LLNL and the reactor can be produced. A low density plastic foam shells are also fabricated by the same emulsion method [29]. The foam structure is 3D network one with network size of less than 1 μm and mass density of less than 50 mg/cm^3. The foam layer can be prepared both inside and outside of normal density plastic shell. Plastic capsules with foam layer inside or outside are used for making uniform DT/D_2 solid or liquid layers and for the improvement of irradiation uniformity, respectively. The plastic shells are characterized with spatial resolutions of 2 μm and the thickness of 0.01 μm by a laser interferometric method.

A W/O/W (water/oil/water) emulsion method is used to make polystyrene capsules. Mass density of each phase is adjusted to eliminate gravitational effect so that uniform thickness shells are obtained. For mass-production of shells with required size and thickness, a droplet making machine is developed [28]. It consists of a double nozzle arranged coaxially to make W/O/W emulsion in the surrounding flowing water as shown in Fig. 6 with a photo of produced shells. The inner nozzle (1st orifice) supplies water to be core with aiming diameter and the outer nozzle (2nd orifice) does oil phase which includes polystyrene polymer. The produced W/O/W emulsions are transferred to the heated water bath to evacuate solvent in oil phase through a guiding tube (3rd orifice). The thickness of the shell is controlled by

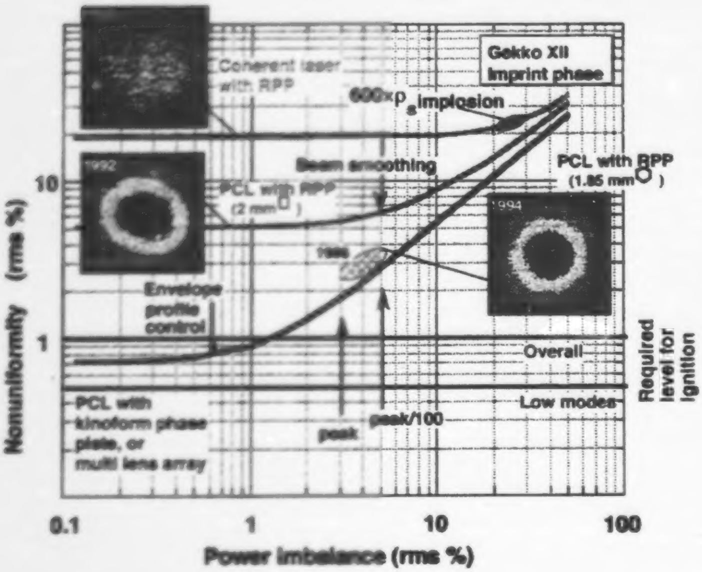

Figure 5. Present status of irradiation uniformity of Gekko XII laser system in green in original color picture.

adjusting the polystyrene density in the oil phase and the diameter of second orifice. The controllable range of diameter and thickness are 0. 1–7 mm and 5–150 μm, respectively. The attained quality so far is >99% in sphericity, 99% in wall uniformity for <1 mm diameter and 98% and <10 nm in surface roughness for >1 mm diameter [30].

Two methods of target levitation are developing. One is magnetically suspension method in which a thin nickel layer (about 10 nm) coated shell is dynamically held at the balance point of magnetic force and gravity using a magnetic pole piece [31]. The horizontal vibration is suppressed by irradiating a weak He-Ne laser. The other one is a method using electrostatic force for the magnetic force. In this case three pairs of electrodes are used to stabiiize the horizontal position. Target must be charged up in this case so that it is used for DT target. In pellet injector the acceleration and tracking methods are investigating [32].

For the cryogenic target technology a foam layer method and a plasma layering method [33] are developing. The plasma layering method is that inner surface of the nonuniform DT or D_2 solid layers are heated impulsively by a plasma produced inside the shell with a microwave. The evaporated gas condenses thicker at the thinner part than at the thicker part since the shell is kept in uniform temperature environment and then the thinner part temperature falls faster than the thicker part. The advantages of this method are to be attained shorter layering time and better surface smoothness comparing the β decay [34] and IR radiation heating [35] methods. This method is useful for the fuel pellets production of an experimental reactor and a fusion plant.

5. FUTURE PROSPECT

In Japan we are mainly involved in direct drive IFE where multi laser beams are directly irradiated onto the fuel pellets. The required laser irradiation uniformity is estimated to be 1%

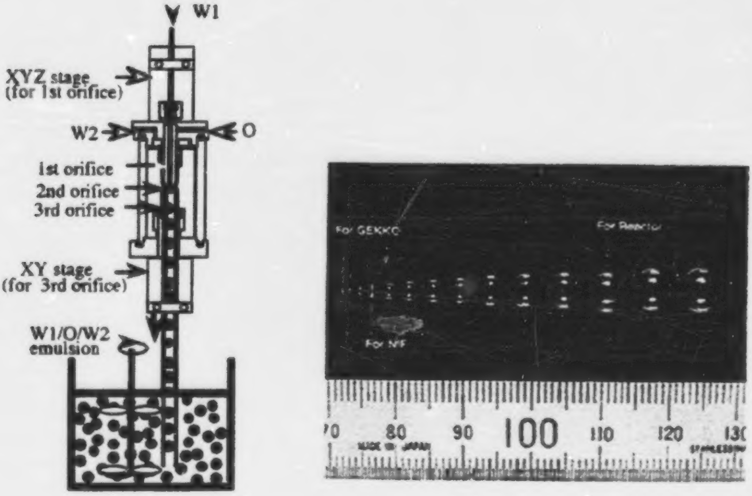
W1
XYZ stage
(for 1st orifice)
W2
O
1st orifice
2nd orifice
3rd orifice
XY stage
(for 3rd orifice)
W1/O/W2
emulsion
For GEKKO
For Reactor
For NIF
70
80
90
100
110
120
130

Figure 6. Continuous production method of plastic shells by means of droplet method, and polystyrene shells of which diameter are 0.5 – 7 mm.

for the isobaric implosion, but no one prove that value by experiments, although the high density compression up to 1000 times solid density without a hot spark at the center is demonstrated with the irradiation uniformity of ÷ 18% and the knowledge on hydrodynamic instability has progressed. And also by the recent progress of ultra-high intensity laser technology presents a new approach of the fast ignition which moderates irradiation uniformity and higher gain than the central ignition method by isobaric implosion.

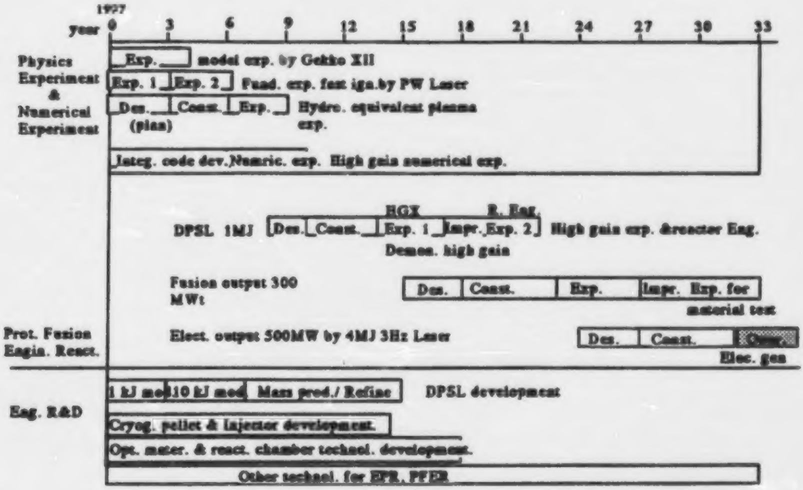

Figure 7. Future plan of IFE research proposed by Japanese scientists.

The high gain experiments with gain meeting the power plant requirement may be demonstrated using conventional laser technology with the cost for NIF which is considerably low compared to conventional Tokamak. But this way is not so good way at the present circumstances. And also we do not have a laser technology meeting to the experimental reactor which follows the high gain demonstration. DPPSL is one of the promising candidates for a reactor driver and its feasibility can be demonstrate by making a 10 kJ class one beam machine.

Figure 7 is a proposal obtained by the Inertial Fusion Energy Assessment Committee composed by Japanese scientists involved in ICF research, laser engineering and fusion technology [2] under the above mentioned arguments. It is proposed that the fundamental experiments to complete an integrated code for the design of high gain experiments with high accuracy and the technology developments such as energy driver, fuel pellet, etc., which can be used for experimental reactor, should be investigated in these 10 years. High gain experiments are pursued using a DPPSL system. At ILE Osaka University which is a key institute of ICF, feasibility study experiments of the fast ignition, model experiments for high gain and hydrodynamic equivalent plasma experiments are promoting to complete an integrated code as well as developing works of DPSSL and fuel pellets.

6. SUMMARY

Inertial fusion energy, especially laser fusion, is an absolutely alternative method of Tokamak device and can make an attractive developmental scenario for fusion energy. Recent progress of laser diode pumped solid state laser has contributed to sketch an attractive scenario for the inertial fusion energy. The promotion of laser fusion energy research will contribute to the industries in 21st century in which photonics is considered to be one of the key technologies and open new approaches for fundamental science. In these 10 years physical data to complete an integrated simulation code for a design of high gain experiments and the scientific feasibility study of the fast ignition are required with reactor related technology developments for an attractive inertial fusion power plant.

REFERENCES

1. T. Yamanaka et al. Particle Accelerators, Gordon and Breach Science Publ. (1992). p. 534.
2. Report of the Inertial Fusion Energy Assessment Committee, Institute of Laser Technology (1996), in Japanese.
3. Y. Kitagawa et al. Seventh International Conference On Emerging Nuclear Energy Systems p. 81; World Scientific (1994); M. Yamanaka et al. ibid p. 145; Y. Kosaki et al. ibid; p. 76.
4. M. Taback et al. Phys. Plasma 1, 1626. (1994); T. Yamanaka, Internal Rep. ILE Osaka Univ. (1983) p. 5, in Japanese (unpublished).
5. H. Takabe at al. Phys. Fluids, **28**, 3676 (1985).
6. H. Azechi et al. Phys. Plasmas, 4, 4079 (1997).
7. M. Nakai et al. 1995 Ann. Progr . Rep. ILE Osaka Univ. (1996) p. 141.
8. H. Shiraga et al. 1995 Ann. Progr. Rep. ILE Osaka Univ. (1996) p. 143.
9. T. Endo et al. Phys. Rev. Lett., 74, 3608 (1995).
10. H. Shigemori et al. 1995 Ann. Progr. Rep. ILE Osaka Univ. (1996) p. 133.
11. R. Ishizaki et al. 1996 Ann. Progr. Rep. ILE Osaka Univ. (1997) p. 224.

12. R. Kodama et al. Phys. Rev. Lett., **24**, 4960 (1996); K. Takahashi et al. SPIE **3156**, 146. (1997).
13. H. Azechi et al. Appl. Phys. Lett., **49**, 555 (1986).
14. H. Nakaishi et al. Appl. Phys. Lett., **55**, 2072 (1989).
15. H. Nakaishi et al. Appl. Phys. Lett., **54**, 1308 (1989).
16. M. Katayama et al. Rev. Sci Instrum., **62**, 124 (1991).
17. H. Shiraga et al. Rev. Sci. Instrum., **66**, 722 (1995).
18. Y. Chen et al. IEICE TRANS. ELECTRON. E78-C, 1787 (1995); N. Miyanaga et al. Ionizing Radiation, **19**, 21. (1992) in Japanese.
19. N. Miyanaga. et al. Rev. Sci. Instrum., **68**, 621 (1997).
20. Idem., **61**, 3591 (1990).
21. N. Izumi et al. Proc. 12th Int. Conf. on Laser Interaction and Related Plasma Phenomena AIP Conf.Proc. 369 eds. S. Nakai, G.H. Miley (1995) p. 550.
22. H. Nishimura et al. Plasma Phys. Rep. **24**, 114 (1998). Major diagnostic instruments in ILE Osaka Univ. are summarized here.
23. Y. Kato et al. Phys. Rev. Lett., **53**, 1057 (1988).
24. N. Miyanaga et al. Laser Interaction with Matter, Inst. Phys. Conf. Series #140, Inst. Science Pub. (1995) p. 81.
25. N. Miyanaga et al. Proc. Second Annual International Conference on Solid State Lasers for application to Inertial Confinement Fusion, Ed. by M. L. Andre', SPIE, **3047**, 746 (1997).
26. T. Yamanaka et al.World Scientific, p. 20 (1997).
27. U. Kubo et al. Ann. Prog. Rep. ILE Osaka Univ. ILE-APR-78, 137. (1978); U. Kubo et al. J.Vac. Sci. Technol., A **4**, 1134. (1986).
28. M. Takagi et al. J. Vac. Sci. Technol., A **9**, 820 (1994).
29. T. Norimatsu et al. J. Vac. Sci. Technol., A **12**, 1293 (1994).
30. T. Norimatsu et al. 11th Target Fabrication Specialists' Meeting, Orcas Island, Washington, Sept 8–12,1996.
31. H. Yoshida et al. Laser and Particle Beams, **11**, 455 (1993).
32. A. Hochi et al. 1996 Ann. Prog. Rep. ILE Osaka Univ., 213 (1997).
33. C. Chen et al. J. Vac. Sci. Technol., A **11**, 509 (1993); C. Chen et al. J. Vac. Sci. Technol., A **13**, 2908 (1995).
34. J.K. Hoffer et al. Phys. Rev. Lett., **60**, 1310 (1988).
35. D. Bittner et al. 11th Target Fabrication Specialists' Meeting, Orcas Island, Washington, Sept. 8–12, 1996.

INERTIAL FUSION TARGETS IGNITION BY HYPERVELOCITY PLASMA JETS

J.M. Martinez-Val, P.M. Velarde and S. Eliezer*

Institute of Nuclear Fusion
ETSII, Madrid Polytechnic University
Madrid, Spain

ABSTRACT

A new method to trigger ignition in highly compressed Inertial Fusion targets is proposed. The method belongs to the general class of fast-ignited targets, in which a fusion burn-wave is created from one or two spots and rums across the fuel as a detonation wave. In this way, very high energy gains can be achieved, because the size of the ignited spots can be much smaller than the target mass.

Ignition is achieved in this case by the impact of hpyersonic plasma jets on one or two spots of the target (Two ignitors could be adivsable by symmetry constraints).

The hypersonic plasma jets are generated in the collapse of conical hollow-charges. Very small jet mass is required to trigger ignition but the jet speed must be well over 10^6 m/s.

Estimates are given about the energy gain that could be achieved with this scheme.

The most critical issue of this proposal is jet generation, and it is also addressed in this paper. Although there is not experimental evidence so far on hypervelocity jet formation, numerical analysis point out that it will be possible for certain hollow-charge designs.

1. INTRODUCTION

Ignition requirements to launch a fusion burning wave from a small spot within a target will be analyzed first. Those requirements will set up a threshold in jet energy, below which ignition will not be possible [1].

Once jet requirements have been determined, the problem of jet generation will be addressed. Due to the very high collapsing velocities needed to reach the threshold, extremely high pressures will have to be generated in the outer surface of the conical hollow-charge. In order to do it, standard Inertial Fusion drivers could be used. In particular, the conical collapse could be driven by the high-temperature thermal radiation generated inside a hohlraum. The cone vertex will point outward the hohlraum and the jet will be ejected inward.

2. JET-IGNITION REQUIREMENTS

High energy gains can be achieved in Inertial Fusion targets if a fusion burning wave is

Current Trends in International Fusion Research — Proceedings of the Second Symposium
Edited by E. Panarella. NRC Research Press, National Research Council of Canada, Ottawa, ON K1A 0R6, Canada. 1999.

triggered from a small volume of fusionable fuel. A standard way that has been suggested to trigger such a wave is to create a central hot spark in the center of a spherical target at the end of the implosion process. The implosion must be tailored to get such a configuration where about one tenth of the fuel is at very high temperature and moderate density, while the rest of fuel is at lower temperature and much higher densities.

Another option to trigger ignition in Inertial Confinement is to use an additional heater beam to ignite a small volume of the compressed target, so launching a fusion burning wave. Such a type of heater can be a ultra-intense laser, a particle beam or a cumulation jet. The so called Fast Ignitor concept is based on this idea [2]. A fuel capsule is imploded according to the isochoric model (uniform final density) to keep the temperature as low as possible. Once the fuel has reached maximum compression, a ultra-short and intense laser beam is aimed at the center of the capsule. The beam has to dig a microhole in the surrounding plasma corona. Additionally, a small region of the capsule reaches ignition temperature by energy deposition of the fast electrons generated in the relativistic regime of this interaction, and a fusion burning wave is launched from there outwards.

The physics of the interaction of the igniting beam with the compressed fuel depends on the type of beam used for this purpose [3].

In our case, jets will be hypersonic and therefore not cohesive. They will be made o very many droplets of sizeable density surrounded by rarefied plasma [4].

The jet droplet interaction with the target will be a complex process with two main competing mechanisms. On one hand, each droplet will be as a macrocluster, and the interaction mechanisms will be the same as those reported before (fragmentation, explosion, and correlated slowing down). On the other hand, each droplet will be as a microjet with a target-piercing capability [5]. In the case of cohesive jets (as those from chemical explosive hollow charges with subsonic velocity), the penetration length would typically be much longer than the range of a cluster o ions initially flying at the same speed. In our case, as in the case of CIF, each jet droplet will penetrate a short length in the target and will produce a little crater before becoming fragmented and stopped [6,7].

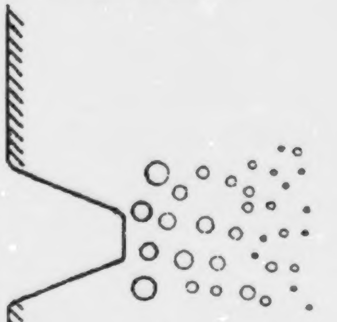

Figure 1. A jet microdroplet interacts with a compressed target by making a microscopic crater. The subsequent droplet fragments will penetrate a short distance (in a similar way as molecular clusters).

A qualitative description of the interaction of a microdroplet with a target is depicted in Fig.1. The droplet penetrates a distance l_p before becoming fragmented and ionized, because of the plastic deformation of the target material. Afterward, the fragments undergo Coulomb explosions and additional fragmentation until they arrive at the equilibrium ionization [6,7] which is governed by rate equations among charge states. Both the ionized microparticles and the final individual ions will be slow down by the plasma components. The stopping power by electrons will be dominant both for cold matter and regular plasmas. For very hot plasma ($T_e > 40$ keV), the ion contribution will become dominant [8,9].

The penetration length of a droplet can be calculated with the same energy and momentum conservation equations used to calculate the penetration of cohesive jets, but in our case, the jet length will be very short because it is equal to the droplet diameter (in a first approach).

If the jet droplet diameter is called l_j and the penetration length is called l_p, a Bernouilli equation can be established in the penetration front, in a frame of reference moving with that point. If the pressure terms are neglected (because of the very high speed of the jet), we can write

$$\rho_j w_j^2 = \rho_t w_t^2 \tag{1}$$

where
j = jet (or droplet)
t = target
w_j = jet speed in this frame of reference
w_t = target speed.

Of course, if v_0 is the penetration speed in the laboratory frame, we have

$$w_t = -v_0 \tag{2}$$

and

$$w_j = v_j - v_0 \tag{3}$$

The penetration length will be the penetration time t_p times the penetration speed [5, 10].

$$l_p = \tau_p w_t = l_j(\rho_j / \rho_t)^{1/2} \tag{4}$$

In the case of $\rho_j = \rho_t$, the penetration length is equal to the jet droplet diameter, and in the case of compressed targets ($\rho_t > \rho_j$), the penetration length becomes very small. From our simulations $\rho_j << \rho_t$ (actually ρ_j/ρ_t may be as samll as 10^{-3} or less). In any case, the penetration length does not depend on the jet speed, which is a surprising effect that was underlined by Birkhoff et al [5] in the first paper on hollow charges after World War II. This surprising effect can be explained because of the fact that the penetration time is inversely proportional to the jet speed, while the penetration speed is directly proportional to it. The penetration length linearly depends on the jet length (or on the droplet diameter for noncohesive jets).

Unfortunately, there is not experimental information good enough to know the spectrum of the droplet size in the collapse of a conical liner in supersonic flow. It seems the jet can be almost atomized [10] in certain cases where hydroinstabilities have a very small scale length. In slightly supersonic cases, a jet with oscillating shape can be formed. Our numerical simulations reported afterwards give also a very distorted shape for the jet.

Note that the energy loss during the penetration phase is very small because the energy required to put the target material aside (–PdV) is very small compared with the droplet kinetic energy [11,12]. This effect is used in armor-piercing hollow charges, where most of the jet energy is lost inside the armored vehicle (by heating the air and internal components to very high temperatures).

In our case, a hot spot can be created by the energy deposition of droplet fragments during the slowingdown phase.

From the data available in the literature and from the physical analysis of the mechanisms governing the stopping process of charged particles, it is obvious that the range of the fragments will be much smaller that the range of the fragments will be much smaller than the range of the fusion-born charged particles which are born individually and uncorrelated [7,13]

The ignitor critical size must be of the order of the range of the fusion-born charged particles unless a huge energy flux comes in from an external source (as the cumulation jet). The power density in the jet/target interaction zone will be

$$\dot{\mathcal{E}}=\frac{\dot{m}v_j^2}{2\mathcal{R}_j} \tag{5}$$

where

$\dot{m}_j$ = mass flow rate (g/cm^2.s

R_j = range (cm), and R_j can be approximately approached by [14]

$$R_j(\mu m) = 8E_n \times 10^{23}/n_e \tag{6}$$

where

n_e= electron density (cm^{-3}) of the target

E_n = energy per nucleon (MeV/amu)

This value is valid for stopping powers dominated by ion/electron interactions in the case of ions moving with correlated speeds. For instance, 1-MeV macroparticles of protons moving in a D-T plasma would have a range of 3.2×10^{-4} g/cm^2. The actual range could still be smaller in highly correlated megacluster fragments. Straggling and skewness of the droplets and their fragments are an additional source of uncertainties in this field. As a matter of fact, they also affect the accuracy of stopping-power data for single (uncorrelated) stiff ions [6]. Although more accurate range values are needed to exactly compute the critical size of a fusion ignitor, current estimates are useful for a qualitative description of the process and to calculate in a first approach the performance of targets ignited by cumulation jets.

In summary, the jet droplet interaction with the target will be governed by two main effects: energy deposition and momentum transfer. The former is given by Eq. (5), and the latter is governed by the direct pressure effect given by Eq. (1) and (3). Reference [14] shows

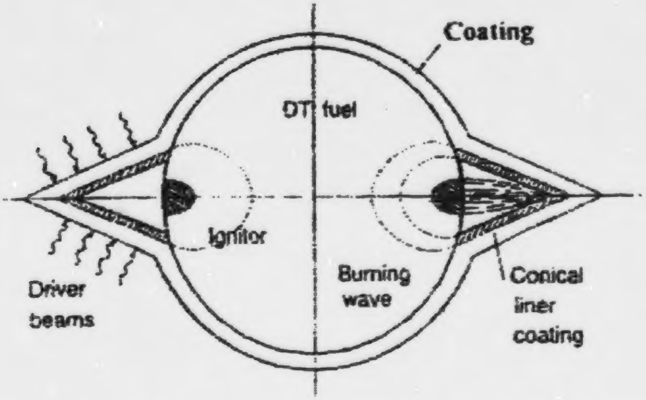
Coating
DT fuel
Ignitor
Driver beams
Burning wave
Conical liner coating

Figure 2. A simple sketch of the igniting jets triggering a fusion burning wave in a target.

that energy deposition will dominate over momentum transfer except in the hammer model case, which is not applicable to this proposal because the jet mass will be much smaller than the target mass.

Energy deposition will produce direct heating of the interaction region and target ablation. Our model needs supersonic heating of the ignitor to launch the heat-detonation wave. This means that ablation will not play an important role in the ignitor performance, unlike in other proposals [15,16] of hypervelocity impact, where target ablation is sought to implode the inner core of the target.

A sketch of a deuterium-tritium target ignited from two conical liners is depicted in Fig. 2. The main problem, as will be seen later on this paragraph, lies in the need of very high density in the main fuel. Hence, driver beams must compress the fuel slightly before the jets are generated in the conical liners. Another approach is to use the same hohlraum to compress the fuel and to generate the jets, as can be seen in Fig. 3.

Requirements to ignite a burn wave with the help of an external source of energy can be expressed as follows:

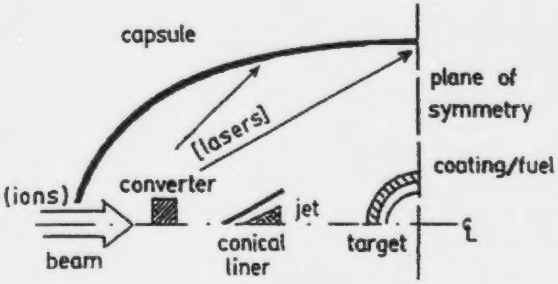
capsule
plane of symmetry
(lasers)
coating/fuel
(ions)
converter
jet
beam
conical liner
target
℄

Figure 3. An indirect-drive hohlraum. Thermal radiation is produced either by laser beams or particle beams. The same field is used for compressing the central target and to generate the igniting jets.

1. The ignitor temperature must be higher than the dynamic ignition temperature (which is slightly above 5 keV for DT)
2. The heating process must be faster than the ignitor disassembly.
3. The energy fluence from the external source heating the ignitor must be about F = 200 MJ/cm^2 or higher (which is the energy needed to heat 0.25g/cm^2 of DT up to 7.5 keV) [9].
4. The cross section of the heating beams must have a radius of the order of the alpha particle range at 5 keV (~0.3 g/cm^2)

   In a first approach we can take with ρ the target density in g/cm^3.

$$S = \pi\left(\frac{\rho R_\alpha}{\rho}\right)^2 = 0.31\rho^{-2}\ ;\ E_j(\mathrm{MJ}) = \mathrm{SF} = 62\rho^{-2} \tag{7}$$

Hence, E_j decreases as density increases. The ignitor volume V_i and mass M_i also depend on the density

$$V_i = SR_\alpha = 0.093\rho^{-3};\ M_i = V_i\rho = 0.093\rho^{-2} \tag{8}$$

The jet mass has to be much smaller than the ignitor mass. If we fix, for instance, $m_j = M_i/10$, we get

$$v_j = \left(\frac{2E_j}{M_i/10}\right)^{1/2} = 3.65\times10^8\ \mathrm{cm/s} \tag{9}$$

This value does not depend on the target density because both E_j and M_i have the same dependence. At this speed, a deutron has a kinetic energy of 140 keV and a triton 210 keV. Their ranges will be smaller than the 3.5 MeV alpha-particle range, which means that electron heat conduction will play an important role in heating the ignitor.

The ignitor heating must be supersonic. Hence, the heating time must be shorter than t_h.

$$t_h = \frac{R_\alpha}{c_s} \cong \frac{R_\alpha}{5\times10^7} = \frac{0.3}{5\times10^7}\rho^{-1} = 6\times10^{-9}\rho^{-1} \tag{10}$$

where c_s is the sound speed in ionized DT (= $3.7\times10^7\,\mathrm{T(keV)}^{1/2}$)

The jet power (E_j/t_h) will then behave as r^{-1}. Of course, higher compressions in the target mean higher ablation pressures, which also mean faster conical collapse.

From the foregoing analysis it is seen that both the ignitor and the igniting beam are defined once the density of the compressed target is given. This fact is described in Table I.

Table 1. Igniting Jets in Isochoric Targets

Density (g/cm^3)	Fuel mass (mg)	Ignitors mass (μg)	Igniting energy (kJ)	Ignition time ps)	Compression energy (kJ)	Fusion Yield (MJ)	Internal Gain
20	1	466	310	300	2.21	20.5	66
20	10	466	310	300	22.1	413	1240
20	100	466	310	300	22.1	7780	14700
200	1	4.66	30	30	10.2	78	5850
200	10	4.66	30	30	102	1320	12600
200	100	4.66	30	30	1020	19500	19100
2000	1	0.046	3	3	47.4	196	4130
2000	10	0.046	3	3	474	2510	5310
2000	100	0.046	3	3	4740	29000	6120

3. JET GENERATION

The collapse of a conical hollow charges is known to generate a jet as a consequence of the energy and matter cumulation effect produced around the cone inner vertex [4,5]. In the case of subsonical collapsing speeds in the frame of reference of the moving vertex, a jet always appear, and a good explanation for this physical phenomenon is given by non-compressible fluid analysis [5]. However, in the planar case of supersonic collapse, compressibility plays a fundamental role in this phenomenon, and an attached shock-wave can appear in such a way that no jet is produced. The attached wave is only possible if the collapsing angle is small. For each supersonic speed, there is a threshold in the angle value above which a jet is always formed. Nevertheless, this is of little help because the jet speed becomes [1,5]

$$v_j = v_p\left(\frac{1}{\tan\alpha} + \frac{1}{\sin\alpha}\right) \tag{11}$$

where v_p is the collapsing speed of the plates (normal to the plates) and α is the half-angel. Hence, when α becomes large, the speed multiplication (v_j/v_p) becomes very small.

A complete theoretical analysis of the supersonic conical case has not been described yet. Some physical hints point out that a jetless case is not possible because it can imply infinite cumulation of mass around the vertex. In fact, a qualitative explanation can be given on the basis of a distortion of the conical half-angle, in such a way that it becomes higher than the original one [10]. A distortion of that type can be explained in terms of a detached shock wave followed by a Prandtl expansion wave. A Mach disc (or stern) could eventually be formed as a sequel of the expansion.

An important point in this extent is the fact that the collapsing matter after the detached shock wave will be very hot and thus the actual vertex collapse will be subsonic and very hot. Jet generation has been studied by computational simulation by means of the ARWEN code [17] and some important conclusions have been drawn from our study. It has been based on the hollow charge scheme given in Fig. 4. In the outer part of the cone, a pressure of 450 Gpa is applied. In the case of a hohlraum, it would correspond to a radiation temperature of 115 eV.

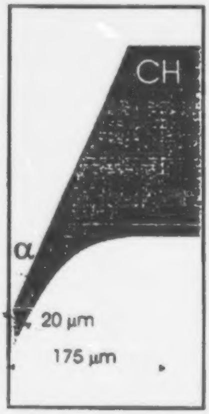

Figure 4. Target geometry of an experiment proposal to study plasma jet generation. It was used in the calculation reported in this paper.

The conical half-angle has been varied from 10° to 40°. In Fig. 5, the evolution of the $\alpha = 27.5\,°$ case is given. At 3 ns the jet is already formed. At 4 ns, it is escaping from the cone basis at a speed of 170 km/s and a density ranging between 0.1 and 5 kg/m^3.

It is worth pointing out that matter speed inside a plastic foil (CH, density $\rho = 1$ g/cm^3) to which a pressure shock of 450 GPa is applied correspond to

$$U_m = \sqrt{\frac{Pa}{1.44\rho}} = 0{,}18\times10^5 \text{ m/s} \tag{12}$$

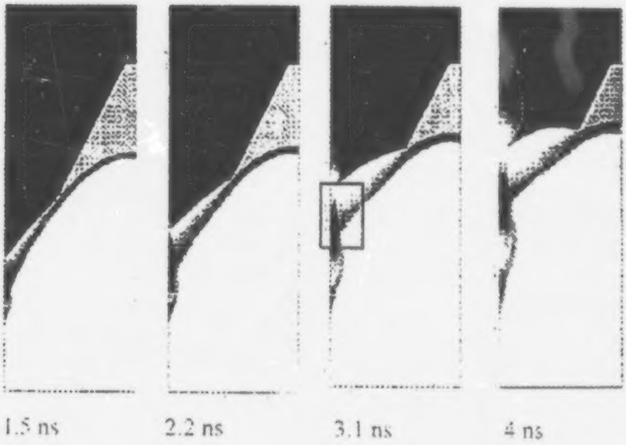

Figure 5. Density contours of the evolution of a case as the one depicted in Fig. 4, with $\alpha = 27.5\,°$. Note the shock-wave in the box area.

When the shock arrives to the opposite border of the plate (a free border with zero pressure) the outermost matter layer escapes at a speed twice as large as the matter speed, i.e., 36 km/s in this case.

For the $\alpha = 27.5°$ cone, the speed multiplication factor would be

$$\left(\frac{1}{\sin\alpha}+\frac{1}{\tan\alpha}\right)=\left(\frac{1}{0.46}+\frac{1}{0.52}\right)=4.1 \tag{13}$$

which is very close to the jet speed over collapsing speed ratio (170/38) = 4.4. In fact, 170 km/s is the speed of the jet at the forefront, where the density is rather small. The bulk of the jet is moving at about 155 km/s.

The main effect of compressibility is not speed reduction but density reduction. In the case reported, the total mass of the jet was about 10^{-9} g. Although this is a very low value, it could be increased by using thicker liners and higher driving pressures.

4. ENERGY GAIN

The total energy gain of this system must take into account the efficiency in

- target compression
- jet generation

A realistic simulation of the whole system is difficult to carry out with the computation tools already available. Compression efficiencies in Direct-drive targets can reach 10%, over the total driver beam energy. In Indirect-drive, efficiencies will be smaller, of a few percent (2 – 3%).

For jet generation there is not yet enough body of evidence as to ease the optimization of the process, i.e., to maximize energy efficiency, provided that the required jet speed is attained.

For the case formerly reported with a half-angle $\alpha = 27.5°$, the efficiency was 0.4%. It must be remembered that it was through conversion of laser beam into thermal radiation inside a hohlraum, and the shape and thickness of the conical liner was not optimized. It is therefore possible to assume a jet generation efficiency of 1%, maybe somewhat higher.

An internal gain (*G*) can be defined more accurately as the total fusion yield (*Y*) divided by the energy contained in the target fuel (*Ec*) plus the energy of the igniting beams.

It must be remembered that the compressed fuel would have to be as cold as possible. A good estimate for E_c would thus be the energy of an Ideal Fermi Fluid.

$$E_c(J)=3\times10^5\rho^{2/3}M_f \tag{14}$$

where M_f must be in (g) and (ρ) in (g/cm^3)

For the igniting beams, we use our former estimates (for two ignitors) $E_i(J) = 2 \times 62 \times 10^6\,\rho^{-2}$. The fusion yield will depend on the burnup fraction f, given by $\rho R_f/(7+\rho R_f)$,

$$Y(J)=3.34\times10^{11}\,M_f\,\frac{\rho R_f}{7+\rho R_f} \tag{15}$$

The internal gain is then defined by

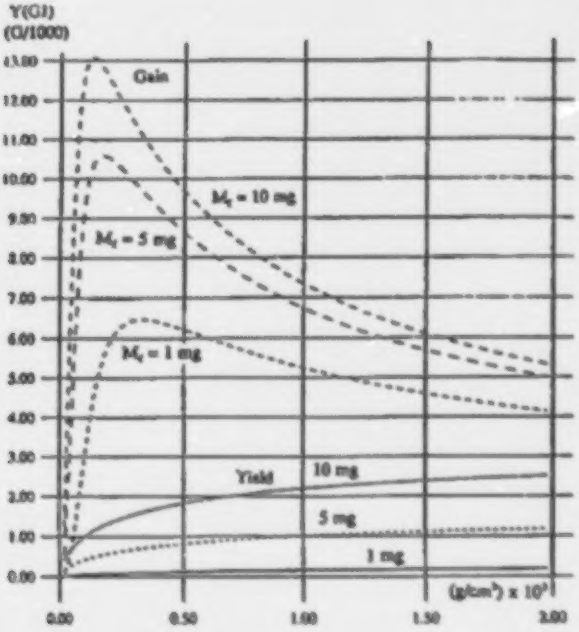

Figure 6. Internal gain (G) and Fusion Yield (Y) of a target, vs. compressed target density at the ignition onset. Curves rorrespond to various DT mass values.

$$G = \frac{Y}{E_c + E_i} \tag{16}$$

and depends on two parameters, ρ and M_f. Of course, the energy terms involved in this case depend at least on ρ(E_i odes not depend on M_f).

Table 1 presents some results of our estimates for a few cases. Figure 6 depicts the dependence of G on ρ and M_f. It is important to note that for very high ρ, $E_c >> E_i$. Then , the limit of G as $\rho \to \infty$ is $G = c\rho^{-2/3}f$.

On the contrary, for small ρ (and not very large mass) $E_i >> E_c$ and thus $G = cM_f\rho^2 f$

It is worth pointing out that for a very large range of parameters G is higher than 10^4. It means that even with a capsule efficiency on only 1%, overall gains of 100 could be achieved.

From Fig. 6, it can be seen that maximum gain is reached for moderate densities (within the framework of Inertial Fusion) namely ~200 g/cm³, which have already been achieved in experiments at ILE of Osaka University (Japan) and LLE of Rochester University (U.S.A.)

5. SUMMARY

A totally new scheme to exploit Nuclear Fusion by Inertial Confinement has been presented. It is based on triggering ignition in a compressed (and relatively cold) target by means of plasma jets impinging on small spots of the target, which act as ignitors of the whole fuel.

The most critical part of this scheme is the generation of plasma jets in the collapse of conical liners. Jet speed must be very high in order to trigger ignition, and this requirement means that the conical collapse will be highly supersonic. Detached shock-waves around the cone vertex will play a very important role in this context, but it seems possible according to our computational simulations- to generate this type of jets. Nevertheless, laser intensities of 10^{16} W/cm^2 will likely be needed instead of 10^{13} W/cm^2, as was assumed in the calculations presented here, aimed at presenting an experimental proposal to C.E. Limeil-Valenton laboratory (CEA-France) where the laser PHEBUS can deliver that intensity for large spots (over 1 mm^2)

The potentiality of this scheme is really high, inspite of the low efficiency of jet generation on the one hand, and cold compression on the other hand. It was seen that the internal gain *G* could be about 10^4. Hence, an overall efficiency of 1% from beam energy conversion to target and jet energy would give a total target gain of 10^2, which is high enough for any Inertial Fusion reactor scenario.

ACKNOWLEDGMENTS

One of the authors (S.E.) is "Iberdrola Chair" Visiting Professor at ETSII, Madrid.

REFERENCES

*"Iberdrola Chair" Visiting Professor, from Soreq National Research Council, Israel
1. J.M. Martinez-Val and M. Piera. Fusion Tech., **32**, 131 (1997).
2. M. Tabak et al. Phys. Plasmas, **1**, 1626 (1994).
3. J.M. Martinez-Val, S. Eliezer, M. Piera and G. Velarde. Phy. Lett. A, **216**, 142 (1996).
4. J.M. Walsh, R.G. Shreffler and F.J. Willig. J. Appl. Phys., **24**, 349 (1953).
5. G. Birkhoff, D.P. MacDougall, E.M. Pugh, and G. Taylor. J. Appl. Phys., **19**, 563 (1948).
6. P. Sigmund and A. Mårmann. Ladr Part. Beams,**13,** 281 (1995).
7. C. Deutsch, Phys. Rev. E, **51**, 335 (1995).
8. Z. Zinamon G. Velarde, Y. Ronen and J.M. Martínez-Val, Eds. Nuclear Fusion by Inertial Confinement, Ch. 5, CRC Press, Boca Ratón, Florida (1993).
9. J.J. Honrubia G. Velarde, Y. Ronen and J.M. Martínez-Val, Eds. Nuclear Fusion by Inertial Confinement, Ch. 9, CRC Press, Boca Ratón, Florida (1993).
10. E. Zababakhin and I. Zababakhin. Unlimited Cumulation Phenomena, Ch. 1, Nauka Publishers, Moscow (1990).
11. E.M. Pugh, R.J. Eichelberger and N. Rostoker. J. Appl. Phys., **23**, 532 (1952).
12. R.J. Eichelberger and E.M. Pugh. J. Appl. Phys., **23,** 537 (1952).
13. C. Deutsch and P. Fromy. Phys. Rev. E, **51**, 632 (1995).
14. S. Eliezer, J.M. Martinez-Val and C. Deutsch. Laser Part. Beams, **13,** 43 (1995).
15. F. Winterberg. J. Plasma Phys, **10**, 55 (1968).
16. F. Winterberg. J. Plasma Phys., **18**, 473 (1977).
17. P.M. Velarde. J. Comput. Phys., **108**, 27 (1993).

NUMERICAL SIMULATION OF ICF EXPERIMENTS AND CONCEPTUAL DESIGNS

Pedro Velarde

Instituto de Fusión Nuclear
ETSII, José Gutiérrez Abascal 2
28006 Madrid, Spain

We present numerical simulations of ICF conceptual design and experiments. Three types of targets are considered:

1. Externally guided targets [1] driven by ion or laser beams, where we show the influence of the border effects and the stability of the implosion foil [2]. We will present the conditions of illumination in order to avoid preheating and assure stability of the foil;
2. Fast jet production in conical hollow-charges driven by X rays. We predict jet speed close to 40 Km/s with cones of 60° aperture with densities much lower than in the incompressible case. Recently, experiments have been conducted in CEL-V Phebus Laser with radiation temperatures between 100 and 130 eV and Au targets with 3 μm thickness with cone angles covering the two main cases.
3. Richtmyer-Meshkov instability experiment proposals driven by X rays. We design the target in order to measure the velocity of fingers in the front side low density plasma. We will present several configurations that could be appropriate for these experiments.

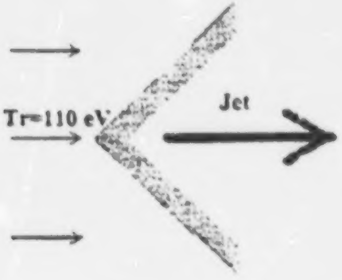

Current Trends in International Fusion Research — Proceedings of the Second Symposium
Edited by E. Panarella. NRC Research Press, National Research Council of Canada, Ottawa, ON K1A 0R6, Canada. 1999.

For these problems we use the code Arwen [2,3,4] developed during the last years at the Institute. Arwen is a Eulerian code with multimaterial capability and multigroup radiation diffusion. Opacities are obtained from SNOP [5] code in LTE and NLTE conditions. The equation of state is obtained from SESAME library or from QEOS [6] program when necessary. The numerical scheme implemented in Arwen use a Riemann solver suited for 2 temperature equation of state (EOS). We pay attention in the thermodynamic data in order to check consistency and to identify regions that could be problematic, for example, with $\frac{\partial^2 P}{\partial v^2}\Big|_s \leq 0$ or very high $\Gamma = \rho c^2/p$.

Radiation diffusion use the improved multifrequency-gray method [7] with flux limited diffusion coefficients.

The cases here presented cover target types that can be numerically simulated by the Arwen code, both reactor size and experimental designs.

REFERENCES

1. J.M. Martinez-Val and M. Piera Fusion Technology **L9**, 134 (1996).
2. P. Velarde et al. to appear in Laser Part. Beams.
3. P. Velarde. J. Comput. Phys. **108**, 27 (1993).
4. P. Velarde et al. Arwen '96, DENIM 402 (1997).
5. K. Eidmann. Laser Part. Beams **12**, 223 (1994).
6. R.M. More et al. Phys. Fluids **31**, 3059 (1988).
7. A.M. Winslow. J. Comput. Phys. **117**, 262 (1995).

PROSPECTS FOR INERTIAL FUSION ENERGY BASED ON A DIODE-PUMPED SOLID-STATE LASER (DPSSL) DRIVER: OVERVIEW AND DEVELOPMENT PATH

Charles D. Orth

Lawrence Livermore National Laboratory
L-472, P. O. Box 808
Livermore, CA 94550-0808, U.S.A.

ABSTRACT

It is now known with certainty that the type of fusion known as inertial fusion will work with sufficient energy input, so inertial fusion is really beyond the "scientific breakeven" point in many respects. The most important question that remains for inertial fusion energy (IFE) is whether this type of fusion can operate with sufficiently low input energy to make it economically feasible for energy production. The constraint for low input energy demands operation near the inertial fusion ignition threshold, and such operation creates enormous challenges to discover a target design that will produce sufficient energy gain. There are also multiple issues relating to the scientific feasibility of using a laboratory-type "driver" to energize a target, such as those concerning bandwidth and beam smoothing for "direct drive," and extension of hohlraum plasma physics to the IFE scale for "indirect drive." One driver that appears as though it will be able to meet the IFE requirements, assuming modest development and sufficient target gain, is a diode-pumped solid-state laser (DPSSL). We give an overview of this type of laser system, and explain what development remains for the economic production of electricity using this type of driver for IFE.

1. INTRODUCTION

With the ever-present demand for electrical power in the modern world, the technical community must prepare a development path for a technology that will be able to meet future energy demands within appropriate cost guidelines. With the ever-declining natural resources of fossil fuels and the increasing environmental impact of burning fossil fuels, the technologies of interest are primarily those having an essentially inexhaustible and environmentally tolerable fuel source–breeder fission reactors, solar power, or fusion. The key questions for any technology development relate to whether the technology provides a practical solution. Such practicality involves acceptable technological risk and sufficiently low environmental impact.

Current Trends in International Fusion Research — Proceedings of the Second Symposium
Edited by E. Panarella. NRC Research Press, National Research Council of Canada, Ottawa, ON K1A 0R6, Canada. 1999.

In this paper, we consider only the fusion technologies. Of these, inertial fusion has already proved itself to be viable, but for input energies much above the amount that would permit economic operation. Although this fact is not well known, the scientific feasibility at such energies has already been demonstrated in underground nuclear tests in Nevada. What remains is to demonstrate that inertial fusion can operate for much smaller input energies, where economic feasibility can be achieved, but where scientific feasibility issues arise in connection with using a laboratory driver.

Because of relatively recent research, an advanced type of driver has emerged that appears to be capable of providing inertial fusion with a practical driver solution. This driver is a diode-pumped solid-state laser, i.e., a DPSSL (pronounced "dip-sol"). In this paper, we explain what inertial fusion is, and provide an overview and development path for a power plant driven by a DPSSL. Such a development path shows that economic feasibility for IFE depends primarily on the achievement of high target gain.

2. WHAT IS FUSION?

Fusion is the nuclear process in which very light nuclei like hydrogen are combined ("fused") to make a slightly heavier nucleus such as helium. Fission, in contrast, is the nuclear process in which very heavy nuclei like uranium are broken up through radioactivity. Both fusion and fission release energy through the well-known Einstein equation $E = mc^2$, because the combined mass of the products is less than the sum of the masses of the starting nuclei–hence, mass has been converted into energy. One difference between fusion and fission is that fusion releases about four times more energy per unit mass, so fusion is preferred from an energetics standpoint. Fusion also involves less radioactivity because, unlike fission, the process itself is not inherently radioactive, and any induced radioactivity (e.g., from neutron emissions activating nearby structures) can be kept to a minimum by the use of non-activating materials. Fusion is also not subject to explosion (as at Chernobyl). Fusion is also not subject to the "China syndrome" (where the uranium fission fuel can melt down through its containment if emergency cooling fails); no China syndrome is possible for fusion because only light elements are used, so the fuel heat content is very low. Fusion thus offers many advantages over fission.

The drawback for fusion has been the difficulty in developing the technology. In order for fusion to occur, the temperature of the constituents must be raised to about 100 million degrees K. At this temperature, the fusion material cannot be contained by ordinary mechanical vessels (which would melt), but must be confined either magnetically or inertially. The length of time that the fuel must be confined depends on the density to which the constituents are compressed, because the reaction rate is proportional to the product of the confinement time and the square of the density. Magnetic confinement involves a low-density gaseous fuel, so it needs seconds or more of confinement; inertial confinement involves densities nearly a thousand times liquid hydrogen densities, so it requires confinement times of 10^{-9} second or less. The different types of fusion are therefore designated by the type of confinement. Fusion occurs in the center of the sun, where gravitation provides the confinement and the high temperatures.

3. WHAT IS INERTIAL FUSION?

For inertial fusion, a capsule is prepared that is essentially a spherical "fuel" shell of hydrogen isotopes surrounded by what is called an ablator (i.e., a layer that can be burned away). Such a capsule is irradiated with beams of energy from a "driver." If the irradiation is directly on the capsule, the type of drive is said to be "direct drive." If the driver beams are focused into a small metallic cylinder (a hohlraum) that heats up and irradiates the capsule with x rays, the type of drive is said to be "indirect drive," and the hohlraum with the capsule mounted inside are said to be the "target."

The driver beams (or the x rays) heat up the surface of the ablator to such an enormous temperature that the surface material blows off radially at great speed. Because for every (momentum) action there is a (momentum) reaction, the blow off causes an inward compression (implosion) of the capsule. As the capsule implodes, the density and temperature at its center increase to the point at which the fusion reactions begin (i.e., the fuel "ignites"). At this time, the inward-moving fuel is confined by its own inertia, because the inward-moving fuel tends to continue moving inward. This type of fusion thereby goes by the name inertial confinement fusion (ICF).

As the fusion fuel "burns," the nuclei fuse together and release energy in the form of fast (14-MeV) neutrons, x rays, and particulate kinetic energy (the energy of the moving products). This sudden release of energy stops the implosion, and reverses it to form a miniature explosion.

For a power-plant application, an ICF capsule is about the size of a marble, and its energy release is about 1/4 ton of TNT equivalent. Such explosion sequences are repeated at the rate of about 5 to 10 targets every second. The energy from such explosions is collected as heat in the wall of a spherical fusion chamber that contains the explosions. This heat can be used to operate a power plant with a steam turbine in much the same way as a coal-fired plant. A fusion plant is hence very similar to a regular power plant, except that a fusion plant needs a driver to generate beams of energy to compress the fusion fuel to the required conditions, and a fusion chamber.

It is noteworthy that inertial fusion will work with different fuels, although the type easiest to ignite consists of equal amounts of two isotopes of hydrogen: deuterium (D), whose nuclei contain one proton and one neutron, and tritium (T), whose nuclei contain one proton and two neutrons. Although tritium is somewhat radioactive, and hence DT fuel is somewhat radioactive, the next generation of inertial fusion could use just deuterium (DD). This type of fuel is not radioactive, and can be extracted from sea water at the rate of about 1/15 gram per gallon, which has the releasable energy content of nearly 2 tons of TNT equivalent (i.e., about 8 capsules worth). The vastness of the oceans therefore provides an essentially inexhaustible supply of fusion fuel. The disadvantage of DD fuel is that it is harder to ignite, requiring about 3 times the ignition temperature (and hence a larger power plant to gain economy of scale and preserve economic feasibility, and a different target design).

4. THE ADVANTAGES OF ICF

At this time, ICF has many advantages over magnetically confined fusion (MCF). First, ICF is now known to work with sufficient energy input. Underground experimental tests in Nevada have allowed the demonstration of excellent performance, putting to rest the fundamental questions about the basic feasibility of achieving significantly more energy output than input (i.e., of achieving high gain). Basic scientific feasibility is therefore no longer an issue for ICF, with sufficient energy input.

Second, DT fusion produces fast neutrons whose energy content can be collected and the environment shielded from induced radioactivity only by the introduction of shielding. For ICF, this shielding is minimal because the source of the neutrons is essentially a point (the center of the imploded capsule). The shielding can therefore be placed around the exterior wall of the fusion chamber as a spherical shell, and can even be designed to serve both as shielding and as (or in conjunction with) an absorber of neutron energy for the transfer of heat energy to a heat exchanger. For MCF, however, the source of the neutrons is a large extended source (e.g., the entire doughnut-shaped interior cavity of a tokamak). Consequently, the geometry of the shielding for MCF cannot be a spherical shell, so considerably more shielding is required. Third, because of the low-density nature of the MCF fuel, and the large amount of shielding required, a power plant utilizing MCF is much larger and hence much more expensive than we think a power plant utilizing ICF will be.

Fourth, ICF has greater physical separability between the location of the fusion reactions and the emplacement of the high-technology equipment that energizes the fusion fuel. Fifth, ICF offers a clearer approach to maintenance — continuous beam maintenance may even be feasible by including extra driver beams. Sixth, ICF offers more control, because one driver can feed multiple fusion chambers, and variable repetition rate can be employed. Seventh, ICF has an attractive development path.

5. WHY DON'T WE HAVE AN ICF POWER PLANT NOW?

Before utility companies will become interested in inertial fusion energy (IFE) — that is, to make energy in a power plant based on ICF — we must demonstrate that IFE can be economically feasible. The main problem for IFE (and fusion in general), other than the complex nature of the technology itself, is the great difficulty in designing a power plant that has a low enough construction cost to permit economic feasibility. The reason for this is that an IFE plant includes extra equipment that a fossil-fuel plant does not have. An IFE plant has a driver and a fusion chamber in addition to the thermal (steam-turbine balance-of-plant) equipment that is common to IFE as well as to other types of power plants. Because the fuel costs for IFE should be almost negligible, the combined cost of the driver and the fusion chamber for IFE must be compared with the cost of the boiler in a fossil-fuel plant and the operational cost of securing fossil fuel. Such a comparison indicates that IFE must demonstrate economic feasibility by designing a driver and a fusion chamber that are low enough in cost.

The size, and therefore the cost, of a fusion chamber is dependent primarily on the plant's thermal power, and only weakly dependent on the energy that the driver beams must focus on the target. In contrast, the cost of the driver is highly dependent on the delivered energy. Thus, for a given size of power plant, the economic competitiveness of IFE depends on whether the technology will function reliably at a driver energy that is low enough to permit the cost of the driver to be minimal. The amount of driver energy required is in turn determined by the target gain (i.e., the ratio of the energy produced by the target and the energy delivered to the target by the driver beams). One key to the economic feasibility of IFE is therefore the ability to operate ICF as close to its ignition threshold as is possible and still maintain reliability. Such operation introduces technology constraints on finding the target design that will produce a high-enough energy gain (>100) to allow a small-enough driver (1 to 2 megajoules).

The lack of sufficient target gain has made another issue become a key to the economic feasibility of IFE. This secondary key is the scientific feasibility of using a laboratory driver to energize an available type of target. Targets requiring more energy require a larger driver, which is more difficult to develop because of the technological constraints in generating more energy in temporally shaped spatially smooth beams and in delivering this energy efficiently to a target. Because the most reliable target designs deliver calculated gains significantly less than 100 for small driver energies, a larger (~2 megajoule) driver had to be developed. It is the difficulties with the technological challenges dealing with target gain and the feasibility of the required driver that have constrained the early development of IFE.

6. DIFFERENT ICF DRIVER OPTIONS AND ISSUES

The pursuit to find an inexpensive driver has focused primarily on a heavy-ion accelerator that will deliver beams of fast-moving heavy ions (e.g., lead ions). The interest in such machines arises from their high efficiency (about 35%) when used for high-energy physics research, because an efficiency of ≥10% is thought to be needed for economic feasibility for IFE. Considerable research effort has therefore been directed to try to discover by how much (if any) the efficiency will be degraded in generating, transporting, and focusing a high-current heavy-ion beam on a target. So far, although positive results are expected, it is not known whether the potential problems associated with the accelerator plasma effects and target space-charge effects will be resolved. Uncertainty arises primarily because of the lack of development — no machines have been built that deliver the applicable beam intensities, energies, and pulse widths, and no one has directed such driver beams onto a target. There are also research efforts for KrF lasers and light-ion accelerators, but these efforts today suffer from uncertainties arising from technologies that are even less developed. KrF systems have many development problems (optics damage, etc.) associated with producing a high-power beam on target, and with the short lifetime of some of its components. Light-ion technologies are only in their infancy. Thus, these other technologies may eventually prove fruitful, and progress is being made, but it is too early to know with certainty whether conceptual solutions to all of the problems will be found.

Research conducted at the Lawrence Livermore National Laboratory (LLNL) over the past several years (see below) enabled us to conduct a full systems analysis of an IFE power plant based on a different type of driver — a diode-pumped solid-state laser (DPSSL) [1]. This study includes the essential concepts for irradiating a target with driver beams, and is hence a comprehensive systems study. Such a study was possible because of the significant commonality that DPSSLs have with the flashlamp-pumped solid-state lasers (SSLs) currently being employed in ICF research. We expect that added understanding will come through research on the National Ignition Facility (NIF) now under construction at LLNL. We are therefore concerned in this paper with a DPSSL driver.

Nevertheless, our systems study identified many issues that must be addressed for DPSSLs (particularly target gain — see below), so research at LLNL is being pursued on both heavy ion beams coupled to indirect-drive targets and DPSSLs for either direct or indirect-drive targets. This dual track approach is justified by the present uncertainties in (1) the target performance that will eventually be achievable, and (2) the driver technology development. Assuming that suitable high-gain targets can be developed, we believe that our study indicates that the DPSSL technology will be suitable for the IFE mission.

Recall that the word "laser" is an acronym meaning Light Amplification by Stimulated Emission of Radiation. A laser thus works by having a "gain medium" with a special dopant that can be energized up to an excited state by a light source such as a flashlamp (which is similar in concept to the strobe light used to time automobile engines). The gain medium can then be stimulated to release its energy by the passage of a light pulse whose photon energy matches the energy difference between the excited state and the ground state in the gain medium. Such stimulation adds energy to the light pulse, and thus provides amplification.

Our DPSSL driver is similar to the flashlamp-pumped lasers currently being operated at the University of Rochester (the Omega laser) and at LLNL (the Nova laser), where laser beams have imploded capsules. The only significant exceptions are that our DPSSL uses crystals as the gain medium instead of the usual neodymium-doped glass (Nd:glass), and it uses light-emitting laser diodes instead of flashlamps to pump the gain medium. These substitutions are needed for the rep-ratable operation required for an IFE driver.

The importance of the similarity of a DPSSL to an ordinary SSL is far-reaching. Because a DPSSL is related to existing SSLs in terms of its basic architecture and optical components (other than the gain medium and pumping optics), the experimental success for a DPSSL can draw from the significant experimental base already established with existing SSLs. This means that, in essence, target physics and laser operation have already been investigated to a considerable degree for a DPSSL.

7. ADVANCES MADE SINCE THE 1ST SYMPOSIUM IN NOVEMBER 1994

Significant advances have been made over the past several years in both laser design and target-physics design. The research advances at LLNL that have permitted the DPSSL to achieve credence as a potential IFE driver are the following.

1. The development of a novel laser gain medium with better thermo-mechanical properties, Yb^{3+}-doped $Sr_5(PO_4)_3F$ [called Yb:S-FAP], whose ≥ 1.10-ms storage lifetime is at least four times longer than the 0.3-ms lifetime for Nd:glass, thereby reducing the diode pump array expenditure by roughly a factor of 4.
2. The manufacture of efficient laser diode pump sources to pump the new gain medium up to its excited state, so that laser operation at efficiencies of $\geq 10\%$ are possible (instead of the $\leq 1\%$ attainable now with Nd:glass). Such laser diode manufacturing techniques make it feasible to eventually scale to acceptably low manufacturing costs at power-plant-level production volumes.
3. The conceptualization of fused-silica final laser optics heated to temperatures of 400°C or more to continuously anneal out the structural defects and optical discoloration induced by neutron interactions, thereby circumventing the low-lifetime constraint on the use of these optics in environments with high neutron fluences which would otherwise quickly turn the optics opaque. (This solution works for a DPSSL, but not for KrF wavelengths.)
4. The development of a large-aperture gas-cooled Pockels cell that permits the realization of a compact multi-pass amplifier architecture by serving as an optical switch to switch a beam out of a multi-pass amplifier cavity.
5. The calculational and experimental validation of gas-cooling techniques to cool the gain medium crystals, thereby showing that the thermally induced optical distortions in the gain medium can be reduced to a simple beam-steering effect, while removing the waste heat.
6. The experimental operation at LLNL of a 2 joule DPSSL prototype with a single $2\times2\times0.5$-cm Yb:S-FAP crystal with helium gas cooling operated with a 1-ms diode pump pulse in a free-running long-pulse (1-ms) mode that verified the basic thermal operation of this type of DPSSL. These experiments [2] demonstrated an intrinsic laser slope efficiency of 67% (theoretical limit is 86%), 25-Hz operation (more than twice that needed for IFE), and facial thermal fluxes several times that needed for 10-Hz IFE operation.

These research results provide potential solutions to all of the issues previously thought to preclude the use of a solid-state laser driver for IFE. The Mercury Project at LLNL, to be described below, will demonstrate the short-pulse extraction and rep-ratability of a DPSSL at 100 joules output. Thus, a DPSSL is well on its way to the actual experimental demonstration of the capabilities required for an IFE driver. Nevertheless, the price of laser diodes to pump the DPSSL gain medium is currently a factor of about 100 too high to permit economic feasibility at the target gain expected for an IFE target. Consequently, there is a need to promote the manufacture of lower-price diodes, and a need to encourage the development of higher-gain targets. On the other hand, we believe that the semiconductor industry will be able to adequately respond to the IFE cost goals for laser diodes, given the existence of a large-enough market, because the price of diodes is falling in the same way that was observed for the cost of semiconductor integrated circuits. As a result, most of the burden for economic feasibility of IFE may fall on the need for higher-gain targets.

The research advances over the past several years that have permitted enhanced credence in our ability to design ICF targets are the following.

1. Experimental demonstration, primarily at LLNL's Nova laser, of our ability to control laser-plasma instabilities (e.g., stimulated Raman scattering and stimulated Brillouin scattering), hohlraum energetics, capsule symmetry, and capsule hydrodynamic instabilities for targets that were operated at tens of kilojoules of blue laser light, but considered to be hydrodynamic equivalents to those at IFE scale.
2. Enhanced experimental validation of Lagrangian and quasi-Eulerian modeling codes used to simulate laser-hohlraum drive, symmetry, and capsule implosions, thereby improving the credence in the modeling predictions for targets at NIF and IFE scales.
3. Demonstrated understanding on Nova of implosions of capsules having high NIF-like convergence ratios (i.e., capsules that implode to a small fraction of their initial radius).
4. Demonstrated understanding on Nova of hydrodynamic (Rayleigh-Taylor) instabilities in quantitative agreement with numerical modeling for planar foils and deliberately perturbed 3D capsule surfaces.
5. The theoretical introduction of a "fast ignitor" target that may be capable of gains well above 100. Such a target employs standard capsule compression, but then the use of a 100-picosecond 10^{18} W/cm^2 laser pulse to "channel" through to the fuel core, and a 5-picosecond 10^{20} W/cm^2 laser pulse to ignite the fuel through the channel.

Although much progress has been made, more development is of course required.

8. NEAR-TERM DEVELOPMENT – THE MERCURY PROJECT

Extension of the current research base to an IFE application requires development in both target physics and DPSSL technologies. Although our IFE design for a DPSSL [see ref. 1] is based rather extensively on the mature experimental technologies for solid-state lasers, the data do not always pertain to the realm of interest for IFE. The same is true for targets. The key issues remaining at this time therefore relate to the extension of this experimental base to the relevant realm, and for a DPSSL, to the particular use of the Yb:S-FAP gain medium. These issues can be addressed and the risk for a DPSSL driver can be reduced through a development path that begins with small-scale experiments in the near term, and then expands greatly with the startup of the National Ignition Facility (NIF).

For the near term, Mercury is a three to four-year project at LLNL to design (FY97), build (FY98–FY99), and operate (FY99–FY00) a 100-joule 10-Hz 1-ns DPSSL that will demonstrate efficient rep-rated short-pulse extraction. Mercury will also demonstrate compatibility with scaling to >1 kilojoule in future single-beam systems, and eventually to IFE systems at the megajoule scale. The goals include an overall electrical efficiency of ≥10%, a final focus less than 5 times the size for a diffraction-limited beam, and pulse lengths of 1 to 10 ns. What this means is that the Mercury laser will demonstrate the utility of a DPSSL as an IFE power plant driver in many respects, but not in total energy output — it will demonstrate the relevant pulse duration, the needed laser efficiency, and the required thermal management at a repetition rate of 10 times every second. It will also address the issues relating to the fabrication of large diode arrays.

It is important to note that the efficiency of interest for an IFE driver is the total efficiency in driving a target, which should be ≥10% (actually, it is the product of the efficiency and the target gain that should be roughly ≥10). This means that the efficiency must include the efficiency factor for the coupling of the beam energy to the fusion target. Such a factor, which depends on the quality and lateral spread of the beams at the target, is about 90% for a DPSSL, based on experiments at Nova and at other laser facilities.

9. INTERMEDIATE-TERM DEVELOPMENT: THE ROLE OF THE NATIONAL IGNITION FACILITY (NIF)

The NIF is a single-shot 192-beam facility under construction at LLNL to demonstrate that a driver with ≤1.8 megajoules can ignite a capsule and provide moderate target gains of 1 to 10. (The NIF also has missions relating to stockpile stewardship for thermonuclear weapons.) This facility is expected to come on line in the year 2002, and continue operation for one or two decades. Although the NIF will be implemented with Nd:glass lasers, the results for both the target physics and laser multi-pass architecture will apply directly for a DPSSL-driven IFE plant.

The NIF is expected to be a pivotal facility for ICF research, because one of its missions is to demonstrate ignition and propagating burn in the laboratory. Its most significant accomplishment relating to IFE is expected to be the determination of the exact ICF ignition threshold for each major type of ICF target, and hence the operating point for reliable IFE operation. Next in importance for IFE should be the insight relevant for the design of an IFE target with a gain ≥100. Research on the NIF is expected to provide the needed understanding for such things as the precise requirements for shaping each laser pulse in time, how spatially smooth each laser beam must be (i.e., the required bandwidth), whether direct or indirect drive is better, and complete understanding of the relevant plasma instabilities inherent in the coupling of the laser energy into a hohlraum and generating x-rays to implode a capsule in a stable manner.

To be certain that DPSSL gain-medium crystals can be grown to large enough sizes for IFE applications, and to test the operation and thermal management of rep-ratable DPSSLs at the kilojoule scale needed for IFE, a sequence of single-beam intermediate-term DPSSL prototype facilities is being considered as one option: Venus offering about one kilojoule, Terra offering 10 to 30 kilojoules, and (eventually) Helios being a rep-rated producer of net electrical power. These facilities could be operated in parallel with the operation of the NIF, whose single-beam energy is about 10 kilojoules.

Note that only single-beam facilities are required for most DPSSL development activities because a DPSSL system is entirely modular. DPSSL functionality can therefore be validated at the component level or at the single-beam level, thus permitting experimental verification at reduced development cost. In addition, many of the novel laser-diode technologies envisioned for an IFE driver are relevant to a variety of scientific, industrial, and military applications and will therefore continue to advance in parallel with ICF developmental efforts.

10. FUTURE DEVELOPMENT PATH: WHAT ARE THE REMAINING ISSUES?

After the NIF and the DPSSL developmental facilities have been operated, the fusion community needs to construct a complete engineering demonstration facility (EDF) to test the engineering issues for IFE, and to prove the effectiveness of fabricating and delivering targets at the rate of roughly 10 targets every second to be tracked and then illuminated with DPSSL beams at the center of the fusion chamber. There are also issues connected with the lifetime of the first wall of the fusion chamber that could involve significant engineering problems, as well as issues pertaining to the clearing of plasma debris from one explosion prior to the next shot 100 ms later. There are also significant issues relating to the final optics that would be exposed to neutron (as well as x-ray and plasma-debris) emissions.

One particularly important issue concerns whether DPSSL optics can withstand the 10^{10} pulses expected during the 30-year lifetime of an IFE plant, even if the potential problems regarding neutron and x-ray damage can be completely solved. Even though a DPSSL operates at fluences only a factor of about 4 higher than off-the-shelf lasers capable of $>10^8$ pulses, more data are needed to convince us that a DPSSL can operate without damage at the IFE conditions identified in our systems study (e.g., a peak fluence of ~20 J/cm^2 at ~9 ns effective square pulse duration at a wavelength of 349 nm for the final optic).

There are also issues relating to the design of a fusion chamber that can accommodate a laser driver. Laser beams are usually expected to enter a fusion chamber at large cone angles, instead of in two opposing small-angle clusters, but such a beam configuration is not thought to be compatible with liquid first wall designs that permit a high plant availability fraction. This issue, however, is directly associated with the amount of target gain — if sufficient target gain is achieved, narrow cone angles can be used and the issue becomes inconsequential. This is one more argument that emphasizes the need for higher-gain target designs. Other issues that must be resolved concern target injection (and the associated beam-alignment tolerances), and pulsed-neutron damage to materials.

11. CONCLUSIONS

The interest in a DPSSL as an IFE driver is growing steadily. ICF is now *known* to work at sufficient energy input. Scientific feasibility for IFE would therefore seem to be assured in many respects, with the main issue being primarily economic feasibility. Unfortunately, all of the known designs for reliable targets require so much driver energy that such economic feasibility has become an issue of scientific feasibility both for the targets and for the ability of the driver to supply the appropriate beams to the targets. In particular, the economic demand for small driver energies forces IFE to operate just above the ignition threshold, whereas target gain there is insufficient even for driver energies above one megajoule. The larger driver energy introduces technological constraints in generating more energy in temporally shaped spatially smooth beams and in delivering this energy efficiently to a target. Great effort must therefore be expended to improve target gain for near-threshold implosions and to understand these technological constraints of a laboratory driver. The NIF is meant to provide most of the answers to the remaining questions relating to this current challenge for laboratory IFE research efforts.

Meanwhile, the DPSSL has emerged as a candidate driver that appears as though it will be able to meet the IFE mission requirements, given modest future development and suitable target gains. With the research advances over the past several years at LLNL, we now know that a DPSSL need not be subject to the major issues thought to restrict the use of a solid-state laser as an IFE driver. The main inhibiting factor for the use of a DPSSL today is the high price of the laser pump diodes, but that is expected to drop as the market for laser diodes expands. Consequently, the only known potential problems for the use of a DPSSL as an IFE driver are (1) the development of targets that have sufficient gain to offset both a target operation near ICF ignition threshold and the reduced-cone-angle beam illumination suitable for wetted-wall fusion chambers, and (2) the development of good solutions for final optics protection. In other respects, DPSSL technology relies on the mature solid-state laser experimental base derived from two decades of experience. DPSSL technology is also a natural extension of the NIF towards IFE applications. There remains, of course, the demonstration that DPSSL technology will work at the IFE scale, but the related questions are not at the conceptual level. In addition, the Mercury Project is poised to demonstrate the rep-ratable short-pulse-extraction characteristics of the Yb:S-FAP gain medium for a 100-joule output, as well as gas-cooling and fabrication of large laser diode arrays. It would therefore appear that DPSSLs are indeed a viable candidate for an IFE driver.

ACKNOWLEDGMENTS

We acknowledge that the Mercury Project is being researched by a team of colleagues at LLNL that includes R. Beach, C. Bibeau, M. Emanuel, E. Honea, K. Schaffers, J. Skidmore, S. Sutton, and the Project Leader, C. Marshall, all under the supervision and leadership of S. Payne, H. Powell, and W. Krupke. This research is being performed under the auspices of the US DOE by LLNL under contract number W-7405-Eng-48.

REFERENCES

1. C.D. Orth, S.A. Payne, and W. F. Krupke. Nuclear Fusion **36**, 75 (1996).
2. C.D. Marshall, L.K. Smith, S. Sutton, M.A. Emanuel, K.I. Schaffers, S. Mills, S.A. Payne, W.F. Krupke, B.H.T. Chai. Diode-pumped gas-cooled-slab laser performance. OSA Trends in Optics and Photonics on ADVANCED SOLID STATE LASERS, ed. S.A. Payne and C.R. Pollock, **1** (1996) pp. 208-212.

STATUS OF DIRECT-DRIVE INERTIAL CONFINEMENT FUSION RESEARCH AT THE LABORATORY FOR LASER ENERGETICS

Robert L. McCrory, and John M. Soures

University of Rochester
Laboratory for Laser Energetics
250 East River Road
Rochester, NY 14623, U.S.A.

ABSTRACT

A major role of the University of Rochester's Laboratory for Laser Energetics (LLE) in the U.S.A. Inertial Fusion Program is to explore the direct-drive approach to inertial confinement fusion. In this paper, details of LLE's Inertial Confinement Program (ICF) are presented with major emphasis in the role of the laboratory to the National Ignition Facility (NIF) program.

1. INTRODUCTION

The U.S.A. Inertial Confinement Fusion program is a dual-mission program that has as its near-term goal to support the U.S. stockpile stewardship program. A longer-term objective of the ICF program is to demonstrate the scientific and engineering feasibility of inertial fusion energy production. Key to both of these objectives is the demonstration of ignition and burn; this achievement is the mission of the 1.8 MJ National Ignition Facility — currently in the detailed design and construction stage. The NIF is a partnership among Lawrence Livermore National Laboratory (LLNL), Los Alamos National Laboratory (LANL), Sandia National Laboratory, and the LLE.

Success of the NIF mission is critically dependent on several physics experiments and technology development efforts currently underway in the U.S. ICF laboratories. Significant progress was made over the last decade in the validation of inertial fusion using laser drivers (Fig. 1). The specific accomplishments include:

- Success of the NOVA hohlraum-driven target experiments; the NOVA technical contract achieved most of its objectives [1].
- Cryogenic-capsule direct-drive experiments demonstrated 200 times liquid-DT density on the OMEGA facility at an energy of 1500–2000 J [2].

Current Trends in International Fusion Research — Proceedings of the Second Symposium
Edited by E. Panarella. NRC Research Press, National Research Council of Canada, Ottawa, ON K1A 0R6, Canada. 1999.

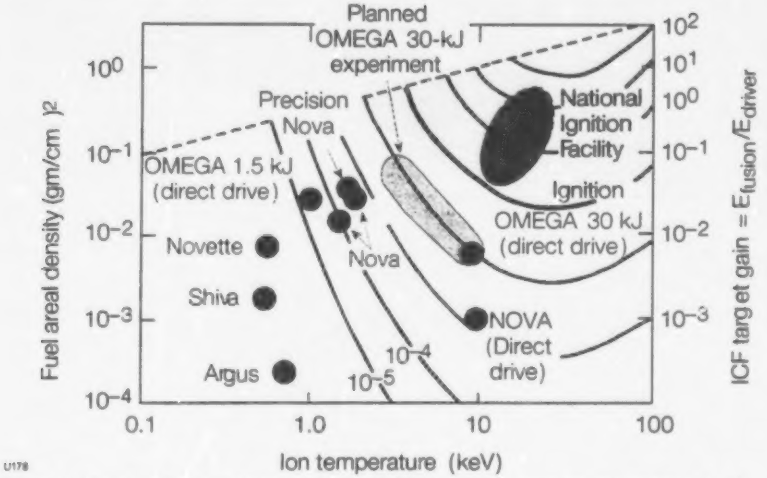

Figure 1. Inertial confinement fusion experiments show steady progress toward ignition and gain. Shown on this graph are the fuel areal density and temperature achieved in experiments to date on laser facilities and the projected performance of the NIF.

- Beam-smoothing techniques were developed and implemented on the glass laser system that have the potential for achieving the irradiation uniformity requirements for high-performance capsules [3].
- Advanced capsule diagnostic techniques were developed and implemented and are now used to make precision measurements of compressed capsule fuel core conditions [4].
- Thermonuclear yield in excess of 1% of the laser energy on target was achieved on OMEGA at 30,000 J of UV energy on target [5].
- Laser science and technology advanced sufficiently to initiate design and construction of the NIF.
- Target fabrication and characterization techniques have made rapid progress toward meeting the requirements for ignition capsules.
- Capsule modeling with advanced computer codes is making remarkable progress in predicting capsule performance.

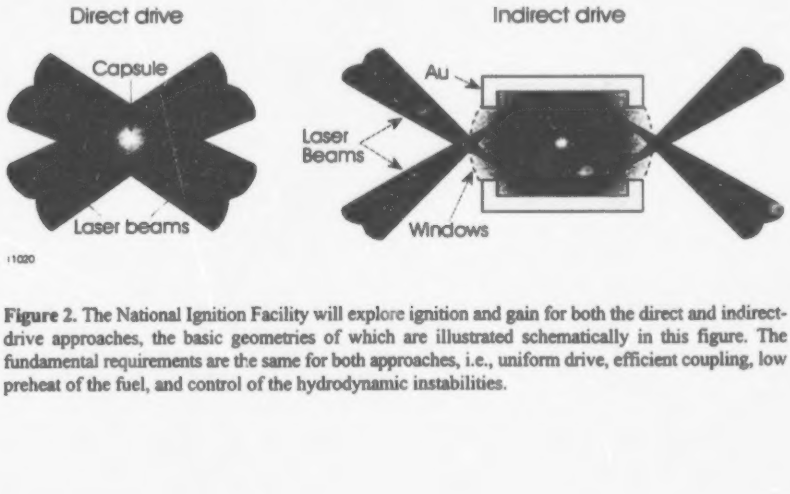

Figure 2. The National Ignition Facility will explore ignition and gain for both the direct and indirect-drive approaches, the basic geometries of which are illustrated schematically in this figure. The fundamental requirements are the same for both approaches, i.e., uniform drive, efficient coupling, low preheat of the fuel, and control of the hydrodynamic instabilities.

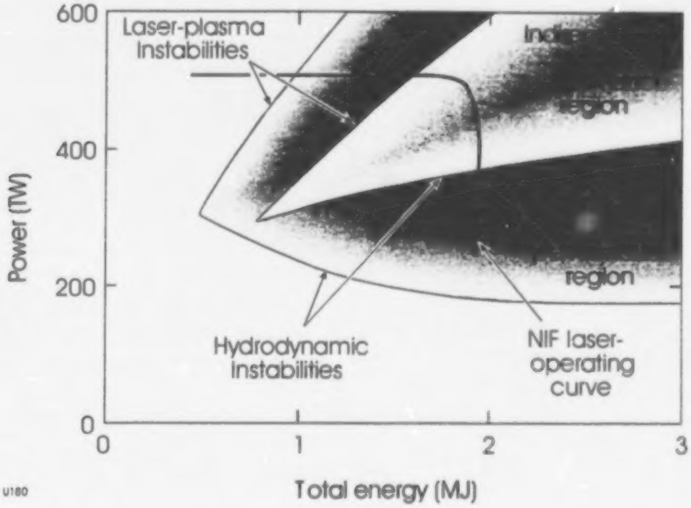

Figure 3. Direct-drive has a larger accessible ignition region with NIF than indirect drive.

In this paper, we briefly discuss some of these ICF program accomplishments as they relate to the NIF project.

The steady progress made toward ignition and gain is illustrated in Fig. 1. With the start of the NIF project, a facility is now in design and the early stages of construction that has a high probability of demonstrating ignition and modest gain. Two approaches are being explored to achieve the NIF objectives: indirect drive (the primary approach) and direct drive. These approaches are illustrated schematically in Fig. 2. The primary advantage of indirect drive is that it may be easier to attain a high degree of drive uniformity with this approach compared to direct drive. On the other hand, indirect drive does not couple energy as efficiently to the capsule as direct drive and may lead to higher levels of nonlinear scattering instabilities such as Raman scattering. These instabilities can cause significant loss of laser energy and may also lead to the production of high levels of high-energy electrons that can preheat the fuel.

Theoretical modeling of both direct and indirect-drive capsules lead to the conclusion that direct drive offers the potential for higher gains on the NIF than indirect-drive targets. Figure 3 illustrates the accessible ignition region expected with direct as well as indirect-drive targets on NIF. The margin for ignition and gain is significantly greater for direct drive than for indirect drive. The main issue for both approaches is control of hydrodynamic instabilities.

2. DRIVE UNIFORMITY

The principal physics issue for direct drive is drive uniformity. Perturbations at the ablation surface arising from nonuniformities in the drive (or capsule imperfections) can act as sources for growth due to hydrodynamic instabilities. If the source magnitude and/or the growth rate are high enough, the hydrodynamic instability can disrupt the capsule implosion and lead to failure of the capsule to reach ignition conditions. Specifically, there are four

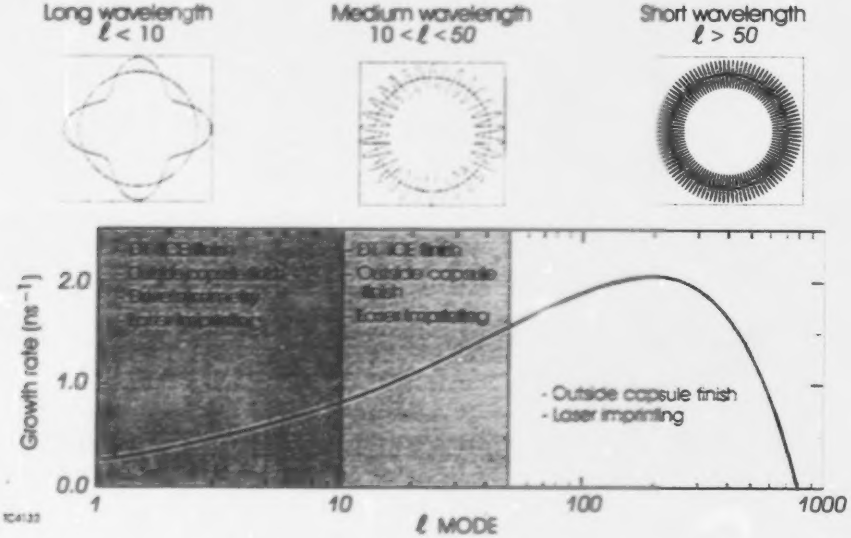

Figure 4. The effect on capsule performance of the four sources of perturbations is influenced by the perturbation wavelength. Shown in this figure is the perturbation growth rate as a function of the perturbation ℓ mode. Short-wavelength modes (high-frequency, large-ℓ modes) arise from imperfections in the outside capsule finish and from laser imprinting. Long-wavelength perturbations (low-frequency, small ℓ's) arise from drive symmetry, laser imprinting, outside capsule finish, and the DT-ice finish on the inside of the capsule.

sources of perturbations a capsule must be able to tolerate in order to reach ignition and burn conditions:

- perturbations in the DT-ice surface (on the inside of the capsule),
- defects in the outside capsule finish,
- irradiation variations due to the drive symmetry, and
- pressure variation due to laser imprinting.

The wavelength and amplitude of these perturbations (see Fig. 4) determine their effect on capsule performance. During the next five years, the experiments required to validate high-performance, direct-drive capsules will be conducted on the OMEGA laser at LLE. The elements of this experimental campaign include (a) laser experiments including development and testing of beam-smoothing techniques, development of power balance control and measurements capability, and high-dynamic-range pulse shaping; (b) capsule physics experiments including absorption and energy transport, long-scale-length plasma physics experiments, hydrodynamics instability experiments, symmetry control and requirements, integrated surrogate cryogenic capsule-implosion experiments; and (c) integrated cryogenic capsule-implosion experiments.

3. BEAM SMOOTHING

The development and testing of beam-smoothing techniques is one of the major aspects of the LLE program. In 1988, LLE developed and patented a unique beam smoothing technique for frequency-converted, solid-state lasers — smoothing by spectral dispersion (SSD). In its original manifestation, SSD was a means of introducing a controlled bandwidth

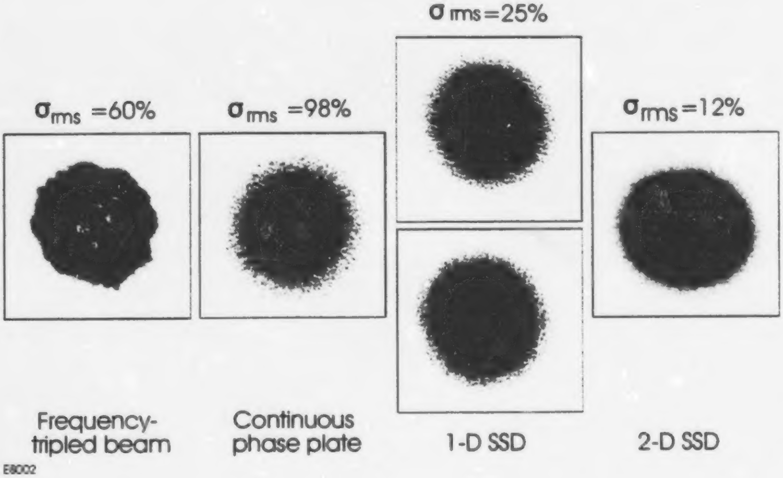

Figure 5. An illustration of the effect of (SSD) on beam uniformity from the OMEGA laser. The typical beam pattern of a high-power UV beam is shown on the left. By using distributed phase plates, it is possible to symmetrize the beam pattern on target as shown in the second photograph from the left. Some of the high-frequency speckle pattern is reduced when 1-D (SSD) is used (third photo from left). By using full, 2-D (SSD), the high-frequency speckle is significantly reduced.

in the laser beam and then dispersing the spectrum spatially using gratings. The resulting beam was propagated through the laser system and frequency converted. The wavelength dispersion was adjusted to partially compensate for the wavelength mismatch at the frequency-conversion crystal. When the resulting beam was passed through a phase converter (in the form of a distributed phase plate or its equivalent) and the beam focused onto a target, the amplitude modulation due to the high-frequency speckle pattern was ameliorated (Fig. 5).

2-D SSD has been implemented on the OMEGA 60–beam, 40 kJ laser at LLE. Continued improvements of SSD and the implementation of distributed polarization rotators are expected to produce the required level of uniformity on OMEGA to validate the performance of direct-drive capsules prior to the implementation of direct drive on the NIF.

4. OMEGA EXPERIMENTS

The experimental program on OMEGA is focused on the direct-drive program. To support the program elements mentioned in the second section, a variety of capsule diagnostics are required. During the last three years, a full suite of ICF plasma diagnostics has been implemented on the OMEGA facility. The placement of some of these diagnostics in the OMEGA target chamber is shown in Fig. 6.

The diagnostics complement currently installed on OMEGA includes x-ray, nuclear, optical, and charged-particle detector systems. The x-ray diagnostics include time-integrated as well as time-gated (using 40 ps gated cameras) x-ray pinhole cameras and x-ray microscopes, time-integrated and time-resolved (with streak cameras) x-ray spectroscopy, and x-ray calorimeter systems.

Nuclear diagnostics include several neutron-counting instruments including Cu activation, In activation, scintillators with photomultiplier tubes for neutron time-of-flight

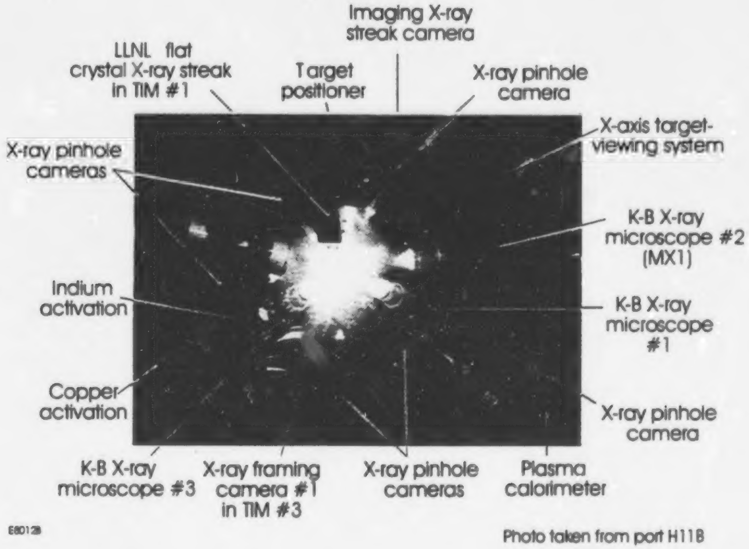
Imaging X-ray streak camera
LLNL flat crystal X-ray streak in TIM #1
Target positioner
X-ray pinhole camera
X-axis target-viewing system
X-ray pinhole cameras
K-B X-ray microscope #2 (MX1)
Indium activation
K-B X-ray microscope #1
Copper activation
X-ray pinhole camera
K-B X-ray microscope #3
X-ray framing camera #1 in TIM #3
X-ray pinhole cameras
Plasma calorimeter
E8012B
Photo taken from port H11B

Figure 6. Photograph of the inside of the OMEGA chamber during a direct-drive target experiment. Several currently installed and operating plasma diagnostics are shown.

detection, a 962-element single-hit neutron detector array for fuel temperature and areal density measurements, knock-on particle detector arrays, and high-energy charged-particle spectrometers. The temperature-density parameter space covered by the nuclear diagnostic systems is shown in Fig. 7. The nuclear diagnostic systems should be able to measure the target

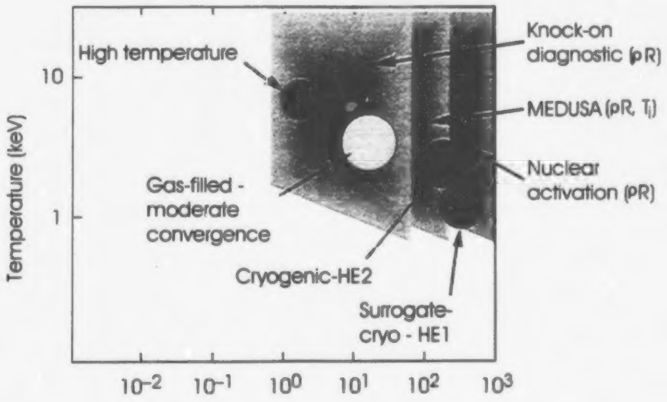

Figure 7. Nuclear diagnostics will be used to assess the core conditions for the principle OMEGA implosion experiments.

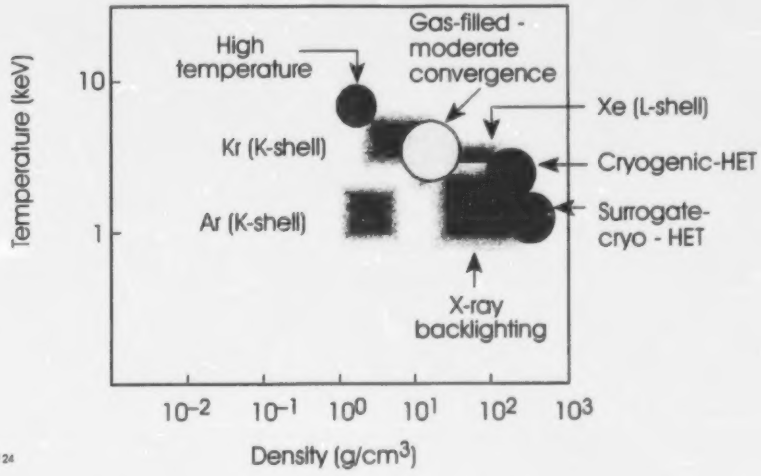

E7124

Figure 8. X-ray diagnostics can assess the core conditions for some of the OMEGA implosion experiments.

conditions anticipated for the principal OMEGA implosion experiments also delineated in Fig. 7.

In addition to nuclear diagnostics, x-ray diagnostics are used to probe the high-energy-density conditions of the OMEGA capsules. High-Z dopants included in the capsules can be used to assess the electron density of the compressed fuel via Stark broadening of the x-ray spectral lines emitted by the constituent elements in the capsule. Ar, Kr, and Xe doping are routinely used for such diagnostics. For densities that are so high as to preclude the use of self-

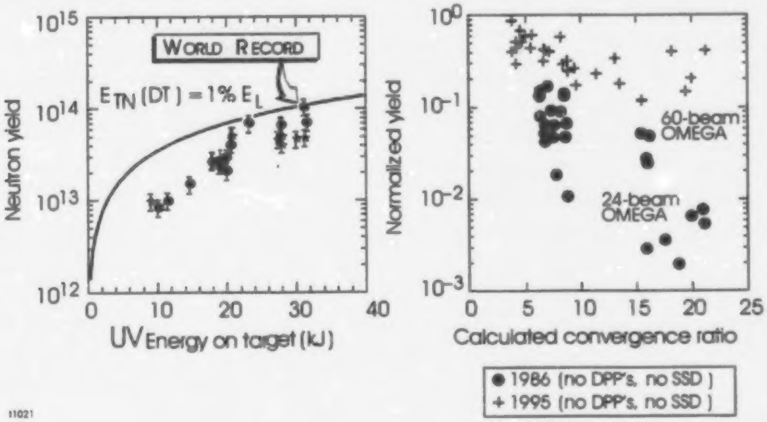

11021

Figure 9. DT-filled glass-shell implosions on the 60-beam OMEGA show record neutron yields. On this graph, the DT-neutron yield is plotted as a function of UV energy on target. Thermonuclear energy equal to 1% of the laser energy on target was achieved for the first time on these implosion experiments.

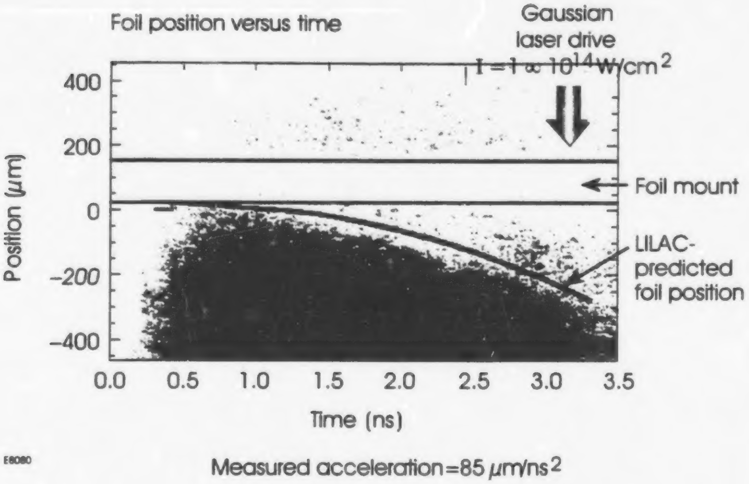

Figure 10. Time-resolved photograph (streak record) of a foil acceleration experiment on OMEGA. The target foil is backlit by X-rays from an X-ray backlighting source. The curved line shows the hydrodynamic-code-predicted foil trajectory. The inferred acceleration from this measurement was 85 μm per square nanoseconds.

emission as a diagnostic or for capsules that do not contain high-Z dopants, x-ray backlighting can be used to probe the density, size, and shape of the compressed cores. Figure 8 shows the parameter space accessed by x-ray core diagnostics.

The first set of implosion experiments conducted on OMEGA was designed to test many of the diagnostics systems including nuclear measurement systems. In early 60-beam experiments on DT-filled glass shell capsule implosions, neutron yields as high as 1.3×10^{14} were achieved — a record for inertial fusion experiments. These experiments (see Fig. 9) produced thermonuclear energy release equal to 1% of the laser energy — also a record high figure for inertial fusion experiments.

In addition to spherical implosion experiments, planar-foil-target experiments of various types are conducted on OMEGA. One such series is designed to investigate hydrodynamic instability physics for direct-drive capsules. Figure 10 shows the results from one such experiment in which a polymer foil was driven by several OMEGA laser beams at an average intensity of 10^{14} W/cm^2. The position of the foil in time was measured by spatially resolved x-ray backlighting and corresponded closely to the calculated position as predicted by the hydrodynamic simulation code LILAC.

In future OMEGA experiments, liquid and solid-DT-fuel layers will be produced by means of a cryogenic-target-delivery system currently under construction by a team composed of scientists and engineers from LLE, LLNL, LANL, and General Atomics. This system will be ready for target experiments in 1999. The direct-drive cryogenic implosion experiments will play a critical role in the national ICF program. These experiments will be conducted using NIF relevant beam numbers, power/energy balance, beam-smoothing techniques, and pulse shaping. They will provide critical data on the inside-surface-finish requirements for high-performance targets and will generate a database against which ICF implosion and mix codes can be tested before conducting NIF experiments.

ACKNOWLEDGMENTS

This work was supported by the U.S. Department of Energy Office (DOE) of Inertial Confinement Fusion under Cooperative Agreement No. DE-FC03-92SF19460, the University of Rochester, and the New York State Energy Research and Development Authority. The support of DOE does not constitute an endorsement by DOE of the views expressed in this article.

REFERENCES

1. J.D. Lindl. Phys. Plasmas **2**, 3933 (1995).
2. R.L. McCrory, J.M. Soures, C.P. Verdon, F.J. Marshall, S.A. Letzring, S. Skupsky, T.J. Kessler, R.L. Kremens, J.P. Knauer, H. Kim, J. Delettrez, R.L. Keck, and D.K. Bradley. Nature **335**, 225 (1988).
3. S. Skupsky, R.W. Short, T. Kessler, R.S. Craxton, S. Letzring, and J.M. Soures. J. Appl. Phys. **66**, 3456 (1989).
4. J.D. Kilkenny, M.D. Cable, C.A. Clower, B.A. Hammer, V.P. Karpenko, R.L. Kauffman, H.N. Kornblum, B. J. MacGowan, W. Olson, T. J. Orzechowski, D. W. Phillion, G. L. Tietbohl, J. E. Trebes, B. Chrien, B. Failor, A. Hauer, R. Hockaday, J. Oertel, R. Watt, C. Ruiz, G. Cooper, D. Hebron, L. Leeper, J. Porter, and J. Knauer. Rev. Sci. Instrum. **66**, 288 (1995).
5. J.M. Soures, R.L. McCrory, C.P. Verdon, A. Babushkin, R.E. Bahr, T.R. Boehly, R. Boni, D.K. Bradley, D.L. Brown, R.S. Craxton, J.A. Delettrez, W.R. Donaldson, R. Epstein, P.A. Jaanimagi, S.D. Jacobs, K. Kearney, R.L. Keck, J.H. Kelly, T.J. Kessler, R.L. Kremens, J.P. Knauer, S.A. Kumpan, S.A. Letzring, D.J. Lonobile, S.J. Loucks, L.D. Lund, F.J. Marshall, P.W. McKenty, D.D. Meyerhofer, S.F.B. Morse, A. Okishev, S. Papernov, G. Pien, W. Seka, R. Short, M.J. Shoup III, M. Skeldon, S. Skupsky, A.W. Schmid, D.J. Smith, S. Swales, M. Wittman, and B. Yaakobi. Phys. Plasmas **3**, 2108 (1996).

MAGNETIC COMPRESSION/MAGNETIZED TARGET FUSION (MAGO/MTF) – AN UPDATE

Ronald C. Kirkpatrick and Irvin R. Lindemuth

Los Alamos National Laboratory
Los Alamos NM 87544, U.S.A.

ABSTRACT

Magnetized Target Fusion (MTF) was reported in two papers at the First Symposium on Current Trends in International Fusion Research [1,2]. MTF is intermediate between two very different mainline approaches to fusion: inertial confinement fusion (ICF) and magnetic confinement fusion (MCF). The only US MTF experiments in which a target plasma was compressed were the Sandia National Laboratory "Phi-targets" [3]. Despite the very interesting results from that series of experiments, the research was not pursued, and other embodiments of MTF concept such as the Fast Liner [4] were unable to attract the financial support needed for a firm proof of principle. A mapping of the parameter space for MTF [5] showed the significant features of this approach. The All-Russian Scientific Research Institute of Experimental Physics (VNIIEF) has an on-going interest in this approach to thermonuclear fusion, and Los Alamos National Laboratory (LANL) and VNIIEF have done joint target plasma generation experiments relevant to MTF referred to as MAGO (transliteration of the Russian acronym for magnetic compression). The MAGO II experiment appears to have achieved on the order of 200 eV and over 100 KG [6], so that adiabatic compression with a relatively small convergence could bring the plasma to fusion temperatures. In addition, there are other experiments being pursued for target plasma generation and proof of principle. This paper summarizes the previous reports on MTF and MAGO and presents the progress that has been made over the past three years in creating a target plasma that is suitable for compression to provide a scientific proof of principle experiment for MAGO/MTF.

1. INTRODUCTION

Magnetized target fusion (MTF) provides a development path for fusion energy that is mid-way between the two dominant approaches to fusion energy. An unambiguous demonstration that compression of a magnetized plasma heats it in accord with MTF theory is desired. Previous MTF studies [5,7] have emphasized that existing pulsed power technology is adequate for a scientific proof of principle (i.e., an unambiguous demonstration), and probably sufficient for experimental exploration beyond. This would allow an economical and

Current Trends in International Fusion Research — Proceedings of the Second Symposium
Edited by E. Panarella. NRC Research Press, National Research Council of Canada, Ottawa, ON K1A 0R6, Canada. 1999.

significant advance of fusion science and technology. The reasons for this assertion have been previously presented [1,2], but will be summarized here.

It should be noted that MTF is a concept that may have many diverse embodiments, some purely for experimental investigation of MTF, and potentially others for applications such as fusion power production and space propulsion. We take the position that the most important first task for research on any fusion concept is to provide a proof of principle. Once that is done, the concept becomes a candidate for consideration as a possible approach to fusion energy production or other application. Therefore, we are reluctant to divert our effort from the first task, but concede that it is necessary to provide a plausible embodiment of MTF for fusion power production and will do so at the end of this paper. However, it should be remembered that there may be many unanticipated applications of fusion. We shall try to anticipate only a few.

2. MTF PHYSICS

Magnetized target fusion is based on the fact that a magnetic field suppresses electron thermal conduction in a sufficiently hot plasma. Electron thermal conduction is the major energy loss mechanism for the wall confined, unmagnetized plasmas produced in most designs for fusion ignition targets in inertial confinement fusion (ICF) [8]. However, for ICF simply imposing a magnetic field on existing ignition target designs does little to suppress electron thermal conduction, because the density is so high that the mean collision time in the plasma is short, leading to a small magnetization parameter, the cyclotron frequency - collision time product $\omega\tau$. Even if the magnetization were sufficient to erase the conduction loss, the next most important loss mechanism, bremsstrahlung, would take over. Therefore, MTF must operate in a lower density regime than ICF, so that both conduction and radiation losses are reduced. For similar fusion plasma mass, this leads to a larger target containing a gaseous DT fusion fuel at a density of about 0.01 to 1 mg/cc.

The required level of magnetic field for insulation of the fusion fuel from loss to the surrounding wall is sufficiently low that synchrotron radiation and magnetic field energy are only perturbations on the fusion fuel dynamics. If the plasma initially has a high ratio of internal energy to magnetic energy β, then it will always be so as the plasma is compressed. With sufficiently reduced energy loss rates the plasma can be compressed relatively adiabatically to fusion temperatures by reducing the volume of the confining vessel. With the reduced energy loss rates, the rate of compression as determined by the implosion velocity and geometry of the confining vessel can be much lower than needed for ICF. In ICF the confining vessel is a spherical shell that is symmetrically and rapidly imploded to a very small final radius. One embodiment of MTF would be similar, except the implosion velocity would be over an order of magnitude lower.

Fusion ignition is not required for all fusion energy schemes, but ignition is what makes ICF a viable fusion energy concept. Fusion ignition relies on "self-heating", which means that the fusion energy release in the form of neutrons and/or energetic charged particles is at least partially deposited in the fusion plasma as these particles pass through it. For ICF the critical parameter that determines whether the fusion self-heating overbalances the energy losses from the fusion plasma is the areal density ρR. It must exceed approximately 0.3 gm/cm^2 for fusion ignition to occur. For this very low value of areal density, the neutrons deposit very little energy, so the DT alpha particles are the major source of self-heating. The efficiency of the burn that follows also depends on an areal density, but that of the imploding part of the target (fusion fuel plus imploded confining vessel), and therefore, the target gain depends on the ρR as well.

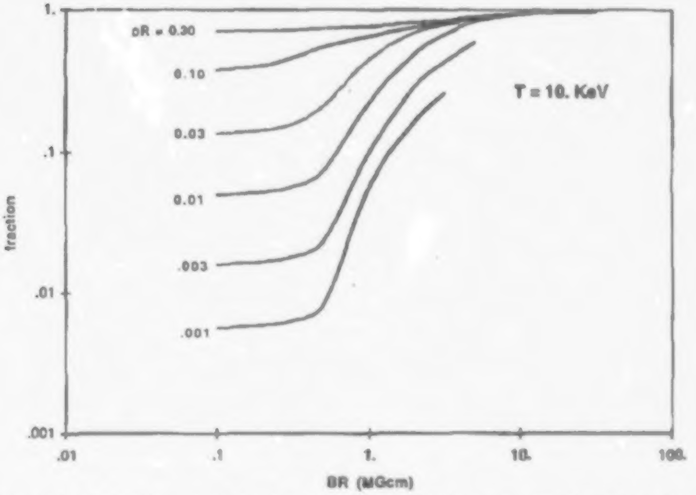

Figure 1. Fractional energy deposition as a function of BR for various areal densities (ρR).

Because the energetic charged particles in a magnetized plasma are turned in the field, their path in the fusion fuel is lengthened. Since in a hot plasma the magnetic field is essentially frozen in place relative to the plasma, the compression of the plasma by the imploded confining vessel also compresses the field. These compressed fields can reach many Megagauss. The critical parameter for self-heating is the gyroradius. If it is much smaller than the fusion plasma radius, then a significant part of the energy of charged fusion products will be deposited to self-heat the plasma. The critical value corresponds to a field times radius product (BR) of 0.3 MG-cm, but the higher the better. The very low ρR typical of MTF is significantly augmented by the high BR, which makes it possible for fusion ignition to occur for MTF at lower ρR than required for ICF. In one study [9] a particle tracking code was used to calculate the fraction of DT alpha particle energy deposited in spherical volume of homogeneous magnetized plasma with a pure azimuthal field. Some results for that study are shown in Figure 1. Figure 2 shows the dependence of the fractional deposition on temperature for a ρR of 0.001 gm/cm^2.

3. THE MTF ADVANTAGE

Because MTF targets are larger and can be imploded slower, the power and intensity for driving the target to fusion ignition are potentially orders of magnitude lower. However, for the same mass of fusion fuel the energy required for ignition is about the same, simply because the same thermal energy must be supplied to the fusion fuel to raise it to the ignition temperature [7]. Ignition of a given design of fusion target requires that the fusion driver (laser, particle beam, or otherwise) supply simultaneously sufficient energy, power, and intensity. For example, at this time lasers are sufficiently powerful and intense to drive appropriate designs of ICF targets to ignition, but are not sufficiently energetic. The anticipated National Ignition Facility at Livermore, California, is intended to provide all three,

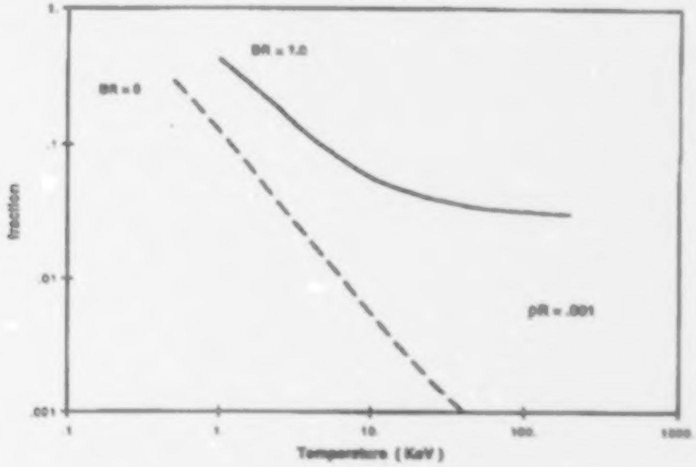

Figure 2. Fractional energy deposition as a function of T_e for given ρR with BR=0 and BR=1 MC-cm.

that is, sufficient energy, power, and intensity on target. The attractiveness of MTF is that the reduced power and intensity requirements needed for MTF targets admit as potential drivers for fusion targets existing and near-term pulsed power machines. Direct pulsed power has never been a contender as an ICF driver, because of an inability to supply the necessary power and intensity on target. However, pulsed power machines can easily supply sufficient energy, power, and intensity for MTF and are more efficient overall than laser or other beam drivers.

4. TARGET PLASMA GENERATION

The benefit promised by MTF is not without cost. It is necessary to create a target plasma that is sufficiently warm, magnetized, and long lived that it can be compressed to fusion temperatures with the slower implosion provided by pulsed power drivers. Because the MTF concept relies on compression of the warm plasma from its initial temperature to fusion temperatures, the energy that resides in the warm plasma before compression is modest. For example, 100 μg of DT at 50 eV has only 500 J of internal energy, but at the temperature required for fusion ignition (~ 5 KeV) 100 μg would have 50 KJ, the bulk of which would have been added through compression following the target plasma creation. There are potentially several ways to create a target plasma.

In the Sandia "Phi" targets [3], an electrical discharge through the deuterium inside the plastic shell that acted as the confining vessel left a target plasma that was about 20 eV with a 10 KG field. In the Fast Liner experiments [4] at Los Alamos a 30 eV plasma with a field of 10 KG was produced with a Marshall gun. Our survey calculations [5] indicated that a 50 eV plasma with a 50 KG field is necessary for reaching fusion ignition. It should be noted here that there is a trade-off between initial target plasma temperature and the convergence required to reach fusion temperatures. While lower values of target plasma temperature and field can provide useful experimental data, the MAGO experiments have been interpreted as providing about 200 eV with a magnetic field of about 100 KG, and these values are what the MHD codes predict [6]. Therefore, the MAGO experiments appear to have demonstrated one method of creating a target plasma that is more than adequate for an MTF scientific proof of principle. However, we are still trying to better assess the life time of the MAGO plasmas.

Because of the important implication of successful target plasma generation experiments regarding an MTF proof of principle, we present here some details of our progress in this area.

5. ANALYSIS OF THE MAGO EXPERIMENTAL DATA

While some other yet untried approach may suffice to produce a target plasma, the MAGO experiments presently appear to provide a plasma with more than adequate properties, and no other approach has yet been experimentally demonstrated to give a more appropriate target plasma. Therefore, we have focused on a better characterization of the MAGO plasma. This is because a proof of principle experiment will tax the small resources presently devoted to MTF, so we don't want to proceed without some assurance that we have a valid starting point. The MAGO experiments use an explosively driven magneto-cumulative pulsed power generator. Therefore, necessarily some of the detectors on these experiments are expended. While some smaller scale experiments using fixed capacitor banks in the lab have been demonstrated, there is insufficient data for an assessment of the plasma temperature and density for these experiments. For this reason, there are only three experiments (all explosively driven MAGO shots) where we have data from a full set of diagnostics.

We note in passing that there is nothing inherent in MTF or the MAGO plasma formation system that requires the generation of electrical current through the use magnetic flux compression generators driven by high explosives. In the former Soviet Union, economic considerations prevented the development of advanced capacitor bank technology such as is now available in the US. Hence, Russian scientists concentrated on the much cheaper flux compression technology. In the process VNIIEF scientists developed a capability that can produce higher electrical currents and energy (albeit, slower) than is available elsewhere. For the fusion scientist, flux compression technology enables experimentation that simply could not be performed in any other manner.

The plasma behavior in the MAGO experiments is complex. Here, we describe the

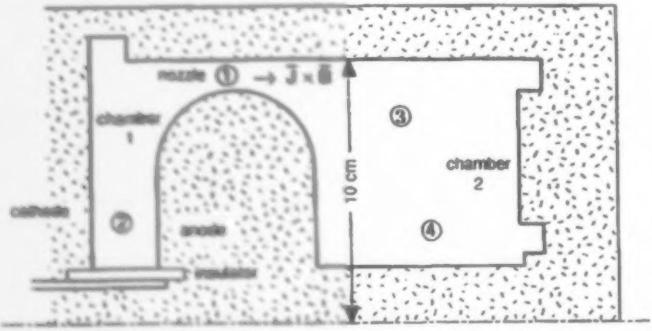

Figure 3. Design of the MAGO plasma formation chambers. The numbers in circles mark sequence of key operation process: 1) Electrical breakdown of the pre-magnetized gas occurring initially in the "nozzle" drives a shock into the right chamber. 2) A weaker breakdown follows about 1 µs later at the insulator and drives an inverse pinch toward the nozzle. 3) Plasma in left-hand chamber is accelerated through the nozzle, thermalizing to ~ 1 KeV when it encounters the previously shocked plasma and producing neutrons. 4) After 3-4 µs dynamic phase, the bulk of the plasma has relaxed to a "warm" (100-300 KeV) magneto-thermally insulated plasma.

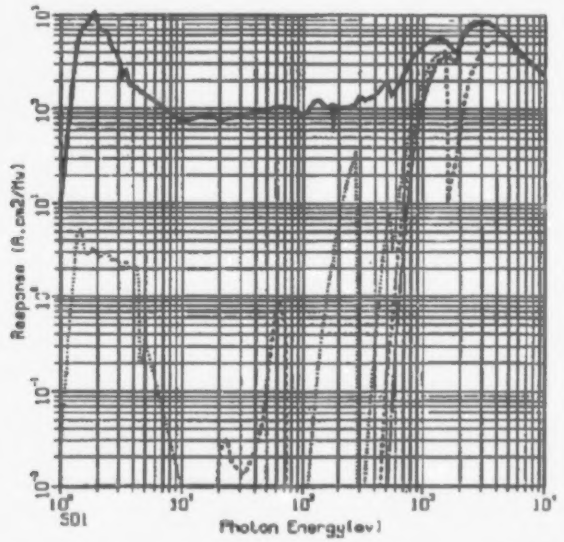

Figure 4. Filtered silicon diode spectral responses. The bold solid curve is for an unfiltered diode. The unfiltered diode was over-driven, so the data was not useful.

computational picture as modeled by a 2-D MHD code at Los Alamos [10,11]. The cylindrical copper plasma chamber is divided into two parts as illustrated in Fig. 3. Initially a slowly rising current of about 1-2 MA is introduced which flows around the chamber and through the center rod that supports the copper barrier between the chambers. This current creates a

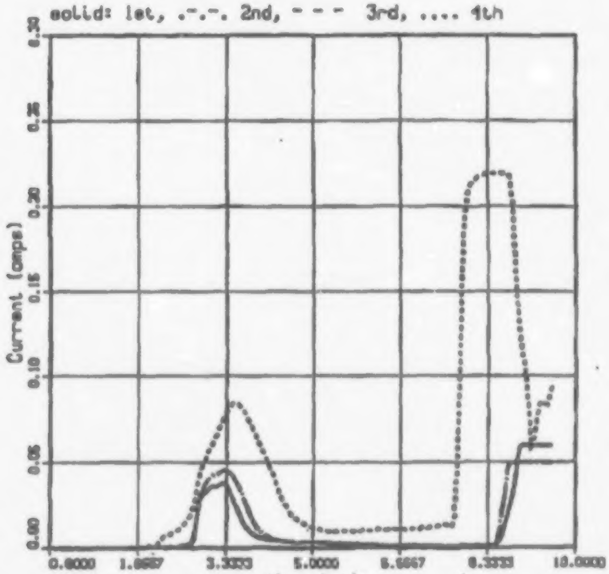

Figure 5. MAGO II Filtered silicon diode signals.

magnetic field throughout both chambers, but the rise time is too long to induce any ionization. A switch isolates the chamber from the explosive pulsed power generator while it continues to operate, building the current to about 10 Ma. At that time an opening switch abruptly introduces a high voltage (an inductive "kick") to the chamber. The high voltage ionizes the deuterium-tritium (DT) gas inside and causes discharges, first between the barrier and the cylindrical wall, and then across the insulator in the first chamber. The discharge across the nozzle weakly shocks the neutral magnetized gas in both chambers and weakly ionizes it. An inverse pinch in the first chamber drives the ionized plasma from that chamber through the annular nozzle where it is accelerated to velocities approaching 100 cm/us by the j × B forces. This fast flow shocks down into the magnetized plasma in the second chamber, initially heating a small portion to temperatures exceeding 1 KeV in hot spots. This plasma quickly relaxes to a warm few hundred electron volts (~ 200 eV), but the brief high temperature hot spots provide on the order of 10^{13} neutrons in a half-microsecond burst. This burst of neutrons is incidental to the creation of the warm magnetized plasma. It is this warm, late time plasma in chamber 2 that we are interested in as a possible target plasma for MTF.

Because of quality of data, we have focused on the MAGO II experiment, which was performed at Los Alamos in October of 1994. Thus far, the most telling data regarding temperature history of the plasma generated appears to be the filtered silicon diode data for a line of sight through the second chamber, parallel to, and 6 cm from its axis [12]. The silicon diodes we used have a spectral response spanning photon energies from about 1 eV to 10 KeV and viewed the plasma along four lines of sight at the same radius through the second chamber. One diode had no filter, and both single material and composite filters were used to give different band passes for the other three. Only the three filtered diode signals could be used in an analysis of the plasma temperature history because the unfiltered diode saturated before any of others gave signals. Figure 4 shows the spectral responses of an unfiltered diode

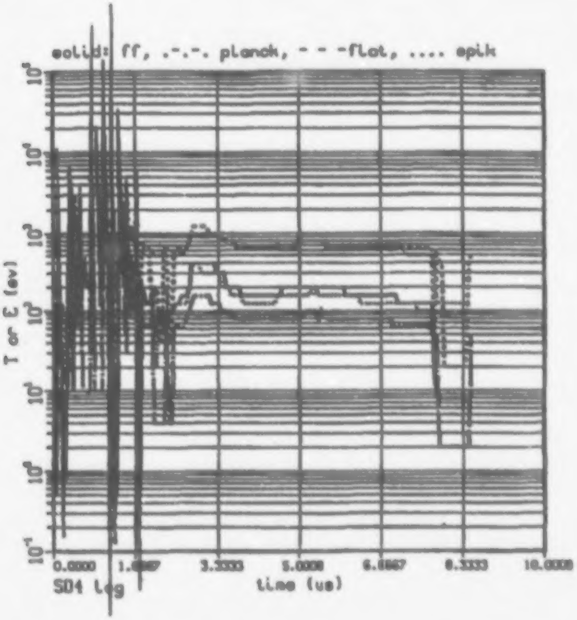

Figure 6. Best fit temperatures for MAGO II data.

and the three filtered diodes. Figure 5 shows the signals for the three filtered diodes. It should be noted that the peak in the approximately 10^{13} neutron output from MAGO II occurred near the time of the first peaks in the signals from these diodes and lasted less than a microsecond. With data for enough spectral band passes it would be possible to reconstruct the spectral history of the emission, but because of the data is very limited it is necessary to assume a spectral shape and test to see what shape provides the best fit to the data.

Figure 6 shows the characteristic plasma temperatures or energies deduced from the data for five assumed spectral types. While all the resulting temperatures and energies (with offsets) track together, that which has the best fit to the data is for an assumed bremsstrahlung spectrum. The second best is for an exponential. In addition, using the 1-D non-LTE radiation transport code ZAP to simulate the spectra expected from the MAGO II plasma (which had a 0.01 % neon impurity), the inferred temperature history of the plasma can again be inferred. It does not differ significantly from that for a bremsstrahlung spectrum. Figure 7 shows these results compared with the spatially averaged temperature calculated using a 2-D MHD code [10] to compute the expected plasma dynamics. Figure 8 shows the estimated density based on analysis of the data compared with the spatially averaged value from the MHD code. Both the temperature and density comparisons are remarkably close, suggesting an average plasma temperature of about 200 eV and an average density of about 10^{18} / cc for a few microseconds after the peak in the diode signals.

After about five microseconds, the diode signal levels rise abruptly and the inferred plasma temperatures all drop sharply. This could be due to a drastic change in the nature of the plasma, but it could also be due to a failure in the filtered silicon diode diagnostics. We did a detailed study of the generation of shocks in the diagnostic access holes for the filtered silicon diodes and concluded that the sharp rise in signals could be reasonably explained by destruction of the filters when a shock generated by an oscillating MHD piston arrives at the diodes. However, we must confirm this hypothesis in another experiment. The MAGO III

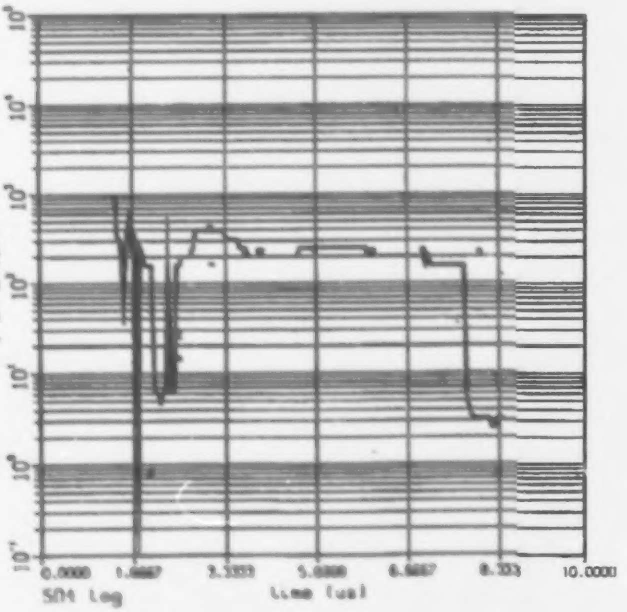

Figure 7. Temperature history using ZAP spectra.

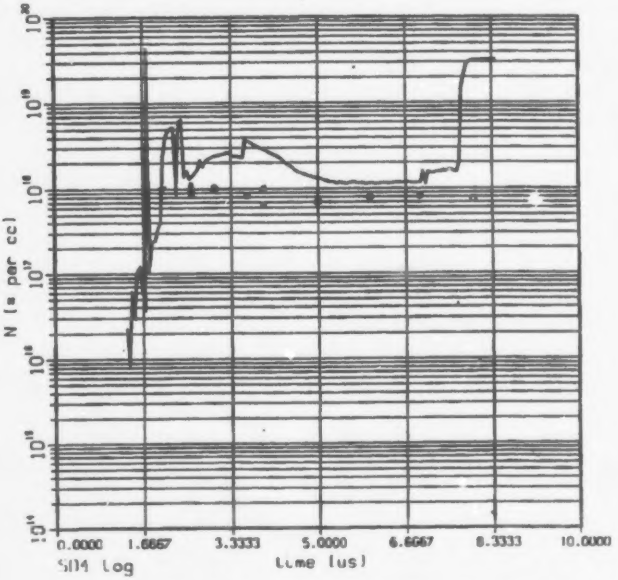

Figure 8. Estimated history of average density along the diagnostic line of sight using ZAP spectra and N^2 scaling.

experiment at VNIIEF in September of 1995 used three sets of seven filtered silicon diodes each to diagnose the plasma, but unfortunately the extensive data was not useable, partly because of saturation of the signals, and possibly because of shock arrival at the diodes. In the MAGO III experiment it appears that the supposed shocks arrived earlier than for MAGO II, which correlates with the higher calculated average temperature for the MAGO III plasma.

6. OTHER TARGET PLASMA APPROACHES

In the Sandia Phi target experiments the target plasma was created in a much simpler way than in the MAGO experiments. These targets contained either a CD_2 fiber or deuterium gas inside a small plastic shell and was driven by a relativistic electron beam, which had a non-relativistic precursor. An electrode was mounted on the cathode side of the target to intercept the non-relativistic precursor. This created an electric field that weakly ionized the gas or deuterated polyethylene (CD_2) fiber inside, leading to a discharge that created a warm magnetized plasma inside. The resulting 20 eV, 10 KG plasma was below the 50eV and 50 KG values, which (in the light of the survey calculations done a few years later [5]) we now think are needed for MTF. The main pulse deposited about 4 KJ of energy in the plastic shell, ionizing it and providing an exploding pusher behavior that compressed the target plasma inside [3]. The conditions created by the discharge in the Phi target were adequate to provide measurable neutron output (~ 5 to 25×10^6) at the end of the compression phase. It should be noted that this was energetically a very low level experiment in comparison to the MAGO experiments. Later, Sandia performed experiments using a capacitive discharge to confirm the initial target plasma conditions. No attempt was made by Sandia National Laboratory to

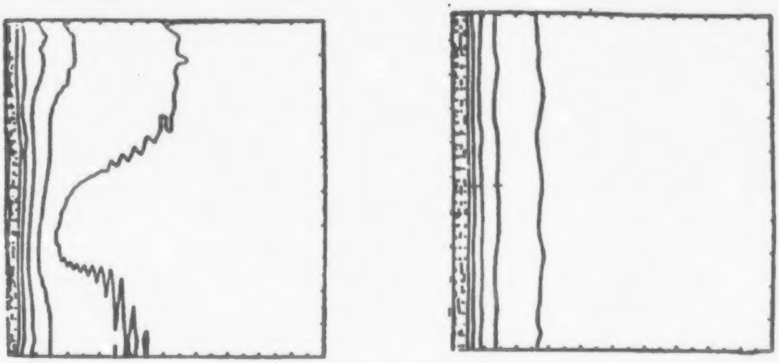

Figure 9. Computed axial current contours (r-z 2 cm by 2 cm): left early (1.1 μs) unstable, expanding phase; (right) later (2.4 μs) stable, wall supported phase. Most of the current is concentrated near the axis of symmetry along the left side of each frame. The curved contour on the left is indicative of an m=0 instabilility.

improve on these conditions. A decision was made to abandon magnetized targets, because at the time they did not appear to scale to high gain. A later study indicated otherwise [13].

The seeming simplicity of the Phi target plasma generation and our interim experience with cryogenic fiber-initiated Z-pinches led us to recently re-examine the physics of the fiber-initiated Z-pinch. The intent of our initial work on cryogenic fiber-initiated Z-pinches (and that of ongoing research elsewhere) was to ohmicly heat and magnetically compress an initially cryogenic DT fiber to fusion temperatures (i.e., "direct fusion"). Sheehey et al., found that the fiber became very unstable [14], thwarting the goal of direct fusion. More recently, Sheehey has examined the role of a nearby cylindrical conducting wall in stabilizing the m=0 unstable modes [11]. The configuration examined was a 2 cm long cryogenic DT fiber inside a 2 cm radius copper cylinder with closed ends (a conducting can). The external circuit with parameters that approximate our small Colt capacitor bank introduce current between the fiber and the conducting walls of the can across an insulator that hydrodynamically closes the can. The current rises to 1 or 2 MA in 1 or 2 μs, a much slower rise than for the initial Z-pinch approach mentioned above. Sheehey found that when the unstable plasma expands out to the wall, it becomes wall supported and settles down to a sporadically re-adjusting Kadomtsev stable profile as shown in Figure 9. As the drive current dies away, the average plasma temperature remains high due to the continuing magnetothermal insulation maintained by internal currents.

We have initiated laboratory experiments to confirm this predicted behavior, but have no definitive results yet. The calculated target plasma generated in this manner appears to be suitable as a target plasma for MTF, and both the experimental results and computational analysis for the Phi targets provides some confidence that this effort will ultimately be successful.

7. COMPRESSION OF THE TARGET PLASMA

Following creation of a warm magnetized target plasma, it is necessary to compress it to fusion temperatures. In the Phi target, this was accomplished by the main electron beam exploding the plastic shell and thereby driving the inner aspect inward to act as a pusher that compressed the target plasma. According to the computational analysis done after the experiments [3], in order to explain the observed neutron yield it was necessary for the plasma to attain about 400 eV at peak compression (corresponding to a convergence of about 20 according to calculations). VNIIEF has proposed to start with a current driven (j × B) cylindrical liner for compressing the MAGO target plasma and to do subsequent experiments with a quasi-spherical geometry.

When the apparent parameters for the MAGO target plasma are used as the initial condition for a calculation with the survey code previously mentioned, a gain of more than 10 is predicted for an initial liner kinetic energy of 65 MJ [6]. We would not propose to use the large MAGO systems for energy production, but the result certainly suggests that MAGO might offer a very affordable approach to a proof of principle and provide useful experiments for studying the physics of MTF.

Because the goal was generation of soft X-rays [15], in past, work on current driven liners focused on fast, low mass liners that become plasmas during the rapid acceleration phase. This is related to the level of current density necessary to reach a very high implosion velocity. The thinner the liner, the higher the current density. For given homogeneous liner properties above a certain implosion velocity the liner becomes a plasma. Because of the significant early ohmic heating of the liner, the imploding liner does a lot of work on itself during the final convergence. This provides high implosion velocity, but has an unfortunate consequence for fusion ignition. This is because near the peak compression when the fusion plasma energy loss rates are rising rapidly, it is not possible for a plasma liner to quickly couple its kinetic energy into the plasma to provide a compressional work rate that outstrips the losses. As the plasma liner becomes thick, the sound speed and thickness limit the compressional work rate to a relatively low value. Also, because of the high self-work by the plasma liner, the coupling efficiency between the liner and the plasma inside is low, leading to a low gain for any fusion energy scheme based on compressing the fusion fuel with a fast, magnetically imploded liner.

8. SOLID LINERS

At Los Alamos both computational and experimental work has been done on empty solid liner implosions using fixed capacitor bank and explosive pulsed power current sources, although not in an MTF context. More recently there has been a renewed interest in magnetically imploding liners that remain solid at the inner aspect throughout the implosion, so that they can be used as shock impactors [16]. Material strength delays some hydrodynamic instabilities and a cold, dense liner can couple better to a target inside. Two approaches are used for solid liners. One is to simply keep the implosion velocity below the limit, above which the liner vaporizes. Another is to use a composite liner for which an outer conductor vaporizes, but an inner insulator remains solid. Initial experiments that are relevant to MTF have used simple liners driven to about 10 Km/s, which is the limit for solid aluminum liners.

High energy liner (HEL) experiments continue at VNIIEF in collaboration with LANL. In these experiments an empty liner is driven by large modular disk explosive pulsed power generators (DEMGs). Several DEMG modules are stacked together to provide the desired current delivery to the liner load. These generators operate on a time scale similar to the liners that they drive, leading to efficient electrical energy transfer into the dynamic load represented by a liner. In one experiment more than 20 MJ of kinetic energy was coupled to a liner that achieved a velocity of 7–8 Km/s [17].

At Los Alamos and elsewhere experiments on solid liners must use fixed capacitor banks and are consequently limited in energy delivery capability to the energy of the bank. The USAF Phillips Lab (now, Air Force Research Lab) has for many years operated an important pulsed power facility called SHIVA STAR. It has a 9 MJ, 25 MA capability, and has been used to drive the implosion of a quasi-spherical liner [18]. A magnetized warm (a few eV) plasma was injected through vanes that removed the magnetic field produced by the plasma gun into the space between the liner and a central rod. This provided a warm unmagnetized plasma that was used as a working fluid for transferring the energy from the liner to the rod. This was imaged by an X-ray backlighter. The liner symmetry was very good and the compression of a hollow central rod used as a diagnostic was very apparent. The MHD simulations of this process with the Mach-2 code compare favorably with the radiograph images.

Phillips Lab has proposed an experiment which would capitalize on their unique experience, that is, study the interaction of a magnetized plasma with the inner aspect of a liner.

9. LINER STABILITY

2-D MHD studies of magnetic Rayleigh-Taylor (MRT) instability for the high energy liner experiments indicate that MRT instability is not a major factor in the HEL-1 liner behavior [16]. However, these studies show that problems can arise where the liner slides along stationary electrodes that make contact with the cylindrical liner. Proper design of these contacts is potentially crucial to the success of a proof of principle based on compression of a target plasma by a cylindrical liner. In the Phillips Lab experiments the contact design appears to have been very successful.

10. PLASMA / WALL INTERACTION

Some 1-D and 2-D MHD calculations of compression of the target plasma are underway. One major concern, the plasma wall interaction problem, is being investigated, both analytically and computationally. The major concern is the introduction of impurities into the fusion plasma that could increase radiative losses from the plasma. While the ZAP code mentioned earlier can provide reliable calculations of enhanced radiation once the impurity level is known, we need to establish some measure of what impurity levels to expect. The Phi-target and MAGO experimental results might suggest that the level of impurities introduced is tolerable, since the calculations, which have had no impurities, agree with the experimental data. However, it is possible that the target plasma formation phase is not as sensitive to impurities as the compression phase that follows. This aspect mainly depends on atomic number (Z) of the impurity.

There are other possible problems associated with the plasma/wall interaction. One is that the cooling of the plasma adjacent to the wall leaves that part of the plasma at lower b, so that the magnetic pressure of that part becomes more important in the compression of the magnetized plasma. Also, because the regions of higher magnetic field in an inwardly accelerated plasma have a mass deficiency, buoyancy forces come into play that can create convection that enhances cooling. Also, the magnetic field has a tendency to diffuse into the wall, which generates ohmic heating (mainly in the wall) and reduces the strength of the field in the magnetized plasma. We have some modeling codes that include this physics, so the greatest modeling (and experimental) uncertainty is potentially the impurity problem mentioned in the previous paragraph.

11. ANALYTIC DT ALPHA TRANSPORT RELATIONS

We have done some work on quantifying the enhancement of the DT alpha energy deposition due to the magnetic field in a fusion plasma. In the past, several methods have been used to compute alpha confinement in a magnetically confined plasma [19], but the combination of accuracy and efficiency for these methods is not sufficient for the dynamic MTF plasma, in which the Larmor radius can be a substantial fraction of the plasma size, that is, span many gradient lengths. In principle, particle tracking (which was used to produce Figures 1 and 2) should be most accurate, but it becomes very expensive for a highly magnetized plasma, even for the case of a static plasma. There have been many DT alpha transport studies for ICF [20], but for ICF any magnetic fields that may accidentally occur are generally negligible, with the exception of the fast igniter [21]. In some MHD capable codes that account for the effect of the field on charged particle transport, a Fokker-Planck formulation is used, which is diffusion-like in space. This becomes a poor approximation when the Larmor radius becomes long compared to the gradient lengths in the problem. Therefore, we have sought to devise a transport method that is at once sufficiently accurate and efficient to handle the dynamic MTF problems that we expect to encounter in the target design process.

Most numerical MHD models discretize the plasma, using many zones or cells to approximate a continuous distribution of plasma and field. To the first order, these zones may be approximated as homogeneous. For a homogeneous medium it is possible to obtain some useful analytic solutions that can greatly speed up the computation of the DT alpha trajectory through the plasma. By stringing together piece-wise the solutions for a set of homogeneous regions, it is possible to get an approximate result for the passage of the alpha through an inhomogeneous plasma. It may be possible to extend the analytic solutions to the case of linear gradients within a zone, which would greatly improve the accuracy, but the simpler problem is already challenging. In a hot fusion plasma the DT alphas loose energy to both electrons and ions, but to avoid complicating the mathematics, here we illustrate the approach by making the assumption that the DT alpha particles do not interact with the plasma ions. In such a case in a plasma above 1 KeV, the velocity decreases exponentially with time:

$$v(t) = v_o\, e^{-t/\tau},$$

where v_o is the initial velocity and t is the relaxation time due to Rutherford scattering with electrons. In an (x.y,z) coordinate system with the magnetic field B in the z direction and the x direction in the direction of v × B,

$$\begin{aligned} v_y(t) &= v_{yo}\, e^{-t/\tau} \cos(\omega t), \\ v_x(t) &= v_{yo}\, e^{-t/\tau} \sin(\omega t), \text{ and} \\ v_z(t) &= v_{zo}\, e^{-t/\tau}, \end{aligned}$$

so that the path of a DT alpha particle entering a homogeneous region at the origin will be:

$$\begin{aligned} x(t) &= v_{yo}t\,(wt - e^{-t/\tau}(\sin\omega t + \omega\tau\cos\omega t\,) / (1+\omega^2\tau^2) \\ y(t) &= v_{yo}t\,(\,1 - e^{-t/\tau}(\cos\omega t - \omega\tau\sin\omega t\,) / (1+\omega^2\tau^2) \\ z(t) &= v_{zo}t\,(\,1 - e^{-t/\tau})\,. \end{aligned}$$

The equation for a plane in that coordinate system is $A\,x + B\,y + C\,z = D$, where $A = d_x/d$, $B = d_y/d$, $C = d_z/d$, and $D = d$. Here, d is the distance between the point of entry into a computational cell at (0,0,0) and the plane defining one side of the cell. Defining the coefficients

$$\begin{aligned} C_1 &= v_{yo}\tau\,(A\omega t + B) / (1+\omega^2\tau^2) + C\,v_{zo}t - D, \\ C_2 &= v_{yo}\tau\,(A - B\omega t) / C_1\,(1+\omega^2\tau^2), \end{aligned}$$

$$C_3 = v_{yo}\tau\,(B + A\omega t) / C_1\,(1+\omega^2\tau^2),$$
$$C_4 = C\,v_{zo}t / C_1$$

solving $e^{-t/\tau}$ [C_3 sin ωt + C_3 cos ωt + C_4] = 1 for the minimum crossing time t (there are potentially several crossings), and substitution into the previous equations, provides the exit point (x,y,z). Since there are more than one plane that define the cell, the minimum time among all of them must be found.

Tables can be made for the solutions to a sin x + b cos x + c = e^{qx}, and interpolation used to efficiently find solutions. This procedure should be extendible to the case of slowing by ions and electrons, but becomes more complicated simply because the paths for the DT alpha can't be expressed analytically for that case. The mathematics becomes more involved, but some results are possible, and some transformation properties allow us to restrict the number of numerical integrations to just two per zone. Thus, the prospect for a method that will be suitable for application to MTF is good.

12. MTF FOR FUSION POWER

As noted in the Introduction, we are reluctant to spend much effort on MTF reactor concepts, because it detracts from the first priority: proof of principle. Here we provide one plausible embodiment of the MTF concept as a fusion power system. It is based on a target driven by a beam, so it has many of the features that one would expect in an ICF based fusion power system. The targets must be manufactured with at least one electrical connection, that for the anode. The fabrication tolerances are not a problem, because the target convergence will be only 10—15. We adopt the target designs studied by Sweeny and Farnsworth [13], which included both electron beam and ion beam variants. In these targets, the target plasma is created *en situ* by a discharge. Then the beam energy is deposited in such a manner that a symmetrical compression ensues. Because of its high efficiency, an electron beam is preferred, but the ion beam has better coupling to the target. This constitutes an obvious trade-off that needs study.

The target must provide a substantial yield, but the close-in parts of the system must be protected, or be expendable, without serious economic consequences. There is a trade-off between the target yield and the shot rate necessary to provide the power to the electrical grid, but the average power of the energy dissipated in the close-in parts of the system remains the same for a given system power rating. The energy dissipation power must be handled primarily by heat removal, and this constitutes an opportunity for a heat based power generation approach.

In addition to the heat loading on the system, even for the advanced fuels such as D_2 and D^3He, neutrons from DT fusion reactions that occur must be used to regenerate the amount of tritium needed for MTF ignition. Because the cost of tritium from diverse sources is highly variable, and the system envisioned regenerates the tritium it needs, except for startup, it is not necessary to consider the commercial value of tritium, only the cost of regeneration. The cross section for transmutation of ^6Li to tritium is high for thermal neutrons, but low for energetic (e.g., 14 MeV) neutrons, so that the regeneration of tritium requires thermalization of the neutrons. Through this process the energy of the neutrons is delivered to the material that moderates them, again providing an opportunity for a heat based power generation approach. Also, the transmutation reaction is exothermic (~ 4 MeV, versus the 3.5 MeV carried by a DT alpha particle) which releases additional heat. Running the fusion reactor requires as fuel the isotopes deuterium (^2H), which is naturally occurring, and lithium-6 (^6Li). It may also be desirable to add material to the moderator that acts as a neutron multiplier through (n, 2n) reactions. Ralph Moir has discussed the details of target chambers for ICF and the above processes have been researched exhaustively, e.g., [22].

The drivers must be capable of repetitive operation at an average power that is some fraction of the grid power supplied. Also, they must provide a beam that penetrates a high heat and particle flux environment in order to reach the target, possibly through some residual debris. Some parts of these drivers may have to endure an attenuated version of the target chamber environment. Therefore, drivers that are robust and have no costly precision parts near or inside the target chamber are preferred. An electron beam machine seems to be the most robust driver, but the beam transport or transmission lines that deliver the electrical current may be susceptible to damage in the near-chamber environment.

The simplest heat based power generation approach uses a heat exchanger to transfer the heat from a working fluid such as FLIBE [22] to produce steam. Beyond this step the technology is standard electrical utility fare. While there are potentially more efficient direct conversion schemes, they are not proven and rely on direct interaction of fields and currents with the fusion-heated plasma. Unless the ρR of the fusion plasma is very high, the energy that comes out in the form energetic neutrons and the exothermic heat of transmutation is missed by direct conversion, and must be handled in some way, preferably to make electrical power rather than to be treated as waste heat. Therefore, direct conversion may be more attractive for relatively aneutronic fusion power systems. The high magnetic fields in MTF should enhance energy deposition by the 14.6 MeV D^3He fusion proton in low ρR targets, so there is potential for an aneutronic MTF target. However, at this time it is premature to advocate MTF as an aneutronic approach to fusion energy, and indeed we have reluctantly provided the MTF based reactor concept discussed here.

Because any diagram of the electrical power generating system described above would be very similar to one for ICF (with appropriate substitutions), there is no need to present one here. If ICF is plausible as a fusion power approach, so is MTF. However, it should be remembered that the system discussed here is only one of many possible embodiments of the MTF concept. MTF has qualitative differences from the traditional ICF or MCF approaches to fusion (i.e., characteristic densities and time scales); therefore the tradeoffs in designing an MTF based reactor will be different and conceivably superior to traditional approaches.

13. OTHER APPLICATIONS OF FUSION

Besides regeneration of the tritium needed for a plausible MTF fusion power approach, the thermalized neutrons may have other valuable uses. For a long time nuclear fission reactors have been used to produce medical isotopes. Wide spread use of fusion could have a tremendous impact on the availability of currently rare isotopes for many uses. This prospect should not be overlooked. Also, pulsed exposure to high fluences of neutrons can create different sets of isotopes than those produced in the continuous, low flux nuclear fission reactors. This prospect needs further exploration.

In addition, the economics of energy production don't apply to some potential applications of fusion. One of these is space propulsion. Here, the propulsion system weight is an important factor in mission planning. This is because the propulsion system, payload, fuel, and other necessary items must be lifted into low earth orbit and the cost per unit weight is very high. In addition, the exhaust velocity plays an important role in determining the mass of propellant that must be expended to achieve a given velocity. A fusion propulsion system has a potential for very high exhaust velocities. Therefore, if a fusion system is developed that can be configured as a space propulsion system, then it would become very attractive for many missions that are now impractical.

14. CONCLUSION

MTF is a relatively unexplored fusion technology that is intermediate between two extremes, ICF and MCF. The prospect for MTF advancing fusion energy science is very good. Until a proof of principle is obtained, the questions about the viability of MTF as a reactor concept will abound. Therefore, the most pressing need is for a scientific proof of principle. The facilities necessary for obtaining this are available now, and with relatively modest funding, we could move quickly to attempt such a proof of principle experiment.

REFERENCES

1. R.C. Kirkpatrick and I.R. Lindemuth. Magnetized Target Fusion, An Ultrahigh Energy Approach to an Unexplored Parameter Space. Current Trends in International Fusion Research, ed. E. Panarella, Plenum Press, New York (1997).
2. I.R. Lindemuth and R.C. Kirkpatrick. Magnetized Target Fusion, An overview of the Concept. Current Trends in International Fusion Research, ed. E. Panarella, Plenum Press, New York (1997).
3. I.R. Lindemuth and M.M. Widner. Phys. Fluids **24**, 746 (1981).
4. A.R. Sherwood, B.L. Freeman, R.A. Gerwin, and T.R. Jarboe et al. Fast Liner Proposal. Los Alamos Scientific Laboratory report LA-6707-P (August 1977).
5. I.R. Lindemuth and R.C. Kirkpatrick, Nuclear Fusion **23**, 263 (1983).
6. I.R. Lindemuth et al. Phys. Rev. Lett. **75**, 1953 (1995).
7. R.C. Kirkpatrick, I.R. Lindemuth, and M.S. Ward. Fusion Technology **21**, 201 (1995).
8. J.D. Lindl. Physics of Ignition for ICF Capsules. Inertial Confinement Fusion Course and Workshop (ed. A. Caruso and E. Sindoni, Varenna, Italy, 1988).
9. R.C. Kirkpatrick and D.P. Smitherman. Energetic Alpha Transport in a Magnetized Fusion Target. Proceedings of the 12th Topical Meeting on the Technology of Fusion Energy (1996 American Nuclear Society Annual Meeting) Reno, NV (1996).
10. I.R. Lindemuth, The Animal Code. Lawrence Livermore Laboratory report UCRL-52492 (1979); P.T. Sheehey. Magnetohydrodynamic Simulation of Solid Deuterium Initiated Z-Pinch Experiments. Thesis (UCLA) and Los Alamos report LA-12724-T (1994).
11. P. Sheehey, J. Hammel, I. Lindemuth. et al. Phys. Fluids **B 4**, 3698 (1992).
12. R.C. Kirkpatrick and G. Idzorek. ICOPS and Megagauss pprs (1997 & 1996).
13. M.A. Sweeny and A.V. Farnsworth. Nuclear Fusion **21**, 41 (1981).
14. P.T. Sheehey, R.A. Gerwin, R.C. Kirkpatrick, I.R. Lindemuth, R.W. Moses and F.J. Wysocki. Computational Modeling of Wall-Supported Dense Z-Pinches. Dense Z-Pinches, Proceedings of the 4th International Conference on Dense Z-Pinches, Vancouver, B.C., Canada (1997).
15. V.E. Fortov, K.S. Dyabilin, M.E. Lebedev et al., Double Liner Z-Pinch as the Source of a Powerful Pulse of Soft X-Rays for the Shock Wave Physics Experiments. 11th IEEE International Pulsed Power Conference, Baltimore, MD, U.S.A. (1997) p. 45.
16. R.J. Faehl, P.T. Sheehey, R.E. Reinovsky, and I.R. Lindemuth. Modeling and Analysis of the High Energy Liner Experiment HEL-1. Proceedings of the 11th IEEE International Pulsed Power Conference, Baltimore, MD, U.S.A. (1997).

17. R.E. Reinovsky, B.G. Anderson, V.K. Chernyshev, V.N. Mokhov et al. HEL-1: A DEMG Based Demonstration of Solid Liner Implosions at 100 MA. Proceedings of the11th IEEE International Pulsed Power Conference Baltimore, MD, U.S.A. (1997).
18. J. Degnan et al. Phys. Rev. Lett. (Feb 1995).
19. Wang and Qui, Nuclear Fusion **36**, 557 (1996); Zweben et al. Nuclear Fusion **35**, 893 (1995); Redi et al. Nuclear Fusion **36**, 1193 (1996).
20. R. Cooper and F. Evans. Phys. Fluids **18**, 332 (1975); M.J. Antal and C.E. Lee, Nucl. Science & Engineering **64**, 379-383 (1977); E.G. Corman, W.E. Lowe, G. Cooper and A. Winslow. Nucl. Fusion **15**, 377 (1975); S. Atzeni, Plasma Phys. Control. Fusion **29**, (1987) p. 1535; M.M. Basko. Nucl. Fusion **30**, (1990)p. 2443; A.M. Oparin, S.I. Anisimov, J. Meyer-Ter-Vehn. Nucl. Fusion **36**, (1996) p. 443.
21. S.C. Wilks, W.L. Kruer, P.E. Young, and M. Tabak. Ultra-Intense, Short -Pulse Laser-Plasma Interactions with Application to the Fast Igniter. Laser Interaction and Related Plasma Phenomena (Proc. of the 12th Int. Conf., Osaka, 1995), (AIP Conf. Proc. 369, AIP Press, NY, 1996), p. 590.
22. R. Moir et al. Fusion Technology **25**, 5 (1994).

STAGED Z PINCHES FOR CONTROLLED THERMONUCLEAR FUSION: THEORETICAL STUDIES

H.U. Rahman, P. Ney, J. Wessel[1] and N. Rostoker[1]

Institute of Geophysics and Planetary Physics
University of California
Riverside, CA 92521, U.S.A.
[1]Department of Physics and Astronomy
University of California
Irvine, CA 92697-4575, U.S.A.

A Staged Z-Pinch is comprised of a high-Z plasma shell (driver) that implodes onto an intervening azimuthal and/or axial magnetic flux and coaxial (DT or DD) target plasma, initially supplied as a cryogenic fiber. Such pinches are projected to achieve high-gain thermonuclear fusion at low cost in a small-size machine. The basic idea is to transfer energy at successive stages and deliver it to the load on an extremely short time scale (1–3 nanoseconds). In this manner the loss rates by radiation or thermal conduction are negligible. Moreover, the multi-MG, trapped-magnetic field prevents alpha-particles from escaping the core plasma, recycling part of the fusion energy, and may help to mitigate typical pinch instabilities, leading to enhanced radial compression.

We will present the results of our comprehensive studies on the Staged Z-Pinch, based on O-D and the LLNL MHD TRAC-2 numerical code run in I-D and 2-D. TRAC-2 computes the dynamic interaction of a multi-component plasma, with separate electron and ion temperatures, three components of magnetic field, and a simplified radiation-loss model for bremsstrahlung (free-free) and recombination (free-bound) radiation. Two classes of pulsed-power drivers are computed: 1.8 msec risetime, 2 MA peak current (characteristic of the UCI ZOT Pinch Facility) and 100 nsec risetime, 20 MA peak current (characteristic of the Sandia National Laboratories PBFA-Z Facility).

The highest thermonuclear yields are obtained with a thin, dense-plasma shell imploding onto a 50:50 DT target plasma with an embedded magnetic field (B_θ and B_z). For the UCI machine the yield is: $Y_n = 6 \times 10^{14}$ with an energy gain (fusion output energy/bank energy) of the order of 0.03. Calculations for PBFA-Z are underway and will also be presented. Conclusions drawn from these studies will be used to project machine designs that operate in the regime of breakeven and beyond.

Funded by the US DoE OFES, and LANL.

Current Trends in International Fusion Research – Proceedings of the Second Symposium
Edited by E. Panarella. NRC Research Press, National Research Council of Canada, Ottawa, ON K1A OR6, Canada. 1999.

UCI STAGED Z-PINCH

F. J. Wessel, B. Moosman, N. Rostoker, Y. Song, A. Van Drie,
P. Ney[1] and H. U. Rahman[1]

University of California,
Department of Physics and Astronomy,
Irvine, CA. 2697-4575, U.S.A.
[1]University of California
Institute of Geophysics and Planetary Physics
Riverside, CA 92521, U.S.A.

ABSTRACT

The Staged Z-pinch couples energy to a target plasma, dynamically in stages. The present UCI (University of California Irvine) experiment provides stable, multishell Z-pinches at 1.2 MA and 1μs implosion time. Test-stand studies of an exploded-fiber target indicate that the fiber core is not ionized, due to current channeling in the high conductivity ablated plasma.

1. INTRODUCTION

In the Staged Z-pinch a plasma liner implodes onto a fiber-target plasma. The fiber is initially preionized by a current pulse that turns it into a uniform, high-density plasma before the Z-pinch liner implodes; the current pulse also injects an azimuthal-magnetic field (B_θ) inside the pinch, in addition to an axial-magnetic field provided by external Helmholtz field coils. The magnetic fields compress differentially, providing dynamic shear, a means to inductively amplify current in the target, and confinement of fusion-reaction products. The unique feature of the Staged Z-pinch is the near-term prospect for thermonuclear break-even in a laboratory device [1] (http://mainpinch.ps.uci.edu).

2. RESULTS

The UCI Staged Z-Pinch Facility [2] is schematically shown in Fig. 1*a*. Two capacitor banks, consisting of ten, 2.5 μF, 50 kV capacitors each, are mounted on the top of the facility and attached to the ends of a plate-transmission line; peak energy 50 kJ. The banks are

Current Trends in International Fusion Research — Proceedings of the Second Symposium
Edited by E. Panarella. NRC Research Press, National Research Council of Canada, Ottawa,
ON K1A 0R6, Canada. 1999.

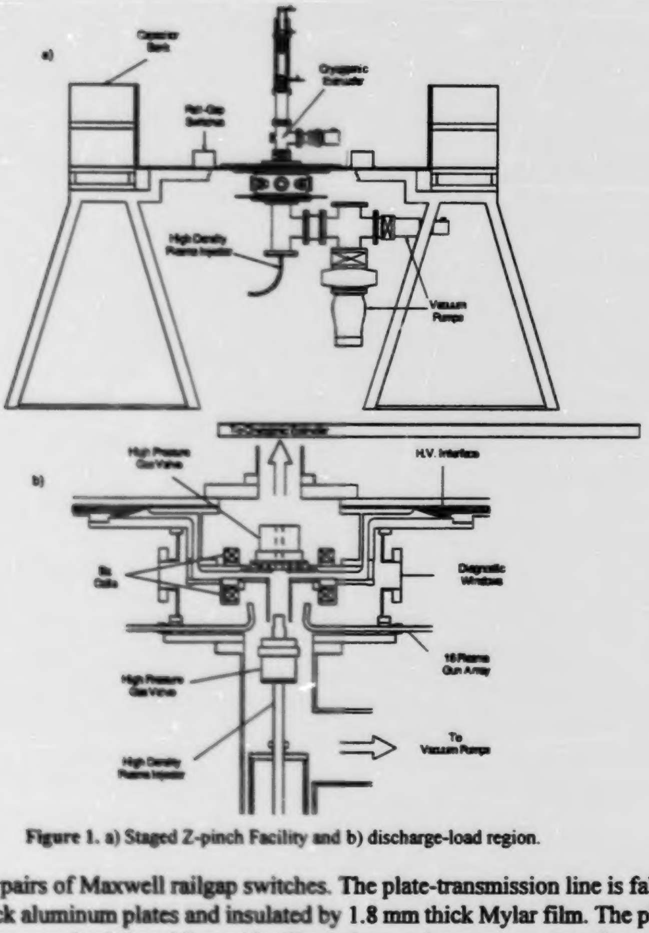
a)
Capacitor Bank
Rail-Gap Switches
Cryogenic
High Density Plasma Injector
Vacuum Pumps
b)
High Pressure Gas Valve
H.V. Interface
Bz Coils
Diagnostic Windows
16 Plasma Gun Array
High Pressure Gas Valve
To Vacuum Pumps
High Density Plasma Injector

Figure 1. a) Staged Z-pinch Facility and b) discharge-load region.

switched by two pairs of Maxwell railgap switches. The plate-transmission line is fabricated from 6.4 mm thick aluminum plates and insulated by 1.8 mm thick Mylar film. The plate line is 1.25 m long (between banks) and 2 m wide. The polypropelene vacuum interface provides an 0.11 m long vacuum path-length between H.V. electrodes; the anode-cathode (pinch) gap is 15 mm. The total-circuit inductance is 28 nH and the short-circuit current is 2 MA with a 1.8 μs quarter-period risetime. Vacuum is maintained by a 0.254 m diameter cryopump and a 0.15 m diameter liquid-nitrogen-baffled oil-diffusion pump; base vacuum is 1×10^{-4} Pa.

The pinch-discharge load-region is illustrated in Fig. 1*b*. The pinch is a multishell configuration, consisting of a 0.10 m diameter low-density hydro-carbon plasma imploding onto a 0.04 m diameter gas annulus and target plasma. Two Helmholtz field coils inject a DC, axial-magnetic field in the discharge-load region prior to energizing the pinch ($B_Z \leq 0.005T$).

The gas-shell load mass is injected by a two-stage, high-pressure gas valve ($P \geq 6.8 \times 10^6$ Pa) and annular-nozzle (0.05 m diameter, 200 μm throat) that are integrated into the cathode electrode. The gas-injection system was characterized by piezoelectric probes to measure the flow-rate. The profile was imaged using a electron-beam scattering diagnostic to generate a time resolved $r - z$ profile of the gas-jet [2]. The nominal flow characteristics for argon are: risetime 60–80 μs, gas-exit velocity ~800 m/s, Mach number 4.5, and mass-per-unit

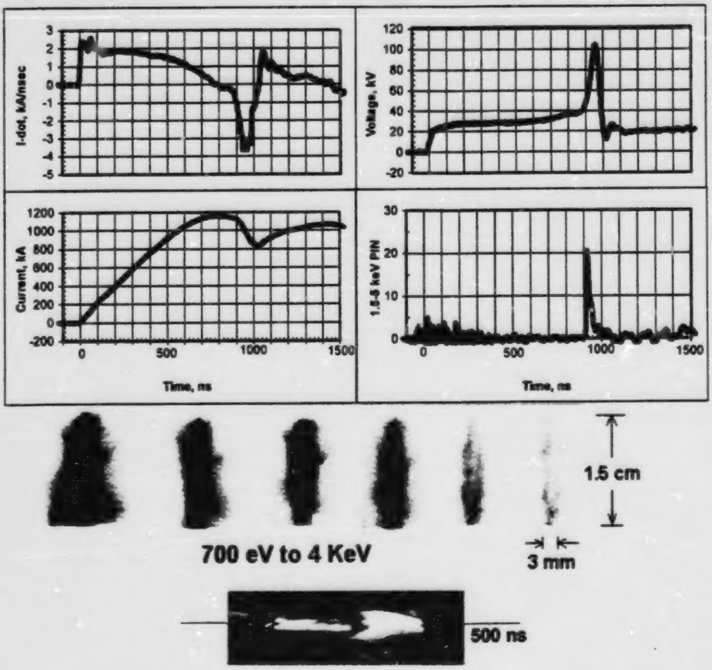

Figure 2. dI/dt, I, V, 1.5-5 keV PIN, 0.7 - 4 keV pinhole, streak images for Ne.

length ~10^{-6} kg/m, 100 μs after injection.

The low-density plasma, injected outside the annular-gas shell, effects a rapid-transfer of current to, and preionization of, the gas shell near peak current. Current coupling occurs by a "dynamic snowplow" of the low-density hydro-carbon plasma onto the load-gas shell [3]. The plasma is injected by semi-rigid, coaxial-cable "flashover" guns with nominal parameters, $T_e \sim 1$ eV and $n_e \sim 10^{22}$ m^{-3}. Z-pinch diagnostics include: current and voltage probes, Ross-filtered PIN diode array, multichannel x-ray pinhole camera, x-ray crystal spectrometer (KAP and LiF crystals), optical-framing and laser-backlit streak-camera imaging, liquid-scintillator neutron time-of-flight detectors, and neutron foil-activation (analyzed by a 0.20 m^2 active area EG&G drifted Germanium detector). An aluminum K-shell x-ray backlighter [4] and N_2 laser-interferometer [5] are used to characterize exploded-fiber targets on a separate test stand.

Pinch experiments involve a bank energy of 35 kJ. Figure 2 displays current, voltage, and x-ray PIN waveforms for a multi-shell neon pinch, and no target plasma. At approximately 750 ns there is a slight dip in the I-dot signal, indicating contact between the low-density plasma and the neon-gas shell as the current attains a peak value of 1.2 MA. The neon-gas shell implodes during the next 200 ns, generating 30 ns wide, broad-band (0.5–5 keV) x-ray pulses; only the 1.5–5 keV signal is shown here. Our experiments primarily involve neon, which provides a simpler-emission spectra and is easier to image than Kr for the parameters of our machine.

Time-integrated, x-ray pinhole images are displayed at the bottom of the Fig. 2, where the average filtered-photon energy of the image increases from left-to-right in the range,

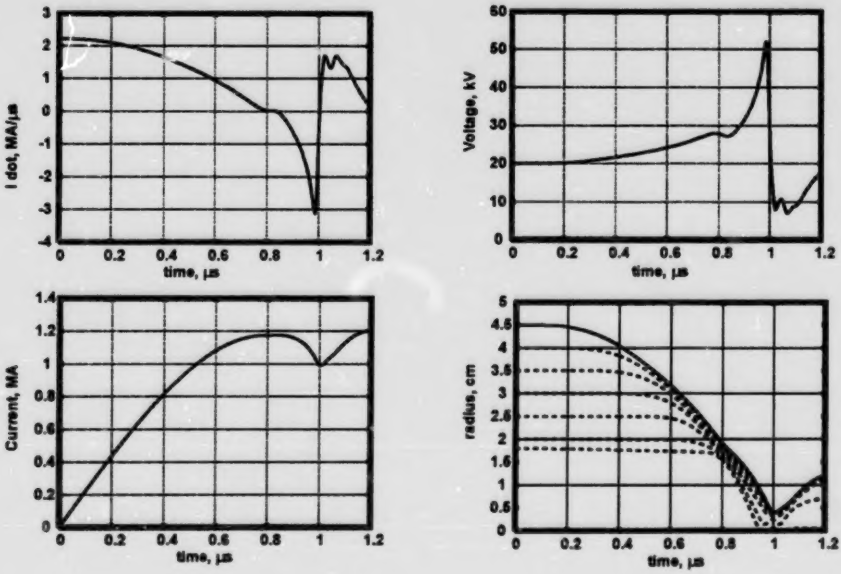

Figure 3. 1-D calculations for the actual parameters of Fig. 2.

0.7–4 keV. Of particular significance is the axially uniform, and slightly hollow neon pinch at higher-filtration energy, due to the presence of a trapped, axial-magnetic field. Optical streak images of the Z-pinch confirm that the pinch remains hollow during most of the implosion. From these data we estimate the following peak-implosion parameters: 0.3–0.4 m/µs implosion velocity, 10^{26} m^{-3} density, and 500 eV temperature, with a K-shell yield of the order of a kJ.

A modified version of the LLNL (Lawrence Livermore National Laboratory) TRAC2 code was used to compute wave forms [6] for the preceding load configuration and lumped-circuit parameters; the results are displayed in Fig. 3, where the outer shell is assumed to be, $1.66 \times 10^{23} m^{-3}$ density and 1 eV temperature, and the neon-plasma shell, $2.5 \times 10^{23} m^{-3}$ density and 0.2 eV temperature. The close match between the computed wave forms and the data instills confidence in the predictions of the TRAC2 code.

The cryogenic-fiber extruder [7] utilizes a closed-cycle, liquid-helium refrigerator and has been used to successfully extrude 100 µm diameter, 0.38 m long fibers of hydrogen, deuterium and neon; length-limited by the vacuum-chamber. Freely-hanging fibers sublimate in vacuum for up to 20 min. A fiber-guiding system was also tested to co-axially position the fiber within a 0.002 m diameter, inside the pinch.

Preionization of a 100 µm diameter D_2 cryogenic fiber requires a coupled-input energy of the order of one Joule, and precise timing to limit the radial expansion of the fiber prior to pinch initiation. On a separate vacuum-test stand we are evaluating fiber-preionization techniques using 25 to 100 µm diameter dielectric (polyethylene) and metallic fibers. The preionization pulse is provided by a compact Marx generator that has an adjustable output in the range: $E_o < 2$ kJ, $I_{peak} = 15 - 45$ kA and $V_o = 20 - 40$ kV with a $\tau_{1/4} = 0.65$ µs. The fiber expansion is time and space resolved using a 337 nm, 0.5 ns, TEA N_2 laser interferometer and a 30 ns pulsewidth, 0.5 J, aluminum K-shell, x-ray backlighter.

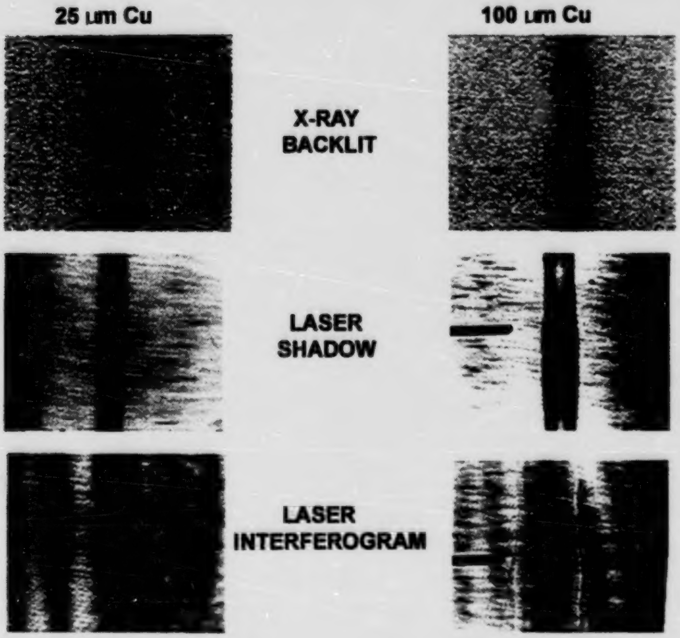

Figure 4. Laser shadow, interferogram, and x-ray radiography images for a 25 μm diameter and 100 μm diameter copper fiber; $E_{input} \sim 10$ MJ/kg.

Figure 4 compares images for 25 and 100 μm diameter copper fibers energized by a 12 kA, 20 kV pulse. The input-energy was $E_{input} \sim 10$ MJ/kg for both fibers, (i.e., $E_{vaporization}$ for the solid) [8] and was adjusted by varying the image time relative to the discharge pulse. The electric-pulse timescale is sufficiently long to fully diffuse to the core of the fiber. The nitrogen laser is highly attenuated in the shadowgram and interferogram images for both fibers. Whereas, in the radiograph images the core of the fiber is absent for the 25 μm diameter fiber, but not for the 100 μm diameter fiber.

Thus, energy coupling to the fiber core is not observed, due to current channeling in the high-conductivity plasma that is ablated from the fiber during energy input. Varying the initial-fiber conductivity, using copper, iron, and aluminum-coated dielectric fibers, causes more energy to be channeled outside the fiber core for lower conductivity. Pulsed-energy coupling to a cryogenic fiber that is sublimating in vacuum is expected to be even more difficult and alternate approaches are under investigation.

ACKNOWLEDGMENTS

Thanks to Drs. E. Ruden, J. Degnan, and J. Bailey for their assistance with various equipment. This work was supported by U.S. DoE (Department of Energy), OFES (Office of Fusion Energy Secretariat) and in part by LANL (Los Alamos National Laboratory).

REFERENCES

1. H.U. Rahman, F.J. Wessel, and N. Rostoker. Phys. Rev. Lett. **74**, 714 (1995).
2. F.J. Wessel, V.M. Bystritskii, B. Moosman, N. Rostoker, Y. Song, T. Tierney, A. Van Drie, P. Ney, and H.U. Rahman. 10th Pulsed Power Conference. Albuquerque, NM, 1995. p. 112.
3. S.M. Goldberg, and A.L. Velikovich. AIP Conf. Proc. **299**, 1994.
4. B. Moosman. Ph.D. thesis, University of California Irvine. 1997.
5. B. Moosman, V.M. Bystritskii, C. Boswell, and F.J. Wessel. Rev. Sci. Inst. **67**, 1. (1995).
6. H.U. Rahman, P. Ney, B. Moosman, N. Rostoker, Y. Song, A. Van Drie, and F.J. Wessel. These Proceedings.
7. H.U. Rahman, E.L. Ruden, K.D. Strohmaier, F.J. Wessel, and G. Yur. Rev. Sci. Inst. **67**, 3533 (1996).
8. H. Knoepfel. Pulsed High Magnetic Fields. North Holland Pub. Co., London, (1970).

STUDY OF ICF-ENERGY CONVERSION SCHEMES WITH MAGNETIC FIELD IN A LASER-PRODUCED PLASMA — EXPERIMENTS AND PIC-SIMULATION

Yu.P. Zakharov, A.G. Ponomarenko, H. Nakashima[1] and Y. Nagamine[1]

Institute of Laser Physics
Novosibirsk 630090, Russia.
[1]Department of Energy Conversion Engineering,
Kyush University
6 -1 Kasuga-Kouen Kasuga, Fukuoka 816, Japan

Due to recent progress in ICF study carried out by "NOVA" [1] or another high- power lasers as well as in developing of related programs of ICF ignition at NIF, LMJ, "KONGOH" and other facilities now is opened a new possibility to realize rather old idea [2,3] of ICF application based on interaction of D-He^3 fusion plasma with various magnetic B-field systems. Such systems could provide the direct conversion of fusion energy into electrical [3–6] or mechanical [2,9] ones due to the diamagnetic effect, i.e. complete exclusion of the external magnetic field by the thermonuclear plasma cloud. Thereby in comparing with more traditional magnetic fusion systems (tokamak, stellarator, etc.), principally impulsive character of ICF-energy' releases in a form of expanding plasma cloud allows to use them by more simple and effective way at expense of its deceleration (probably without confinement) by external B-field. According to our idealized PIC2D-simulation [6,9], efficiency of such energy conversion both in uniform (by pickup coils) and magnetic mirror field (for rocket propulsion) can exceed 50%, but neglected effects of flute instabilities or Joule heating of plasma could essentially decrease it [10]. To study a real influence of those effects the experiments [5,7,10] at " KI-1" facility (Institute of Laser Physics) are carried out for the first time with Laser-produced Plasma Clouds (LPC) under conditions being enough close to future ICF ones in relation of the main similarity criteria of the problem (ion magnetization level, Alfven - Ma or Knudsen numbers, etc.). The results of such experiments with "usual" LPC in various B-fields are analyzed on the base of PIC/2D-model [6,9] and used for testing of up-grade 3D-model [12] in the frame of our ICF-collaboration program [13] as well as for providing of a "small-scale" experimental background for proposed testing of Laser Fusion Rocket' concept [9] at the National Ignition Facility [13].

a) Experimental Set-up and PIC-Simulation Method

The multi-purpose "KI-I" simulation facility [8] was initially designed to study a wide range of non-stationary processes in space plasmas and it includes a large-scale (φ 1.2m*5m), high-vacuum interaction chamber and system of CO_2-lasers with output energies $Qr \geq 1$ kJ

Current Trends in International Fusion Research – Proceedings of the Second Symposium
Edited by E. Panarella. NRC Research Press, National Research Council of Canada, Ottawa, ON K1A OR6, Canada. 1999.

for producing quasispherical LPC of a large mass ≥ 0.01 mg and energy Eo ~ 0.5 kJ need for ICF simulation (by two-sided and multi-staged irradiation of the spherical Nylon6 pellet). The chamber is supplied by sources of an axial uniform *B*- field up to 1 kG and internal dipole *B*-field as well (with moment M ≥ 10 MG*CM^3). There is also a quasi-stationary source of background plasma to fill a volume ~ 1m^3 of a chamber by highly-ionized density up to n^* ~ 10^{14} cm^{-3} . To calculate the ICF-plasma [12] a 3D hybrid code [16], which treats ions as a particle and electrons as inertialess fluid. The Darwin limit or non-radiative Maxwell equations are solved for electromagnetic field calculation.

b) Results on Simulation of ICF-Plasma Dynamics in Magnetic Fields

Within the scope of LPC-experiments related to discussed ICF-problems we study the following items:

a) diamagnetic cavity formation, non-MHD flute instability development and suppression , across-*B* deceleration and along-*B* field motion of plasma cloud in the uniform *B*-field [7,10];
- interaction [8] of such cloud with ionized magnetized background for ICF system with the first wall protection by gas medium [4];
- dynamics [14] and effective recoil momentum of plasma cloud expanding in the "magnetic nozzle field" under conditions of the Laser Fusion Rocket [9,12,13].

Due to simulation of ICF-processes in such LPC-experiments and by PIC-calculation as well we have obtained the next results. It was established for the first time that in vacuum magnetic field, under condition of high-level ion magnetization $Lb \leq 0.5 - 1$ (= Larmor/radius of plasma deceleration) LPC or ICF plasmas could really decelerate by uniform *B*-field [7] and create a cavity which size is corresponding to the theoretical one [6] and therefore they are enable to convert a main part of their kinetic energy Eo into electrical one [5,6,11]. Since during such interaction a lot of plasma could reach to first wall of a target chamber (due to development [7,10] of flute instability) we test a method [10] of its protection by neutral gas (via flutes suppression) and taking into account X-ray-ionization of gas in a real ICF-system [4], we had studied [8] a possibility of LPC interaction with background plasma via curl electrical field' mechanism (insensate to $Ma \geq 1$ at $L \leq 1$). As a result of a new class LPC experiments [8,14,15] on the plasma expansion in non-uniform (dipole) *B*-field we have obtained the confirmation of calculations [9,12,13] that under condition of Laser Fusion Rocket with diamagnetically expanding plasma (with $Lb \leq 1$ and Eo ~ M^2/R^3 near the pole of dipole, at distance *R* from its center) LPC could escape field in a form of quasi-directed plasma flow having average velocity comparable with initial (non-directed) one. All this experimental data and corresponding PIC-simulation' results prove that future ICF based power station or rocket propulsions could be very perspective indeed and that our common approach (**LPC+P1C**) is rather productive for development of their design [5,6,9–13].

REFERENCES

1. J. Lindl. Prepr. LLNL, UCRL-JC-I 19015/L-19821-1 (1995), p. 140.
2. R. Hyde, L. Wood and J. Nuckolls. AIAA Paper N 72-1063 (1972), p. 15.
3. G.H. Miley. Fusion Energy Conversion (ANS: Hinsdale, IL 1976).
4. I.O. Bohachevsky et al. Nucl.Tech. Fusion **1**, 390 (1981).
5. Yu.P. Zakharov et al. Soviet Fusion Research News **1**(43), 10 (1987) - In Russian.
6. H. Nakashima et al. Fusion Eng.and Design **15**, 255 (1992).
7. Yu.P. Zakharov et al. Sov. J. Plasma Phys. **12**, 674 (1986).
8. Yu.P. Zakharov et al. In "Laser Interaction and Related Plasma Phenomena" (AIP Conf.

Proc. N.Y. 1996), 369, Pt. I, 347.
9. H. Nakashima et al. Ibid. Pt. II, 117.
10. Yu.P. Zakharov et al. Proceed. of 1996 Intern. Conf. on Plasma Physics (Nagoya, 1996), **2**, 1674 (1997).
11. Ibid. **2**, 1670 (1997).
12. Y. Nagamine et al. Ibid. Paper 12C 15, p. 4.
13. H. Nakashima et al. Proceed. of IAEA Techn. Meet. on "Drivers and Ignition Facilities for Inertial Fusion" (Osaka, 1997) p. 4.
14. I.F. Shaikhislamov et al. Journ. Appl. Mech. and Techn. Phys. **36**, N6 (1995).
15. S.A. Nikitin and A.G. Ponomarenko. Ibid. **34**, 745 (1993).
16. J.E. Horowitz et al. J. Comput. Phys. **84**, 279 (1989).

THE COLLIDING BEAM FUSION REACTOR I. SOLUTION TO THE PROBLEM OF ANOMALOUS TRANSPORT WITH BEAMS IN A FIELD REVERSED CONFIGURATION PLASMA

N. Rostoker, M.W. Binderbauer and H.J. Monkhorst[1]

University of California, Irvine, CA 92697, U.S.A.
[1]University of Florida, Gainesville, FL 32611, U.S.A.

ABSTRACT

In this paper aspects of conceptual reactor designs are investigated that are based on the FRC configuration for D-T, D-He^3, and p-B^{11} reactions. The fuel ions are of sufficient energy that the orbit size is large enough so that classical transport should prevail in the absence of long wavelength instabilities.

We begin by reviewing briefly some evidence for classical confinement in such a system. Next we address the key issue of current maintenance by injecting beams of neutral atoms into an FRC. Although there are many theoretical papers on this subject, there are no experiments. Our investigation of this issue starts with a discussion of FRC experiments, the current carried by ions and the decay of current due to Coulomb interactions of electrons and ions. We then consider periodic pulses of injected neutrals in order to maintain a steady state ion current in the FRC. The injected neutrals constitute a source of ions and electrons and for a steady state there must be a sink. For a burning plasma the dominant sink is the fusion reactions.

We have previously shown that the sources and sinks of a burning plasma dominate the equilibrium distributions [1]; i.e. the equilibrium is quite different from the self-consistent solution of the Vlasov-Maxwell equations without fusion reactions. In this paper we illustrate some of the changes in the kinetic description of a burning plasma due to the inclusion of sources and sinks. For example the electrons are injected at relatively low energy. Electrons leave along with fusion product ions in a steady state. The electrons leave after being heated and this constitutes a significant heat transfer mechanism that can be more important than radiation. Source and sink modifications to previous reactor kinetic calculations are included to arrive at quantitative estimates for key operating parameters.

Current Trends in International Fusion Research — Proceedings of the Second Symposium
Edited by E. Panarella. NRC Research Press, National Research Council of Canada, Ottawa, ON K1A 0R6, Canada. 1999.

1. MOTIVATION: CLASSICAL CONFINEMENT OF IONS

A plasma consisting of large orbit non-adiabatic ions and adiabatic electrons is considered. Experimental evidence with energetic beams injected into Tokamaks for heating in DIII-D and TFTR and with energetic fusion products in JET indicates that such a plasma does not suffer from the anomalous transport characteristics usually observed in fusion devices. In fact the diffusion of these large orbit ions is consistent with classical estimates while at the same time the thermal population diffuses anomalously. In addition to Tokamak experiments numerical simulations support the fact that large orbit particles feel predominantly low frequency field fluctuations with wavelengths that exceed the Larmor radius. The physical reason for this is that ions, over the course of such a large orbit, average the fluctuations so that only long wavelengths (compared to gyro-radius) and small frequencies (compared to gyro-frequency) cause transport. Thus if the particle orbit radius is large and the plasma has gross stability at long wavelengths, anomalous transport can in principle be avoided.

Such classical diffusion would result in a much smaller reactor. An estimate of the reduction in size can readily be obtained by comparing classical diffusion with Bohm diffusion:

where D_B and D_C are the Bohm and classical diffusion coefficients, respectively; Ω_e is the electron cyclotron frequency, τ_{ei} is the electron-ion collision time, B is the magnetic field in kG, T_e the electron temperature in keV and n the density in cm^{-3}. For typical numerical data of $n \sim 10^{15}$cm^{-3}, $T_e \sim 100$ keV and $B \sim 100$ kG, $D_B \sim 10^8 D_C$. The magnitude of the anomalous diffusion coefficient in current Tokamaks is of the order $D_B/1000$ so that classical diffusion involves a further reduction of 10^5 which corresponds to a reduction in the smallest linear scale from meters to centimeters.

2. CONCEPTUAL REACTOR DESIGN

The basis of the design for the reactor discussed here is a modified FRC as described by Rostoker *et al* [2]. The modification to the usual FRC lies in the fact that almost all the ions are considered to be non-adiabatic and to possess high coherent energy and, thus, large orbits (for typical data the worst case fuel ion orbit size is on the order of 1 cm – slightly larger than the minimum orbit size of the classically diffusing particles in the previously mentioned tokamak experiments). With this alteration the system can essentially be thought of as an ion beam confined to an annular region encircling the axis of symmetry. The electrons are thermal and as such respond also to short wavelength turbulence. However, their loss is limited by positive charge accumulation in the plasma. A nice feature of the FRC configuration is that the plasma is surrounded by a natural divertor, i.e., the region of near vacuum between the walls and the plasma exhibits an open magnetic field line topology – allowing particles that reach this region to scatter and leave along the field lines much faster than it would take to diffuse across. A schematic of the model is depicted in Fig. 1.

3. CURRENT MAINTENANCE

A key issue of whether the envisioned reactor can sustain a steady state equilibrium is current drive and current maintenance by injecting beams of neutral atoms into the FRC system. Although there are many theoretical papers on this subject, there are no experiments for the type of closed magnetic topology setup discussed here. This section is intended to

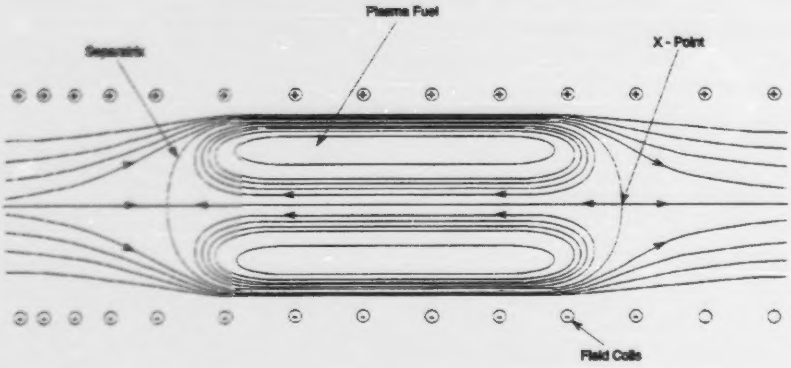

Figure 1. Computer model of the flux surfaces in 2 dimensions. The beam is confined by the self-field. Separatrix and X-points are clearly visible. Outside the separatrix there are open field lines.

illustrate the problems and indicate some possible solutions.

3.1 Creation of FRC and Origin of Ion Current

Typically an FRC is formed by the inductive or θ-pinch method which preferentially heats ions by compression. After the compression the current is carried by electrons and the ions have zero net drift velocity and a temperature of about 500 eV. After reconnection there is a radial magnetic field at the ends which is focusing for ions that rotate in the diamagnetic direction and defocusing for those that rotate in the opposite direction. This leads to selective confinement of the ions and causes about half of them to escape along with an adequate number of electrons. The resultant net ion current causes electrons to be collisionally accelerated towards zero net drift – in this period the ion velocity changes are negligible compared to those of the electrons. Thus the total current changes little but the electron current decreases until at the end of this "formation phase" the current is carried about equally by ions and electrons.

3.2 Lifetime of FRC and Current Decay

After the FRC is established as described in the previous section, the lifetime is determined by the decay of the current. In typical experiments carried out at LANL [3] the parameters of the produced pure hydrogen plasma are $n_i = n_e \approx 5\times10^{15}\ \mathrm{cm}^{-3}$, $T_e \approx 100$ eV and $T_i \approx 500$ eV. The ratio of plasma scale to ion orbital radius is on the order of 2 and about half the current is carried by ions. The observed lifetime is between 100 to 500 μsec.

To see whether these numbers are in agreement with classical predictions, we assume that the current decay is due to coulomb collisions between electrons and ions. For the initial conditions given by the LANL data we find that the electron-ion and ion-electron momentum exchange times are, respectively, $t_{ei} \approx 4$ nsec and $t_{ie} \approx 7\mu\sec$. Recasting the conservation of energy during this process in the form of a circuit equation gives

$$\left(L+L_I\right)\frac{dI}{dt}+IR=0$$

where, respectively, $L \approx 2\pi^2 r_o^2 / c^2$, $L_I = (2\pi r_o)^2 m m_i / N_e e^2 (m + m_i)$ and $R = (2\pi r_o)^2 m / N_e e^2 t_{ei}$ are the inductance/unit length of the ring, the inertial inductance/unit length ($L_I << L$), and the plasma resistance/unit length. N_e is the line density of electrons and r_o the radius of peak density. From the time scales given by t_{ei} and t_{ie} we can see that the current decay is mainly due to an increase in the average azimuthal electron velocity, $V_{e\theta}$ i.e., $dI / dt = -(eN_e / 2\pi r_o) dV_{e\theta} / dt$.
The decay time of the current is, thus, given by

$$\tau \cong \frac{L + L_I}{R} \cong \frac{1}{4} \frac{r_o \Delta r}{(c / \omega_{pe})^2} t_{ei} \cong 300 \mu\,\text{sec}.$$

$N_e = 2\pi r_o \Delta r n_e$ and $\omega_{pe}^2 = 4\pi n_e e^2 / m$. This time is much greater than the momentum exchange time t_{ei} because of the large inductance. Its value is within the range given by the LANL measurements. For large density values (on order of 10^{16} cm^{-3}) classical diffusion theory is also consistent with the observed particle confinement time as reported by Aso *et al* [4].

3.3 Current Neutralization Issues

The main question for current maintenance is fast current neutralization of a beam. The time scale for this would be much shorter than neutralization by collisions. When a beam is injected into a plasma with axial symmetry the initial current increase induces an electric field E_θ which makes electrons drift in the radial direction $V_r = cE_\theta / B_z$. This electron drift perturbs the charge density causing a radial electric field in response to E_θ. The radial electric field then produces a drift $V_\theta = cE_r / B_z$ of electrons which neutralizes the current of the beam. This can take place on a fast time scale described by the Vlasov-Maxwell equations. If the magnetic field has open field lines, electrons can move along the field lines and prevent the development of E_r. In this case current neutralization is due to Coulomb collisions and the time scale is L / R. If the magnetic field involves closed field lines and axial symmetry prevails it is predicted that fast current neutralization can take place [5]. It is also predicted that it can be prevented by breaking the axial symmetry for example with the addition of a weak quadrupole field. It can also be prevented by instabilities [6]. There are no experiments in which a beam of neutrals or a neutralized ion beam is injected into an FRC. It is a fact that fast current neutralization does not take place in an FRC. However, an FRC usually does have a weak quadrupole field. It does not seem likely that a complete answer to the questions of current neutralization in an FRC can be attained without some new experiments. For the present investigation, we assume that fast neutralization cannot take place although this may involve breaking the symmetry.

3.4 Current Maintenance by Neutral Beam Pulses

We consider the injection of pulsed beams as illustrated in Fig. 2. They may be pulsed neutral beams or neutralized beams with a pulse duration $\Delta t << t_{ei}$. The injected electrons

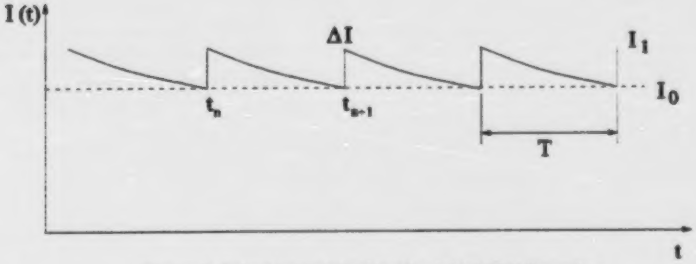

Figure 2. Pulsed beam injection after initial FRC formation.

have a negligible energy and do not speed up during Δt while the ion velocity changes. From $t = t_n + \Delta t$ until $t = t_n + T$ the current decays as previously discussed; the change in ion velocity $V_{i\theta}$ is negligible and although $V_{e\theta}$ changes significantly the energy $N_e m V_{e\theta}^2/2$ is negligible. Therefore, from energy conservation

$$\frac{1}{2}LI^2\Big|_{t_n+\Delta t}^{t_n+T} = -\int_{t_n+\Delta t}^{t_n+T} I^2 R\,dt,$$

i.e., the dissipated energy comes from the stored magnetic field energy. Thus, the injected beam has to have sufficient energy to also resupply the loss in stored magnetic energy (the beam loses this energy due to the inductive electric field after trapping). A steady periodic state can, therefore, be maintained by injecting and trapping ΔN_i particles (particle losses due to diffusion out to the separatrix and due to fusion reactions must be balanced with $\Delta N_i/T$) with a proper choice of $V'_{i\theta}$ (determined by the dissipation $I_o^2 RT$) such that

$$\sum_i \tfrac{1}{2}\Delta N_i m_i\left[(V'_{i\theta})^2 - V_{i\theta}^2\right] = \tfrac{1}{2}L\left[I^2 - (I-\Delta I)^2\right] \cong I_0^2 RT$$

4. SINK ISSUES

In order to describe the injection and trapping of particle beams as well as fusion reactions and diffusion, it is necessary to add sources and sinks to the Vlasov/Fokker-Planck equation:

$$\frac{\partial f}{\partial t} + v\cdot\frac{\partial f_i}{\partial x} + \frac{e_i}{m_i}\left(E + \frac{1}{c}v\times B\right)\cdot\frac{\partial f_i}{\partial v} = \frac{\partial}{\partial v}\langle\Delta v\rangle_i f_i + \frac{1}{2}\frac{\partial}{\partial v}\cdot\frac{\partial}{\partial v}\langle\Delta v\Delta v\rangle_i f_i + Q_i - S_i$$

Q_i is the source due to beam injection; S_i is the sink. In the last section we discussed the injection source and its role in maintaining the equilibrium. In this section we show an example of the strong effect sinks have on the plasma kinetic equations and in particular on the determination of ion and electron temperatures.

Consider for instance the electron temperature. Electrons are injected along with the fuel beams and enter the plasma with negligible energy and temperature. With each fusion reaction two fusion fuel ions disappear; they are replaced by fusion products which leave the plasma if there is to be a steady state. To maintain charge neutrality $Z_1 + Z_2$ electrons must also leave. Since there is a potential barrier (the plasma is positively charged in equilibrium) only the high energy electrons can escape. They expend energy to get over the barrier, but get it back after they leave the plasma completely along the open field lines. To escape the electrons must go over a potential barrier of height T_e/e. The average energy of particles that leave is

$$T_e + \frac{\int_c^{\infty} \frac{1}{2} m v^2 f_e(v) dv}{\int_c^{\infty} f_e(v) dv} \cong 5T_e,$$

where $f_e(v)$ is a one dimensional Maxwell distribution. Thus a sink in the form of a cooling term must be added to the Fokker-Planck equation which is of the form

$$-5T_e \sum_j \frac{N_j Z_j}{t_{Fj}}.$$

This cooling term may be more important than the Bremsstrahlung because it is proportional to T_e rather than $T_e^{1/2}$. Similarly there are cooling terms for the fuel ion beams if the temperatures of the beams at injection are less than the steady state temperatures. Although the cooling term above helps to reduce electron temperature and therefore Bremsstrahlung it does represent an energy loss. However, the electron energy can be recovered with high efficiency whereas Bremsstrahlung can only be recovered with an efficiency of at most 40%.

5. MODES OF OPERATION

We consider fuel systems with two types of ions of mass m_1, m_2 and atomic number $Z_1 = 1$ and $Z_2 > 1$ such as D-T, D-He^3 and p-B^{11}. The fusion cross section for each case has a resonance. The reactivity $\langle \sigma v \rangle$ can be calculated by

$$\langle \sigma v \rangle = \int dv_1 dv_2 F_1(v_1) F_2(v_2) |v_1 - v_2| \sigma(| v_1 - v_2 |)$$

where

$$F_i(v_i) = \left(\frac{m_i}{2\pi T_i}\right)^{3/2} \exp\left[-\left(\frac{m_i}{2T_i}\right)(v_i - V_i)^2\right].$$

In the first mode of operation $V_1 = V_2$ and $T_1 = T_2$. The distribution functions are thermal in a moving frame of reference. The thermal reactivities designated in Fig. 3 are applicable and are no better than a purely thermal reactor. V_1 and V_2 are large enough to avoid anomalous diffusion but as small as possible consistent with this to minimize the circulating power. The injection energy $\frac{1}{2} m_1 V_1^2 + \frac{1}{2} m_2 V_2^2$ is the price to be paid for avoiding anomalous diffusion.

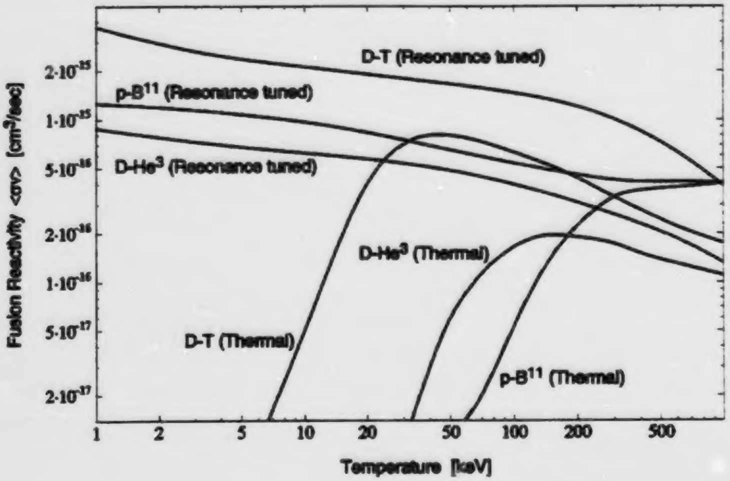

Figure 3. Reactivities for various fusion reactions.

The advantages of this mode are that both fuel ions are in thermal equilibrium (ion-ion collisions assure this but do not contribute to transport), that there is no anomalous transport and that current drive is accomplished. In this paper we will only give examples for this mode since we are still in the process of evaluating the second mode discussed below.

The second mode of operation involves $V_1 \neq V_2$ and $\frac{1}{2}m_1(V_1 - V_2)^2 = \varepsilon_R$ the resonant energy. The temperatures of the beams should be as low as possible to enhance the reactivity as illustrated in Fig. 3. In this case the steady state electron velocity would be $V_e = (n_1V_1 + n_2Z_2^2V_2)/(n_1 + n_2Z_2^2)$ where n_1, n_2 are fuel ion densities. The steady state current is the Ohkawa current

$$j_\theta = \frac{en_1n_2}{n_1 + n_2Z_2^2}\left(Z_2^2 - Z_2\right)\left(V_1 - V_2\right)$$

Provided that V_1 and V_2 can be maintained this takes care of current drive. If $Z_2 = 1$ as it is for D-T reactions $j_\theta = 0$. However, current could possibly be maintained considering the net current of the α-particles produced by fusion which would be selectively confined in an FRC. The reactivity enhancement depends on the beam temperature. It is significant for D-He^3 at $T_1 = T_2 \approx 100$ keV. The price to be paid is in the additional input energy of the fuel ions in order to maintain V_1 and V_2. Additional problems arise because of the requirement of low beam temperatures to take advantage of the resonance.

6. SAMPLE DATA

In this section we would like to summarize the results of a systematic treatment of all aspects of reactor kinetics for D-T (shown in Table 1), D-He^3 (shown in Table 2) and p-B^{11} (shown in Table 3) fuel cycles for a reactor operating in the first mode. The calculations are

Table 1. D-T Reactor Parameters

$n_e = 10^{15}$ cm^3		$n_1 = n_2 = .5\times 10^{15}$ cm^{-3}
$\frac{1}{2}m_1V_1^2 = 200$ keV		$\frac{1}{2}m_2V_2^2 = 300$ keV
$\tau_{F1} = 1/n_2\,\langle\sigma v\rangle = 25$ sec		$\tau_{F2} = 1/n_1\,\langle\sigma v\rangle = 25$ sec
$\langle\sigma v\rangle 8\times 10^{-16}$ cm^3/sec		$\varepsilon_F = 18$ MeV
$T_e = 100$ keV		$T_i = 96$ keV
$P_N = 576$ W/cm^3	$P_S = 173$ W/cm^3	$P_C = 55$ W/cm^3
$\eta_A = .8$	$\eta_B = .4$	$\eta_N = .4$
$Q = 86$	$Q' = 18$	$Q_o = 2.27$

Table 2. D-He^3 Reactor Parameters

$n_e = 10^{15}$ cm^3		$n_1 = n_2 = \frac{1}{3}\times 10^{15}$ cm^{-3}
$\frac{1}{2}m\,V^2 = 200$ keV		$\frac{1}{2}m_1V_1^2 = 300$ keV
$\tau_{F1} = 1/n_2\,\langle\sigma v\rangle = 15$ sec		$\tau_{F2} = 1/n_1\,\langle\sigma v\rangle = 15$ sec
$\langle\sigma v\rangle 2\times 10^{-16}$ cm^3/sec		$\varepsilon_F = 18.4$ MeV
$T_e = 185$ keV		$T_i = 217$ keV
$P_N = 64.5$ W/cm^3	$P_S = 36.6$ W/cm^3	$P_C = 32.5$ W/cm^3
$\eta_A = .8$	$\eta_B = .4$	$\eta_N = .9$
$Q = 2.65$	$Q' = 3.03$	$Q_o = .958$

based on the power flow schematic illustrated in Fig. 4.

The figures of merit are $Q = P_N / P_B$ and $Q' = P_N / P_I$ where P_I is the input power. Q indicates the Bremsstrahlung power which can only be recovered with a rather low efficiency. Q' indicates the input power that is related to the circulating power. Q_o is the minimum value of Q for net power $P_S > 0$. For D-T reactions $Q' = 18$ and $Q = 86$. The difference is due to the loss of energetic electrons described by the cooling term of the previous section. This energy loss reduces the temperature and therefore the Bremsstrahlung.

Table 3. p-B^{11} Reactor Parameters

$n_e = 10^{15}$ cm^3	n_1=.5×10^{15}cm^{-3}	$n_2 = 10^{14}$cm^{-3}
$\frac{1}{2}m_1V_1^2$ =50 keV		$\frac{1}{2}m_2V_2^2$ =550 keV
$\tau_{F1} = 1/n_2 \langle\sigma v\rangle = 25$ sec		$\tau_{F2} = 1/n_1 \langle\sigma v\rangle = 5$ sec
$\langle\sigma v\rangle 4\times10^{-16}$ cm^3/sec		$\varepsilon_F = 8.68$ MeV
$T_e = 125$ keV		$T_i = 234$ keV
$P_N = 27.9$ W/cm^3	$P_S = 2.2$ W/cm^3	$P_C = 34.1$ W/cm^3
$\eta_A = .8$	$\eta_B = .4$	$\eta_N = .9$
$Q = 1.07$	$Q \doteq .794$	$Q_0 = .97$

The reduced temperature increases $P_I = I^2R = \Sigma_{i=1,2}n_im_i(V_i - V_e)^2/t_{ie}$. The energy of these energetic electrons can be recovered with high efficiency. For the D-T reaction Q' and Q are quite adequate for a reactor. However, only about 30% of the nuclear power is for sale – indicative of the low efficiency in converting the neutrons. Apart from this the energetic neutrons are the cause of a variety of other problems.

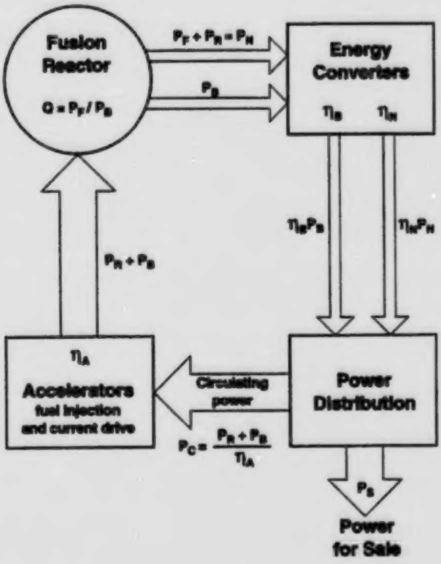
Fusion Reactor
$Q = P_F / P_B$
$P_F + P_R = P_N$
P_B
Energy Converters
η_B η_N
$\eta_B P_B$
$\eta_N P_N$
$P_R + P_B$
η_A
Accelerators
fuel injection
and current drive
Circulating power
$P_C = \frac{P_R + P_B}{\eta_A}$
Power Distribution
P_S
Power for Sale

Figure 4. Power flow schematic

For the D-He^3 reaction $Q = 2.65$ and $Q' = 3.03$. The electron cooling term is less important than Bremsstrahlung because of the low fusion reactivity and the heating from high energy protons is important. The relatively high temperature reduces the input P_I so that $Q' > Q$. The values of Q' and Q are much less for D-He^3 than for D-T because $\langle \sigma v \rangle$ is less by a factor of 4. Also Coulomb scattering and Bremsstrahlung increase because He^3 has $Z = 2$. However, considering the higher efficiency of energy conversion of 14 MeV protons compared with 14 MeV neutrons and the other problems with neutrons the values of Q' and Q may be adequate for a reactor. This is illustrated by the fact that more than half of the nuclear power is available for sale.

For the p-B^{11} reaction $Q = 1.07$ and $Q' = .794$. In this case the electron cooling is significant and fusion product heating is less important than it is for D-He^3, which accounts for the fact that $Q' < Q$. The electron cooling is enhanced by the fact that $Z = 5$ for Boron so that with each fusion reaction, 3 α-particles must escape confinement along with 6 electrons. The fact that $Z = 5$ for Boron is also important for Coulomb scattering and Bremsstrahlung and it is the fundamental reason for the low values of Q and Q'. For this reaction there would be a net power for sale, but it is too small for a reactor, and the circulating power is too large.

In the resonant mode the reactivity could be increased by a factor of about 2 if the beam temperatures are below about 100 keV. With spin polarization [7] of the fuel another factor of 1.6 could be anticipated. One or both of these innovations may be required for a practical reactor.

7. SUMMARY

The purpose of the ion beams is two fold: to provide the current to sustain the equilibrium; to avoid anomalous diffusion of ions by endowing most of the ions with a sufficiently large gyro-radius.

The latter objective is met by using an FRC for magnetic confinement which is a very high β device which implies a relatively small internal magnetic field. In addition ions are accelerated outside of the device to a high energy (100's of keV). The choice of energy (e.g. 200 keV and 300 keV for D-T and D-He^3) is not a well defined choice because the ion orbit size to avoid anomalous transport has not been quantified. The cost of avoiding anomalous transport is in the ion input energy and consequently in the input power P_I. There has been a controversy in the fusion community about whether or not a beam of neutrals injected into a plasma produces a current because of various processes that make electrons catch up to ions and the general theorem known as Lenz's law. For a plasma with open field lines there is little disagreement and there are supporting experiments. For a plasma with closed field lines (i.e., an FRC) there are no experiments. We have analyzed this problem in some detail and concluded that a repetitively pulsed beam will drive current.

We have developed a systematic theory of reactor kinetics that includes the sources and sinks of a burning plasma. We have previously shown that the sources and sinks are quite important in the determination of the equilibrium. In this paper we have presented the results of reactor kinetic calculations and illustrated the importance of sources and sinks in D-T, D-He^3 and p-B^{11} reactions for a mode of operation that can be described as thermal in a moving frame of reference. A mode of operation that takes advantage of the resonance in the fusion cross section has been suggested and the possible gains indicated.

ACKNOWLEDGMENTS

This work was supported by the Office of Naval Research under contract N00014-96-1-1188.

REFERENCES

1. N. Rostoker, M.W. Binderbauer and H.J. Monkhorst. Science **278**, 1419 (1997).
2. N. Rostoker et al. Phys. Rev. Lett. **70**, 1818 (1993).
3. M. Tuszewski. Nucl. Fusion **28**, 2023 (1988).
4. Y. Aso, S. Himeno and K. Hirano. Nucl. Fusion **23**, 751 (1983).
5. H. Berk, H. Momota and T. Tajima. Phys. Fluids **30**, 3548 (1987); J.H. Hammer and H. Berk. Nucl. Fusion **22**, 89 (1982).
6. A. Reimann and R.N. Sudan. Comm. Plasma Phys. and Controlled Fusion **5**, 167 (1979).
7. H.J. Monkhorst et al. this conference.

AN OVERVIEW OF REVERSED-FIELD PINCH RESEARCH

D.A. Baker and J.A. Phillips

Los Alamos National Laboratory
Los Alamos, New Mexico 87545, U.S.A.

ABSTRACT

The reversed-field pinch RFP concept has an extensive history evolving from the fast z-pinches in the early fifties to the present. The tokamak relies on a high toroidal field to exclude the globally unstable sausage and kink modes. The RFP utilizes a conducting shell and a much smaller highly sheared magnetic field, reversed in direction at large radii, to give the global MHD stability. A chief aim of the RFP approach is to allow a small compact fusion reactor with simple ohmic heating to obtain ignition. This paper gives an overview of the history, potential advantages, critical issues for reactor feasibility, and present status of the international RFP research.

1. INTRODUCTION

This paper gives an overview of the current status and areas of investigation of the reversed-field pinch (RFP) approach to a fusion reactor. This overview provides an update of previous RFP reviews [1–9]. The structure of this review is guided by the stated aims of this conference. At the first conference of this series we suggested a line of research aimed at giving improved operation making use of a small versatile RFP experimental device [10].

This paper presents a brief review of RFP history in Sec. 2. The potential advantages and parameters of an RFP fusion reactor are presented in Sec. 3 followed by the critical issues in Sec. 4. A summary of experimental RFP achievements and present investigations relating to the critical RFP reactor issues are reported in Sec. 5. Finally, concluding comments, observations and recommendations are presented in Sec. 6.

2. BRIEF CHRONOLOGY

A brief chronology of the notable steps leading to the present RFP concept are as follows: In 1934 the pinch effect was first described mathematically by W.H. Bennet. During the early fifties the interest in controlled fusion was an outcome of the successful testing of fission ignited fusion energy release in nuclear explosions. The early z-pinch work was done using small fast discharges and a large slow experiment in the UK called Zeta. The latter

Current Trends in International Fusion Research – Proceedings of the Second Symposium
Edited by E. Panarella. NRC Research Press, National Research Council of Canada, Ottawa, ON K1A OR6, Canada. 1999.

experiment, after some initial excitement, was discontinued when the observed neutron emission was found to be generated in local regions of accelerated deuterons rather than by a thermonuclear plasma. Guided by the theoretical sharp boundary equilibrium model of the axial current pinch (z-pinch), many experiments were made on the rapidly formed shock-heated, small linear and toroidal discharges. The results showed rapidly growing unstable disturbances. In 1954 an idealized, sharp boundary, linear stability theory predicted improved behavior if an added axial magnetic field and perfectly conducting boundary was used. During later portions of the 50's decade, the experiments on these "stabilized pinches" showed that an initially sharp boundary diffused rapidly and the stability behavior, while improved, was far from acceptable.

During the time up to the early 70's it was found theoretically that diffuse pinch configurations in which the axial field reversed direction in the outer region of the plasma can exist which are stable to both ideal MHD and resistive tearing modes. The reversed toroidal field configuration was then named the reversed field pinch (RFP). Experiments also demonstrated that under proper conditions the pinch would produce the field reversal automatically (self reversal). The RFP experiments showed improved behavior but with low and high frequency plasma and field fluctuations. Theoretically the RFP configuration is not totally MHD stable; the regions unfavorable field line curvature give rise to unstable g (resistive interchange) modes. In 1974 the RFP self reversal action was proposed to result from a relaxation to a lowest energy state subject to the constraint of constant magnetic helicity The magnetic helicity K is defined as the integral of **A**·**B** over the plasma volume where **B** is the magnetic field and **A** is a corresponding vector potential whose curl is **B**. K is a measure of the knottedness of the field lines. Although the magnetic helicity is not strictly constant, arguments have been given that it decays on a significantly longer time scale than the magnetic field energy. The original concept of a totally stable shock-heated plasma column magnetically confined away from the walls was abandoned.

From the late 70's to present the research has focused on slow ohmically heated RFP's utilizing programmed and self-reversed toroidal magnetic fields. As discussed in later sections, the present emphasis is on lowering the turbulence and energy transport losses.

3. THE RFP REACTOR

The RFP concept of a fusion reactor has the following potential advantages:

1. The observed high beta confinement > 15% obtained in RFP's allows small compact reactor designs, which predict a lower cost of development and cost of electricity [11].
2. The high current density of the RFP gives the possibility of ohmic heating to ignition avoiding the expensive rf or beam injection heating of the tokamak approach.
3. The low value of the toroidal magnetic field at the outer edge of the RFP reactor results in moderate forces on field coils.
4. The relaxation process leads to the possibility of low frequency (≈ 1-5 kHz) steady-state current drive [12,13].
5. Since the RFP does not rely on the safety factor q> 1 stabilization, the aspect ratio can be chosen large enough to give good access.
6. The RFP can be free from current disruptions.

A list of parameters for a compact RFP reactor [11] is shown in Table I.

Table I. RFP reactor parameters

Titan II Design Point	
Major Radius (m)	3.9
Minor Wall Radius (m)	0.60
Fusion Power (MW)	2290
Net Electric Power (MW)	900
Toroidal Current (MA)	17.8
Ignition Temperature (KeV)	4.0
Burning Temperature (KeV)	10
Energy Confinement time (s)	0.2
Peak Electron Density (m^{-3})	5×10^{20}
Plasma Beta	0.2

4. CRITICAL ISSUES

Essential critical issues that need to be addressed for the successful achievement of a fusion reactor based on the RFP concept are as follows:

1. The primary objective that needs to be accomplished is the achievement of an **increased energy confinement time.** A portion of this can be attained by an increase in size but if the reactor is to remain small and compact most of the increase will have to be attained as the current is increased. As discussed below, various measures are being studied to reduce the transport losses and increase the energy confinement time in present experiments.
2. The second issue is expected to come with suitably improved confinement, namely the reaching of **ignition temperatures.**
3. The reactor must have a **viable first wall** capable of withstanding the high heat loading of a compact design while maintaining an acceptable release of impurities to the main plasma core. Moreover, for a D-T fuel the wall must be capable of standing the neutron damage from the fusion reactions with an economically acceptable wall replacement time. In order to reduce the radioactive waste, the wall materials are to be chosen to minimize the neutron induced radioactivity.
4. Because of the fatigue of metals due to the pulsed forces from cyclic pulsing of the current and accompanying magnetic fields, engineers generally agree that the reactor must run in a steady current mode. This means one must replace the present pulsed inductive systems with a **steady-current drive**.
5. A final important critical issue that will need research is the **confinement and fueling properties of an burning plasma.**

5. EXPERIMENTAL STATUS

5.1 Present RFP Experiments

The present major RFP experiments are shown in Table II.

Table II. RFP Experiments

Experiment Focus	R (m)	a (m)	I (KA)	Location	Recent Experiment
RFX	2.0	0.46	550-900*	(IGI) Padua, Italy	Modification for enhanced operation. Attempting to mitigate mode locking and hot spots.
MST	1.5	0.50	300-600	U. Wisconsin Madison, WN	Enhanced temp. and confinement using inductive poloidal current drive. Spontaneous high theta mode.
TPE-1RM20	0.75	0.19	100-270	ETL Tsukuba, Japan	Plasma properties for q ranging from an RFP to a tokamak (-0.2 to 2.5). Improved confinement high theta mode.
TPE-1RM	0.73	0.19	100-200	ETL Tsukuba, Japan	Toroidal and Poloidal divertor studies.
EXTRAP-T2	1.24	0.18	70-260	RIT Stockholm, Sweden.	Exploration of resistive shell operation. Comparison of data with a collisional radiative model.
REPUTE-1Q	0.55	0.15	50-150	Univ. Tokyo Tokyo, Japan	Plasma properties for q values ranging from -.2 to 2.5 (RFP to tokamak)
EXTRAP-T1	0.50	0.057	40-100	RIT Stockholm, Sweden.	Dynamo and power balance studies with reactor-like current densities.
STE-2	0.40	0.10	20-40	KIT Kyoto, Japan	Response of RFP plasma to external helical perturbations. Poloidal divertor
SWIP	0.48	0.10	50-70	SIP Sichuan, China	Recent startup; discharge cleaning, titanium gettering, and controlled wall conditions allowed good RFP formation.
IFTES	0.30	0.043	10-25	Iwate Univ. Morioka, Japan	Recent startup has produced high current density RFP configurations.

---

*Design value 2 MA

ETL - Electrotechnical Laboratory

IGI - Institute of Gas Ionizzati

KIT - Kyoto Institute of Technology

RIT - Royal Institute of Technology

SIP - Southwest Institute of Physics

5.2 Energy Confinement Time

A major effort in RFP investigations is presently focused on the lengthening of the energy confinement time τ_E. It has become customary to demonstrate the status of each RFP by plotting its best value of τ_E *vs* the quantity $a^2I^{3/2}(I/N)^{3/2}$ where a is the plasma minor radius, I the toroidal current and N is the line density $n_e a^2$. This is motivated by the RFP "scaling law"

$$\tau_E \sim [\beta_p^{5/2}/Z^* \ln\Lambda]\, a^2I^{3/2}(I/N)^{3/2},$$

where β_p is the poloidal beta $\equiv 2\mu_o\langle p\rangle/B^2(a)$, $\ln\Lambda$ is the coulomb logarithm and Z^* is the enhancement factor of the plasma resistance over the classical value for a uniform column of purely hydrogenic plasma. The quantity Z^* includes the contribution of impurities (Zeff]), the increased length of the helical field lines and any anomalous resistivity. If β_p, Z^* and (I/N) remain nearly constant as the size and/or current is increased the $I^{3/2}a^2$ scaling, often referred to as constant beta scaling[14,15], is favorable from the fusion reactor point of view. The RFP experiments to date regularly demonstrate operation with β_p of 10% and above. Thus the success in achieving favorable confinement times, as reactor size and current levels are approached, lies in keeping the impurities and anomalous resistivity at acceptable levels. The determination of the scaling of τ_E as the toroidal current is increased toward the design goal of 2 MA is a primary goal of the RFX experiment [16].

The current status of the RFP energy confinement time achievements are shown in Fig.1. The best τ_E obtained for each of the experiments shown is placed on the plot.

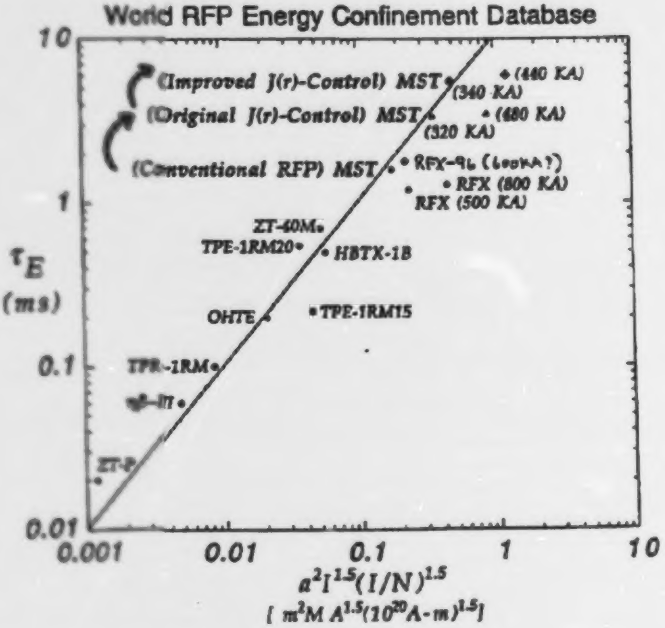

Figure 1. A plot of the best energy confinement time for past and present RFP devices.

5.3 Approaches to Improve RFP Energy Confinement Time

5.3.1 Current profile control

Numerical simulations and experiments suggest that the RFP fluctuations result from the resistive MHD turbulence that is associated with departures from the stable relaxed state [17] for which the quantity $\lambda \equiv \mathbf{J}\cdot\mathbf{B}/B$ is a constant. The RFP experiments normally deviate from the λ = constant near the wall where the colder and more resistive plasma reduces the current density. In order to overcome this effect, experiments have been performed in which the plasma current density near the wall was increased by inductively driving the current with a pulse of negative poloidal voltage [18]. This drives the reversed toroidal field more negative, inducing a corresponding plasma current, and is called pulsed poloidal current drive PPCD. It was found that during the time the reversed field was driven more negative at the plasma edge, the observed field fluctuations were much reduced and the corresponding τ_E was increased up to a factor of five [19,20] with a record T_e of 600 eV. The reduced fluctuation level during PPCD is shown Fig. 2. Corresponding results have been reproduced in the RFX experiment [21]. Since the negative voltage pulse is inductively driven, the period of the time for driving the poloidal edge current is of necessity limited. Efforts are presently being explored to produce a sustained poloidal current drive in order to maintain the outer region current and a flattening of the λ spatial distribution. The use of electron gun injection of current has shown some positive results [22]. A program to produce a sustained poloidal current drive by injecting lower hybrid waves is underway [23,24]. The sustaining of the current drive in the outer plasma region is needed to verify that the improved operation can be maintained and is not just a transient dynamic effect.

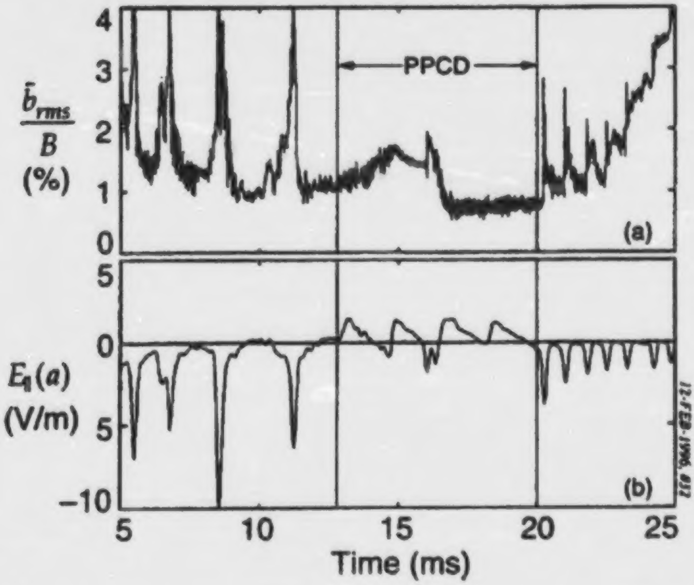

Figure 2. The measured values of (a) rms magnetic fluctuations and (b) plasma edge parallel electric field showing the reduced fluctuations during inductively driven pulsed poloidal current drive PPCD on MST.

5.3.2 Reduction of field errors

It is well recognized that it is important to minimize field errors due to port holes and gaps in the shell. Field errors near the wall promote mode locking and can destroy ideal magnetic surfaces in the outer annular region giving the field lines a stochastic behavior resulting in a reduced plasma confinement. Even in the absence of stochasticity the field errors can direct field lines to the wall allowing outward plasma and heat flow to the walls. Proposals for minimizing field errors are as follows:

1. Minimize the size and number of pump and diagnostic ports in the shell. In MST, for example, the pump port field error is reduced by pumping through many small holes rather than using one or more large ones. There is always a trade off between good diagnostic access and reducing the number and size of the diagnostic ports.
2. Use specially designed [25,26] tapered overlapping gaps. This was implemented in ZT-40M and is was found that mode locking to the wall was avoided [27].
3. Utilize active field correction at the gaps. This was implemented in the RFX experiment with favorable results [28].
4. Use a smart shell [29-31] consisting of a mesh of conductors having a feedback correction in each loop of the mesh so as to force the flux in each loop to zero thus approximating an ideal flux conserving shell. Some preliminary studies on this concept were done on the Reversatron RFP[32] but much more research on this concept is needed.
5. Use a resistive shell having no gaps [33]. Resistive shells have been studied in the OHTE [34] and EXTRAP-T2 experiments [35]. These experiments had shell gaps which lead to mode locking. An experiment having no gaps is needed to answer the following questions: Are the residual modes propagating? If so, the question arises: can the resistivity and shell thickness be chosen that can both limit the amplitude of propagating modes and their associated transport losses to an acceptable level while allowing adequate slow startup and equilibrium sustaining fields? In this regard we note that some operating tokamaks (for example Alcator-C and Doublet III-D) have fairly thick stainless-steel vacuum vessels without gaps.

All reversed-field pinches to date have one or more cuts (gaps) in their conducting stabilizing shells. These are introduced in order to allow the pulsed driving fields to enter the plasma region interior to the conducting stabilizing shell. The energy principle [36], ideal MHD stability analyses [37,38] and Taylor relaxation [17] all assume closed, perfectly conducting boundaries. These analyses therefore magnetically shield the plasma from the world outside the closed conducting shell. Actual shells with gaps allow magnetic coupling to the outside driving circuits that can affect the stability and associated dynamic behavior of the plasma. These considerations have been ignored in past stability analyses and nonlinear simulations under the assumption that, for small shell gaps, the plasma external coupling effects are negligible as far as MHD plasma fluctuations are concerned. Experiments conducted by the present authors demonstrated that indeed the plasma-circuit coupling can have important effects. For example the observed magnetic fluctuation level in the ZT-40M RFP was drastically reduced when the 12 sets of toroidal field windings, which were normally connected in three parallel circuits consisting of four series connected windings each, were reconnected with all 12 windings sets in parallel [39]. Similar experimental studies were done on the Reversatron [40]. There it was found that the m=0, and n ranging from 6 to 12 magnetic activity was reduced during startup and later in the discharge there was a significant reduction in the external kink modes. Adequate experimental and theoretical studies are lacking in this area.

5.3.3 The parameter search for improved RFP operating modes

Tokamaks behave differently under particular sets of operating parameters, (e.g. L and H modes) allowing a choice for improved performance. Likewise different operating modes have been observed in RFP experiments. For example, an improved high theta mode IHTM of operation for which sawteeth fluctuations have been surpressed has been found in the TPE-1RM20 experiment [41]. A comparison of this operating mode with normal operation is shown in Fig. 3. The parameters important for good reproducibility of the IHTM were keeping Θ below 1.95 and a choice of an adequate current decay rate. During this sawteeth-free operation, the significant improvements were an increase in n_e, an increase in the poloidal beta from 8% to 20% and a doubling of τ_E.

Spontaneous periods of sawteeth-free operation have been found in MST [42]. The conditions for this behavior involved operating at low electron density, deep field reversal and good wall conditioning. Under these conditions the energy confinement time increased from 1 ms to 4 ms.

5.4 The First Wall and Impurity Control

5.4.1 Wall conditioning and protection

It is standard practice to clean the walls of RFP experiments with glow and/or standard discharges before taking data. The walls of many RFP experiments are protected by either partially or totally covering them with carbon tiles. Carbon limiters have also been used. For

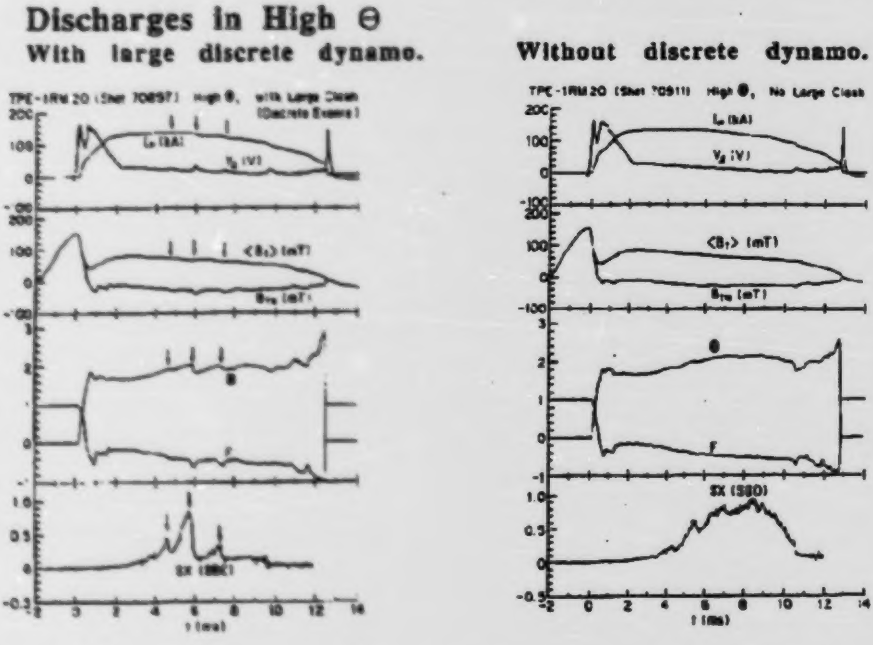

Discharges in High Θ

With large discrete dynamo.

Without discrete dynamo.

Figure 3. Comparison large sawteeth and sawteeth-free high theta discharges obtained on TPE-1RM20l.

the planned new RFP experiment TPE-RX there are plans to utilize Molybdenum limiters.

5.4.2 Wall boronization

The earliest RFP studies on low Z (Boron) wall coatings were done on Repute-1 [43,44]. It was found that the partial pressure of hydrogen, oxygen and water were reduced. The plasma number density became higher and nearly constant and the high frequency (50-250 kHz) magnetic oscillations decreased.

Boron wall coatings have been used on RFX [45] and MST [46]. In both Repute-1 and RFX an amorphous boron layer (~60 nm thick) containing hydrogen and carbon was deposited by glow discharge in a mixture of trimethylboron $B(CH_3)_3$ and He. A general improvement in the plasma performance of RFX was observed. There was a reduction of a factor of four of the influx of oxygen and a factor two of carbon. The radiated power was reduced a factor of two. The boronization allowed a higher density operation and resulted in higher τ_E (~1.4 ms) and β_p (13%).

The boronization of the wall of MST was done by a different technique of plasma ablation of a hot-pressed boron carbide rod. This method of boronizing the wall was deemed safer and easier to implement. As in RFX, reductions of the oxygen and carbon impurities as well as the radiated power were obtained.

5.4.3 Divertors

In a manner similar to that used for Tokamaks, the RFP fusion reactor designs include a magnetic divertor to deflect the field lines and plasma flow near the wall through an exit space into an outer plasma dump chamber. In this way wall impurities and spent fuel are removed from the active plasma core.

Two general types of magnetic divertors for the RFP have been considered: a poloidal divertor PD and a toroidal divertor TD named after the component of magnetic field which is redirected. Each have their advantages and drawbacks. The PD has the property that it can maintain toroidal symmetry but requires large divertor coils and current. This is because, in contrast to the tokamak, in the RFP the poloidal field component is much larger than the toroidal component at the wall position. The TD on the other hand has the engineering advantage of diverting a smaller field but will necessarily perturb the toroidal symmetry. In both cases there are important questions as to what degree the divertor perturbations effect the RFP energy and particle confinement as well as the field configuration sustaining dynamo.

(a). Poloidal Divertor Experiments: An early study [47] used four conducting field divertor rings which had the effect of positioning the plasma away from the non-circular cross-section conducting vacuum chamber. With this arrangement a large stationary asymmetry developed. This "first look" study made a large departure from the usual RFP configurations and without an appropriate stability analysis left the stability properties of this poloidal divertor uncertain.

A second PD experiment was done on the STE-2 device [48,49]. It was concluded that the divertor configuration had no deleterious effect on the plasma for the range divertor-coil current I_d and plasma current I_p studied ($I_d/I_p \leq 0.3$). The dominance of the m=1 tearing modes in the magnetic fluctuations was not influenced by the presence of the PD fields.

The most recent PD studies were done using the TPE-2M device [50]. The first experiments were performed without a space to lead the diverted plasma out of the main confining region and the current discharge duration was limited by the buildup of impurities.

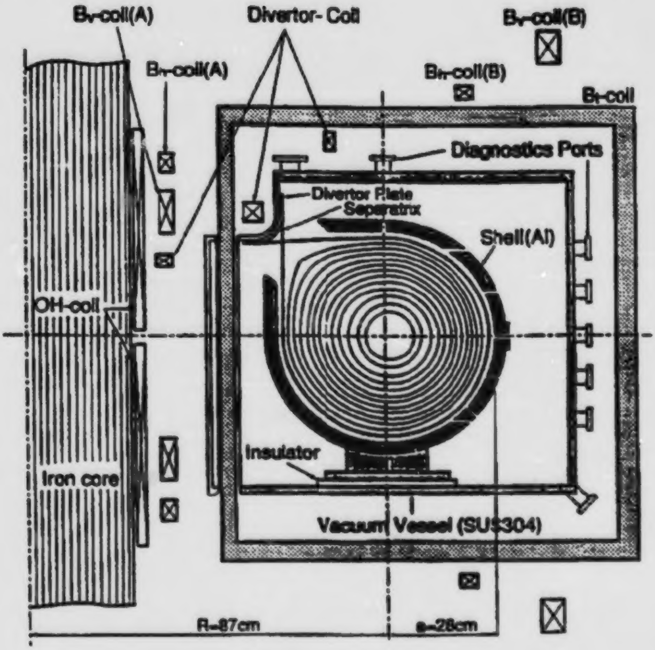

Figure 4. A cross-section view showing the geometry and field lines for poloidal divertor in TPE-1RMC.

To alleviate this problem, a shell was placed inside the vacuum chamber, see Fig 4, so that the outermost space acted as a sink for the diverted plasma. With this improved version TPE-2MC, the sustainment of the poloidally diverted RFP discharge was achieved without impurity buildup.

(b). Toroidal Divertor Experiment: Research on toroidal divertors has also been made using the TPE-2M device[50]. The toroidal field was diverted at four equally spaced positions the long way around the torus using four local poloidal coils outside the torus. It was observed that the dynamo field sustainment remained operative, but the mode structure of the fluctuations was altered. Rather surprisingly, the energy confinement with this TD was somewhat improved. This was attributed to a shift from the dominant m=1 MHD activity to a dominant m=0 mode. The m=1 modes tend to transport energy from the hot plasma core to the cooler outer region while The m=0 disturbances tend to be located at the reversal surface and cause less severe transport than the m=0 fluctuations.

The results for both poloidal and toroidal divertors are encouraging and more detailed studies are forthcoming.

5.5 Current Drive and Burning Plasma

The most desirable current drive from an engineering and economic basis is the low frequency oscillating field current drive OFCD. Preliminary experiments [51,52] with this technique showed predicted effects but must wait for a hotter and reduced loss RFP plasmas for steady current sustainment to be demonstrated. In a like fashion, the issues of fueling and fusion reacting RFP plasma physics must wait for improved higher temperature RFP plasmas. For example, pellet injection has been performed on RFP's [28,53] but must wait for reactor-like plasmas to assess its eventual viability.

6. CONCLUSION

As a result of the concerted international effort, considerable progress is being made on the RFP critical issues. Several engineering issues are common to the tokamak and information is coming from that highly funded program which can carry over to RFP applications.

Considerable effort is being expended in the comparison of theory and experiment particularly in the areas of fluctuations, the plasma dynamo and transport losses. The increased physics understanding resulting from that research will lead to a more rapid progress toward the reactor goal.

Finally, we point out two areas of RFP research that the authors feel are high priority: (1) the development of a viable non-invasive method of measuring the magnetic field (or current density) time dependent spatial distributions in the hot RFP plasmas. Currently too much dependence on field and plasma pressure profile modeling (which is not unique) is being relied upon to obtain quantities such as beta and energy confinement time. Likewise, direct time dependent field fluctuation measurements deep inside the plasma core would be invaluable in delineating the precise nature of the RFP dynamo mechanisms and sawteeth behavior. (2) The increasing capability of plasma simulations should be used to attack the problem of coupling the plasma MHD dynamics to the outside field-producing circuitry. This should include the modeling of the shell gaps, instead of using prescribed oversimplified boundary conditions.

ACKNOWLEDGMENTS

This paper is a broad overview based upon the results of the extensive research of the entire reversed-field pinch community. We thank the many who were very cooperative in supplying data and information during the preparation of this manuscript.

The colleagues of co-author Jim Phillips are saddened by his recent sudden death. His presence is sorely missed. Jim's character trait was to spend countless hours analyzing any RFP data he could get his hands on. He would then often come up with innovative interpretations which often did not follow the popular party line. Some of his ideas including those contained in this paper are discussed in more detail in a manuscript presently in final preparation [54].

REFERENCES

1. S. Glasstone and R. Loveberg. Controlled Thermonuclear Reactions. D. Van Nostrand, NY (1960) p.p. 225-289.
2. D.A. Baker et.al. Los Alamos Scientific Lab. Report, LA-UR-77, 459 (1977).
3. H. Dreicer (compiler). Los Alamos Scientific Lab. Report, LA-7527-MS (1978).
4. H.A.B. Boden and A.A. Newton. Nucl. Fusion **20**, 1255 (1980).
5. D.A. Baker and W.E. Quinn. Fusion 1, Part A, (Edward Teller ed.) Academic Press N.Y., p. 437–475 (1981).
6. H.A.B. Bodin, R.A. Krakaowski and S. Ortolani. Fusion Technology **10**, 307 (1986).
7. S. Ortolani. Energy Independence Conference on Fusion Energy, World Scientific Pub., Singapore p. 620 (1988). D.A. Baker. ibid p.730.
8. H.A.B. Bodin. Nuclear Energy **29**, 57 (1990).

9. S.C. Prager. Plasma Physics and Controlled Fusion Research **34**, 1875 (1992).
10. J.A. Phillips, D.A. Baker and R.F. Gribble. 1st Symp. on Current Trends in Int. Fusion Res. (E. Panarella Ed.) Plenum Press N.Y. (1997) p. 375.
11. The Titan Reversed-Field Pinch Fusion Reactor Study, Univ. Calif. Los Angeles Rep. UCLA-PPG-1200 (1990).
12. M.K. Bevir and J.W. Gray. Proc. Reversed-Field Pinch Theory Workshop Los Alamos Rep.LA-8944C, 176 (1981).
13. K.F. Schoenberg, R.F. Gribble and D.A. Baker. J. Applied Physics **56**, 2519 (1984).
14. M.M. Pickrell et al. Proc. 15th European Conf. on Controlled Fusion and Plasma Physics, Venice Italy (1989).
15. R. Veerasingam et al. Phys. Fluids **B4**, 3241 (1992).
16. RFX Team. Plasma Phys. and Cont. Fusion Research 1992 (Proc. 14-th Int. Conf. Wurtzburg, 1992, IAEA, Vienna) (1993). p. 583
17. J.B. Taylor. Physical Review Letters **33**, 1139 (1974).
18. J.S. Sarff and A.F. Almagri et al. Phys of Plasmas **2**, 2440 (1995).
19. M.R. Stoneking. Bul. Amer. Phys. Soc. **41**, 1558 (1996). S.C. Prager et al. Ibid. p. 1409.
20. D.J. Den Hartog et al. Fusion Energy 1996 (Proc. 16-th Int. Conf. On Fusion Energy IAEA) **2**, 83 (1997).
21. P. Martin et al. Bul. Amer. Phys. Soc. **42**, 2049 (1997).
22. D. Craig et al. Bul. Amer. Phys. Soc. **41**, 1407 (1996).
23. E. Uchimoto et al. Phys. Plasmas **1**, 3517 (1994).
24. S. Hokin et al. Nuclear Fusion **34**, 1447.
25. R.W. Moses. Proc.of the Int. Workshop on Engineering Design of Next Step Reversed-Field Pinch Devices. D.B. Thomson Ed., Los Alamos Lab. Rep., LA-113-C (1987) p. 343.
26. R. Watt et al. Tapered Poloidal Field Gap Results in ZT-40M. Los Alamos Lab. Rep., LAUR-85-3895.
27. J.A. Phillips. et al. Bul. Amer. Phys. Soc. **41**, 1411 (1996)
28. V.Antoni et al. Fusion Energy 1996 (Proc. 16th Int. Conf. On Fusion Energy IAEA) **2**, 711 (1997).
29. C. M. Bishop. Plasma Physics and Controlled Fusion **31**, 1179 (1989).
30. T.H. Jensen and R. Fitzpatrick. Physics of Plasmas **4**, 2997 (1997).
31. R. Fitzpatrick and T.H. Jensen. Physics of Plasmas **3**, 2641 (1996).
32. S. Robertson. Private communication.
33. D.A. Baker and J.A. Phillips. IEA Workshop on Reversed Field Pinches. Oct. 14–16, 1996 Madison, WI., p. 726.
34. R.R. Goforth et al. Nucl. Fusion **26**, 515 (1986).
35. J.R. Drake et al. Fusion Energy 1996 (Proc. 16-th Int. Conf. On Fusion Energy IAEA) **2**, 193 (1997).
36. I.B. Bernstein et. al. Proc Royal Soc. **A244**, 17 (1958).
37. B.R. Suydam,. Proc.U.N. Int. Conf. on Peaceful Uses Of Atomic Energy, IAEA Vienna, **31**, 157 (1958).
38. W.A. Newcomb. Annals of Phys. **10**, 232 (1960).
39. J.A. Phillips et al. Nuclear Fusion **28**, 1241 (1988).
40. D. Alexander and S. Robertson. Plasma Phys. and Controlled Fusion **36**, 1671 (1994).
41. Y. Hirano et al. Fusion Energy 1996 (Proc. 16th Int. Conf. On Fusion Energy IAEA) **2**, 95 (1997).

42. J.S. Sarff for MST Group. IEA Workshop on Reversed Field Pinches. Oct. 14-16, 1996, Madison, WI., p. 421.
43. S. S. Shinjiro et al. J.Physical Soc. of Japan **59**, 1232 (1990).
44. S. Shinohara et al. J. Physical Soc. of Japan **61**, 3030 (1992).
45. J Winter et al. J. Nuclear Materials **176-177,** 486 (1990).
46. D.J. Den Hartog et al. J. Nuclear Materials **200**, 177 (1993).
47. J.S. Sarff et al. Nuclear Fusion **29**, 104 (1989).
48. M. Iida et al. Plasma Phys. and Cont. Fusion **36**, 153 (1994).
49. D. Ishijima et al. Plasma Phys.and Cont. Fusion **37**, 657 (1995).
50. K. Hattori et al. Fusion Energy 1996 (Proc. 16-th Int. Conf. On Fusion Energy IAEA) **2**, 213 (1997).
51. K.F. Schoenberg et al. Phys. Fluids **31**, 2285 (1988).
52. S. Shinohara et al. J. Physical Soc. of Japan **59**, 1232 (1990).
53. G.A. Wurden et al. Nucl. Fusion **27**, 857 (1987).
54. J.A. Phillips, D.A. Baker and R.F. Gribble. The Reduction of Low Frequency Fluctuations in RFP Experiments. Final manuscript in final preparation for publication in Nuclear Fusion.

THE COLLIDING BEAM FUSION REACTOR II. ATOMIC AND NUCLEAR PHYSICS OF SPIN POLARIZED H AND B^{11} FUEL BEAMS

Hendrik J. Monkhorst, Michl W. Binderbauer[1] and Norman Rostoker[1]

Department of Physics
University of Florida
Gainesville, Florida, 32611-8435, U.S.A.
[1] Department of Physics
University of California
Irvine, California, 92717, U.S.A.

ABSTRACT

In order to make an assessment of the practical possibilities of the Colliding Beam Fusion Reactor (CBFR), it is necessary to quantify the relevant nuclear and atomic physics to a greater degree of precision.

Using the most recent data, we present a greatly improved p-B^{11} fusion reactivity. In addition we calculated the energy dependence of the fusion cross section in the strongest resonance region. The contaminating side reactions and their cross sections are tabulated and their occurrences are quantified, confirming the attractiveness of the p-B^{11} option.

Nuclear polarization enhancements to the fusion cross section are discussed. Besides a spin enhancement factor of 1.6, a further enhancement is possible due to the B^{11} quadrupole moment. This is only feasible in a CBFR-like device, because of its cylindrical symmetry. It is argued that the nuclear shape enhancement can be quite large, and thus warrants an experimental determination.

A discussion and derivation of nuclear depolarization is given. It is shown that its rate is many orders of magnitude smaller than fusion (or other relevant) rates, thus posing no discernible negative effects for CBFR reactions. Resonant wave depolarization can be excluded in a FRC plasma such as in the CBFR, in contrast to Tokamak plasmas where this depolarization mechanism can be appreciable.

1. INTRODUCTION

In another contribution to this Proceedings [1], it was argued that in a Field Reversed Configuration (FRC) plasma with energetic particle beams, the problem of anomalous diffusion can be eliminated. The self-confining property of a FRC will avert this problem due to several properties inherent to our design. Its strong poloidal magnetic field enclosing the

Current Trends in International Fusion Research — Proceedings of the Second Symposium
Edited by E. Panarella. NRC Research Press, National Research Council of Canada, Ottawa, ON K1A 0R6, Canada. 1999.

rotating plasma will enable the device to achieve the high densities required. This provides the opportunity to build much more compact reactors. Their linear geometry will hold additional engineering benefits. In particular, all reactor components can be mounted on rails and thus can be easily separated for repairs and maintenance. Moreover, the power output scales almost linearly with the length of the reactor chamber. Therefore, reactors with a range of total power outputs can be built which should be of an engineering as well as a commercial advantage. We refer to a reactor operating under these conditions as a Colliding Beam Fusion Reactor (CBFR). It was also shown in [1] how the reaction

$$p + B^{11} \rightarrow 3\,He^{4} + 8.681 \text{ MeV} \tag{1}$$

can be used in a CBFR. This reaction has a broad peak in its cross section near 600 keV in the c.m. frame, reaching a value of 1.15 barn [2]. This value is considered more accurate than the one previously recommended [3] and is larger by more than forty percent. Using various techniques, and exploiting the physical properties of FRC plasmas, it can be shown that it is possible to maintain fast hydrogen and slow boron beams, with a collision energy near 600 keV, and for a time at least comparable to the burn time of reaction (1). Most of the fusion energy will be carried by the helium-4 nuclei into a Direct Energy Converter (DEC). This can give a very high overall efficiency for the CBFR, theoretically exceeding that of any known thermal power generation device by at least a factor of two.

Because p and B^{11} have nuclear spins, it is possible to enhance the fusion cross section by spin polarization. This was proposed by Kulsrud et al. [4] for use in tokamaks burning D and T; its applicability includes FRCs. A further enhancement is possible because of the quadrupole moment of the B^{11} nucleus. This can only happen in highly nonthermal, colliding beam-type systems such as the CBFR, and can not occur in a thermal device such as a Tokamak. This quadrupole enhancement was first suggested by Perkins [5].

The question arises whether the spins stay polarized inside plasmas for times at least as long as the burn time. One might think that the intense electromagnetic fields would cause rapid depolarization. This turns out to be invalid. Depolarization rates are found to be several orders of magnitude smaller than burn rates. This is particularly true for FRCs, unlike depolarization rates of triton nuclei in tokamaks which can be fast compared to fusion rates [6]. Because of the attractiveness of the p-B^{11} option for fusion with a CBFR , we undertook a study of the atomic and nuclear physics of the reaction (1). In the following two sections we present the calculation of an improved reactivity, and a summary of side reactions. The next section contains the theory of the fusion cross section enhancements resulting from spin polarization. This is followed by a discussion of depolarization. The unique advantages of FRCs in exploiting these effects will be demonstrated.

2. THE REACTIVITY

In the CBFR, fusion reactions occur among co-rotating beams of p and B^{11} ions confined within the FRC plasma. In any point x the distribution functions are assumed to have the form

$$F_p(x, v_p, t) = n_p(x,t)\left(\frac{m_p}{2\pi T_p}\right)^{\frac{3}{2}} \exp\left[-m_p \frac{(v_p - V_p)^2}{2T_p}\right] \tag{2}$$

for protons, and

$$F_B(x,v_B,t)=n_B(x,t)\left(\frac{m_B}{2\pi T_B}\right)^{\frac{3}{2}}\exp\left[-m_B\frac{(v_B-V_B)^2}{2T_B}\right] \tag{3}$$

for B^{11}. Additional t dependence can occur in the temperatures T_p and T_B, but these are ignored in the present treatment. n_p and n_B are particle densities, and V_p and V_B are drift velocities.

$$\begin{aligned}<\sigma_F v>=&\left(\frac{m_P}{2\pi T_P}\right)^{3/2}\left(\frac{m_B}{2\pi T_B}\right)^{3/2}\int d^3v_P d^3v_B|v_p-v_B|\sigma_F(|v_P-v_B|)\\ &\times\exp\left[-\frac{m_P}{2T_P}(v_P-V_P)^2-\frac{m_B}{2T_B}(v_B-V_B)^2\right]\end{aligned} \tag{4}$$

σ_F is the total p-B^{11} fusion cross section, and thus depends only on the relative speed. A substantial simplification is possible with the coordinates

$$\begin{aligned}&v=v_p-v_B;\quad MV=m_Pv_P+m_B\left(\frac{T_P}{T_B}\right)v_B\\ &M=m_P+\left(\frac{T_p}{T_B}\right)m_B\end{aligned} \tag{5}$$

v is the relative velocity vector, and V can be called the "temperature weighted" center-of-mass velocity, and M the "temperature weighted" total mass. The exponent in Eq. (3) then transforms into

$$\begin{aligned}&\frac{m_P}{2T_P}(v_P-V_P)^2+\frac{m_B}{2T_B}(v_B-V_B)^2=\frac{m}{2T_P}(v-V_{pB})^2+\frac{M}{2T_P}(V-V_0)^2\\ &\frac{m}{T_P}=\frac{m_Pm_B}{m_BT_P+m_PT_B};\quad \frac{M}{T_P}=\frac{m_p}{T_P}+\frac{m_B}{T_B}\\ &V_{pB}=V_p-V_B;\quad V_0=\frac{m_PT_BV_P+m_BT_pV_B}{m_PT_B+m_BT_P}\end{aligned} \tag{6}$$

The Jacobian of the transformation is unity, and the V integration is trivial. $\langle\sigma_F v\rangle$ now reduces to

$$<\sigma_F v>=\left(\frac{m}{2\pi T_P}\right)^{3/2}\int d^3v v\sigma_F(v)\exp\left[-\frac{m}{2T_P}(v-V_{pB})^2\right] \tag{7}$$

The angular integration in spherical coordinates can also be carried out:

$$<\sigma_F v>=2\left(\frac{m}{2\pi T_P}\right)^{1/2}\frac{\exp(-mV^2_{pB}/2T_P)}{V_{pB}}\int_0^\infty dv\,v^2\sigma_F(v)\sinh\left(\frac{mvV_{pB}}{T_P}\right)\exp\left(-\frac{mv^2}{2T_p}\right). \tag{8}$$

because σ_F is the total fusion cross section. When the differential cross section $d\sigma_F/d\Omega$ becomes available, due to the B^{11} nonspherical shape and under nuclear polarized conditions (see Sections 4 and 5), this step will probably be done numerically.

An accurate total fusion cross section was extracted from the work of Becker et al. (BRT, Ref.[2]), who published the astrophysical factor. The maximum value is found

$$\sigma_m \equiv \sigma_F\,(\varepsilon_R \cong 580\ \text{keV}) = 1.15 \pm 0.05\ \text{barn} \tag{9}$$

and the width (at half maximum)

$$\Gamma \cong 280\ \text{keV}. \tag{10}$$

ε_R and Γ are slightly different from those reported in BRT (620 and 300 keV, respectively), apparently due to the use of different numerical fits. On the other hand, σ_m and Γ differ substantially from those reported in Ref. [3], which were based on experiments through 1979. In particular, σ_m of Eq. (9) is about forty percent larger. This was first pointed out by TUNL scientists (Drs. Ludwig and Brune, private communication).

$$\begin{gathered} \varepsilon = \mu v^2/2 \\ \mu = \frac{m_p m_B}{m_p + m_B},\ \text{the reduced mass} \end{gathered} \tag{11}$$

In Figure 1 we reproduce σ_F versus the center-of-mass energy over the most important ε range covering the largest resonance.

Since σ_F is tabulated as a function of ε, it is most convenient to use it as the integration variable; Eq. (8) then takes on the form

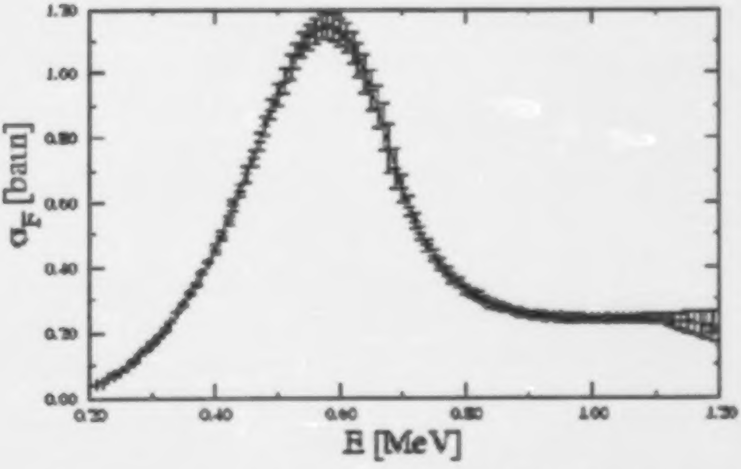

Figure 1. Inelastic total cross section $\sigma(\varepsilon)$ (in barns) versus energy ε(MeV) of the B^{11} (p, $\alpha\alpha$)α reaction. Errors include experimental uncertainties, but not the overall error in the cross section normalization, estimated to be about 6%.

$$<\sigma_{pF} v> = \sqrt{\frac{m/\mu}{2\pi\mu T_p \varepsilon_R}} \int_0^\infty d\varepsilon \sqrt{\varepsilon}\, \sigma_F(\varepsilon) \{\exp[-\frac{m}{\mu}(\sqrt{\varepsilon} - \sqrt{\varepsilon_R})^2 / T_p] - \exp[-\frac{m}{\mu}(\sqrt{\varepsilon} + \sqrt{\varepsilon_R})^2 / T_p]\} \tag{12}$$

with $\varepsilon_R = \mu V^4_{pB}/2$. V_p and V_B are adjusted such that $\varepsilon_R \approx 580$ keV. Since $\sigma_F v$ applies to fusion between (co-rotating) colliding beams, we can call it *beam-on-beam reactivity*.

Dependence on T_B enters through m; we can write

$$\mu \cong m = \frac{m_p}{1 + (m_p T_B)/(m_B T_p)} \cong m_p, \tag{13}$$

thus we notice that this dependence is weak: $m_p/m_B \approx 0.1$ and $T_B/T_p \sim 1$. Therefore we can write approximately

$$<\sigma_F v> \cong \frac{1}{\sqrt{2\pi m_p T_p \varepsilon_R}} \int_0^\infty d\varepsilon \sqrt{\varepsilon}\, \sigma_F(\varepsilon) \{\exp[-(\sqrt{\varepsilon} - \sqrt{\varepsilon_R})^2 / T_p] - \exp[-(\sqrt{\varepsilon} + \sqrt{\varepsilon_R})^2 / T_p]\} \tag{14}$$

If we put $V_p = V_B = 0$, we arrive at the usual *thermal reactivity* expression:

$$<\sigma_F v> = \frac{4}{\sqrt{2\pi m_p T^3_p}} \int_0^\infty d\varepsilon\, \varepsilon\, \sigma_F(\varepsilon) \exp(-\varepsilon / T_p) \tag{15}$$

Since $\varepsilon_R > T_p$, the second term in Eq. (14) contributes insignificantly.

In Figure 2 we plotted various reactivities. The p-B^{11} curves correspond to Eqs. (14) and (15), with σ_F taken from BRT. The reactivities for D-T and D-He^3 are plotted as functions of mean temperatures of the Maxwell distributions of the two reactions involved.

We note that for $T_p \approx 25$ keV the p-B^{11} beam-on-beam reactivity equals the maximum $<\sigma_F v>_T$ for D-T, is twice the maximum $<\sigma_F v>_T$ for p-B^{11}, and four times the maximum $<\sigma_F v>_T$ for D-He^3.

It is of some interest to extract the limiting behaviors of the reactivities as the temperatures approach zero. For the thermal reactivities this is easily found to be

$$\lim_{T_p \mapsto 0} <\sigma_F v>_T \cong 4\sigma_F(0) (\frac{T_p}{2\pi m_p})^{1/2} \tag{16}$$

The slope near $T_p = 0$ is therefore

$$\lim_{T_p \mapsto 0} (\partial / \partial T_p) <\sigma_F v>_T \cong 2\sigma_F(0) (\frac{1}{2\pi m_p T_p})^{1/2} \tag{17}$$

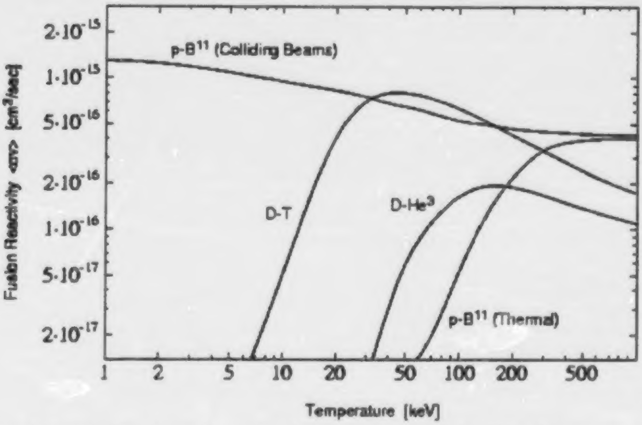

Figure 2. Reactivities $<\sigma_F v>$ for various fusion reactions: as a function of the proton temperature T_p for p-B^{11}, and of the mean temperature of the reactants for D-T and D-He^3.

We see that the slope of the thermal reactivity diverges like $T^{-1/2}$.

On the other hand, the beam-on-beam reactivity has a very different behavior. Its derivation is more subtle. Starting from Eq. (14), we drop the second term: its contribution in the limit $T_p \mapsto 0$ vanishes like $\exp(-4\varepsilon_R/T_p)$ relative to the first one.

We also approximate the fusion cross section by a Breit-Wigner formula,

$$\sigma_F(\varepsilon) = \frac{\sigma_m(\Gamma/2)^2}{(\varepsilon-\varepsilon_R)^2+(\Gamma/2)^2} \tag{18}$$

Although this expression is globally quite inappropriate, because of the multiple-resonance character of the fusion cross section [3], it is appropriate locally around $\varepsilon=\varepsilon_F$ where the integrand peaks like a delta function in the small $-T_p$ limit. Eq. (18) introduces the effect of the local curvature on the slope of $<\sigma_F v>$ for small T_p.

Defining

$$R(T_p) \equiv \frac{<\sigma_F v>}{\sigma_m v_R}, \quad v_R \equiv (2\varepsilon_R/m_p)^{1/2} \tag{19}$$

we have

$$<\sigma_F \pi v> \cong \frac{\Gamma^2}{8\varepsilon_R\sqrt{\pi T_p}} \int_0^\infty d\varepsilon\sqrt{\varepsilon}\exp\left[-\frac{(\sqrt{\varepsilon}-\sqrt{\varepsilon_R})^2/T_p}{(\varepsilon-\varepsilon_R)^2+\frac{\Gamma^2}{4}}\right] \tag{20}$$

$$\frac{\partial R(T_p)}{\partial T_p} = -\frac{R(T_p)}{2T_p} + \frac{\Gamma^2}{8\varepsilon_R\sqrt{\pi T_p^5}} \int_0^\infty d\varepsilon\sqrt{\varepsilon}\frac{(\sqrt{\varepsilon}-\sqrt{\varepsilon_R})^2\exp[-(\sqrt{\varepsilon}-\sqrt{\varepsilon_R})^2/T_p]}{(\varepsilon-\varepsilon_R)^2+\frac{\Gamma^2}{4}} \tag{21}$$

To simplify the reduction of the integrals, yet without loss of accuracy in the limit $T_p \mapsto 0$, we write

$$(\varepsilon-\varepsilon_R)^2 \mapsto 2\varepsilon_R(\sqrt{\varepsilon}-\sqrt{\varepsilon_R})^2.$$

Changing variable $t=(\sqrt{\varepsilon}-\sqrt{\varepsilon_R})/\sqrt{T_p}$, and extending the lower limit in the t integration from $(-\sqrt{\varepsilon_R}/\sqrt{T_p})$ to $(-\infty)$ (the associated error vanishes like $\exp(-\varepsilon_R/T_p)$ as $T_p \mapsto 0$), we notice the dependence on the parameter

$$x=\frac{\Gamma}{4\sqrt{\varepsilon_R T_p}}. \tag{22}$$

This parameter has to be large for a valid asymptotic expansion of R and $\partial R/\partial T_p$ The following result is obtained:

$$R(0)=1 \tag{23}$$

$$R'(0)\equiv \lim_{T_p\mapsto 0}\ \frac{\partial R}{\partial T_p}=-\frac{8\varepsilon_R}{\Gamma^2}+\frac{3}{4\varepsilon_R} \tag{24}$$

Eq. (23) is a trivial result. Eq. (24) can not be obtained through differentiation of the asymptotic expansion of $R(T_p)$: the integral lacks uniform convergence when T_p approaches zero.

$$R'(0)\cong(-5.9+0.13)\times 10^{-2}/\text{keV}$$
$$\text{or} \tag{25}$$
$$R'(0)\cong -5.8\times 10^{-2}/\text{keV}$$

This is a large value: already at $T_p = 8.6$ keV we would estimate $R(T_p) = 0.5$. However, this estimate is invalid because the asymptotic condition

$$x \gg 1$$

or

$$T_p \ll \frac{\Gamma^2}{16\varepsilon_R} \cong 6.2\ \text{keV}$$

is not satisfied. Although the drop in $R(T_p)$ is initially very steep, terms to higher order in T_p become rapidly significant. Put mathematically, since $T_p=0$ is a nonanalytic point of $R(T_p)$ (the integrands of Eqs. (20) and (21) have essential singularities for $T_p=0$), a power series expansion in T_p is at best asymptotic. On the other hand, it is difficult to obtain higher order terms in this expansion. We conclude that only a numerical evaluation, with carefully chosen grids in ε (or t), can be reliable.

The present situation does not arise for the thermal reactivity limit: the essential singularity in Eq. (15) appears at the end of the ε integration, whereas in Eqs. (20) and (21) it appears at $\varepsilon=\varepsilon_R$. Therefore, to the extent that the fusion cross section can be expanded in powers of ε around $\varepsilon=0$ (which is doubtful), a convergent expansion in powers of T_p could be derived for the thermal reactivity.

3. CONTAMINATING SIDE REACTIONS

Although we propose to use pure hydrogen and boron-11 fuels, some contamination with the boron-10 isotope can be expected. In addition, the He^4 ions will react with boron in secondary reactions and produce some low energy neutrons. Finally, there are gamma-ray producing reactions.

We will assess the extent of such contaminating side reactions, and draw conclusions regarding the required purity of boron-11 and any shielding requirement. We will start by tabulating all side reaction data relevant for our p-B^{11} reactor, and compare them to the main reaction B^{11} (p,αα)α. No B^{11} polarization was assumed. All cross sections were culled from references reviewed by Azjenberg-Selove [8]. Most entries were obtained by analyzing tabulated or curved data in these references, or by combining numbers in their texts and tables.

Of the p-B^{11} reactions, only the reaction 2, producing gamma rays, could pose any concern. These emissions, carrying about 10 kW for a 100 MW fusion reactor, will be absorbed in just a few centimeters of heavy metal. The stainless steel reactor chamber wall, its exterior cooling system to carry off the Bremsstrahlung heating and the surrounding superconducting magnets should provide ample absorption without additional shielding. This should also be relevant for the gammas escaping into the direct energy converter. Reaction 7 is innocuous for the same reason.

The neutron-producing reactions 3 and 8 are closed since their thresholds far exceed the collision energy of less than 1 MeV. On the other hand, the secondary reactions 4 and 10 occur very rarely, have a small Q, and thus carry only a small power, even if a substantial B^{10} admixture were to occur.

The only reaction of potential concern is reaction 6, producing radioactive and poisonous Be^7. In fact, for this reason only the removal of B^{10} is required. Using chemical isotope separation alone [9] can already provide better than 99% purity of B^{11} [9]. This will suppress reaction 6 to insignificant levels. Moreover, the Be^7 ions will pass through the DECs (because they are tuned to α particles only), and can be easily collected at their collector plates.

We conclude that isotope purification to only 99% of the B^{11} can reduce all contaminating side reactions to insignificant levels. The 15.96 MeV gamma photons of reaction 2 are harmlessly absorbed in the walls and cooling system of the reaction and DEC chambers.

Table 1: Data on the most relevant side reactions and their comparison to the main reaction 1. σ_1 is the cross section for the reaction 1 at $\varepsilon=\varepsilon_R=620$ keV. n_p and n_α are the proton and He^4 densities, and V_p and V_α are their respective velocities. $\sigma(\varepsilon_R)$ is the cross section for the various side reaction rates and the main reaction rate.

Reaction	Q(MeV)	$\sigma(E_R)/\sigma_1$	$n_\alpha\sigma(E_R)V_\alpha/(n_p\sigma_1 V_p)$
1: B^{11}(p,αα)α	8.681	1	
2: B^{11}(p,γ)C^{12}	15.956	$\sim 5\times10^{-5}$	
3: B^{11}(p,n)C^{11}	–2.764	$[1.5\times10^{-5}]$	
4: B^{11}(α,n)N^{14}	0.157	$< 10^{-4}$	$< 10^{-12}$
5: B^{11}(α,p)C^{14}	0.784	$< 10^{-5}$	$< 10^{-13}$
6: B^{10}(p,α)Be^7(β^+)Li^7	1.146	$\sim 6\times10^{-3}$	
7: B^{10}(p,γ)C^{11}(β^+)B^{11}	8.690	$\sim 1.2\times10^{-7}$	
8: B^{10}(p,n)C^{10}	–4.433		
9: B^{10}(p,He^3α)α	–0.442	10^{-4}	
10: B^{10}(α,n)N^{13}	1.0589	10^{-4}	$< 10^{-12}$
11: B^{10}(α,p)C^{13}	4.0616	10^{-4}	$< 10^{-12}$
12: B^{10}(α,d)C^{12}	1.3399	$<< 10^{-4}$	$<< 10^{-12}$

4. NUCLEAR POLARIZATION

The fusion reactions have the form

$$A(I_A)+B(I_B)\rightarrow C^*(I_C)\rightarrow \text{products} \tag{26}$$

They proceed through a compound nuclear (CN) state C^*, with spin I_C; the reacting nuclei have spins I_A and I_B. D-T and D-He^3 reactions in FRCs would be at low energies, and since they then occur in (rotating) thermonuclear plasmas, only the l=0 relative angular momentum state reacts. The same holds for the H-B^{11} reaction, but now the negligible involvement of l=1 and higher states results from the averaging of the relative velocity directions in the x-y plane.

Possible I_C values range from (I_A-I_B) to (I_A+I_B). However, all three reactions proceed through an $I_C=I_A+I_B$ CN state at the collisions energies considered (only D-T would undergo some I_C=1/2 fusions, but these account for at most a few percents).

Consider A-B fusion reactions with non-polarized nuclei, for which the cross sections have been measured. Given the spin multiplicities (2I+1) for each reaction species, the fraction of close A-B collisions that can contribute to the fusion cross section is given by

$$f_{AB}\,(C^*)=\frac{2I_C+1}{(2I_A+1)(2I_B+1)} \tag{27}$$

If both A and B are polarized with say their maximum spin components parallel to the injected beam direction, all close encounters can contribute. As a result a *nuclear spin enhancement* of the experimental cross section, $E^S{}_{AB}$, can occur equal to

$$E^S{}_{AB}=\frac{1}{f_{AB}(C^*)}=\frac{(2I_A+1)(2I_B+1)}{2I_C+1} \tag{28}$$

In D-T fusion, I_D =1 and I_T=1/2. The fusion proceeds through a CN state He$^5(3^+/2)^*$ at about 100 keV. We thus find

$$E^S{}_{DT}=1.5 \tag{29}$$

In D-He^3 fusion, I_{He3}=1/2, and the fusion proceeds through Li$^5(3^+/2)^*$ around 250 keV. Thus,

$$E^S{}_{D\text{-}He^3}=1.5 \tag{30}$$

The H-B^{11} fusion reaction involves spins $I_p=1/2, I_{B11}=3/2$ and $I_{C12}=2$ near the resonance at 580 keV in the c.m. frame. Therefore

$$E^{S}_{HB^{11}} = 1.6 \tag{31}$$

Kulsrud et al. [10] considered possible mechanisms for depolarization in a magnetic fusion reactor. These mechanisms apply equally to Tokamaks and to our FRC plasmas. It was found that all these mechanisms lead to depolarization rates orders of magnitude slower than burn or diffusion rates. This will be discussed in the next section.

There can be an additional enhancement if nuclei A and/or B have electric quadrupole moments Q. This requires that I_A and/or $I_B \geq 1$. This is true for D in D-T and D-He^3 reactions, but the Q_D =0.27 fm^2 is too small for a significant effect. On the other hand, the value Q_{B11}=4.06fm^2 for B^{11} is considered substantial for a nucleus with this size and charge.

How can we understand this enhancement and how large could it be? Nonspherical nuclei have electric quadrupole moments. Most commonly they have either a prolate (Q>0) or oblate (Q<0) ellipsoidal shape. According to the physics of nuclear magnetism [11], the principal quadrupole axis of such nuclei tends to align with the polarization direction of the magnetic dipole moment. This alignment increases with the spin component I_1 parallel to the field. It induces NMR level shifts which are different for different I_1 values. This results in NM line results that are proportional to the product of the electric gradient q at the nucleus and the electric quadrupole moment Q.

Proceeding semi-classically, consider a proton that approaches a B^{11} head on along a direction that makes an angle Θ with the quadrupole moment axis. According to a model by Wong [12], fusion cross sections involving nonspherical nuclei can exhibit dramatic variations with Θ for collisions at or just below the Coulomb barrier. Physically this is related to the lower barrier at the ends of the prolate nucleus B^{11} (Θ = 0 or π), which in turn gives an easier barrier penetration for a proton, i.e., a larger fusion cross section. Sub-barrier cross sections vary exponentially with the collision energy, becoming most rapid at near-barrier energies. Therefore even small variations in barrier heights (as in B^{11} with Θ changes) can result in relatively large variations of fusion cross sections.

Following Wong's model, these cross sections have the dependence

$$\sigma_F(\theta) = \sigma_F(P_2(\cos\theta)) \tag{32}$$

on the angle θ. Therefore experimental cross sections without quadrupole alignment can be related like

$$\sigma_F = <\sigma_F(\theta)>_\Omega \tag{33}$$

where the average is over the sphere. In a Tokamak, with or without nuclear polarization, the same holds true: because of the thermonuclear nature of its plasma, all orientations on the sphere arise for the relative velocity vector. On the other hand, in our CBFR the relative velocity vector between H and B^{11} is largely in the plane perpendicular to the z axis. Therefore, with the principal quadrupole axis in that plane(which would be the case if it is aligned to the beam directions) the averaging of $\sigma_F(\theta)$ is on the circle. Then the relevant quadrupole modified fusion cross section is

$$\sigma^Q{}_F \equiv \frac{1}{2\pi}\int_0^{2\pi}\sigma_F(\theta)d\theta \qquad (34)$$

The nuclear shape for *I* 1 is expressed as

$$R(\theta) \approx R_{ave}(1 + \beta_2 Y_{20}(\theta))$$

with R_{ave} the average radius, and $R(\theta)$ is the distance to the nuclear surface in direction θ. Prolate and oblate nuclei are characterized by positive and negative β_2 values, respectively. For B^{11} we have the relationship between the quadrupole moment and β_2 (assuming a uniform charge density)

$$Q_{B^{11}} = \frac{3Z}{\sqrt{5\pi}} R^2_{ave}\beta_2[1+(\frac{20}{49}\pi)^{1/2}\beta_2 \ldots] \qquad (35)$$

with

$$R_{ave} \cong 1.07\, A^{\frac{1}{3}}\, fm = 2.2\, fm \qquad (36)$$

with A=11 the atomic number; we compute

$$\beta_2 = 0.22 \qquad (37)$$

According to Wong's model, since

$$\frac{1}{2\pi}\int_0^{2\pi} P_2 \cos(\theta)d\theta = \frac{1}{2} \qquad (38)$$

we conclude for B^{11}

$$E^Q{}_{HB^{11}} \equiv \frac{\sigma^{Q_F}}{\sigma_F} \succ 1 \qquad (39)$$

Spin enhancement can also occur independently of nuclear shape enhancement despite magnetic and electric quadrupole moment alignment. There are no experiments available to determine the shape effect for H-B^{11} fusion. However, a rather old but reliable series of measurements of fusion cross sections for the reaction

$$O^{16} + Sm^A \longrightarrow \text{products} \quad A = 148,150,152,154 \qquad (40)$$

by Stokstad et al. [13] may bear witness to our assertion that the nuclear shape enhancement in H-B^{11} fusion can be substantial (see also Leigh et al. [14] for a confirmation of Stokstad's results). The physical characteristics relevant for comparison with H-B^{11} reaction are:

1. O^{16} has zero spin, therefore the variation in fusion cross sections for various A values is not influenced by any spin polarization or Sm^A spin states.
2. The Sm^A collision energies range from 54 MeV to 68 MeV in the center of mass frame [13]. The associated closest b_1 range from 12 fm to 10 fm. This is to be compared with the closest approach in H-B^{11} collisions at the $E_R \approx 580$ keV resonance energy of $b_2 \approx 12$ fm.
3. Using the formula of Eq.(36) for nuclear sizes R we find

$$\begin{aligned} R_1 &\equiv R(O^{16}) + R(Sm^A) \approx 8.4\,fm \\ R_2 &\equiv R(p) + R(B^{11}) \approx 3.3\,fm \end{aligned} \tag{41}$$

   $b_1/R_1 \approx 1.3$ expresses the fact that the $O^{16} - Sm^A$ reactions are non resonant at sub-to-near Coulomb barrier energies. On the other hand, $b_2/R_2 \approx 3.6$ reflects a below-Coulomb barrier resonance characteristic of H-B^{11} fusion reactions.
4. Stokstad et al. [13] found a dramatic spread in $O^{16} - Sm^A$ fusion cross sections for A values of Eq.(38) at the low end of the collision energy range that can not be explained by the variations of the Sm^A nuclear sizes. σ_F increases steadily with increasing A, giving rise to an enhancement of a factor 20 for A=154 compared to A=148. This enhancement is attributed to the non-spherical shapes of the Sm^A nuclei: the shape parameter β_2 varies from β_2=0.00 for A=148 to β_2=0.20 for A=154. The upper end of the collision energy range yields fusion cross sections which are nearly independent of A, occurring slightly above the Coulomb barrier [14].

It should be pointed out that these experiments were without nuclear polarization. The effects would have been much larger if Sm^A were polarized, as stressed by Mosel [15].

These results should be juxtaposed with H–B^{11} fusion: the β_2=0.22 for B^{11} and its sub-barrier character 580 keV, strongly suggest a large shape enhancement to the fusion cross section upon polarization. Moreover, in section 3 we found a ratio of 6×10^{-3} of the fusion cross sections for p–B^{10} and p–B^{11} fusion reactions (entry 6 in the table), considered to be a very small value. In view of the findings above, particularly point 4., the enhancement could be enormous. On the other hand, the B^{10} nucleus has a larger Q value (by nearly a factor 2), which is at odds with Wong's model: it would have predicted a smaller p–B^{11} fusion cross section than that for p–B^{10}. This illustrates limitations of this model. *In light of this empirical data, experimental verification of this effect would be highly desirable.*

5. NUCLEAR POLARIZATION

5.1 Seven Steps Towards Fuel Trapping

From the formation of highly polarized nuclear spins to the capture of the nuclei in the steady state FRC plasma, we can identify different steps, with their respective polarization/depolarization physics. These steps are as follows:

- **Step 1 - Polarization of Atomic Beams.**
  Several techniques can be used, that range from optical pumping to Stern-Gerlach separation, RF re-populations, and any of their combinations. This publication will not address these techniques. A study is currently under way to find the most sturdy, simple and energy efficient method.

  Spins will be polarized in a holding field $\boldsymbol{B}_h = \boldsymbol{B}_h^{\perp}$, i.e., perpendicular to the FRC axis, and (most likely) to the beam direction.

- **Step 2 - Exiting the Holding Field.**
  The polarized atomic beams will exit the holding field in about 1 μsec, of which the direction remains unchanged while its magnitude drops to zero.

- **Step 3 - $\vec{H}$ and (possibly) $\vec{B}^{11-}$ Formation.**

  In order to accelerate $\vec{H}$ and maybe $\vec{B}^{11}$, we should produce negative ions. Several charge exchange methods exist for this purpose.

  In any case, the polarized atomic beams enter and exit some charge exchange device, while retaining their velocities. No magnetic field will be present.

- **Step 4 - Acceleration of Ions.**
  Standard techniques will be used, capable of preserving the polarization (see below).

- **Step 5 - Neutralization of Ions through Electron Stripping.**
  Optimal techniques are required for ion neutralization, and this process needs further study. However, no depolarization is expected (see below).

- **Step 6 - Passage of Neutrals through Intense Magnetic Field in Vacuum before Entering FRC Plasma.**
  After exiting the neutralization stage the neutral atoms enter the 'return' field of the FRC, reaching a strength of about 10 T in less than 1 μsec. The vacuum field $B_v^{\parallel}$ is by definition directed parallel to the FRC axis, and is perpendicular to the holding field $B_h^{\perp}$ to polarize the nuclei.

  As we will see below, polarization will be maintained during this step.

- **Step 7 - Complete Ionization of Neutrals and Subsequent Trapping by FRC Plasma.**

  As soon as the beam atoms enter the plasma a rapid cascade of ionization for $\vec{B}^{11}$ begins (a single one for $\vec{H}$); the presence of a high T_e makes the ionization complete. Each ionization event will take $t_i \sim a_0/v_e = a_0/(2T_e/m_e)^{1/2}$ or about 10^{-18} sec. Little heating of the p and B^{11} occurs in the process. Heating will happen 'later' through ion-ion collisions.

Atom-ion collisions provide the largest cross section (~ 10^{-15} cm^2), thus with n ~ 10^{15}/cm^3 the ionization length l_{ion} ~ cm, which is sufficient.
The ions are now trapped by the FRC plasma, and they will start betatron oscillations about the magnetic-null surface. The $\vec{p}$ and $\vec{B}^{11}$ ions will have different betatron frequencies consistent with their different azimuthal velocities so as to 'stay' on the fusion resonance (see Section 2).

It is worth estimating the various characteristic frequencies with which the $\vec{p}$ and $\vec{B}^{11}$ are oscillating in the three cylindrical directions. The azimuthal frequencies are

$$\nu_{p\theta} \equiv \frac{\omega_p}{2\pi} = 7.0 \text{ MHz}; \nu_{B\theta} \equiv \frac{\omega_B}{2\pi} = 1.0 \text{ MHz} \tag{42}$$

According to the theory of betatron oscillations in FRC's we can relate $\upsilon_{i\theta}$ to the $\upsilon_{ir,}$ the betatron frequencies (i=p, B^{11}):

$$\nu_{ir} = \sqrt{1-s_o}\,\nu_{i\theta} \tag{43}$$

where

$$s_0 = -\left(\frac{dB_Z}{dr}\right)\left(\frac{r_o}{B_o}\right) \tag{44}$$

is the field index in the interior of the FRC at radius $r=r_o$, about which the betatron oscillations occur. In our FRC

$$s_0 = -\frac{2r_0}{\Delta r}\sqrt{\beta} \sim -926 \tag{45}$$

and it follows therefore

$$\nu_{pr} = 213 \text{ MHz}, \nu_{Br} = 30 \text{ MHz} \tag{46}$$

The axial frequencies ν_{iz} arise due to the ion temperature; a reasonable measure is

$$\nu_{iz} = \frac{\left(\frac{2T_i}{m_i}\right)^{\frac{1}{2}}}{2L} \tag{47}$$

where L is the length of the FRC plasma. It corresponds to the bounce frequency between the

FRC ends for an ion temperature T_i. The results are

$$\nu_{pz} = 0.8 \text{ MHz}, \nu_{Bz} = 0.2 \text{ MHz}. \tag{48}$$

The $v_{i\theta}$ and v_{ir} will be rather well-defined, but the v_{iz} velocity distribution shows higher dispersion.

5.2 Physics of Beam and Plasma Depolarization

In order to quantify any depolarization during the above steps, we first summarize the theory of the dynamics of initially polarized nuclear spins in electromagnetic fields. We will rely heavily on a series of papers on spin polarized plasmas by Kulsrud et al. [10]. We also consulted the classic book on magnetic resonance by Slichter [16].

Formally, the treatment of polarized plasmas requires a quantum description for the i-th particle magnetic moment $\boldsymbol{\mu}_i$ in the magnetic field, and a classical description for its position $\mathbf{x}_i$ and velocity $\mathbf{v}_i$. This method employs a quasi-classical approximation.

In a plasma, because of its relatively low density, the spin dynamics of the particles are practically uncorrelated. If the spins of a plasma of density $10^{15}/\text{cm}^3$ were perfectly aligned, a field of 10^{-8} Gauss would be produced which is a factor 10^{-13} smaller than the conventional plasma confining fields. Spin-spin interactions, although occurring continually, are negligible in mean behavior. We conclude that the plasma spins can be treated as independent.

The magnetic moment operator for the i-th spin is

$$\mu_i = \gamma_i \hbar \mathbf{I}_i \tag{49}$$

where γ_i is the gyromagnetic ratio, often expressed as (in cgs units)

$$\gamma_i \hbar = g_i \frac{e\hbar}{2 m_p c} = g_i \mu_N \tag{50}$$

where μ_N is the nuclear magneton (m_p is the proton mass). $\mathbf{I}_i$ is the dimensionless spin operator. g_i is of the order of unity. The Hamiltonian for the spin-field interaction is

$$H = -\mu_i \cdot B_i \tag{51}$$

with

$$B_i = B(x_i, t) - v \times E(x_i, t)/c, \tag{52}$$

the field 'seen' by the i-th particle at $\mathbf{x}_i, \mathbf{v}_i, t$. The Heisenberg equation of motion for $\boldsymbol{\mu}_i$ is

$$\frac{d\mu_i}{dt} = \frac{i}{h}[H,\mu_i] \tag{53}$$

the field 'seen' by the *i*-th particle at $\mathbf{x}_i$,$\mathbf{v}_i$,t. Using the commutation relation among spin components yields

$$\frac{d\mu_i}{dt} = \mu_i \times \gamma_i \boldsymbol{B}_i \tag{54}$$

Using Eq.(52) we also write

$$\frac{d\boldsymbol{I}_i}{dt} = \boldsymbol{I}_i \times \gamma_i \boldsymbol{B}_i \tag{55}$$

Now consider the *i*-th particle spin state $|\psi_i>$. We can define the polarization vector

$$\mathbf{p}_i = \langle \psi_i | \boldsymbol{I}_i | \psi_i \rangle \tag{56}$$

or the expectation value of $\boldsymbol{I}_i$. Taking such a value of the operator equation (54) we get

$$\frac{d\mathbf{p}_i}{dt} = \mathbf{p}_i \times \gamma_i \mathbf{B}_i \tag{57}$$

This equation is the same as for the classical time evolution of magnetic moments immersed in a magnetic field. Among others, it shows that

(a) $p_i = |\mathbf{p}_i|$ is constant;

(b) $\mathbf{p}_i$ precesses about $\hat{\mathbf{b}}_i = \mathbf{B}_i/\mathrm{B}_i$ with frequency $\gamma_i B_i$ and a constant angle with $\hat{\mathbf{b}}_i$;

(c) if $\mathbf{p}_i$ is parallel to $\mathbf{B}_i$, $d\mathbf{p}/dt = 0$, regardless of any time change of $\mathbf{B}_i$;

(d) since

$$\delta\mathbf{p}_i = \mathbf{p}_i \times (\gamma_i \mathbf{B}_i \delta t) \tag{58}$$

and p_i is of order unity, $\delta p_i << p_i$ if

$$\gamma_i B_i \delta t \ll 1 \tag{59}$$

i.e., Eq.(62) is the condition for an insignificant change of $\mathbf{p}_i$, or depolarization, under brief field fluctuations.

The $\mathbf{p}_i$ above are somewhat different from those used in [10]. It has the advantage that it applies to any I_i, and that the relationship to classical dynamics is most transparent [16].

In the above treatment it was assumed that the spin Hamiltonian $\mathcal{H}$ for all particles is separable, i.e., $\mathcal{H}=\Sigma_i \mathcal{H}_i$; instantaneous spin-spin interactions were ignored. This makes the system's spin wavefunction of the form

$$|\psi\rangle = \prod_i |\psi_i\rangle \tag{60}$$

i.e.,$|\psi>$ is a pure state. If spin-spin interactions are included, $|\psi>$ becomes a mixed state. In Ref. [10] it is shown that $|\psi>$ becomes 'impure' at a rate orders of magnitude slower than the depolarization rates from other sources. Therefore, from now on we will ignore mixed states: we will ignore any effects to the spin wavefunction due to direct interactions between spins.

We are now ready to introduce a generalization to the Fokker- Planck (and Vlasov-Maxwell) equations, including polarization. Each particle is described in a nine-dimensional phase space spanned by *x*, *v* and *p* (we drop the subscript "*i*" for convenience). We define a distribution function in this space by

$$\delta n(\mathbf{x},\mathbf{v},\mathbf{p},t) = f(\mathbf{x},\mathbf{v},\mathbf{p},t)\,\delta^3 x\,\delta^3 v\,\delta^3 p \tag{61}$$

where δn is the number of particles in the volume element $\delta^3 x\ \delta^3 v\ \delta^3 p$ at $(\mathbf{x},\mathbf{v},\mathbf{p})$. The equations of motion are

$$\begin{aligned} \frac{dx}{dt} &= v \\ \frac{dv}{dt} &= \frac{q}{m}(\boldsymbol{E}+v\times\boldsymbol{B}/c) \\ \frac{dp}{dt} &= p+\gamma(\boldsymbol{B}-v\times\boldsymbol{E}/c) \end{aligned} \tag{62}$$

From Liouville's equation in this extended space we get the conservation equation

$$\frac{df}{dt} = \frac{\partial f}{\partial t} + v\cdot\nabla_x f + \frac{q}{m}\left(\boldsymbol{E}+\frac{\mathbf{v}\times\boldsymbol{B}}{c}\right)\cdot\nabla_v f + p\times\gamma\left(\boldsymbol{B}-\frac{v\times\boldsymbol{E}}{c}\right)\cdot\nabla_p f + \left(\frac{\partial f}{\partial t}\right)_{\mathrm{coll}} = 0 \tag{63}$$

If $(\partial f/\partial t)_{\mathrm{coll}} = 0$, we have the generalized Vlasov-Maxwell equation. Again, this equation applies to any spin *I*.

We observed that even totally aligned nuclear magnetic moments contribute negligibly to the internal field **B**. In contrast, the equation of motion for ***p*** is determined by **B** and **E**, arising in turn from the external and induced fields. Therefore the dynamics of **p** is strongly coupled to the **B** and **E** of the plasma related through the second and third terms in Eq. (63).

We should also point out that **E** ~ (v/c)**B** in plasmas, therefore the second term in the dp/dt equation is usually negligible for non-relativistic plasmas. However, during close collisions between plasma particles this term can be large, and its effect on **p** must be considered. The zero-th moment is defined as

$$F_l \equiv \int d^3 p f \tag{64}$$

We can easily verify that the term involving $_{\rho}f$ integrates away, and F_l is seen to satisfy the normal FP equation, as expected.

The first moment, defined as

$$P \equiv \int d^3 p \, p f \tag{65}$$

satisfies the equation

$$\frac{\partial P}{\partial t} + (\mathbf{v} \cdot \nabla_x) P + \{\frac{q}{m}(E + \frac{\mathbf{v} \times B}{c}) \cdot \nabla_v\} P + \gamma(B - \frac{v \times E}{c}) \times P = -(\frac{\partial P}{\partial t})_{coll} \tag{66}$$

5.3 Analysis of the Polarization Physics in each Step

We will now apply the above definitions, insights and equations to the physical conditions present in all steps, and determine their impact on the polarization and depolarization.

Step 1: We assume that the proper technique will be developed to achieve near 100% polarization in the holding field $\mathbf{B}_h$. P will be parallel to this field, and for typical B_h~0.1 T we have precession frequencies

$$\begin{aligned} \Omega_{ph} &= \gamma_p B_h \cong 4.3\text{MHz} \\ \Omega_{Bh} &= \gamma_B B_h \cong 1.4\text{MHz} \end{aligned} \tag{67}$$

We may have to make sure that the densities are less than $10^{12}/\text{cm}^3$ to avoid significant depolarization due to fine structure level quenching. We will investigate whether this limit can be exceeded with adiabatic beam cooling, a technique to reduce atom-atom collisions. This should not be necessary for $\vec{H}$ beams.

Step 2: When the beams exit the holding field the spins will cease to precess, and **P** will be unchanged, provided that the direction of the 'dying' field stays constant while exiting. This is evident from Eq. (55). If there are 'stray' fields with directions different from that of $\mathbf{B}_h$ the time of passage δt_r through such fields should satisfy Eq. (59) for redirection of **P** not to occur. This is possible to arrange.

Step 3: The attachment of an electron to $\vec{H}$ and $\vec{B}^{11}$ seems like a violent event to the electromagnetic environment of the polarized nuclei. Indeed, the momentary change of the $v \times E/c$ in Eq. (50) is large; it can be estimated from considering an electron suddenly appearing at a distance or r~1Å with velocity $v \sim 10^9$ cm/s. We then find

$$\frac{vE}{c} \cong \frac{v}{c}\left(\frac{e}{r^2}\right) \cong 20 \text{ Tesla} \tag{68}$$

However, the extra electron either 'flies by' in δt 10^{-16} sec, or is bound in an orbital in that time, giving only a small $\delta p_i/p_i$.

This contribution to collisional depolarization was studied more precisely in [10], and a formula was derived for the associated cross section. The result was

$$\sigma^{so}{}_{sp} \cong \frac{\pi}{3I} g^2 r_p^2 \ \ln \Lambda \tag{69}$$

I is the nuclear spin (in units of), g is defined in Eq. (48), $r_p = 1.529 \times 10^{-16}$ cm, the classical proton radius, and $\ln \Lambda$ 20, the Coulomb logarithm. Notice that $\sigma^{so}{}_{dp}$ is independent of the mass of the scattered particle, and it depends only weakly on its velocity through $\ln \Lambda$ [10]. Typical values for $\vec{H}$ and $\vec{B}^{11}$ are

$$\sigma^{so}{}_{dp,p} \cong 10^{-29}\,\text{cm}^2, \sigma^{so}{}_{dp,B} \cong 3 \times 10^{-31}\,\text{cm}^2 \tag{70}$$

These cross sections are very small compared to fusion cross sections (about 10^{-24} cm^2) and electron ionization or attachment cross sections (1 to 10 Å^2). We conclude that no significant depolarization takes place due to these encounters.

We attached the superscript 'so' to the cross section to indicate that this contribution arises from a spin orbit-like interaction. Since all the beam particles carry spin, there is also a spin-spin contribution: a rapidly passing spin induces a magnetic field with arbitrary direction. Scattering particles which are unpolarized, can then induce nuclear depolarization. This spin-spin depolarization cross section was found to be [10]

$$\sigma^{ss}{}_{dp} \leq f_{ij}(m_i, m_j)\pi r^2{}_p \tag{71}$$

where the i and j refer to the target and projectile particles, and m_i and m_j are their respective azimuthal quantum numbers. In Ref. [10] all f_{ij} are given for a D-T plasma. Their values range from 10^{-2} to 10. Inspection of their analytic dependence on $(g_i, g_j, I_i, I_j, m_i, m_j)$ shows that a similar range will occur for our p-B^{11} plasma. We thus express conservatively

$$\sigma^{ss}{}_{dp} \leq 10\ \pi r^2{}_p \cong 10^{-30}\,\text{cm}^2 \tag{72}$$

Finally, the B^{11} nuclei have a quadrupole moment, and thus have quadrupole interactions with $\vec{H}$ and electrons. It was found in [10] that electrons give a vanishingly small cross section to B^{11} depolarization (in fact, at least a factor $(m_e/m_p)^2$ smaller than $\sigma^{so}{}_{dp}$). The p-B^{11} quadrupole depolarization cross section $\sigma^{eq}{}_{dp}$ is not greater than the associated $\sigma^{so}{}_{dp}$ and almost certainly orders of magnitude smaller [10]. In summary, we can state

$$\sigma^{\text{coll}}{}_{dp} = \sigma^{so}{}_{dp} + \sigma^{ss}{}_{dp} + \sigma^{eq}{}_{dp} \cong \sigma^{SO}{}_{dp} \leq 10^{-29}\ \text{cm}^2 \tag{73}$$

for $\vec{H}$, $\vec{B}^{11}$, $\vec{H}^-$, $\vec{B}^{11-}$, and their positive ions including the bare polarized nuclei.

This sweeping result arises due to the smallness of the effect of the ($\mathbf{v} \times E$/c) term in the equation of motion for **p**. The interaction on the order of 10^{-16} sec occurs during passage of a charged particle (e, $\vec{p}$, $\vec{B}^{11}$) within atomic range of the above particles. The dependence on the relative velocity, and thus collision energy, is weak as it appears in ln Λ, thanks to the Coulomb nature of the SO interaction. The main difference between $\sigma^{ss}{}_{dp}$ and $\sigma^{so}{}_{dp}$ is the absence of the Coulomb logarithm in the former (this is also true for $\sigma^{eq}{}_{dp}$). This results from the $1/r^3$ behavior of the spin-spin interaction.

Step 4 and 5: It is clear from the discussion under Step 3 that acceleration and electron stripping do not affect polarization. In the absence of magnetic fields $\mathbf{p}_i$ does not precess, and $\mathbf{P}_i$ is constant throughout these steps.

Step 6: When the beams enter the strong chamber vacuum field (B_v 10 T) the nuclear spins start processing with frequencies

$$\Omega \quad 420\ \text{MHz},\ \Omega_{Bv} \quad 137\ \text{MHz} \tag{74}$$

As a result, the $\mathbf{p}_i$ rotate at these frequencies in the plane perpendicular to $\mathbf{B}_v{}^{\parallel}$.

The $\mathbf{P}_i$=$\mathbf{P}_i(x)$ are also in this plane, but do not rotate. Instead, $\mathbf{P}_i$ changes direction as **x** advances along the beam's path, with a rate of change characteristic of $\mathbf{V}_i$ and γ_r. In the absence of collisional depolarization (a good assumption in this case: the FRC-surrounding vacuum has low background ion density), P_i=constant.

We conclude that the $\vec{p}$ and $\vec{B}^{11}$ enter the FRC plasma becoming trapped in betatron-like orbits with an unchanged $\mathbf{P}_i$ from vacuum values but with

$$\cos\Theta_{pB}(r) \equiv \hat{P}_p \cdot \hat{P}_B(r) \tag{75}$$

where $\hat{P}_i = P_i/P_r$. In general

$$-1 \leq \cos\Theta_{pB}(r) \leq 1 \tag{76}$$

In fact, there is no guarantee that $\cos\Theta_{pB}(r_o)$=1, where r_o is the radius of the FRC plasma, unless the holding fields $\mathbf{B}^{\perp}{}_{hp}$ and $\mathbf{B}^{\perp}{}_{hB}$ in the spin polarization step make a certain angle $\Theta_{pB}{}^h$.

Therefore it will be necessary to tune $\Theta_{pB}{}^{h}$ such that the $\cos\Theta_{pB}(r_o)$ is near unity: only then can we obtain the maximum fusion cross section enhancement. This tuning obviously poses no difficulties.

The discussion thus far ignores effects from the finite length of the FRC. The particles bounce back-and-forth between the ends of the FRC plasma volume, with bounce frequencies v_{ii} that are much smaller than Ω_{ip} even for very small distances from the magnetic-null surface ($\Omega_i=0$ occurs with measure zero). The plasma density maximum falls very near this surface, but never coincides with it ($((r-r_o)\quad 10^{-2}$ cm). Therefore, the great majority of the plasma ions have $\Omega_{ip} >> v_{iz}$.

But v_{iz} is a measure for the rate of change of the fields near the FRC ends. The above inequality states then the condition for an adiabatic change in P_i.

In this situation the adiabatic theorem in magnetic resonance is applicable [16]. For plasmas it amounts to the applicability of the guiding center approximation in the generalized FP theory including polarization, in particular the moment equation (66). This was analyzed in Ref.[10]. The conclusion is that the component **P** along the plasma magnetic field $\boldsymbol{B}_p(\boldsymbol{x})$ is independent of **x** to a good approximation when the rate of change of the field direction is small compared to the precession frequency.

For our purposes the most important consequence is that $\cos\,\Theta_{pB}$ is essentially independent of z along the magnetic-null surface. This is important since by adjusting $\cos\Theta_{pB}(r_o)$ to unity we can look forward to a maximum fusion enhancement in the entire length of the FRC plasma, hence the form of Eq. (54).

We can now discuss the collisional depolarization rate. Since the electrons are the fastest particles in the plasma, the collisional depolarization rate is dominated by the electron-ion collisions. With $\upsilon_e=(T_e/m_e)^{1/2} \approx 2 \times 10^{10}$cm/s, we compute ($n_e=10^{15}$ cm^3, $\sigma^{coll}{}_{\phi}\quad 2 \times 10^{-4}\ \mathrm{s}^{-1}$)

$$\lambda^{coll}{}_{\phi}\quad \lambda^{coll,e}{}_{\phi} = n_e\,\sigma^{coll}{}_{\phi}\,\upsilon_e \approx 2 \times 10^{-4}\ \mathrm{s}^{-1} \tag{77}$$

Two more plasma-peculiar depolarizations should be considered. The first one was called *gyro-collisional* (GC) depolarization by Kulsrud et al.[10]. During gyromotion in a sheared magnetic field, particles experience variations of the magnetic field. Thus, superimposed on the precessional motion is a small periodic oscillation component of **p**. Gyromotion and this small oscillation are correlated until a collision changes the gyrocenter, leading to small, nonperiodic changes in **p**. Many collisions can cause diffusion in **p** space, and thus shrinkage of **P**: depolarization occurs. Kulsrud et al. [10] estimate $\lambda^{gc}{}_{\phi}$-$10^{-3}\ \mathrm{s}^{-1}$ for tokamak densities of 10^{15}/cm^3.

We believe, however, that GC depolarization does not occur at all in FRC plasmas, because

(a) the ions follow betatron orbits, crossing the magnetic null-surface repeatedly;

(b) these motions are not correlated with the precessional motion since the $\mathbf{B}^{I}{}_{p}(\mathrm{r})$ oscillates in r at MHz frequencies;

(c) for most of the FRC plasma (except near the end points) the shear length is infinite. Each of these reasons alone can preclude GC depolarization.

The second type can be called *resonant-wave* (RW) depolarization. It can occur whenever a plasma fluctuation wave propagates along magnetic field lines about which polarization precesses. Such a wave would have an oscillatory magnetic field perpendicular to these field lines, and thus could be capable to flip **p** (see Eq. (57)). If its frequency is ω, and k^l and v^l are its wavenumber and velocity, depolarization can occur if ω satisfies (see [10])

$$\omega - k_{\|} v_{\|} + n\omega_l = \Omega_j \tag{78}$$

Here ω_l is the Larmor frequency appropriate for an adiabatic, small gyration plasma. In Ref.[10], Eq. (45) gives the expression for the associated depolarization. For tokamak D-T plasma a possibly serious depolarization for tritons is pointed out ([6],[10]).

We will now show that RW depolarization is not a problem in our FRC plasma. Firstly, in Eq.(78) we should replace the term '$n\omega_l$' by '$nv_{i\theta}$' where $v_{i\theta}$ are the azimuthal frequencies. Secondly, because the FRC plasma has finite length, ω and k_l are 'quantized': the axial waves, if occurring, are standing waves. ω_m and k_{lm} are related by a dispersion relation; here it is only important that $(\omega_m - k_{lm} v_l)$ have only discrete values.

Thirdly, and most importantly, because the betatron-like oscillations of the particles, the precession frequencies in the FRC plasma Ω_{jp} vary like

$$\Omega_{jp}(t) = \Omega_{jp0}\cos(\omega_{ir} t) \tag{79}$$

We now find the FRC-type resonance condition

$$\omega_m - k_{\|m} v_{\|} + n\,\omega_{i\theta} = \Omega_{jp}(t) \tag{80}$$

This is an important result. Since $n,m = 0,1,2$ there will be typically only a few values of t within a period satisfying Eq. (78). Notice that all pairs $i,j=p$,B^{11} have to be considered. If we now take the collisional depolarization into account, the condition (78) is somewhat relaxed:

$$\Omega_{jp} - 2\frac{\pi}{T_1} < (\omega_m - k_{\|m} v_{\|} + n\,\omega_{i\theta}) < \Omega_{jp} + \frac{2\pi}{T_1} \tag{81}$$

where $2\pi/T_1 \sim 10^{-3}$ rad/s, (T_1 is the spin-relaxation time[16]), to be compared with $\omega_{pr} \sim 10^8$ rad/s. We see that no more than a fraction 10^{-11} of the betatron oscillation period will RW depolarization be active.

The actual amount of depolarization will, of course, depend on the wave's amplitude. This in turn, will depend on the damped or undamped nature of the wave. In [10] it was found that already with $\delta B/B \sim 10^{-4}$ and on resonance frequency ω, a RW depolarization rate value $\lambda^{rw}_{dp} \sim 0.1$ s^{-1} was found for triton in a D-T plasma. However, in the PhD thesis of one of us (MWB, unpublished), it was pointed out that only a few axial modes were observed in FRCs (m_z m 2). These were typically stabilized by various means, i.e., the associated $\delta B/B$ must be smaller. We thus conclude that in our FRC plasma

$$\lambda^{rw}{}_{dp} \prec \frac{2\pi}{T_1\,\omega_{pr}}\nu_{pr} = \frac{1}{T_1} \tag{82}$$

$$\lambda^{rw}{}_{dp} \prec 10^{-4}\,s^{-1} \tag{83}$$

5.4 Concluding Remarks

We have shown that the total depolarization rate in a FRC plasma is negligibly small; for n=10^{15}/cm^3,

$$\lambda^{tot}{}_{dp} \quad \lambda^{coll,e}{}_{dp} + \lambda^{gc}{}_{dp} + \lambda^{rw}{}_{dp} \quad 2 \times 10^{-4}\,\mathrm{s}^{-1}. \tag{84}$$

We have also shown that FRCs are less prone to wave depolarization, largely due to the dramatically varying precession frequencies Ω_{jp} of the spins as they oscillate radially through the null surface on their betatron orbits(see Eq. (78)). Therefore, unlike tokamak conditions [6],[10], resonance with any finite number of particular waves can not occur.

As pointed out by Kulsrud et al. [10], an additional problem in tokamaks is depolarization due to spin interactions with wall metal atoms. Because of the superior confinement of our FRC plasma, their densities on walls are smaller by many orders of magnitude, leading to negligible wall-induced depolarization.

Therefore, we conclude that nuclear depolarization in FRC plasma can be ignored on the fusion time scale τ_F~1 to 10 sec.

REFERENCES

1. N. Rostoker, M.W. Binderbauer and H.J. Monkhorst. (This proceedings p. 291).
2. H.W. Becker, C. Rolfs and H.P. Trautvetter. Z. für Physik **A327**, 341 (1987).
3. R. Feldbacher and M. Heindler. Nucl. Instr. and Meth. **A271**, 55 (1988).
4. R. Kulsrud et al. Phys. Rev. Letters, **49**, 1248 (1982).
5. L.J. Perkins et al. Current Trends in International Fusion Research (Plenum, New York, 1997), pp. 365-372.
6. B. Coppi et al. Phys. Fluids, **29**, 4060 (1986).
7. G. Hale. LANL, private communication.
8. F. Azjenberg-Selove. Nucl.Phys. **A449**, 70-80 (1986); **A506**, 1 (1990).
9. A.A. Palko. ORNL5418 (Contract No.W-7405-eng-26) (1978).
10. R.M. Kulsrud, E.J. Valeo and S.M Cowley. Technical Report PPPL (1986); S.M. Cowley, R.M. Kulsrud and E.J. Valeo. Phys. Fluids **29**, 430 (1986), and refs. cited
11. A. Abragam. The Principles of Nuclear Magnetism (OUP, London, New York, 1962).
12. C.Y. Wong. Phys. Rev. Letters, **31**, 766 (1973).
13. R.G. Stokstad et al. Phys Rev. **C21**, 2427 (1980).
14. Y.R. Leigh et al. Phys. Rev. **C47**, R437 (1993).
15. U. Mosel. Treatise on Heavy Ion Science (D.A. Bromley, Ed.) Plenum, (1984), Vols. 2 and 3.
16. C.P. Slichter. Principles of Magnetic Resonance, Harper and Row Inc. (1963), Chs. 1 and 3.

KINETIC BALLOONING MODES IN TOKAMAKS

A. Hirose, M. Elia, M. Yamagiwa[1] and L. Zhang[2]

Plasma Physics Laboratory
University of Saskatchewan
Saskatoon, Saskatchewan, Canada
[1]Naka Fusion Research Establishment
Japan Atomic Energy Research Institute
Naka, Ibaraki, Japan
[2]Advanced Laser and Fusion Technology
Hull, Quebec, Canada

ABSTRACT

Recent progress in understanding the ballooning mode in tokamaks is reviewed. Analysis based on two-fluid and kinetic formulation has revealed the existence of the ballooning mode in parameter regimes where the ideal MHD ballooning mode is stable. Both the so-called second stability regime and negative shear regime are subject to kinetic ballooning instabilities driven by a finite ion temperature gradient η_i . Relevance of the theoretical studies to recent experimental observation of the ballooning mode and enhanced tokamak performance with negative shear will be discussed.

1. INTRODUCTION

The ballooning mode is an electromagnetic instability in magnetically confined plasmas driven by excessive plasma pressure gradient combined with unfavorable magnetic curvature. It is qualitatively described by the following local MHD dispersion relation,

$$\omega(\omega+\omega_{*pi})=(k_\parallel V_A)^2-\frac{2c_s{}^2}{L_pR}, \tag{1}$$

where $\omega_{*pi}=(1+\eta_i)\omega_{*i}$ is the ion diamagnetic drift frequency, V_A is the Alfven speed,

Current Trends in International Fusion Research — Proceedings of the Second Symposium
Edited by E. Panarella. NRC Research Press, National Research Council of Canada, Ottawa, ON K1A 0R6, Canada. 1999.

$c_s = \sqrt{(T_e + T_i)/M}$ is the sound speed, L_p is the pressure gradient scale length and R is the magnetic curvature radius. In a toroidal plasma such as tokamaks, both ingredients are intrinsically present, at least locally, and the ballooning mode is expected to impose an upper limit on the maximum pressure gradient that can be stably confined. For this reason, extensive theoretical and numerical investigations have been made in the past. Earlier studies were based on the ideal MHD approximation. In the original work [1] by Furth et al., the toroidicity (magnetic curvature) was mocked by an effective gravity with periodic variation. The critical plasma pressure gradient estimated is in the form,

$$\frac{d\beta}{dr} > f(U)\frac{1}{q^2 R},$$

where $\beta = 8\pi p / B^2$ is the normalized plasma pressure, q is the safety factor against the kink mode, and $f(U)$ is a function of relative magnetic well depth U. In the analysis, only the normal magnetic curvature was considered and the geodesic curvature, which plays an important role in actual toroidal plasmas, was not implemented. The magnetic shear s does not explicitly appear in the criterion either.

In 1977, with the advent of numerical equilibrium and stability codes, the problem of tokamak stability against low mode number ballooning mode was revisited [2,3]. It was found that for small shear, the ballooning mode occurs if

$$\frac{d\beta}{dr} \geq \frac{0.3}{q^2 R}, \text{ or } \alpha = -q^2 R \frac{d\beta}{dr} \geq 0.3, \tag{2}$$

where α is the ballooning parameter. Theoretical explanation to the instability found numerically was subsequently given by Connor et al. [4] in terms of the ballooning transformation [4–6] which has enabled rigorous stability analysis of the ballooning mode in tokamaks. For a tokamak discharge with circular magnetic surfaces with Shafranov shift, the mode equation at marginal stability is given by

$$\frac{d}{d\theta}\left([1+(s\theta-\alpha\sin\theta)^2\frac{d\phi}{d\theta}\right)+\alpha[\cos\theta+(s\theta-\alpha\sin\theta)\sin\theta]\phi = 0, \tag{3}$$

where θ is the extended poloidal angle. The second term represents the ballooning drive, the $\cos\theta$ term due to the normal curvature and $\sin\theta$ term due to the geodesic curvature. The stability boundary emerging from the mode equation is shown Fig. 1 as dotted line. For a given shear s the onset of the ballooning mode occurs at the first boundary. Further increase in the ballooning parameter results in stabilization (second stability region) [7–10]. This may be attributed to deactivation of the ballooning drive

$$\alpha\int[\cos\theta+(s\theta-\alpha\sin\theta)\sin\theta]\phi^2 d\theta,$$

which could become negative for large α and appropriate eigenfunction $\varphi\theta$.

The validity of ideal MHD approximation applied to the ballooning mode has largely

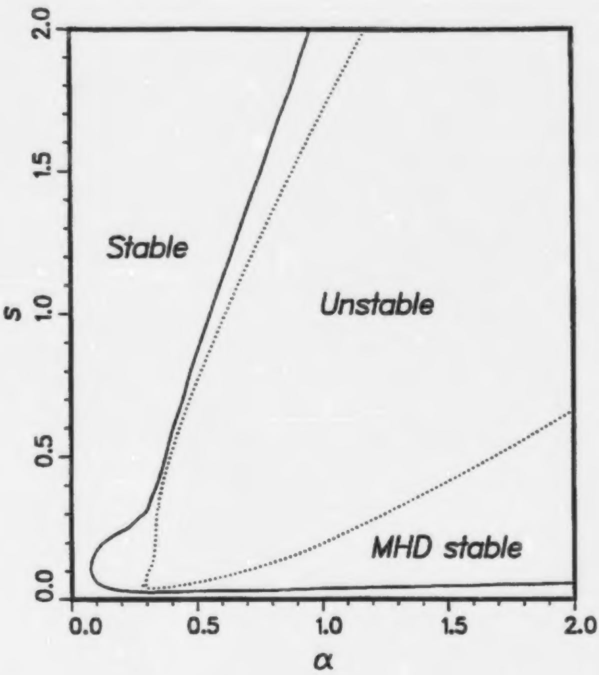

Figure 1. Stable-unstable boundaries in the (s, α) plane from ideal MHD approximation (dotted line) and kinetic analysis (solid line) when $b_0 = 0.01$, $\tau = 1$, $\varepsilon_n = 0.175$, $\eta_i = \eta_e = 2$.

been confirmed by Cheng [11] who has developed a gyro-kinetic stability code. In particular, stabilization in the MHD second stability regime has been recovered in the kinetic analysis as well. More recently, Nordman et al. [12] have re-analyzed the ballooning mode in terms of two-fluid approximation and also recovered the results based on ideal MHD. However, Hirose et al. have shown that if the ion temperature gradient η_i is finite, the MHD second stability regime essentially disappears [13]. This pessimistic finding has later been confirmed in two-fluid approximation as well [14]. The kinetic ballooning mode (KBM) persists even in negative shear region [15] $s < 0$ where the ideal MHD mode has been known to be stable. The driving mechanism of the KBM is attributed to the kinetic resonance due to the ion magnetic drift which is enhanced by the ion temperature gradient.

In contrast to extensive theoretical investigations, experimental observation of the ballooning mode has been rare largely because tokamaks are usually operated at α (ballooning parameter) well below the critical value. Recently, in TFTR DT supershot discharges, low mode number magnetic fluctuations have been identified as the KBM for a ballooning parameter $\alpha \simeq 0.05$. [16] This exceeds the MHD critical α and the ideal MHD ballooning mode is expected to be unstable. Use of kinetic ballooning theory is needed to predict the frequency and identify the most unstable mode. The kinetic ballooning theory applied to the TFTR parameters predicts that the most unstable mode occurs at n (toroidal mode number) ≈ 6 in a favorable agreement with the experimental observation [17].

2. FORMULATION OF KINETIC BALLOONING THEORY

The ballooning mode is a destabilized Alfven mode and its frequency falls in the so-called intermediate frequency regime, $k_\parallel v_{Ti} < |\omega| < k_\parallel v_{Te}$ where $k_\parallel v_{Ti(e)}$ is the ion (electron) transit frequency. In this regime, electron inertia plays no role and the electron density and parallel current perturbations can be found from the following hydrodynamic equations,

$$(\partial_t + V_{De} \cdot \nabla) n_e + \nabla \cdot [n_0 (v_E + v_{De})] - \frac{1}{e} \nabla \cdot J_{\parallel e} = 0,$$

$$0 = -e n_0 E_\parallel - \nabla_\parallel p_e - \frac{1}{B} B_\perp \cdot \nabla p_{e0},$$

$$\nabla_\parallel T_e' + \frac{1}{B} B_\perp \cdot T_e = 0,$$

where $v_E = cB \times \nabla\phi / B^2$ is the E × B drift, V_{De} is the electron magnetic drift, v_{De} is the perturbed electron magnetic drift due to temperature perturbation T_e', $E_\parallel = -ik_\parallel \phi + i\omega A_\parallel$ is the parallel electric field, $p_e = n_0 T_e' + n_e T_e$ is the pressure perturbation, and $B_\perp = \nabla \times A_\parallel$ is the magnetic perturbation. Elimination of the temperature perturbation yields

$$n_e = \left(\phi - \frac{\omega - \omega_{*e}}{ck_\parallel} A_\parallel \right) \frac{e}{T_e} n_0, \tag{4}$$

$$J_{\parallel e} = \frac{n_0 e^2}{k_\parallel T_e} \left((\omega_{*e} - \omega)\phi + \frac{(\omega - \omega_{*e})(\omega - \omega_{De}) + \eta_e \omega_{*e} \omega_{De}}{ck_\parallel} A_\parallel \right), \tag{5}$$

here ω_{*e} is the electron diamagnetic drift frequency, ω_{De} electron magnetic drift frequency, $\eta_e = d \ln T_e / d \ln n_0$ and electron temperature gradient. Trapped electrons which are known to be weakly stabilizing the ballooning mode are ignored in the analysis to follow.

For ions, the gyro-kinetic distribution function is

$$f_i = -\frac{e\phi}{T_i} f_{Mi} + \frac{\omega + \hat{\omega}_{*i}(v^2)}{\omega + \hat{\omega}_{Di}(v,\theta) - k_\parallel v_\parallel} J_0{}^2(x) \left(\phi - \frac{v_\parallel}{c} A_\parallel \right) \frac{e}{T_i} f_{Mi}, \tag{6}$$

where f_{Mi} is Maxwellian,

$$\hat{\omega}_{*i}(v^2) = \omega_{*i} \left[1 + \eta_i \left(\frac{Mv^2}{2T_i} - \frac{3}{2} \right) \right],$$

$$\hat{\omega}_{Di}(v,\theta) = \frac{Mck_\theta}{eBR} \left(\frac{1}{2} v_\perp{}^2 + v_\parallel{}^2 \right) [\cos\theta + (s\theta - \alpha \sin\theta) \sin\theta],$$

and $J_0(x)$ is the Bessel function with an argument

$$x = \frac{k_\perp v_\perp}{\omega_{ci}} = \frac{k_\theta v_\perp}{\omega_{ci}} \sqrt{1+(s\theta - \alpha \sin\theta)^2}.$$

The ion density and parallel current perturbations are to be evaluated from the integrals,

$$n_i = \int f_i dv, \quad J_\| = e \int v_\| f_i dv.$$

Imposing charge neutrality $n_e = n_i$, the parallel Ampere's law can be cast into the following mode equation,

$$\frac{d}{d\theta}\left([1+(s\theta-\alpha\sin\theta)^2] \frac{d\phi}{d\theta} \right) + V(\theta)\phi = 0, \tag{7}$$

where

$$V(\theta) = \frac{q^2\beta_e}{2{\varepsilon_n}^2}\left((\hat{\omega}-F)(\hat{\omega}-1) + \eta_e F - \tau\delta^2 M_{i2} - \frac{(\hat{\omega}-1-\tau\delta M_{i1})^2}{1+\tau(1-M_{i0})} \right), \tag{8}$$

$$\hat{\omega} = \omega / \omega_{*e}, \tau = T_e / T_i, \varepsilon_n = L_n / R, \delta = \bar{k}_\| v_{Ti} / \omega_{*e}, F = \omega_{De}(\theta) / \omega_{*e}$$
$$= 2\varepsilon_n [\cos\theta + (s\theta - \alpha\sin\theta)\sin\theta],$$

$$M_{in} = \left\langle \left(\frac{v_\|}{v_{Ti}} \right)^n \frac{\omega + \hat{\omega}_{*i}}{\omega + \hat{\omega}_{Di} - k_\| v_\|} {J_0}^2(x) \right\rangle_v, \tag{9}$$

and $\langle \cdots \rangle_v$ indicates velocity averaging with Maxwellian weighting for the ions. The quantity δ perturbatively implements effects of the finite ion transit frequency with $\bar{k}_\|$ the effective norm of the parallel gradient of the scalar potential $\varphi(\theta)$,

$$\bar{k}_\| = \sqrt{\left\langle {k_\|}^2 \right\rangle_\theta}, \quad \left\langle {k_\|}^2 \right\rangle_\theta = -\frac{1}{(qR)^2} \int \phi^* \frac{d^2\phi}{d\theta^2} d\theta.$$

For the ballooning mode with $|\omega| \cong \omega_A = V_A / qR$ (the Alfven frequency), δ may be ignored. However, in investigating finite β effects on the predominantly electrostatic drift type modes, such as the η_i mode, δ should be retained.

If the ion density perturbation is approximated by that found from electrostatic fluid dynamic approach, [12]

$$n_i = M_{if}\frac{e\Phi}{T_i}n_0,$$
$$M_{if} = \frac{\omega'(\omega_{*e} - \omega_{De} - [\omega + \omega_{*i}(1+\eta_i)](k_\perp \rho_s)^2) + (2/3 - \eta_i)\omega_{*e}\omega_{Di}}{\omega'^2 - (10/9)\omega_{Di}{}^2} \tag{10}$$

with $\omega' = \omega + (5/3)\omega_{Di}$, a resultant two-fluid ballooning mode equation without ion transit effects is

$$\frac{d}{d\theta}\left([1+(s\theta - \alpha\sin\theta)^2]\frac{d\phi}{d\theta}\right) + V_f(\theta)\phi = 0, \tag{11}$$

where

$$V(\theta) = \frac{q^2\beta_e}{2\varepsilon_n{}^2}\left((\hat{\omega}-F)(\hat{\omega}-1) + \eta_e F - \frac{(\hat{\omega}-1)^2}{1+\tau-M_{if}}\right), \tag{12}$$

Two-fluid approximation does not involve velocity space integrations and for qualitative assessment of the eigenfrequency ω it provides a quick estimate. In fact, two-fluid approximation does predict instabilities outside the MHD regime. However, in detail, eigenvalues from two-fluid approximation deviate significantly from kinetic assessment.

3. POSITIVE SHEAR REGIME

The kinetic ballooning mode equation is to be solved with a shooting code in which full ion velocity integrations must be evaluated at each mesh point. An efficient shooting code has been developed at the University of Saskatchewan based on the Gaussian-Hermite quadrature approximation for the velocity integrations. The accuracy of this integration scheme has been checked with an exact integration.

Figure 2 shows the frequency eigenvalues ω (complex) normalized by the Alfven frequency $\omega_A = V_A / qR$ as functions of the ballooning parameter α found from three approaches, ideal MHD, two-fluid approximation and fully kinetic analysis. The growth rate of the ideal MHD ballooning mode is qualitatively recovered by both two-fluid and kinetic analyses. However, in the MHD second stability regime $\alpha > 1.5$, both two-fluid and kinetic analyses predict an instability. The growth rate is comparable with that of the ideal MHD mode. Two-fluid approximation predicts an instability even below the first stability boundary $\alpha < 0.3$. However, this instability is spurious, for it cannot be recovered from kinetic approach. The frequency of the ballooning mode (which ideal MHD approximation is unable to assess accurately) is a large fraction of the Alfven frequency and exceeds the estimate often used, $\omega_r = -(1+\eta_i)\omega_{*i}/2$ by nearly one order of magnitude. Therefore, the ballooning mode is not purely growing as predicted from ideal MHD theory and in this respect the instability is not really strong. The instability may enhance transport but is not expected to destroy plasma confinement entirely.

The KBM in the MHD second stability regime requires a finite ion temperature gradient. This is illustrated in Fig. 3. The mode labeled "MHD" is in the MHD unstable region recovered from kinetic analysis. It does not require a finite η_i. The mode in the second stability

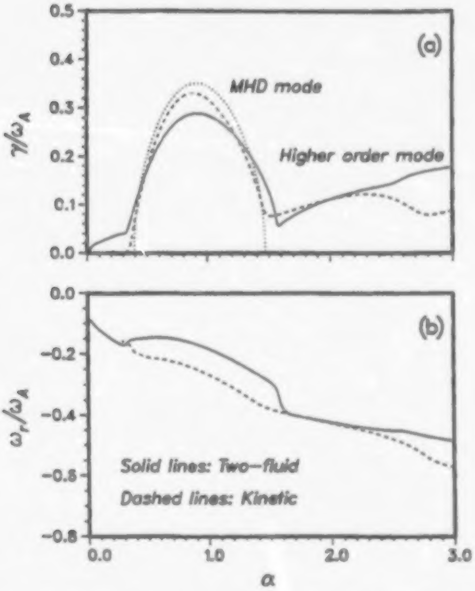

Figure 2. Growth rates (a) and mode frequencies (b) from ideal MHD (dotted line), two-fluid approximation (solid lines and kinetic analysis (dashed lines). S = 0.4. Other parameters are the same as in Fig. 1.

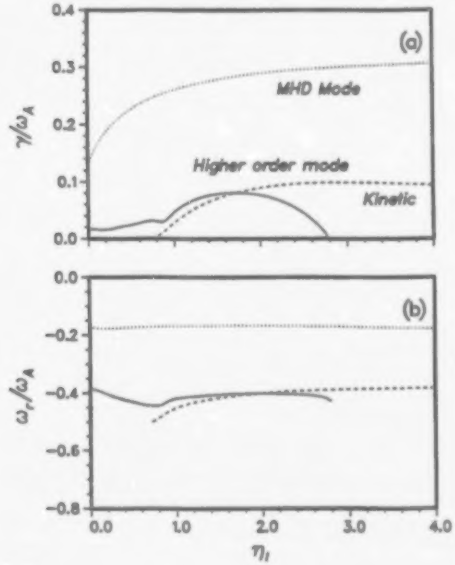

Figure 3. Dependence of the eigen-frequencies on η_i. MHD-like mode (dotted lines) recovered from kinetic analysis when α = 0.9 has no threshold. For modes in the MHD second stability regime α = 1.7 two-fluid approximation (solid lines) yields results qualitatively different from the kinetic analysis (dashed lines).

regime (labelled "higher order mode") is activated if $\eta_i > 0.8$. One would be attempted to regard the mode as the toroidal η_i mode corrected for finite β. However, this is not the case. The η_i mode is predominantly electrostatic and effectively stabilized when the ballooning parameter α approaches the first stability boundary. Also, the mode frequency of the η_i mode remains of order $\omega_{Di} \approx 2\varepsilon_n \omega_{*i}$, far smaller than that of the KBM. In two-fluid approximation (solid line in Fig. 3), the threshold in η_i disappears but stabilization occurs at $\eta_i > 2.8$. Two-fluid approximation may thus yield eigenvalues qualitatively incorrect and its use must be made with some care.

Recently, in TFTR D-T supershot discharges, relatively high frequency magnetic fluctuations have been observed and identified as a kinetic ballooning mode. Result of kinetic stability analysis for TFTR-like hot ion discharge parameters is shown in Fig. 4. The ballooning parameter in TFTR is approximately 0.5 and for the shear parameter $s = 0.5$, the discharge is in the ballooning unstable regime. The growth rate peaks at $b_i = (k_\theta \rho_i)^2 = 0.02$, which translates to n (toroidal mode number) = 6, in favorable agreement with the experimental observation.

4. NEGATIVE SHEAR REGIME

It is well known that the ideal MHD ballooning mode is stable if the magnetic shear is reversed $s < 0$. Qualitatively, this may be seen from the norms of the differential operators in the MHD mode equation for the lowest order ballooning function $\phi(\theta) = 1 + \cos\theta, |\theta| \leq \pi$

$$\left\langle k_\parallel k_\perp{}^2 k_\parallel \right\rangle_\theta = \frac{k_\theta{}^2}{(2qR)^2}\left(1 + 2.79s^2 - 2.67s\alpha + 0.75\alpha^2\right),$$
$$\left\langle \omega_D \right\rangle_\theta = 2\varepsilon_n \omega_* (0.67 + 0.56s - 0.42\alpha),$$

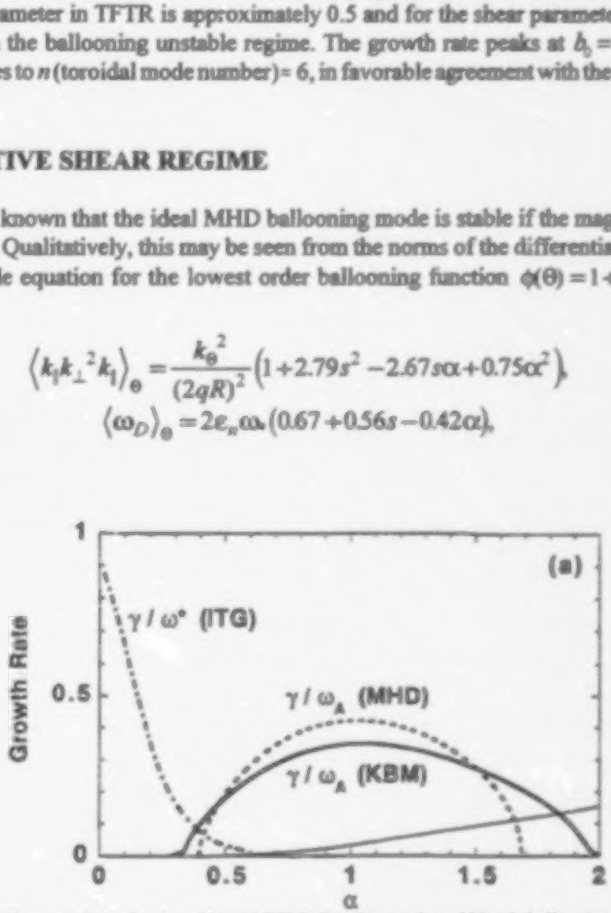

Figure 4. Growth rates of ideal MHD ballooning mode and kinetic ballooning mode for TFTR-like hot ion discharge. Stabilization of the η_i mode by finite β (or α) is also shown. ε=0.2, s=0.2, τ=1, η_i=2, b_i=0.02, α=1 unless chosen as a variable.

and consequent dispersion relation at marginal stability,

$$1+2.79s^2-2.67s\alpha+0.75\alpha^2-4\alpha(0.67+0.56s-0.42\alpha)=0. \qquad (13)$$

When $s<0$ there is no real solution for α and the MHD ballooning mode is stable in that region. Negative shear tends to deactivate ballooning drive and also effectively increase the Alfven frequency.

However, as recently shown, the ion temperature gradient driven kinetic ballooning mode persists even when the shear is reversed. The characteristics of the instability are similar to those of the KBM in the MHD second stability regime with positive shear including the threshold in η_i and extended eigenfunctions in the ballooning space. The growth rate is of order ω_* the diamagnetic drift frequency, and the frequency hovers at around $\omega_r \approx -V_A/2qR$.

Results of shooting code analysis for the mode equation in negative shear regime is summarized in Fig. 5. Fig 5 (a) shows the dispersion relation (ω vs. $b_0=(k_\theta\rho)^2$) when $s=0.2$, $\alpha=1.2$. The growth rate peaks at relatively long wavelength $b_0\approx 0.02$ and the maximum growth rate is approximately ω_*. The magnitude of the eigenfunction $|\phi(\theta)|$ is depicted in Fig. 5 (b). As in the case of kinetic ballooning mode in the MHD second stability regime with positive shear, the eigenfunction extends to large value of θ. The ion FLR parameter $(k_\perp\rho)^2=(k_\theta\rho)^2[1+(s\theta-\alpha\sin\theta)^2]$ exceeds unity because of the extended eigenfunction which necessitates employing kinetic analysis for satisfactory assessment of the eigenvalue although both two-fluid and gyro-fluid approximations are able to reveal the instability qualitatively. Fig. 5 (c) demonstrates the existence of a threshold in the ion

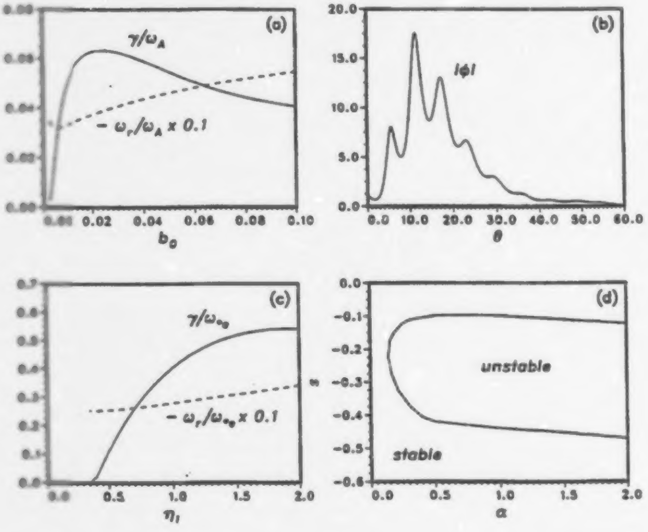

Figure 5. Kinetic ballooning mode in the negative shear regime. (a) Dispersion relation. (b) Eigen-function. (c) Dependence of the eigen frequency on η_i. (d) Stable-unstable boundry in the (s,α) plane. $\varepsilon_n=0.1$, $s=0.2$, $\tau=1$, $\eta_e=\eta_i=2$, $b_o=0.02$, $\alpha=1$unless chosen as a variable.

temperature gradient for the kinetic ballooning mode. The critical η_i is modest, η_i>0.5, which is satisfied in most tokamaks. Finally, instability boundary in the (s, α) plane is shown in Fig. 5 (d) for the case $\eta_i = \eta_e = 1, \varepsilon_n = 0.1, b_0 = 0.01$. The critical α for s = —0.2 is 0.1. For α > 0.3, the unstable window in s resides in the region —0.4 < s < —0.1.

5. CONCLUSIONS

It has been shown that an ion temperature gradient driven kinetic ballooning mode exists in tokamak parameter regions where the ideal MHD ballooning mode is expected to be stable. Both the MHD second stability regime with positive shear and negative shear regime are subject to the instability provided the ion temperature gradient η_i exceeds a critical value (η_i>0.8 when $s > 0$, η_i>0.5 when $s < 0$). The driving mechanism of the instability is attributed to ion magnetic drift resonance which is enhanced by the ion temperature gradient.

ACKNOWLEDGMENTS

This research has been sponsored in part by the Natural Sciences and Engineering Research Council of Canada.

REFERENCES

1. H.P. Furth et al. in Plasma Physics and Controlled Nuclear Fusion Research 1966, (IAEA, Vienna, 1967), Vol. 1, p. 127.
2. A.M.M. Todd et al. Phys. Rev. Lett. **38**, 826 (1977).
3. D. Dobrott et al. Phys. Rev. Lett. **39**, 943 (1977).
4. J.W. Connor, R.J. Hastie and J. B. Taylor. Phys. Rev. Lett. **40**, 396 (1978).
5. Y.C. Lee and J.W. van Dam. Proc. Finite Beta Theory Workshop, (U.S. Department of Energy, Washington, D.C., 1977).
6. D. Lortz and J. Nuhrenberg. Phys. Lett. **68**, 49 (1977).
7. C. Mercier. In Plasma Physics and Controlled Nuclear Fusion Research 1978, (IAEA, Vienna, 1978), Vol. 1, p. 701.
8. A. Sykes et al. *ibid.*, p. 625.
9. L. E. Zakharov. *ibid.*, p. 689.
10. B. Coppi et al. Nucl. Fusion **19**, 715 (1979).
11. C. Z. Cheng. Phys. Fluids **25**, 1020 (1982); Nucl. Fusion **22**, 773 (1982).
12. H. Nordman, B. Jhowry and J. Weiland. Phys. Fluids B **5**, 3465 (1993).
13. A. Hirose, L. Zhang and M. Elia. Phys. Rev. Lett. **72**, 3993 (1994).
14. *Idem.* Phys. Plasmas **2**, 859 (1995); H. Nordman et al. Phys. Plasmas **2**, 3440 (1995).
15. A. Hirose and M. Elia Phys. Rev. Lett. **76**, 628 (1996).
16. Z. Chang et al. Phys. Rev. Lett. **76**, 1071 (1996).
17. M. Yamagiwa, A. Hirose and M. Elia. Plasma Phys. Controlled Fusion **39**, 561 (1997).

THE ROLE OF MAGNETIC TURBULENCE IN THE SAWTOOTH RELAXATION PROCESS IN SINP TOKAMAK

Amit Kumar Hui, Ratan Kumar Paul and Dipak Banik

Plasma Physics Group, Saha Institute of Nuclear Physics
1/AF Bidhannagar
Calcutta 700 064, India

The importance of magnetic turbulence in the enhanced transport processes in the region around the core of a tokamak leading to various disruptive activities is fast becoming apparent. In SINP tokamak the part played by these fine scale magnetic phenomena in the internal sawtooth relaxation process is being studied. The sawtooth activities in this tokamak has several characteristics. Those indicating a mechanism additional to the usual m = 1 tearing mode are being presented in this initial report. SINP tokamak is a small iron-cored machine with R = 30 cm, a = 7.5 cm, B(T) = 2T (max) and I(plasma) = 75 kA (max). It has an aluminum shell with several cuts in addition to a set of stabilizing field coils. The machine generally works in three regimens, a) low and ultra low q, b) low current shots so that probes can be inserted for physics studies and c) the normal q discharges in which the present set of experiment were performed.

The machine has several characteristics which can be traced back to its construction: It has a large initial current ramping, about 50 MA in low q mode and about half that value in normal q, very large current density, about 5MA/squared M at the highest rated current and like in all machines of its size, large toroidal electric field and pressure gradient. Many of the peculiarities in the observations [1–5] in different regimes is thought as due to some turbulent phenomena or the other which have their origin in the above machine characteristics.

The sawtooth activities in the SINP tokamak is studied with an array of soft x-ray detector. The tomographic reconstruction is performed with the usual assumption of solid rotation. Other diagnostics used are magnetic pickup loops and a visible light detector array and foil absorption technique for temperature estimation. Unfortunately, at present a density diagnostic is not available on SINP tokamak. Sawtooth oscillations were observed in SINP tokamak in most shots where electron temperature exceeded about 150 eV.

In many respect the results on these oscillations conform to the classical (Kadomstev) description. However, the part of the results interesting for the present purpose are summarized as follows:

a) Tomographic reconstruction of the soft image of m = 1 tearing island was performed in many shots. However, in no reconstruction the island size was found to be large enough to engulf the core.

Current Trends in International Fusion Research – Proceedings of the Second Symposium
Edited by E. Panarella. NRC Research Press, National Research Council of Canada, Ottawa, ON K1A OR6, Canada. 1999.

b) SINP tokamak does not have any control for current profile, and consequently the there is a large variation of inversion radius (from about 2.4 cm down to about 0.5 cm). The sawtooth period seem to be very insensitive to inversion radius and for about five-fold increase of the inversion radius only about 50% increase in the sawtooth period was observed.

c) The above observation is corroborated by the fact that the size of the m = 1 tearing mode island obtained on tomographic reconstruction of emissivity data just before a sawtooth crash is independent of the inversion radius.

The results of yet unconfirmed experiment on the stabilization of sawtooth instability indicate that the sawtooth activity can be stabilized by a strong gas puffing without affecting the mhd mode.

Small scale magnetic phenomena are thought about as being responsible for the limited island size at the sawtooth crash in TFR [6]. There are various experimental and theoretical works to indicate the excitation of magnetic turbulence as the size of the tearing mode island grows large enough [7,8]. In SINP tokamak this critical size, because of large current density and other discharge parameters, is thought as being small and smaller than the inversion radius in most cases. The sawtooth crash is being triggered by the onset of magnetic turbulence enhancing the transport processes when the critical size of the m = 1 tearing mode island is reached. Inclusion of such turbulence in the simulation model has been used to explain various experimental observation on sawtooth phenomena [9,10]. This readily accounts for the constant size of the island at the crash and the insensitivity of the sawtooth period on inversion radius.

The stabilization of the sawtooth instability by gas puffing is perhaps due to damping of the turbulence.

Since the runway electrons are hardly affected by electrostatic effects, their transport is governed by magnetic turbulence. Therefore the latter can be correlated hard x-ray emissivity. With this aim, the hard x-ray emissivity in SINP tokamak is being carefully studied recently. Whenever the hard x-ray signals are measurable, these initial works show either a clear sawtooth in hard x-ray with some phase delay with the soft x- ray sawtooth or a strong modulation of hard x-ray intensity oscillation at the sawtooth frequency. The hard x-ray data are being analyzed.

REFERENCES

1. S. Lahiri et al. Nuclear Fusion **36**, 254 (1996).
2. A.N.S. Iyenger et al. Pramana **39**, 181 (1989).
3. N. Ray. Europhys. Letts. **32**, 482(1995).
4. R. Paletal. Proc. TCM-RUST, Serra Negra,SP, Brazil, 1993, pp **88**.
5. P.K. Chattopadhyay. Ph. D. Dissertation, Jadavpur University, 1996.
6. M.A. Dubois et al. Nuclear Fusion **20**, 565(1980).
7. V.J. Simic et al. Phys. of Fluids **B5**, 1576 (1993).
8. M. Dubois and A. Semain. Nuclear Fusion **28**, 565 (1988).
9. W.J. Goedheer and E. Westerhof. Nuclear Fusion **28**, 565 (1988).
10. F.A. Haas and A. Thyagaraja. Europhys. Letts. **19**, 285 (1993).

BREAKEVEN CRITERIA FOR DT PLASMAS IN REACTOR-TYPE CONDITIONS*

E. Panarella[1]

Advanced Laser and Fusion Technology, Inc.
189 Deveault Street, Unit No. 7
Hull, PQ J8Z 1S7, Canada
[1]Also with the Department of Electrical Engineering
University of Tennessee
Knoxville, Tennessee, U.S.A.
and the National Research Council
Ottawa, Canada

E-mail: editor@physicsessays.com

ABSTRACT

A previous study (E. Panarella. Current Trends in International Fusion Research, Plenum Press, New York, 1996, pp. 211–244) extended Lawson's analysis on the breakeven criteria for fusion by introducing conduction losses from heat transfer theory rather than through the $3nkT/\tau_E$ term, and found that breakeven depends on particle density, plasma temperature, and character of the temperature evolution both when the α particles escape from the plasma, and when they are retained. The analysis, while confirming a threshold temperature for breakeven, added another threshold element, a particle density in excess of 10^{16} cm^3, below which breakeven cannot be obtained under realistic reactor conditions.

On the basis of this finding, a complete and rigorous analysis is now carried out of the ignition conditions for a pulsed DT plasma magnetically confined, where again the conduction losses are taken from heat transfer theory, rather than from the empirically defined energy confinement time. It is shown that the magnetic field required for ignition exceeds any of those presently considered for major machines. It will also be shown that ignition is independent of particle density in this case. On the basis of these results it is argued that ignition is facilitated in an inertially confined plasma, both of the classical type with lasers, or with the Spherical Pinch, or the Magnetized Target Fusion concept.

The analysis has then been extended to the ITER machine, starting from the design temperature profile, machine dimensions, and particle density. It is assumed that ITER requires a power input of 400 MW to bring it towards ignition, and that the reactor works with an efficiency of 30% of conversion of thermal energy into electricity.

It is considered that, at regime, the alpha particle heat and that part of the power input

Current Trends in International Fusion Research – Proceedings of the Second Symposium
Edited by E. Panarella. NRC Research Press, National Research Council of Canada, Ottawa, ON K1A OR6, Canada. 1999.

that goes into the plasma, as determined by an energy transfer coefficient a, has necessarily to be transferred to the liquid blanket of the reactor in the form of heat and bremsstrahlung. For simplicity, it is assumed that the blanket is made up of water at 300 °C, for which the thermal conductivity is well known. Other types of blanket do not significantly change the results.

On the basis of the above data and assumptions, one finds that the power deficit for ignition can range from 3.73×10^{7} to 8.87×10^{8} watts. Moreover, one finds that the temperature of the first wall is 40 eV for an energy transfer efficiency $a = 13.1\%$, or 60 eV for $a = 37.5\%$. When one integrates over the entire volume of the plasma the energy balance, i.e., energy produced by neutrons and alpha particles, and losses by bremsstrahlung and heat, one finds that the machine cannot reach ignition.

1. INTRODUCTION

For 40 years, since J.D. Lawson in 1957 published a paper in the Proceedings of the Physical Society by title "Some Criteria for a Power Producing Thermonuclear Reactor," [1] the plasma physics community has been guided in its quest for fusion by the directions provided by the 'Lawson criteria' for energy breakeven conditions. These are general criteria, applicable to an idealized situation where a plasma of particle density n is brought instantaneously to a temperature T, which is maintained for a time τ_E after which it is allowed to cool to the original temperature. The criteria state that for breakeven, the temperature has to be above 30 million °K and the product $n\tau_E$ must exceed 10^{14} cm^{-3} sec in deuterium-tritium reactions. The reaction products are not retained in the plasma of the Lawson analysis, and conduction losses are neglected during the plasma burning time. These criteria apply to the case of 'scientific breakeven', in which the energy supplied to heat the plasma and maintain the bremsstrahlung losses is returned to the system, together with the reaction energy, with a recovery efficiency η of 1/3. No allowance is made for the fact that the energy used to heat the plasma and supply the bremsstrahlung losses must come from a conventional source, and that the transfer efficiency is normally much less than 100 percent. Were this considered, the Lawson criteria would become even more difficult to satisfy. Mills [2] has generalized the 'scientific breakeven' conditions by considering several energy recovery efficiencies η, from 2.5 to 60 percent. Some discussion regarding terms in the energy balance equation of Lawson has been carried out in Refs. 3 and 4. Several generalizations of the Lawson criteria are also reported in the standard textbook literature on fusion energy [5–11].

In the present work, the complete system is examined in detail, i.e., source of energy and plasma sink, and various energy transfer efficiencies are considered from the first to the second, as well as from the second to the first. The energy from the source is deposited in a pulse, and the plasma experiences a cycle of temperature values. The analysis departs from the conventional one, in that heat conduction losses are introduced from heat transfer theory, rather than through the $3nkT/\tau_E$ term, thus changing the role played by the energy confinement time in the ignition conditions. In order to ease the inclusion in the energy balance equation of conduction losses, the geometry considered here is spherical. More specifically, it is the spherical pinch geometry [12–14]. However, the analysis can be extended to other geometries, including the toroidal, when the appropriate heat conduction loss term is used. The particular case of ignition of a magnetically confined plasma is considered here. Previously, the most general criteria for breakeven or ignition were provided, including the effect of the shape of the plasma temperature excursion [15]. A most important result is now found that ignition does not depend on particle density. In other words, any attempt to have more fusion energy by increasing the fuel (particle) density leads to greater conduction losses. This can be offset by an increase of the magnetic field that confines the plasma. However, it is found that, for a plasma of normal radius, i.e., a centimeter or so, the strength of the magnetic field required for ignition is well above any of the present machines. The analysis has then been extended to a simple model of the ITER machine (International Thermonuclear Experimental Reactor). It will be shown that this machine, as presently designed, might not be able to reach either ignition or power breakeven. It is concluded that, because of the large cost and long time frame of the ITER program, no doubt should exist that the machine must reach its stated goal of ignition. Consequently, as long as these doubts persist, and cannot easily be dissipated, it is recommended that the ITER program is put on hold, and fusion alternative concepts are pursued.

2. ANALYSIS

Figure 1 illustrates the system under consideration. Energy E from a source is released in a pulse of power $W(t)$. A fraction E_i of the energy ($E_i = aE$ where a is the efficiency of energy transfer from the source to the sink) is deposited in a spherical chamber containing a plasma core and an ionized gas blanket, while the rest $(1 - a)\,E$ is dissipated in the components of the energy transfer system. The energy $a\int_0^t W(t)dt$ that reaches the chamber at time t is used to heat the plasma core, and to provide for the radiation and conduction losses. In the absence of other energy inputs, the energy balance equation is:

$$a\int_0^t W(t)dt = \int_0^t \left[H(t) + R(t) + C(t)\right]dt \qquad (1)$$

where $H(t)$ is the rate of heat energy change in the plasma core, and $R(t)$ and $C(t)$ are the rate of energy loss by radiation and heat conduction, respectively. Other losses, such as synchrotron or inverse Compton radiation production, are not included here.

A 50 percent mixture of deuterium and tritium is considered here as making up the

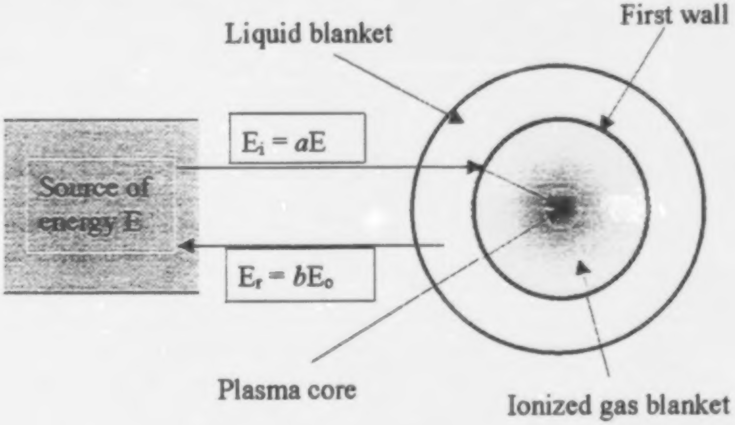

Figure 1. Energy flow system.

plasma and surrounding gas. The fusion nuclear reaction taking place in the plasma core is:

$$D + T = \mathrm{He}^4\ (3.5\ \mathrm{MeV}) + n\ (14.1\ \mathrm{MeV}) \tag{2}$$

where 3.5 MeV is the energy carried by the α particle He^4, and 14.1 MeV is the energy carried by the neutron n.

At the end of the life t_o of the plasma core, when this has cooled down and returned to the original temperature, an amount of energy E_o is available from the liquid blanket for return to the source. A fraction E_r of this energy ($E_r = bE_o$, where b is the efficiency of energy transfer from the liquid blanket to the source) is the amount that actually reaches the source. Breakeven or ignition require that $E_r = E$. The aim of this study is to find the conditions for ignition of a magnetically confined plasma as a function of the strength of the confining magnetic field, given the temperature T, particle density n, and radius r of the plasma, and the coefficients a and b of transfer efficiency from the energy source to the sink, and viceversa, respectively, when conduction losses are introduced from heat transfer theory rather than through the $3nkT/\tau_E$ term.

The rate of energy released in the form of α particles and neutrons will be designated as $P_\alpha(t)$ and $P_n(t)$, respectively. Only the α particles may remain in the plasma and further heat it, whereas the neutrons will escape and be absorbed by the liquid blanket. The case considered here is the one in which the α particles are retained (ignition).

2.1 α Particles Are Retained

Only the neutrons escape, and the energy available at time t from the liquid blanket for return to the source is:

$$E_o(t) = \int_o^t \left[P_n(t) + R(t) + C(t)\right]dt \tag{3}$$

Ignition requires that, at the end of the time t_o:

$$\int_o^{t_o} W(t)dt = b\int_o^{t_o}\left[P_n(t) + R(t) + C(t)\right]dt \tag{4}$$

Since the α particles remain in the plasma core, this is a new energy source, and the energy balance equation becomes:

$$a\int_o^t W(t)dt + \int_o^t P_\alpha(t)dt = \int_o^t \left[H(t) + R(t) + C(t)\right]dt \tag{1A}$$

which can be written as:

$$a\int_o^t W(t)dt = \int_o^t \left[H(t) + R(t) + C(t) - P_\alpha(t)\right]dt \tag{1B}$$

From Eqs. (4) and (1B) one gets:

$$\frac{1}{a}\int_o^{t_o}\left[H(t) + R(t) + C(t) - P_\alpha(t)\right]dt = b\int_o^{t_o}\left[P_n(t) + R(t) + C(t)\right]dt \tag{5}$$

which transforms into:

$$\int_{o}^{t_o} H(t)dt = ab\int_{o}^{t_o}\left\{P_n(t)+\frac{1}{ab}P_\alpha(t)+\left(1-\frac{1}{ab}\right)[R(t)+C(t)]\right\}dt \tag{6}$$

At the end of t_o, the plasma core returns to the original temperature. No heat energy remains and therefore:

$$\int_{o}^{t_o} H(t)\,dt = 0 \tag{7}$$

Hence:

$$ab\int_{o}^{t_o}\left\{P_n(t)+\frac{1}{ab}P_\alpha(t)+\left(1-\frac{1}{ab}\right)[R(t)+C(t)]\right\}dt = 0 \tag{8}$$

or:

$$\int_{o}^{t_o}\left\{P_n(t)+\frac{1}{ab}P_\alpha(t)+\left(1-\frac{1}{ab}\right)[R(t)+C(t)]\right\}dt = 0 \tag{9}$$

If eq. (9) is satisfied, ignition is achieved.

The first three terms $P_n(t)$, $P_\alpha(t)$ and $R(t)$ in the integral (9) are functions of plasma temperature T, particle density n, and plasma volume V_p. Specifically, for a 50% D-T mixture, one has [16]:

$$P_n(n,T,V_p) = 8.31 \times 10^{-24}\frac{n^2}{4}T^{-\frac{2}{3}}e^{-\frac{19.94}{T^{1/3}}}V_p \tag{10}$$

$$P_\alpha(n,T,V_p) = 2.06 \times 10^{-24}\frac{n^2}{4}T^{-\frac{2}{3}}e^{-\frac{19.94}{T^{1/3}}}V_p \tag{11}$$

$$R(n,T,V_p) = 2.14 \times 10^{-30}\frac{n^2}{4}T^{\frac{1}{2}}V_p \tag{12}$$

where P_n and P_α are expressed in watts, T in kV, V_p in cm^3, and n in cm^{-3}.

The rate of heat conduction loss $C(t)$ from the plasma core to the liquid blanket can be derived from heat transfer theory [17] as follows. The rate of heat transfer in a hollow sphere with surface temperature T_1 at r_1, and T_2 at r_2, where r_1, r_2 are the radii of the inner and outer surfaces, respectively, is given by:

$$C_1(r_1,r_2,T_1,T_2) = \frac{4\pi K\, r_1 r_2}{r_2 - r_1}(T_1 - T_2) \tag{13}$$

where K is the thermal conductivity of the material that makes up the hollow sphere.

In the present case, heat transfer takes place from the plasma core of radius r_1 and temperature T_1 to the liquid blanket of radius r_2 and temperature T_2. The medium through which heat propagates before reaching the liquid blanket is the ionized gas blanket made up of deuterium and tritium, and the first wall, usually made up of stainless steel [18]. The latter easily transfers heat, so that only the thermal conductivity of the former needs to be considered. Eq. (13) expresses the rate of heat transfer from the entire volume of the plasma core $V_p = \frac{4}{3}\pi r_1^3$. The rate of heat transfer per unit volume is obtained by dividing (13) by V_p. Since the temperature T_1 of the plasma core is much larger than the temperature T_2 of the liquid blanket, one has $T_1 - T_2 \approx T_1 = T$. Likewise, since $r_2 \gg r_1 = r$, one has $r_2 - r_1 \approx r_2$. Eq. (13) thus leads to:

$$c(r\ ,T\ ) = \frac{4\pi\ K r_1 r_2 T_1}{(r_2 - r_1)} \Big/ \frac{4}{3}\pi\ r_1^3 \approx \frac{3\ KT}{r^2} \tag{14}$$

and the heat conduction loss rate appearing in (9) is given explicitly by:

$$C(r,\ T\ \ ,V_p) = \frac{3\ K\ T}{r^2} V_p \tag{15}$$

where $C(r,\ T,\ V_p)$ is expressed in watts, when T is expressed in kV, r in cm, and K in W/cm kV.

Eq. (15) shows that the rate of heat conduction loss from the plasma core of radius r and temperature T to the liquid blanket is a function of the thermal conductivity K of the ionized gas blanket. In the following, we shall provide the formula for the thermal conductivity of a plasma immersed in a magnetic field.

Plasma Blanket with Magnetic Field. The thermal conductivity is given by [19]:

$$K = 3.54x\, 10^{25} \frac{A_i^{1/2} Z^2 n_i^2 \ln\Lambda}{T^{1/2} B^2} \frac{cal}{\sec {}^o K\, cm} \tag{16}$$

where A_i is the atomic weight of the positive ions of density $n_i = n/2$ (in cm^{-3}), B is the magnetic field (in gauss), and $Z = 1$ for deuterium and tritium. Taking $A_i = 2.5$ (averaged for a 50% D-T plasma), and $ln\ \Lambda \sim 20$ for a hot plasma, expression (16) transforms into:

$$K = 3.99x\, 10^{20} \frac{n^2}{T^{1/2} B^2} \frac{W}{cmkV} \tag{17}$$

The thermal conductivity in this case decreases with temperature T and magnetic field B, and increases with particle density n. Heat losses are now controlled mainly by the plasma layer with the lowest conductivity. This is the one in contact with the hot plasma core, which can therefore be identified as having the same parameters as the core itself, i.e., the same n and T.

Introducing (17) into (15), one gets:

$$C(r\ ,T\ ,V_p) = 1.61x\, 10^{19} \frac{n^2 T^{1/2}}{r^2 B^2} V_p \tag{18}$$

If one now inserts the previous expressions for $P_n(t)$, $P_e(t)$, $R(t)$, and $C(t)$ from (10), (11), (12), and (18), respectively, into (9), and divides by V_p, one gets an explicit expression for ignition:

$$\int_o^{t_o}\left\{\begin{array}{l}\left(8.31\times10^{-24}+\dfrac{2.06\times10^{-24}}{ab}\right)\left[\dfrac{n^2}{4}\mathcal{T}(t)^{-\frac{2}{3}}e^{-\frac{19.94}{\mathcal{T}(t)^{1/3}}}\right]_n\\+\left(1-\dfrac{1}{ab}\left[2.14\times10^{-30}\dfrac{n^2}{4}\mathcal{T}(t)^{1/2}+1.61\times10^{-19}\dfrac{n^2\mathcal{T}(t)^{1/2}}{r^2\mathcal{B}^2}\right]\right)\end{array}\right\}dt=0 \qquad (19)$$

The interesting aspect of this expression is that n^2 appears in all terms of the integrand as common factor, which therefore cancels out. This makes the integrand independent of particle density, and ignition is not a function of *n*. This is an important result. The integral (19) becomes:

$$\int_o^{t_o}\left\{\begin{array}{l}\left(8.31\times10^{-24}+\dfrac{2.06\times10^{-24}}{ab}\left[\dfrac{1}{4}\mathcal{T}(t)^{-\frac{2}{3}}e^{-\frac{19.94}{\mathcal{T}(t)^{1/3}}}\right]_n\right)\\+\left(1-\dfrac{1}{ab}\right)\left[2.14\times10^{-30}\dfrac{1}{4}\mathcal{T}(t)^{1/2}+1.61\times10^{-19}\dfrac{\mathcal{T}(t)^{1/2}}{r^2\mathcal{B}^2}\right]\end{array}\right\}dt=0 \qquad (19')$$

In (19') it has been assumed that, during the short time t_o, only the temperature *T* of the plasma core changes, whereas *n* and *r* remain constant. In other words, it is assumed that the plasma is confined by some means during time t_o, and therefore the plasma radius *r* and particle number density *n* do not change. The formulation of the conditions for ignition, however, as expressed by (19'), has general validity and remains the same if *n* and *r* also are a function of time. It can have even more validity if *n* is also a function of space within the plasma core volume. In this case, clearly the integration has to be performed over space and over time.

The three functions that appear in the integral (19') are positive functions, the latter two being subtracted from the first. The integral can therefore have positive or negative values. If the integrand, which is the sum of these three functions, is negative, the integral will also be negative. Likewise, if it is positive, the integral will be positive. One can examine the trend of the integrand by calculating and plotting it as a function of one of its variables, assuming prescribed values for the others. In this way, one is able to find for which value of the variable the function (integrand) from negative becomes positive, i.e., assumes a value equal to zero. For this value, or for any positive value of the integrand, ignition can be achieved. The geometry to which these results apply is the spherical geometry. For other geometries, such as the toroidal, the proper expressions for the conduction loss must replace the one used here. In the following figures, plots of the integrand of (19') are provided as a function of the magnetic field *B*. Two parameters are kept constant, namely the coefficient $b = 0.3$, and the radius of the plasma $r = 1$ cm. Each figure refers to a specific plasma temperature, ranging from 5 to 20 kV, and contains three plots for $a = 0.05$, 0.10, and 0.15, respectively.

Figure 2 shows that, for $T = 5$ kV, the integrand is always negative, no matter what value of the magnetic field up to 2×10^5 gauss = 20 Tesla. This means that ignition cannot be obtained for the plasma parameters considered in the figure. If one increases the temperature to $T = 10$ kV, Fig. 3 shows that still ignition cannot be obtained. Only when one pushes the

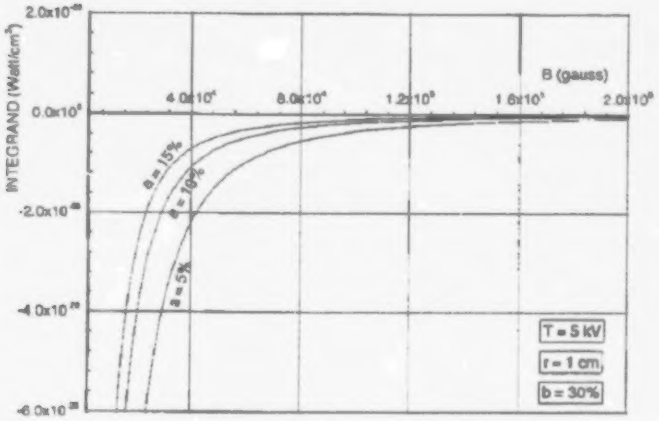

Figure 2. Plot of the integrand of Eq. (19') as a function of confining magnetic field. Ignition cannot be achieved with a confining field of up to 2x10^5 gauss (20 Tesla) for a plasma temperature T=5 kV.

temperature to T = 15 kV (Fig. 4), and to T = 20 kV (Fig. 5), then ignition can be obtained at a value of B around 1.8 x 10^5 gauss (18 Tesla), and B = 1.5 x 10^5 gauss (15 Tesla), respectively. These are very high values of the magnetic field, probably higher than any of those considered for future machines.

The ignition condition derived here as a function of the confining magnetic field is certainly necessary, but by no means sufficient. The reason is that, in a pulsed reactor, the plasma core is subjected to a temperature cycle during the pulse. When the temperature is above threshold for breakeven, there is a gain of energy and a loss of energy when it is below

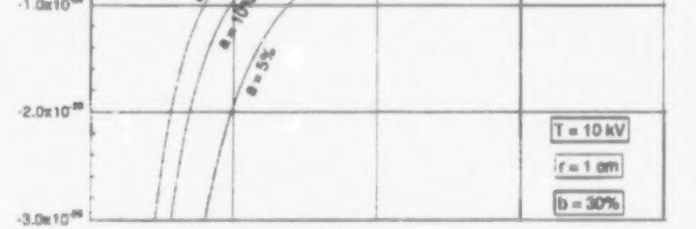

Figure 3. Plot of integrand of Eq. (19') as a function of confining magnetic field. Ignition cannot be achieved with a confining field of up to 2x10^5 gauss (20 Tesla) for a plasma temperature T=10 kV.

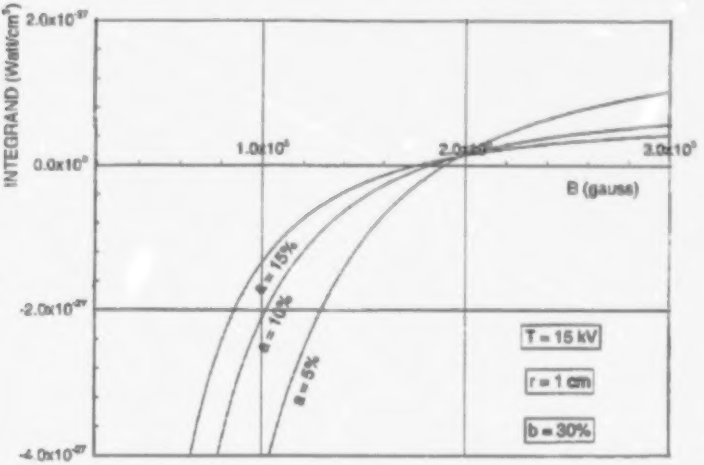

Figure 4. Plot of the integrand of Eq. (19') as a function of confining magnetic field. Ignition can now be achieved with a confining field of 1.8x10^5 gauss (18 Tesla) for a plasma temperature *T*=15 kV.

threshold. The plasma temperature excursion must therefore be shaped in such a way that the energy gained during the time when the temperature is above threshold compensates for the energy lost when it is below this value.

3. THE PRESENT APPROACH TO FUSION [20]

Figures 6, 7, and 8 show drawings of the ITER (International Thermonuclear Experimental Reactor) device, a machine that has been proposed as a reactor of the magnetic confinement type to demonstrate the scientific and technological feasibility of fusion power.

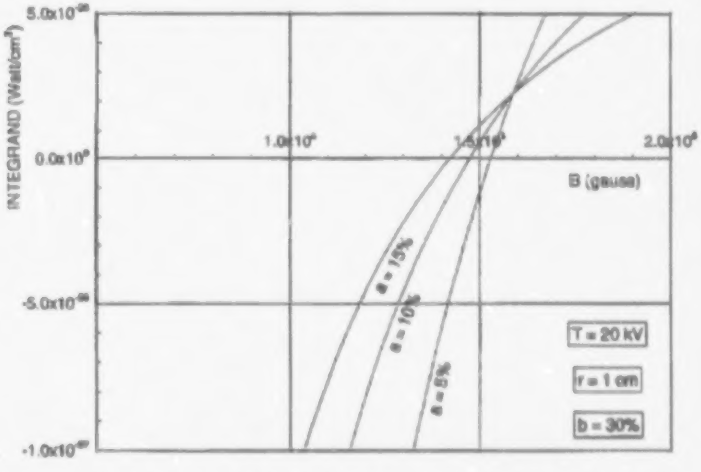

Figure 5. Plot of the integrand of Eq. (19') as a function of confining magnetic field. Ignition can now be achieved with a confining field of 1.5x10^5 gauss (15 Tesla) for a plasma temperature *T*=20 kV.

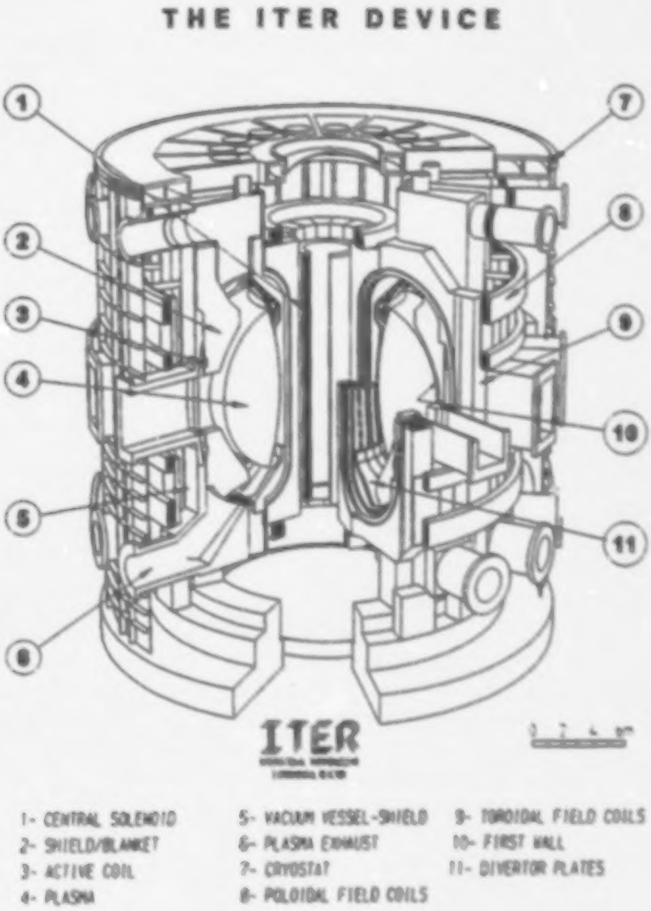
THE ITER DEVICE
1
2
3
4
5
6
7
8
9
10
11
ITER
0 2 4 6m
1- CENTRAL SOLENOID
2- SHIELD/BLANKET
3- ACTIVE COIL
4- PLASMA
5- VACUUM VESSEL-SHIELD
6- PLASMA EXHAUST
7- CRYOSTAT
8- POLOIDAL FIELD COILS
9- TOROIDAL FIELD COILS
10- FIRST WALL
11- DIVERTOR PLATES

Figure 6. The ITER device.

It is a machine of about 30 m diameter, and 36 m height. To accommodate it, a facility of ~30,000 m^2 for a total cost of ~U.S. $\$10^{10}$ will be required. Its construction should begin around the year 2000, with completion by about 2010. An intense debate has been going on within the fusion community about the desirability of building such a machine. Specifically, the magazine *Physics Today* reported in its June 1996 issue an opinion piece titled "Build the International Thermonuclear Experimental Reactor?" in which Andrew M. Sessler and Thomas H. Stix on one side, and Marshall N. Rosenbluth on the other side, debated the issue. The opinion piece best represents the two sides of the issue. The arguments were as follows:

Arguments against ITER (by Sessler and Stix)
- The ITER machine would be genuinely huge.
- The toroidal field coils would be 17 m high.

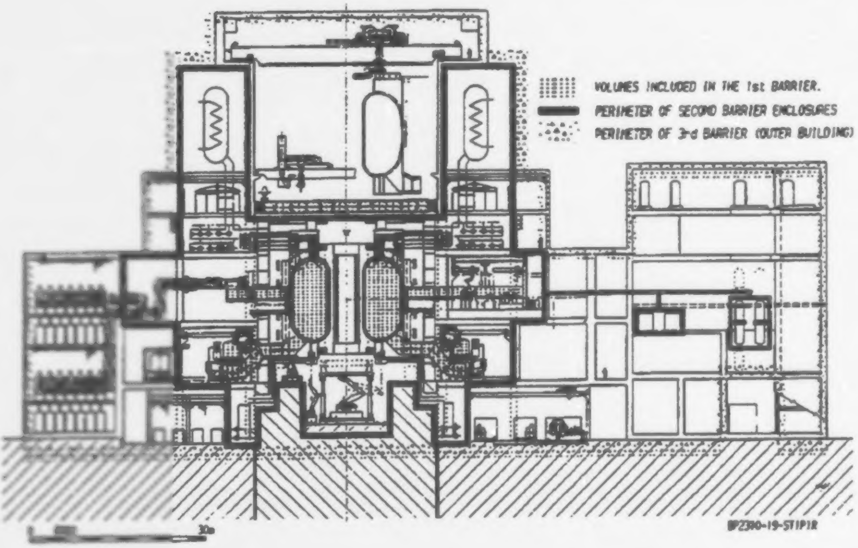
VOLUMES INCLUDED IN THE 1st BARRIER.
PERIMETER OF SECOND BARRIER ENCLOSURES
PERIMETER OF 3rd BARRIER (OUTER BUILDING)
30m
8P2310-19-STIP1R

Figure 7. The ITER facility (vertical cross section).

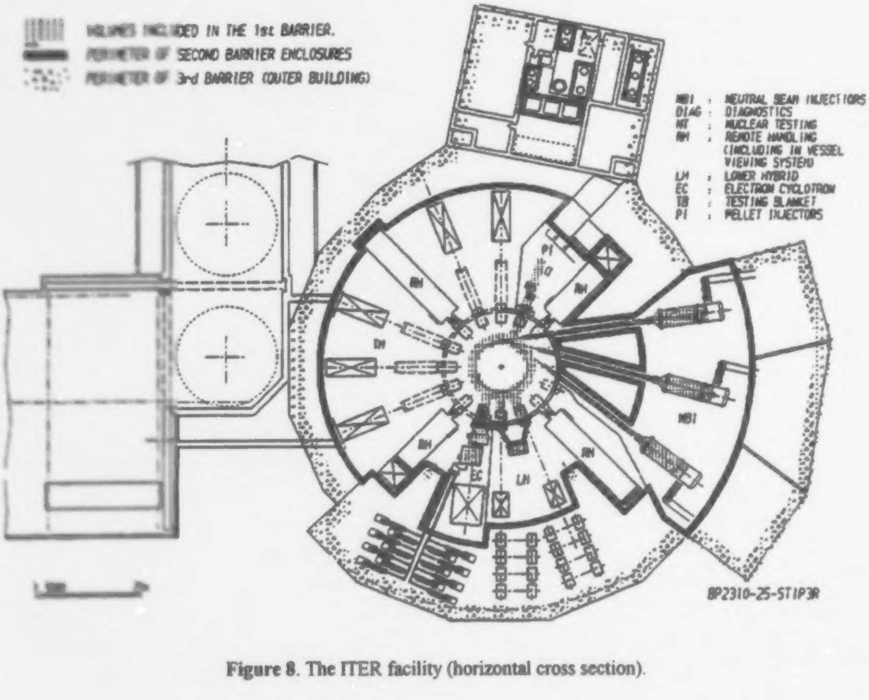
VOLUMES INCLUDED IN THE 1st BARRIER.
PERIMETER OF SECOND BARRIER ENCLOSURES
PERIMETER OF 3rd BARRIER (OUTER BUILDING)
NBI : NEUTRAL BEAM INJECTIONS
DIAG : DIAGNOSTICS
NT : NUCLEAR TESTING
RH : REMOTE HANDLING (INCLUDING IN VESSEL VIEWING SYSTEM)
LH : LOWER HYBRID
EC : ELECTRON CYCLOTRON
TB : TESTING BLANKET
PI : PELLET INJECTORS
PI
RH
RH
DH
RH
RH
NBI
EC
LH
8P2310-25-STIP3R

Figure 8. The ITER facility (horizontal cross section).

- The plasma volume would be 20–40 times larger than that of today's largest tokamaks.
- Construction time has been estimated at 10–12 years.
- Construction costs, in 1996 dollars, has been estimated at $10 billion.
- Although the magnetically confined plasmas most closely approaching fusion conditions have been produced in tokamaks, an eventual fusion reactor will look very different. Proceeding with ITER may not only preempt funding for alternative concepts, but also could freeze reactor design and engineering at a premature stage.
- Finally, the construction of ITER would be a poor choice for the following reasons:
  - The machine's untested attributes and unresolved technical issues.
  - Questions of science policy, including the narrowed focus on conventional tokamak.
  - Diversion and dedication of great human, scientific and fiscal resources to this single project.
  - The 10 or more years to "first plasma".
  - The time periods typical for fusion innovation and for political change of will.
  - The negative impact on future research that would rebound from a mechanical or physics failure in this single device.

In short, Sessler and Stix conclude, the step is too large and the overall concept, for all its attractiveness, is both premature and over ambitious with respect to current knowledge.

Arguments in Favor of ITER (by Rosenbluth)

- The nonlinear physics and novel engineering issues of fusion are so complex that only a real experiment at the approximate parameters required for ignition will ever resolve them quantitatively.
- Fusion research requires a test bed such as ITER that could be used to design a desirable reactor by interpolation rather than continual extrapolation from undersized experiments.
- If Japan assumes the major financial role in constructing ITER, with U.S. support at about its present level of 20% ($55 million) of the annual U.S. fusion budget, this is a wonderful bargain, because, for 5% of the cost, the U.S. could participate in designing and experimenting on fusion's flagship experiment.
- The U.S. fusion community should not turn its back on an internationally agreed upon experiment designed as the first exploration of the burning plasma experiment.

4. SCIENTIFIC CONSIDERATIONS ON THE POSSIBILITY FOR ITER TO REACH IGNITION

The above debate is indicative of the uncertainties surrounding this major fusion program. The debate is at the level of opinions and speculations. It would be desirable if the analysis of the performance of ITER were done at a scientific level. The purpose of the following section is to provide such scientific analysis. We remind that instabilities [21], and turbulence [22] have already been mentioned as significantly serious to preclude ignition for ITER. I shall give an account, from a different perspective, of the reason why ITER might have some difficulties in reaching ignition with the present design parameters of this machine. The calculations presented here are based on a simple model of the machine. They are nonetheless sufficiently convincing to show that the present design of ITER is not reassuring. The design parameters of ITER are: [23]

Temperature profile	20 kV at center decreasing linearly towards the periphery
Driver power	400 MW

Particle density	10^{14} cm^{-3}
Major radius	8 m
Minor radius	2.8 m to 4 m.

The most elementary definition of ignition is that plasma condition for which bremsstrahlung and conduction losses cannot cool the plasma because the α particles heating is able to compensate for these losses and maintain the plasma at a constant temperature. We shall refine this definition later on.

One can verify if ignition is achieved by analyzing the temporal evolution of the plasma through the following relation:

$$aW(t)+P_{\alpha}(t)=H(t)+R(t)+C(t) \tag{20}$$

where $W(t)$ is the power available from a driver to heat the plasma core, a is the efficiency of coupling the driver power to the plasma core, $P_\alpha(t)$ is the α particle power, $H(t)$ is the rate of heat energy change in the plasma core, and $R(t)$ and $C(t)$ are the rate of energy loss by radiation and heat conduction, respectively. Other losses, such as synchrotron or inverse Compton radiation production, are not included here.

Let us consider the case when one has a driver of maximum power W_{max}. As soon as it is turned on, the driver power will rise within a certain time until W_{max} is reached, after which it remains constant. At that time equilibrium is established, the plasma will have reached a certain constant equilibrium temperature, and P_α, R, and C will also have constant values. However, $H = 0$, because the plasma has now constant temperature. During this steady-state condition we have:

$$aW_{max} + P_{\alpha} = R + C. \tag{21}$$

Eq. (21) is satisfied for any steady-state driver input W_{max}. However, ignition is not achieved with a driver input for which $P_\alpha < R + C$. Only when

$$P_{\alpha} = R + C \tag{22}$$

ignition is achieved, and one can turn the driver power off at that time. It is not advisable to keep the driver power W_{max} on after ignition, because the reactor might be damaged from the combined action of W_{max} and P_α.

The objective of this analysis is not to derive from (20) the conditions to be satisfied in order to reach ignition. Rather, it is to verify if, for the ITER design parameters provided above, ignition can be achieved. In other words, since it has been claimed that, for the design parameters listed above, ITER should reach ignition [23], we first want to derive from (21) some additional operating parameters of ITER, and then we want to proceed to verify if ignition can be achieved for those parameters.

4.1 Determination of the Temperature of the First Wall

The following analysis aims at deriving the temperature of the first wall (Fig. 9). We assume that the first wall is surrounded by a liquid blanket which absorbs whatever heat leaks out from the plasma, as well as the neutron and bremsstrahlung powers (the bremsstrahlung absorption in the first wall converts into heating of the latter with heat transfer to the liquid blanket). For simplicity the liquid blanket is considered to be made up of water at 300°C, whose thermal conductivity is [24]

$$K_{LB} = 6.27 \times 10^{4} \frac{W}{cm \cdot keV} \qquad (23)$$

Eq. (21), which is valid at the time immediately before the driver power is turned off at ignition, can be converted into:

$$C = P_{\alpha} - R + aW_{\max} \qquad (24)$$

In the toroidal geometry of ITER, the total heat conduction loss rate C flowing into the liquid blanket is given by [25]

$$C = 4\pi^{2} RM \frac{KLBT1}{\ln(r2/r1)} \qquad (25)$$

where $R_M = 8$ m is the major radius of the torus, T_1 is the temperature of the first wall located at $r_1 = 2.8$ m or 4 m, and r_2 is the radius of the external wall of the liquid blanket container. We assume $r_2 = 6$ m. Eq. (24) becomes:

$$4\pi^{2} RM \frac{KLBT1}{\ln(r2/r1)} = \int_{0}^{Vp} (p_{\alpha} - r_B) dV_p + aW_{\max} \qquad (26)$$

where V_p is the plasma volume, and p_α and r_B are the α particle and bremsstrahlung power per unit volume, respectively.

Let us convert the integral in (26) over volume V_p into an integral over minor radius r_1 of the torus:

$$dV_p = 4\,\pi^{2} R_M\, r\, dr$$

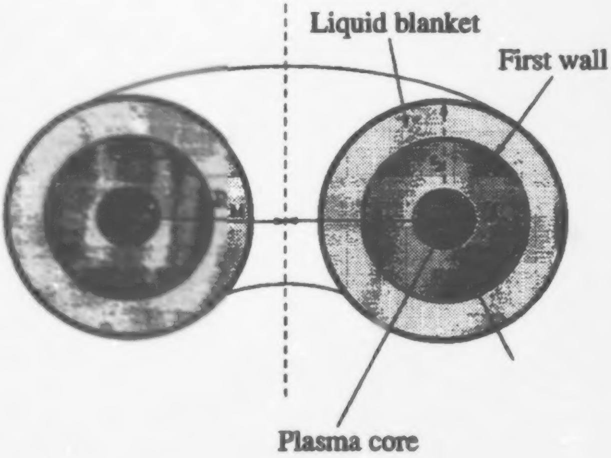

Figure 9. Simplified configuration of the ITER machine.

$$4\pi^2 R_M \frac{K_{LB} T_1}{\ln\left(r_2/r_1\right)} = 4\pi^2 R_M \int_0^{2.8\,m\,or\,4\,m} \left(p_\alpha - r_B\right)_r \, dr + aW_{\max}$$

$$\frac{K_{LB} T_1}{\ln\left(r_2/r_1\right)} = \int_0^{2.8\,m\,or\,4\,m} \left(p_\alpha - r_B\right)_r \, dr + \frac{aW_{\max}}{4\pi^2 R_M} \tag{27}$$

Inserting in (27) the known numerical values of the various parameters, one can get the temperature T_1 (in keV) of the first wall:

$$T_1 = \frac{\int_0^{280cm} \left(p_\alpha - r_B\right)_r \, dr + 1.27x10^4 a}{8.23x10^4} \quad \text{for } r_1 = 2.80 \text{ m} \tag{28}$$

$$T_1 = \frac{\int_0^{400cm} \left(p_\alpha - r_B\right)_r \, dr + 1.27x10^4 a}{1.55x10^5} \quad \text{for } r_1 = 4.00 \text{ m} \tag{29}$$

The α particle power and bremsstrahlung power per unit volume for a 50% D-T mixture are given by the following expressions, respectively: [16]

$$p_\alpha = 2.06x10^{-24} \frac{n^2}{4} T(r)^{-(2/3)} e^{-\frac{19.94}{T(r)^{1/3}}} \tag{30}$$

$$r_B = 2.14x10^{-30} \frac{n^2}{4} T(r)^{1/2} \tag{31}$$

where p_α and r_B are expressed in watt/cm^3, $T(r)$ is the plasma temperature in keV, and n is the particle density in cm^{-3}.

Inserting (30) and (31) in (28) and (29), with $n = 10^{14}$ cm^{-3}, one gets:

$$T_1 = 3.04x10^{22} \int_0^{280cm} \left[2.06x10^{-24} T(r)^{-(2/3)} e^{-\frac{19.94}{T(r)^{1/3}}} - 2.14x10^{-30} T(r)^{1/2} \right]_r dr$$

$$+ 1.54x10^{-1} a \qquad \text{for } r_1 = 2.80 \text{ m} \tag{28'}$$

$$T_1 = 1.61x10^{22} \int_0^{400cm} \left[2.06x10^{-24} T(r)^{-(2/3)} e^{-\frac{19.94}{T(r)^{1/3}}} - 2.14x10^{-30} T(r)^{1/2} \right]_r dr$$

$$+ 8.19x10^{-2} a \qquad \text{for } r_1 = 4.00 \text{ m} \tag{29'}$$

The plasma temperature $T(r)$ is a function of the minor radius r of the torus, starting at 20 keV in the central core and decreasing linearly towards the periphery, where it reaches T_1 at the first wall. [23] Hence:

$$T(r) = 20 - \frac{20 - T_l}{280} r \qquad \text{for } r_l = 2.80 \text{ m} \qquad (32)$$

$$T(r) = 20 - \frac{20 - T_l}{400} r \qquad \text{for } r_l = 4.00 \text{ m} \qquad (33)$$

and (28'), (29') transform, respectively, into:

$$T_l - 1.54 x 10^{1} a$$

$$= 3.04 \times 10^{22} \int_0^{280cm} \left[2.06 \times 10^{-24} \left(20 - \frac{20 - T_1}{280} r\right)^{-(2/3)} e^{-\frac{19.94}{\left(20 - \frac{20 - T_1}{280} r\right)^{1/3}}} - 2.14 \times 10^{-30} \left(20 - \frac{20 - T_1}{280} r\right)^{1/2} \right] r dr$$

$$\text{for } r_l = 2.80 \text{ m} \qquad (28")$$

$$T_l - 8.19 x 10^{2} a$$

$$= 1.61 \times 10^{22} \int_0^{400cm} \left[2.06 \times 10^{-24} \left(20 - \frac{20 - T_1}{400} r\right)^{-(2/3)} e^{\frac{19.94}{\left(20 - \frac{20 - T_1}{400} r\right)^{1/3}}} - 2.14 \times 10^{-30} \left(20 - \frac{20 - T_1}{400} r\right)^{1/2} \right] r dr$$

$$\text{for } r_l = 4.00 \text{ m} \qquad (29")$$

Eqs. (28") and (29") can be solved numerically for T_l as a function of a. Table 1 reports the results

In the Table we have highlighted the first wall temperature when $a \approx 1$. It is 0.181 keV for $r_l = 2.80$ m, and 0.111 keV for $r_l = 4.00$ m.

4.2 Verification of Ignition

Although the most general definition of ignition is the one provided by Eq. (22), a more appropriate one for ITER stems from the consideration that this machine is designed to be a proof-of-principle reactor. Therefore, the reaction product, namely the neutron output power, should be taken into account in the energy balance equation. This is because this power will help in achieving the goal of the reactor, which is production of electricity.

Since the neutrons escape from the plasma and are absorbed by the liquid blanket, together with the heat and bremsstrahlung radiation losses, the power available from the liquid blanket W_{LB} for conversion into electricity is:

$$W_{LB} = P_n + R + C \tag{34}$$

where P_n is the neutron power.

A fraction b of this power is converted into electricity, where b is typically 30%. Hence:

$$W_{electr.} = b(P_n + R + C) \tag{35}$$

ITER is supposed to be able to reach ignition. If this is so, at ignition $W_{max} = 0$, and Eq. (21) becomes:

$$W_{max} = \frac{1}{a}(R + C - P\alpha) = 0. \tag{21'}$$

The electricity production, if any, from ITER is obtained by subtracting (21') from (35):

$$W_{electr} = b(P_n + R + C) - \frac{1}{a}(R + C - P\alpha) \tag{36}$$

This general expression is justified because, if indeed ignition is achieved, the second term on the right-hand side of (36) is equal to zero, and (36) reduces to (35).
Equation (36) transforms into:

$$\frac{W_{electr}}{b} = P_n + \frac{1}{ab}P\alpha + (1 - \frac{1}{ab})(R + C) \geq 0 \tag{37}$$

where $P_n = p_n V_p$, and p_n (neutron power per unit volume) is given by [16]

$$p_n = 8.31 x 10^{-24} \frac{n^2}{4} T(r)^{-(2/3)} e^{-\frac{19.94}{T(r)^{1/3}}} \tag{38}$$

Inserting (25), (30), (31), and (38) in (37), one has:

$$4\pi^2 R_M \int_0^{2.8m \text{ or } 4m} \left[\begin{array}{c} \left(8.31 \times 10^{-24} + \dfrac{2.06 \times 10^{-24}}{ab}\right)\left(\dfrac{n^2}{4} T(r)^{-(2/3)} e^{-\frac{19.94}{T(r)^{1/3}}}\right) \\ + \left(1 - \dfrac{1}{ab}\right)\left(2.14 \times 10^{-30} \dfrac{n^2}{4} T(r)^{1/2}\right) \end{array} \right] r\,dr$$

$$+ 4\pi^2 R_M \left(1 - \frac{1}{ab}\right) \frac{K_{LB} T_1}{\ln(r_2/r_1)} \geq 0 \tag{39}$$

Inserting in (39) the values of a and T_i reported in Table 1, and of $T(r)$ as given by (32) or (33) for $n = 10^{14}$ cm^{-3}, and carrying out the operations on the left-hand side of the above inequality, one finds that the inequality is not satisfied. One always gets negative numbers,rather than positive numbers, or at most zero. In (39) we have assumed $b = 30\%$. Table 2 reports the results.

Table 1. Temperature of the first wall as a function of the energy transfer efficiency *a* from driver to plasma, for two minor radii, i.e., r_1=2.8 m and r_1=4.0 m.

T_i (keV)	*a*	
	r_1=2.80 m	r_1=2.80 m
0.181	**0.996**	-
0.15	0.796	-
0.111	0.543	0.997
0.10	0.472	0.860
0.09	0.407	0.739
0.08	0.343	0.617
0.07	0.278	0.496
0.06	0.213	0.374
0.05	0.148	0.252
0.04	0.084	0.131
0.03	0.019	0.008

Table 2. Values of the left-hand side of inequality (39), as a function of *a* and *b*, for two minor radii, i.e., r_1=2.8 m and r_1=4.0.

T_i (keV)	*a*		*b*	Left-hand side of (39)	
	r_1=2.80 m	r_1=4.00 m		r_1=2.80 m	r_1=4.0 m
0.181	**0.996**	-	0.3	$-4.91\text{x}10^8$	-
0.15	0.796	-	0.3	$-5.73\text{x}10^8$	-
0.111	0.543	**0.997**	0.3	$-6.77\text{x}10^8$	$-3.73\text{x}10^8$
0.10	0.472	0.860	0.3	$-7.13\text{x}10^8$	$-1.02\text{x}10^8$
0.09	0.407	0.739	0.3	$-7.34\text{x}10^8$	$-1.41\text{x}10^8$
0.08	0.343	0.617	0.3	$-7.56\text{x}10^8$	$-1.93\text{x}10^8$
0.07	0.278	0.496	0.3	$-7.87\text{x}10^8$	$-2.45\text{x}10^8$
0.06	0.213	0.374	0.3	$-820\text{x}10^8$	$-2.91\text{x}10^8$
0.05	0.148	0.252	0.3	$-846\text{x}10^8$	$-3.42\text{x}10^8$
0.04	0.084	0.131	0.3	$-8.59\text{x}10^8$	$-3.78\text{x}10^8$
0.03	0.019	0.008	0.3	$-8.87\text{x}10^8$	$-3.00\text{x}10^8$

Since the above table shows that ignition is not achieved, this means that Eq. (21') is not zero but greater than zero. Despite this, one can still verify if ITER can reach power breakeven, i.e., $W_{electr} = W_{max}$, provided, of course, that the driver power W_{max} is kept on. Subtracting (21') from (35), one gets:

$$W_{electr}-W_{\max}=b(P_n+R+C)-\frac{1}{a}\left(R+C-P_{\alpha}\right) \tag{36'}$$

which becomes, for power breakeven:

$$\frac{W_{electr}-W_{\max}}{b}=P_n+\frac{1}{ab}P_{\alpha}+(1-\frac{1}{ab})(R+C)=0 \tag{40}$$

Eq. (40) is the same as (37), and the negative numbers of Table 2 show that ITER might not even reach power breakeven for the design parameters provided before.

5. CONCLUSIONS

The present study has provided on overview of the main direction of the fusion program in magnetic confinement and has found that the magnetic field required for ignition exceeds any of those presently considered for major machines.

The analysis has then been extended to the ITER (International Thermonuclear Experimental Reactor) machine, and found that serious doubts persist about its scientific validity. The analysis carried out on a simple model of the machine, as presently designed, has shown that ITER might not be able to reach either ignition or power breakeven. The large cost and the long time frame of the ITER program, on the other hand, do not allow for any doubt that the machine must reach its stated goal of ignition. Consequently, as long as these doubts persist, and cannot easily be dissipated, the ITER program should be put on hold, and fusion alternative concepts should be pursued.

We want to suggest here that a healthy fusion program should rely on a good mix of conventional and alternate concepts, in order to diversify the risks involved in the solution of the fusion problem. The tokamak program should not be abandoned, provided it is centered on reasonable size machines, such as the Ignitor [26], which promises to reach ignition at a fraction of the cost of ITER. At the same time, alternate concepts should be vigorously pursued. To quote just a few of these concepts deserving of support, one should mention the dense Z-pinch, magnetized target fusion, muon catalyzed fusion, plasma focus, reversed field pinch, spherical pinch, spheromak, staged Z-pinch, etc. Moreover, one should leave the door open to exploratory concepts, which might very well prove to be decisive in the fusion problem. All of these concepts have been presented in a previous conference dedicated to an overview of the fusion arena [27], as well in the present conference.

REFERENCES

1. J.D. Lawson. Proc. Phys. Soc. **B70,** 6 (1957).
2. R.G. Mills. IEEE Trans. Nucl. **NS-18,** 205 (1971).
3. B.C. Maglich, and R.A. Miller. J. Appl. Phys. **46,** 2915 (1975).
4. F.F. Chen, J.M. Dawson, B.D. Fried, H.P. Furth and M.N. Rosenbluth. J. Appl. Phys. **48,** 415 (1977).
5. T.J. Dolan. Fusion Research. Principles, Experiments and Technology. (Pergamon Press, New York, 1982), pp. 73–100.
6. R.A. Gross. Fusion Energy. (John Wiley & Sons, New York, 1984) pp. 38–41.
7. T. Kammash. Fusion Reactor Physics. Principles and Technology. (Ann Arbor Science Publishing, Ann Arbor, 1975) pp. 21–23.
8. G.H. Miley. Fusion Energy Conversion. (American Nuclear Society, 1976) pp. 393–394.

9. J.R. Roth. Introduction to Fusion Energy. (Ibis Publishing, Chalottesville, Virginia, 1986) pp. 223–282.
10. J. Raeder, K. Borrass, R. Bünde, W. Dänner, R. Klingelhöfer, L. Lengyel, F. Leuterer and M. Söll. Controlled Nuclear Fusion, (John Wiley & Sons, Chichester, 1986) pp. 210-212.
11. J. Wesson. Tokamaks. (Clarendon Press, Oxford, 1987) pp. 8–11.
12. E. Panarella and P. Savic. J. Fusion Energy **3**, 199 (1983).
13. E. Panarella. J. Fusion Energy **13,** 45 (1987).
14. H. Chen, J. Chen, B. Hilko and E. Panarella. J. Fusion Energy **13**, 45 (1994).
15. E. Panarella. Current Trends in International Fusion Research. (Plenum Press, New York, 1996) pp. 211-244.
16. S. Glasstone and R.H. Lovberg. Controlled Thermonuclear Reactions. (D. Van Nostrand, 1960), pp. 20–32.
17. Lindon C. Thomas. Fundamentals of Heat Transfer. (Prentice-Hall, Englewood Cliffs, N.J., 1980) p. 9.
18. R.W. Conn. J. of Nuclear Materials **76 & 77**, 103 (1978).
19. L. Spitzer, Jr. Physics of Fully Ionized Gases, (Interscience Publishers, 1962) p. 144.
20. A.M. Sessler, T.H. Stix and M.N. Rosenbluth. Physics Today, (June 1996) pp. 22-25.
21. B. Coppi, F. Bombarda, P. Detragiache, S. Migliuolo and L.E. Sugiyama. Evolution of global modes and magnetic reconnection in fusion burning plasmas. Proceedings of the 17th IAEA Fusion Energy Conference, Montreal, Canada, (7-11 October 1996).
22. James Glanz. Science **274**, 1600 (1996).
23. L. John Perkins. ITER Team (private communication).
24. Ref. 17, p. 653.
25. L.R. Ingersoll, O.J. Zobel and A.C. Ingersoll. Heat Conduction, (McGraw-Hill, New York, 1948) p. 38.
26. F. Pegoraro. Ignition Physics and the Ignitor Project. Current Trends in International Fusion Research, Emilio Panarella, ed. (Plenum Press, New York, 1997) p. 125.
27. E. Panarella. Current Trends in International Fusion Research, Plenum Press, New York (1997).

ISSUES OF FUSION BURN CONTROL

Hans Persson

Group of Theoretical Electrotechnics
Department of Materials Science
Box 534
S - 751 21 Uppsala, Sweden

ABSTRACT

A critical discussion is provided of several factors and circumstances relevant to the dynamics and control of the burn of a thermonuclear reactor, particularly based on the tokamak concept. Notably, the following issues are considered: separate density and temperature control versus integrated design, influence of delays in energy deposition and fuel supply, control based on variation of density alone, notably "fusion choking", controlled setpoint changes, comparing a conventional gain scheduling controller with a suggested, nonlinear controller obtained by complete linearization. The latter is shown to have superior properties, except a lack of robustness against modeling errors. Kalman filters are suggested for automatic discrimination between confinement modes and for avoidance of thermal runaway.

1. INTRODUCTION

A fusion reactor is likely to require a device for control of its burn. In a tokamak you normally have two equilibrium points, a low-temperature equilibrium which is thermally unstable, and a high-temperature equilibrium which is stable. In the former case you will need to control the instability, and in the case of a stable operating point you will still need to control the working point against various unforeseen influences and perturbations, and to perform any required change of the operating point. In a power-producing reactor the low-T equilibrium may be a preferred alternative, since you may get a higher power.

In this paper a few critical issues of burn control are discussed, and a few new results are included, notably a discussion of set point changes and a suggestion regarding a certain nonlinear controller with some desirable properties.

2. BURN INSTABILITY AND CONTROL

The stability situation is for instance illustrated in Fig. 6 in [1]. The diagram is a phase space plot obtained in a strongly simplified, zerodimensional model. The low-T equilibrium is an unstable saddle point, and there is also a stable equilibrium. The figure was drawn for

Current Trends in International Fusion Research – Proceedings of the Second Symposium
Edited by E. Panarella. NRC Research Press, National Research Council of Canada, Ottawa, ON K1A OR6, Canada. 1999.

given values of injection rate and auxiliary heating.

The burn of a fusion reactor can be influenced in many different ways. One important possibility is to vary the supply of fuel, another to vary the auxiliary heating. Influencing the burn with the injection rate is in fact an old idea. There is also the opposite school where you regard the density as something you should keep constant for itself, and then you control the temperature separately, e. g., by the auxiliary heating. Now the fact is that the burn depends, in a coupled way, on both the particle injection and the auxiliary heating; therefore, it seems rational to control the burn using both in an integrated fashion, without giving a priori preference to one or the other.

When you design a controller you will then, conventionally, linearize the evolution equations describing your system around the working point and design a controller for a linear system. In simplest cases you use pole placement techniques, or perhaps linear-quadratic (LQ) optimization:

Minimize the performance index

$$J = \int_0^\infty (x^T Qx + u^T Ru)dt$$

with the closed system evolution equation $d\mathbf{x}/dt = \mathbf{Ax} + \mathbf{Bu}$ as a constraint. Here, **Q** and **R** are penalty matrices associated with the deviation **x** from the working point and the control signal **u**, respectively. The problem gives a Riccati equation for the controller **K**; ($\mathbf{u} = -\mathbf{Kx}$).

There also exist a few modern techniques, like H-infinity theory or μ-analysis, that guarantee that you get a reliable control even when your system is not well known or your diagnostic information is incomplete.

3. SEPARATE VS INTEGRATED N AND T CONTROL

Already on the linearized level you gain efficiency by optimizing with respect to *n* and *T* in an integrated way, rather then optimizing each of them separately. This can be shown by actually calculating the penalty functional for the two cases. It also follows from the property of the LQ-minimal solution of actually providing the minimum value of J. You get a faster control and a lower J-value. But this is far from the only improvement; even greater gain by considering both n and T is obtained nonlinearly, in particular, in connection with the phenomenon of actuator saturation; this will be discussed more in detail below.

An illustration of how actuator saturation influences the control is found in Fig. 14 in [1]. The region of control extends in a certain surrounding of the working point. For low *T* and n there is a region of quench, where the maximum available power is too low to bring the plasma up to the working temperature. There is also a region of runaway for high *T* (and n), where turning the heating down to zero is not enough to prevent a thermal excursion.

4. DELAYS

Delays may be important in connection with burn and burn control. For instance, delays associated with the energy deposition of fast particles need in principle to be considered. The delay in the energy transfer from fast alpha particles to the plasma tends to act stabilizing, because the energy runaway will be delayed. On the other hand, the delayed energy deposition from a neutral beam will be less efficient as a means for control. It would seem that such energy deposition delays, usually of the order of one second, would simply be too short to produce any dramatic effects; there seems to be a marginal influence. However, for modulation of the particle supply rate the delay is longer, and it may be quite important. Before going into details, it is worthwhile stating a general principle for delays in the context of control actuations:

Delays in control actions are of limited importance, provided that

a) the delay is known to you, and you have a good, reliable model of your "process", based upon which you can take countermeasures, and
b) no disastrous nonlinearities are being encountered. The general method is, in accordance with the famous Otto Smith controller, to base the control not upon the present state of the system but on the state predicted by the model one delay time later.

The control becomes less efficient, but may still be linearly acceptable. For instance, in linear-quadratic optimal control the cost functional is increased by a term given by the delay time.

Thus, the major disadvantage with delayed control is that the system becomes sensitive to modeling errors, making predictions less reliable, and that the control becomes more vulnerable to nonlinearities. This is the main reason why control by fuel injection rate only is unfeasible, except under very special conditions. In [1], Sec. VI F a few cases of delayed density actuation are studied; If, with LQ-optimal control, too high penalty is placed on the magnitude of the control signals, too large deviations of the state of the plasma from the working point are accepted, and the system trajectories become wiggly and the control inefficient. However, when larger control signals are accepted, the control becomes acceptable.

5. FUSION "CHOKING"

In Fig. 17 in [1] an interesting property of the control was illustrated. The working point was located close to the ignition curve, and it was found that control of the burn can be obtained in a reasonably large region with moderate or small densities even above the ignition curve. The controller prescribes a quick addition of a lot of fuel in order to cool the plasma; the term "fusion choking" was coined to describe this mechanism. The figure was constructed without considering any delay, but it was also found that some 60 % of the controlled region above the ignition curve was preserved even with a delay of 7 seconds. Similar results were later reported by Hui et al. [2].

6. CONTROL WITH FUEL INJECTION

It was felt for some time that modulation of the fuel injection rate alone would not be quite sufficient to control the burn of a fusion reactor. This was then proved, in a convincing way, in [2]. Their paper is fundamentally important, because a number of effects were included, like delays, recycling and effects of helium ash. Furthermore, the controller has a robust, modern design. In essence, even if thermal runaway can be prevented in a region outside the ignition curve, this region is limited, due to the delay involved in the cooling by density increase. In addition, reducing the injection to meet a negative temperature perturbation will not be feasible when the reactor operates under conditions leading to a strong wall recycling because it makes reduction of the fuel supply rate difficult, a reduction that would be necessary to bring the temperature up again.

Clearly, one has to combine the fuel injection with other methods. The control region could be extended upwards in T, either by using fast pellet injection, or perhaps by impurity injection (see e.g. [3]. A too low T, on the other hand, could be controlled by additional heating. In any of these cases, one should use an integrated approach.

7. DELAY IN ALPHA PARTICLE ENERGY DEPOSITION

The conjecture above that the delay in alpha particle deposition only has a marginal importance can be demonstrated by a simulation. See Figs 1a and b, showing phase space plots valid for a simple zerodimensional model, with the working point given by $n_0 = 0.9 \times 10^{14}$ /cm^3; $T_0 = 7$ keV; ITER 89-P scaling, with an H-mode enhancement factor of 2.2. At the start of each curve, the alpha power is assumed to be equal to its undelayed value at the starting point. Fig. 1a corresponds to neglect of this delay, and in Fig. 1b a delay of 1 sec is included. A similar diagram appears if the delay is assumed to be as long as 2 secs. The working point is strongly unstable, situated near the ignition curve. In spite of the short runaway time (approximately 5 secs), the delay is still too short to produce more than a marginal change of the phase portrait; the location of the separatrices is changed by small amounts, and the inclusion of the delay makes the trajectories in the upper right part of the picture tend to large values less steeply.

It is concluded that the delay in the energy deposition of fast alpha particles can usually be disregarded, except in careful, quantitative calculations.

8. INFLUENCE OF HELIUM ASH

As is well known, the presence of helium ash has a profound influence on the burn, notably by the resulting fuel dilution. The equilibrium state is indeed influenced by a helium content of the order of 10%, and there should also be a significant influence on the global,

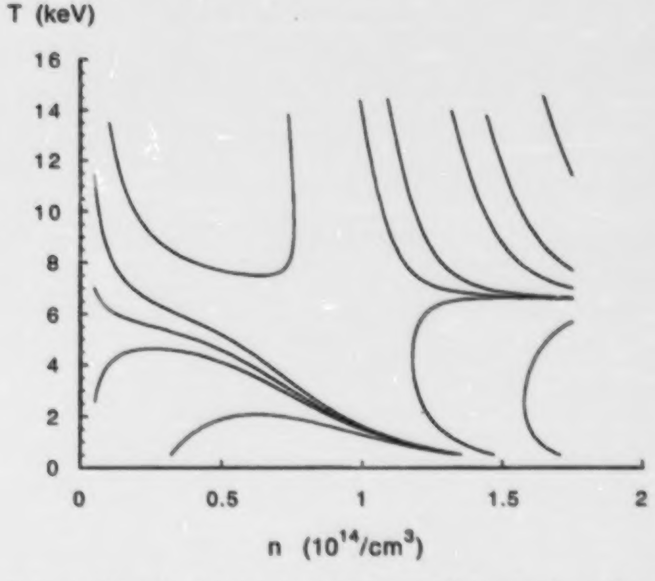

Figure 1a. Phase plot of fusion plasma obeying ITER89-P scaling law, with an unstable equilibrium at n_0=9x10^{14}/cm^3, T_0 = 7 keV. No delay in alpha particle energy deposition considered.

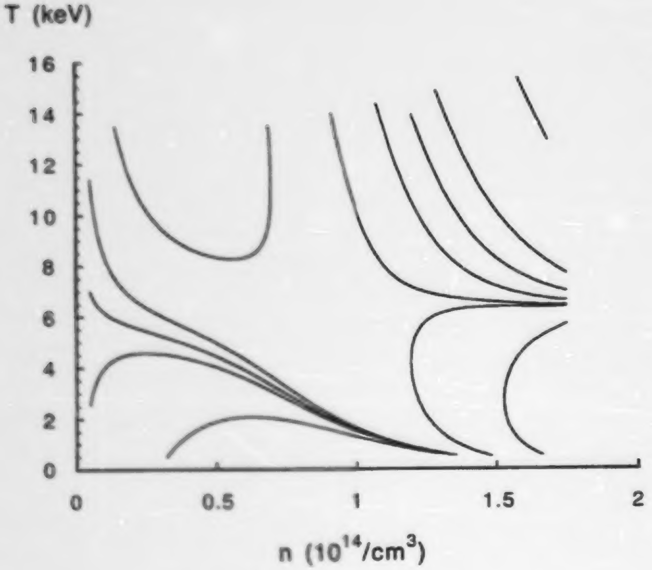

Figure 1b. A delay of one second included.

nonlinear dynamics of the plasma. Linearly, however, we do not expect a strong influence on the dynamics, due to the long time scale (burn-up time) involved in the helium generation, compared to the energy runaway time.

It is perhaps less well known that the helium ash can, in an indirect way, provoke a thermal runaway, at least for low densities. This is shown by simulations, and the physical mechanism behind it can be described as follows: The presence of helium necessitates a higher additional heating to keep the plasma at a given operating point, in order to compensate for the decrease in alpha power connected with the fuel dilution. This leads to an overcompensation for low densities, where the alpha power is less important, and a thermal runaway results.

9. CONTROLLED CHANGE OF SET POINT

For the operation of a fusion reactor it is also necessary to have means for controlled startup and shutdown and any changes of set point necessitated e.g. by the requirements of the grid. The system then has to work well for global changes of the parameters, passing stability borders, the Cordey pass and mode transitions, with their well known hysteresis. An interesting study within this area is reported in a paper by Werley and Bathke [4]. Here, we wish to illustrate some matters of principle in a simplified model, without a mode transition (cf. Sec. 11 below for a brief discussion of the latter phenomenon).

In a simulation, the set point was assumed to vary, from a constant state at $n_0 = 0.1\text{x}10^{14}/\text{cm}^3$; $T_0 = 2$ keV to another constant state at $n_0 = 0.9\text{x}10^{14}$ /cm^3; $T_0 = 7$ keV, with a linear increase with time between, the rate of which could be varied. In this parameter interval the plasma varies strongly, and "gain scheduling" was first used; i.e., a bank of five linear, LQ-optimal 2x2 controllers were designed, each of which to be used for a particular

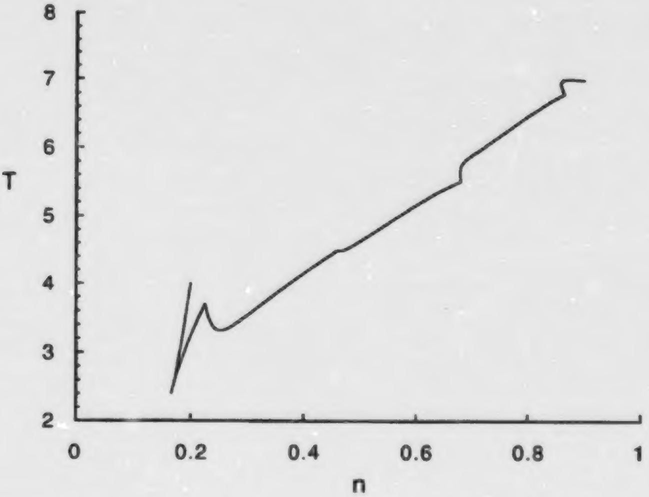

Figure 2. Phase trajectory of plasma controlled with a bank of five LQ-optimal controllers. The set point is varied linearly in time.

range of set points. The resulting trajectory of a plasma starting at $n(0) = 0.2\text{x}10^{14}/\text{cm}^3$; $T(0) = 4$ keV is shown in Fig. 2; it corresponds to a total time of about 10 minutes. If the ramping is made too fast, the curve gets worse.

Clearly, the result is not impressive; the curve wiggles and has kinks, and the set point is not being well followed. There exist systematic procedures for improvement, but this adds to the complication. Straightforward means to take would be to use more controllers or make them robust in order to meet the varying properties of the plasma.

One particular disadvantage with gain scheduling is the necessity to design a new bank of controllers, if another curve than a straight line in parameter space is to be followed. In principle, one might need to fill the entire parameter space with linear controllers.

In this situation it seems reasonable to use a nonlinear approach, e.g., try a full nonlinear optimization – which may lead to complications. In the next section we shall present a simple nonlinear controller that appears to be promising.

10. NONLINEAR CONTROLLER

It was briefly stated in [1] that, at least for the simplified system considered, it was possible to carry out a "complete linearization", i.e., design a nonlinear controller by which the nonlinearity of the system is eliminated, and the closed system becomes linear. This possibility has now been investigated, and a control scheme designed and tested. It turns out that one obtains a closed-form, analytical expression for the controller, valid over the entire parameter space. Any desired change of set point along any curve can be conveniently carried out with this controller, and perturbations are eliminated with dynamics of the choice of the operator. One serious flaw still exists: Since the controller rests upon an elimination of the process dynamics, it has no robustness against modeling errors. However, already in its present form it is felt to be an interesting starting point for design of a controller without this drawback.

Denoting the density and temperature by *n* and *T*, respectively, the transport losses of particles and energy by F_p and P_t, the alpha particle heating by P_α and the Bremsstrahlung loss by P_b, we define

$$f_1 = -(F_p - F_{p,0})$$
$$f_2 = [(P_\alpha - P_{\alpha,0}) - (P_b - P_{b,0}) - (P_f - P_{f,0}) + T(F_p - F_{p,0})]/n$$
$$f = \begin{pmatrix} f_1 \\ f_2 \end{pmatrix}$$

Here, index 0 refers to the values of the functions at the set point. Then, using S for the particle injection rate and P_{aux} for the auxiliary heating, we introduce

$$x = \begin{pmatrix} n \\ T \end{pmatrix}$$
$$u = \begin{pmatrix} S - S_0 \\ P_{aux} - P_{aux,0} \end{pmatrix}.$$

Here, **x** is the state vector and **u** the vector of control signals.

$$B = \begin{bmatrix} 1 & 0 \\ -T/n & 1/n \end{bmatrix}$$

The matrix **B** describes the occurrence of **u** in the evolution equations.
Then the evolution equation for the closed system takes on the form

$$\frac{dx}{dt} = f + Bu .$$

In this case **B** is invertible, and we choose

$$u = B^{-1}[-f(x) + g(x)] \tag{1}$$

where **g** is any suitably chosen function of the state vector.
This then gives $\frac{dx}{dt} = g(x)$.
That is to say, the dynamics given originally by **f** have been replaced by those of **g**, which can be chosen at will, e. g., linear. In the present case we have

$$B^{-1} = \begin{bmatrix} 1 & 0 \\ T & n \end{bmatrix}.$$

For **g** we choose a matrix **G** such that we get dynamics corresponding to the standard 135 degrees pole placement for the difference between the state vector and the setpoint. Thus, the dynamics are made independent of the setpoint:

$$\frac{d}{dt}\begin{pmatrix} n - n_0 \\ T - T_0 \end{pmatrix} = G\begin{pmatrix} n - n_0 \\ T - T_0 \end{pmatrix}$$

Thus, $\frac{d}{dt}\begin{pmatrix} n \\ T \end{pmatrix} = G\begin{pmatrix} n - n_0 \\ T - T_0 \end{pmatrix} + \begin{pmatrix} \frac{dn_0}{dt} \\ \frac{dT_0}{dt} \end{pmatrix}$

One finds $G = k\begin{bmatrix} -1 & -n_0 / T_0 \\ T_0 / n_0 & -1 \end{bmatrix}$.

Here, the scalar constant k determines the characteristic time of the control. Introducing this into Eq. (1), one gets

$$\begin{aligned} deltaS &\equiv S - S_0 = -f_1 - k[(n - n_0) + n_0(T - T_0)/T_0] \\ deltaP &\equiv P_{aux} - P_{aux,0} = -Tf_1 - nf_2 - k[(T - T_0 n / n_0)(n - n_0) + \\ &+ (n + n_0 T / T_0)(T - T_0)] \end{aligned}$$

Furthermore,

$dn/dt = f_1 + deltaS + dn_0/dt$ (f_1 is eliminated); $dT/dt = f_2 - (T deltaS - deltaP)/n + dT_0/dt$ (f_1 and f_2 are eliminated).

This controller was then tested with the set point variation described in the previous section. One result appears from Fig. 3, showing the set point temperature T_0 (dashed curve) and plasma temperature T (solid curve) as functions of time. Near T = 5 keV a positive temperature step perturbation of 0.7 keV was artificially introduced. Clearly, the controller works well and takes care both of the off-setpoint initial state and the temperature perturba-

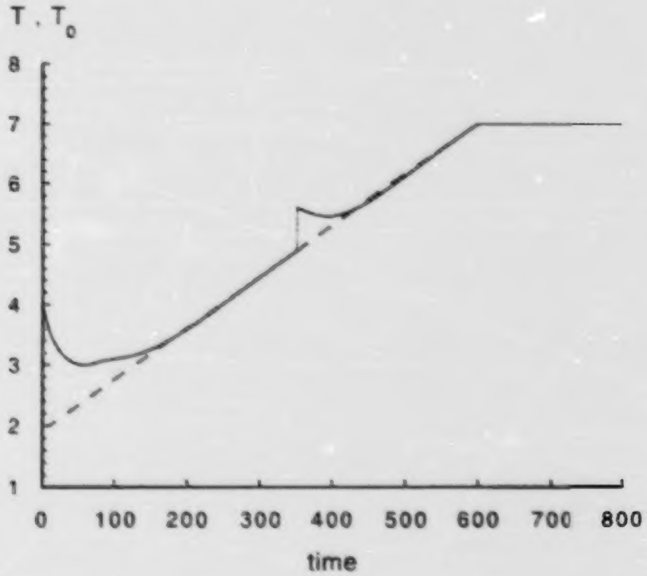

Figure 3. Set point temperature T_0 (dashed) and plasma temperature T (solid) versus time for nonlinear controller obtained by complete linearization. A temperature step of +0.7 keV was artificially introduced near T=5 keV.

tion. The jump in T occurs in the stable region where the auxiliary heating needs to be increased to increase T_0. A similar step was introduced in the unstable region, where the auxiliary heating diminishes with increasing T_0. The strategy of the controller is a bit different in the two cases. The auxiliary heating is suddenly decreased, but the soft reduction of the particle injection in the stable case is preceded by a sharp positive injection spike in the unstable case – apparently a form of "fusion choking".

It is easy to show that the controller, in spite of several attractive properties, does not work well when the model disagrees with the one assumed. However, it is felt that it could still serve as a starting-point to construct an attractive controller with sufficient robustness.

11. IDENTIFICATION

In order to control a process, you must know its dynamics. If the latter are unknown, it becomes necessary to find them out. The paper by Anderson et al. [1] contains an example of simulated parameter identification. In that simulation numerically integrated data were scrambled by noise and then introduced as the only information (together with the system order) into an identification algorithm. It turned out that the system parameters could be reconstructed with good accuracy. Needless to say, such a simulation cannot model all the complications and pitfalls of a real experiment, but the result is encouraging.

It would be of interest to integrate an identification with the control to form an adaptive control scheme. For burn control this has been made by Miley and Varadarajan [5]. It appears that there are different attitudes to adaptive control among control experts. Many of them seem to prefer to have the human mind as a link in the entire process, because the properties of nonlinear closed systems can sometimes be difficult to predict. Here, we will only like to suggest an automatic control scheme that can handle mode transitions: Kalman filters are used to predict new values of the phase space quantities from old ones. One would then use two different Kalman filters, one for each mode, with its respective dynamics. The filters should then not be used for control – at least not if complete diagnostic information exists. Instead the predictions should be compared with measured values after some time, and this would tell which mode is present. Then the controller is chosen accordingly.

It appears feasible to simulate this setup numerically, testing - among other things - the robustness against limited perturbations of the models, and against noise.

If something unforeseen happens during high-Q operation (e.g., a sudden improvement of the confinement, discovery of unknown, systematic measuring errors, etc.) then it is necessary to identify the situation and take countermeasures. One will then only have a few secs, or maybe 10-20 secs, to identify, take action and wait for the result. This implies that the protection must be automatic. A Kalman filter is known to be superior to the human eye to eliminate noise and identify systematic changes, and could be used for this purpose. Moreover, the controller should be designed in such a way that the ignition curve is avoided. This then suggests more sophisticated dynamics than those of the standard design chosen after linearization in the previous section.

ACKNOWLEDGMENTS

I wish to thank Dr. K. Nordström for stimulating discussions of control theory issues.

This work was carried out within the Swedish-Euratom association and supported by the Swedish Natural Science Research Council (NFR), Grant No. F-AA/FU 06481-309.

REFERENCES

1. D. Anderson, T. Elevant, H. Hamnén, M. Lisak and H. Persson. Fus. Tech. **23**, 5 (1993).
2. W. Hui, B. Bamieh and G. H. Miley. Fus. Tech. **26**, 1151 (1994).
3. W.M. Stacey Jr. Fus. Tech. **23**, 157 (1993).
4. K.A. Werley and C.G. Bathke. Fus. Tech. **26**, 582 (1994).
5. G.H. Miley and V.Varadarajan. Fus. Tech. **22**, 425 (1992).

FUSION OF DEUTERIUM NUCLEI AND OTHER NUCLEAR PROCESSES IN A METALLIC LATTICE*

David W. Kraft and Lloyd Motz[1]

Division of Natural Sciences and Mathematics
University of Bridgeport
Bridgeport, CT 06601, U.S.A.
[1]Department of Astronomy
Columbia University
New York, NY 10027, U.S.A.

ABSTRACT

Experiments reporting the observation of cold nuclear fusion in metallic lattices have excited much interest and controversy [1–3]. Although these experiments indicate the presence of an unexplained source of energy, there are no satisfactory fusion or other theoretical models to account for these observations. In the present work we analyze possible mechanisms that, either enhance the fusion of deuterons in Pd and Ti lattices or that affect other energy-releasing nuclear processes, and we study the extent to which these mechanisms account for the experimental results. We consider the following:

- The electrostatic interaction of the D_2 molecule with neighboring metal atoms;
- The role of Li nuclei as participants in fusion reactions, as facilitators to enhanceother mechanisms and as a source of deuterons;
- The increased effective mass of D_2 binding electrons in a metallic lattice;
- The role of the metallic nuclei as participants in nuclear reactions, with emphasis on deuteron stripping reactions.

Of these, only the first mechanism proves significant. For a D_2 molecule suitably positioned within a Pd lattice, the electrostatic interaction with neighboring Pd atoms can reduce the D_2 internuclear separation from the free-molecule value to 0.1018 Å, corresponding to a fusion rate of 10^{-14} fusions/molecule/second. This rate is adequate to account for the observations of Jones et al. [1] .

The Li nuclei provide a small enhancement of the electrostatic mechanism but they play no significant role for nuclear processes in a metallic lattice. The reduction of the D_2 internuclear separation by the increased effective mass of the D_2 binding electrons is, by itself, not adequate to account for the claimed cold fusion rates. The contributions of nuclear

Current Trends in International Fusion Research — Proceedings of the Second Symposium
Edited by E. Panarella. NRC Research Press, National Research Council of Canada, Ottawa, ON K1A 0R6, Canada. 1999.

reactions involving the Pd or Ti nuclei directly, and the effects of stripping of deuterons by these nuclei are negligible.

1. INTRODUCTION

Experiments reporting the observation of cold nuclear fusion in metallic lattices have excited much interest and controversy [1-3]. Although these experiments indicate the presence of an unexplained source of energy, there are no satisfactory fusion or other theoretical models to account for these observations. In the present work we analyze possible mechanisms that, either enhance the fusion of deuterium nuclei in Pd and Ti lattices, or that affect other energy-releasing nuclear processes, and we study the extent to which these mechanisms account for the experimental observations. We consider the following:

- The electrostatic interaction of the D_2 molecule with neighboring metal atoms;
- The role of Li nuclei as participants in fusion reactions, as facilitators to enhance other mechanisms and as a source of deuterons;
- The increased effective mass of D_2 binding electrons in a metallic lattice;
- The role of the metallic nuclei as participants in nuclear reactions, with emphasis on deuteron stripping reactions.

2. ELECTROSTATIC ENHANCEMENT OF FUSION RATE

2.1 Electrostatic Interaction of Deuterons with Metallic Atoms

The probability for nuclear fusion is enhanced when the separation between the interacting nuclei is reduced. In the free D_2 molecule, the separation between the two deuterium nuclei is 0.7417 angstroms (Å), and fusion rates for this separation have been estimated at 10^{-64} to 10^{-62} fusions per molecule per second [4,5]. Such rates are far too low to account for cold fusion in metallic lattices. If such fusion processes occur, there must be some mechanism functioning to reduce the internuclear distance when the deuterons are embedded in the lattice. We examine here an electrostatic mechanism for the reduction of the deuteron internuclear distance in palladium (Pd) and titanium (Ti) lattices..

For our purpose, we need not distinguish between deuterium entering the metallic lattice as a D_2 molecule, a D_2 ion, a D atom or as deuterons since we are concerned only with the internuclear separation. For brevity, we will refer to a deuteron pair as a D_2 molecule. Consider such a molecule situated halfway between two metal atoms such as Pd, as shown in Figure 1. The line joining the deuterium nuclei is perpendicular to and bisected by the line joining the Pd nuclei, so that the two deuterons are each equidistant from the two-Pd nuclei. The half-distance, *d*, between the Pd nuclei is related to the lattice constant, *a*, and depends on the location of the D_2 molecule within the lattice.

We model the Pd electron distributions by concentrations of charge on the line joining the atoms, an assumption justified by the symmetry of the situation. For each Pd atom, we take the electrons to be concentrated at two points, one on either side of the nucleus, with half the electronic charge at each point. The distance of these charges from the nucleus is specified as a fraction of the metal atom radius, bR_A, where R_A is the atom radius and $0 < b < 1$. As a nominal value for this distance we use the radius enclosing one-half of the metal atom volume; thus $b = 2^{-1/3} = 0.7937$. We also examine the sensitivity of the results to variations in *b*.

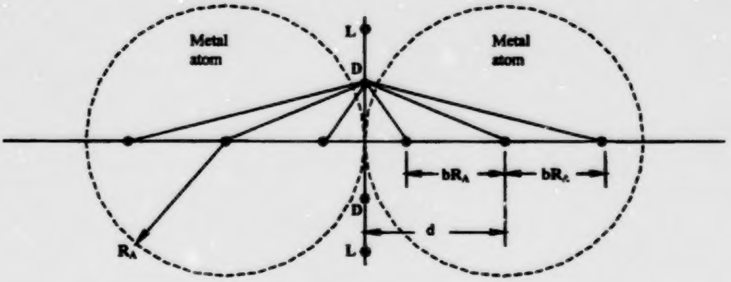

Figure 1. Deuterons in a metallic lattice. Deuterons are situated at points D, a distance R apart. The nuclei of the metal atoms are at distance d from the D-D axis. For each atom, the electronic charge is concentrated at two points $d \pm bR_A$ where R_A is the radius of the Pd atom and $0 < b < 1$. Li nuclei are located at points L.

The total electrostatic force acting on either deuteron consists of attractive forces exerted by the two Pd atoms' concentrations of electronic charge, and of repulsive forces exerted by the two Pd nuclei and by the other deuteron. By symmetry, the only nonvanishing component of the force is that exerted along the line joining the deuterons. For the net force acting on each deuteron when their separation is R, we obtain

$$F = \frac{4Z_1Z_2e^2}{R^2}\left[\frac{2}{(1+m^2)^{3/2}} - \frac{1}{(1+k_1^2)^{3/2}} - \frac{1}{(1+k_2^2)^{3/2}} + \frac{Z_1}{4Z_2}\right] \tag{1}$$

in which Z_1 and Z_2 are the atomic numbers respectively of deuterium and of the metal atom and e is the electronic charge. The quantities m, k_1 and k_2 are dimensionless distances defined by $m = 2d/R$, $k_1 = 2(d + bR_A)/R$ and $k_2 = 2(d - bR_A)/R$. The attractive forces are represented by negative terms and the repulsive forces by positive terms.

The lattice structures of Pd and Ti are, respectively, face-centered cubic and hexagonal close-packed, and in each structure the assumed location of the deuteron pair is between nearest-neighbor atoms. Thus, in Pd, the assumed location of the deuterons is between atoms at a corner and the face-center, while in Ti the deuterons are taken to be in the face plane, halfway between atoms at a corner and the center. The half-distance, d, between nearest-neighbor atoms is related to the lattice constant, a, by $d = a/2^{3/2}$ in Pd and $d = a/2$ in Ti. In units of angstroms we have $R_A = 1.376$ and $a = 3.8907$ in Pd, $R_A = 1.54$ and $a = 2.9504$ in Ti [6]. Substituting these values in Eq. (1) we find that, in each lattice, at the free-molecule internuclear separation, the net force on each deuteron is attractive and therefore the deuterons should approach each other.

The equilibrium separation is determined by the condition $F = 0$, i.e., when the attractive and repulsive forces are in balance. An approximate value for the equilibrium value of R can be obtained approximating the terms in Eq. (1) in the limit of small R. With the above values for R_A and a, we note that the terms containing m and k_1 can be neglected for small R, so that we obtain for this approximation,

$$F \approx \frac{4Z_1Z_2e^2}{R^2}\left[\frac{Z_1}{4Z_2} - \frac{1}{\left(1+k_2^2\right)^{3/2}}\right] \tag{2}$$

and therefore, for $F = 0$,

$$R \approx \frac{2(d - bR_A)}{\left[(4Z_2 / Z_1)^{2/3} - 1\right]^{1/2}} \tag{3}$$

With $b = 2^{-1/3}$, values for the equilibrium separation calculated from Eq. (3) for Pd and Ti are, respectively, 0.101 Å and 0.137 Å . These compare well with precise calculations based on Eq. (1); for example, for Pd, setting $F = 0$ in Eq. (1) yields $R = 0.1018$ Å. These values are substantial reductions from the free-molecule deuteron separation and the corresponding fusion rates are calculated below.

2.2 Nuclear Fusion Rates

Early calculations of cold nuclear fusion rates were performed by Jackson [7] and by Zel'dovich and Gershtein [8]. More recent work includes that of Picker [4], Van Siclen and Jones [9], and Koonin and Nauenberg [5]. We employ the development of Koonin and Nauenberg (KN) who calculated fusion rates for isotopic H_2 molecules of various composition, and for enhancements of the mass of the H_2 binding electrons such as might occur when they are subjected to the fields in a crystal lattice.

The fusion reaction rate for the deuterons in a D_2 molecule is given by

$$\Lambda = B|\Psi(R)|^2 \tag{4}$$

where Λ is the number of fusions per molecule per second, B is the nuclear reaction constant obtained from measured cross sections for low-energy collisions between hydrogen nuclei, and $\Psi(R)$ is the normalized molecular wave function at the deuteron interaction distance, R. KN obtained the wave function for s-wave nuclear motion, for which the fusion rate is largest, by numerical integration of the Schrödinger equation using the diatomic molecular potential of Kolos and Wolniewicz [10]. They obtain for the fusion reaction rate

$$\log_{10} \Lambda = 6.5 + \log_{10} \frac{B}{a_0^3} + \log_{10} \left(\frac{\mu}{M_n}\right)^3 - 79\left(\frac{\mu}{M_n}\frac{m_0}{m}\right)^{1/2} \tag{5}$$

where μ is the reduced mass of the interacting nuclei, M_n is the nucleon mass, and a_0 is the Bohr radius. The ratio m_0 / m is the ratio of the free-electron mass to the effective mass of the binding electron when the D_2 molecule is in a crystal lattice. For deuteron-deuteron reactions, KN list $B = 1.5\times10^{-16}$ cm^3-s^{-1}. With $\mu \approx M_n$ for D_2, the reaction rate formula then reduces to

$$\log_{10} \Lambda = 15.5 - 79\ (m_0 / m)^{1/2} \tag{6}$$

In Section IV we use Eq. (6) for the analysis of the role of the effective mass of the D_2 binding electrons in the enhancement of fusion rates.

We adapt the KN formula, Eq. (6), to include the internuclear separation explicitly. Since the internuclear distance varies inversely with the mass of the binding particles, we replace m_0 / m by R/R_0 where R_0 is the equilibrium internuclear separation in the free D_2 molecule. Hence Eq. (6) becomes

$$\log_{10} \Lambda = 15.5 - 79(R / R_0)^{1/2}. \tag{7}$$

Setting either m_0 / m or $R/R_0 = 1$ leads to the fusion rate in a free D_2 molecule quoted above, i.e. $\Lambda \approx 10^{-64}$ s^{-1}. We use Eq. (7) to calculate the fusion rate resulting from the reduction of the value of R in a metal lattice. The equilibrium values of R calculated above and the resulting fusion rates are given in Table I below:

Table I. Deuteron Fusion Rates in Metal Lattices. Calculations of the deuteron fusion rate from Eq. (7) for deuterium in Pd and Ti lattices. The electronic charge distributions are assumed to be concentrated at points corresponding to $b = 0.7937$.

Lattice	R (Å)	$\log_{10} \Lambda$	Λ (s^{-1})
Pd	0.101	−13.7	$\approx 10^{-14}$
Ti	0.137	−17.3	$\approx 10^{-18}$

It is seen from Eq. (3) that the deuteron equilibrium separation is sensitive to the value of the parameter b, the assumed location of the electronic charge concentration. Table II lists the value of the equilibrium separation and of the corresponding fusion rate in Pd for various vales of b.

Table II. Variation of R and Λ with electron location. Calculations of equilibrium separation and fusion rate in Pd for various assumed locations of the electron charge.

b	R (Å)	$\log_{10} \Lambda$	Λ (s^{-1})
0.5	0.246	−30.0	$\approx 10^{-30}$
0.6	0.196	−25.2	$\approx 10^{-25}$
0.7	0.147	−19.7	$\approx 10^{-20}$
0.8	0.0982	−13.2	$\approx 10^{-13}$
0.9	0.0490	−4.81	$\approx 10^{-5}$

2.3 Discussion

The fusion rates reported by Jones et al. [1] for deuterium in Pd and Ti lattices range from 10^{-23} to 10^{-20} fusions/molecule/second. The rates computed here exceed these values by several orders of magnitude, indicating that the electrostatic mechanism for the reduction of the deuteron equilibrium separation can account for these experimental results. However, the energy releases reported by Fleischmann and Pons (FP) [2], if attributed to fusion, imply a fusion rate of $\approx 10^{-9}$ fusions/molecule/second for which the above mechanism cannot account; to obtain such a rate, the equilibrium separation would have to be reduced to 0.0713 Å. Below and in subsequent Sections we explore whether the electrostatic mechanism can be enhanced by other mechanisms to achieve reductions to this level.

Table II exhibits the dependence of R and Λ upon the assumed location of the electronic charge. Smaller values of b lead to larger values of R and hence to lower fusion rates, and vice-versa. There is a range of values of b which can account for the Jones data; for example, for $b = 0.7$, $\Lambda \approx 10^{-20}$ s^{-1}. However, to account for the FP data would require the position of the electrons to correspond to $b = 0.86$, a position too near the outer edge of the atom to seem physically feasible.

Calculations of the contributions by other metal atoms along the symmetry axis found their effects to be negligible. However, preliminary analysis indicates that other nearby Pd atom pairs not on the symmetry axis may contribute to further diminution of R. This requires a more detailed analysis of the geometric arrangement Also, we chose only one location and orientation of the D_2 molecule in the Pd lattice, this choice being based on a preliminary analysis of situations which would result in the largest effect. However, other locations and orientations of the D_2 molecule in the Pd lattice may also result in effects that cannot be dismissed and therefore should be investigated further.

Our analysis did not take into account the polarization of the metal atom charge by the electric field of the deuterium nuclei. Such polarization would have the effect of drawing the positions of the electron charge closer to the D_2 molecular axis, thus increasing the differential effect of the forces exerted by the metal nuclei and electrons on the D_2 nuclei and resulting in a further reduction of R. On the other hand, it could be argued that if the lattice became saturated with deuteron pairs, each lodged as described above, their combined effects on the electrons could cancel and there would be no polarization of the metal atoms.

The curve of potential energy vs. internuclear separation for the free D_2 molecule has a potential well minimum of -4.74 eV at the equilibrium separation. When the molecule is situated in the metal lattice there is an additional contribution to the electrostatic potential energy given by

$$V = \frac{4Z_1Z_2e^2}{R}\left[\frac{2}{\left(1+m^2\right)^{1/2}} - \frac{1}{\left(1+k_1^2\right)^{1/2}} - \frac{1}{\left(1+k_2^2\right)^{1/2}}\right]. \qquad (8)$$

For D_2 in Pd and using the nominal value for b, Eq. (8) yields a minimum of ≈ -3.2 keV at the equilibrium separation, i.e. three orders of magnitude deeper than the well for the free molecule. Thus the D_2 molecule in a metal lattice has a much higher binding energy than does the free molecule, a result consistent with the reduction of the internuclear separation.

3. THE ROLE OF LITHIUM

3.1 Introduction

We consider a role for Li because the cold fusion experiments were performed with strongly alkaline solutions containing 0.1 mole of lithium hydride (deuteride), so that ^{7}Li nuclei and deuterons are driven into the metal lattice. We examine here roles for Li nuclei as participants in nonfusion energy-releasing nuclear processes, as facilitators to enhance other mechanisms, and, in the form of lithium hydride, as a source of deuterons.

3.2 Nuclear Processes Involving Li Nuclei

Three energy-releasing reactions in which ^{7}Li nuclei can react with the protons in deuterons are radiative resonance capture of 0.37 MeV protons by ^{7}Li, capture of protons with energy > 1.63 MeV, and capture of a proton to produce ^{8}Be in the ground state with immediate decay into two α-particles. We dismiss the first two processes because the energy requirements on the protons are far greater than the available thermal energies of deuterons in a metal lattice. The third process is constrained by conservation of parity and of angular momentum. Since α-particles are Bose particles, they have zero spin and therefore their parity is even. Because of their zero spin, their total angular momentum consists entirely of orbital angular momentum and, since parity is determined by orbital angular momentum, the angular momentum must also be even. Therefore the only ^{8}Be state that can decay into two α-particles must have even parity and even angular momentum. This is a severe constraint and therefore the likelihood for this process is very small [11].

The possibility for Li nuclei of thermal energies to react with each other can be dismissed because of their high Coulomb barrier. Thus there is no process involving Li nuclei directly in a nuclear reaction that can account for the observed energy releases.

3.3 Enhancement of Electrostatic Mechanism

We examine whether suitably-placed Li nuclei can enhance the reduction of the deuteron separation calculated in the Section II. Consider two Li nuclei situated on the line with the deuterons as in Figure 1. The additional force exerted on either deuteron by the two Li nuclei is

$$\begin{aligned} F_{Li} &= Z_1 Z_3 e^2 \left[\frac{1}{(L+R/2)^2} - \frac{1}{(L-R/2)^2} \right] \\ &= -\frac{32 Z_1 Z_3 e^2 LR}{(4L^2 - R^2)^2} \end{aligned} \tag{9}$$

where Z_3 is the atomic number of Li, and L is the distance of the Li nuclei from the line joining the metal atoms. We add Eq. (9) to the terms in Eq. (1) to obtain the total force on each deuteron and again equate the force to zero to find the new equilibrium separation. The result depends on the distance of the Li nuclei from the deuterons. If we assume the Li nuclei are one angstrom from the deuterons, i.e., $L - R/2 = 1$ Å, we find the deuteron separation in Pd reduced to 0.1016 A. Thus, for this arrangement, the reduction in the deuteron separation has been enhanced by the presence of Li nuclei by only two parts per thousand. The resulting fusion rate is increased by ≈ 7%. If the Li nuclei were closer to the deuterons, the internuclear distance would be reduced further. However, with the assumed one Å distance, we are probably close to the limit of approach.

3.4 Electrostatic Interaction of LiD Molecule with Metal Atoms

We assume here that Li is present in the form of LiD molecules and we examine whether electrostatic forces exerted by the metal atoms can reduce the separation of the deuterons in these molecules. For this calculation, we replace the deuterons in Fig. 1 by LiD molecules. The total force exerted on each LiD molecule is given by Eq. (1) with the modification that $Z_1 e$ now represents the charge on the LiD nucleus: thus $Z_1 e = 4e$. For the equilibrium separation in Pd we obtain $R = 0.165$ Å and a corresponding fusion rate of $\approx 10^{-22}$ fusions/molecule/second. Since this is substantially smaller than the rate calculated for fusion of the D_2 molecule in Pd, we do not pursue this case further.

3.5 Conclusion

Apart from providing a small enhancement of the electrostatic mechanism for the reduction of the deuteron separation, Li nuclei play no significant role for fusion or for other nuclear energy-releasing processes in a metal lattice.

4. ENHANCEMENT OF FUSION BY INCREASED EFFECTIVE MASS

4.1 Dependence of the D_2 Bond Distance on Electron Mass

The internuclear separation in a molecule varies inversely with the mass of the binding particles. This accounts for the muon-induced fusion in the D_2 molecule when the binding electron is replaced by a muon [12]. This dependence of the molecular bond distance on the mass of the binding particle can be understood from the following rough argument. We set $E = h\nu$, where E is the molecular binding energy, h is Planck's constant and ν is the frequency of the electron exchange and we assume the exchange takes place in a time given by ν^{-1} and over a distance equal to the intermolecular separation, R. If the electron velocity is u, then $u = R\nu$. We introduce the electron mass, m, b[illegible]tting $E = mu^2/2$. Eliminating u and ν from these expressions yields $R = h/(mE)^{1/2}$. Since E [illegible]portional to m, we see that R is inversely proportional to the mass of the electron.

4.2 Electron Effective Mass in a Crystal Lattice

It is well known that an electron in a crystal lattice behaves as though it were more massive than a free electron. This enhanced mass, denoted m, is known as the effective mass and is a result of the periodic potential of the lattice. Values of m can be obtained experimentally from measurements of the de Haas-van Alphen effect or theoretically from the band structure [13]. The effective mass in Pd was determined by Vuillemin from de Haas-van Alphen measurements; for two orientations of the applied magnetic field, Vuillemin obtained $m = 2.1\ m_0$ and $m = 2.3\ m_0$, where m_0 is the free electron mass [14]. A theoretical estimate obtained from the density of states at the Fermi surface is $2.31\ m_0$ [15].

We assume that the electrons of a D_2 molecule in a Pd lattice experience the same electric fields as do the Pd electrons and therefore we can take the mass of the D_2 binding electrons to be the effective mass of the Pd electrons. Hence, the bond distance of D_2 in Pd should be reduced from that in the free molecule by a factor of m_0 / m.

4.3 Discussion

Using $m = 2.31\ m_0$, the D_2 equilibrium internuclear separation in Pd is reduced to 0.321 Å and the corresponding fusion rate, as computed from Eq. (6), is $\approx 10^{-37}\ s^{-1}$. This rate is many orders of magnitude below those reported experimentally. KN [5] pointed out that a mass enhancement of $5\ m_0$ is required to bring cold fusion rates into the range claimed by Jones et al. [1] and $10\ m_0$ is required for the FP [2] observations. We conclude that the reduction of the D_2 internuclear distance in Pd by the increased mass of the D_2 binding electrons is, by itself, not adequate to account for the claimed cold fusion rates. This, however, does not preclude the possibility that this mechanism may act in concert with some other mechanism to provide the necessary reduction in the D_2 internuclear distance.

5. PROCESSES INVOLVING METALLIC NUCLEUS

5.1 Introduction

In cold fusion experiments, the observed energy release is accompanied by detection of free neutrons and heating of the metal electrode. To account for these results, one must consider interactions involving the nucleus of the metal atom. We consider a two-step process in which, first, by the Oppenheimer-Phillips (OP) process, [16,17] the electrostatic field of the metallic nucleus splits a deuteron into its constituent proton and neutron particles, and then the nucleus absorbs either particle. Whichever particle is absorbed, energy will be released and the metal electrode will appear heated. Neutrons that are not absorbed are available to be detected as free neutrons.

In the usual nuclear reaction an incident nucleus enters a target nucleus to form a compound nucleus which then readjusts itself to a state of minimum energy with the emission of various particles. If however, the incident nucleus is a deuteron, the probability of capture of the entire deuteron is small compared to that of the splitting of the deuteron outside the target nucleus since, before the deuteron can enter the target (metal) nucleus, it must come within the break-up distance, defined below, and therefore must split before absorption can take place [18].

One can also see from general physical considerations that the splitting process, called stripping, is favored over capture because the deuteron binding energy is small compared to the kinetic energy required to penetrate the Coulomb potential barrier of the target nucleus. This is certainly so for nuclei with $Z > 25$, for then the proton in the deuteron is strongly repelled, even at fairly large distances from the target nucleus, whereas the neutron is not repelled [17]. If this repulsion of the proton leads to the splitting of the deuteron, the neutron is free to be absorbed by the target nucleus, while the proton carries off the excess energy and momentum. Owing to the electrostatic repulsion, the probability for proton absorption is much smaller than that for neutrons and therefore may be neglected.

5.2 Deuteron Stripping

The electrostatic potential energy of a deuteron at a distance r from a target (Pd) nucleus is $V(r) = Ze^2/r$, where Z is the Pd atomic number. Figure 2 shows schematically the potential energy of a deuteron with total energy E in the field of a Pd nucleus. The proton in the deuteron experiences an increasing electrostatic repulsion as the deuteron approaches the nucleus, thereby slowing the deuteron and bringing it to a halt at the classical turning point,

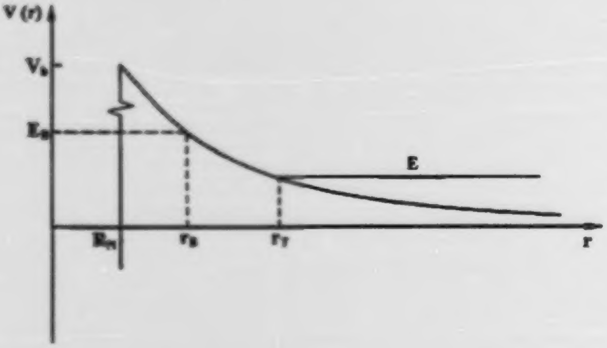

Figure 2. Potential energy function. $V(r)$ is the potential energy of a deuteron at distance r from the center of a metal nucleus. The nucleus has radius R_N and an incident deuteron approaches with total energy E. For $r < R_N$ the short-range nuclear force results in a deep potential well. For $r > R_N$, the Coulomb potential barrier of maximum height V_b dominates. E_B is the deuteron binding energy and r_B is the distance at which $V(r) = E_B$. We consider stripping to occur if the deuteron approaches to within r_B. Deuterons with energy $E < E_B$ approach up to the classical turning point, r_T.

r_T, i.e., the distance for which the total energy equals the potential energy. We assume that the deuteron will split if its total energy exceeds its binding energy, i.e., $E > E_B$, for at such kinetic energies the deuteron will be brought sufficiently close to the Pd nucleus for the proton to be torn loose. We find the threshold for break-up by equating the potential energy to E_B from which we obtain $r = r_B \equiv Ze^2/E_B$. For Pd, $E_B = 2.23$ MeV and $Z = 46$, leading to $r_B = 30$ fermi, which is consistent with the value obtained from Bethe's quantum mechanical analysis [17]. At this and closer separations, the electrostatic repulsion is sufficient to tear the proton loose.

We assume that most of the deuterons in the Pd lattice have thermal energies, kT, where k is the Boltzmann constant and T is the temperature in kelvins (K). For $T = 300$ K, we obtain $kT \approx 0.026$ eV, i.e., eight orders of magnitude less than the deuteron binding energy. The corresponding classical turning point is then eight orders of magnitude larger than r_B and therefore we do not expect the stripping of deuterons by Pd nuclei to be of significance. The situation is only slightly improved if we consider Pd at its melting point, ≈ 1800 K, for which $kT \approx 0.16$ eV. However, since the deuteron energies are distributed according to the Maxwell-Boltzmann law, we should obtain an estimate for the fraction with energy $E > E_B$. Also, if the deuteron energy is not large enough to bring it to within r_B, i.e. if $E < E_B$, it can still tunnel through the barrier to reach this distance. The probability for this process depends on the magnitude of the deuteron wave function within the barrier. We calculate each of these cases below.

5.3 Deuterons with $E > E_B$

We use classical statistical mechanics to determine the number of deuterons that have the necessary kinetic energy to approach the Pd nucleus to within r_B. The fractional number density of deuterons with energy $E > E_B$ is given by the Maxwell-Boltzmann formula

$$2\pi^{-1/2}(kT)^{-3/2}\int_{E_B}^{V_b} E^{1/2}\exp(-E/kT)\,dE,$$

where the infinite upper limit has been approximated by the potential barrier height, V_b. This is given by $V_b = Ze^2/R_N$, where R_N is the radius of the target nucleus. For a nucleus with mass number A, $R_N \approx 1.2 \times A^{1/3}$ fermi. Thus for ^{108}Pd, $R_N = 5.7$ fermi and $V_b \approx 1160$ MeV. For $T = 1800$ K, the Maxwell-Boltzmann integral then becomes

$$\int_{E_B}^{V_b} E^{1/2}\exp(-6.4E)\,dE,$$

where energies are expressed in eV. A numerical integration yields essentially zero. Thus we do not have an appreciable number of deuterons with energy $E > E_B$ and hence the number of stripped deuterons ≈ 0.

5.4 Deuterons with $E < E_B$

A deuteron whose kinetic energy is too low to bring it to within r_B can still tunnel through the barrier to reach this distance. We calculate here the probability of a deuteron penetrating the Pd potential barrier to the break-up distance, r_B. The quantum mechanical probability per collision [19] for a nucleus of charge Z_1e and energy E to penetrate the potential barrier of another nucleus of charge Z_2e is $W = \exp(-2G)$, where G is the Gamow exponent which, for

$E << V_b$, is given by

$$G = \frac{\pi Z_1 Z_2 e^2}{\hbar} \left(\frac{\mu}{2E}\right)^{1/2}, \tag{10}$$

where μ is the reduced mass of the interacting particles. The quantity W, called the transparency of the potential barrier, represents the probability of a particle with energy E to tunnel through the barrier to reach the surface of the target nucleus, i.e. to a distance R_N. Since the classical turning point for most of the incident deuterons is several orders of magnitude larger than r_B, we can approximate r_B by R_N and therefore use the above formula to calculate the probability of tunneling to distance r_B.

For a deuteron incident upon a Pd nucleus, the reduced mass ≈ mass of the deuteron ≈ 3.3 × 10^{-24} gm, so the transparency becomes $W \approx \exp(-5 \times 107\, E^{-1/2})$, where E is in eV. Since W increases with E, we first consider the most favorable case, $E = E_B$, for which we obtain $W \approx \exp(-10^4) \approx 0$. As shown above, the number of deuterons at this energy is vanishingly small. A more typical case is a deuteron with thermal energy corresponding to the Pd melting point for which $E \approx 0.16$ eV. Substituting this value yields $W \approx \exp(-10^8) \approx 0$. Therefore, deuterons which do not possess kinetic energy sufficient to reach the break-up distance while still outside the Pd nucleus have negligible probability of reaching this distance by tunneling.

5.5 Discussion

We conclude that the stripping of deuterons by Pd nuclei contributes very little, if anything at all, to the energy release observed in cold fusion experiments. However, these broad analyses must be modified in certain details to take into account the following features of the dynamical process involved:

If the kinetic energy of the deuteron is larger than the critical break-up potential energy, the break-up will occur with the certain absorption of the neutron and emission of the proton. But if the deuteron kinetic energy is smaller than the critical potential energy, stripping will occur only if some (partial or total) penetration of the nuclear potential barrier by the entire deuteron occurs. However, the amplitude of the deuteron wave function within the potential barrier falls off exponentially with the inverse half-power of the deuteron kinetic energy and therefore stripping may not occur even if partial penetration is effected. Only if the amplitude of the deuteron wave function is sufficiently large to give an appreciable probability for finding the deuteron at the nuclear surface will the probability for the stripping reaction be significant. This will occur only at deuteron energies that are substantially higher than the thermal energies employed in our calculation. Bethe has calculated this wave function using the Gamow theory.

The stripping analysis has been carried out for a free deuteron, but the deuterons in the palladium lattice may be bound in molecules. This may be neglected, however, since the molecular binding energy of the D_2 molecule, which is of the order of a few eV, is negligible compared with the binding energy of the deuteron.

6. SUMMARY AND CONCLUSIONS

The electrostatic effect of one pair of Pd or Ti atoms on a suitably positioned and oriented D_2 molecule reduces the internuclear separation and increases the deuteron fusion rate. For a wide range of assumed average positions of the metal atoms' electrons, the increased fusion rates are adequate to account for the observations of Jones et al. [1] but, by itself, this mechanism cannot account for the fusion rate implied by the data of Fleischmann and Pons [2]. The electrostatic interaction results in a potential well in which the two deuterium atoms in the D_2 molecule are bound is much deeper than the binding potential well of the free molecule and this increase in the D_2 binding energy is in qualitative agreement with the reduction of the deuteron separation. Apart from providing a small enhancement of the electrostatic mechanism for the reduction of the deuteron separation, Li nuclei play no significant role for fusion or for other nuclear energy-releasing processes in a metal lattice. The reduction of the D_2 internuclear distance by the effective mass of the D_2 electrons in a metal lattice is, by itself, not adequate to account for the claimed cold fusion rates. This, however, does not preclude the possibility that this mechanism may act in concert with some other mechanism to provide the necessary reduction in the D_2 internuclear distance. The effects of reactions involving the Pd or Ti nucleus directly and the stripping of deuterons are negligible.

The success of the electrostatic mechanism to account for some of the experimental observations suggests that further study of this mechanism is merited. In particular, the following avenues of analysis may prove profitable:

- The electrostatic interaction of the D_2 molecule with additional metal atom pairs;
- Consideration of other locations and orientations of the D_2 molecule in the lattice;
- The effects of metal-atom polarization, lattice vibrations, and vibrational states of the D_2 molecule.

REFERENCES

* Supported in part by Department of Defense contract no. N60921-90-C-0187.

1. S.E. Jones et al. Nature **338**, 737 (1989).
2. M. Fleischmann and S. Pons. Journal of Electroanalytical Chemistry **261**, 301 (1989).
3. E. Storms. Technology Review 20, May/June 1994.
4. H.S. Picker. Nukleonika **25**, 1491 (1980).
5. S.E. Koonin and M. Nauenberg. Nature **339**, 690 (1989).
6. C.A. Hampel, ed. The Encyclopedia of the Chemical Elements, (Reinhold, New York, 1968).
7. J.D. Jackson. Physical Review **106**, 330 (1957).
8. Ya. B. Zel'dovich and S.S. Gershtein. Soviet Physics Uspekhi **3**, 593 (1961).
9. C. DeW. Van Siclen and S.E. Jones. Journal of Physics **G 12**, 213 (1986).
10. W. Kolos and L. Wolniewicz. Journal of Chemical Physics **49**, 404 (1968).
11. J.M. Blatt and V.F. Weisskopf. Theoretical Nuclear Physics (John Wiley & Sons, New York, 1952), pp. 499-501.
12. S.E. Jones. Nature **321**, 127 (1986).
13. A.P. Cracknell and K.C. Wong. The Fermi Surface (Clarendon, Oxford, 1973).
14. J.J. Vuillemin. Physical Review **144**, 396 (1966).
15. V.L Moruzzi. J.F. Janak and A.R. Williams. Calculated Electronic Properties of Metals (Pergamon, New York, 1978), p. 144.
16. J.R. Oppenheimer and M. Phillips. Physical Review **48**, 500 (1935).
17. H.A. Bethe. Physical Review **53**, 39 (1938).
18. Ref. 11, pp. 504-511.
19. S. Chandrasekhar. An Introduction to the Study of Stellar Structure (Dover, New York, 1967) p. 457.

NEW PHYSICS FOR FUSION ENERGY

J. Reece Roth

UTK Plasma Sciences Laboratory
Department of Electrical Engineering
University of Tennessee
Knoxville, Tennessee 37996-2100, U.S.A.

ABSTRACT

As the field of magnetic fusion energy has become more narrowly focused on the Tokamak, and inertial fusion on weapons-related concepts, the original goal of socially responsible, inexpensive and inexhaustible energy for all nations appears to have receded further and further into the future, if it has not been lost sight of altogether. Rather than discuss approaches of long standing, I hope to make a contribution to the debate on the future of fusion energy by calling attention to little-known (in the fusion community) physical processes or plasma-related phenomena which may give rise to fusion reactor concepts different in kind from those now being considered, or concepts with features which cannot now be envisioned with currently-understood fusion physics. This paper will consider five principal "new" inputs of possible fusion relevance, including: 1) magnetoelectric toroidal confinement; 2) the Bohr-van Leeuwen Theorem; 3) Buckingham's Pi Theorem; 4) ball lightning; and 5) atmospheric glow discharges. It is hoped that awareness of these inputs will contribute to the revitalization of fusion research and preparations for the post-Tokamak era.

1. INTRODUCTION

During the last two of nearly five decades of fusion research, the field of magnetic fusion energy has become more and more narrowly focused on the Tokamak, and inertial fusion on weapons-related concepts. The original goal which attracted many of those currently working in the field, of socially responsible, inexpensive, and inexhaustible energy for all nations, appears to have been lost sight of altogether in the programmatic imperatives of government supported fusion research.

The status of magnetic fusion research is identified in the minds of most members of the technical community with that of Tokamak experiments, which have recently been reviewed by Wolf (1996). The current goal of most national magnetic fusion programs is the International Thermonuclear Experimental Reactor (ITER) a steady state, DT Tokamak fusion reactor which is hoped to be capable of scientific break-even, of generating at least 500 mega-

Current Trends in International Fusion Research — Proceedings of the Second Symposium
Edited by E. Panarella. NRC Research Press, National Research Council of Canada, Ottawa, ON K1A 0R6, Canada. 1999.

watts of thermonuclear power, and possibly of operating in the "ignited" regime, in which the cold incoming fuel will be heated to the operating temperature by charged particle energy deposited in the plasma by fusion reactions. A fundamental controversy has recently arisen, however, whether known scaling laws for the containment time in existing Tokamak fusion reactors can be extrapolated to the size and scale of the ITER reactor. The ITER reactor is expected to cost somewhere between 5 and 10 billion dollars to construct, and will likely preempt all available sources of governmental support for magnetic fusion energy. This has caused several senior members of the fusion community to question whether ITER should proceed (Glanz, 1996).

At the basis of this controversy about the future of the ITER reactor are the phenomenological scaling laws for the energy containment time in Tokamak reactors, which have been obtained by empirical collation of a wide variety of data from existing Tokamak experiments (Messiaen, 1996). This phenomenological approach is not restricted to the Tokamak concept, but has been applied also to other toroidal magnetic fusion concepts such as the Stellarator/Torsatron (Stroth et al., 1995). Advocates of this approach as a basis for building a five to ten billion dollar magnetic fusion reactor are in a weak logical position, in that the phenomenological correlations described by Messiaen and Stroth et al. are not predicted or supported by any physical theory based on first principles. Indeed, the physical processes primarily responsible for radial transport of particles and energy have not yet been identified after nearly five decades of toroidal magnetic confinement research, and at least thirty-five years of research on Tokamaks. At the same time that the Tokamak concept has grown to dominate magnetic fusion research, and weapons-related concepts to dominate inertial fusion, many alternative magnetic and inertial fusion concepts have been put forward and progressed to a point which has been, in most cases, limited only by the availability of additional funding.

At this time, and at this Symposium, it is appropriate to take stock of the direction in which fusion energy is headed, and to consider alternate conceptual approaches to the magnetic and inertial confinement of fusion plasmas based upon the body of plasma physical knowledge developed by the fusion community over the past five decades. Even within this body of knowledge, there are many alternate concepts, the merits of which have never been fully exploited as the result of historical accident or the unavailability of funding. It is appropriate at this Symposium to revisit these concepts in light of the serious difficulties in which the Tokamak program and the proposed ITER reactor now find themselves.

In this paper, however, I hope to make a contribution of a different kind, by calling the attention of my fusion colleagues to little known (in the fusion community), or little utilized physical processes or plasma related phenomena, which may be capable of contributing to fusion reactor concepts different in kind from those now being considered, or fusion reactors with features which cannot now be envisioned under the constraints of current fusion physics. I have selected five concepts for discussion as potentially new physics for fusion energy, as follows.

2. MAGNETOELECTRIC TOROIDAL CONFINEMENT

In conventional approaches to magnetic fusion, gross plasma confinement is provided by strong, static magnetic fields which do no work on the plasma because the velocity vectors of individual charged particles are at right angles to the magnetic field. In this situation, the second law of thermodynamics assures that the plasma will expand radially outward toward the walls, thus increasing its entropy. This expansion may be driven by classical diffusion, which is the slowest rate, in principle, at which a magnetized plasma can diffuse toward the walls. The plasma can be transported outward at higher rates by other processes, such as the fluctuations and turbulence associated with MHD or electrostatic instabilities. In Tokamak plasmas, for example, radial transport rates are several orders of magnitude greater than those predicted by classical diffusion. In order to counter this radial diffusion of the plasma across a static magnetic field, one must do work on the plasma, to prevent the increase in entropy associated with plasma expansion.

Magnetoelectric toroidal confinement (Roth, 1973, 1983; Roth et al. 1977) is accomplished by using a strong toroidal magnetic field to provide gross plasma confinement, while biasing the plasma to high potentials in a way which creates a strong (kV/cm) electric field along the minor radius. This radial electric field does work on the plasma and provides both E/B drift heating of the ions (Roth, 1973) and radially inward transport of ions against the density gradient (Roth et al. 1977, 1983).

A minor cross section of a magnetoelectrically contained toroidal plasma is shown in Fig. 1. The toroidal plasma is biased to high (preferably) negative potentials by an electrode in contact with the outer boundary of the plasma at one or more locations on its circumference. Over the entire surface of the toroidal plasma, except that part immediately under the biasing electrodes, the electric field will point radially inward, creating a toroidal electrostatic potential well for ions and "pushing" ions radially inward against the density gradient. This radial electric field is preferably on the order of kilovolts per centimeter, and at right angles to a toroidal magnetic induction on the order of several tesla pointing into the plane of the diagram in Fig. 1. The crossed electric and magnetic fields lead to a azimuthal drift velocity given by

$$v_o = \frac{\boldsymbol{E}_r \times \boldsymbol{B}}{B^2} = \frac{E}{B} \quad \text{meters/sec.} \tag{1}$$

The radial electric field heats the ions and electrons to kinetic energies given by

$$\mathcal{E} = \frac{1}{2} m\, v_o^2 = \frac{m}{2} \frac{E^2}{B^2} \quad \text{Joules.} \tag{2}$$

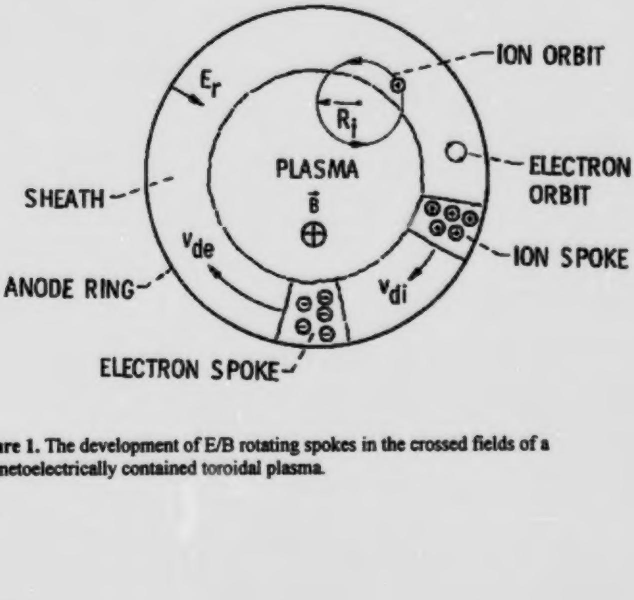

Figure 1. The development of E/B rotating spokes in the crossed fields of a magnetoelectrically contained toroidal plasma.

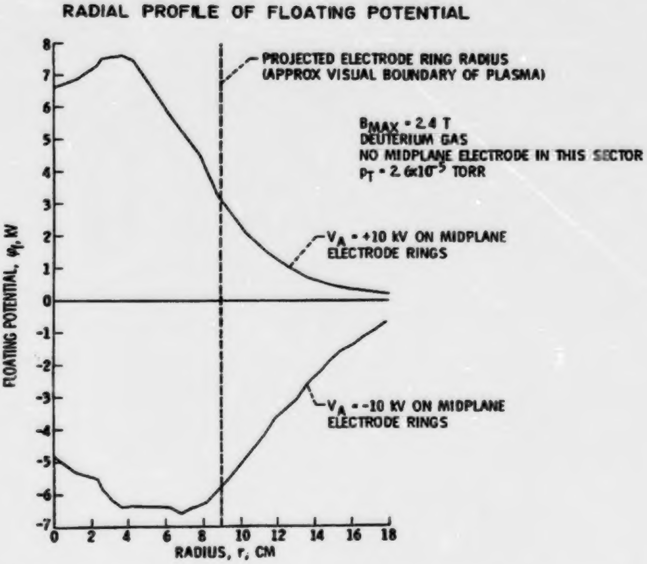

Figure 2. Radial profile of floating potential, with positive and negative biasing polarity, of a magnetoelectrically contained toroidal plasma. Biasing electrode rings were maintained at potientials of + or - 10 keV for the upper and lower profiles, respectively. Data nearer than 4 centimeters to the plasma minor axis may have been affected by the probe pertubation.

Equation 2 is basic to the magnetoelectric heating of plasmas. It has the significant property, for fusion applications, that the energy deposited in the individual particles is proportional to the mass: i.e. the energy from the DC power supply which biases the plasma goes preferentially into the heavy ions, rather than into the electron population. This is just where one would wish to have the energy deposited in heating a plasma of fusion interest.

A characteristic example of radial potential profiles of a positively (top half of the graph) and negatively biased (lower half of the graph) magnetoelectrically contained toroidal plasma is shown in Fig. 2. The electric fields at the boundary of the plasma approach values of several kilovolts per centimeter, which lead to deuterium ion energies between 100 eV and one keV in this experiment.

Once the ions achieve the drift velocities described by Equation 1 and acquire the energies of Equation 2, the high radial electric fields drive strong electrostatic turbulence, an example of which is shown in Fig. 3 (Roth, 1983). This figure shows the spectrum of electrostatic potential fluctuations between a frequency of 100 kHz and one MHz. Ions undergoing E/B drift are subject to the diocotron instability, which causes them to bunch up into azimuthally rotating spokes with the E/B drift velocity shown in equation 1, but reduced by the fraction of time, indicated in Fig. 1, which these ions spend in the strong electric field of the plasma sheath. Fig. 3 illustrates an example in which the diocotron spoke frequency was about 300 kilohertz. Above and below this energy input frequency, the spectrum of electrostatic potential fluctuations has a characteristic power law form with the same slope. Below the energy input frequency, there is a cascade of energy from the large scale motions of the rotating spoke to

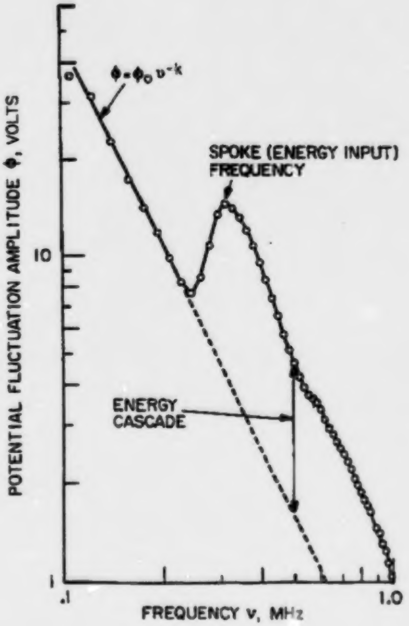

Figure 3. Autopower spectrum of electrostatic potential fluctions in a magentoelectrically heated plasma. The spoke (energy input) frequency produces an energy cascade responsible for maxwelling the E/B drift energy of the ions.

smaller and smaller scale vortices until the input energy at 300 kHz is finally dissipated as thermal motions of the plasma ions.

The result of magnetoelectric heating is typically ions which are both energetic and maxwellianized by the strong electrostatic turbulence. An example of a charge exchange neutral detector measurement of the ion energy distribution function in a magnetoelectrically heated E/B helium plasma, taken from Roth (1983), is shown in Fig. 4. The open circles are measured data and the open triangles are the best fitting maxwellian with a helium ion kinetic temperature of 2500 eV. The energy distribution function of these ions was maxwellian out to energies of at least 22 keV as a result of the electrostatic turbulence.

The energy fed into E/B drift of the plasma not only induces strong electrostatic turbulence which thermalizes the directed E/B motion, but it also allows the ions to undergo fluctuation-induced transport radially inward against the density gradient (Roth, et al., 1977; Roth, 1986). Two examples of magnetoelectrically induced radial fluctuation-induced transport have been taken from Roth, et al. (1977) and are illustrated in Fig. 5. Figure 5a was taken in a magnetoelectrically contained toroidal plasma which was biased to high positive potentials. The upper graph in Fig. 5a is the transport spectrum, which shows the amount of outward fluctuation induced transport occurring at frequencies between 0 and 500 kHz. In this case, nearly all of the fluctuation induced transport was confined to three peaks below 100 kHz. The bottom graph on Fig. 5a shows the cumulative transport spectrum as a function of frequency. This gives the total outward flux of ions in units of 10^{16} ions per square meter per second. Figure 5b is a case in which a magnetoelectrically contained plasma was biased to high negative potentials. In this case, the transport was in the opposite direction, i.e. radially inward. The top graph in Fig. 5b shows the transport spectrum as a function of frequency,

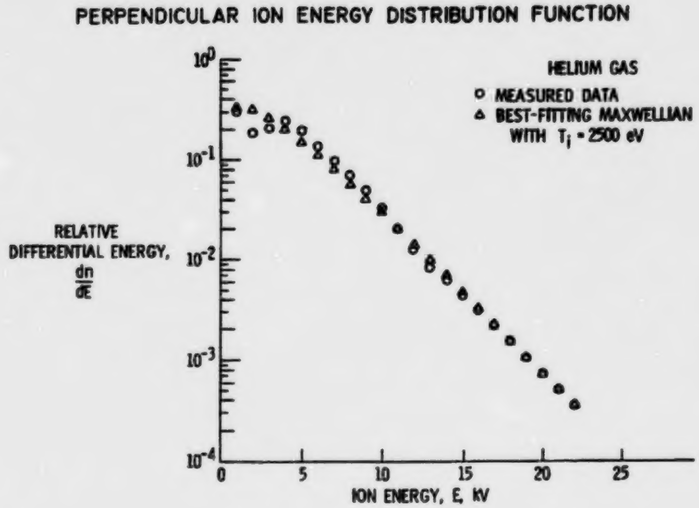

Figure 4. A characteristic example of the ion energy distribution function of a magnetoelectrically heated E/B plasma. Open circles are measured data, open triangles are the best-fitting maxwellian. Data shown were taken in helium gas and produced a helium ion kinetic temperature of 2500 eV. Energetic helium ions were detected with a charge exchange neutral energy analyzer out to ion energies of 22 keV.

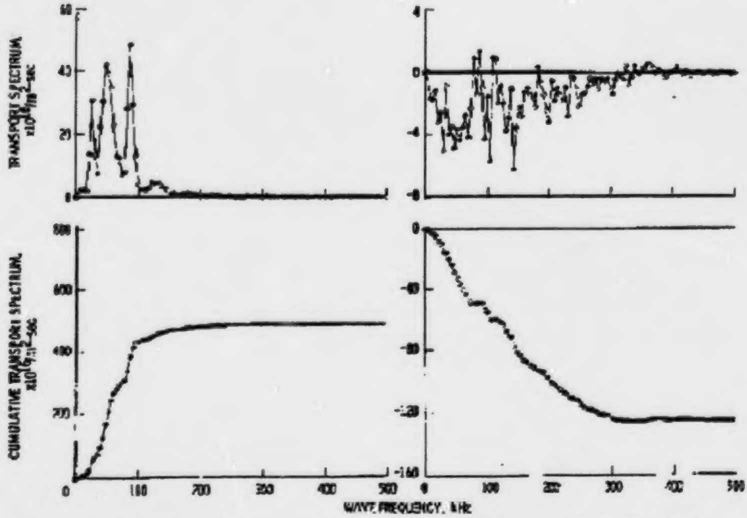

a) NEGATIVE ELECTRODE POLARITY I_A = 0.75 A.

b) POSITIVE ELECTRODE POLARITY I_A = 0.75 A.

Figure 5. Transport spectra at the top of the figure and cumulative transport spectra of the bottom for a) negative and b) positive electrode polarity, illustrating reversal of the direction of radial ion transport with a change of the polarity of the biasing direction of the minor radial electric field.

which was radially inward over the entire frequency range from 0 to more than 300 kHz in this case. The cumulative transport spectrum below this in Fig. 5b shows the total flux on the ordinate up to the frequency shown on the abscissa The inward flux of ions in this case reaches an asymptotic value at about 300 kHz.

Magnetoelectric toroidal confinement therefore has the demonstrated capability of doing work on a toroidal plasma in such a way that the ions are preferentially heated rather than the electrons, while at the same time doing work on the plasma ions in such a way that they are infused radially inward against the density gradient. This ability to control the radial transport is not available with plasmas contained solely by a static magnetic field, and is an important potential advantage of magnetoelectric toroidal confinement.

3. THE BOHR-VAN LEEUWEN THEOREM

This theorem from solid state physics (van Vleck, 1937) can be applied to the interior, but not the edges, of magnetically confined plasmas (Alfven and Falthammar, 1963; Roth, 1986). This theorem states that a plasma in local classical kinetic equilibrium will evolve to a state in which its diamagnetism is zero, a theorem which was originally developed by Neils Bohr to explain why metals are not diamagnetic when inserted into a static magnetic field.

As applied to plasmas, one consequence of the Bohr-van Leeuwen theorem is that if a magnetically confined plasma is confined for a sufficiently long period of time to reach a stable equilibrium, then the diamagnetic current density $\mathbf{J}_\perp$ in the plasma interior will approach zero. That is,

$$J_\perp = \frac{nmv_\perp^2}{2\gamma B^2} B \times \nabla \ell n \left[\frac{nmv_\perp^2}{2\, B^\delta} \right] = 0, \tag{3}$$

which is derived in Roth (1986), where the parameter δ is the *isotropy* index and is given by

$$\delta \equiv 1 - \frac{2\, v_\parallel^2}{v_\perp^2}. \tag{4}$$

This parameter is equal to zero for an isotropic plasma velocity distribution, is negative for a beam-like velocity distribution, and is positive for a mirror-like distribution of trapped ions containing a loss cone. The parameter γ is given by

$$\gamma \equiv 1 + \delta \left[\frac{\mu_o n m v_\perp^2}{2\, B^2} \right]. \tag{5}$$

A sufficient condition for equation 3 to be zero is that the term in square brackets be a constant, independent of position,

$$\frac{nm v_\perp^2}{2 B^\delta} = \text{constant}. \tag{6}$$

In most plasmas to which the Bohr-van Leeuwen Theorem applies, the velocity distribution will be isotropic, rendering Equation 6 independent of magnetic field. In any case, the radial profile of magnetic induction is slowly varying in most toroidal magnetic containment systems. Equation 3 implies that as plasmas deplete their reservoirs of free energy, their energy density gradient perpendicular to the magnetic field becomes smaller, and the radial profile of kinetic pressure becomes flatter. Equation 6 cannot be satisfied all the way to the wall, since infinite temperatures would be required to compensate for the decrease of number density at the plasma edge. In local classical kinetic equilibrium, the individual radial profiles of plasma number density and kinetic temperature can have any shape, provided that their product is constant along the radius. As Tokamak and Stellarator plasmas become more stable and confined for longer periods, the constant kinetic pressure profile predicted by Equation 6 should become more widely observed. Another implication of Equation 6 is that the heating and confinement mechanisms of a successful magnetic containment configuration should be designed to produce a constant kinetic pressure profile across as much of the plasma diameter as possible.

A second consequence of the Bohr-van Leeuwen Theorem is that the interior of a stable, confined plasma should satisfy the magnetically force-free condition

$$\mathcal{F}_m = \mathcal{J} \times \mathcal{B} = \mathcal{J}_\perp \times \mathcal{B} = 0 \qquad (7)$$

This theorem sheds light on the futility of generating plasmas with net diamagnetism or volumetric body forces in their interior, and it suggests that the path of least resistance to a macroscopically stable plasma is to arrange for its kinetic pressure (but not necessarily its density or kinetic temperature profile) to be constant across the plasma diameter.

4. BUCKINGHAM'S Pi THEOREM

Buckingham's Pi Theorem has been used for nearly a century to correlate experimental data for which the physics is not well understood, which is nonlinear, or which does not yield simple analytical expressions for comparison with experiment. This theorem has been successfully used in aerodynamics, hydrodynamics, heat transfer, the strength of materials, electrical discharge physics, and other fields (Samaras, 1971). Buckingham's Pi Theorem can also be applied to magnetically contained plasmas to predict a confinement time scaling law (Roth, 1986 pp. 91 to 94).

In the formalism of Buckingham's Pi Theorem, a dependent variable (such as the energy or particle confinement time) is correlated in terms of a multiplicative product (hence the operator π) of a canonical number of independent power-law variables. Each of these variables has an exponent selected on the basis of rules designed to assure dimensional consistency in terms of the fundamental dimensions of mass, M; length, L; time, T; and electrical charge, Q. All variables are either in appropriate dimensionless form (such as the Reynolds number in aerodynamics, for example) or, if dimensional, the numerical coefficient of the correlation must be dimensionless. A dimensional coefficient for a correlation or phenomenological expression is inconsistent with a formalism based on Buckingham's Pi Theorem, and implies at least one "hidden variable" in the application. Buckingham's Pi Theorem requires dimensional consistency of both sides of an equation describing a correlation of interest, and it places constraints between the number of independent variables of the problem, and the fundamental dimensions involved.

Although the phenomenological scaling relationship for the confinement time of Tokamaks discussed by Messiaen (1996) and for Stellarators/Torsatrons discussed by Stroth, et al. (1995) have a general form suitable for application of Buckingham's Pi Theorem, this formalism has not been applied by the fusion community. The available phenomenological scaling laws discussed by Messiaen and Stroth et al. have, of necessity, been empirically derived from a large experimental database, because the physical processes responsible for toroidal radial transport have not yet been identified. It is not encouraging to note that the scaling laws for toroidal magnetic confinement not only are inconsistent with Buckingham's

Pi Theorem, but also that they have progressively diverged over the history of magnetic fusion research away from the dimensionless numerical coefficient consistent with Buckingham's Pi Theorem. Examples of this worsening situation in toroidal transport theory are taken from Roth (1986), Messiaen, (1996), and Stroth, et al., (1995).

The earliest phenomenological scaling law for toroidal confinement was Bohm scaling, which was applied to early (prior to 1965) Stellarators. The Bohm confinement law is given by

$$\tau_b = C_1 \frac{eBa^2}{kT_e} \text{ sec}, \tag{8}$$

where the independent variables on the right include the magnetic induction and the kinetic temperature of the plasma, the dimensions of which are

$$|B| = \frac{M}{QT}; \; |kT_e| = \frac{L^2 M}{T^2}. \tag{9a,b}$$

The vertical bars indicate that the entity on the right-hand side is the fundamental dimensions of the SI quantity involved. Substituting Equations 9a, b into Equation 8, and recognizing that the Bohm confinement time has the dimensions of time (T), Equation 8 becomes

$$T = C_1 Q \frac{M}{QT} \; \frac{L^2 T^2}{L^2 M}, \tag{10}$$

from which it follows that

$$|C| - \text{Dimensionless}. \tag{11}$$

Expression 11 indicates that the constant C_1 appearing in the Bohm confinement scaling law is dimensionless, as it should be. This early scaling law is the only one used in the field of controlled fusion which is consistent with Buckingham's Pi Theorem.

Another early confinement time scaling law which was applied to ohmically heated Tokamaks in the period around 1970 was *Mirnov scaling*, which had the form

$$\tau_2 = C_2 A_i^{0.5} I_t \text{ sec}. \tag{12}$$

Substituting for the dimensions of ion mass, current, and containment time, one obtains the dimensions of the coefficient C_2, given by

$$|C_2| = \frac{T^2}{QM^{0.5}}. \tag{13}$$

The Mirnov coefficient does not obey Buckingham's Pi Theorem. The fundamental dimensions which it contains strongly imply that one or more hidden variables remain imbedded in the constant C_2.

During the period from approximately 1975 to 1980, Alcator scaling of ohmically heated Tokamaks was described by the phenomenological expression

$$\tau_a = C_3 a^2 \bar{n}_e q^{0.5} \text{ sec,} \tag{14}$$

which contains the dimensionless safety factor q, the electron number density, and the minor radius of the Tokamak plasma. Substituting the fundamental dimensions of the variables on both sides of Equation 14, one obtains the dimensions of the Alcator scaling constant C_3,

$$|C_3| = LT. \tag{15}$$

Again, Alcator scaling does not satisfy Buckingham's Pi Theorem, and the dimensions of its coefficient imply at least one hidden variable in the correlation.

During the period from approximately 1979 to 1985, the confinement time scaling of ohmically heated Tokamaks was described by the *neo-Alcator* scaling law, given by

$$\tau_{na} = C_4 \bar{n}_e q^{0.5} a^{1.05} R^{2.04} \text{ sec.} \tag{16}$$

which contains the dimensionless safety factor q, the average electron number density, and the major and minor toroidal radii. When one substitutes the fundamental dimensions on both sides of this equation, one obtains the dimensions of the neo-Alcator scaling constant C_4,

$$|C_4| = \frac{T}{L^{0.09}} \tag{17}$$

Here again, the constant C_4 is not dimensionless and neo-Alcator scaling is inconsistent with the requirements of Buckingham's Pi Theorem.

When neutral beam and/or RF heating significantly exceed the power input from ohmic heating in Tokamaks, the *Goldston L-mode Tokamak scaling* (circa 1983) was found to hold. One version of the Goldston L-mode Tokamak scaling law is given by

$$\tau_{lm} = C_5 A_i^{0.5} \mathrm{I} \mathrm{P}_{tot}^{-0.5} R^{1.75} a^{-0.37} \kappa^{0.5} \text{ sec,} \tag{18}$$

where the independent variables include the dimensionless cross-sectional elongation of the plasma κ, the major and minor toroidal radii, the input power, the toroidal current I, and the ion mass. Substituting fundamental dimensions on both sides of Equation 18 yields the dimensions of the Goldston L-mode scaling coefficient C_5,

$$|C_5| = \frac{T^{3.5}}{MQL^{2.38}} \tag{19}$$

The Goldston scaling constant C_5 satisfies Buckingham's Pi Theorem less well than either of the predecessor Alcator scaling laws.

Finally, as Messiaen (1996) discussed, the ITER H90-P Tokamak scaling law, (one of the recent correlations used in designing the ITER facility), has the form

$$\tau_{iter} = C_6 I^{0.87} R^{1.82} a^{0.12} B^{0.15} n_e^{-0.09} P_{tot}^{-0.50} \kappa^{0.30} A_i^{0.5} \text{ sec,} \tag{20}$$

where the independent variables on the right side of the equation include the toroidal current I, the major and minor toroidal radii, the magnetic induction B, the electron number density, the total heating power input, the dimensionless vertical elongation κ, and the ion mass in the plasma. Substituting the fundamental dimensions of the parameters on both sides of the equation yields the dimensions of the ITER correlation parameter C$_6$,

$$|C_6| = \frac{T^{0.52}}{Q^{0.72} L^{0.67} M^{0.15}}. \tag{21}$$

This correlation coefficient is involves charge, mass, length, and time, but the exponents of each of these variables, while a physically irrational (that is they are not simple whole numbers or ratios of whole numbers) is closer to the requirement of Buckingham's Pi Theorem than the previous Goldston L-mode Tokamak scaling of Equation 18.

Confinement time correlations inconsistent with Buckingham's Pi theorem are not confined to Tokamak research. The energy confinement scaling derived from the international Stellarator database has been discussed by Stroth, et al., and is

$$\tau_{st} = C_7 a^{2.21} R^{0.65} P_{\text{tot}}^{-0.59} \overline{n}_e^{0.51} B_t^{0.83} \ell^{0.4}. \tag{22}$$

which involves the major and minor toroidal radii, the plasma input power, the average electron number density, the toroidal magnetic induction, and the dimensionless rotational transform angle,ℓ. If the respective fundamental dimensions are substituted in both sides of Equation 22, the correlation coefficient for the international Stellarator database has the dimensions.

$$|C_7| = \frac{T^{0.06} Q^{0.83}}{L^{3.80} M^{0.24}}, \tag{23}$$

a situation not much improved from that of Tokamak research.

The dimensions of the scaling law coefficients, all of which should be dimensionless according to the requirements of Buckingham's Pi theorem, are summarized in Table 1 for the scaling laws considered above. It is clear from Table I that the scaling laws for the Tokamak energy containment time have progressively diverged over the history of magnetic fusion research from the dimensionless numerical coefficient consistent with Buckingham's Pi Theorem. These examples indicate that over the history of toroidal magnetic fusion research, workers in the field have not only lost sight of the requirements of Buckingham's Pi Theorem, but also they have allowed a situation to develop which has (in architectural terms) gone from the classical, to the baroque, to the rococo. The dimensions of the numerical coefficients of

Table 1. Dimensions of scaling law coefficients for toroidal plasma containment times.

Equation	Scaling Law	Circa	Coefficient	M	L	T	Q
8	Bohm	< 1965	C$_1$	0	0	0	0
12	Mirnov	1972	C$_2$	-0.5	0	2	-1
14	Alcator	1975	C$_3$	0	1	1	0
16	Neo Alcator	1979	C$_4$	0	-0.09	1	0
18	Goldston L-mode	1983	C$_5$	-1	-2.38	3.5	-1
20	ITER 89O-P	1990	C$_6$	-0.15	-0.67	0.52	-0.72
22	Int. Stellarator	1996	C$_7$	-0.24	-3.80	0.06	0.83

the confinement time scaling laws have evolved from small or zero exponents to progressively larger, more irrational (in the mathematical sense), more fractional, (not integers or simple integer ratios) and more aphysical exponents. The confinement time correlations are not evolving to the dimensionless coefficients consistent with Buckingham's Pi Theorem. These exponents have evolved in the opposite direction, and now have values which imply hidden variables and physical processes not accounted for by the independent variables correlated.

It is disturbing not only that the dimensions of the numerical coefficients are becoming more complex with the passage of time, but also that the numerical coefficients for the phenomenological confinement time scaling laws for Tokamaks and Stellarators are so different. One would suppose, by application of Occam's razor, that the radial transport process in both types of device (whatever it is) would be the same.

5. BALL LIGHTNING

Ball lightning has been widely observed, but has not been accessible to scientific study because it has not until recently been possible to reproducibly generate it in the laboratory. It has many features, including stable existence in atmospheric air for up to 90 seconds, which are of fusion interest (Roth, 1995a). Although no measurements are available to shed light on the ion energies or number densities in ball lightning, it has many characteristics of fusion relevance, as indicated in Table 2. These characteristics include lifetimes from one to more than 90 seconds, energy densities higher than a DT fusion plasma, diameters greater than one meter, and kinetic pressures of the same magnitude as that of DT fusion reactors.

Possibly the most interesting characteristic of ball lightning is that its energy source apparently arises from stored magnetic energy, rather than chemical reactions. The reasoning behind this statement is based on Fig. 6, taken from Barry (1980). Figure 6 shows the cumulative distribution function the energy density 13 of ball lightning events, for which enough information was available to calculate the energy density in each case. These data lie on a straight line, indicating a log normal distribution of energy density. The fact that the data lie along a single straight line indicates that all ball lightning events arise from a single physical cause, since it is likely that if two distinct physical processes were responsible, there

Table 2. Relevant Characteristics of Ball Lightning (see Roth, 1995b).

Characteristics	Ball Lightning Observations	Self-Sustaining DT Fusion Requirements
Duration	1 sec to > 90 sec	1 to 10 sec.
Energy Density	10^{-3} to 10^{5} J/cm^3	1 J/cm^3
Diameter	~ 1 cm to 2 meters	> 1 meter
Kinetic Pressure	~ 1 atm.	1.6 to 10 atm.
Number Density	Poorly known	~ 10^{14}/cm^3
Kinetic Temperature	Poorly known > 0.025 eV	10^4 eV

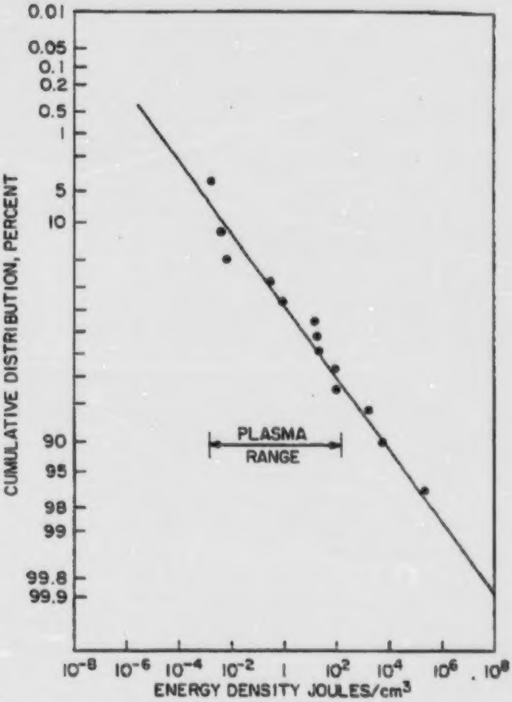

Figure 6. The cumulative probability of observing ball lightning of the energy density shown on the abscissa. The thirteen data points shown are rare examples of ball lightning in which information about their diameter and energy content was available.

would be a change in slope of the curve, at the point where one physical process left off, and the other took over. The data on Fig. 6 is usually used to rule out chemical explanations of ball lightning, since one of the most energetic explosives known, TNT, has an energy density of 2,000 Joules per cubic centimeter, and examples of ball lightning have been observed well above this value. If ball lightning is not an example of chemical energy storage, then stored magnetic energy is one of the very few remaining possibilities. The stable magnetic configuration which makes the long lifetime of ball lightning possible is surely of fusion interest.

Table 3. Fusion implication of ball lightning.

- Reactors of small size and power output
- Mobile applications of fusion reactors
- Simple formation and confinement equipment
- Power output controlled by surrounding pressure
- Long plsama containment times
- Stable operation for tens of seconds

A second significant characteristic of ball lightning is its ability to maintain itself for up to 90 seconds in air at one atmosphere. If a fusion reactor could also do this, a vacuum system would not be necessary. In a powerplant context, the ability to operate without a vacuum system would eliminate the expense of a major subsystem, as well as a source of unscheduled outages associated with failure of the vacuum system. Beyond that, applications of fusion energy outside the field of powerplant reactors might also be feasible, and include fusion powered turbojets for aircraft, and fusion rockets capable of taking off from the surface of the earth, rather than having to initiate their operations in the vacuum of earth orbit.

Some of the fusion implications of ball lightning are listed in Table 3. First, fusion reactors of small size and power output may be possible, if ball lightning plasmas can be made capable of supporting fusion reactions. The small size of a ball lightning fusion reactor implies mobile applications of fusion reactors. As previously discussed, ball lightning fusion reactors should be capable of operation at one atmosphere of pressure. In addition, ball lightning fusion reactors should require only simple formation and confinement equipment, since natural ball lightning has been observed to occur in an open field without any man-made apparatus whatever. The viral theorem must apply to ball lightning fusion reactors, so the plasma energy density and fusion power output should be controllable by adjusting the pressure surrounding the ball lightning plasma to be above or below one atmosphere, thus, compressing or rarifying the plasma. Consistent with observations of natural ball lightning, long plasma containment times and stable operation for long periods (tens of seconds) should be possible.

Natural ball lightning has been described in the monograph by Barry (1980), and the implications of ball lightning for fusion energy and the plasma research community has been discussed previously by the present author (Roth, 1995a).

6. ATMOSPHERIC GLOW DISCHARGES

One of the operational problems of fusion powerplant reactors as they are now understood is the requirement that the plasma of both magnetic and inertial fusion powerplants operate in a vacuum system. This requirement imposes the additional cost of a vacuum system, and introduces a catastrophic mode of failure if the vacuum wall is breached. Fossil fuel and nuclear fission reactors do not require a vacuum subsystem and do not have these problems, placing fusion reactors at a competitive disadvantage. As discussed previously, ball lightning is one indication that high energy density, magnetically confined plasmas can be operated at one atmosphere in air, thus eliminating the requirement of a vacuum system for fusion reactors.

A second indication that glow discharge plasmas can be operated in air at one atmosphere is the recent development of the One Atmosphere Uniform Glow Discharge Plasma (OAUGDP), at the UTK Plasma Sciences Laboratory (Roth, 1995b; Roth, et al. 1995a, 1995b) and is now being licensed to industry for vacuum-free industrial plasma processing. The physics which makes the OAUGDP possible includes two factors; one is that the electron energy is not constant in time during the discharge operation. The electrons are energetic enough to ionize the background gas only during a brief period, and cold, (or attached to form negative ions) during most of the discharge duration. In addition, the OAUGDP traps ions, on electric field lines in the plasma (Roth, 1995b). The concept of gas insulation of a fusion grade plasma is not a new one, and was put forward, among others, by Alfven and Smars (1960).

7. SUMMARY AND CONCLUSIONS

The isolation of the magnetic fusion community from the rest of the physics community - and even from their colleagues working in the field of industrial plasma engineering - has placed it in a position where perhaps not all relevant information is being brought to bear in the search for fusion energy. If nothing else is clear after nearly 50 years of fusion energy research, it is obvious that the achievement of fusion energy is a very difficult problem, and all available tools and approaches must be brought to bear. Several additional principles and concepts, including those described in this paper, should be incorporated in the mainstream of fusion physics because they imply possibilities or constraints which may facilitate progress toward a socially and economically acceptable fusion reactor.

Two of the phenomenon discussed above, ball lightning and the one atmosphere uniform glow discharge plasma, suggest that it may be possible in principle for a fusion reactor to operate in air or at one atmosphere, rather than in a vacuum system. The ball lightning literature suggests that it may be possible to create a small, long-lived plasma of fusion interest much more easily and cheaply than is possible with current approaches. Even if the phenomenon of ball lightning proves not to be a viable fusion concept, the ability of glow discharge plasmas to exist in the steady state in atmospheric air could lead to significant savings in the capital cost of vacuum systems, eliminate a catastrophic mode of failure, and open up the possibility of applications, such as fusion powered turbojets, which require operation at one atmosphere.

Significant advances in the theoretical understanding of fusion plasmas may follow from application of the Bohr-van Leeuwen and/or Buckingham's Pi Theorems, or from a detailed understanding of physics of ball lightning, one of the oldest unsolved problems in the field of plasma physics. Any advances stemming from application of the Bohr-van Leeuwen Theorem and/or Buckingham's Pi Theorem require only that they capture the attention of the fusion community; a detailed understanding of the physics of ball lightning is not available at present, but should become available now that ball lightning can be reproducibly generated in the laboratory for scientific study.

Much more control over the heating, transport, and confinement of fusion grade plasmas should be possible by using magnetoelectric confinement, because it allows one to do work on the confined plasma, unlike the plasmas normally used in magnetic fusion research which are confined by magnetic fields alone. Some of the benefits of magnetoelectric heating and containment have already been observed in Tokamak biasing experiments (Roth, 1993), including electron heating at the level of two megawatts, and increases in particle containment times of a factor of 10. The magnetoelectric containment provided by Tokamak plasma biasing probably has not been followed up with the vigor which its very promising results would appear to justify; in any case, the magnetoelectric confinement of a bumpy toroidal plasma has demonstrated ion heating to kinetic temperatures above 2500 eV, increases in particle containment time of up to a factor of 10, and, perhaps most importantly, radially inward transport of ions against the density gradient (Roth, et al., 1977).

Finally, if the field of fusion energy is to progress, it will be necessary not only to identify and pursue new and promising principles and conceptual approaches, but to correct long standing errors, including the phenomenological approach to correlating confinement time data used in Tokamak and other toroidal confinement experiments. When basic physical processes are not known or understood (which is the case with Tokamak radial transport) it is justified, as a second best approach, to use a phenomenological correlation of large amounts of data in order to simplify it. This phenomenological approach has been useful in correlating data in the field of aerodynamics, heat transfer, strength of materials, and many other areas. However it is important not to lose sight of the fact (as the fusion community appears to have done) that the correlation laws so derived are good only over the data set correlated, and extrapolations beyond the correlated data set are highly questionable. Extrapolation of such scaling laws become even more questionable when the physics changes, as in the transition from ohmically heated to externally heated Tokamak operation, or the transition from externally heated

Tokamak operation to burning plasmas, or the further transition from burning plasmas to ignited plasmas. The value of a phenomenological correlation is further compromised when the correlation is not conducted according the principles of Buckingham's Pi theorem, as has been done in the correlation of confinement time scaling laws for both Tokamak and Stellarator geometries.

REFERENCES

1. H. Alfven and C.-G. Falthammar. Cosmical Electrodynamics, 2nd Edition, Oxford, Clarendon Press (1963) p. 203.
2. H. Alfven and E. Smars. Nature. **188** (1960) pp. 801-802.
3. J D. Barry. Ball Lightning and Bead Lightning: Extreme Forms of Atmospheric Electricity. Plenum Press, New York, NY (1980).
4. J. Glanz. Science. **274** (1996) pp 1600-1602.
5. A.M. Messiaen. Transactions of Fusion Technology. ISSN: 0748-1896, **29**, 2T (1996) pp. 216-223.
6. J.R. Roth. Phys. of Fluids. **16**, 2 (1973) pp. 231-236.
7. J.R. Roth, W.M. Krawczonek, E.J. Powers, J.Y. Hong and Y.C. Kim Phys. Rev. Lett. **40**, (1977) pp. 1450-1453.
8. J.R. Roth. Nuclear Instruments and Methods. **207**, 1,(1983) pp. 271-299.
9. J. R. Roth. Introduction to Fusion Energy, IBIS Publishing, Charlottesville, VA., ISBN 0-935005-07-2 (1986) pp 91-94,111-113.
10. J.R. Roth. Fusion Technology. **23** (1993) pp. 246-252.
11. J.R. Roth. Magnetoelectric Toroidal Confinement. Proceedings of the First International Symposium on Evaluation of Current Trends in Fusion Research, Washington, D. C., November 14-18, 1994.
12. J.R. Roth. Industrial Plasma Engineering, Volume I: Principles. IoP Publishing, Bristol, England ISBN 0-7503-0317-4 (1995a).
13. J.R. Roth. Fusion Technology. **27** (1995b) pp. (255-270).
14. J. R. Roth, P.P. Tsai, and C. Liu. Steady-State, Glow Discharge Plasma. U.S. Patent 5, 387,842, February 7, 1995.
15. J.R. Roth, P.P. Tsai, C. Liu, M. Laroussi, and P.D. Spence. One Atmosphere, Uniform Glow Discharge Plasma. U.S. Patent 5,414,324, May 9, 1995.
16. D.G. Samaras. Theory of Ion Flow Dynamics. Dover Publications, Inc. New York, NY, ISBN 0-486-60309-1. (1971) See Section 6.6.
17. U. Stroth, M. Murakami, R.A. Dory, H. Yamada, S. Okamura, F. Sano, and T. Obiki. Energy Confinement Scaling From the International Stellarator Database. National Institute for Fusion Science Research Report NIFS - 375, Nagoya, Japan, Sept. 1995 (Equation 13).
18. J.H. Van Vleck. The Theory of Electric and Magnetic Susceptibilities. Oxford, Clarendon Press, (1932) p. 94.
19. G.H. Wolf. Fusion Technology. **29**, 2T, (1996) pp 392-399.

THE LOS ALAMOS INTENSE NEUTRON SOURCE

R.A. Nebel, D.C. Barnes, R. Bollman, G. Eden, L. Morrison,
M.M. Pickrell and W. Reass

Los Alamos National Laboratory
Los Alamos, New Mexico 87545, U.S.A.

ABSTRACT

The Intense Neutron Source (INS) is an Inertial Electrostatic Confinement (IEC) fusion device presently under construction at Los Alamos National Laboratory. It is designed to produce 10^{11} neutrons per second steady-state using D-T fuel. Phase I operation of this device will be as a standard three grid IEC ion focus device. Expected performance has been predicted by scaling from a previous IEC device. [1]

Phase II operation of this device will utilize a new operating scheme, the Periodically Oscillating Plasma Sphere (POPS). This scheme is related to both the Spherical Reflex Diode [2] and the Oscillating Penning Trap. [3] With this type of operation we hope to improve plasma neutron production to about 10^{13} neutrons/second.

1. INTRODUCTION

While electrostatic confinement has received interest for a number of years, it is only recently that sufficient insight has been gained to realize the important and unique capability of creating a high intensity fusion neutron source this way. The first suggestion to use electric fields for heating and confining fuel for nuclear fusion reactions was made by Salisbury [4]. Later and better concepts were proposed by Elmore, Tuck and Watson [5] in 1959, and Farnsworth [6] in 1956-66. Such concepts have come to be known as inertial-electrostatic confinement (IEC) schemes. They all envision that ions (Salisbury, Farnsworth) or electrons (Elmore, et al) projected radially inward will provide a negative potential well for the confinement of fusion-reactive ions in a core region. In the work of Elmore, et al., their original interest was piqued by their theoretical result that a 100 A electron current could maintain a potential well depth of 100 kV in a device size the order of one meter. Furth further explored this configuration in a theoretical study in 1963[7]. In this study he concluded that an anisotropic electron distribution in a medium of neutralizing ions could lead to a pinch-type instability possessing a perturbation magnetic field, which could grow if the particle density maintained in the field was too large. Even so, later numerical calculations suggested that

Current Trends in International Fusion Research — Proceedings of the Second Symposium
Edited by E. Panarella. NRC Research Press, National Research Council of Canada, Ottawa, ON K1A 0R6, Canada. 1999.

net power might be achieved if the density distribution could be kept to at least an inverse-square dependence on the radius of the system.

Following this work additional experimental, theoretical and a few computational studies were completed [8–12]. Perhaps the most intriguing of these was an experiment done by Hirsch [1], which demonstrated a much larger rate of neutron production was occurring than could be accounted for by theoretical and computational models. In this work Hirsch, following the lines conceived by Farnsworth [5], modified the Elmore et al scheme by using ion beams injected into a sphere to bring in electrons which, in turn, set up the negative potential well structure desired to trap the ions internally.

Hirsch used six symmetrically-placed ion beams of 10 mA in a background of electrons emitted by a spherical cathode. No instabilities were observed. At least two virtual electrodes were implied (but not measured directly). Reproducible neutron output that increased linearly with current for fixed potential and pressure was produced. A higher neutron yield resulted from lowering the pressure, probably by reduction of beam degradation from neutral-ion and charge exchange reactions at high background pressures. Hirsch observed 2×10^{10} n/s at densities between $1\times10^{12}/\text{cm}^3$ and $1\times10^{14}/\text{cm}^3$ with 10 keV and 100 keV ion beams in volumes between 0.1 cm^3 and 10 cm^3.

The work described in this paper builds and expands upon Hirsch's basic ideas. Instead of using ion guns to supply the ions, we are building a three grid IEC. A three grid IEC device confines a plasma inside a potential well that is formed from a set of spherical concentric electrodes (see Fig. 1). The center grid is charged to a high potential, relative to the outer grids,

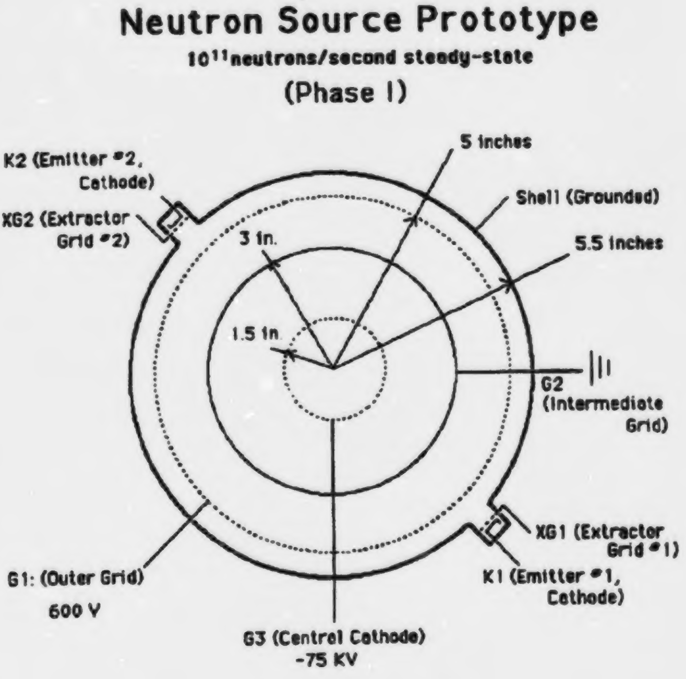
Neutron Source Prototype
10^{11}neutrons/second steady-state
(Phase I)
K2 (Emitter #2, Cathode)
XG2 (Extractor Grid #2)
3 in.
5 inches
Shell (Grounded)
5.5 inches
1.5 in.
G2 (Intermediate Grid)
XG1 (Extractor Grid #1)
K1 (Emitter #1, Cathode)
G1: (Outer Grid) 600 V
G3 (Central Cathode) -75 KV

Figure 1. 3 Grid IEC Device

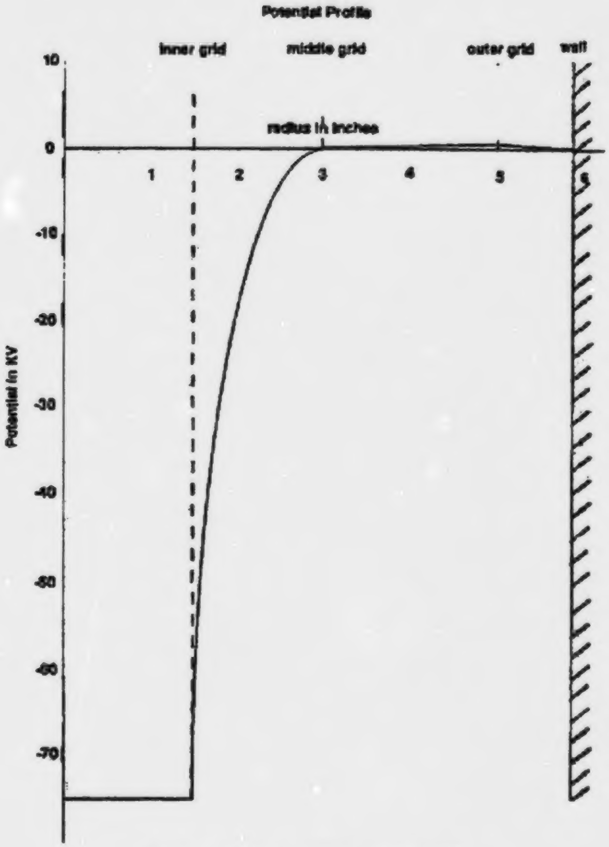

Figure 2. Typical vacuum potential profile

on the order of 10's of kilovolts. The center grid is charged negative, such that it takes on the role of a cathode. Any ions present in the region between the middle grid and the center grid will be attracted to the cathode. If the cathode is highly transparent, this spherical beam of ions will pass through the grid several times before being captured by the grid. The source of ions in a three grid system is from a background fill gas which is ionized between the two outermost grids. The middle electrode and the outermost electrode form a potential well which confines electrons. The outermost grid is held at about 600V while the middle grid is at ground (same as the wall). Electrons then oscillate around the outermost grid and ionize the background gas. Ions formed between the outermost grid and the middle grid will then be accelerated through the central grid and focused at the center. As the ions focus into the center, they interact with one another through space charge effects. A typical potential profile is shown in Fig. 2.

IEC has potential for immediate application as a portable neutron source. Applications for neutron sources in this range include safeguards and proliferation, assaying of nuclear and chemical waste, well logging, and detection of high explosives. These applications require a compact, portable, intense and inexpensive neutron source. IEC devices have significant advantages over present neutron sources in terms of both cost and ES&H.

The goal of phase I of the Intense Neutron Source project is to build an IEC similar to

Hirsch's that is capable of producing 10^{11} neutrons per second steady-state. The parameters for this device are scaled directly from Hirsch's data base. This device is described in the Phase I Device section. The goal of Phase II is to operate the IEC in a new regime, one that will hopefully greatly increase the gain and possibly even reach breakeven. The physics of this device and neutron yield projections will be discussed in the Phase II Device section.

2. PHASE I DEVICE

As stated above, the goal of Phase I of the INS project is to build a 10^{11} neutrons/second steady-state neutron source based on a three grid IEC design (see Fig. 1). Source parameters have been scaled from Hirsch's data [1]. Pessimistic and optimistic scalings have been assumed in order to bracket the expected performance of the device. Experimental parameters have been chosen so that the desired plasma parameters can be achieved even under the pessimistic assumptions.

Figure 3 shows the projected current vs voltage curves required for a $1\text{x}10^{11}$ source assuming that the neutron yield scales like the current (top curve) or as the current squared (bottom curve). We have sized our power supplies at 75 KV and 335 mA which should allow us to produce a $1\text{x}10^{11}$ source even if the pessimistic assumptions prevail.

Table I is a summary of the device parameters.

Table I

Chamber diameter	12 inches
Number of grids	3
Inner grid radius	1.5 inches
Middle grid radius	3.0 inches
Outer grid radius	5.5 inches
Number of e-guns	6
Maximum current per e-gun	12 Ampere
e-gun grid voltage	100 V
Maximum e-gun grid current	15 Amperes
Maximum grid voltage	75 kV
Maximum current rating	335 mA
Anticipated fill pressure	.1 mtorr
Anticipated base pressure	10^{-8} torr
High voltage feedthroughs	2

Figure 4 shows the front view of the chamber layout, including all of the ports and their purposes. The chamber is disassembled along its equator. This is how grids are placed and accessed. The top and bottom halves of the chamber are identical. They are rotated 60 degrees with respect to each other so the e-guns sit on the faces of a cube.

Since the device has up to 25 kW of continuous input power, active cooling is required. The shell is a double jacketed design with the coolant flowing between the chamber wall and the outer jacket. Note that the High voltage feedthrough port is cooled along with the chamber.

The innermost grid is also actively cooled. This is the high voltage grid and shares the

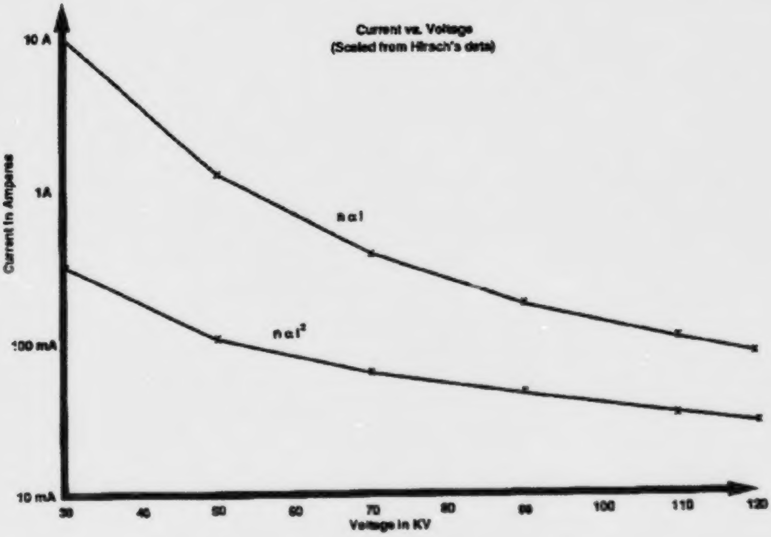

Figure 3. Empirical data scaling for current required for 1e11 source

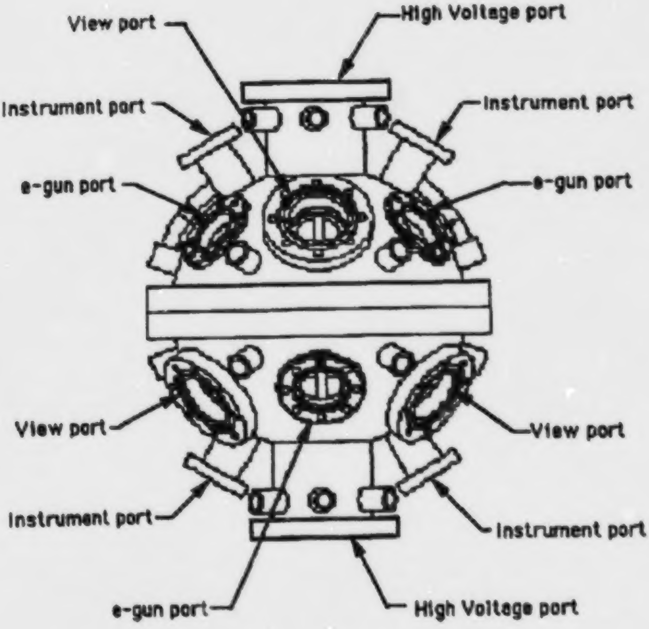
View port
High Voltage port
Instrument port
Instrument port
e-gun port
e-gun port
View port
View port
Instrument port
Instrument port
e-gun port
High Voltage port

Figure 4. Front view

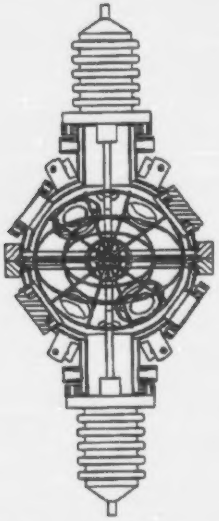

Figure 5. Cutaway view showing grids

dominant heat load with the wall. Figure 5 shows a cutaway view of the innermost grid along with the high voltage feedthroughs. The high voltage feedthroughs and the innermost grid are constructed of hollow tubing so they can carry coolant (deionized water). Once again, the coolant flows from the bottom to the top of the device. Coolant system and heat transfer parameters are listed in Table II. The power split between the innermost grid and the wall depends on the secondary emission rate of electrons from the innermost grid. This number is somewhere between 1 and 10, depending on the ion impact energy and the grid material (Copper in our case). Consequently, we anticipate that somewhere between 50% and 90% of the energy will be deposited on the chamber wall. Both the chamber and the grid are designed to handle the full 25 kW of power with substantial safety factors. (Heat transfer is not a major problem).

Table II

Maximum coolant flow rate	4 gallons/minute
Maximum temperature rise	100° F
Maximum head drop across grid	< 1 psi
Maximum head drop across chamber	< 1 psi
Maximum head available from pump	55 psi
Number of grid tubes	12
Inner diameter of grid tubes	.096 inches
Outer diameter of grid tubes	.125 inches
Maximum Reynolds number in chamber flow	670
Maximum Reynolds number in grid flow	200000
Chiller size	25 KW
Maximum grid temperature	335° C

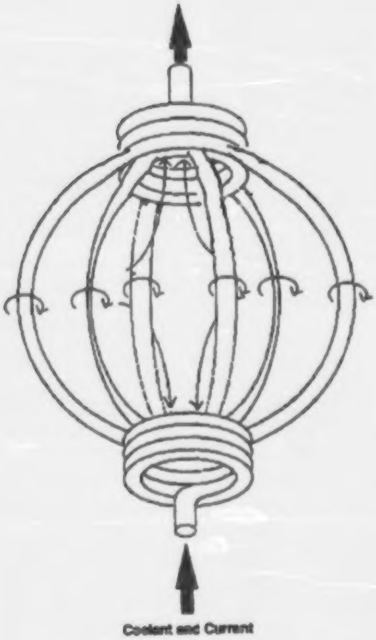

Figure 6. Magnetically insulated grid

The outer two grids will be made of tungsten and will radiatively cool. Anticipated loads on these grids is less than 1KW per grid. The middle grid will be covered with a fine tungsten mesh (~1mm grid spacing) to isolate the electrons in the gun from the high voltage region.

It is anticipated that this device will operate in a hot cell at NIS-5. Initial operation will be with deuterium in a continuous feed pumped system. Optimal operational parameters will be determined during this phase. Final operation will be with tritium in a hermetically sealed gettered device. Full neutron production is anticipated in this phase.

3. PHASE II

The goal of Phase II is to increase the neutron yield by a factor of 100 and to provide these neutrons in 200 picosecond bursts at a repetition rate of about 10^7 Hertz. This source will be suitable for time-of-flight imaging schemes and also will test the physics required to scale IECs to net power producing systems.

For Phase II we are proposing to operate the INS device as an electron-based IEC rather than as a spherical ion focus device as was done in phase I. We plan to replace the ion beam character of the device with an oscillating thermal (Maxwellian) plasma. The scheme is called the Periodically Oscillating Plasma Sphere (POPS) and is a combination and extension of two previous ideas; the Spherical Reflex Diode [2] and the Oscillating Penning Trap. [3]

For Phase II, the three grid system will be replaced by a single grid. A conceptual design for this grid is in Fig. 6. The grid is magnetically insulated in order to increase its transparency. Table 3 summarizes the grid parameters.

Table III

Grid radius	4 inches
Maximum grid voltage	75 KV
Maximum current rating (Grid to wall)	335 mA
Current for magnetic insulation	6 KA
Maximum coolant flow rate	4 gallons/minute
Maximum temperature rise	100° F
Maximum head drop across grid	< 1 psi
Number of grid tubes	6
Inner diameter of grid tubes	.096 inches
Outer diameter of grid tubes	.125 inches

Figure 7 shows the placement of the grid in the chamber. The grid is placed near the guns to maximize defocussing of the electrons. As in the case of the Spherical Reflex Diode, the goal is to spread the electrons as uniformly as possible over the volume enclosed by the grid. If the charge density is uniform, then the resulting potential well is a harmonic oscillator potential:

$$\phi = \phi_0 \left(1 - (r/r_{grid})^2\right) \tag{1}$$

where r_{grid} is the grid radius and ϕ is the electrostatic potential. The ion response to the harmonic oscillator potential can be calculated using the fluid equations in 1-D:

$$\partial n_i/\partial t + \partial(n_i V_r)/\partial r = 0 \tag{2}$$

$$m_i n_i \partial V_r/\partial t + m_i n_i V_r \partial V_r/\partial r = q_i n_i E_r - \partial p_i/\partial r \tag{3}$$

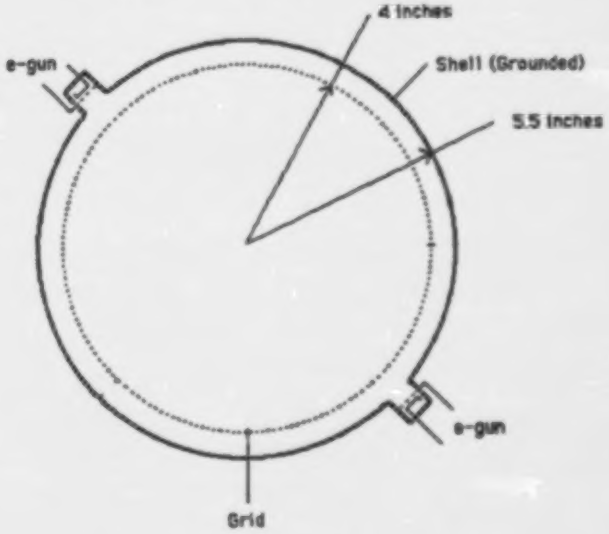

Figure 7. POPS grid placement

along with the ideal gas law:

$$p/n_i^{5/3} = \text{constant} \tag{4}$$

and Poisson's equation:

$$1/r^2\partial(r^2E_r)/\partial r = 4\pi(q_i n_i - en_e - en_b) \tag{5}$$

where n_i is the ion density, V_r is the ion radial velocity, m_i is the ion mass, p_i is the ion pressure, n_e is the thermal electron density, n_b is the background electron density generated by the grid and the e-guns, and E_r is the radial electric field where:

$$E_r = -\partial\phi/\partial r. \tag{6}$$

A set of self-similar solutions exist for these equations of the form:

$$n_i = n(\xi)\alpha(t) \tag{7}$$

$$V_r = V(\xi)\beta(t) \tag{8}$$

$$E_r = E(\xi)\gamma(t) \tag{9}$$

$$p_i = p(\xi)\eta(t) \tag{10}$$

where $\xi = r/a(t)$ and $a(t)$ is the moving radius of a sharp boundary plasma sphere. Substituting eqs (7)–(10) into eqs (1)–(6) yields:

$$n(\xi) = 1.0 \text{ for } \xi < 1.0 \text{ and } n(\xi) = 0.0 \text{ for } \xi > 1.0, \tag{11}$$

$$\alpha(t) = n_0(a_0/a(t))^3, \tag{12}$$

$$V(\xi) = \xi, \tag{13}$$

$$\beta(t) = \partial a/\partial t\,, \tag{14}$$

$$E(\xi) = \xi, \tag{15}$$

$$\gamma(t) = 4/3\pi q_i a(t)[n_0(a_0/a(t))^3 - n_e - n_b] \tag{16}$$

$$p(\xi) = (1 - \xi^2) \tag{17}$$

$$\eta(t) = p_0(a_0/a(t))^5 \tag{18}$$

where n_0, p_0 and a_0 are the initial density, pressure and plasma radius respectively. These solutions reduce the problem to the following ordinary differential equation for the plasma radius:

$$\partial^2 a \partial t^2 + 4/3\pi q i^2/m_i n_b a = 4/3\pi q_i^2/m_i[n_0(a_0/a(t))^3 - n_e] + 2p_0/(m_i a_0 n_0)(a_0/a(t))^3 . \tag{19}$$

Note that if the right hand side of equation (18) is ignored, the equation reduces to a simple harmonic oscillator equation. For now, we will assume that $en_e = q_i n_i$ and $T_0 = .025$ ev.

Assuming that the acceleration voltage is large (~75kV) compared to T_0, equation (19) reduces to a harmonic oscillator equation except in the region of $a(t)/a_0 << 1$:

$$\partial^2 a \partial t^2 + 4/3\pi q i^2/m_i n_b a = 0 \tag{20}$$

The pressure potential is very steep in the region of $a(t) \sim 0$ and its dominant effect is to cut the oscillation frequency in half. (This has been verified numerically.)

Note that nothing has been assumed about the time dependence of n_b. If one makes n_b sinusoidal then:

$$n_b = n_b^0 + n_b^1 \cos(\omega t) \tag{21}$$

and equation (19) becomes a Mathieu equation [13]:

$$\partial^2 a \partial t^2 + 4/3\pi q i^2/m^i(n_b^0 + n_b^1 \cos(\omega t))a = 0. \tag{22}$$

Phase locking is achieved by driving the system near one of the resonances. The lowest (and most efficient) resonance is:

$$\omega = 2\omega_h \equiv 2(4/3\pi q_i^2 n_b^0/m_i)^{1/2} \tag{23}$$

It is well known that a harmonic oscillator driven at resonance (with a small amount of dissipation, here provided by collisions with either the electrons or the background gas) will phase lock to the driver. The oscillation in n_b can be provided in one of two ways: either by

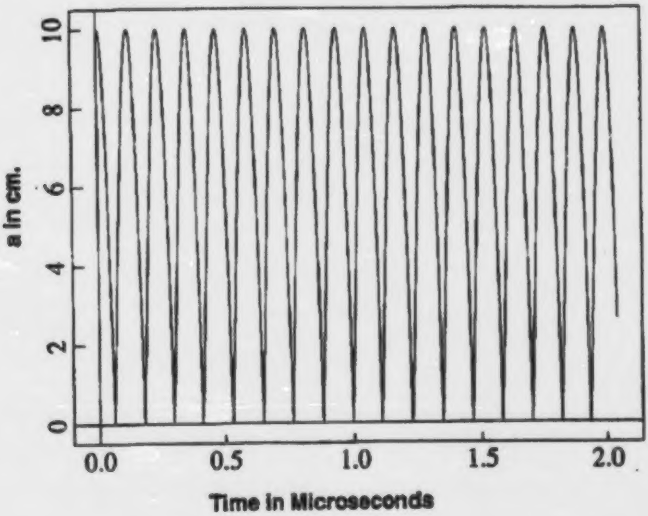

Figure 8. Plasma radius vs. time

oscillating the high voltage grid potential or by oscillating the extractor grid potentials (see Fig. 7). It can also be shown that these oscillations are stable to multi-dimensional perturbations. [14]

Numerical solutions of equation (19) are shown in Figures 8–12. Figure 8 shows a typical time dependence of the plasma radius. Note that the radius collapses to almost zero. An expansion of one of the collapses is shown in Fig. 9. The minimal plasma radius is about 60 microns. The plasma density and temperature increase as the radius shrinks. This is shown in Figures 10 and 11 respectively. Maximum density is about $10^{22}/\mathrm{cm}^3$ and the maximum temperature is 75 KeV (same as the applied potential). Figure 12 shows the time averaged neutron production rate. These curves assume D-D fusion. The D-T rate would be about 200 times larger. These curves asymptote to a production rate of about $6\mathrm{x}10^{16}$ neutrons/second. Each spike up in the production rate is caused by a burst of neutrons produced by the plasma compression. These neutron bursts are about 200 picoseconds in width and occur at a rep rate of approximately 10^7 Hertz.

Figure 13 show the expected D-D neutron yields vs. the normalized current. The normalized current is the total current which passes through the grid, including that which intercepts the grid (labeled as I_{grid}). The vertical dashed lines indicate where the INS device should operate, given different assumptions for the grid transparency. These curves are drawn for both steady-state and pulsed, assuming for the pulsed case that there is 1 kJ of capacitor energy storage. Note that there is almost no yield unless the transparency is better than 99.9%. Consequently, a magnetically insulated grid is imperative to see an effect (see Fig. 6).

The small numbers beside the curves are n_{i0}/n^b. If this number is much greater than 1, that is an indication that the effective Debye length has become shorter than the device size and the validity of these curves is questionable. It is therefore quite possible that we will not be able to exceed 10^{11} neutrons/second in D-D or 10^{13} neutrons/second in D-T with the Phase II device. However, if we are able to access the high density regions of parameter space, then it is easy to show that:

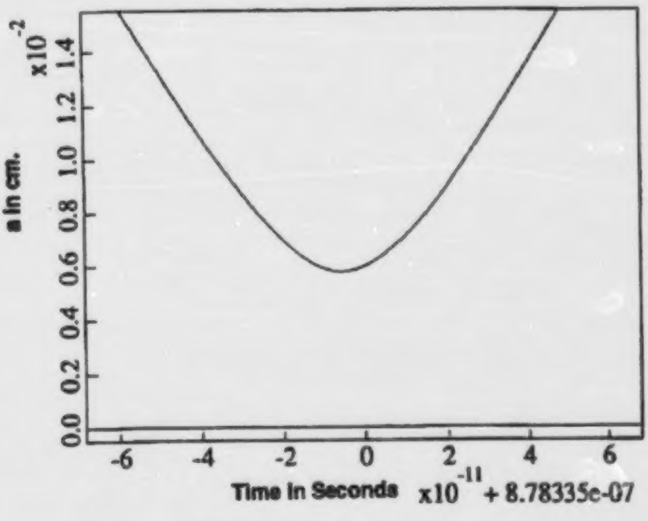

Figure 9. Plasma radius vs. time

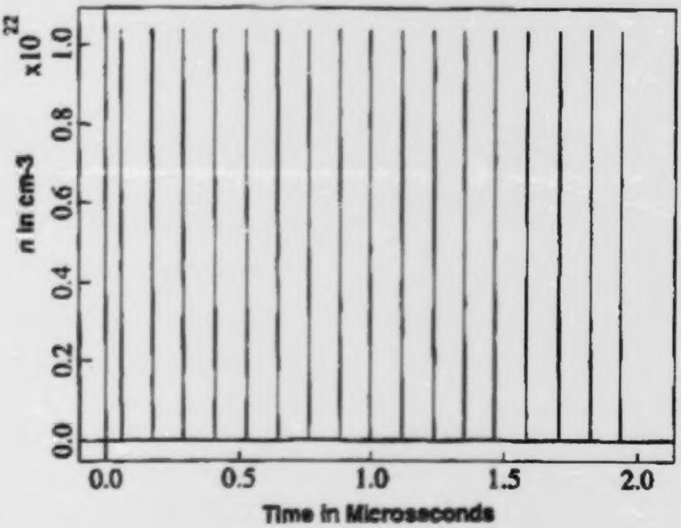

Figure 10. Plasma density vs. time

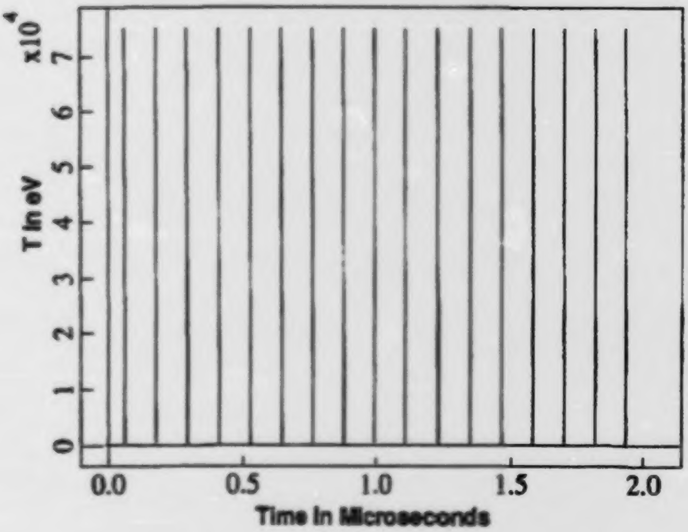

Figure 11. Plasma temperature vs. time.

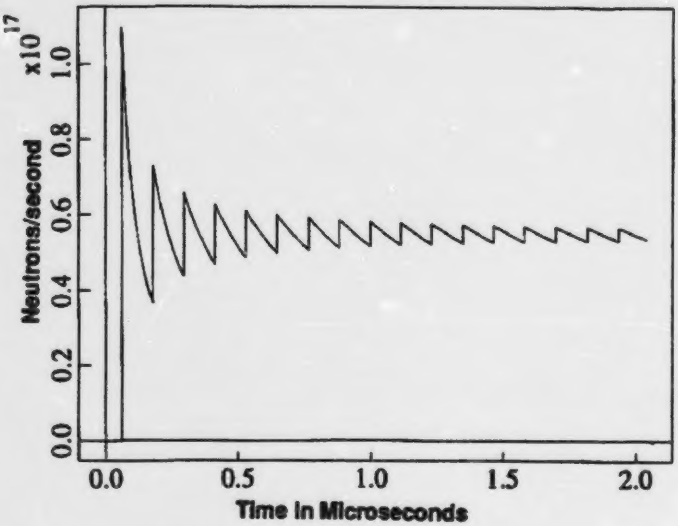

Figure 12. Average neutron yield.

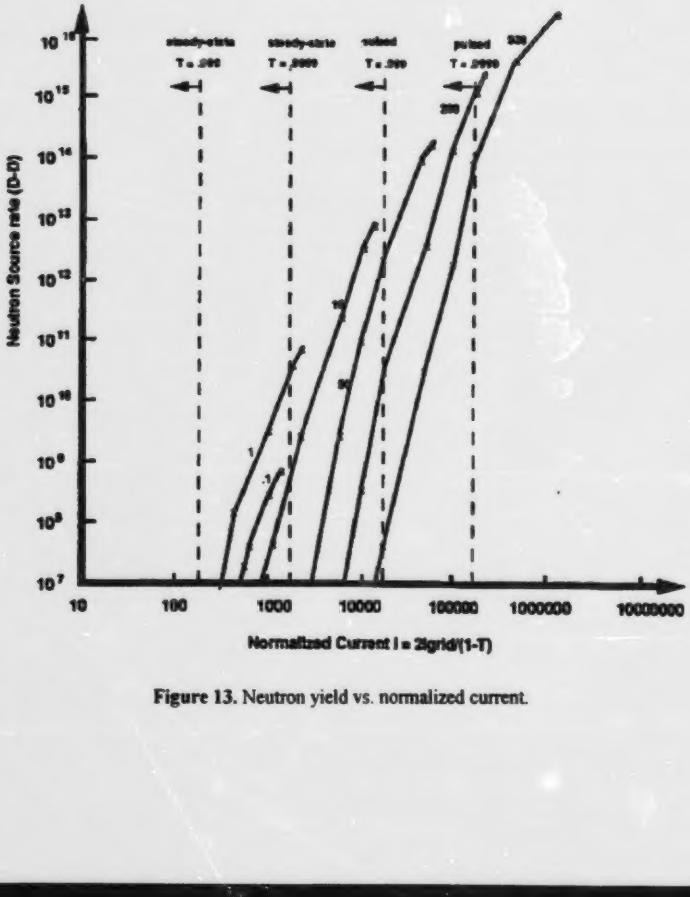

Figure 13. Neutron yield vs. normalized current.

$$n_{i0} \sim I_{grid} \tag{24}$$

so

$$P_{fusion} \sim I_{grid}^{\ 2} \tag{25}$$

and

$$Q_{fusion} \sim I_{grid}. \tag{26}$$

The uppermost point on Fig. 13 is the breakeven point if the plasma were operating with D-T instead of D-D. Thus, breakeven is possible, but it isn't very likely.

Even if the high density plasmas are not obtainable, the POPS operating scheme still has attractive reactor possibilities. Either the voltage can be increased, or the size can be shrunk down to a Penning Trap. If one decreases the size at constant voltage, then:

$$n_{i0} \sim 1/r_{grid}^{\ 2} \tag{27}$$

and

$$P_{fusion} \sim 1/r_{grid}. \tag{28}$$

Penning Traps are gridless systems, so one will probably also gain an another order of magnitude in Q_{fusion} due to the effective increase in the grid transparency.

4. SUMMARY

The Intense Neutron Source (INS) is an Inertial Electrostatic Confinement (IEC) fusion device presently under construction at Los Alamos National Laboratory. It is designed to produce 10^{11} neutrons per second steady-state using D-T fuel. Phase I operation of this device will be as a standard three grid IEC ion focus device. The design parameters for the phase I device indicate that expected yield should be realized even under conservative assumptions. Expected performance has been predicted by scaling from a previous IEC device.[1] Even if the presently utilized power supplies fall short of the desired yield, the thermal hydraulics and heat transfer are over-designed by almost a factor of 10 so all that will be necessary to reach the desired goal would be to use a larger power supply and chiller.

Phase II operation of this device will utilize a new operating scheme, the Periodically Oscillating Plasma Sphere (POPS). With this type of operation we hope to improve plasma neutron production to about 10^{13} neutrons/second. It is estimated that this scheme also will give 200 picosecond bursts of neutrons at a repetition rate of about 10^7 Hertz. This source should have applications for imaging using time-of-flight techniques.

The Phase II device will also test the physics required to obtain high gain using the POPS operating scheme. How well this works should give an indication as to the possibilities of using this scheme for net power production.

REFERENCES

1. R.L. Hirsch. J. Appl. Physics **38**, 4522 (1967).
2. B. Edwards. Phd Thesis, University of Illinois (1980).
3. D.C. Barnes and L. Turner. Phys Fluids **B4**, 3890 (1992).

4. W.W. Salisbury. Method and Apparatus for Producing Neutrons, U. S. Patent No. 2,489,436, issued Nov. 29, 1949, filed Dec. 17, 1947.
5. W. Elmore, J. Tuck and K. Watson. Phys. Fluids **2**, 239 (1959).
6. P.T. Farnsworth. Electric Discharge Devide for Producing Interactions Between Nucleii, U.S. Patent No. 3,358,402, issued June 28, 1966, initially filed May 5, 1956, rev. Oct. 18, 1960, filed Jan. 11, 1962.
7. H.P. Furth. Phys. Fluids **6**, 48 (1963).
8. T.J. Dolan, J.T. Verdeyen, D.J. Meeker and B.E. Cherrington. J. Appl. Physics **43**, 1590 (1972).
9. D.A. Swanson, B.E. Cherrington and J.T. Verdeyen. Appl. Phys. Lett. **23**, 125 (1973).
10. *Idem*. Phys. Fluids **16**, 1939 (1973).
11. W.M. Black and J.W. Robinson. J. Appl. Phys. **53**, 2497 (1974).
12. D.C. Baxter and G.W. Stuart. J. Appl. Phys. **53**, 4601 (1982).
13. See, M. Abramowitz and I. Stegun, Handbook of Mathematical Functions, 721 (1964).
14. R.A. Nebel and D.C. Barnes. to be submitted to Physics of Plasmas.

ON THE POSSIBILITY TO DUPLICATE IN THE LABORATORY FUSION RELEVANT BALL LIGHTNINGS

Mircea Sanduloviciu and Erzilia Lozneanu

"Al. I.Cuza" University of Iasi
Iasi 6600, Romania

The first requirement to duplicate in laboratory space charge configurations (SCC) similar to ball lightnings (BLs) is the knowledge of a realistic model able to describe in detail the physical process involved in its formation [1]. In this context we have proposed a new model [2], suggested by laboratory experiments [3]. This model considers the BL as the result of a self-organization process [3] that begins with a lightning stroke and ends with a BL after proceeding through the following series of sequential steps:

- generation of a well localized hot plasma by a lightning stroke;
- spatial separation of the opposite electrical charges owing to the difference between the mobility and diffusivity of electrons and positive ions (during this sequential step a nucleus enriched in positive ions is formed, immediately outside it there is a partially ionized gas which fades off into the surrounding neutral atmosphere);
- acceleration of the surrounding thermalized electrons toward the nucleus (which acts as a gas anode) and, consequently, symmetry breaking and spatial separation of the excitation and ionization cross section functions;
- accumulation of the electrons in the region where the neutral cross section function suddenly increases and, as a result, formation of a negative shell which surrounds the positive nucleus;
- long-range order produced by the induced electrostatic forces which act between the adjacent net opposite space charges; and
- self-assemblage into a complex SCC whose coherence is assured by a spherical self-consistent DL. The self-assemblage process takes place spontaneously without expenditure of energy because the resulting spherical SCC corresponds to a local minimum of the free energy.

The final product of such a self-organization process is a gaseous SCC whose luminosity is produced by the de-excitations of the neutrals placed at its external spherical border, i.e., in the region where the electrons accelerated toward the nucleus lose their kinetic energy after neutrals' excitation. In Fig. 1 is presented the SCC formed after self-organization. The persistence of the BL, for a short time interval after its birth, is related to the property of each

Current Trends in International Fusion Research — Proceedings of the Second Symposium
Edited by E. Panarella. NRC Research Press, National Research Council of Canada, Ottawa, ON K1A 0R6, Canada. 1999.

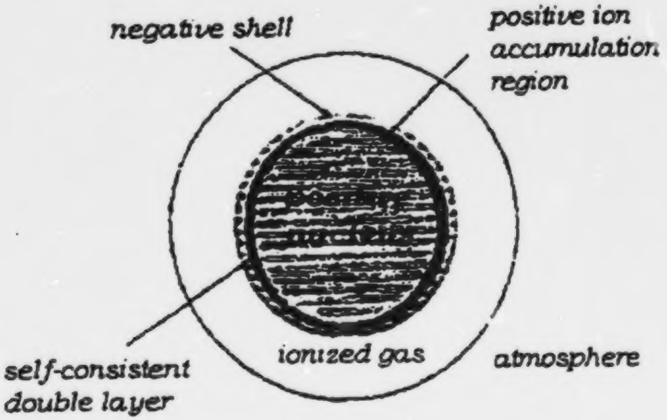
negative shell
positive ion accumulation region
self-consistent double layer
ionized gas
atmosphere

Figure 1. Ball lightning according to the model grounded on self-organization

complexity resulting after self-organization to memorize its past history [3]. The prolonged existence of the BL occasionally observed can be explained taking into account that a SCC bordered by a spherical DL behaves as a cavity able to absorb at resonance electromagnetic energy [4]. In nature such radiation sources are linear lightnings [4].

For the above briefly described model process two phenomena are essential in the potentiality of a SCC to operate as a fusion reactor. Firstly, there is the self-confining mechanism and the stability assured by the DL at its border. Secondly, there is the ability of such a stable SCC to self-modify the structure and dimensions so that electromagnetic energy from external sources is trapped at resonance.

For testing the above model process we have used the experimental device presented in Fig. 2. In the plasma produced by a plasma source was immersed an electrode E whose voltage was chosen a little smaller that the critical value for which a nearly spherical SCC, atached at the E surface appears [3]. Producing an electrical spark one observes, at its impact point on the E surface, the appearance of a luminous spot that develops in the nearly spherical SCC [3]. If under such conditions in the region in front of E a h.f. electric field is created, it becomes possible to determine the detachment of the SCC from the E surface and its transition into a free floating SCC sustained only by the h.f. electric field when the d.c. voltage of E is removed. The investigation of the internal structures of both above mentioned SCC (the free floating one and that attached at the E surface) relieves the same space charge configuration whose essential part is a spherical DL at its border.

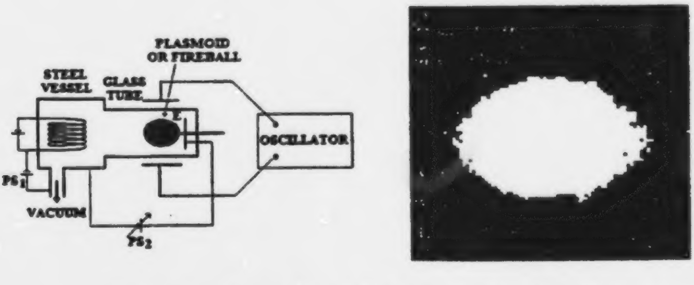

Figure 2. Experimental device and photograph of the plasmoid

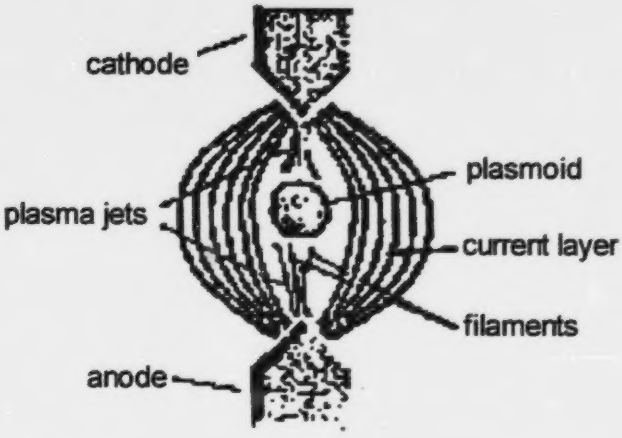

Figure 3 SCC formed in Z-pinch device [from reference (6)]

Although performed under conditions far away from those existent in nature (low gas pressures and low energies) our experiment is able to justify a self-organization physical scenario able to create in laboratory SCC with characteristics usually attributed to BL [1,5].

The validity of a self-organization physical scenario under conditions close to those existent in nature seems to be confirmed by recent experiments performed in Z-pinch and plasma focus devices [6,7]. In the experiment described in Ref. 6 it was reported that a pulsed discharge produced in Argon between two con shaped electrodes at pressures around KPa a stable spherical SCC in the form of a plasmoid with (1;2)*10^{25} m^{-3} electron density, 3 – 5 min diameter and (1:2)μs life time was spontaneously generated. The disintegration of such a SCC is very implosive and this fact improves the high energy density in the plasmoid. Fast ions of energy above 50 KeV are emitted in the first moment of the SCC formation. The number of fast ions per one shot was evaluated at 6*10^{11} and the half-width pulse is lower that 100 μs. The scheme of the electrodes configuration and the discharge containing the spherical SCC is presented in Fig. 3. An experiment similar to that described in Ref. 8 with the essential difference that the formation of the fireball is initiated by an electrical spark is under consideration in our laboratory.

REFERENCES

1. R. Roth, Fusion Technology **27**, 255 (1994).
2. M. Sanduloviciu and E. Lomeanu. Romanian Rep. In Phys. **48**, 751 (1996).
3. M. Sanduloviciu, C. Borcia and G. Leu. Phys. Lett **A 208**, 136 (1995).
4. X.H. Zheng. Phys. Lett **A**, 436 (1990).
5. D.J. Turner. Phy. Trans R. Soc. London **347**, 83 (1994).
6. P. Kubes. 2nd Nat. Symp. Plasma 95 (Polish Academy of Sciences), Inv. paper 79.
7. M. Sanduloviciu and E. Lozneanu. Int. Conf. Plasma Phys., 1996 Nagoya, Japan, p. 1610.
8. Y.H. Ohtsuky and H. Ofuruton. Nature **350**, 139 (1991).

ADVANCED ANALYZERS AND PROBES FOR FUSION-PLASMA DIAGNOSTICS

Edbertho Leal-Quiros and Mark A. Prelas[1]

Polytechnic University of Puerto Rico
P.O. Box 192017-2017
San Juan, Puerto Rico 00919-2017
[1]Nuclear Engineering Program
University of Missouri-Columbia
Columbia, MO 65211, U.S.A.

ABSTRACT

Various novel analyzers and probes were designed, built and successfully tested in the Cusp-Mirror machine in the Fusion Research Laboratory at University of Missouri-Columbia. We will discuss four of them: The Variable Energy Analyzer (VEA), the Magnetic Dipole Moment Meter (The μ-Meter), The Double Energy Analyzer (DEA), and the Hyperbolic Energy Analyzer (HEA). The main advantage of these analyzers is that they are very small (about 7 mm diameter) and they are made of materials that resist high temperature, high plasma flux and they are shielded for RF signals. All of them have a probe driver in such way that they can move back and forward inside the machine. For that reason it is possible to map the plasma at almost all points inside the device.

Plasma parameters in both directions parallel and perpendicular to the axial magnetic field have been measured. Among of them: plasma density, electron temperature, ion temperature, and μ-dipole moment, velocities of ions and electrons, plasma flux, local fl parameter, Larmor radii, local magnetic fields. Some of these analyzers like VEA are used as a reference for the construction of other analyzers.

1. INTRODUCTION

The Modified Missouri Magnetic Mirror eXperiment (M4X) is a device that uses two solenoid magnets parallel to each other to provide the magnetic field. The coils can be run with complementary or opposing fields. Hence, it is possible to run M4X as a simple mirror, or as a spindle cusp (see Fig. 1), which is an advantage over other conventional devices of this kind.

The microwave and RF heating sources available to the M4X device are a 2.45 GHz, 5 kW CW microwave source, a 2 to 5 MHz, 10 kW RF source, and a 0.1–1 MHz, 1 kW RF power supply. Only the 2.45 GHz source has been used on a routine basis, for ECRH (electron

Current Trends in International Fusion Research — Proceedings of the Second Symposium
Edited by E. Panarella. NRC Research Press, National Research Council of Canada, Ottawa, ON K1A 0R6, Canada. 1999.

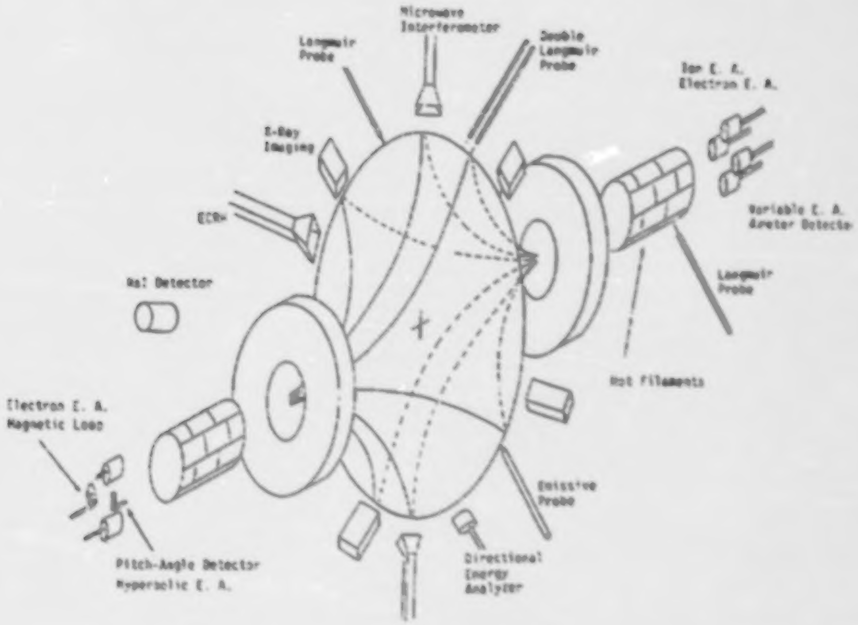
Microwave Interferometer
Langmuir Probe
Double Langmuir Probe
Ion E. A.
Electron E. A.
X-Ray Imaging
ECRH
Variable E. A.
Ameter Detector
NaI Detector
Langmuir Probe
Hot Filaments
Electron E. A.
Magnetic Loop
Emissive Probe
Pitch-Angle Detector
Hyperbolic E. A.
Directional Energy Analyzer

Figure 1. Diagnostic in Modified Missouri Magnetic Mirror Experiment (M4X)

cyclotron resonance heating) in the X-mode. The design of M4X, allows studies of basic plasma physics and it has easy access for new diagnostic tools. These probes were used in a series of experiments in the cusp and mirror mode in which we studied the properties of the plasma while varying either magnetic field strength or microwave power, for different gases that are published elsewhere. This paper is more about the probes themselves, than about the Cusp-Mirror experiments.

However, the data was compared with data of other plasma diagnostics measurements with acceptable agreement.

2. THE VARIABLE ENERGY ANALYZER (VEA)

The Variable Energy Analyzer (VEA) was first described by Leal-Quiros in 1981 [1]. The VEA is an electrostatic multigrid (ion or electron) energy analyzer in which the geometry can be changed externally with a micrometer control. This new type of diagnostic probe is an improvement over conventional ion energy analyzers because the resolution of ion spectra is improved by a factor of two, and the sensitivity is improved by a factor of two. As an example, the ion energy analyzer developed by Taylor [2] was able to measure ion temperatures as low as 0.3 eV. A prototype VEA built and tested by Leal-Quiros was able to measure ion temperatures as low as 0.125 eV.

Geometric parameters such as the separation distance between the grids, the aperture diameter, the transparency of the grids, and the space charge all influence the characteristic curve of the diagnostic probe (collector current vs. the retarding potential on the discriminator grid).

2.1 Theoretical Discussion

A simple plane Langmuir probe yields information on the electron density and temperature. An ion energy analyzer, using additional electrodes to eliminate the electron contribution, is required to measure the ion temperature. After the electrons have been screened out by the retarding potential of the discriminator grid (φ), the ion current I (φ) reaching the plate collector (of area A), is given by:

$$I(\phi) = eA \int_{V_{\min}}^{\infty} VF(v)\,dv$$
$$I(\phi) = \frac{eA}{M} \int_{e\phi}^{\infty} F(V)\,dE \qquad (1)$$

where:

$$V_{\min} = \left(\frac{2e\phi}{M}\right)^2 = \text{minimum velocity},$$
$$E = \frac{1}{2} Mv^2$$

Differentiating equation (1) with respect to ϕ, we get an expression for the velocity distribution function $F(v)$ in terms of the first derivative of the current-voltage characteristic, ($I(\phi)$ vs. ϕ).

$$F(v) = -\frac{M}{e^2 A}\frac{dI}{d\phi} \qquad (2)$$

In order to calculate the ion temperature, assuming that $F(v)$ is approximately Maxwellian, we can manipulate equation (1):

$$I(\phi) = (\text{constant})\exp\left(-\frac{e\phi}{kT_i}\right)$$
$$\ln(I\phi) = (\text{constant}) - \left(\frac{e\phi}{kT_j}\right) \qquad (3)$$
$$KTi = -\frac{e}{\frac{d}{d\phi} Ln(I(\phi))}$$

From the plot of, Ln(I (ϕ)) vs. ϕ, the inverse of the slope gives the ion temperature kT_i directly.

The assumption of a Maxwellian distribution function for the plasma is not necessarily valid. For this reason, the plot of ln(I(ϕ)) vs. φ is not always a straight line, but using the Kudyan method [38] the effective ion temperature can still be obtained. The plasma potential can be deduced from the characteristic curve of the VEA. This potential is related to the point where all of the ions are collected . Experimentally, the potential is given by the value at which

$\frac{dI(\phi)}{d\phi}$ becomes zero .

Even when the effects introduced by the grids, secondary electrons, and space charge are neglected, the measurement of the distribution function would be in error unless the analyzer is: infinite in extent or particle flow, one dimensional, and aligned parallel to the retarding field. The error arises because the apertures, in the electrodes of the analyzer, block some particles that have sufficient energy or momentum to be collected.

The analyzer with its three electrodes is shown. The grids in the analyzer are separated by a distance, *D*.

Assuming that the plasma is Maxwellian and isotropic, the potential on the first grid reflects the other charged species (i.e, $V_o < 0$), and the variable potential V_{RET} on the second grid defines a lower limit in the energy of the collected particles.

3. THE VEA ANALYZER

We have designed a test analyzer with variable geometry using an external micrometer control. The analyzer has two separate components which are placed in separate boxes that are linked together by an axis which acts like a transmission line. The first component is located

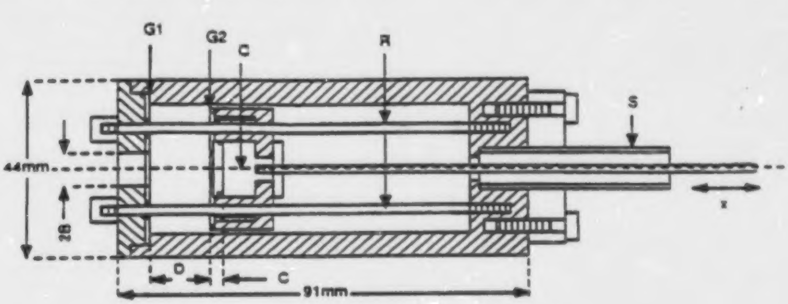

a) Prototype Variable Energy Analyzer tested by the authors

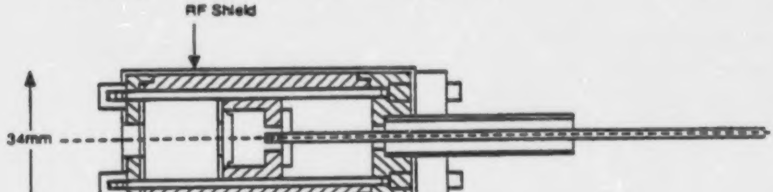

G1 – Entrance Grid
G2 – Discriminator Grid
C – Collector

R – Rails
S – Support

The set G2 - Collector can separate from G1 using the bar BA which is connected to a micrometer control that is not shown.

Figure 2. a) The design of the prototype Variable Energy Analyzer and b) The design of the Modified Variable Energy Analyzer. (VEA) in the vacuum chamber and has direct contact with the plasma. This component contains the three electrodes (Grid 1, Grid 2 and the collector), their associated insulators, the other electrical connections, and the rail mechanism to move G_2 and the collector back and forth (see Fig. 2).

The second component is located outside of the vacuum chamber and it contains the mechanism to move the transmission bar back and forth by adjusting the micrometer. In this manner we can vary the separation distance, (D), between the Grid G1 and the Grid G2 from (0.00 ± 0.01) mm to (12.00 ± 0.01) mm. It is also possible to change the apertures (2A and 2B) of the Grids G1 and G2. We used a mesh of 500 lpi, and Grids with aperture diameters of 7 and 10 mm, respectively.

3.1 Results From The Prototype Variable Energy Analyzer

The first set of results (see Fig. 3) generated different characteristic curves (I vs V_{RET}) for the various separation distances (D) between Grids G1 and G2, when the Grid aperture diameters constant. Grid G1 was held at the floating potential in order to attract the ions and repel the electrons.

These characteristic curves also allowed the ion temperature (T_i) as a function of the

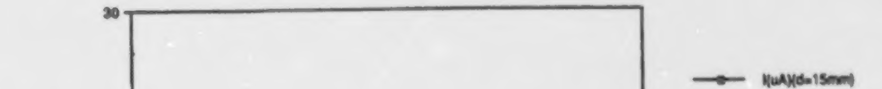

Figure 3. Characteristic I vs. V_{RET} from the Variable Energy Analyzer. Each one of the characteristic curves corresponds to one D value. The aperture diameters 2A = 2B = 10 mm are constants $p_o = 6 \times 10^{-4}$ Torr; $n_o = 10^9$ cm^{-3}.

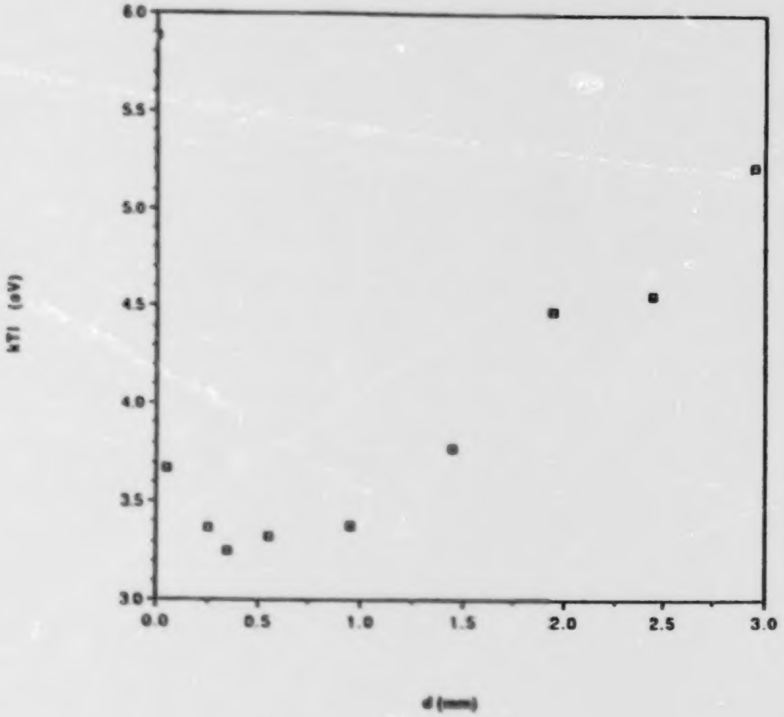

Figure 4. Apparent ionic temperature vs the separation distance between grid 1 and grid 2.

separation distance (*D*) to be deduced from the theory described above (see Fig. 4). We have found that a grid mesh of 500 lpi was approximately 5 to 10 times more sensitive (i.e., able measure lower ion temperatures) than a grid mesh of 100 lpi holding all other geometric factors constant. The optimum separation distance (*D*) between the Grids depends upon the aperture sizes.

When the aperture sizes of the two Grids were 10 mm, the optimum separation distance was $D = 0.4$ mm (See Fig. 4).

The measured ion density apparently decreases almost linearly with the separation distance. This is due to the influence of the geometric parameters of the Ion Energy Analyzer, such as the blocking of the particles by the finite size of the apertures [3].

The resolution of the energy analyzer ($\Delta V/V$) is found by using the method of Stenzel [4]. From $\Delta V/V$ vs D the optimum separation distance is obtained; this is accomplished by locating the minimum value of $\Delta V/V$ on the curve. This minimun is important because as the separation distance changes, the apparent ion temperature reading changes (see Fig. 3). The resolution of the analyzer for particle energy also decreases when Grid G2 is very close to Grid G1 (i.e., when D is smaller than the optimum separation distance).

It is important to note that the optimum spacing between G1 and G2 is different from the minimum spacing . Therefore, with the VEA working at the optimum D, this means that it has the best resolution .The separation distance between G1 and G2 can be varied from zero to one hundred times the Debye length ($0 \le D \le 100\ \lambda_D$).

The VEA shows agreement with the measurement of the plasma density using the

Langmuir probe in two different ways: a) through the plasma frequency and b) through the probe characteristics. The increase or decrease from this optimum *D* appears as a false increase in the ion temperature, and also as a reduction of the current on the collector. When the VEA was working at the optimum *D*, the characteristic curves of current versus retarding potential were very similar to the well known ideal curves generated from theory. The ion temperature measured at optimum spacing *D*, with the VEA, is the most accurate measurement to date because it is able to correct for errors caused by the geometric parameters and the space charge.

3.2 Results from the Modified Variable Energy Analyzer

For this experiment, an Ar (Argon) plasma was produced in M4X as mirror, with an ECH power of only 2.2 kW transmitted. Then a study of the influence of the geometric parameters in the ion collection was performed.

The experiment was done in such way that, for each separation distance between Grid 1 and Grid 2, a characteristic curve *I* vs VG2 was taken. After that, a Ln *I* vs VG2 was made for each separation distance. Also the ion energy distribution function was plotted for each separation distance.

The temperature was evaluated and the ion density was calculated. The area of the grids was 0.385 cm^2 because both grids had an aperture of 0.7 cm in diameter. We found that the optimum separation distance was $d_{op} = 0.40$ mm.

After finding the optimum separation distances between Grid 1 and Grid 2, the VEA was used to measure the plasma parameters such as the plasma density, the ion temperature, and the ion energy distribution function. The parameters have the following definitions:

d (mm) = the separation distance between G1 and G2. This distance can be changed with the micrometrical control between 0.00 mm and 20.00 mm with a resolution of 0.01 mm.
T_i (eV) = the ion temperature .
I_0 (A) = the ion saturation current.
n (m^{-3}) = the ion density .

The VEA had very high sensitivity. Also, it was possible to measure the ion distribution function at the minimum separation distance $d = 0.00$ mm and at the optimum separation distance $d = 0.4$ mm (see fig. 5). The differences between both distribution functions are shown clearly in the same figure.

Conclusions from use the modified VEA

A new energy analyzer called the Modified Variable Energy Analyzer clearly showed the influence of the geometric parameters in the measurement of the plasma properties.

For a grid aperture diameter of 7 mm, the existence of an optimum value for the grid separation was found: $d_{op} = 0.40$ mm. The optimum value d_{op}, was found to be the same for all kinds of plasmas . The plasma parameters should be measured when the VEA is working at the optimum separation distances d_{op}.

The modified VEA could sensitively analyze very weak ionized plasma, such as plasma produced in the M4X as mirror with only 120 Watts of ECRH power. The good performance of VEA in magnetized and RF plasmas was clearly demonstrated in M4X .

The small size and the RF shield makes the VEA a very important tool in the analysis

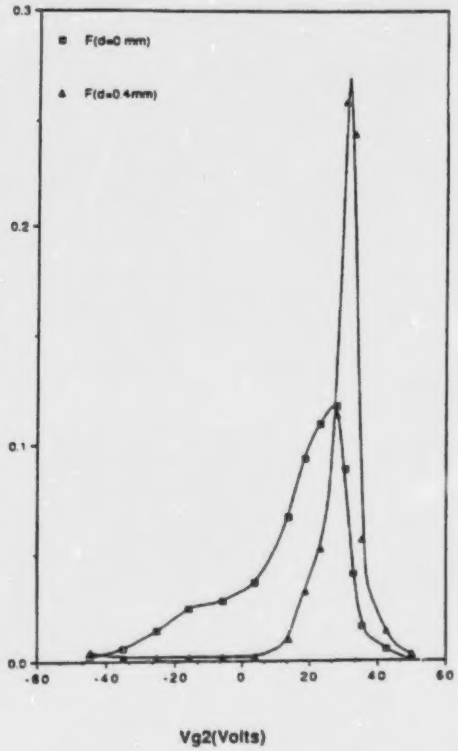

Figure 5. Comparison of Distribution Functions for d = 0.00 mm and d = 0.4 mm the optimum separation distance enter grid 1 and grid 2, using VEA.

of plasmas at low density .

The high sensitivity and good resolution may suggest the use of VEA as a standard for calibrations of other Energy Analyzers.

4. THE DOUBLE ENERGY ANALYZER (DEA)

The double energy analyzer is a new analyzer formed by two directional energy analyzers perpendicular to each other. One goal of this analyzer was to study the axial and radial loses of plasma, in mirrors and in cusps.

The configuration of the double energy analyzer is such that one directional energy analyzer allows the measurement of the charged particles, for example, in the direction parallel to the magnetic field. The second analyzer then measures the velocity of the particles in the direction perpendicular to the magnetic field, (if the correct orientation of the analyzer with the magnetic field is made). Because directional energy analyzers are in the same small case, very close to each other, this allows the measurement of both average velocities $V_{\parallel}$ and $V_{\perp}$, at almost exactly the same point.

When the double energy analyzer is inside a magnetized plasma, so that the parallel analyzer is aligned with the magnetic field and the other analyzer is perpendicular to the magnetic field, then the pitch angle α for particles with perpendicular average velocity $V_\perp$, and parallel average velocity $V_\parallel$ could be measured instantaneously.

4.1 Theoretical Considerations

In order to study the confinement of the plasma in magnetized devices, the pitch angle, the adiabatic invariant, the loss cone and the trapping mechanism should be defined.

The pitch angle α is defined as :

$$tn\alpha(l) = \frac{v_\perp(l)}{v_\parallel} = \frac{\sqrt{W_\perp(l)}}{W_\parallel(l)} \tag{4}$$

Although there are many authors that treat the pitch angle theory, we prefer to use the approach by Chamberlain [36] and Stacey [25].

The relationship between total kinetic energy of the particle (*W*) the local magnetic field B, the pitch angle α, and the dipole moment is:

$$\mu \equiv \frac{W \sin^2 \alpha}{B} = \text{constant} \tag{5}$$

A study of the Dipole moment μ and a proof that m is an adiabatic invariant is possible. If there is no electric field acting on the particle, so that

$$w = \frac{1}{2} m\left(v_\parallel^2 + v_\perp^2\right) = \text{constant}$$

then at a given point (l_1) on the trajectory, the field and angle of pitch are B_1 and α_1 respectively. Then the particle will be magnetically reflected when the field seen by the particle increases to the value

$$B_m = \frac{B_1}{\sin \alpha_1{}^2} \tag{6}$$

4.2 Double Energy Analyzer Design

The double energy analyzer is formed by two directional energy analyzers, independent but in the same case. See Fig. 6. The directional Energy Analyzers are mutually perpendicular.

4.2.1 The directional energy analyzer

In Fig. 7, a directional energy analyzer is shown with the components and dimensions. The directional energy analyzer is a two grid component analyzer of retarding field design with the characteristic property that the first component selects only ions (or electrons) with

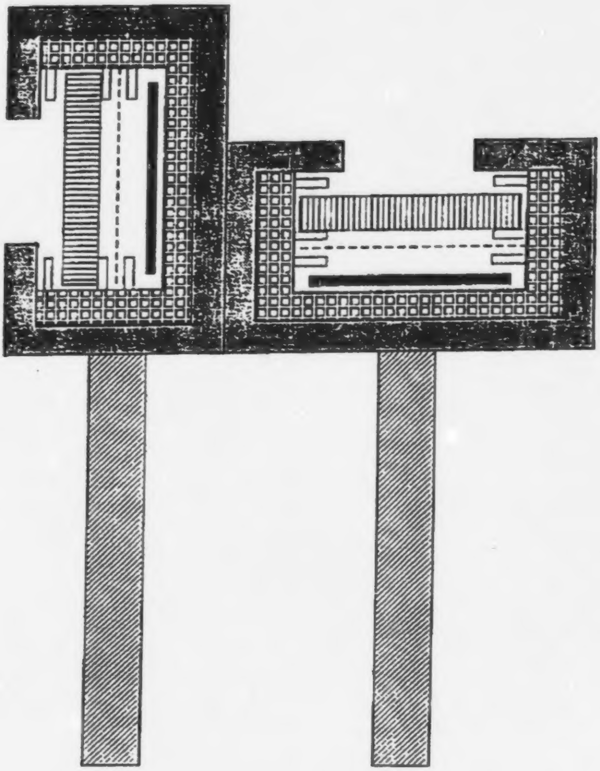

Figure 6. Double Energy Analyzer (DEA)

paraxial velocity to the analyzer to be detected, which means that it is possible to measure only ion (or electron) velocity in one direction. That direction should be parallel V_{II} (in one case), and perpendicular to the magnetic field $V_{\perp}$ (in the other case).

The directional energy analyzer follows the Stenzel [6] criteria in order to detect in the collector plate only the charged particles (electrons or ions, depending on the mode of operation of the analyzer) whose velocity is perpendicular to the collector in the analyzer. This measurement is possible because the first component is a microchannel plate facing the plasma. For ions, the first grid is electronically floating, i.e. reflects most electrons, collects most thermal ions, and passes beam ions moving along the direction of the microchannels. In the Stenzel analyzer [6], the microchannels have a diameter $d \sim 13$ mm and length $L \sim 0.6$ mm. This gives a geometric acceptance angle for ions of:

$$\theta = + \arctan (d/2L) = +0.6°$$

The transparence of the multichannel grid is about 60%. Therefore, only ions which pass the channels without impact with the walls will contribute to the collector current.

The collected ion current [7][38] is given by:

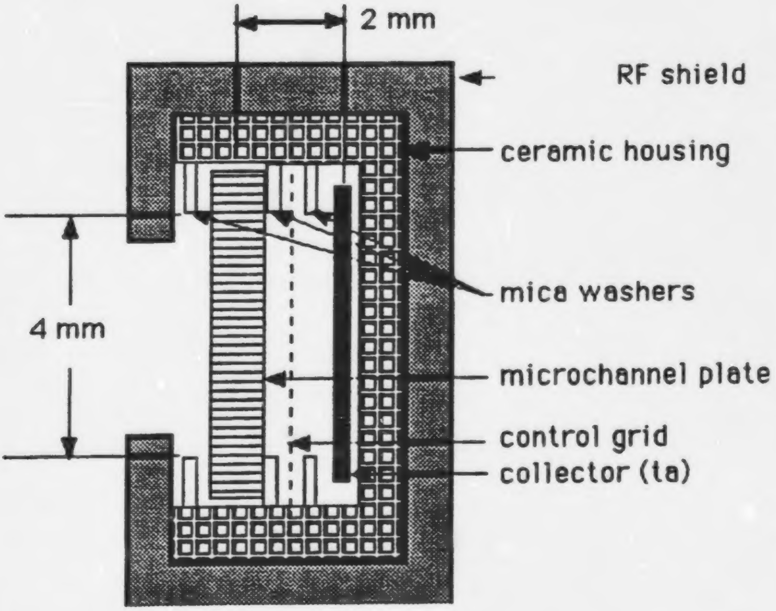
2 mm
RF shield
ceramic housing
mica washers
4 mm
microchannel plate
control grid
collector (ta)

Figure 7. Directional Energy Analyzer

$$l = Aen \int_{\infty}^{\infty} \int_{\infty}^{\infty} \int_{v_{zm}}^{\infty} v_z f(v) dv_x dv_y dv_z$$

(ignoring grid transparency factors) where A is the collector area, n the density, and *f(v)* the distribution function,

$$v_z \min = \left(2eV_g / m_i\right)^{1/2}$$

V_z min is the minimum velocity component normal to the collector surface of ions traversing the control grid potential V_g (retarding potential) in G_2.

If the ions have only one velocity component V_z, the one-dimensional distribution function is given by:

$$\frac{dl_c}{dv_g} = Aenf\left(v_{z\min}\right)$$

for the ion temperature Ti_z and a Maxwellian distribution function:

$$KT_i = \frac{e}{\dfrac{d(\ln l)}{dVg}}$$

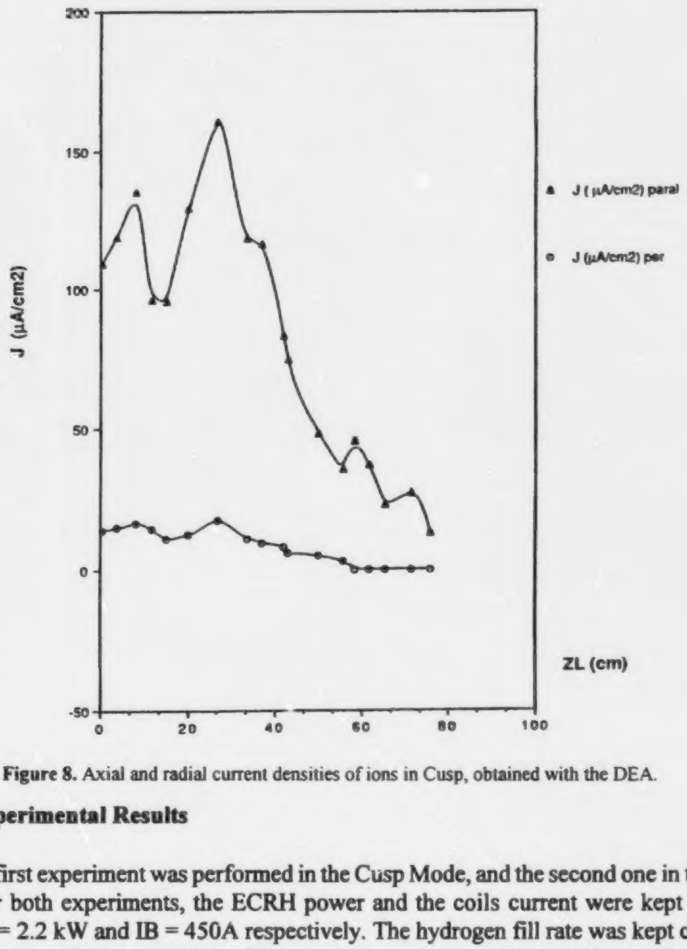

Figure 8. Axial and radial current densities of ions in Cusp, obtained with the DEA.

4.3 Experimental Results

The first experiment was performed in the Cusp Mode, and the second one in the Mirror Mode. For both experiments, the ECRH power and the coils current were kept the same, P(ERCH) = 2.2 kW and IB = 450A respectively. The hydrogen fill rate was kept constant at 5.5×10^{-5} torr, and the separation of the magnets was kept constant at 30 cm. The magnetic surface of 875 Gauss, that corresponds to an electron cyclotron frequency of 2.45 GHz, was always present.

The double energy analyzer was moved axially between the center ($ZL = 0$ cm) and the end ($ZL = 90$ cm) of the device inside the plasma at a radial position of $r = 8$ cm with respect to the center line in both cases.

From the plasma produced in the Cusp. Measurements of the plasma density n, and the ion temperature T_i, with ZL = the axial separation distance between the center of the machine and the head of the double energy analyzer were done. Fig. 8 shows J plasma current density which is proportional to plasma Flux vs. ZL.

Variations in the average kinetic energy and therefore the ion temperature in the

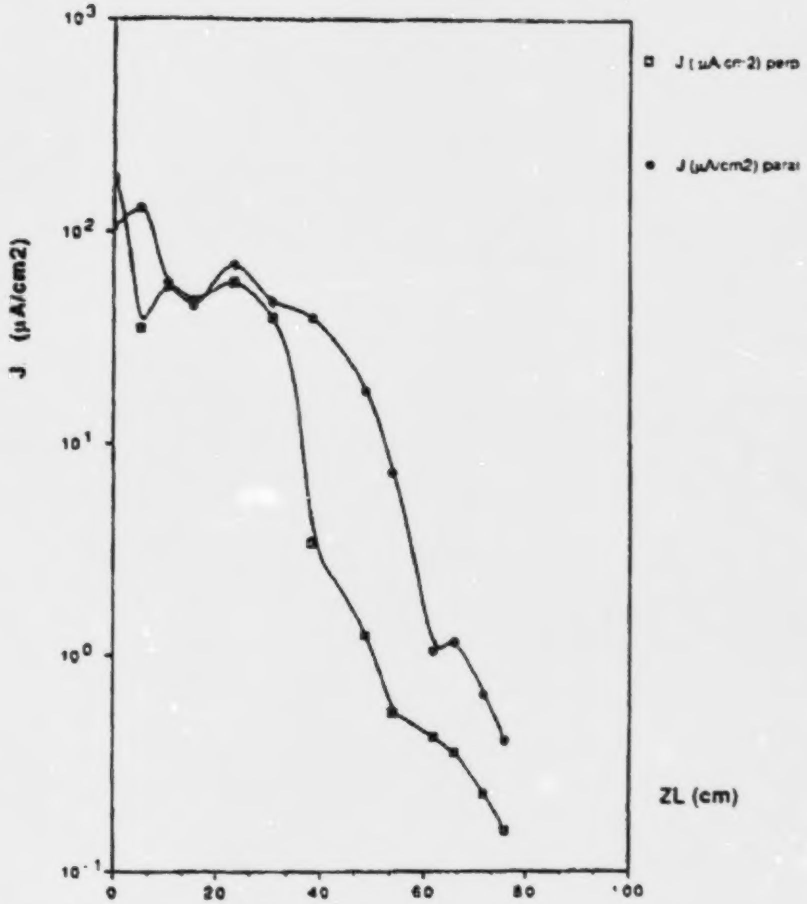

Figure 9. Axial and radial current densities of ions in mirror, obtained with the DEA.

perpendicular and in the parallel directions were measured between 1.1 eV and 7.7 eV. Densities between 1.0 × 10^{11} (m^{-3}) and 5.8 × 10^{14} (m^{-3}) were obtained with the double energy analyzer in the cusp. The same kind of experiment as just mentioned were done for the mirror configuration.

With the double energy analyzer, the perpendicular density varied from 2.3 × 10^{11} (m^{-3}) and 6.2 × 10^{13} (m^{-3}), and the parallel density varied from 1.5 × 10^{13} (m^{-3}) and 2.4 × 10^{14} (m^{-3}).

From both experiments it is clear that at the plasma edge, the perpendicular density is less than the parallel density. This fact, for the mirror and for the cusp, is clearly shown with the double energy analyzer.

In addition, Fig. 9 shows the variations of the plasma current density versus the axial separation distance are shown.

One of the more interesting results from these experiments is that the plasma is much better confined in the cusp than in the mirror. This fact can be noticed by making a comparison between the results at the same *ZL* (approximately 71 cm) from the center of the machine.

The parallel densities and the temperatures have about the same order of magnitude. But the density in the parallel direction to the axis is 2.2×10^{13} (cm^{-3}) in the mirror, and only 5.6×10^{11} (cm^{-3}) in the cusp. The axial losses are also larger in mirror.

The current density J is defined as:

$$J = e \cdot n \cdot v \text{ (Amp/cm}^2\text{)}$$

where e, is the electron charge, n is the plasma density, v is the average velocity.

A comparison at the same $ZL = 71$ cm for both machines gives:

$$\frac{J(\text{Mirror})}{J(\text{Cusp})} \text{ is approximately equal to 50}$$

4.4 Conclusions

In the cusp and mirror configurations, losses of the plasma were also measured with the double energy analyzer. Most of the particles escape from the magnetic confinement device following the magnetic field lines, however, a small fraction of particles still escape in the perpendicular direction to the magnetic field.

Although the goal of the double energy analyzer was to measure ion densities and temperatures mutually perpendicular simultaneously at the same point, information about the physics of the losses of the particles from the mirror and from the cusp has been measured directly.

The double energy analyzer is a powerful tool that helps measure the trapping and losses of plasma particles in the cusp and mirror of the M4X. This helps us understand magnetic confinement in general.

One important conclusion is that cusp confines the plasma much better in the axial direction than the Mirror. The axial losses in the mirror are approximately fifty times more than in the cusp, for the same external parameters of the machine, the same ECRH power, coil

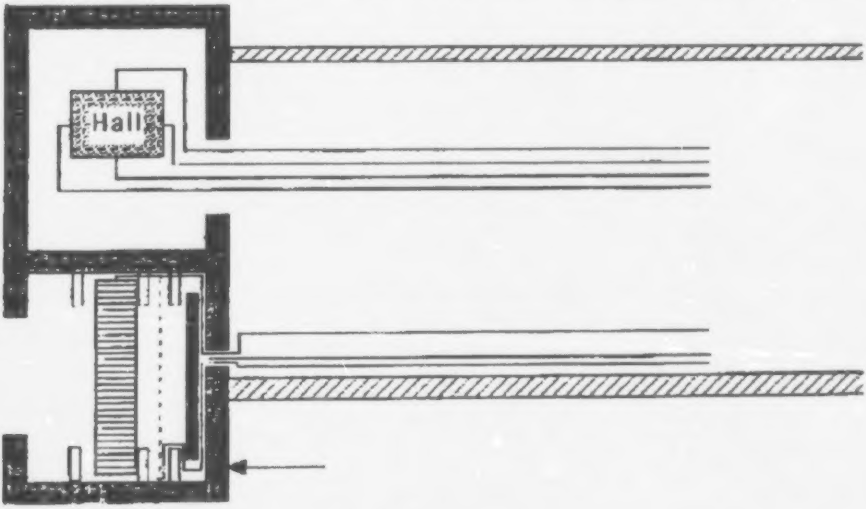

Figure 10. Diagram of the µ-Analyzer

current, hydrogen fill rate, and separation distances between the coils.

5. THE MAGNETIC MOMENT ANALYZER

The Magnetic Dipole Analyzer (μ-Analyzer) consists of two small devices measuring key parameters at the same time and location. The directional energy analyzer measures the particle kinetic energy perpendicular to the magnetic field ($W_\perp$), and the plasma density (n). The Hall probe (about 3 mm) measures the local magnetic field (B). These three parameters ($W_\perp$, n, B) are used to calculate the magnetic dipole moment (μ), the local ratio of thermal energy density to magnetic energy density (β), and the Larmor Radius ($r_\perp$).

The μ-Analyzer consists of a directional energy analyzer (miniature) [4] and a small Hall probe in the same detector case, see Fig. 10.

The μ -Analyzer can be used in Tokamaks, Stellerators, Reverse Pinch, Spheromaks, Cusps, and in Mirrors to measure μ or β directly. To the authors' knowledge, this μ-meter is the first diagnostic tool that allows such micro-measurements to be made at localized points.

This is very important for magnetized plasma systems and magnetic fusion research. Diamagnetic properties of the plasma due, for example, to hot electron ring formations may be studied with this Analyzer.

5.1 Theoretical Considerations

Definitions:

The first adiabatic invariant μ is defined [8, 9] as :

$$\bar{\mu} = \frac{W_\perp(l)}{B(l)} \hat{n}_{\parallel}$$

where:

$$\hat{n}_{\parallel} = \frac{\bar{B}}{B} = \text{unit vector parallel to the magnetic field } B,$$

and

$W_\perp = \frac{1}{2} m v_\perp^2$ is the kinetic energy of the ion mass m in the perpendicular direction to the magnetic field, $B(l)$ at the point l.

The Larmor radius is defined as $r_L = \frac{V_\perp}{|\Omega|}$ where Ω is the cyclotron frequency, and has the following values: $\Omega_2 = 1.5 \times 10^7\ B$ (Tesla) for protons and $\Omega_e = 2.3 \times 10^{10}\ B$(Tesla) for electrons.

The Larmor radius is calculated by:

$$r_L(m) = 1.5 \times 10^{-4} \frac{\sqrt{W_\perp}}{B} \qquad \text{(for protons)}$$

and

$$r_L(m) = 3.0 \times 10^{-6} \frac{\sqrt{W_\perp}}{B} \qquad \text{(for electrons)}$$

β is the thermal to magnetic energy density ratio:

$$\beta = \frac{nW_{\perp}}{\frac{B^2}{2\mu_0}}$$

where *n* is the density of the plasma (found with the energy analyzer). $W_{\perp}$ is the perpendicular kinetic energy,

$$W_{\perp} = \frac{1}{2} m v_{\perp}^2$$

and μ_o is the magnetic permeability in free space,
Also,

$$\frac{\delta B}{B} = \frac{\mu_0 2n\mu}{B} = \frac{nW_{\square}}{\frac{B^2}{2\mu_0}} = \beta$$

Thus, the gyromotion of the particles in a plasma produces a diamagnetic effect of a magnitude of approximately β.

Let α be defined as the pitch angle between the total velocity vector and the magnetic field. Also define *W* as the Kinetic energy of the particle. Thus:

$$W = \frac{1}{2} m\left(v_{\parallel}^2 + v_{\perp}^2\right) = \frac{1}{2} mv^2$$

The magnetic moment constant may then be expressed as [9, 10]:

$$\mu = \frac{\mu v_{\perp}^2}{2B} = \frac{mv^2 \sin^2 \alpha}{2B} = \frac{W \sin^2 \alpha}{B} = \text{const.}$$

5.2 The μ -Analyzer Design

The μ-Analizer consists of a directional energy analyzer beside a Hall probe. Fig.10 shows a diagram of the Analizer.

The Hall probe is inside a copper case, protected against heat from radiation and convection. The diameter of the Hall probe is les than 3 mm.

The Hall probe has been found quite useful in measuring both static and time-dependent magnetic fields.

5.3 The Directional Energy Analyzer

The directional energy analyze was described above, with the DEA.

5.4 Experimental Results

Simultaneous measurements of the plasma parameter have been made using the μ-Analyzer inside of the M4X device. These include the average kinetic energy in the perpendicular direction ($W_\perp$), the ion temperature, plasma density (n), local radial magnetic field strength (B_r), magnetic dipole moment (μ), plasma beta ($\beta_\perp$) and the Larmor radius (r_L).

Several experiments were performed using the μ-Analyzer, one of them is shown below.

This experiment was performed in the cusp mode, holding the current in the magnetic coils constant and varying the ECRH power. In all four experiments the location of the μ-Analyzer was held constant and was aligned so it measured magnetic field components parallel to the central axis of the device, and the ion energy perpendicular to the axis . The μ-Analyzer was located at $z = 8$ cm and $r = 11$ cm from the null point at the center ($z = 0$; $r = 0$), as shown in Fig. 11.

In each position, the magnetic field and the ion characteristics were measured with the μ-Analyzer, inside the plasma.

The results of measurements of the above parameters for this first experiment in the cusp configuration are shown in Table 1.

The definition of the parameters in all of the Tables are :
P (kW) = the ECH transmitted power .
Current (A) = I_B (A) = the magnet coil current .
W (eV) = the perpendicular kinetic energy of the ions
I_s (mA) = the saturation current in the collector of the Analyzer..
n (m^{-3}) = the ion density measured with the Analyzer
V Hall (mV) = the output voltage from the Hall probe.
B_r (Tesla) = the Magnetic field measured with the μ-Meter inside the plasma.
μ (A-m^2) = the local Magnetic Dipole Moment.
β (%) = the local relation between the perpendicular kinetic presure and the magnetic presure in (%).
r_L (cm) = is the local Larmor radius.

Remember that the magnetic field in the center of the cusp or null point is zero, hence one would measure a beta of infinity at the null. Values for the Larmor radius between 0.32 cm. and 1.08 cm were obtained. The Debye length of this plasma was $\lambda D = 8.5 \times 10^{-2}$ cm.

The values of μ and the Larmor radius agree with the theoretical estimates, however this experiment was the first attempt to measure locally these parameters. With regard to the

Table I. Cusp configuration with constant coil current.

Power (kW)	Current (A)	W (eV)	n (m^{-3})	B_r (Tesla)	μ (A-m^2)	β (%)	r_L (cm)
3	420	3.25	1.6×10^{14}	0.115	4.5×10^{-18}	16.31	0.36
2.5	420	3.35	1.7×10^{14}	0.095	5.6×10^{-18}	25.00.	0.45
2	420	3.37	1.7×10^{14}	0.085	6.3×10^{-18}	31.54	0.50
1.5	420	4.50	2.2×10^{14}	0.08	9.0×10^{-18}	63.62	0.61
1	420	3.63	1.8×10^{14}	0.08	7.3×10^{-18}	41.40	0.55
0.5	420	3.25	1.6×10^{14}	0.08	6.5×10^{-18}	33.26	0.52

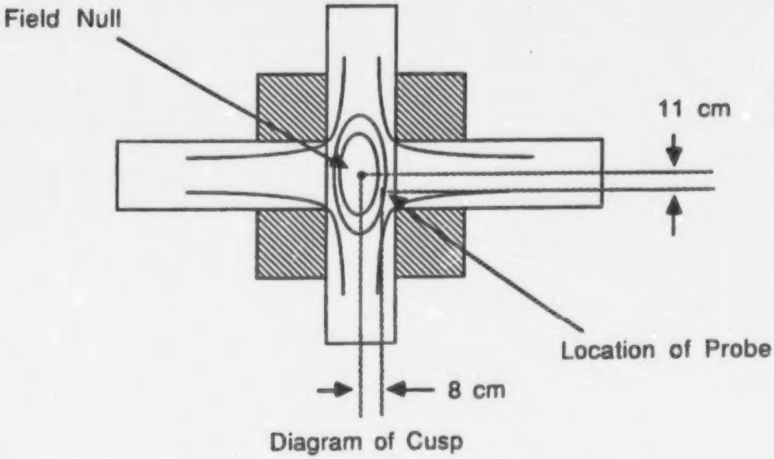

Figure 11. Location of the μ-analyzer in the plasma vessel.

measurements of β, there are several definitions of it, but this experiment with the μ- Analyzer, is the first attempt to measure locally the β-parameter.

5.5 Conclusions on μ-Analyzer

The μ-Analyzer, allows simultaneous measurement of the ion temperature and the magnetic field at the same spot, and at the same time. The operational performance was observed experimentally inside magnetized plasmas.

The local Magnetic Dipole Moment obtained in the cusp experiment while holding constant the coil current of 420A and varying the ECRH power, was less than 9×10^{-18} (A-m^2), a local beta maximum of 63.62%, and a Larmor radius less than 0.61 cm.

The μ-Analyzer is a very important tool for studies of the magnetic confinement in plasma devices that are used in fusion research: tokamacks, stellerators, cusps, tandem mirrors, reverse pinch mirrors, etc.

The μ-Analyzer has, in a localized point, the ability to find the β-parameter, and the μ diamagnetic moment (first adiabatic invariant) of the plasma, with these parameters we can calculate the Larmor radius.

6. THE HYPERBOLIC ENERGY ANALYZER (HEA)

This new energy analyzer consists of three components: a plane parallel disc with interchangeable diameter orifices for rejection of electrons and collimating the ion beam, a hyperbolic lens for particle energy selection and beam focusing, and a Faraday Cup as the collector (see Fig. 12).

A hyperbolic cross-section lens was chosen because we know from electron optics [12–14] that equipotential surfaces in the vicinity of a diaphragm are hyperboloids of revolution, and the saddle point is crossed by straight lines. An angle of 54°–44' between the straight lines and the axis at the saddle point was used for design the hyperbolic lens.

If a potential, V_R, which can be calculated, is imposed on the saddle point, then only

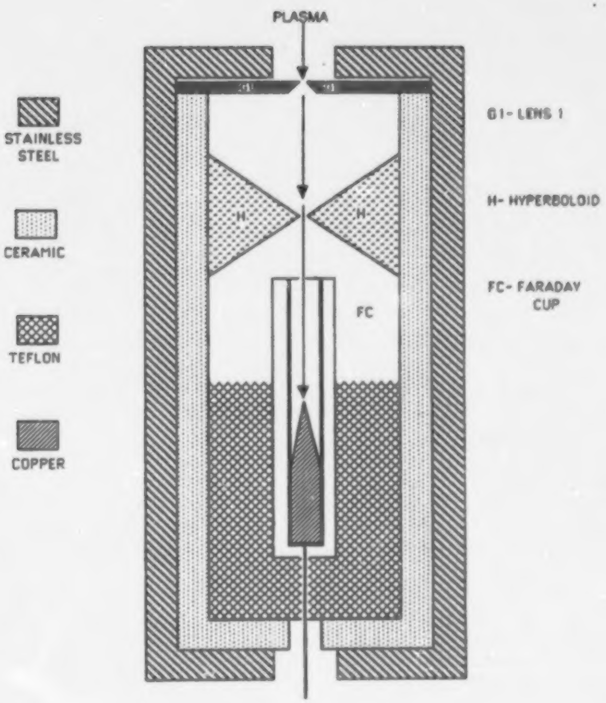

Figure 12. Design of the Hyperbolic Energy Analyzer (HEA)

paraxial ions with energy greater than qV_R can pass through the lens into the Faraday Cup. The remainder of the ions are discriminated against by the repulsive electric field resulting from the adjustable voltage applied to the hyperboloidal lens. Thus, the use of grids is avoided. The hyperbolic energy analyzer has none of limitations of gridded energy analyzers. It can be used to measure hot and thermal electron and ion temperature, electron and ion density, plasma potential, and electron and ion distribution functions.

All of these parameters can be measured by externally changing only the polarity and magnitude of the potential applied to the hyperboloic lens.

This Hyperbolic lens will function essentially the same as an Einzel lens.

In this way, a lens that has the Hyperbolic shape will have convergent properties like the Einzel lens because the equipotentials are parallel to the surfaces of the hyperbolic lens, and with only one external bias will give a potential at the saddle point. Therefore, a sweep potential on the Hyperbolic lens provides a sweep potential on the saddle point. In other words, the Hyperbolic Lens will produce selection of energy of the beam, and will focus it at the same time, with only one bias.

Use of only one bias by the Hyperbolic lens is an additional practical advantage over the Einzel lens.

Applying a retarding potential, V_{Ret}, to the hyperbolic lens is the same as applying it to the saddle pointis. Then, only paraxial charged particles with larger kinetic energy than the electrostatic retarding potential energy of the saddle point can reach the Faraday Cup.

The Hyperbolic energy analyzer will focus and select the beam energy like a retarding potential analyzer.

6.1 Design

Figure 10 shows the design of the hyperbolic energy analyzer. The lens L1 or collimator aperture and Faraday Cup are inside a stainless steel box for shielding from external RF fields. The hyperbolic lens are made of copper .

6.2 Experimental Arrangement

The set up of the circuit follows the idea of using a sweep voltage to the hyperbolic lens in order to produce the retarding potential. We have done these experiments using a BOP (Bipolar operational power) for the sweep voltage, between –1000 V and 1000 V

The aperture L1 can be at a floating potential for ions or at the plasma potential for electrons.

The Faraday Cup was biased to +67.5 Volts for electrons and to -67.5 Volts for ions, in order to collect the current.

The plasma parameters and the ion energy distribution function were obtained with the HEA.

6.3 Results

Several experiments were performed using the M4X as a cusp, and also as a mirror. Only results from two of them are shown bellow.

The HEA was used for detection of electrons and ions in the mirror ring (the region between the two coils where the hot ions or electrons are formed, normally off the axis in the radial direction). In our experiment, the HEA was located in a mirror ring of $R = 30$ cm from the center

Additionally, the HEA was used to study hot electron rings in the cusp mode at various radial distances from the null point, which results will be published elsewhere.

In all cases the plasma was at steady state and stable.

We assumed that the plasma outside and inside the analyzers obeyed the Vlasov equation, and therefore the distribution functions were Maxwellian.

6.4 First Experiment

The first experiment was set up in order to analyze electrons produced from the Mirror, with the current in the coils kept constant at 450A, and 2.4 kW of ECRH transmitted power. The neutral pressure of hydrogen was kept constant at 5.7×10^{-5} Torr.

The lens L1 of the HEA was biased at $V_L = 10$ Volts, the Hyperbolic lens were swept with a bipolar operational power (BOP), from -200 Volts to +200 Volts. The Faraday Cup was biased at +67.5 Volts. The current collected from the Faraday Cup was plotted on an X-Y recorder against the retarding potential of the Hyperbolic lens.

The Energy distribution function for electrons and the Characteristic curves of the HEA are shown in Fig. 13.

The main findings from this experiment at P (ECRH) = 2.4 kW is the fact that two populations of electrons were found. The warm electron population with a temperature of

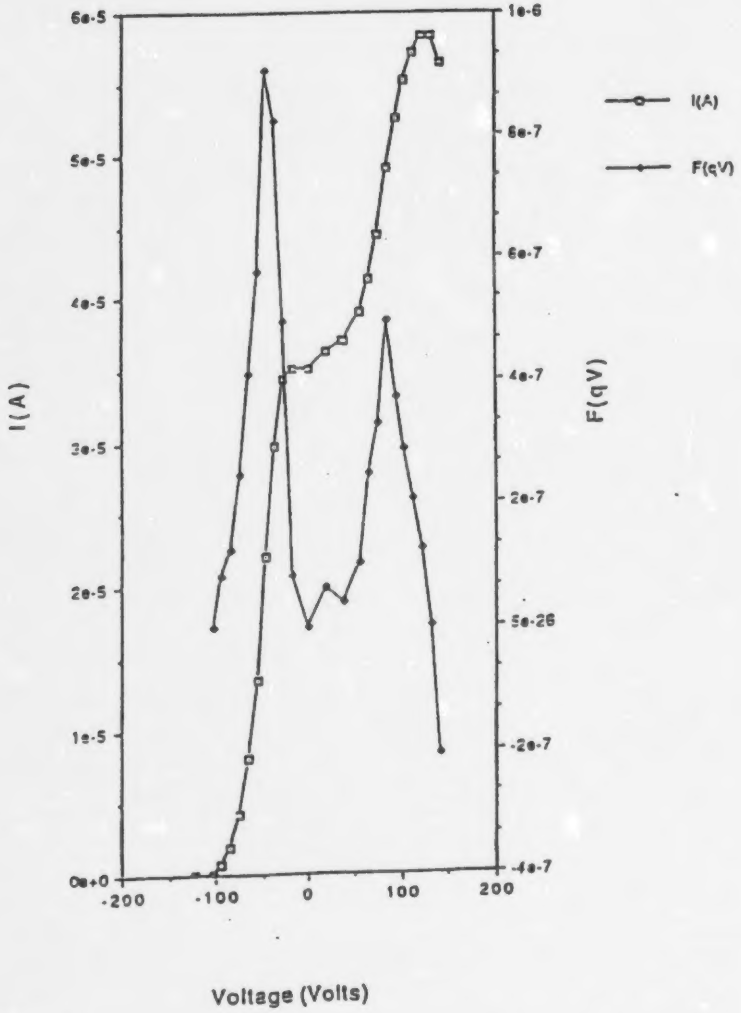

Figure 13. Characterustuc *I* vs *V* and energy distribtion function for electrons using the HEA in the mirro mode of M4X, at 2.4 kW of ECRH power.

106 eV and a density of 2.4×10^{15} (m^{-3}), and the cold electrons with a temperature of 15 eV and density of 4.2×10^{15} (m^{-3}) were measured with the HEA for the case of 2.4 kW in the mirror ring.

6.5 Second Experiment

The second experiment was performed in the cusp mode with the same current in the coils as before, but for ions.

Ion's temperature are measured using HEA. Fig. 14 shows that the Ion Temperature

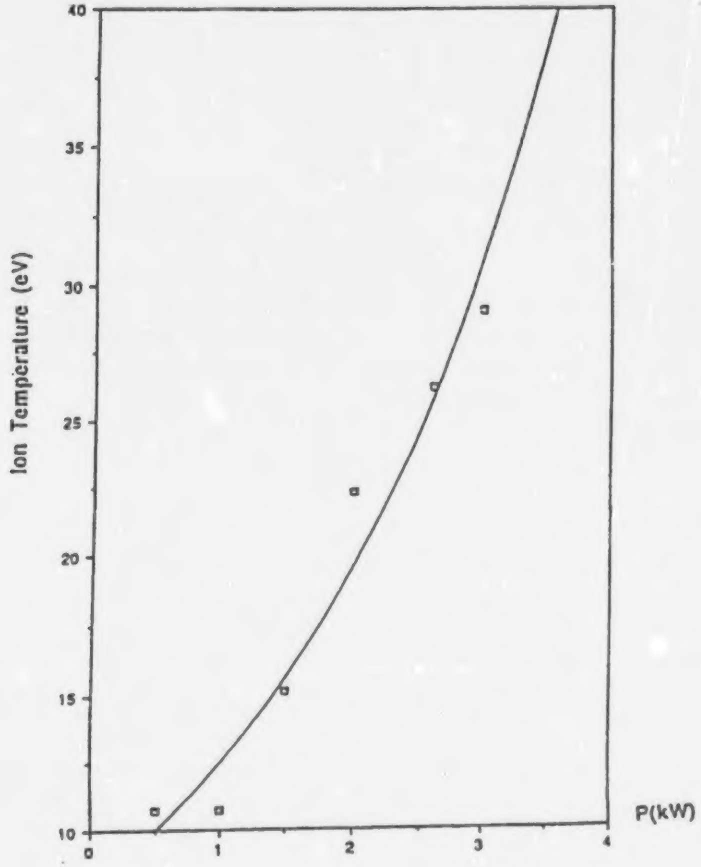

Figure 14. Ion temperature in cusp line, for different ECH power.

increases with the ECRH power.

6.6 Conclusions from the HEA

The novel analyzer called the Hyperbolic Energy Analyzer (HEA), has been tested, showing clearly the detection of electrons and ions. Results from the HEA have also shown agreement with the VEA, the Langmuir probe, the ion energy analyzers, and the electron energy analyzers.

The goal of this work was to demonstrate that the HEA performs as an energy analyzer. The existence of two populations of electrons in the Mirror Mode was measured clearly with the HEA.

The warm electrons have a temperature of 106 eV, and a density of $2.4 \times 10^{15}(m^{-3})$, and the cold electrons have a temperature of 15 eV and a density of $4.2x\ 10^{15}\ (m^{-3})$ as measured by the HEA for the case of 2.4 kW in the mirror ring. The HEA is the only analyzer that we have used as an electron and ion analyzer. Without any internal modification, the HEA may be used for high density plasma diagnostics, because it does not requires meshes.

Table 2 shows a comparison of the measurements of several plasma parameters in the cusp mode using the different Analyzers. The results show a good agreement in the values measured with each one of them.

Table 2. Comparison of several plasma parameter measured with VEA, DEA, and μ-analyzer

ANALYZER	P (kW)	I_B (A)	n (m^{-3})	T_i (eV)	r (cm)	Z (cm)
VEA	2.2	398	6.7×10^{14}	3.3	11	12
DEA	2.2	450	1.1×10^{14}	3.5	11	8.1
MUA	2.4	420	4.2×10^{14}	4.3	11	8.0

REFERENCES

1. E. Leal-Quiros. Geometry Variable Energy Analyzer of Retarding Field, USB, 81, 39. Physics Department, Simon Bolivar University, Caracas, Venezuela.
2. R.J. Taylor. Ph.D. Thesis, UCLA (1970); H. Ikezi and R.J. Taylor. J. Appl Phys. **41**, 738 (1970).
3. De Neef and Theiss. Rev. Sci. Instrum. **50**, 3 (1979).
4. R.L. Stenzel, R. Williams, R. Aguero, K. Kitazaki, A. Ling, T. McDonald and J. Spitzer. Rev. Sci. Instrum. **53**, 7 (1982).
5. G. Donoso. (Private Communication).
6. J.T. Tate., Phys. Rev. **17**, 394 (1921).
7. H.M. Kudyan, Rev Sci Instrum. **49**, 8 (1979).
8. N.A. Krall and A.W. Trivelpiece. Principles of Plasma Physics, McGraw Hill (1973).
9. Weston M. Stacey. Fusion Plasma Analysis, John Wiley (1981).
10. F. Chen. Plasma Phys. **214** A, B and C Lecture notes, UCLA, 1985–86.
11. J. F. Kunze, M. A. Prelas, T. J. Dolan, P. Bennet, J. Freeman, L. Haynes, J. Hwaug, S. McGhee and R. Roberts. Nuclear Tech. Fusion **10**, 1034 (1986).
12. F. Ollendorff. Technische Elektrodynamik Band II/1, Elecktronik Des Einzelelektron. Wien, Springer Verlag (1955).
13. K. R. Spangenberg. Vacuum Tubes. New York, McGraw-Hill (1948).
14. M. Wilmers Instrumentation I, and II. Lecture notes Department of Physics, National University of Colombia, Bogota (1974).
15. E. Leal-Quiros. Geometry Variable Energy Analyzer of Retarding Field, Spring College on Plasma Physics, ICTP, Trieste (1983).
16. R.L. Stenzel et al. Rev Sci Instrum **53**, 10227
17. Kwok Leung Lam. Private communication.

CENTRIFUGALLY CONFINED PLASMAS: ENHANCED STABILITY SCENARIOS

M.G. Jackson[1], B.R. Osborn, R.F. Ellis and A.B. Hassam

Institute for Plasma Research
University of Maryland, College Park
College Park, Maryland 20742, U.S.A.
[1]Duke University
Durham, North Carolina 27708, U.S.A.

ABSTRACT

Centrifugally Confined Plasmas (CCP) are desirable as fusion reactors because they can be made steady state, are disruption-free, may exhibit enhanced confinement, and have a simpler magnetic configuration. The disadvantage of CCP's is required circulating power. The simple magnetic configuration comes from the fact that the toroidal magnetic field, B_t required could be smaller than the poloidal field, B_p. In previous work, it was estimated that $B_t \sim B_p$ would be required to suppress a residual MHD wobble. By taking advantage of plasma elongation, we argue that the residual wobble could be eliminated for modest Mach numbers and that the resulting configuration could be stabilized completely for $B_t \ll B_p$. This makes CCP's considerably more attractive for fusion.

1. INTRODUCTION

Centrifugally confined plasmas [1–4] (CCP) are of much interest to fusion because they have several advantages over tokamak-based designs. The basic idea is that the inertial forces $\rho\mathbf{u}\cdot\nabla\mathbf{u}$ provide confinement along the field lines, allowing one to re-examine "open" magnetic confinement systems such as mirrors. In simple schemes, the plasma is confined to the outboard side of the torus as a result of the centrifugal confinement. This allows the possibility that a current-carrying coil can be positioned on the inboard side of the torus resulting in a steady-state device. This confinement feature is in addition to the other desirable aspects of a CCP, namely, that velocity shear suppresses macro- and microinstabilities, with associated improved transport [3, 5–7], as recent experimental evidence has shown [8]. The fact that MHD instabilities might be suppressed, in particular the dangerous flute instability, implies that one may be able to operate with a weak toroidal field, or perhaps without one. This results in a greatly simplified coil design [3].

In previous work [3], two basic designs for CCP's for thermonuclear fusion were

Current Trends in International Fusion Research — Proceedings of the Second Symposium
Edited by E. Panarella. NRC Research Press, National Research Council of Canada, Ottawa, ON K1A 0R6, Canada. 1999.

explored. These designs are the single and multicoil geometries, shown in Figs. 1 and 2. The grey shade in these figures indicates centrifugally stratified plasma. Both these geometries are susceptible to the flute instability but the idea was that velocity shear, v', would stabilize this mode. A model numerical simulation was carried out to test this notion [3,7] (the theoretical basis for this is described in the next section). The simulation showed that v' was very effective in stabilizing flute instabilities, but that the stabilization was not complete: there was a residual wobble that seemed unavoidable. It was therefore concluded that a toroidal magnetic field, of order $B_t \sim B_p$, would have to be included in the design. Though this is a weaker field than in a tokamak (wherein $B_t \approx 3$–$4\, B_p$), a finite toroidal field is nonetheless undesirable from the viewpoint of simplicity.

In this report, we present subsequent work which suggests that the amount of B_t required might actually be considerably less than B_p. This conclusion is based on three aspects that we have examined more thoroughly since the first paper. These aspects are: (A) a plausible reason for the underlying cause of the residual wobble mentioned above; (B) utilization of the stabilizing effect of elongation on the interchange mode; (C) a detailed understanding of the Kelvin-Helmholtz instability. We use (A)–(C) above in optimal fashion to present a greatly improved design and to suggest a possible path for a CCP fusion reactor.

The outline of this report is as follows. In the next section, we give a theoretical background to elucidate aspects (A)–(C). In section 3, we present the improved design.

2. THEORETICAL BACKGROUND

In this section, we expand on items (A), (B), (C) discussed in the introduction.

2.1 The Residual Wobble in the v' Stabilized Flutes

The flute interchange mode is related to the Rayleigh-Taylor (RT) instability. This mode is the ideal MHD interchange of flux tubes resulting in a release of gravitational potential energy if the density gradient is inverted with respect to the gravitational acceleration **g**. The growth rate for this mode is $\sqrt{g/L_n}$ where L_n is the density gradient scale. As detailed in [6], in the presence of a velocity shear, v', the stability criterion is

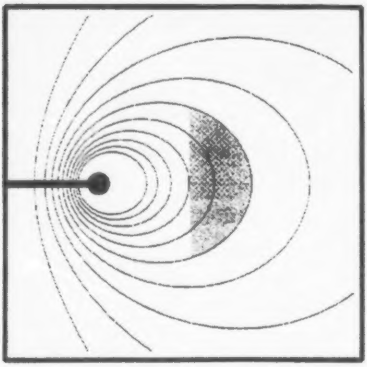

Figure 1. Single Coil Design

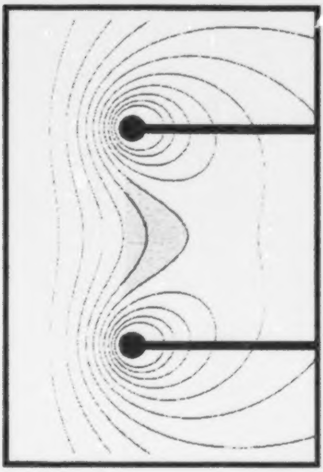

Figure 2. Double Coil Design

$$|v'| > \sqrt{(g/L_n)\ln R} \tag{1}$$

where $R \gg 1$ is the Reynolds number defined roughly as

$$R = L_n c_s / \mu \tag{2}$$

and μ is the viscosity. For rotating plasmas, the **g** is now due to the thermal centripetal acceleration, c_s^2 / L_n, and the velocity shear is of the same order as v/L_n. (There is also a centripetal acceleration from the rotation itself. Instability from this acceleration is related to instability of Couette flow. We discuss the latter in more detail in Section 3.3.) Hence (1) can be rewritten as

$$v/L_n \geq c_s / L_n \sqrt{\ln R} \tag{3}$$

$$\Rightarrow M_s > \sqrt{\ln R} \tag{4}$$

For a typical reactor $R \approx 10^8$, making $\ln R \approx 18$. Hence $M_s \geq 4$.

In previous work, we studied numerically the v' stabilization of RT type modes[3,7]. We ran cases for $M_2 \approx 1$–2.5 and found much stabilization from v' but there was a residual wobble that could not be eliminated. Based on the ln R factor above, we now believe that it is quite possible we did not go to large enough M_s. In what follows, we will take as our working assumption that the residual wobble comes from the ln R effect.

In our previous paper, we concluded that a toroidal field, $B_t \leq B_p$, would be needed to suppress the wobble. This was based on the idea that, for $M_s^2 > 1$, the centripetal acceleration above goes from $c_s^2 / L_n \rightarrow v^2 / L_n$. Thus, the corresponding equation to (3) would suggest no stability for any M_s. We therefore concluded that only magnetic shear would suppress the wobble - a simple Suydam type analysis then resulted in $B_t \leq B_p$ as a requirement.

2.2 Effect of Elongation

In the literature on FRC's [9], it is well known that an elongated plasma cross-section is favorable for MHD stability. Consider an elongated cross section of dimensions a and b with $a < b$. Then the maximum field-line curvature is of order a. Thus $g_{\max} \approx c_s^2 / a$. However, in the "straight section", the curvature is very small. Thus, $\langle g \rangle \sim g_{\max}(a/b) \sim c_s^2/b$. Since $L_n \sim a$, the RT growth rate $\sim c_s^2/ab$. Now $v' \sim v/a$. Thus, if we use all this in (1), we find we need

$$M_s > \sqrt{(\ln R)/E} \tag{5}$$

where $E \equiv b/a$ is the elongation.

In this paper, we have taken into account the advantage of having $E > 1$. In a reactor design, $E \sim \ln R \approx 18$ may not be out of the question. A possible fusion reactor design, shown in Fig. 3, is constructed to exploit this feature. The straight section is, in fact, desirable for a fusion reactor.

2.3 The Kelvin-Helmholtz Instability

One concern in a large aspect ratio design, like the one in Fig. 3, is the Kelvin-Helmholtz (KH) Instability [10]. Our geometry of Fig. 3 is almost the same as the geometry for Taylor-

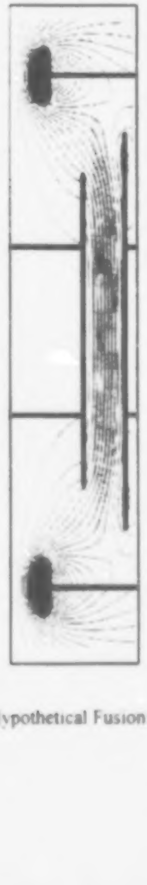

Figure 3. Hypothetical Fusion Reactor Design

Couette Flow or "Dean Flow". It is well known that Taylor-Couette Flow is unstable for wavenumbers non-zero in the direction of our magnetic field [10]. Since **B** is strong in our case, these wavenumbers will not be unstable. If the KH, or Taylor-Couette, were unstable, the maximum growth rate of the KH would be of $O(v/a)$. Since there is no inflection point in $v(R)$, the KH does not grow at the above "ideal" rate; rather, $\gamma_{KH} \sim (v/a)R^{-\alpha}$, $0 < \alpha < 1$, where R is the Reynolds number. Thus, in the Fig. 3 design, the KH might be unstable *but only weakly so*. As such, B_t might still be needed, but $B_t \sim B_p/R^{\alpha}$ might be sufficient. This toroidal field is extremely weak and should present no significant complication in coil design.

3. MODIFIED DESIGN FOR CCP

We have investigated the design of a CCP fusion reactor which takes advantage of the enhanced understanding of the three aspects described in the previous section. Specifically, we proceed on the assumption that the residual wobble seen in the numerical simulations results from the fact that M_s is not large enough to overcome the ln R effect to date. Very large M_s is undesirable. We, therefore, use elongation E to reduce the growth rate and weaken the requirement on M_s. The resulting design is of an elongated geometry as in Fig. 3. The desirable Mach number requirement for stability is

$$M_s > \sqrt{(\ln R)/E} \tag{6}$$

Hence the flute may be completely suppressed for mildly supersonic flow, and any KH could be eliminated by a very weak B_t.

The fact that all MHD instabilities would be eliminated for very small B_t implies a coil design that is very much simplified. A reactor with this coil structure (Figure 3) is very desirable.

ACKNOWLEDGMENTS

Work supported by Department of Energy (DOE), MGJ supported by NUF Fellowship from Princeton Plasma Physics Laboratory (PPPL).

REFERENCES

1. J.M. Wilcox. Rev. of Mod. Phys. **31**, 1045 (1959).
2. B. Lehnert. Nucl. Fusion **11**, 485 (1971).
3. A.B. Hassam. Comments in Plasma Phys. Controlled Fusion **18**, 263 (1997).
4. R.F. Ellis and A.B. Hassam. ICC Workshop, PPPL, Princeton (1998).
5. H. Biglari, P.H. Diamond and P.W. Terry. Phys. Fluids B **2**, 1 (1990).
6. A.B. Hassam. Phys. Fluids B **4**, 485 (1992).
7. A.B. Hassam and Ramin Sina. ICC Workshop, PPPL, Princeton (1998), under preparation for publication.
8. R.J. Groebner. Phys. Fluids B **5**, 2343 (1993).
9. M. Tuszewski. Nucl. Fusion **28**, 2033 (1988).
10. S. Chandrasekhar. Hydrodynamic and Hydromagnetic Stability, (Oxford University Press, Oxford, England, 1961).

CONFINEMENT OF A ROTATING DEGENERATE GAS OF IONS IN A MAGNETIC FIELD

Vincenzo Molinari and Domiziano Mostacci

Laboratorio di Ingegneria Nucleare
Università di Bologna
Via dei Colli 16
40136 Bologna, ITALY

A cylindrically symmetric, rotating gas of ions (e.g., Deuterium ions) in an axial magnetic field is considered, of density and temperature such that degeneracy effects cannot be neglected. In the framework of Bose-Einstein statistics, starting from the quantum modified Boltzmann equation, as obtained by Uehling and Uhlenbeck, [1,2] with the help of Boltzmann's H-theorem a relation is obtained between density and self- consistent electric field (analogous to the Boltzmann factor of the classical case), and a necessary condition for confinement is derived: confinement is found to depend on the difference between rotation frequency and cyclotron frequency. The relation between density and self-consistent electric field can be solved together with Poisson's equation, at least in principle, yielding the potential and density distributions in space. Quantum mechanical effects are shown to produce an increase in the equilibrium density of ions in the core of the rotating column, at temperatures not greatly exceeding Bose's critical temperature. The results give indications that could be useful in the confinement problems arising in fusion studies. As quantum effects become more and more important as temperature decreases, and as they lead to the above mentioned marked increase in density in the core of the column, this may suggest that a beam of Deuterium ions could be made very dense by keeping its temperature close to Bose's condensation point.

REFERENCES

1. E.A. Uehling and G.E. Uhlenbeck. Phys. Rev. 43, 552 (1933).
2. R.L. Liboff. Kinetic Theory: Classical, Quantum and Relativistic Descriptions (Englewood Cliffs, USA, 1991).

Current Trends in International FusionResearch — Proceedings of the Second Symposium
Edited by E. Panarella. NRC Research Press, National Research Council of Canada, Ottawa, ON K1A 0R6, Canada. 1999.

MAGNETIC COMPRESSION/MAGNETIZED TARGET FUSION (MAGO/MTF): A MARRIAGE OF INERTIAL AND MAGNETIC CONFINEMENT

Irvin Lindemuth, Carl Ekdahl, Ronald Kirkpatrick, Robert Reinovsky, Richard Siemon, Peter Sheehey, Frederick Wysocki, Vladimir Chernyshev[1], Vladislav Mokhov[1], Anatoli Demin[1], Sergei Garanin[1], Victor Korchagin[1], Ivan Morozov[1], Valerii Yakubov[1], James Hammer[2], Dmitri Ryutov[2], Arthur Toor[2], Chris Deeney[3], Dillon McDaniel[3], James Degnan[4], Gerald Kiuttu[4] and Robert Peterkin, Jr.[4]

Los Alamos National Laboratory (LANL)
Los Alamos, NM 87545, U.S.A.
[1]All-Russian Scientific Research Institute of Experimental Physics (VNIIEF)
Sarov, Russia
[2]Lawrence Livermore National Laboratory (LLNL)
Livermore, CA 94551, U.S.A.
[3]Sandia National Laboratories (SNLA)
Albuquerque, NM 87123, U.S.A.
[4]Phillips Laboratory (PL)
Albuquerque, NM 87123, U.S.A.

Intermediate between magnetic confinement (MFE) and inertial confinement (ICF) in time and density scales is an area of research now known in the US as magnetized target fusion (MTF) and in Russia as MAGO (MAGnitnoye Obzhatiye-magnetic compression). MAGO/MTF uses a magnetic field and a preheated, wall-confined plasma within an implodable fusion target. The magnetic field suppresses thermal conduction losses in the fuel during the target implosion and hydrodynamic compression heating process. The high initial adiabat of the preheated, magnetized fuel and the quasi-adiabatic compression of the fuel make it possible in principle to reach ignition temperatures at modest convergence ratios without strong, precisely timed shocks.

MAGO/MTF includes, but is not limited to, some previously reported concepts in imploding liner fusion and impact fusion and includes the electron-beam driven "phi" targets. Although the possible benefit of a magnetic field in a fusion target was recognized in the 40's by Fermi at Los Alamos and at approximately the same time by Sakharov in the former Soviet Union, it is only in light of recent advancements in plasma formation techniques, implosion system drivers, plasma diagnostics, and large scale numerical simulation capabilities that the prospects for fusion ignition using this approach can be evaluated.

In contrast to direct, hydrodynamic compression of initially ambient-temperature fuel,

Current Trends in International Fusion Research — Proceedings of the Second Symposium
Edited by E. Panarella. NRC Research Press, National Research Council of Canada, Ottawa, ON K1A 0R6, Canada. 1999.

MAGO/MTF involves two steps: (a) formation of a warm (e.g., 100 eV or higher), magnetized (e.g., 100 kG) plasma within a fusion target prior to implosion; (b) subsequent quasi-adiabatic compression by an imploding pusher, of which a magnetically driven imploding liner is one example. The magneto-thermal insulation of the fuel permits lower implosion velocities than are required for unmagnetized fuel. Furthermore, because the implosion process is quasi-adiabatic, the radial convergence ratio of a MAGO/MTF target may be lower than 10:1, depending upon the temperature achieved in the formation stage. Because the magnetic field is amplified under implosion conditions, it may become large enough to trap charged fusion products and enhance fuel self-heating. Therefore, the areal density required to achieve fusion ignition potentially is substantially reduced. Because the implosion process substantially reduces the fuel burn time, when compared to non-imploded configurations, simple plasma formation and magnetization schemes can be considered.

Perhaps the simplest plasma formation candidate is a cryogenic fiber z pinch. Two-dimensional computations show that the m=0 instabilities that prevented such a z-pinch from reaching fusion conditions directly [1] actually provide a mechanism for the pinch to form a Kadomtsev-stable, wall-confined plasma suitable for subsequent implosion. Fiber-formed z-pinch experiments are underway on the COLT (LANL) capacitor bank (100 kV, 2 MA, 200 kJ) to confirm these predictions [2].

Liner implosion experiments relevant to MAGO/MTF are being designed for the SATURN (SNLA), SHIVA-STAR (PL), and PEGASUS (LANL) facilities. Integrated liner-on plasma experiments are also being considered for these facilities. SATURN experiments will use a new, "slow" mode of operation that permits experiments on a microsecond time scale. Quasi- spherical liner implosions have already been demonstrated on SHIVA STAR, [3] and an auxiliary plasma formation bank is operational. Precision cylindrical solid-liner implosions have been demonstrated on PEGASUS [4].

A series of experiments using a unique plasma formation chamber have been conducted in the US and Russia [5]. A suite of plasma diagnostics, including inductive probes, plasma interferometry, spectrometry, and x-ray diodes, provides evidence of the formation of a $>10^{18}/cm^3$, 150 – 300 eV, 200 kG plasma, although the impurity content and lifetime of the plasma remain uncertain. During the dynamic phase of the experiment, up to 4×10^{13} isotropic fusion neutrons are produced.

VNIIEF-developed magnetic flux compression generators provide a means for driving target implosions at energy levels more than an order of magnitude higher than any other existing or near-term target driver and appear to provide sufficient energy for tests of the MTF concept at the scale required for significant fusion gain. Generators delivering over 200 MJ of electrical energy have been demonstrated [6] and used to couple more than 25 MJ of kinetic energy to a cylindrical magnetically driven imploding liner.

Near-term experiments with flux compression generators and laboratory pulsed power devices could benchmark calculations and test critical issues such as the mix of wall/insulator material with the fuel. These experiments would be at the appropriate plasma conditions to allow proof- of-principal tests of MTF as a path to fusion. For fusion reactor scenarios, major engineering design and major capital expenditures to replace the one-shot flux-compression generators with a fixed, repetitive pulsed power facility would occur only after ignition and substantial fuel burn-up have been demonstrated.

REFERENCES

1. P. Sheehey et al. Phys. Fluids **B4**, 3698 (1992).
2. R. Kirkpatrick et al. Proposed Generation and Compression of a Target Plasma for MTF, in Digest of Technical Papers – Tenth IEEE International Pulsed Power Conference, edited by W. Baker and G. Cooperstein (IEEE, Piscataway NJ, 1995).
3. J. Degnan et al. Phys. Rev. Lett. **74**, 98 (1995).
4. M. Hockaday et al. Liner Target Interaction Experiments on Pegasus-II, in Digest of Technical Papers-Tenth IEEE International Pulsed Power Conference, edited by W. Baker and G. Cooperstein (IEEE, Piscataway NJ, 1995).
5. I. Lindemuth et al. Phys. Rev. Lett. **75**, 1953 (1995).
6. V. Chernyshev et al. Megagauss Fields and Pulsed Power Systems, edited by V. Titov and G. Shvetsov (Nova Science Publishers, New York, 1990).

HOHLRAUM TARGETS DRIVEN BY CLUSTER ION BEAMS FOR INERTIAL CONFINEMENT FUSION

C. Deutsch, N.A. Tahir, 0. Geb[1] and J.A. Maruhn[1]

Laboratoire de Physique des Gaz et des Plasmas
Bât. 212, Université Paris XI
91405 Orsay, France
[1]Institüt für Theoretische Physik
Postfach 111932, Universitat Frankfurt
60054 Frankfurt, Germany

Correlated ion stopping of charged debris resulting from the fragmentation of energetic cluster ions focused on Au foam converters is considered for driving indirectly a thermonuclear capsule. The 1 D simulation of converter time evolution demonstrates a very high conversion efficiency of projectile energy into hard X-ray photons building up a very hot (Tr > 300 eV) thermal bath. Intense and energetic cluster ion beams thus demonstrate considerable potential as a novel driver for inertial confinement fusion.

Current Trends in International Fusion Research — Proceedings of the Second Symposium
Edited by E. Panarella. NRC Research Press, National Research Council of Canada, Ottawa, ON K1A 0R6, Canada. 1999.

CONCLUDING REMARKS

Emilio Panarella, Chairman of the Steering Committee

Advanced Laser and Fusion Technology, Inc.
189 Deveault St., No. 7, Hull, PQ, Canada and
Department of Electrical Engineering
University of Tennessee
Knoxville, Tennessee 37996-2100, U.S.A.

This 2nd Symposium "Current Trends in International Fusion Research: Review and Assessment" is coming to an end, and I take the podium with a sense of satisfaction for what we have achieved in the past 5 days.

One of the most notable achievements has been the bringing together here of a significant number of representative fusion research programs from all over the world. We have heard of the activities going on in plasma focus in Russia, Argentina, and Mexico, in inertial confinement fusion at Livermore, Rochester, Los Alamos, N.R.L., Japan and Spain, on the spherical pinch in Canada, U.S.A., Italy and New Zealand, on magnetized target fusion in Los Alamos, on the inertial electrostatic confinement at the University of Illinois and Los Alamos, the heliotron program at Kyoto University, the tokamak research program of MIT, Princeton, University of Saskatchewan, and China. The Field Reversed Configuration was well represented with talks from Japan and the University of Washington. The tandem mirror from Japan, the staged Z-pinch from the University of California at Irvine and the Reversed Field Pinch of Los Alamos were also well represented here. Exploratory concepts such as the "linear collider" of Prof. Post, the "Colliding Beam Fusion Reactor" of Prof. Monkhorst and Prof. Rostoker, and the "Centrifugally Confined Plasma" of Prof. Hassam were also welcome as indicative of the "beginning of a new era of fusion research", as Prof. Post so lucidly stated Monday morning in his keynote presentation. Analyses on the issues of fusion burn control of Prof. Persson, on the mechanism for fusion of deuterium nuclei in a metallic lattice of Prof. Kraft, on the new physics for fusion energy of Prof. Roth, and even my own analysis on the ignition criteria of a D-T plasma in reactor-type conditions, and of the relevant consequences for magnetic fusion and the ITER program, were all stimulating studies aimed at bringing a sense of renewal and innovative thinking in this mature field of plasma physics and fusion science.

In the past five days, what has impressed me most has been quality of the presentations from all of you, which I found flawless. However, what has impressed me even more has been the quality of the debate that followed the presentations. The depth and sharpness of the questions were counterbalanced by answers which were just as penetrating and illuminating as the questions. The stimulation that followed from the debate was just as intense as the excitement that followed the presentations.

Current Trends in International Fusion Research – Proceedings of the Second Symposium
Edited by E. Panarella. NRC Research Press, National Research Council of Canada, Ottawa, ON K1A OR6, Canada. 1999.

To summarize the achievements from this symposium, I say without hesitation that, besides bringing together the excellence of several fusion research programs, in a climate of healthy scientific debate and exposure, I have perceived a renewed sense of commitment to work even harder than before in order to increase our understanding of the phenomena governing a plasma under conditions amenable to fusion burn.

As I am sure you have all noticed, this 2nd Symposium has proceeded smoothly from beginning to end, and the merit has to go to all the people of the Steering Committee and International Advisory Board, who have dedicated many hours of their valuable time to make this happen. My thanks go to all of them. In particular, I would like to thank Ron Kirkpatrick and Julio Herrera who have closely worked with me in the last, most hectic days before the Symposium.

Our works are now in the hands of the Panel of Distinguished Scientists and Engineers who will evaluate them. I am confident that their response will be favourable, thus reflecting on their desire to promote fusion science for public acceptance and support.

The success of the 1st and 2nd Symposium leads me to believe that interested governments will receive strong recommendations from us that fusion needs to be supported is a sustained way, and in diversified approach. We have to be vigilant however, and not to lose the momentum that we have acquired with the first two Symposia. For this reason, there will be a third Symposium, which will be held again here in Washington. Although I cannot tell you the exact date when it will be held, because it will be decided in the coming months, I can however tell you that it will be held no later than two years from now.

In conclusion, I would like to thank all of you for having been part of this Symposium and for having made it such a success story as we have all witnessed. Thank you again.

REPORT OF THE EVALUATORS*

Stirling A. Colgate, Edward C. Creutz, Arthur R. Kantrowitz (Chairman), Joseph E. Lannutti, Hans J. Schneider-Muntau, Glenn T. Seaborg and Frederick Seitz

The charge to the panel of reviewers of this symposium is to reflect on the presentations made at the Symposium, using them as a basis on which to make informed observations concerning the present status and possible future course of fusion research.

Given the above interpretation of the panel's charge the following comments are offered:

Fusion research in the late 1990's is nearing its "Golden Anniversary," having been launched mid-century. During this period enormous progress has been made, both in the understanding of the basic plasma physics issues encountered in the fusion quest, and in the development of the advanced technology required in the pursuit of this goal. In fusion research based on magnetic confinement the concept itself has been shown to be a viable one, although involving far more complex issues than was initially thought when the idea was first put forward. Similarly, in pellet fusion (inertial confinement fusion), first estimates of the energy required to implode and heat a pellet of fusion fuel to the point that more fusion energy is released than that required to ignite it were found to be far too low, when the full complexity of the process was understood.

Viewed now in terms of the final goal, both magnetic and inertial confinement fusion research must deal with three distinct areas: (1) the physics of the high-temperature plasma state; (2) the quantitative requirement of achieving a net fusion power release, and (3) economic practicality, as measured against alternative sources of energy, be they fossil fuel sources (for the next several decades), energy from nuclear fission, or solar-based energy.

The reality is that, despite nearly 50 years of hard work, and despite the impressive accomplishments that have been made during that period, we cannot at this point in time put the label "solved" on any of these three areas of concern. A second reality is that the growing awareness of this latter circumstance on the part of policy makers, and, to a certain extent, the general public, have put fusion power increasingly "on the back burner" when it comes to budgetary support from the various governments involved.

Viewed as a whole, the papers at the Symposium witnessed to all three of the above areas of concern. There were papers (e.g., the paper by Mazzucato and the TFTR Group entitled: "High Confinement Regime in TFTR Configurations") that dealt with important plasma physics issues, papers that dealt with the quantitative requirements for achieving net fusion power, both in inertial fusion and magnetic fusion, and papers that examined aspects of the economic challenges facing fusion. Another cross-cut of the papers presented was the division between papers reporting progress on well-established "approaches," such as the

---

*This report was prepared by Richard F. Post, in consultation with the Panel of Evaluators.

Current Trends in International Fusion Research — Proceedings of the Second Symposium
Edited by E. Panarella. NRC Research Press, National Research Council of Canada, Ottawa, ON K1A 0R6, Canada. 1999.

tokamak, and those describing proposed, or less-well-known approaches, e.g., electrostatic confinement systems of the type investigated many years ago by Farnsworth and Hirsch.

Also apparent from several of the papers was the dilemma with which both magnetic and inertial confinement researchers are presented: In magnetic fusion research, although it is the most successful magnetic confinement approach, the tokamak is viewed by many as being too large, too complex, and too expensive to meet the goal of economic practicality, based as it is on a brute force approach to achieving ignition through scale-up in its dimensions. Similarly, in inertial fusion, the lasers that have been employed to approach, and, with high probability (in the new NIF facility at Livermore), to achieve, ignition, are not viewed as suitable for fusion-power applications, owing to their low efficiency and low duty-cycle capabilities.

There appears to be a common thread that provides a rationale for establishing a change in course in magnetic fusion research, one that seems essential if the fusion goal is to be reached by this path. The common thread: that there does not exist an adequate knowledge of the plasma state as it interacts with magnetic fields. For example, there is an urgent need for basic experiments aimed at better establishing the conditions under which a quiescent plasma can coexist with a confining magnetic field. Conversely, there needs to be a more basic understanding of those circumstances where magnetically confined plasmas are inherently subject to turbulence, for example owing to the topology of the magnetic field (i.e., either "closed" or "open"). A firm understanding of these basic aspects of plasma behavior would go a long way toward rationalizing the various approaches to magnetic fusion, as follows: Those approaches that have been shown to be capable of achieving a quiescent state can employ theoretical analyses in comparing their performance with a standard based on "classical" calculations, providing a near-sure means for extrapolation to fusion-relevant parameters. Conversely, those approaches (such as the tokamak) which by their nature seem inherently incapable of confining plasma in a quiescent state, will then be understood to have a more restrictive requirement: They can only be made fusion-relevant by scale-up in size to overcome turbulence-enhanced plasma losses or by operation in pulsed regimes that achieve net fusion power in the face of these losses.

The above situation in some way resembles that encountered in the development of the airplane. Until the role of turbulence was understood only empirical methods could be employed to design their wings. With the understanding of turbulence and how to suppress it, came the ability to design airfoils whose performance approached a "classical" optimum.

Hand-in-hand with the experimental approach to dividing confinement systems into either quiescent-capable or turbulence-prone categories should come an increased emphasis on extending the capabilities of computer plasma-simulation codes to perform this separation. In this way the plasma-physics problems of magnetic fusion research could be better defined as they apply to any newly proposed approach.

To summarize these comments on the physics of magnetic confinement, they imply that there should be an increased emphasis in the fusion program on a basic understanding of the confinement process, particularly as it relates to defining those situations where quiescent or near-quiescent states can be achieved, together with the scaling laws that apply in such situations. This change in emphasis should have the effect of clearly defining the task at hand for a given approach, i.e., either to operate in regimes that can be evaluated by classical calculations, or else to chose to operate in a turbulent state where either size scaling or short time scale allows one to hope to achieve net fusion power.

A second area for comments with respect to magnetic fusion research has to do with the issue of programmatic balance. In addition to a need for increased emphasis on basic plasma physics issues, there should be a return to a better-balanced state as between the so-called "mainline" approach (the tokamak) and those approaches that differ substantially from the tokamak. In earlier days, when no one approach had taken the lead, for whatever reason, the world magnetic fusion effort was characterized by a more even distribution of effort among many different approaches to the problem. Today in the U. S., primarily as a result of policy decisions in the 1980's, very little effort is being devoted to anything but the tokamak. Fortunately, those earlier policy decisions are being examined and, to a certain extent, reversed. However, there need to be put in place new means to insure the health of approaches that are "orthogonal" to the tokamak and its relatives, so as to help insure that new and potentially better routes to fusion are not cut off. As an example, in the U. S. there are at present no fusion-related experiments employing the "open" field topology, a major program exploring this approach existed in the mid-1980's.

With respect to the second major area of inquiry for fusion research, namely, the satisfaction of the quantitative requirements for fusion, the situation seems quite different as between the inertial and magnetic fusion approaches. In inertial fusion, ignition of the fusion pellet is an entry-level requirement for that approach, lying beyond which is the requirement for sufficient excess energy production to yield net power after subtracting the power required by the driver, be it lasers or particle beams. These requirements are clearly defined and are being pursued methodically.

By contrast, it seems that in magnetic fusion research there has occurred an unfortunate and premature narrowing of the definition of the requirement for success in achieving the quantitative requirements for fusion. Starting with the use of the Lawson criteria as a standard for success, the concept of plasma ignition has been taken as the goal that must be achieved, where "plasma ignition," in the case of the D-T reaction is taken to mean that situation where the alpha particles from fusion reactions deposit enough of their energy to maintain the plasma at fusion temperatures in the face of both particle and radiation losses. However, magnetic fusion differs from inertial fusion in that it is possible to visualize situations, describable as "driven" systems, where a portion of the power is continuously recirculated back to the plasma to maintain its temperature, and where net power is achieved by paying attention to the efficiency of the heating and energy recovery processes. A thermo-mechanical analog to a driven fusion power system is the gas turbine, where the recirculated power exceeds the net output power by a substantial margin. In magnetic fusion the true goal is net power, not plasma ignition.

In connection with both the quantitative requirements for fusion power and the policy-related need to broaden the concept base of magnetic fusion research is the accompanying need to pursue a broader base of supporting technologies. For example, two decades ago there were active and successful programs looking into means for the direct conversion of particle energy into electricity. In this research conversion efficiencies approaching 90 percent were demonstrated. Direct conversion is a technique that is especially applicable to open magnetic systems, where it enhances the operation of driven systems and opens up the possibility of employing alternative fusion fuels, such as D-He^3, with energy releases coming entirely in the form of charged reaction products. Since the tokamak is inherently unsuited for any known types of direct converters, direct converter research was essentially abandoned when the policy decision to pursue the tokamak to the exclusion of all other approaches was made.

Finally, with respect to the third area that must be taken into account in fusion research, namely, economic practicality, it seems that this requirement has been used in some cases as a two-edged sword. That is, there have been cases where promising approaches have been abandoned or their support has been greatly reduced on the basis of early studies that seemed to indicate that fusion power plants based on this approach would be too expensive to compete in today's market. The first thing wrong with this argument is that it does not take into account the economic situation that may apply at the time such a system is brought into operation. If the CO_2 "greenhouse effect" problem, fossil fuel depletion, or future unsolved concerns with nuclear fission rule out these alternatives, then the fact that a fusion system is projected to be somewhat more expensive than these systems is irrelevant. Second, to rule out a potentially promising approach before there has been a chance for it to evolve toward a more economically attractive form is clearly not a wise move. Economics is, of course, an important issue, but it should not be used prematurely as a criterion for rejecting an otherwise promising approach.

In summary, in considering the status of fusion research, particularly magnetic fusion research, as reflected in the papers at the Symposium, we have the following comments:

- The magnetic fusion program should encourage and support physics-oriented experiments that define those circumstances allowing near-quiescent plasma confinement, and those that are inherently turbulence-prone, better to define the basic nature of the magnetic confinement of plasmas.
- The programmatic balance of the magnetic fusion effort needs to be changed in the direction of a broader and more physics-based effort, employing analysis and computer simulation techniques to aid in the screening out of clearly unpromising approaches.
- The pragmatic goal of magnetic fusion research needs to be clearly focused on the achievement of net power, not on the overly restrictive goal of achieving plasma ignition.
- Along with increasing the breadth of the magnetic fusion program there needs to occur a broadening of its technology base, e.g., direct conversion and high-efficiency ion sources.
- Except for clearly unpromising cases, proposed new fusion approaches should not be prematurely rejected on the basis of perceived economic inferiority.

BIOGRAPHIES OF EVALUATORS

Dr. Stirling A. Colgate
Dr. Edward C. Creutz
Dr. Arthur R. Kantrowitz, Chairman
Dr. Joseph E. Lannutti
Dr. Hans J. Schneider-Muntau
Dr. Glenn T. Seaborg
Dr. Frederick Seitz

STIRLING A. COLGATE

Stirling A. Colgate, an associate staff member and senior fellow at Los Alamos National Laboratory, earned his BA and Ph.D. degrees in physics from Cornell University. He initially worked on accelerator physics at Lawrence Berkeley National Laboratory before joining LLNL at its inception. There he led the fast diagnostics for the weapons test for LLNL as well as LANL for the Castle tests, including the Bravo test in the Pacific in 1954. He then led the helical magnetic fusion confinement program at LLNL for 8 years, started the laser inertial fusion laser program, and initiated calculations of stellar collapse and supernova explosions. In 1959 he became Consultant to the US State Department for the treaty on the Discontinuance of Nuclear Weapons Tests. In 1964 he became President of New Mexico Institute of Mining and Technology, working in atmospheric physics and astrophysics, and astronomy. He joined LLNL in 1976 becoming a group leader in astrophysics and fusion. Research Interests: Nuclear physics (diagnostics and fusion plasma confinement), astrophysics (supernovae, quasars, cosmic rays, solar physics), atmospheric physics (tornadoes, thunderstorms), geotectonic engineering, epidemiology, human complexity.

Present Memberships and Boards: Member National Academy of Sciences; Fellow of the American Physical Society, Fellow of the American Association for the Advancement of Science; Member of: American Astronomical Society, American Meteorological Society; American Geophysical Society, Cosmic Physics Division of APS, International Astronomy Union, American Academy of Arts and Sciences; Founding Board, Santa Fe Institute, Member of the Aspen Center for Physics.

Prizes and Awards: Rossi Prize, American Astronomical Society for Cosmic Ray Theory, Wehterhill Prize, Franklin Institute for Supernova Theory and the Importance of Neutrino Physics.

25 patents and 250 papers.

Current Trends in International Fusion Research — Proceedings of the Second Symposium
Edited by E. Panarella. NRC Research Press, National Research Council of Canada, Ottawa, ON K1A 0R6, Canada. 1999.

EDWARD CHESTER CREUTZ

Edward Chester Creutz: Education: B.S. Mathematics and Physics, University of Wisconsin, 1936; Ph.D. Physics, U. of Wisconsin, 1939; Thesis: Resonance Scattering of Protons by Lithium.

Professional Experience: 1977-1984, Director, Bishop Museum, Honolulu, HI; 1976-1977, Acting Deputy Director, National Science Foundation, Washington, DC; 1975-1977, Assistant Director for Mathematical and Physical Sciences, and Engineering, National Science Foundation; 1970-1975, Assistant Director for Research, National Science Foundation (Presidential appointee); 1955-1970, Vice President, Research and Development, General Atomic, San Diego, CA; 1955-1956, Scientist at large, Controlled Thermonuclear Program, Atomic Energy Commission, Washington, DC; 1948-1955, Professor and Head, Department of Physics, and Director, Nuclear Research Center, Carnegie Institute of Technology, Pittsburgh, PA; 1946-1948, Associate Professor of Physics, Carnegie Institute of Technology; 1944-1946, Group Leader, Los Alamos, NM; 1942-1944, Group Leader, Manhattan Project, Chicago, IL; 1939-1942, Instructor of Physics, Princeton University, Princeton, NJ.

1945 ff, Consultant to AEC, NASA, Industry.

1960 ff, Editorial Advisory Board: American Nuclear Society, Annual Reviews, Handbuch der Physik, Interdisciplinary Science Reviews, Handbook of Chemistry and Physics.

Publications: 65 in fields of Physics, Metallurgy, Mathematics, Botany, and Science Policy.

Patents: 18 Nuclear Energy Applications.

Honors: Phi Beta Kappa; Tau Beta Pi; Sigma Xi; National Science Foundation Distinguished Service Award; University of Wisconsin, College of Engineering, Distinguished Service Citation; American Nuclear Society, Pioneer Award.

Memberships: National Academy of Sciences; AAAS, Fellow; American Physical Society, Fellow; American Association of Physics Teachers; American Nuclear Society.

ARTHUR R. KANTROWITZ

Arthur R. Kantrowitz, Professor of Engineering at the Thayer School of Engineering of Dartmouth College, earned his B.S., M.A., and Ph.D. degrees in physics at Columbia University. He taught aeronautical engineering and engineering physics at Cornell for ten years, and then founded and was CEO of the Avco Everett Research Laboratory. He is a member of the National Academy of Sciences and the National Academy of Engineering, and a fellow of the American Academy of Arts and Sciences, the American Physical Society, the American Institute of Aeronautics and Astronautics, the American Association for the Advancement of Sciences, and the American Astronautical Society. He was a Fulbright and Guggenheim Fellow, and recipient of the Roosevelt Medal of Honor for Distinguished Service in Science. He is an honorary trustee of the University of Rochester, an honorary life member of the Board of Governors of the Technion, and an honorary professor of the Hauzhong Institute of Technology in Wuhan, China. He holds 21 patents, and has published extensively. He is a director of the Hertz Foundation, and a member of the advisory board to television's popular "Nova" program. He has served our government on advisory boards to the Ford White House, the Department of Commerce, NASA, the General Accounting Office, and the National Science Foundation.

JOSEPH E. LANNUTTI

Joseph E. Lannutti: Born May 4, 1926, Malvern, PA; married with three children. High Energy Experimental Particle Physicist, Ph.D. 1957, University of California at Berkeley.

Served in the U.S. Army, 28th Infantry Division, European Theater, in WWII 1944–46; Worked in Motive Power Division of the Pennsylvania Railroad Company 1943–44 and 1946–47.

Worked as a theoretical physicist designing guided missile autonavigation systems, at the North American Aviation, Inc., Downey, CA 1952–53; and as a research assistant at the University of California Radiation Laboratory 1953–57.

Came to Florida State University (FSU) as Assistant Professor in September 1957; promoted to Professor of Physics in 1965; appointed Associate Vice President for Academic Affairs in 1984.

Established laboratory for High Energy Particle Physics research at FSU and has been principal investigator since 1957. Continuous research funding from U.S. Department of Energy with FY93 budget over $1M; present personnel approximately 30.

Published more than 150 scientific articles and abstracts.

Established FAMU/FSU College of Engineering in 1982 and co-directed it until September 1984. Enrollment in 1992–93 approximately 2,000 students.

Established Supercomputer Computations Research Institute (SCRI) in 1984 and was Director 1984–1993. SCRI is the first federal/state/industry computations research institute of its kind in the United States and has a FY93 budget of approximately $10M; present personnel approximately 70.

Appointed Associate Vice President for Research 1992.

National organization memberships:

Past

- High Energy Physics Advisory Panel, U.S. Department of Energy
- Oak Ridge Associated Universities, Board of Directors, Chairman of Council
- University Research Association, Board of Trustees, Chairman of Physics Committee
- Southeastern University Research Association, Board of Trustees
- Users Executive Committee, Fermi National Accelerator Laboratory

Present

Member of User Organizations at

- Brookhaven National Accelerator Laboratory, Long Island, NY
- Fermi National Laboratory, Batavia, IL
- Stanford Linear Accelerator Laboratory, Palo Alto, CA
- Center for Nuclear Research for Europe, Geneva, Switzerland
- University of Research Association Fermilab Review Committee

HANS J. SCHNEIDER-MUNTAU

Professional Interests:	Advancement of magnet technology, development of state-of-the-art magnet systems, laboratory management
Education:	Ph.D., Electrical Engineering, University of Munich, 1967 M.S., Electrical Engineering, University of Stuttgart, 1962 B.S., Electrical Engineering, University of Stuttgart, 1958

Professional Experience:

1991 - Present	Deputy Director, National High Magnetic Field Laboratory. Director, Magnet Development and Technology Group, NHMFL.

Professor of Mechanical Engineering:

1972-1991	Chief Engineer, High-Field Magnet-Laboratory, Grenoble, of the Max-Planck-Institute für Festkörperforschung, Stuttgart. Responsible for magnet development and administration, worked on development of resistive, pulsed and hybrid magnets and facility improvements.
1967-1972	Head of the Development Laboratory, European Space Research Institute, Frascati. Worked on space simulation experiments, development of high-voltage ns discharges, capacitor banks and pulsed laser sources.
1962-1967	Scientist, Institut für Plasmaphysik, Garching, of the Max-Planck-Gesellschaft, Munich. Worked on fusion technology, developed pulsed neutron sources, and fast high voltage discharges.

GLENN T. SEABORG

Glenn T. Seaborg is currently University Professor of Chemistry (the most distinguished titled bestowed by the Regents), Associate Director-at-Large of the Lawrence Berkeley Laboratory, and Chairman of the Lawrence Hall of Science at the University of California, Berkeley.

He received his A. B. in Chemistry from UCLA in 1934 and his Ph.D. in Chemistry from Berkeley in 1937. He has served on the faculty of the Berkeley campus since 1939 and was Chancellor of that campus 1958-1961. In 1961 Dr. Seaborg was appointed Chairman of the

Atomic Energy Commission by President John F. Kennedy. He was subsequently reappointed by both Presidents Johnson and Nixon, serving in that position until 1971.

Winner of the 1951 Nobel Prize in Chemistry (with E. M. McMillan) for his work on the chemistry of the transuranium elements, Glenn Seaborg is one of the discoverers of plutonium (element 94). During World War II he headed the group at the University of Chicago's Metallurgical Laboratory which devised the chemical extraction processes used in the production of plutonium for the Manhattan Project. He and his coworkers have since discovered none more transuranium elements: americium (element 95), curium (96), berkelium (97), californium (98), einsteinium (99), fermium (100), mendelevium (101), nobelium (102), and Element 106. He has been honored by the recommendation by the co-discoverers of Element 106 that it be named "seaborgium," with the symbol Sc. He holds over 40 patents, including those on elements americium and curium (making him the only person ever to hold a patent on a chemical element).

In 1944, Dr. Seaborg formulated the actinide concept of heavy element electronic structure which accurately predicted that the heaviest naturally occurring elements together with synthetic transuranium elements would form a transition series of actinide elements in a manner analogous to the rare earth series of lanthanide elements. This concept, one of the most significant changes in the periodic table since Mendeleev's 19th century design, shows how the transuranium elements fit into the periodic table and thus demonstrates their relationships to other elements.

His co-discoveries include many isotopes which have practical applications in research medicine and industry (such as iodine-131, technetium-99m, cobalt-57, cobalt-60, iron-55, iron-59, zink-65, cesium-137, manganese-54, antimony-124, californium-252, americium-241, plutonium-238), as well as the fissile isotopes plutonium-239 and uranium-233.

Dr. Seaborg continues to work as an active research scientist, with a research group in the search for new isotopes and new elements at the upper end of the periodic table, including a search for the "superheavy" elements. The group is also investigating the mechanism of the reactions of heavy ions with heavy element target nuclei. Another aspect of the research program is concerned with the determination of the chemical properties of the heaviest chemical elements.

Dr. Seaborg is the author of numerous books. During the spring of 1994, he published three books: *Chancellor at Berkeley*, a memoir about developments on the Berkeley campus during his chancellorship, *Modern Alchemy: The Selected Papers of Glenn T. Seaborg*, and *The Plutonium Story: The Journals of Professor Glenn T. Seaborg 1939-1946*, which describes his discovery of plutonium and work on the Manhattan Project. *Elements Beyond Uranium* (1990) is a comprehensive summary of all aspects of transuranium elements. He has written a trilogy about his service as chairman of the Atomic Energy Commission: *Kennedy, Khrushchev, and the Test Ban* (1981), *Stemming the Tide: Arms Control in the Johnson Years* (1987), and *The Atomic Energy Commission under Nixon: Adjusting to Troubled Times* (1993); the first two books focus on arms control issues, while the Nixon book is more general. He has also authored over 500 scientific articles and guided the graduate studies of more than 65 successful Ph.D. candidates. In addition to the Nobel Prize and a great many other awards for his work in chemistry, science education and community service, Dr. Seaborg has been awarded 50 honorary doctoral degrees.

Among his many interests are international cooperation in science, history of science (documenting the early history of nuclear science), nuclear arms control (advocating a comprehensive test ban treaty), and hiking. A member of the National Commission on

Excellence in Education which published the much-publicized report *A Nation At Risk* in 1983 and Chairman of the Lawrence Hall of Science, Dr. Seaborg is recognized as a national spokesman on education, addressing in particular the crisis in the mathematics and science education.

FREDERICK SEITZ

Frederick Seitz was born in San Francisco on July 4, 1911. He received his bachelor's degree from Stanford in 1932 and his Ph.D. from Princeton in 1934. He has written some classic works in physics including *Modern Theory of Solids* (1940), was co-editor of the series *Solid State Physics* (started in 1954), and examined the evolution of science in *The Science Matrix* (1992).

Seitz's early career included positions at the University of Pennsylvania, the Carnegie Institute of Technology, and General Electric. During World War II, he worked for the National Defense Research Committee, the Manhattan District, and as a consultant to the Secretary of War. From 1946 to 1947 he was director of the training program on peaceful uses of atomic energy at Oak Ridge National Laboratory. Appointed professor of physics at the University of Illinois in 1949, Seitz became department chair in 1957 and dean and vice president for research in 1964. He joined the Rockefeller University as its president in 1968.

Dr. Seitz was elected to the National Academy of Sciences in 1951, serving as part-time president for three years before assuming full-time responsibility in 1956. He has served as advisor to NATO, the President's Science Advisory Committee, the Office of Naval Research, the National Cancer Advisory Board, the Smithsonian Institution, and other national and international agencies. He has been honored with the Franklin Medal (1965), the Compton Medal - the highest award of the American Institute of Physics (1970), the National Medal of Science (1973), two NASA Public Service Awards (1969 and 1979), the National Science Foundation's Vannevar Bush Award (1983), as well as honorary degrees from 32 universities worldwide. In 1993, the University of Illinois renamed its Materials Research Laboratory in Dr. Seitz's honor. Stanford University has honored him with the Hoover Medal and Princeton University with the Madison Medal.

PARTICIPANTS

Dr. D. A. Baker
P-4 MS E554
Los Alamos National Laboratory
LOS ALAMOS, NM 87545
U.S.A.

Dr. John Blewett
7405 Sweetbriar Dr.
COLLEGE PARK, MD 20740
U.S.A.

Dr. Stephen Bodner
Code 6730.
Naval Research Laboratory
WASHINGTON, DC 20375
U.S.A.

Dr. Derek Boyd
Department of Physics
University of Maryland
COLLEGE PARK, MD 20742
U.S.A.

Dr. Stirling A. Colgate
MS B27
Los Alamos National Laboratory
LOS ALAMOS, NM 87545
U.S.A.

Dr. Bruno Coppi
Department of Physics
Massachusetts Institute of Technology
Rm. 26-217
CAMBRIDGE, MA 02139
U.S.A.

Dr. Edward C. Creutz
P.O. Box 2757
RANCHO SANTA FE, CA 92067
U.S.A.

Dr. Ben Cross
Westinghouse Savannah River
Company
Strategic Programs and
Mission Development - Fusion Programs
Bldg. 773-41A
AIKEN, SC 29808
U.S.A.

Dr. James Degnan
USA Philips Laboratory, PL/WSP
High Energy Plasma Division
3550 Aberdeen SW
KIRTLAND AFB, NM 87117-5776
U.S.A.

Dr. Claude Deutsch
Laboratoire de Physique des Gaz et des
Plasmas
Unité de Recherche Associée au CNRS
Université Paris XI
Bat. 210
91405 ORSAY CEDEX
FRANCE

Dr. Francesco Giammanco
Department of Physics
University of Pisa
Piazza Torricelli, 2
56126 PISA
ITALY

Dr. George Goldenbaum
Office of the Dean
College of Computer, Mathematical
and Physical Sciences
University of Maryland
COLLEGE PARK, MD 20742
U.S.A.

Dr. Seiichi Goto
Plasma Physics Laboratory
Osaka University
2-1 Yamadaoka Suita
OSAKA 565
JAPAN

Dr. Victor Granatstein, Director
Laboratory for Plasma Research
University of Maryland
COLLEGE PARK, MD 20742
U.S.A.

Dr. Adil B. Hassam
Laboratory for Plasma Research
University of Maryland
COLLEGE PARK, MD 20742
U.S.A.

Dr. Julio Herrera
Instituto de Ciencias Nucleares
Universidad Nacional Autonoma de Mexico
Circuito Exterior C.U.
A.P. 70-543
04510 MEXICO DF
MEXICO

Dr. Akira Hirose
Department of Physics
University of Saskatchewan
SASKATOON, SK S7N OWO
CANADA

Dr. Amit K. Hui
Plasma Physics Group
Saha Institute of Nuclear Physics
1/af Bidhannagar
CALCUTTA 700 064
INDIA

Dr. Ashok Jain
Embassy of India
Scientific Attaché
2536 Massachussetts Ave., NW
WASHINGTON, DC 20008
U.S.A.

Dr. Arthur R. Kantrowitz
4 Downing Road
HANOVER, NH 03755
U.S.A.

Dr. Aleksander Khlunov
Counsellor for Science and Technology
Embassy of the Russian Federation
2650 Wisconsin Ave. N.W.
WASHINGTON, DC 20007
U.S.A.

Dr. Ronald C. Kirkpatrick
MS-B229
Los Alamos National Laboratory
LOS ALAMOS, NM 87545
U.S.A.

Dr. Paul M. Koloc
Phaser Corporation
Box 222
COLLEGE PARK, MD 20740-0222
U.S.A.

Dr. David W. Kraft
School of Science and Engineering
University of Bridgeport
BRIDGEPORT, CT 06601
U.S.A.

Dr. Stephen Kral
Babcock And Wiicox Corp.
P.O. Box 785
LYNCHBURGH, VA 24505
U.S.A.

Dr. V.I. Krauz
RRC "Kurchatov Institute"
Nuclear Fusion Institute
Kurchatov sq. 18
MOSCOW, 123182
RUSSIA

Dr. Rustam Kh. Kurtmullaev
State Research Center TRINITI
TROITSK
RUSSIA

Dr. Joseph E. Lannutti
217E Westcott Bldg.
Florida State University
TALLAHASSEE, FL 32306-4093
U.S.A.

Dr. M. Laroussi
Department of Electrical Engineering
The University of Tennessee
102 Ferris Hall
KNOXVILLE, TN 37996-2100
U.S.A.

Dr. Irvin R. Lindemuth
MS-B259
Los Alamos National Laboratory
LOS ALAMOS, NM 87545
U.S.A.

Dr. Erick L. Lindman
X-1
Los Alamos National Laboratory
LOS ALAMOS, NM 87545
U.S.A.

Dr. Shenggang Liu
The University of Electronic Science
and Technology of China
CHEGDU, SICHUAN PROVINCE,
610054
PEOPLE'S REPUBLIC OF CHINA

Dr. E. Lozneanu
Department of Plasma Physics
"Al. I. Cuza" University of Iasi
Blvd. Copou 11
6600 IASI
ROMANIA

Dr. Julio Martinell
Laboratory for Plasma Research
University of Maryland
COLLEGE PARK, MD 20742
U.S.A.

Dr. José Maria Martinez-Val
Escuela Teorica Superior
de Ingenieria Industrial
José Gutierrez Abascal, 2
28006 MADRID
SPAIN

Dr. Ernesto Mazzucato
Plasma Physics Laboratory
Princeton University
P.O. Box 451
PRINCETON, NJ 08543
U.S.A.

Dr. George H. Miley
216 Nuclear Engineering Laboratory
University of Illinois
103 S. Goodwin Avenue
URBANA, IL 61801
U.S.A.

Dr. H. Momota
National Institute for Fusion Science
Nagoya University
NAGOYA 464
JAPAN

Dr. Hendrik J. Monkhorst
Department of Physics
University of Florida
GAINESVILLE, FL 32611
U.S.A.

Dr. Domiziano Mostacci
Department of Nuclear Engineering
University of Bologna
Via dei Colli, 16
40136 BOLOGNA
ITALY

Dr. Ghulam Murtaza
Head, Fusion Laboratory
Department of Physics
Quaid-I-Azam University
ISLAMABAD
PAKISTAN

Dr. Richard A. Nebel
Los Alamos National Laboratory
MS K717
LOS ALAMOS, NM 87545
U.S.A.

Dr. Tokuhiro Obiki
Plasma Physics Laboratory
Kyoto University
Gokasho Uji, 611
KYOTO 611
JAPAN

Dr. Charles Orth
Lawrence Livermore National
Laboratory
L-490
P. O. Box 808
LIVERMORE, CA 94550
U.S.A.

Tel. (510) 422-8665
Fax (510) 423-6506
E-mail: orth2@llnl.gov

Dr. Emilio Panarella
Advanced Laser and Fusion Technology,
Inc.
189 Deveault Street, No. 7
Hull, P.Q. J8Z 1S7
CANADA

and

Department of Electrical Engineering
University of Tennessee
KNOXVILLE, TN 37996
U.S.A.

Dr. Hans Persson
Fusion Plasma Physics
Alfvén Laboratory
Royal Institute of Technology
S-100 44 STOCKHOLM
SWEDEN

Dr. Mireia Piera
UNED
Ciudad Universitaria s/n
MADRID 28040
SPAIN

Dr. Richard F. Post
Lawrence Livermore National
Laboratory
P.O. Box 808
L-640
LIVERMORE, CA 94550
U.S.A.

Dr. Jorge Pouzo
Instituto de Fisica Arroyo Seco (IFAS)
Azcuenaga 349
(7000) TANDIL
ARGENTINA

Dr. Mark Anthony Prelas
H.O. Croft Professor, Director
Fusion Research Laboratory
Nuclear Engineering
University of Missouri-Columbia
COLUMBIA, MO 65211
U.S.A.

Dr. Edbertho Leal Quiros
Department of Physics
University of Puerto Rico
HUMACAO, PR 00661
U.S.A.

Dr. Hafiz-Ur Rahman
Institute of Geophysics and Planetary
Physics
University of California
RIVERSIDE, CA 92521-0412
U.S.A.

Dr. Norman Rostoker
Department of Physics
University of California
IRVINE, CA 92715
U.S.A.

Dr. Dmitri Ryutov
Livermore National Laboratory
L-630
P. O. Box 808
LIVERMORE, CA 94550
U.S.A.

Dr. J. Reece Roth
Department of Electrical Engineering
The University of Tennessee
316 Ferris Hall
KNOXVILLE, TN 37996-2100
U.S.A.

Dr. Nikos A. Salingaros
Division of Mathematics, Computer
Science and Statistics
The University of Texas
SAN ANTONIO, TX 78249-0664
U.S.A.

Dr. M. Sanduloviciu
Department of Plasma Physics
"Al. I. Cuza" University of Iasi
Blvd. Copou 11
6600 IASI
ROMANIA

Dr. Hans J. Schneider-Muntau
National High Magnetic Field
Laboratory
Florida State University
1800 E. Paul Dirac Drive
TALLAHASSEE, FL 32306-4005
U.S.A.

Dr. Glenn T. Seaborg
Bldg. 70/A Rm. 3307
Lawrence Berkeley Laboratory
1 Cyclotron Road
BERKELEY, CA 94720
U.S.A.

Dr. Frederick Seitz
The Rockfeller University
1230 York Ave.
NEW YORK, NY 10021-6399
U.S.A.

Dr. John Thomas Slough
AERL
University of Washington
Box 352250
SEATTLE, WA 98195
U.S.A.

Dr. John M. Soures
Laboratory for Laser Energetics
University of Rochester
ROCHESTER, NY 14623
U.S.A.

Dr. M. A. Sweeney
Sandia National Laboratory
Mail Stop 1186
P.O. Box 5800
ALBUQUERQUE, NM 87185-1186
U.S.A.

Dr. Teruo Tamano
Plasma Research Center
Tsukuba University
1-1-1 Tennoudai
IBARAGI 305
JAPAN

Dr. Francis Chia Thio
Head, Mathematics Section
Massey University at Albany
Private Bag 102-904
North Shore Mail Centre
AUCKLAND
NEW ZEALAND

Dr. Yukihiro Tomita
National Institute for Fusion Science
NAGOYA 464-01
Japan

Dr. Pedro Velarde-Mayol
E.T.S.I. INDUSTRIALES
Depto. de Ingenieria Nuclear
C/. José Guitiérrez Abascal, 2
28006 MADRID
SPAIN

Dr. Christopher Wallace
BDM International
1801 Randolph Road S.E.
ALBUQUERQUE, NM 87106
U.S.A.

Dr. Kenneth D. Ware
Defence Nuclear Agency
6801 Telegraph Road
ALEXANDRIA, VA 22310-3398
U.S.A.

Dr. Frank J. Wessel
Department of Physics
University of California
IRVINE, CA 92715
U.S.A.

Dr. Tatsuhiko Yamanaka
Institute of Laser Engineering
Osaka University
2-6 Yamada-Oka, Suita
OSAKA 565
JAPAN

Dr. Yuri Zakharov
Institute of Laser Physics
NOVOSIBIRSK, 630090
RUSSIA

INDEX

Abel inversion, 188
Ablation pressure, 215, 216, 221
Absorption, 427
Acceleration, 28, 32
Adiabatic compression, 421
Advanced analyzers, 431
Advanced confinement, 411, 427
Alcator scaling, 403
Alfven ion cyclotron instability (AIC), 200
Alfven-Mach number, 287
Alpha particle heating, 93, 101
Alpha particles, 135, 356, 374, 376, 377, 379
Alternate confinement devices, 411
AMBAL-M, 197
Ambipolar potentials, 23, 24
    Pastukhov theory of end losses, 15, 16
    Ryutov theory of electron transport, 23
Angular momentum, 190, 193
Anomalous transport, 291
Anomalous viscosity, 135
ARTEMIS, 155, 164, 166, 167, 168
Atmospheric glow discharges, 395, 408
Auxiliary heating, 137, 138, 374, 379, 381
Axial loss, 199

Background plasma, 287
Ball lightning, 395, 406, 409, 427
Ballooning mode, 341, 342, 343, 344, 345, 346, 348, 349, 350
Beam phasing, 80
Beam smoothing, 254
Beta layering, 87
Beta value, 72
Blanket of reactor chamber, 214, 217
Bohm scaling, 403
Bohm time, 199
Bohr-van Leeuwen Theorem, 395, 401, 402, 409
Boron coating, 72
Breakdown, 28, 32
Breakeven, 27, 29
    criteria, 353
    in plasma magnetically confined, 358
Bremsstrahlung, 378
Buckingham's Pi Theorem, 395, 402, 403, 404, 409, 410
Burn fraction, 215
Burn-up time, 377

Capacitor storage, 28, 29, 30
Capillary collimator, 185, 186
Capsule, 77, 80, 467
Centrifugal confinement, 455
Charge exchange collisions, 191, 192
Cluster beam, 467
Cluster ion, 467
Coaxial plasma accelerators, 27
Coaxial plasma gun, 116
Cold fuel layer, 123
Colliding Beam Fusion Reactor, 291, 317, 318, 469
    reactivity, 317, 318, 321, 322, 323
    beam-on-beam, for p-B^{11}, 321, 322
    thermal, for D-He^{3}, 322
    thermal, for D-T 6, 322
COLT, 464
Compact tori, 29
Compact toroid (CT), 114
    acceleration, 209
    adjustment methodology, 209
    advanced design on CT, 210
    antiparallel magnetic structure, 209
    application for conceptual design, 210
    applications for solid liner conception, 210
    damping of losses and instabilities, 210
    Double Star system, 210
    formation, shock heating, 209
    long lived, 210
    nontearing connection of field lines, 209
    plasma flows in CT, 209
    programming Compact Torus, 209
    slow energy accumulation, 209
    self-organized mode of CT, 209
    thermalization, 209
    translation and confinement, 210
Compression, 28, 29, 30, 32, 33, 34, 35, 37, 38
    current, 32
    plasma, 28, 29, 35
Confinement, 373, 381
Confinement, 93
    high temperature plasma, 93, 94
Conical liners, 229, 231, 235, 237
Contaminating side reactions, 317, 324
    for alpha-B^{10}, 324
    for alpha-B^{11}, 324
    for p-B^{10}, 8, 324
    for p-B^{11}, 324
Controlled fusion, 27, 29, 39

Converter , 467
Cryogenic fiber, 281, 285
Current drive, 137
Current
    converters system, 31
    discharge, 27, 28, 29, 30
    drive, 149, 312
    generator, 30, 36, 38
    instabilities, 29
    interruption, 36
    jumper, 28
    pulse duration, 30
    switch, 31, 32, 35
    transfer, 30
    transportation, 30
Currentless plasma, 65, 66, 67, 75
Cutoff, 139, 140

D-^{3}He energetic protons, 181
D-^{3}He reactor, 152, 200
Dean flow, 459
DEMO, 27, 39
Dense magnetized plasmas, 59, 60, 61, 63
Dense plasma focus (DPF), 41, 42, 55, 56, 61, 62, 63
Dense plasma, 171, 175
Density or density-radius product ρR, 215, 220
Density-radius product, 215, 220
Depolarization, 317, 318, 326, 329, 331, 332, 333, 334, 335, 336, 337, 338, 339
    gyro-collisional, 337
    in tokamaks, 318, 338, 339
    of plasmas, 331
    quadrupole, 336
    resonant-wave, 317, 337
    spin-orbit like, 335
    spin-spin like, 335
Deuterium, 137
Deuteron stripping, 391
Developing countries, 59, 60, 61, 63, 64
D-He^3 fuel, 168, 287, 473
Diagnostics, 255
    x-ray, 255, 258
Diamagnetic effect, 287
Diode laser pumped solid state laser (DLPSSL), 216, 225
Direct conversion, 9, 18
Direct drive system, 77, 217
Direct energy conversion, 318
Direct ICF-energy conversion, 287
Direct numerical simulation, 81, 82
Dissipative phenomena, 93, 99, 100
DLPSSL, 216, 225
Double Energy Analyzer (DEA), 431, 438
Double potential well, 177, 179, 181, 183, 184, 191, 193
    "characteristic" signature of, 190, 191, 193
    depth, 184, 186, 189, 191, 193
DPF, 61, 62, 63
Drift instability, 199
Drift mode, 341, 345
Drive symmetry, 83
Driven fusion power systems, 8
Driver, 467
Droplet making machine, 222, 224
D-T fusion engine, 153

E × B velocity shear, 137, 142, 143
ECH, 66, 72
Economic considerations of linear colliders, 24
Efficiency of electrical conversion scheme, 287
Efficiency, 30, 32 33, 35, 36
    transfer, 36, 37
Electron collisionality, 68, 69
[illegible]ctron Cyclotron Heating (ECH), 66, 72
[illegible]tron cyclotron resonance heating (ECRH), 198, 199, 200
Electron particle diffusivity, 138, 141
Electron physics of open-ended systems, 23
Electron temperature, 99
Electron thermal diffusion, 93, 95
Electron-ion thermalization time, 96
Electrostatic confinement, 411
Electrostatic drift-type mode, 142
Electrostatic traps, 411, 424
Elongated plasmas, 458
Emulsion method, 222
Energy cumulation, 233
Energy gain, 227, 235
Energy runaway time, 376
Energy transfer, 31, 35, 36, 37, 38
Energy transfer efficiency, 106
EUV lithography, 105
E × B shear flow, 199
Expanding plasma cloud, 287
Experimental facilities, 37
    MARAUDER, 29, 32
    MINIK, 27, 30, 31, 32, 39
    PF-3, 32, 33
    SHIVA-STAR, 29
    TSP, 27, 30, 31, 39
Extreme Ultraviolet Lithography (EUV), 103

Fast flyers, 174
Fast ignition, 213, 214, 215, 216, 217, 219, 221, 224, 225
Fast-ignited targets, 227
Fiber scintillator streak camera, 220
Field Reversed Configuration (FRC), 317, 318, 325, 326, 328, 330, 331, 336, 337, 338, 339, 469
Fireball, 97, 100
Firehose instability limits, 19
    criterion for injected beams, 19, 20
Fission, 241
    defined, 242
    China syndrome, 242
FIX-FRC experiment, 156, 160
Fluctuation-induced transport, 399
Flute instability, 200

Fokker-Planck equation, 296, 333
  generalization, 333, 334
FRC (Field Reversed Configuration), 145, 147, 148, 155, 163, 171, 172, 173, 293, 317, 318, 325, 326, 328, 330, 331, 336, 337, 338, 339
FRTP, 145
Fuel capsule fabrication, 222
Fuel pellets, 213, 214, 215, 216, 217, 222, 223, 225
Fusion "spin-off applications," 177
Fusion applications, 62, 63, 64
Fusion burn time, 220
Fusion burning wave, 227, 228, 231
  fusion chamber, clearing, 249
    ICF, defined, 243
    IFE, defined, 244
    ignition threshold, 241, 244, 248, 249
    indirect drive, 241, 243
    hohlraum, 241, 242, 247, 248
    how it works, 242, 243
    instabilities, 247, 248
      hydrodynamic (Rayleigh-Taylor), 247
      laser-plasma, 247, 248
    known to work, 241, 243
    optics, 245, 246, 249, 250
      cooling, 246, 250
      lifetime, 245, 246, 249
      protection, 250
    power plant, 242, 243, 244, 245, 247
      availability factor, 249
    principle of separability, 244
    target, 241, 243, 244, 245, 246, 247, 248, 249
      convergence ratios, 247
      design issues, 247
      fast ignitor, 247
      gain, 241, 242, 243, 244, 245, 246, 247, 248, 249
    scientific feasibility, 241, 242, 243, 244, 249
  neutron shielding, 243
  technology development, why difficult, 242
  why we don't have a power plant now, 244
Fusion choking, 373, 375, 381
Fusion reaction rate, 183, 190
Fusion reactor, 299, 373, 374, 375
Fusion space propulsion, 177
  fusion, 65, 66, 73, 74, 75, 242
  confinement, types of, 242, 243
    defined, 242
  controlled thermonuclear, 373, 375
  economic feasibility, 242, 243, 244, 246, 247, 249
  engineering demonstration facility (EDF), 248
  enhancement, 390
  environmental impact, 241
  inertial
    ablator, 242
    defined, 242
    development path, 241, 242, 244, 247, 248
    direct drive, 241, 248
    driver, 241, 242
      defined, 243
    DPSSL, 241, 242, 245, 246, 247, 248, 249
    heavy-ion, 245, 246
    KrF laser, 245, 246
    light-ion, 245
  fuels, 242, 243, 244
    DT (deuterium–tritium), 243
    inexhaustible source, 241, 243
  of deuterium nuclei, 383
  plasma diagnostics, 431
  rate, 386
    in metallic lattices, 387
Fusion-grade plasmas, 180

Gain, 252, 253
GAMMA, 10, 197, 198, 199, 20, 201
Gas-dynamic trap, 15, 23
Goals of fusion research, 7
Goldston L-mode Tokamak scaling, 404, 405
Grid effective transparency, 183

HANBIT, 197
Hard X-ray, 467
Heating, 374
Helical axis, 74
Helical system, 65, 66, 72, 73, 74, 75
Heliotron, 65, 66, 67, 71, 73, 74, 75, 469
Helium ash, 375, 376, 377
HIEI, 197, 200
High beta tokamak, 341
High density compression, 213, 215, 221, 224
High density implosion, 214
High ion temperature mode, 73
Hohlraum, 83, 467
Hole boring, 219, 220
Hollow charge, 228, 229, 230, 233
Hot spark energy, 215
Hot spark main fuel mixing, 215
Hot spark, 215, 216, 224
Hybrid method, 219
Hydrodynamic equivalent plasma, 214, 215, 225
Hydrodynamic
  instabilities, 253, 254
  simulation code, 258
Hyperbolic Energy Analyzer (HEA), 448
Hypervelocity impact, 227, 231

ICDMP, 59, 60, 61, 63
ICF, 77, 213, 214, 217, 220, 225, 239, 251, 252, 255, 262
IEC, 177, 178, 179, 180, 181, 182, 183, 186, 190, 194
IFE, 213, 214, 215, 216, 223, 224
Ignition and burn, 215, 222
Ignition, 93, 79, 135, 251, 252, 253, 357, 360, 368, 375, 381
Imploding liner, 172, 173, 174

Implosion dynamics, 117, 125
Implosion, 257, 281
Imprint, 218, 219
Improvement of plasma confinement, 66, 70, 75
Impurities, 375
Indirect drive, 78, 467
Inductive cascade, 31, 36, 37
Inductive storage, 27, 30, 31, 32, 35, 36, 37, 38
  TIN-900, 27, 30, 31, 36, 37
  two-cascaded, 35
Inertial confinement fusion, 77, 213, 251, 252, 255
  laser, 251
    direct drive, 77, 251, 253
    indirect drive, 251, 253
Inertial Electrostatic Confinement (IEC), 177, 178, 179, 180,181, 182, 183, 186, 190, 194
  cylindrical, 179
  development strategy, 180
  spherical, 178
Inertial fusion, 1, 395, 396, 467
Inertial fusion energy, 213, 214, 225
Innovative confinement concepts, 2, 411
INS, 411
Instability, 81, 86, 373
Intense Neutron Source (INS), 411
Interchange instability, 456
International Center for Dense Magnetized Plasmas (ICDMP), 59, 60, 61, 63
Inverse diode, 174, 175
Inward plasma transport, 399
Ion cyclotron heating (ICH), 66, 72
Ion cyclotron resonance heating (ICRH), 198
Ion focus, 183
Ion magnetization, 287
Ion thermal conductivity, 138, 139
Ion trap, 179
Ion-electron coupling, 139
Irradiation uniformity, 213, 214, 215, 216, 221, 222, 223, 224
Isentrope of main fuel, 215
Isochoric targets, 233
ITER, 2, 353, 361, 362, 363, 364, 366, 368, 371, 395, 396, 404, 405, 469
ITG mode, 341

Jet-ignition, 227
Joule heating, 287

Kelvin-Helmholtz instability, 458
KI-1, 287
Kinetic ballooning mode, 341, 343, 344, 346, 348, 349, 350
Kinetic tandem mirror concept, 24

Laboratory experiments of astrophysics, 214
Laboratory simulation of ICF-plasma dynamics, 288
Large Mach number flows, 455, 459
Larmor radius, 140
Laser
  bandwidth and beam smoothing, 241, 248
  defined, 245
  DPSSL (Diode-Pumped Solid-State Laser), 241, 242, 245, 246, 247, 248, 249
    development path, 241, 246, 247, 248, 249
    multiple use, 249, 250
    prototype operation, 246, 248
  efficiency, 246, 247
  KrF, 245, 246
  Mercury laser, 246, 247, 250
  multi-pass architecture, 246, 248
  Nd:glass, 245, 246, 248
  pockels cell optical switch, 246
  pumping of gain medium, 246
    diodes, 246, 249
    flashlamps, 245
  Yb:S-FAP, 246, 247, 250
    crystal growth, 248
    storage lifetime, 246
Laser fusion, 213, 214, 215, 216, 225
Laser Fusion Rocket, 287
Laser irradiation uniformity, 213, 214, 215, 216, 221, 222, 223, 224
Laser-produced plasma, 287
LASNEX, 78, 83, 84, 85
Lawson criterion, 101, 354
  improved, 355
LILAC, 258
Linear colliders, 5, 16, 18, 20, 21, 22, 23, 24, 25
  breakeven length, 21
Linear growth, 142
Loading, 29, 20, 34, 35, 36, 37, 39
Low density plastic foam shell, 222, 224
Lower pressure limit, 50
Low-Q fusion power systems, 7, 9

M4X, 431, 432
Mach number requirement for centrifugal confinement, 459
Magnetic configurations, 137
Magnetic confinement, 65, 74, 75
Magnetic dipole, 287
Magnetic Dipole Moment Meter, 431, 445
Magnetic fusion, 1
Magnetic fusion energy, 396
Magnetic nozzle, 288
Magnetic shear, 457
  suppression of interchange, 457
Magnetic turbulence, 351
Magnetically suspension method, 223
Magnetized Target Fusion, 113, 114, 129, 261, 353, 463
Magnetoelectric heating, 396, 398, 409
Magnetoelectric toroidal confinement, 395, 397, 401
MAGO, 175, 261, 264, 265, 463, 464
Major radius, 137
Mass ablation rate, 217
Matching, 32, 36, 37, 38
Mean free path, 191

MHD interchange modes, 13
MHD, 397
Microlithography, 104
Microwave reflectometry, 139
Minor radius, 137, 140
Mirnov scaling, 403
Mirror confinement and adiabatic invariants, 10, 11
Mirror instability limit, 20
Mirror, 197
MTF (Magnetized Target Fusion), 113, 114, 129, 206, 261, 262, 263, 274, 276
Multiple mirrors, 171, 175
Multi-reactor system, 214

NAA, 177, 178, 179
National Ignition Facility, 251
NBI, 138
NBI, 66, 67, 68, 69, 70
Negative shear, 341, 343, 348, 349, 350
Neo-Alcator scaling, 404
Neoclassical theory, 139
Neutral Beam Heating (NBI), 66, 67, 68, 69, 70
Neutral beam injection (NBI), 138
Neutron Activation Analysis (NAA), 177, 178, 179
Neutron activation method, 220
Neutron knock-on method, 220
Neutron source, 177, 180, 194
  high intensity, 180
  volume, 181
Neutron sources, 411, 413, 414, 424
Neutron yield
Neutron
    cost, 29
    radiation, 30, 35, 39
    scaling law, 41, 42
    source, 28, 29, 31, 39
    yield, 29, 30, 33, 37, 43, 46, 47, 52, 179
Neutrons, 93, 97
Next Generation Lithography (NGL), 103
NGL – Next Generation Lithography, 105
NIF (National Ignition Facility), 77, 88, 89, 245, 247, 248, 249, 250, 251, 252, 253, 258, 287
Nonlinear controller, 373, 378, 380
Non-MHD flute instability, 288
NOVA, 251
Nuclear shape enhancement, 317, 327, 328
Nuclear yield, 100
Numerical simulation, 229

OAUGDP, 408
OMEGA, 251, 252, 255, 256, 258
One Atmosphere Uniform Glow Discharge Plasma, 408
Open-ended fusion systems, 6, 7, 8, 9, 10, 13, 14, 15, 16, 17, 18, 23, 24 25
Oscillating plasmas, 411, 417, 424

PACO, 49, 54
Partially coherent light (PCL), 221
Particle beams, 28, 29, 39
Particle confinement time, 402
PCL, 221
Peaking
    current, 28, 29, 30
    power, 29, 30, 32
    system, 30
PEGASUS, 464
Pellet, 467
Pellet injection, 199, 217, 222
Penning traps, 411, 417, 424
Penumbral coded imaging, 220
Periodic Oscillating Plasma Sphere (POPS), 411
Perveance K, 182
PET Scans, 181
Phenomenological scaling, 402
Phi target, 264
Pick-up coil, 287
PIC-simulation, 287
Pinch, 27, 28, 29, 32, 33, 34, 35, 37
    compression, 35
    current, 29, 37
    dense, 29
    inductance, 37
    phase, 33, 34
    spherical, 93, 94, 103, 133, 469
    Z-pinch, 27, 28
      non-cylindrical, 28, 29
Plasma
    current, 27, 30, 35, 38
    heating, 29
    loading, 30, 37, 38, 39
    switch, 29
Plasma confinement, 198
Plasma current, 137
Plasma-current sheath (PCS), 28, 32, 38
Plasma Focus (PF), 27, 28, 32
    Filippov-type, 27, 28, 30, 39
    Mather-type, 27, 28
Plasma free energy, 401
Plasma jets, 227, 228, 229, 230, 231, 232, 233, 235, 236
Plasma layering method, 223
Plasma liner, 121
Plasma-magnetic field interaction, 287
Plasma recoil momentum, 287
Plasma stability, 200
Plasma transport, 139, 141
Plug/barrier potential, 198, 199, 200
POPS (Periodic Oscillating Plasma Sphere), 411
Potential, 197
Potential confinement, 197
Potential formation, 198, 199, 200
Power amplification, 31, 35
Power balance (of laser beams), 221, 222
Preheat, 215
Pre-ionization, 281
Proton rate density, 188, 191
Proton therapy, 181
Pulse shaping, 80

Pulsed power, 61, 62, 63, 64
Pulsed - high current - discharges, 27, 29, 31, 32, 35

Radial confinement, 199
Radiation diagnostics, 107
Radiation losses, 93
Random phase plate (RPP), 221
Rayleigh-Taylor (R-T) instability, 118, 215, 218
Reflectometer, 139
Relativistic effect (of laser beam), 216, 219
Reversed Field Pinch (RFP), 303, 313
Reversed magnetic shear, 137, 143
RFP reactor, 304, 305, 306, 307, 308, 310
Richtmeyer-Meshkov instability, 239
Ripple shock wave, 219
RMF (Rotating Magnetic Field), 146
RO5, 54, 56
Rotating degenerate gas, 461
Rotational transform, 66, 67, 70, 74
RPP, 221

Safety factor, 137, 138
Sawtooth relaxation, 352
Scaling, 200
Scaling law, 29, 33, 35, 37, 65, 68, 73, 74
Scattered waves, 139
Scientific co-operation, 59, 60, 61, 63
Second stability regime, 341, 342, 343, 346, 347, 349, 350
Secondary reaction method, 220
Self-focusing, 219, 220
Self-organization, 427
Semiconductor proton detector, 185
SESAME, 240
Shafranov shift, 342
Shock heating, 119
Shock wave, 93, 94, 96, 97, 98
    implosion, 93, 98
Shutdown, 377
Similarity criteria, 287
Similarity solutions, 419
Simulation code (IXL), 186, 190
Soft and hard x-ray emissivity, 352
Source, 37, 39
Space charge configuration (SCC), 427
Spherical devices, 411
Spherical liner, 203
Spherical pinch, 93, 94, 103, 133, 469
    geometry, 133
    spin-offs, industrial, 133
Spherical tokamak, 175
Spheromak, 171, 175
SPX (Spherical Pinch X-Ray Generator), 104, 105, 106
SPX machine, 105
SSD, 254, 255
Stand-off energy source, 171, 174
Star Mode plasma, 178, 180, 181, 183
Startup, 377
Stellarator, 402, 405
Stored energy, 28, 30, 32, 33
Supershot regime, 138
Switch, 28, 29, 30, 31, 32, 35, 36, 37, 38
System identification, 381

Tandem mirror, 197, 469
Target confinement, 122
Target gain, 467
Target levitation, 222, 223
Target plasma, 264
Taylor-Couette flow, 459
Temperature measurement, 109
TFTR, 137, 138, 139, 343, 348
Thermal dike, 201
Time of bifurcation, 138, 139
Tokamak, 137, 139, 140, 142, 180, 351, 371, 373, 395, 396, 402, 405, 472, 473
    SINP, 351
Tokamak Fusion Test Reactor (TFTR), 137, 138, 139
Toroidal magnetic field, 137
Torsatron, 402
TRAC2 code, 284
Training, 59, 60, 61, 62, 63
Transport barrier, 138, 139
Trapped ions, 183, 184, 191, 192
Turbulent fluctuations, 137, 139, 141, 142, 143

Ultra-high-intensity laser, 215, 216, 219, 224
Ultra-intense field physics, 214
UNESCO, 60, 63
Upper pressure limit, 48
User facility, 171, 172, 173, 174, 175

Variable Energy Analyzer (VEA), 431, 432, 434, 435, 436
Velocity shear, 455. 456, 457
    suppression of instability, 455
    stabilization of Z-pinch, 455
    residual wobble, 455, 456, 457, 459
Velocity-space instabilities in open systems, 14, 15
Virtual anode, 182, 183, 138, 190, 191
Vlasov-Maxwell equation 291, 333
    generalized, 333
Vlasov-Poisson's equations, 182, 183

Wall boronization, 311
Wavenumber, 139

X-ray
    production, 33
    radiation, 28, 29, 33 39
X-ray imaging camera, 217, 220

Z pinch, 281, 283, 469
    diagnostics, 283, 28
    staged, 279, 281